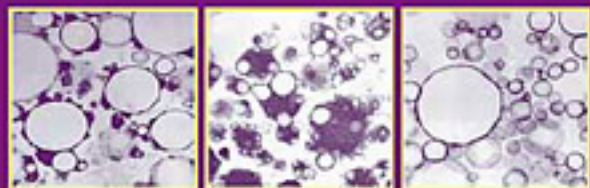


Food Emulsions

Fourth Edition, Revised and Expanded



edited by

Stig E. Friberg

Kåre Larsson

Johan Sjöblom

Food Emulsions

Fourth Edition, Revised and Expanded

edited by

Stig E. Friberg

*University of Missouri–Rolla
Rolla, Missouri
and Clarkson University
Potsdam, New York, U.S.A.*

Kåre Larsson

*Camurus Lipid Research
Lund, Sweden*

Johan Sjöblom

*Norwegian University of Science and Technology
Trondheim, Norway*

The previous edition of this book was published as *Food Emulsions: Third Edition, Revised and Expanded*, edited by Stig E. Friberg and Kåre Larsson, 1997 (Marcel Dekker, Inc.), ISBN 0-8247-9983-6.

Although great care has been taken to provide accurate and current information, neither the author(s) nor the publisher, nor anyone else associated with this publication, shall be liable for any loss, damage, or liability directly or indirectly caused or alleged to be caused by this book. The material contained herein is not intended to provide specific advice or recommendations for any specific situation.

Trademark notice: Product or corporate names may be trademarks or registered trademarks and are used only for identification and explanation without intent to infringe.

Library of Congress Cataloging-in-Publication Data

A catalog record for this book is available from the Library of Congress.

ISBN: 0-8247-4696-1

This book is printed on acid-free paper.

Headquarters

Marcel Dekker, Inc., 270 Madison Avenue, New York, NY 10016, U.S.A.
tel: 212-696-9000; fax: 212-685-4540

Distribution and Customer Service

Marcel Dekker, Inc., Cimarron Road, Monticello, New York 12701, U.S.A.
tel: 800-228-1160; fax: 845-796-1772

Eastern Hemisphere Distribution

Marcel Dekker AG, Hutgasse 4, Postfach 812, CH-4001 Basel, Switzerland
tel: 41-61-260-6300; fax: 41-61-260-6333

World Wide Web

<http://www.dekker.com>

The publisher offers discounts on this book when ordered in bulk quantities. For more information, write to Special Sales/Professional Marketing at the headquarters address above.

Copyright © 2004 by Marcel Dekker, Inc. All Rights Reserved.

Neither this book nor any part may be reproduced or transmitted in any form or by any means, electronic or mechanical, including photocopying, microfilming, and recording, or by any information storage and retrieval system, without permission in writing from the publisher.

Current printing (last digit):

10 9 8 7 6 5 4 3 2 1

PRINTED IN THE UNITED STATES OF AMERICA

FOOD SCIENCE AND TECHNOLOGY

A Series of Monographs, Textbooks, and Reference Books

EDITORIAL BOARD

Senior Editors

Owen R. Fennema University of Wisconsin–Madison
Y. H. Hui Science Technology System
Marcus Karel Rutgers University (emeritus)
Pieter Walstra Wageningen University
John R. Whitaker University of California–Davis

Additives **P. Michael Davidson** University of Tennessee–Knoxville
Dairy science **James L. Steele** University of Wisconsin–Madison
Flavor chemistry and sensory analysis **John H. Thorngate III** University of California–Davis
Food engineering **Daryl B. Lund** University of Wisconsin–Madison
Food lipids and flavors **David B. Min** Ohio State University
Food proteins/food chemistry **Rickey Y. Yada** University of Guelph
Health and disease **Seppo Salminen** University of Turku, Finland
Nutrition and nutraceuticals **Mark Dreher** Mead Johnson Nutritionals
Phase transition/food microstructure **Richard W. Hartel** University of Wisconsin–Madison
Processing and preservation **Gustavo V. Barbosa-Cánovas** Washington State University–Pullman
Safety and toxicology **Sanford Miller** University of Texas–Austin

1. Flavor Research: Principles and Techniques, *R. Teranishi, I. Hornstein, P. Issenberg, and E. L. Wick*
2. Principles of Enzymology for the Food Sciences, *John R. Whitaker*
3. Low-Temperature Preservation of Foods and Living Matter, *Owen R. Fennema, William D. Powrie, and Elmer H. Marth*
4. Principles of Food Science
Part I: Food Chemistry, *edited by Owen R. Fennema*
Part II: Physical Principles of Food Preservation, *Marcus Karel, Owen R. Fennema, and Daryl B. Lund*
5. Food Emulsions, *edited by Stig E. Friberg*
6. Nutritional and Safety Aspects of Food Processing, *edited by Steven R. Tannenbaum*
7. Flavor Research: Recent Advances, *edited by R. Teranishi, Robert A. Flath, and Hiroshi Sugisawa*
8. Computer-Aided Techniques in Food Technology, *edited by Israel Saguy*

9. Handbook of Tropical Foods, *edited by Harvey T. Chan*
10. Antimicrobials in Foods, *edited by Alfred Larry Branen and P. Michael Davidson*
11. Food Constituents and Food Residues: Their Chromatographic Determination, *edited by James F. Lawrence*
12. Aspartame: Physiology and Biochemistry, *edited by Lewis D. Stegink and L. J. Filer, Jr.*
13. Handbook of Vitamins: Nutritional, Biochemical, and Clinical Aspects, *edited by Lawrence J. Machlin*
14. Starch Conversion Technology, *edited by G. M. A. van Beynum and J. A. Roels*
15. Food Chemistry: Second Edition, Revised and Expanded, *edited by Owen R. Fennema*
16. Sensory Evaluation of Food: Statistical Methods and Procedures, *Michael O'Mahony*
17. Alternative Sweeteners, *edited by Lyn O'Brien Nabors and Robert C. Gelardi*
18. Citrus Fruits and Their Products: Analysis and Technology, *S. V. Ting and Russell L. Rouseff*
19. Engineering Properties of Foods, *edited by M. A. Rao and S. S. H. Rizvi*
20. Umami: A Basic Taste, *edited by Yojiro Kawamura and Morley R. Kare*
21. Food Biotechnology, *edited by Dietrich Knorr*
22. Food Texture: Instrumental and Sensory Measurement, *edited by Howard R. Moskowitz*
23. Seafoods and Fish Oils in Human Health and Disease, *John E. Kinsella*
24. Postharvest Physiology of Vegetables, *edited by J. Weichmann*
25. Handbook of Dietary Fiber: An Applied Approach, *Mark L. Dreher*
26. Food Toxicology, Parts A and B, *Jose M. Concon*
27. Modern Carbohydrate Chemistry, *Roger W. Binkley*
28. Trace Minerals in Foods, *edited by Kenneth T. Smith*
29. Protein Quality and the Effects of Processing, *edited by R. Dixon Phillips and John W. Finley*
30. Adulteration of Fruit Juice Beverages, *edited by Steven Nagy, John A. Attaway, and Martha E. Rhodes*
31. Foodborne Bacterial Pathogens, *edited by Michael P. Doyle*
32. Legumes: Chemistry, Technology, and Human Nutrition, *edited by Ruth H. Matthews*
33. Industrialization of Indigenous Fermented Foods, *edited by Keith H. Steinkraus*
34. International Food Regulation Handbook: Policy • Science • Law, *edited by Roger D. Middlekauff and Philippe Shubik*
35. Food Additives, *edited by A. Larry Branen, P. Michael Davidson, and Seppo Salminen*
36. Safety of Irradiated Foods, *J. F. Diehl*

37. Omega-3 Fatty Acids in Health and Disease, *edited by Robert S. Lees and Marcus Karel*
38. Food Emulsions: Second Edition, Revised and Expanded, *edited by Kåre Larsson and Stig E. Friberg*
39. Seafood: Effects of Technology on Nutrition, *George M. Pigott and Barbee W. Tucker*
40. Handbook of Vitamins: Second Edition, Revised and Expanded, *edited by Lawrence J. Machlin*
41. Handbook of Cereal Science and Technology, *Klaus J. Lorenz and Karel Kulp*
42. Food Processing Operations and Scale-Up, *Kenneth J. Valentas, Leon Levine, and J. Peter Clark*
43. Fish Quality Control by Computer Vision, *edited by L. F. Pau and R. Olafsson*
44. Volatile Compounds in Foods and Beverages, *edited by Henk Maarse*
45. Instrumental Methods for Quality Assurance in Foods, *edited by Daniel Y. C. Fung and Richard F. Matthews*
46. *Listeria*, Listeriosis, and Food Safety, *Elliot T. Ryser and Elmer H. Marth*
47. Acesulfame-K, *edited by D. G. Mayer and F. H. Kemper*
48. Alternative Sweeteners: Second Edition, Revised and Expanded, *edited by Lyn O'Brien Nabors and Robert C. Gelardi*
49. Food Extrusion Science and Technology, *edited by Jozef L. Kokini, Chi-Tang Ho, and Mukund V. Karwe*
50. Surimi Technology, *edited by Tyre C. Lanier and Chong M. Lee*
51. Handbook of Food Engineering, *edited by Dennis R. Heldman and Daryl B. Lund*
52. Food Analysis by HPLC, *edited by Leo M. L. Nollet*
53. Fatty Acids in Foods and Their Health Implications, *edited by Ching Kuang Chow*
54. *Clostridium botulinum*: Ecology and Control in Foods, *edited by Andreas H. W. Hauschild and Karen L. Dodds*
55. Cereals in Breadmaking: A Molecular Colloidal Approach, *Ann-Charlotte Eliasson and Kåre Larsson*
56. Low-Calorie Foods Handbook, *edited by Aaron M. Altschul*
57. Antimicrobials in Foods: Second Edition, Revised and Expanded, *edited by P. Michael Davidson and Alfred Larry Branen*
58. Lactic Acid Bacteria, *edited by Seppo Salminen and Atte von Wright*
59. Rice Science and Technology, *edited by Wayne E. Marshall and James I. Wadsworth*
60. Food Biosensor Analysis, *edited by Gabriele Wagner and George G. Guilbault*
61. Principles of Enzymology for the Food Sciences: Second Edition, *John R. Whitaker*
62. Carbohydrate Polyesters as Fat Substitutes, *edited by Casimir C. Akoh and Barry G. Swanson*
63. Engineering Properties of Foods: Second Edition, Revised and Expanded, *edited by M. A. Rao and S. S. H. Rizvi*

64. Handbook of Brewing, *edited by William A. Hardwick*
65. Analyzing Food for Nutrition Labeling and Hazardous Contaminants, *edited by Ike J. Jeon and William G. Ikins*
66. Ingredient Interactions: Effects on Food Quality, *edited by Anilkumar G. Gaonkar*
67. Food Polysaccharides and Their Applications, *edited by Alistair M. Stephen*
68. Safety of Irradiated Foods: Second Edition, Revised and Expanded, *J. F. Diehl*
69. Nutrition Labeling Handbook, *edited by Ralph Shapiro*
70. Handbook of Fruit Science and Technology: Production, Composition, Storage, and Processing, *edited by D. K. Salunkhe and S. S. Kadam*
71. Food Antioxidants: Technological, Toxicological, and Health Perspectives, *edited by D. L. Madhavi, S. S. Deshpande, and D. K. Salunkhe*
72. Freezing Effects on Food Quality, *edited by Lester E. Jeremiah*
73. Handbook of Indigenous Fermented Foods: Second Edition, Revised and Expanded, *edited by Keith H. Steinkraus*
74. Carbohydrates in Food, *edited by Ann-Charlotte Eliasson*
75. Baked Goods Freshness: Technology, Evaluation, and Inhibition of Staling, *edited by Ronald E. Hebeda and Henry F. Zobel*
76. Food Chemistry: Third Edition, *edited by Owen R. Fennema*
77. Handbook of Food Analysis: Volumes 1 and 2, *edited by Leo M. L. Nollet*
78. Computerized Control Systems in the Food Industry, *edited by Gauri S. Mittal*
79. Techniques for Analyzing Food Aroma, *edited by Ray Marsili*
80. Food Proteins and Their Applications, *edited by Srinivasan Damodaran and Alain Paraf*
81. Food Emulsions: Third Edition, Revised and Expanded, *edited by Stig E. Friberg and Kåre Larsson*
82. Nonthermal Preservation of Foods, *Gustavo V. Barbosa-Cánovas, Usha R. Pothakamury, Enrique Palou, and Barry G. Swanson*
83. Milk and Dairy Product Technology, *Edgar Spreer*
84. Applied Dairy Microbiology, *edited by Elmer H. Marth and James L. Steele*
85. Lactic Acid Bacteria: Microbiology and Functional Aspects: Second Edition, Revised and Expanded, *edited by Seppo Salminen and Atte von Wright*
86. Handbook of Vegetable Science and Technology: Production, Composition, Storage, and Processing, *edited by D. K. Salunkhe and S. S. Kadam*
87. Polysaccharide Association Structures in Food, *edited by Reginald H. Walter*
88. Food Lipids: Chemistry, Nutrition, and Biotechnology, *edited by Casimir C. Akoh and David B. Min*
89. Spice Science and Technology, *Kenji Hirasa and Mitsuo Takemasa*

90. Dairy Technology: Principles of Milk Properties and Processes, *P. Walstra, T. J. Geurts, A. Noomen, A. Jellema, and M. A. J. S. van Boekel*
91. Coloring of Food, Drugs, and Cosmetics, *Gisbert Otterstätter*
92. *Listeria*, Listeriosis, and Food Safety: Second Edition, Revised and Expanded, *edited by Elliot T. Ryser and Elmer H. Marth*
93. Complex Carbohydrates in Foods, *edited by Susan Sungsoo Cho, Leon Prosky, and Mark Dreher*
94. Handbook of Food Preservation, *edited by M. Shafiur Rahman*
95. International Food Safety Handbook: Science, International Regulation, and Control, *edited by Kees van der Heijden, Maged Younes, Lawrence Fishbein, and Sanford Miller*
96. Fatty Acids in Foods and Their Health Implications: Second Edition, Revised and Expanded, *edited by Ching Kuang Chow*
97. Seafood Enzymes: Utilization and Influence on Postharvest Seafood Quality, *edited by Norman F. Haard and Benjamin K. Simpson*
98. Safe Handling of Foods, *edited by Jeffrey M. Farber and Ewen C. D. Todd*
99. Handbook of Cereal Science and Technology: Second Edition, Revised and Expanded, *edited by Karel Kulp and Joseph G. Ponte, Jr.*
100. Food Analysis by HPLC: Second Edition, Revised and Expanded, *edited by Leo M. L. Nollet*
101. Surimi and Surimi Seafood, *edited by Jae W. Park*
102. Drug Residues in Foods: Pharmacology, Food Safety, and Analysis, *Nickos A. Botsoglou and Dimitrios J. Fletouris*
103. Seafood and Freshwater Toxins: Pharmacology, Physiology, and Detection, *edited by Luis M. Botana*
104. Handbook of Nutrition and Diet, *Babasaheb B. Desai*
105. Nondestructive Food Evaluation: Techniques to Analyze Properties and Quality, *edited by Sundaram Gunasekaran*
106. Green Tea: Health Benefits and Applications, *Yukihiko Hara*
107. Food Processing Operations Modeling: Design and Analysis, *edited by Joseph Irudayaraj*
108. Wine Microbiology: Science and Technology, *Claudio Delfini and Joseph V. Formica*
109. Handbook of Microwave Technology for Food Applications, *edited by Ashim K. Datta and Ramaswamy C. Anantheswaran*
110. Applied Dairy Microbiology: Second Edition, Revised and Expanded, *edited by Elmer H. Marth and James L. Steele*
111. Transport Properties of Foods, *George D. Saravacos and Zacharias B. Maroulis*
112. Alternative Sweeteners: Third Edition, Revised and Expanded, *edited by Lyn O'Brien Nabors*
113. Handbook of Dietary Fiber, *edited by Susan Sungsoo Cho and Mark L. Dreher*
114. Control of Foodborne Microorganisms, *edited by Vijay K. Juneja and John N. Sofos*
115. Flavor, Fragrance, and Odor Analysis, *edited by Ray Marsili*

116. Food Additives: Second Edition, Revised and Expanded, *edited by A. Larry Branen, P. Michael Davidson, Seppo Salminen, and John H. Thorngate, III*
117. Food Lipids: Chemistry, Nutrition, and Biotechnology: Second Edition, Revised and Expanded, *edited by Casimir C. Akoh and David B. Min*
118. Food Protein Analysis: Quantitative Effects on Processing, *R. K. Owusu-Apenten*
119. Handbook of Food Toxicology, *S. S. Deshpande*
120. Food Plant Sanitation, *edited by Y. H. Hui, Bernard L. Bruinsma, J. Richard Gorham, Wai-Kit Nip, Phillip S. Tong, and Phil Ventresca*
121. Physical Chemistry of Foods, *Pieter Walstra*
122. Handbook of Food Enzymology, *edited by John R. Whitaker, Alphons G. J. Voragen, and Dominic W. S. Wong*
123. Postharvest Physiology and Pathology of Vegetables: Second Edition, Revised and Expanded, *edited by Jerry A. Bartz and Jeffrey K. Brecht*
124. Characterization of Cereals and Flours: Properties, Analysis, and Applications, *edited by Gönül Kaletunç and Kenneth J. Breslauer*
125. International Handbook of Foodborne Pathogens, *edited by Marianne D. Miliotis and Jeffrey W. Bier*
126. Food Process Design, *Zacharias B. Maroulis and George D. Saravacos*
127. Handbook of Dough Fermentations, *edited by Karel Kulp and Klaus Lorenz*
128. Extraction Optimization in Food Engineering, *edited by Constantina Tzia and George Liadakis*
129. Physical Principles of Food Preservation: Second Edition, Revised and Expanded, *Marcus Karel and Daryl B. Lund*
130. Handbook of Vegetable Preservation and Processing, *edited by Y. H. Hui, Sue Ghazala, Dee M. Graham, K. D. Murrell, and Wai-Kit Nip*
131. Handbook of Flavor Characterization: Sensory Analysis, Chemistry, and Physiology, *edited by Kathryn D. Deibler and Jeannine Delwiche*
132. Food Emulsions: Fourth Edition, Revised and Expanded, *edited by Stig E. Friberg, Kåre Larsson, and Johan Sjöblom*

Additional Volumes in Preparation

Handbook of Frozen Foods, *edited by Y. H. Hui, Paul Cornillon, Isabel Guerrero Legarreta, Miang Lim, K. D. Murrell, and Wai-Kit Nip*

Handbook of Food and Beverage Fermentation Technology, *edited by Y. H. Hui, Lisbeth M. Goddik, Aase Solvejg Hansen, Jytte Josephsen, Wai-Kit Nip, Peggy S. Stanfield, and Fidel Toldra*

Industrialization of Indigenous Fermented Foods: Second Edition, Revised and Expanded, *edited by Keith H. Steinkraus*

Genetic Variation in Taste Sensitivity, edited by John Prescott and Beverly J. Tepper

Handbook of Food Analysis: Second Edition, Revised and Expanded: Volumes 1, 2, and 3, edited by Leo M. L. Nollet

Vitamin E: Food Chemistry, Composition, and Analysis, Ronald Eitenmiller and Junsoo Lee

Preface to the Fourth Edition

Food Emulsions has now reached its fourth edition and very much reflects the strength of the original publication. Like the previous editions, this book realizes the value of the long tradition of diversity and excellence of research and development within the food emulsion industry. This is exemplified by [Chapter 12](#) on beverage emulsions (Tan), by [Chapter 2](#) on food emulsifiers (Krog and Sparsø); by [Chapter 4](#) on proteins and polar lipids (Nylander); by [Chapter 1](#) on food emulsions in general (Dagleish), and by [Chapter 13](#) on dressings and sauces (Ford et al.).

There is probably no other emulsion category for which components have more influence on the properties of crystalline and liquid crystalline structures, than lipids—[Chapter 3](#) by Larsson on lipid structures is essential reading.

The first edition of the book introduced advanced chapters on the fundamentals of food emulsion properties, and this aspect is a conspicuous feature of the present book with [Chapter 5](#) on destabilizing mechanisms, [Chapter 6](#) on emulsion stability, [Chapter 9](#) on orthokinetic stability, [Chapter 8](#) on coalescence mechanism, and [Chapter 10](#) on the characteristics of double emulsions.

Finally, this edition shows strength in an area not represented as strongly earlier: namely, the different methods of characterization and analysis of emulsions. [Chapter 14](#) on droplet analysis by Coupland and McClements, [Chapter 7](#) on surface forces in emulsions by Claesson et al., [Chapter 11](#) on rheology of emulsions by Princen, and [Chapter 15](#) on NMR in food emulsions by Balinov et al. give excellent overviews of these methods.

Needless to say, this book exceeds the quality of its predecessors, and we take this opportunity to recognize the truly outstanding efforts of our colleagues.

*Stig E. Friberg
Kåre Larsson
Johan Sjöblom*

Preface to the Third Edition

The economic and social changes during the last decades have changed the formulation requirements for emulsion systems in the most drastic manner.

Total cost analysis means that the selection of ingredients is no longer just a question of cost per pound, but the efforts to stabilize the system must now be complemented by “hidden” costs for long-term technical or commercial failures—sometimes related only indirectly to stability. Social pressure has meant that new components with little or no nutritional value and with intermolecular interactions different from traditional components must be accommodated, leading to phenomena for which the earlier methods provide no appropriate response.

Taken in total, the consequences of change are that complex food emulsion systems must be analyzed with proper attention to the colloidal structures involved. Hence, the effects of the specific properties and interactions of polymers and proteins included in this book and the association structures of lipids leading to the formation of vesicles have received the attention they merit.

*Stig E. Friberg
Kåre Larsson*

Contents

Preface to the Fourth Edition

Preface to the Third Edition

Contributors

1. Food Emulsions: Their Structures and Properties

Douglas G. Dalgleish

2. Food Emulsifiers: Their Chemical and Physical Properties

Niels J. Krog and Flemming Vang Sparsø

3. Molecular Organization in Lipids and Emulsions

Kåre Larsson

4. Interactions Between Proteins and Polar Lipids

Tommy Nylander

5. Droplet Flocculation and Coalescence in Dilute Oil-in-Water Emulsions

Øystein Sæther, Johan Sjöblom, and Stanislav S. Dukhin

6. Structure and Stability of Aerated Food Emulsions

D. T. Wasan, W. Xu, A. Dutta, and A. Nikolov

7. Surface Forces and Emulsion Stability

Per M. Claesson, Eva Blomberg, and Evgeni Poptoshev

- 8. Coalescence Mechanisms in Protein-Stabilized Emulsions**
George A. van Aken
- 9. Orthokinetic Stability of Food Emulsions**
Siva A. Vanapalli and John N. Coupland
- 10. Recent Developments in Double Emulsions for Food Applications**
Nissim Garti and Axel Benichou
- 11. Structure, Mechanics, and Rheology of Concentrated Emulsions and Fluid Foams**
H. M. Princen
- 12. Beverage Emulsions**
Chee-Teck Tan
- 13. Dressings and Sauces**
Larry D. Ford, Raju P. Borwankar, David Pechak, and Bill Schwimmer
- 14. Analysis of Droplet Characteristics Using Low-Intensity Ultrasound**
John N. Coupland and D. Julian McClements
- 15. NMR in Studies of Emulsions with Particular Emphasis on Food Emulsions**
Balin Balinov, Francois Mariette, and Olle Söderman

Contributors

Balin Balinov Department of Physical and Analytical Chemistry, Amersham Health, Oslo, Norway

Axel Benichou Casali Institute of Applied Chemistry, The Hebrew University of Jerusalem, Jerusalem, Israel

Eva Blomberg Royal Institute of Technology, Stockholm, Sweden

Raju P. Borwankar Kraft Foods, East Hanover, New Jersey, U.S.A.

Per M. Claesson Royal Institute of Technology, Stockholm, Sweden

John N. Coupland Department of Food Science, The Pennsylvania State University, University Park, Pennsylvania, U.S.A.

Douglas G. Dalgleish University of Guelph, Guelph, Ontario, Canada

Stanislav S. Dukhin New Jersey Institute of Technology, Newark, New Jersey, U.S.A.

A. Dutta Illinois Institute of Technology, Chicago, Illinois, U.S.A.

Larry D. Ford Kraft Foods, Memphis, Tennessee, U.S.A.

Nissim Garti Casali Institute of Applied Chemistry, The Hebrew University of Jerusalem, Jerusalem, Israel

Niels J. Krog Danisco, Brabrand, Denmark

Kåre Larsson Camurus Lipid Research, Lund, Sweden

Francois Mariette Cemagref, Rennes, France

D. Julian McClements The University of Massachusetts, Amherst, Massachusetts, U.S.A.

A. Nikolov Illinois Institute of Technology, Chicago, Illinois, U.S.A.

Tommy Nylander Department of Physical Chemistry, Center for Chemistry and Chemical Engineering, Lund University, Lund, Sweden

David Pechak Kraft Foods, Glenview, Illinois, U.S.A.

Evgeni Poptoshev Royal Institute of Technology, Stockholm, Sweden

H. M. Princen Consultant, Flemington, New Jersey, U.S.A.

Øystein Sæther Department of Chemical Engineering, Norwegian University of Science and Technology, Trondheim, Norway

Bill Schwimmer Kraft Foods, Glenview, Illinois, U.S.A.

Johan Sjöblom Department of Chemical Engineering, Norwegian University of Science and Technology, Trondheim, Norway

Olle Söderman Department of Physical Chemistry, University of Lund, Lund, Sweden

Chee-Teck Tan Consultant, Middletown, New Jersey, U.S.A.

George A. van Aken Wageningen Centre for Food Sciences, Wageningen, The Netherlands

Siva A. Vanapalli Department of Chemical Engineering, University of Michigan, Ann Arbor, Michigan, U.S.A.

Flemming Vang Sparsø Danisco, Brabrand, Denmark

D. T. Wasan Illinois Institute of Technology, Chicago, Illinois, U.S.A.

W. Xu Illinois Institute of Technology, Chicago, Illinois, U.S.A.

1

Food Emulsions: Their Structures and Properties

Douglas G. Dalgleish

University of Guelph, Guelph, Ontario, Canada

I. INTRODUCTION

A. General Introduction

The taste and texture of a processed food perceived by the consumer depend on a variety of factors, important among which are the structures formed by the constituent materials. The molecules which make up the food interact to create assemblies of molecules which give the structure and hence to a large extent, determine the texture of the particular food. The ingredients are assembled during processing, and the structure created by the manufacturer is governed by the controlled application of one or more effects: physical (e.g., interparticle forces, phase separations), chemical (e.g., formation of specific covalent bonds between molecules and particles), or biological (e.g., fermentation, enzyme action). It is, of course, the aim of the processor to generate products of predictable properties from materials whose properties are themselves understood and to do this as economically as possible.

Among the structures and structure-forming units within foods, emulsions play a major part. They are known to impart desirable mouthfeel characteristics to the food, but, in addition, they are key ingredients in the formation of structures in certain products, such as whipped toppings and ice creams, and more complex products, such as processed cheeses. Therefore, the understanding of the formation, structures, and properties of emulsions is essential to the creation and stabilization of structures in foods. Food emulsions are widely used and are familiar to almost everyone. In addition to the products just mentioned, whole milk and cream are

emulsions, as are butter, margarine, spreads, mayonnaises and dressings, coffee creamers, cream liqueurs, some fruit drinks and whippable toppings. Many meat products depend on the presence of emulsions for their properties, as does bread dough, although in both cases the emulsion structures can be extremely complex.

The formulation and creation of a food structure involving emulsions is always a compromise, depending on the desired qualities of the food and the materials which can be used to create these qualities. In addition to the essential physical functionality of the materials, it is necessary to take into account nontechnological, but nonetheless important, factors. Foods contain ingredients which are subject to regulation by appropriate agencies. In some cases, the use of certain ingredients may be discouraged because of restrictions imposed by certain religious groups or by public perceptions of health issues. Furthermore, the processor is constrained by economics and cannot use expensive materials in product formulations. Last but not least, the product must be safe from a microbiological point of view; this may have important consequences because of the need for heat treatments, which may affect the stability of an emulsion during processing. All of these factors make the study of the efficient formulation and production of emulsions a key to the structure and behavior of processed foods.

B. Emulsion Types

An emulsion is a suspension of one phase in another in which it is immiscible. One of the phases exists as discrete droplets suspended in the second, continuous, phase, and there is an interfacial layer between the two phases which is occupied by some necessary surfactant material. There are three main types of emulsion which are important, or potentially so, in foods. In oil-in-water (o/w) emulsions, droplets of oil are suspended in an aqueous continuous phase. These are the most versatile of the emulsion types; they exist in many forms (mayonnaises, cream liqueurs, creamers, whippable toppings, ice cream mixes), and their properties can be controlled by varying both the surfactants used and the components present in the aqueous phase. Water-in-oil (w/o) emulsions are typified by butter, margarines, and fat-based spreads in general. These depend for their stability more on the properties of the fat or oil and the surfactant used than in the properties of the aqueous phase, and because of this, there are fewer parameters which can be varied to control their stability. The third of the emulsion types is water-in-oil-in-water (w/o/w), which is, in effect, an o/w emulsion whose droplets themselves contain water droplets (i.e., are w/o emulsions). These are the most difficult emulsions to produce and control, because the water

droplets contained in the oil droplets must be stable, as must the oil droplets contained in the continuous aqueous phase. These emulsions are described in detail in [Chapter 5](#) and will not be described further here.

For convenience of description, we may divide o/w food emulsions into three classes, depending on how they are to be used. The first class contains emulsions which are end products in themselves. Coffee creamers and cream liqueurs are relatively simple emulsions whose only requirement is to remain stable toward creaming and coalescence during their shelf-life (which, however, may have to be considerable, so that sterility is also important). These emulsions present less of a challenge to the processor than do more complex emulsions; there are a few basic rules of formulation which allow successful products to be created. The second class of emulsions contains those which can be used as ingredients that participate in forming the structures of more complex products; that is, other components of the food (proteins, polysaccharides) form a matrix in which the fat globules are trapped or with which they interact. Examples are yogurts, processed cheeses, and other gelled systems containing emulsion droplets which must interact with other components in the food, but are not destabilized in the process. Their effect is to alter the rheological properties of the gel, thus creating texture and mouthfeel. In the third class of emulsion, the droplets are required to create new structures during processing, such as in ice cream or whipped products (1,2), where the emulsion is destabilized and further interacts as a means of creating structure in the product. Some emulsions themselves may also form gels during heating, to create new structures within foods (3). The requirements for the compositions and properties of the emulsion droplets are different in these different cases. However, it is generally necessary for the emulsion droplets to interact with themselves and/or with the other food components to give the required structures.

One of the ultimate goals in studying emulsions is to be able to describe their functionality well enough from first principles to allow the reduction of the amount of fat in a product without, at the same time, adversely affecting its texture and organoleptic properties. Similarly, it is important to anticipate the possibility that emulsions will be used as carriers of flavors or bioactive materials. To best achieve this, we need to understand how the fat functions in the original structure and how any material which is used to replace it should efficiently reproduce all of this function. Ideally, we would like to be able to define the properties of a product and then to construct it from a knowledge of the possible ingredients. At the present time, this is possible for only a few of the simpler systems.

In the text which follows, emphasis has been given to emulsions prepared using milk constituents. This is simply because the milk proteins are

by far the most studied of the food proteins (being easily prepared, soluble, and relatively well behaved once they are in solution) and the emulsions prepared using these materials have a correspondingly voluminous literature, especially on the subject of ice cream. Reports on the basic properties of other proteins in emulsions are more fragmentary; this is not to say that they are unimportant, as the egg-based mayonnaise, to name only one, is a very widely used product.

II. THE BASIS OF THE BEHAVIOR OF OIL-IN-WATER EMULSIONS

A. General Aspects of Emulsions

Oil and water do not coexist comfortably because of the surface energy (Gibbs free energy) of the oil–water interface. Because of the interfacial tension between oil and water, any emulsion will seek to minimize the interfacial energy by making the interfacial area between oil and water as small as possible. In the absence of surfactants, this is achieved by coalescence of the oil droplets, to give separated layers of oil and water. The presence of adsorbed surfactant molecules lowers the interfacial tension between the oil and water phases, so that the driving force for coalescence is reduced, although never to zero. Many surfactants (e.g., proteins) do not simply reduce interfacial tension, but actively inhibit coalescence by altering the viscoelastic properties of the interface. The adsorbed material can also prevent the close approach of oil droplets by causing the surfaces to have sufficient charge to repel one another or by creating an extended surface layer, which also prohibits close approach. Thus, although emulsions tend to be regarded as thermodynamically unstable, it is possible, by judicious use of surfactants, to control the kinetics of destabilization and to produce emulsions with very lengthy shelf lives. Surfactant molecules are amphiphilic; that is, they contain hydrophobic and hydrophilic domains. The former dissolves in, or interacts with, the hydrophobic surface of the fat or oil, whereas the latter dissolves in the aqueous phase. The surfactant therefore forms a layer on the surfaces of the emulsion droplets. Depending on the type of surfactant, the adsorbed layer may have a complex structure, examples of which are described in the following subsections.

The thermodynamic instability leading to coalescence is, however, only one way in which emulsions can be unstable. Coalescence has the most drastic consequences, because it can be reversed only by rehomogenizing the product, but other mechanisms which are important are creaming and flocculation. Both of these may promote coalescence and are generally not to be favored. In creaming, the emulsion droplets do not lose their identity; they simply redistribute in space and can be returned to their

original state by agitation. Flocculation or aggregation arises from a more permanent physical or chemical interaction between droplets. Flocs are often not easily redispersed and may, therefore, have a negative effect on product quality (in soups, sauces, etc.). Because flocs have a long lifetime, the possibility that rupture of the interfacial layers and coalescence can occur is enhanced.

The functional behavior of oil-in-water food emulsions is related to their stability and is controlled by the three parts of the system: the fat or oil in the interior of the emulsion droplets, the interfacial material between this lipid material and the continuous aqueous phase, and the aqueous phase itself. Each of these “phases” may be chemically complex. The lipid may be partly or wholly crystalline and it may be subject to chemical change such as lipolysis or oxidation. The interfacial material can be composed of proteins or of small emulsifiers such as monoglycerides, esters of fatty acids, or phospholipids, or mixtures of a number of these components. Finally, the aqueous phase may contain ions, which may interact with and potentially destabilize the emulsions, or macromolecules such as polysaccharides, which may exert either stabilizing or destabilizing effects. Therefore, to understand the functional properties of the emulsions, it is necessary to understand the properties of these three parts, individually and collectively.

B. Lipids and Emulsion Functionality

In oil-in-water emulsions, the fat or oil used to form the emulsion affects the functionality of the emulsion mainly by its degree of crystallinity, or its ability to crystallize. Oils which are liquid at the temperature at which foods are produced and consumed have little effect on the behavior of the emulsion, because they act essentially as fillers. They can, of course, coalesce if the fat globules are destabilized and the interfacial layer is sufficiently weak, but they have little structural significance apart from that. On the other hand, it is possible for unsaturated liquid oils to undergo oxidation, and this, in turn, can lead to chemical reactions between the oxidized oil and a proteinaceous emulsifier (4). The overall effect of the reaction may be to alter functional properties of the emulsion and the nutritional value of the food, as well as creating undesirable flavors. The details of how the functional properties of the emulsions are altered by these reactions are not known, although it is known that the oxidized material is harder to displace from the interface than the original protein.

Emulsions are nearly always created (e.g., by homogenization) at a temperature at which all of the fat or oil is in a liquid state, and crystallization then occurs as the product is cooled to the temperature at which it is stored. Fats and oils which can crystallize in this way can be very important

in defining the functionality of the emulsion. By far the best known example of this is the involvement of partly crystalline fat in the mechanism of partial coalescence, which stabilizes air bubbles in whipped emulsion products or in ice creams (1). As the fat crystallizes, the growing crystals start to break the interfacial layer of the fat globules (5), and this weakening of the surfaces allows more efficient destabilization of the emulsion (which in ice cream mixes has often helped by weakening the interface by small-molecule surfactants). In addition, the emulsion droplets, because their surfaces are destabilized, are susceptible to being broken by the attachment to the air-water interfaces of the air bubbles as the mixture is whipped (6). The semiliquid fat cannot wholly coalesce as the interfacial layers are broken, because of the limited mobility of the crystalline material, but it will partially coalesce to form a sintered layer around the bubble (7). As long as the crystals are not melted, the layer will remain intact and stable around the bubbles. The fat may, of course, be completely crystallized after the partial coalescence has occurred, but it must be semiliquid for the original phenomenon to take place. Fats that are completely solid at the temperature at which whipping takes place are not efficient at stabilizing the foam. Equally, fat globule membranes that are too viscoelastic are too tough to permit the breakage essential for partial coalescence to occur.

Not all of the lipid components of a food are, however, neutral lipids in the form of triglycerides. Phospholipids (lecithins) are a second class of lipid materials that are important in defining the properties of emulsions. However, in contrast to the fats and oils, which are present in the interiors of the emulsion droplets, phospholipids are found in the interfacial layer (8) or may even not adsorb at all (9). It should be noted that although the lecithins are often described as “emulsifiers,” they are not as efficient on their own as are other small or large molecular emulsifiers. They may, nevertheless, have a moderating effect on the properties of these other materials. It is also probable that although it is popular to designate a whole range of phospholipid materials under the heading of “lecithins,” each individual phospholipid type (with different head groups and fatty acids) will behave in a way unique to itself. Thus, phosphatidylcholines may behave differently from phosphatidylethanolamines, and distearyl phosphatidylcholine will behave differently from dioleoyl phosphatidylcholine. Hence, the source and composition of a lecithin sample will influence its functional properties.

C. The Interfacial Layer

The interfacial layers of many oil-in-water food emulsions contain proteins, which may be mixed with other surfactant materials (Fig. 1). Proteins are often present in the raw materials of the food, and the fact that they are

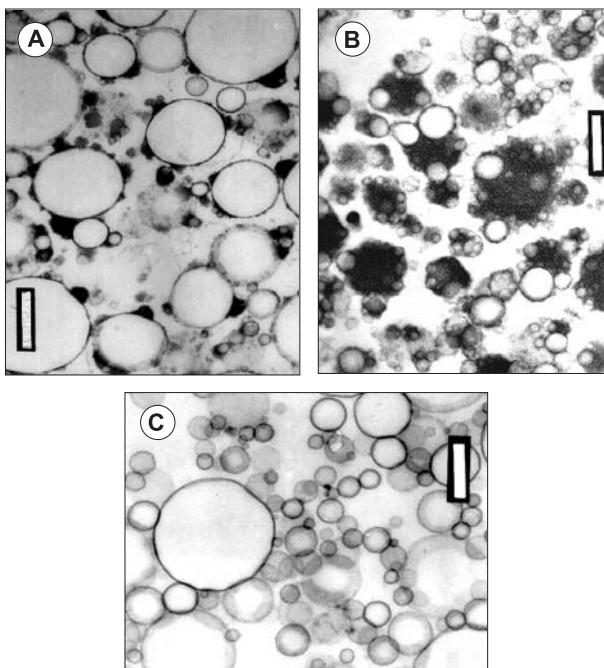


Figure 1 Transmission electron micrographs of emulsion systems. (A) and (B) show milk homogenized using a microfluidizer and centrifuged to separate different populations of particles. (A) represents the larger fat globules, which float during centrifugation (scale bar = 300 nm). (B) shows the sedimenting fraction from the same milk, where very small fat globules are complexed with protein particles (scale bar = 200 nm). (C) shows an emulsion made with soybean oil and sodium caseinate, with only thin protein layers around the fat droplets (scale bar = 200 nm).

excellent emulsifiers enhances their usefulness. The properties of the interfacial layers depend not only on the quantities of materials adsorbed but also on their properties, although we do not completely understand how the composition and structure of an interfacial layer affect the detailed properties of an emulsion.

The composition of the interfacial layer is governed mainly by what is present at the moment the emulsion is formed (10). If proteins are the only emulsifiers present, they will adsorb to the oil interfaces, generally in proportion to their concentrations in the aqueous phase (11). Certain mixtures of caseins are anomalous in this respect, because there is preferential adsorption of β -casein from a mixture of purified α_s - and β -caseins (12).

However, this preferential adsorption does not seem to occur in emulsions made with sodium caseinate, where the caseins adsorb approximately according to their ratios in the original caseinate (11). Why this should be is not clear, although it may be a consequence of the different aggregated states of the caseins in solution (13). It is possible also that the concentration of casein in the emulsion is important (14).

Small-molecule surfactants have important effects on the composition of the interfacial layer. Depending on their nature, they may completely displace adsorbed protein, as in the case of water-soluble surfactants added after the formation of the interface (15), or partially displace the protein, as found for oil-soluble surfactants, which must be added before the interface is formed (16). The effects of these surfactants may not be confined to simply displacing the proteins; there is evidence for binding to proteins (17) or a complex displacement reaction, which has been observed by atomic force microscopy (18). Between the small-molecule surfactants and proteins in size, there are peptides derived from the proteolytic breakdown of protein molecules. These are also capable of stabilizing emulsions, although it appears that larger peptides are more effective at this than smaller ones (19,20). Controlled proteolysis of proteins used as emulsifiers can give increases in their emulsifying efficiency; this has been observed for whey proteins (9,21) and soy proteins (22,23).

The direct or competitive adsorption processes during the formation and storage of an emulsion are, of course, time and path dependent, a subject on which there is little information. This leads to difficulties when interpreting the properties of emulsions produced in laboratory conditions, where it is often the case that ingredients are mixed one at a time, with the normal industrial situation, where many ingredients are mixed and processed at one time. Evidence of time dependence is manifest in the formation of networks of adsorbed whey proteins on the surfaces of emulsion droplets as the emulsion is aged (24). The formation of disulfide linkages between adsorbed proteins is probably responsible for the stability of that adsorbed layer, which is extremely difficult to displace (25). Strong rigid interfacial layers can also be created by deliberate enzymatic cross-linking of adsorbed proteins, the best known example of which is the use of transglutaminase (26).

Details of the structures of the adsorbed layers will be discussed in Section VI. Briefly, a number of methods has been used to estimate the dimensions of adsorbed protein monolayers, among them are dynamic light scattering (27), ellipsometry (28,29), and neutron reflectance (30). The results show that adsorbed layers of protein may be thick compared to molecular dimensions. By forming a hydrodynamically thick layer and because they are generally charged, adsorbed proteins can stabilize emulsion

droplets by both steric repulsion and electrostatic (charge-repulsion) mechanisms.

Many, if not all, adsorbed proteins exist in conformations that are different from their native states (31–33). This is a result of the tendency of hydrophobic parts of the molecules to be adsorbed to the hydrophobic interface, with a consequent distortion or disruption of their secondary or tertiary structures (34). As a result, the properties of the emulsion are not necessarily the same as those of the parent protein. A more drastic manipulation of the adsorbed layer is possible—by the action of proteolytic enzymes on the adsorbed proteins. Although it would be difficult to control on an industrial scale, the partial breakdown of adsorbed casein by trypsin can considerably enhance the stability of the emulsion toward Ca^{2+} (35).

D. The Continuous Phase

If the emulsion droplets are to contribute to the structure of a food, they must interact in some way with the other components which are present. Interactions can occur between the droplets themselves, leading to gelation or flocculation, but other reactions are possible. If the components of the food which are in the aqueous phase tend to form gels, then the emulsion droplets may act in the simplest case as filler particles (i.e., they take up space but do not interact physically or chemically with the gel) (36). On the other hand, the interfacial layer of the emulsion droplets may be capable of interacting with the aqueous-phase components as they gel (37); one obvious example of this is the gelation of whey protein-based emulsions during heating, where the protein in the aqueous phase interacts strongly with the adsorbed whey protein of the emulsion droplet surfaces (38). Similarly, in the acid gelation of milk, which is part of the manufacture of yogurt, the globules of milk fat are homogenized and end up with an interfacial layer that is composed mainly of disrupted casein micelles (39). This allows the droplets to interact with free casein micelles as the acidification proceeds. In yogurt, the interfacial layer remains intact after gelation, but in the related product, cream cheese, the protein-fat emulsion gel is further worked, with the result that the interfacial layers are partially broken down, to give a different structure to the final product.

Interactions between emulsion droplets and macromolecules in solution can be aided by the presence of certain ions, of which calcium is the most important. The presence of these ions may cause flocculation of the emulsions, or gel formation may be enhanced. A general increase in ionic strength can destabilize the emulsions (40), but calcium may form more specific bridges between emulsion droplets and materials in solution (41).

These effects can be greatly enhanced by inducing orthokinetic effects (i.e., by stirring). In such a case, added ions may have a very strong effect (42). The basis of these effects is the fact that proteins generally carry a negative charge in the pH region 5–7 and, therefore, are capable of binding the ions. In addition, the small ions alter the conformations and stabilizing properties of the adsorbed protein layer (43).

Polysaccharides in food systems containing emulsions behave in complex ways, which are being intensively researched at the present time. They may have at least three effects upon emulsions. First, there may be phase-separation effects, because of the thermodynamic incompatibility of the polysaccharides, on the one hand, and the emulsion droplets, on the other (44). This leads to “depletion flocculation” processes, where the emulsion droplets may be driven to form a concentrated emulsion phase, distinct from the aqueous phase containing the polysaccharide. Such depletion flocculation can also be caused by the presence of excess protein (45). This separation can be more pronounced as the concentrations of emulsion and polysaccharide are increased and may be rapid. Second, the polysaccharide may gel, trapping the emulsion droplets and, in effect, stabilizing the emulsion toward flocculation and coalescence (however, the presence of a sufficient quantity of polysaccharide to form a gel may also induce phase separation before gelation occurs). Third, the polysaccharides may interact directly with the adsorbed material on the surface of the emulsion droplet. Because polysaccharides are not hydrophobic in nature, they adsorb poorly, if at all, to lipid surfaces, although some galactomannans do show some surface activity (46). In some cases, such as gum arabic, there is sufficient protein associated with the gum to make it surface active (47–49); in addition, synthetic protein–polysaccharide complexes have been shown to be surface active (50,51).

In addition, charged polysaccharides may interact with adsorbed protein of the opposite charge. It is possible to stabilize caseinate-based emulsion droplets against acid precipitation by interaction with pectin (52), although the presence of pectin in emulsions can also lead to phase separation (53). Caseinate emulsions can also be stabilized against acidification by the presence of κ -carrageenan, which may bind to the κ -casein of the caseinate even though both are negatively charged (52).

It is apparent that the possible interactions between an emulsion droplet and the other components of a food can be very complex. Several ingredients are generally present and they may give rise to final structures which are dependent not only on overall composition, but also on the manner in which the ingredients are added and the time/temperature variations to which they are subjected during manufacture. Of the last two, we have little knowledge, because the kinetics of exchange, phase

separation, and binding reactions have been studied very little, because of the complexity of the reactions and the products.

III. SURFACTANTS

A. Small-Molecule Surfactants

A considerable variety of surfactants is permitted for use in food emulsions, and these are discussed more fully in [Chapter 8](#). Small-molecule surfactants (monoglycerides and diglycerides, sorbitan esters of fatty acids, polyoxyethylene sorbitan esters of fatty acids, phospholipids, and many others) contain long-chain fatty acid residues, which provide the hydrophobic group which binds to the lipid phase of the oil–water interface and causes adsorption. The head groups of these emulsifiers are more varied, ranging from glycerol (in monoglycerides and diglycerides) and substituted phosphoglycerol moieties (in phospholipids) to sorbitan highly substituted with polyoxyethylene chains. Such material can have hydrophilic–lipophilic balance (HLB) values from 3 (oil soluble) to 10 or higher (water soluble). As a general rule, emulsifiers of a low and high HLB are used to form w/o emulsions and o/w emulsions, respectively (54).

Because these molecules adsorb strongly to the oil–water interface and have few steric constraints to prevent them from packing closely, they generate low interfacial tensions (55) and are very effective at lowering the Gibbs interfacial energy. However, they do not generally give highly cohesive or viscous surface layers, so that adsorbed layers of these small molecules may be quite easily disrupted (relative to adsorbed proteins; see Section III.B). This property is indeed used in certain types of emulsion, where limited stability to coalescence is required.

B. Proteins

Proteins, on the other end of the scale of molecular complexity, act as emulsifiers but behave differently from the small molecules, because of their individual molecular structures, and, indeed, it is the particular proteins present which give many food emulsions their characteristic properties. Most, if not all, proteins in their native states possess specific three-dimensional structures (even though we may not know what they are) which are maintained in solution, unless they are subjected to disruptive influences such as heating (56). When proteins adsorb to an oil–water interface, the hydrophobic regions of their structures (created by clusters of appropriate amino acid side chains) lie on, or possibly partially dissolve in, the oil phase. Some structures may be considered as especially important; for example, it is

possible for an α -helical portion of a protein to have a hydrophobic side, created by the hydrophobic side chains which lie outside the peptide core of the helix. However, even proteins such as caseins, which lack large amounts of regular structure, possess many groups of amino acids with hydrophobic side chains which adsorb to the oil–water interface. When a protein is adsorbed, the structure of the protein itself (the polypeptide backbone) will prevent close packing of the points of contact with the interface (the side chains), and as a result, adsorbed protein reduces the interfacial tension less than do small molecules. Although some proteins are excellent emulsifiers, not all proteins can adsorb strongly to an o/w interface, either because their side chains are strongly hydrophilic or because they possess rigid structures that do not allow the protein to adapt to the interface [as in the cases of gelatin (57) and of lysozyme, which although it does adsorb to o/w interfaces, tends to be a poor emulsifier (58)]. However, even apparently very hydrophilic proteins may adsorb strongly, as shown by the egg protein phosvitin, which is a surprisingly good emulsifier (59–62) despite having more than 50% of its residues composed of phosphoserine (63), an amino acid which is charged and hydrophilic. In this case, even the relatively few hydrophobic residues in the protein are sufficient to cause adsorption, so that the protein can cover a large interfacial area with relatively few points of contact.

Because adsorption of proteins occurs via the hydrophobic side chains of amino acids, it has been suggested that a measurement of surface hydrophobicity (64) should allow prediction of the emulsifying power of a protein (65). However, surface hydrophobicity is an ill-defined parameter, which is determined by the binding of probe molecules to the protein in solution (66) and may be a poor predictor of adsorption, especially because adsorbed proteins change conformation during or after adsorption.

C. Adsorption and Protein Conformation

Much research has been aimed at determining the mechanism of protein adsorption, and it is likely that most of the proteins which adsorb well to interfaces are capable of changing conformation either as they adsorb or shortly afterward. The concept of surface denaturation is well established (67,68) because the protein as it adsorbs is affected by spreading pressure, which pulls apart the native structure to maximize the amount of hydrophobic contact with the oil interface (Fig. 2).

A number of methods have confirmed that proteins change their conformations when they adsorb to liquid or solid interfaces. Spectroscopic studies of lysozymes show that adsorption to polystyrene latex causes a decrease in the amount of secondary structure (69) and that the protein

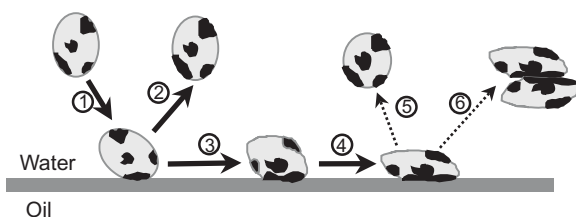


Figure 2 Schematic diagram of the adsorption and desorption of protein. The surface of the protein has hydrophobic (dark) and hydrophilic (light) regions. The protein molecule approaches the interface (1) and begins to adsorb. In principle, it is possible that very rapid desorption may take place (2) without the protein changing conformation. With time, the adsorbed protein changes its conformation to maximize hydrophobic contact with the oil, and this may pass through several stages (4). At this stage, the protein may be hard to displace (dotted arrows), and even if it is displaced, it will have an altered conformation (5) or even be denatured and aggregated (6). The adsorbed protein may itself react with its neighbors to form a network.

may pass through a number of conformational states as the adsorption process continues (70). The Fourier transform infrared (FTIR) spectra of adsorbed α -lactalbumin and β -lactoglobulin have both been shown to differ significantly from those of the native proteins (34,71). Proteins adsorbed to a surface and subsequently desorbed by the action of small molecules have been found to possess an altered conformation (72), showing that adsorption-induced changes may be irreversible; for example, lysozyme and chymosin lose their enzymatic activity on adsorption and do not regain it after being desorbed from the interface (32). It might be expected that the change in the conformation during adsorption is likely to destroy the secondary and tertiary structures of proteins, but it is possible to increase the ordered structure in some cases (73).

Once adsorbed, some proteins are capable of interacting chemically by forming intermolecular disulfide bonds to give oligomers, as has been shown for adsorbed β -lactoglobulin and α -lactalbumin (24,74), although such reactions do not occur in solution unless the proteins are denatured by heating (75). Further evidence for the denaturation of adsorbed proteins comes from differential scanning calorimetry (DSC), suggesting that unfolding on the surface has occurred (33,76,77). In some cases (e.g., lysozyme and α -lactalbumin), this surface denaturation appears to be at least partially reversible, but in others (e.g., β -lactoglobulin), adsorption causes irreversible changes in the protein molecules.

The casein proteins tend to be a special case. Because these proteins appear not to contain much rigid secondary structure (α -helix or β -pleated

sheet) (78) and because they possess considerable numbers of hydrophobic residues (79), they adsorb well (80). However, because of the lack of definition of their original native structures, it is impossible to determine whether conformational changes occur during adsorption, as neither spectroscopic changes nor DSC are capable of demonstrating conformational changes in these proteins.

Reactions between adsorbed protein molecules in emulsions (for instance, disulfide bridging interactions such as those mentioned earlier) will be encouraged by the very high local concentration of protein within the adsorbed interfacial layers. Generally, we know (81,82) that for monolayers of adsorbed proteins, the interfacial concentration (surface excess, Γ) is generally between 1 and 3 mg/m² and that the adsorbed layers are generally less than 5 nm thick (83), so it is simple to calculate that, in the interfacial region, a monolayer of protein has an effective concentration of about 500 mg/mL (i.e., 50%). This is, of course, very much higher than can be achieved by attempting to directly dissolve the proteins because of the extremely high viscosity generated, so direct comparisons between adsorbed and unadsorbed proteins at equal effective concentrations are not possible. However, the protein in the adsorbed layer may be in a favorable position for intermolecular interactions, because the molecules are very close to one another and adsorption holds them in position so that diffusion is slow. We should probably regard the adsorbed layer of protein as being more like a gel than a solution; this is at least partly the reason why many adsorbed proteins form highly viscous interfacial layers. These gels will be essentially two dimensional, with each molecule occupying approximately 11 nm² of interface [calculated on the basis of a molecule of 20,000 Da and a surface coverage of 3 mg/m²; this agrees well with the expected dimensions of a globular protein of this weight (84) and is much larger than the 0.5–2.5 nm² per molecule which has been found for adsorbed modified monoglycerides (85)]. It is, therefore, not surprising that adsorption can alter the structures of proteins. The formation of such concentrated layers has relatively little to do with the overall bulk concentration of the protein in solution, which may give stable emulsions at relatively low bulk concentrations (although this depends on the amount of oil and the interfacial area to be covered).

Caseins form extended layers about 10 nm thick, and even at a Γ of 3 mg/m² have a “concentration” of about 300 mg/mL. Conversely, whey proteins form much thinner layers (about 2 nm thick) and must begin to form multilayers if Γ is more than about 2 mg/m², as there is no further space available for monolayer adsorption beyond that point.

With a few exceptions, most of the detailed research has been performed on relatively few proteins. Of these, the caseins (α_{s1} , α_{s2} , β , and κ)

and whey proteins (α -lactalbumin and β -lactoglobulin) predominate. This is principally because these proteins are readily available in pure and mixed forms in relatively large amounts; they are all quite strongly surfactant and are already widely used in the food industry, in the form of caseinates and whey protein concentrates or isolates. Other emulsifying proteins are less amenable to detailed study by being less readily available in pure form (e.g., the proteins and lipoproteins of egg yolk). Many other available proteins are less surface active than the milk proteins [e.g., soya isolates (86)], possibly because they exist as disulfide-linked oligomeric units rather than as individual molecules (87). Even more complexity is encountered in the phosphorylated lipoproteins of egg yolk, which exist in the form of granules (88), which themselves can be the surface-active units (e.g., in mayonnaise) (89).

IV. FORMATION OF EMULSIONS AND MEASUREMENT OF EMULSIFYING ACTIVITY OF PROTEINS

Food oil-in-water emulsions are generally produced using either colloid mills or high-pressure homogenizers. In the former, the oil–water–surfactant mixture is passed through a narrow gap between a rotor and stator, in which the stresses imposed on the mixture are sufficient to break up the oil into droplets, to which the surfactant adsorbs. This method tends to produce droplets of emulsion which are larger than those produced by high-pressure homogenization, being of the order of 2 μm in diameter. The technique is used to manufacture mayonnaises and salad creams, in which stability depends less on the presence of very small particles than on the overall composition and high viscosity of the preparation. In liquid emulsions, however, smaller particles are required to prevent creaming and possible coalescence.

High-pressure homogenization is used to produce these smaller droplets. A coarse emulsion of the ingredients is formed by blending, and this suspension is then passed through a homogenizing valve, at pressures which are generally in the region of 6.8–34 MPa (1000–5000 psi). This high-pressure flow through the valve creates turbulence, which pulls apart the oil droplets, during and after which the surfactant molecules adsorb to the newly created interface (90). If the adsorption is not rapid, or if there is insufficient surfactant present to cover the freshly formed interface, then recoalescence of the oil droplets rapidly occurs (91). The breakup and recoalescence occurs many times as the droplets pass through the field generated by the homogenizer (92). Apart from the mechanical design of the homogenizer, the sizes of the emerging droplets depend on, among other factors, the homogenization pressure, the viscosity of the suspension, the number of

passes (93), and the amount and types of surfactant present (94). Generally, when the surfactant is present in excess concentration, the particle size is limited by the characteristics of the homogenizer and of the suspension; on the other hand, if only small amounts of surfactant are present, the surfactant concentration limits the sizes of the particles, because insufficiently covered emulsion droplets will recombine. Generally, therefore, as the compositions of products are reformulated, the sizes of the emulsion droplets in them will change.

In addition to recombination and increased droplet size in the presence of insufficient surfactant, the phenomenon of bridging flocculation, in which the emulsion droplets form clusters during homogenization, can be observed. For the bridging to occur, it is necessary to have macromolecular surfactants with at least two sites by which they can adsorb to interfaces. At low surfactant concentrations, such molecules can become adsorbed to two separate oil droplets. Proteins can form bridges in this way (95), and even more commonly, natural aggregates of proteins such as casein micelles can induce clustering of the oil droplets (96). Bridging flocculation may be reversed by incorporating more surfactant (which need not be macromolecular) so as to provide enough material to cover the interface as it is formed. In the case of clustering by particles which themselves can be broken up, a second-stage homogenization at lower pressure can be sufficient to break down the bridging aggregates and to separate the clustered fat globules. Clearly, however, such treatment will be inapplicable to clusters bridged by single macromolecules, which cannot be broken up in this way.

One factor which can have considerable importance on the emulsifying properties of proteins is their quaternary structure. For example, in milk, the caseins exist in aggregates of considerable size (casein micelles) containing hundreds or thousands of individual protein molecules (97), held together by hydrophobic interactions and microparticles of calcium phosphate. The casein micelles act as the surfactants when milk is homogenized (98). During this homogenization, the micellar structure is disrupted, possibly by the forces within the homogenizer (99), but presumably also by the spreading forces which occur when the micelles violently encounter the oil surface. The result is that the oil surface is unevenly coated by partially broken up casein micelles, and not by a monolayer of casein (Figs. 1A and 1B).

In contrast, sodium caseinate (which is prepared by removing the calcium phosphate from the micelles by precipitation at acid pH and then washing the precipitate and redissolving at neutral pH) has much superior emulsifying properties compared to casein micelles (100) (i.e., the amount of oil which can be stabilized by a given weight of casein in either of the two

forms, under identical homogenization conditions). This effect is probably simply because the effective concentration of emulsifier is much less when the casein is in the micellar form, which is relatively resistant to disruption. Therefore, during homogenization, the nonmicellar casein will arrive at the interface more readily than the micelles. Interestingly, sodium caseinate at the concentrations generally used (above about 0.5% w/w protein) is not itself monomeric, but exists in the form of aggregates of the proteins containing about 30 molecules (13), which are held together probably by hydrophobic forces. In contrast to the intact micelles, these particles are believed to create monolayers of casein molecules around the fat globules; that is, the aggregates are pulled apart by the spreading pressure which they encounter as they bind to the interface. This cannot happen to casein micellar fragments, whose integrity is probably maintained by the presence of calcium phosphate.

Molecules such as β -lactoglobulin also show changes in quaternary structure as a function of pH (101), and these may be related to the changes in the protein's surfactant properties at different pH values (102). The denaturation of β -lactoglobulin by heat causes the protein to aggregate, and this decreases the emulsifying power to a considerable extent (103).

Because different proteins are more or less efficient at forming and stabilizing emulsions, and even the same protein may have different efficiencies in different circumstances (as has just been described for casein), it is essential to have methods for estimating the potential of given surfactants for forming emulsions. To achieve this, the required techniques should be method independent; that is, they should give absolute results, or at least give results applicable to specific methods for preparing emulsions. There are two widely used methods, Emulsifying Activity Index (EAI) and Emulsifying Capacity (EC). Neither of these methods is method independent, although they are simple to apply. To measure EC, a known quantity of surfactant is dissolved in water or buffer and then oil is added to it in a blender. This forms a crude emulsion, and further aliquots of oil are added until the emulsion inverts or free oil is seen to remain in the mixture. This ostensibly gives the weight of oil, which can be emulsified by the defined weight of protein. It is evident that this method is dependent on the particular blender because what is important in emulsion formation is not the weight of oil *per se* but its interfacial area. Thus, if the emulsion is made of large droplets, it will consume less surfactant than if small droplets are present. The conditions of emulsion formation are therefore critical to the method, as it is possible to obtain different results at different blender speeds, or with other homogenizing devices. Therefore, the method is not in any sense an absolute measure. As a quality control measure or as an internal method in a single laboratory, it may have considerable usefulness.

To measure the EAI, an emulsion is made and the particle size of the emulsion droplets is estimated. The assumption is then made that all of the protein is adsorbed to the interface, and so a measure of emulsifying potential can be measured. Although it provides more information than EC, the method has two major defects: First, it is very often the case that not all of the available protein is adsorbed, or adsorbed as a monolayer. Indeed, it is known that at concentrations of protein of more than about 0.5% (with oil concentration of 20%), some of the protein remains unadsorbed, even after powerful homogenization where the concentration of protein is the limiting factor in the determination of the sizes of the droplets (11,94). If homogenization is less extensive, then the proportion of protein which is adsorbed decreases. The second major problem in interpretation of the EAI is simply the difficulty of determining the particle sizes and their distribution. There are a variety of methods for measuring the size distribution of suspended particles, and care must be taken to avoid error in this measurement. Traditionally, the particle sizes in determinations of the EAI are measured by determining the turbidity of diluted suspensions of the emulsions, which is a method much subject to error.

Ideally, to fully describe the emulsifying capacity of a surfactant, the particle size distribution of the emulsion and the amounts of individual surfactants adsorbed to the oil-water interface need to be measured. It is possible to measure the amount of adsorbed protein by centrifuging the emulsion so that all of the fat globules form a layer above the aqueous phase and measuring by chromatography the concentration of surfactant left in the latter phase (12). Alternatively, the fat layer after centrifugation can itself be sampled, and the adsorbed protein can be desorbed from the interface by the addition of sodium dodecyl sulfate (SDS) and quantified by electrophoresis on polyacrylamide gels (104). In addition, although this is more difficult to determine, it is desirable to know the state of the adsorbed material (e.g., its conformation, which parts of the adsorbed molecules protrude into solution and are available for reaction, etc.). This represents an ideal which is rarely possible to achieve, but the explanation of the behavior of emulsions and perhaps the design of new ones may depend on this knowledge.

V. MEASUREMENT OF PARTICLE SIZES AND SIZE DISTRIBUTIONS IN EMULSIONS

Once an emulsion has been formed using homogenization or other means, it is often necessary to characterize it, specifically in terms of its average size and its size distribution. This is important in a number of

respects: Knowledge of the size distribution provides information on the efficiency of the emulsification process, and the monitoring of any changes in the size distribution as the emulsion ages gives information on the stability of the system. Regular measurement of particle size can be part of a quality control operation and can also be important when emulsion systems or processes are patented. However, the measurement of true size distributions or even the average sizes of emulsion droplets is not simple, despite the existence of a number of potentially useful and apparently simple methods.

The most direct method and one which is theoretically least subject to errors is electron microscopy (105). This technique measures the number-average size distribution, providing that (a) a fully representative sample of the emulsion is prepared, fixed, mounted, sectioned, and stained without distortion, (b) a sufficient number of particles is measured to ensure statistical accuracy of the distribution, and (c) proper account is taken of the effects of sectioning on the apparent size distribution. All of this requires considerable time, effort, and calculation, so that the technique cannot be used routinely to determine size distributions. It may be used as a standard against which to compare other methods, and it also finds a use in measuring systems where dilution causes changes in the particle sizes, as in micro-emulsions (106).

The most widely used of the rapid methods for particle sizing are based on light scattering. These tend to emphasize large particles in the distribution because larger particles scatter more light than smaller ones. The simplest of these methods depends on the measurement of turbidity at one or a number of wavelengths (107,108). Turbidity, or apparent absorbance of light, is a measure of the total amount of light scattered as it passes through a cuvette containing diluted emulsion (assuming that no component of the emulsion absorbs light of the wavelengths used). Although the method is rapid and may be performed in any laboratory possessing a spectrophotometer, it cannot be used to give the true distribution of particle sizes, but at best to give an average. It can be assumed that the particles form a distribution of known shape, but this, of course, assumes that the distribution is known beforehand.

A number of commercial instruments measure the distributions of particle sizes by determining the intensity of light scattered from a highly diluted sample at a number of specific scattering angles [integrated light scattering (ILS)]. With knowledge of the scattering properties (i.e., the Mie scattering envelope) of the particles (109), software is used to calculate the most probable distribution of particle sizes.

This does not always yield the true absolute distribution, for two main reasons. The first of these is that the angular range is often too restricted to allow measurement of small particles of diameters less than about 50 nm,

which scatter almost isotropically. Large particles preferentially scatter in the forward directions, so that to measure the distribution accurately, ideally measurements have to be made at a span of scattering angles between 0° and 150° (110). This is now available in modern particle sizers, but in older instruments, the angular range used limits the detection of small particles (smaller than $0.1\ \mu\text{m}$). Many food emulsions made by high-pressure homogenization contain particles of this size within their size distribution. A further problem with any light-scattering method is that the accuracy of the calculated distribution depends on how well the optical properties of the emulsion droplets (i.e., their real and imaginary refractive indices, which determine the scattering properties) can be defined. Generally, it is realistic to assume that the emulsion droplets are spherical, but it may be necessary to make assumptions about the structures of the interfacial layers. An emulsion droplet is essentially a coated sphere (111), which is characterized by refractive indices of the core and the coat, and these are likely to differ. Calculations based on of the scattering behavior of emulsion droplets may, therefore, depend on the presumed structures and compositions of the particles.

If the emulsion is unstable, the particle size distribution will change with time, and this will be detected by the light-scattering measurements. However, a simple measure of light scattering cannot distinguish between droplets which have flocculated and those which have coalesced, and other methods of measurement are needed to define which type of instability has occurred. Flocculation introduces another problem relative to the detailed interpretation of light-scattering measurements, because it produces particles which are neither homogeneous nor spherical. To determine the type of instability which has occurred, it is often possible to use light microscopy. Alternatively, the destabilized emulsion can be treated with SDS, which will dissociate any flocs. A second measurement of the particle size after the SDS treatment will show no change if the emulsion had coalesced, but it will revert to the original particle size distribution if the destabilization has been by flocculation (112).

Dynamic light scattering (DLS) offers an alternative means of measurement (113). This technique does not measure the total amount of light scattered, but the dynamics of the scattered light over very short time periods. Usually, the light scattering is measured at a fixed angle of 90° and a correlation function is measured. This is essentially a weighted sum of exponentials, which depend on the diffusion coefficients of the particles through the aqueous medium. As with ILS, the calculation of the true size distribution depends on the knowledge of the detailed light-scattering properties of the emulsion droplets. In addition, the fit of theory to the true correlation function is ill-conditioned (114), so that the size distribution obtained can

depend on the technique used to fit the correlation function. As with other light-scattering techniques, the contribution of larger particles to the size distribution is generally overestimated. This is partly because they tend to scatter more (i.e., have higher weighting factors), but also because of the nature of the correlation function itself, as the information about the small particles is contained only in the short-time part of the function, whereas information about the large particles is contained at all points.

An important demand of both ILS and DLS is that they require the suspensions of particles to be highly diluted. This is necessary because the theories used to calculate the particle sizes demand that the scattered photons have undergone only one scattering event. Multiple scattering distorts the photon statistics and leads to erroneous results. The dilution is not necessarily serious in the case of simple stable emulsions, but in more complex emulsions, it is necessary to ensure that no dissociation of particles is caused by the high dilution required for accurate light-scattering experiments. The dilution may lead to dissociation of flocculated material or to the breakdown of complex interfacial layers (e.g., those formed by casein micelles on the oil-water interfaces in homogenized milk). Conversely, it is possible that dilution into an inappropriate solution may promote aggregation or the emulsion droplets (e.g., dispersing casein-stabilized droplets in a solution containing large concentrations of calcium ions).

Recent advances in instrumentation have allowed some measurements of DLS to be made on more concentrated suspensions. Three methods have been developed. In the first, the optical paths of the incident and scattered beams of the instrument are positioned so that the measurements take place just inside the wall of the cuvette containing the sample. In such a case, the path lengths of the incident and scattered photons in the sample are very short, and up to a volume concentration of as much as 20%, the system may be considered as a simple DLS experiment with no multiple scattering. A second, more complex, but in principle more accurate, method is to use two scattering beams which are cross-correlated with one another (115). This effectively compares two scattering experiments on the same sample and allows the elimination of the contribution of multiply-scattered photons. This technique has been used to study milk (116) but not, so far, emulsions. Finally, a third technique uses the multiply-scattered light rather than trying to eliminate its effects. This is the technique of diffusing wave spectroscopy (DWS). The method is useful for concentrated suspensions such as emulsions (117), but although it can give average sizes of the particles, distributions are harder to obtain. It has, however, been more widely used than the other methods, especially in empirical ways, to detect gelation (118).

These three methods are not as yet widely used, because instrumentation is only now coming on to the market, and most DWS apparatuses tend

to be custom-built in a single laboratory. In using them, it is essential also to be aware of a problem that is not present in diluted solutions. All of the methods of dynamic light scattering depend on the presence of moving particles; in fact, they measure diffusion coefficients, which are then transformed into particle sizes. In turn, diffusion coefficients depend on the viscosity of the continuous phase. When concentrated suspensions are measured, the particles themselves contribute to the viscosity of the suspension, so that care must be taken when evaluating particle sizes from measurements made in concentrated suspensions.

Light-scattering methods are, at present, the most effective and most widely used means of obtaining information about the size distributions of particles in emulsion systems. Like many methods, they are especially useful in a comparative mode to measure changes that occur during processing or storage of the suspensions. All of the light-scattering methods can detect whether aggregation is occurring, so that they may all be used to detect instability of emulsions, and they are almost unique in allowing the kinetics of aggregation to be studied on a real-time basis (119). Simply, the fact that the particle size is increasing can be determined without any particular attributes of the particles needing to be known.

An alternative method of particle sizing, which shows considerable potential although it is not so widely used as light scattering, is based on ultrasonic acoustic spectroscopy. This measurement can easily be made on concentrated dispersions and depends on the fact that the attenuation and velocity of ultrasound of a defined frequency through a suspension depends on the sizes of the particles in the dispersed phase. By measuring the attenuation of sound at a series of different frequencies through the sample, it is possible to calculate the size distribution of the particles in the suspension (120,121). Instruments to perform the measurements are available and they are capable of being compared with the information available from light-scattering measurements (122). Just as the scattering of light depends on the relative refractive indices of the dispersed phase and the continuous phase, so particle sizing by ultrasound also depends on the physical properties of the dispersed phase; for example, the density, viscosity, thermal conductivity, and specific heat are all required to be known to permit the true size distribution to be determined (123). In the absence of these factors, ultrasonic attenuation spectroscopy can give only relative size distributions. However, because of the applicability of the method to real (undiluted) emulsion systems, it is likely that the method will increase in its usage. Ultrasound and its applications are discussed in detail in [Chapter 10](#).

A related method which has been proposed is that of electroacoustic spectroscopy (124). Because the passage of ultrasound through a dispersion

disturbs the double layer which surrounds the dispersed particles, an electric current is set up. Measurement of this current allows the calculation also of the ζ -potential of the particles as well as their size distribution. The measurement may also be performed in reverse; an oscillating electric field causes the emission of ultrasound, which, in turn, permits the size distribution and the ζ -potential to be measured (125,126). Like the simpler ultrasonic spectroscopy, these methods require precise knowledge of the physical characteristics of the medium and the dispersed phase if they are to give absolute, rather than relative, results.

VI. STRUCTURES OF THE ADSORBED LAYERS ON THE SURFACES OF EMULSION DROPLETS

A. Simple Surfactants

The structures of the interfacial layers in emulsion droplets might be expected to be simple when small-molecule emulsifiers are used, but this is not necessarily the case, especially when not one but a mixture of surfactant molecules is present. Although simple interfacial layers may be formed where the hydrophobic moieties of the surfactants are dissolved in the oil phase and the hydrophilic head groups are dissolved in the aqueous phase, it is also possible for multilayers and liquid crystals or even crystals to form close to the interface. This depends on the nature and the concentrations of the different surfactants. Interactions between surfactants generally enhance the stability of the emulsion droplets, because more rigid and structured layers tend to inhibit coalescence. Also, mixtures of different surfactants having different HLB numbers appear to provide structured interfacial layers, presumably because of the different affinities of the surfactants for the oil–water interface. Specifically, phospholipids may form multilamellar structures around the oil–water interface, and presumably these layers will have different spacing depending on the amount of hydration (127). They also depend both on the nature of the oil and of the phospholipid (128). So, although the major adsorption of phospholipids at low concentration is likely to be in the form of monolayers, it may be possible to produce more complex structures when large amounts of phospholipid are present or when other surfactants are coadsorbed to the interface.

B. Interfaces with Adsorbed Proteins

Undoubtedly, the most complex interfacial structures are produced when proteins are used as the surfactants, because of the great range of conformational states accessible to such molecules. This is of interest because of the

implications of conformational change on the reactivity and functionality of the proteins [e.g., it appears that adsorbed β -lactoglobulin cannot form disulfide bonds with κ -casein when heated in the presence of caseinate (129), although this reaction is known to occur between the proteins in solution and in heated milk]. Flexible molecules such as caseins may be considered as adsorbing as if they were heteropolymers (130) because they are presumed to have high conformational mobility (78). As evidence of the presumed conformational change, adsorbed β -casein exhibits different susceptibility to attack by proteolytic enzymes, compared with the protein in solution (131). Further, adsorption to different hydrophobic materials causes differences in the conformation of the adsorbed molecule; for example, the protein seems to have somewhat different conformations when adsorbed to hydrocarbon (*n*-tetradecane) or triglyceride (soya oil)–water interfaces (132). As a result of these measurements, it appears that model hydrocarbon–water systems are not necessarily suitable for describing triglyceride–water systems.

Much is known about the structure of adsorbed β -casein, certainly more than is known for any other food protein. The first evidence from dynamic light scattering showed that β -casein can adsorb to a polystyrene latex and cause an increase in the hydrodynamic radius of the particle by 10–15 nm (133). Small-angle x-ray scattering confirmed this and showed that the interfacial layer was not of even density throughout and that the bulk of the mass of the protein was close to the interface (134). Neutron reflectance studies also showed that most of the mass of the protein was close to the interface (135). From these results, we can infer that a relatively small portion of the adsorbed protein molecule extends from the tightly packed interface into solution, but it is this part which determines the hydrodynamics of the particle and which must be the source of the steric stabilization which the β -casein affords to emulsion droplets (133). All of the studies just described were performed on polystyrene latex particles or on planar interfaces; however, it has also been demonstrated that the interfacial structures of β -casein adsorbed to emulsion droplets resemble those in the model particles (83,134). Although detailed control of emulsion droplets during their formation in a homogenizer is impossible, it is possible to break down the surface layers of protein once they are formed, by the use of proteolytic enzymes (135), and by comparison with the behavior of model systems under similar conditions, it is possible to demonstrate that the proteins seem to have similar conformations in the model systems and emulsions (27).

It is also possible to use proteolytic enzymes to demonstrate which part of the β -casein protrudes into the solution. There are many sites in the protein molecule (lysine and arginine residues) susceptible to attack by

trypsin, and these are almost equally susceptible to attack when the protein is free in solution. In the adsorbed protein, sites close to the N-terminal are most readily accessible, presumably because they form the part of the adsorbed layer which protrudes into solution (131). This region of the molecule is the one which would be expected to behave in this way, being the most hydrophilic and highly charged part of the protein. Thus, for β -casein, it is possible to predict some features of the conformation of the adsorbed protein from a study of its sequence (131). It seems that β -casein is perhaps the only protein for which this kind of prediction can be done; most other proteins (even the other caseins) have much less distinct hydrophilic and hydrophobic regions and, therefore, have conformations which are more difficult to predict (27). From studies of the structure of adsorbed α_{s1} -casein in model systems and in emulsions, it is established that neither the most accessible sites for trypsinolysis (136) nor the extent of protrusion of the adsorbed protein into solution (137) can be readily predicted.

Nevertheless, it is possible to calculate from statistical mechanical principles the approximate conformations of the adsorbed caseins, by assuming that they are flexible, composed of chains of hydrophilic and hydrophobic amino acids (138). The results of these calculations reproduce many of the features of the actual measured properties, especially the tendency of the adsorbed β -casein to protrude further from the interface than the α_{s1} -casein (139). These calculations have, in turn, been used to explain the differing stabilities of the two different types of emulsions toward added salts (140). These calculations have considerable success in explaining both the structure and stability of casein-coated emulsions, but they are less adaptable to explain the behavior of more rigid protein surfactants. However, the same principles have been used to explain the apparently anomalous adsorption of phosvitin (61).

The difficulty of ascertaining the structure of the adsorbed protein is greater for globular proteins. In these cases, the adsorbed layer is much thinner than it is for the caseins, so that layers of β -lactoglobulin appear to be of the order of 1–2 nm thick instead of the value of about 10 nm measured for the caseins (83,104,137). Hydrodynamic and scattering experiments suggest that the thickness of the adsorbed layers is smaller than would be expected from the protein in its natural conformation, so that these simple measurements of the size of the adsorbed protein already suggest that adsorption causes a conformational change. This is confirmed by other techniques. For example, adsorbed β -lactoglobulin forms intermolecular disulfide bonds (24), which does not occur when the molecules are in their native conformations in solution (although the high concentration of protein in the adsorbed layer will certainly enhance any tendency that the molecules have to aggregate). In addition, detailed studies of the DSC of

emulsions containing β -lactoglobulin (33) have shown that (a) the protein when adsorbed to the oil–water interface in emulsions loses its heat of denaturation (i.e., shows no intake of heat which can be associated with denaturation, presumably because the protein is already surface denatured) and (b) if the protein is desorbed from the interface by treatment with detergent (Tween-20), it can be seen to be denatured irreversibly (i.e., no recovery of the denaturation endotherm is seen). This may be contrasted with the behavior of α -lactalbumin, which loses its heat of denaturation when adsorbed but recovers its original thermal behavior when the protein is competitively desorbed by Tween (33,70). These studies confirm that different proteins show quite different degrees of denaturation when they are adsorbed to oil–water interfaces.

Similarly, the use of infrared spectroscopy (FTIR) shows that significant changes in the conformation of β -lactoglobulin occur as a result of adsorption. Detailed interpretation of the spectra is difficult, but changes in the contents of α -helix and β -sheet contents of the protein appear to occur (34). The protein α -lactalbumin is less affected by adsorption (71). However, nearly all of the evidence [chemical, physical, spectroscopic, and enzymological (32)] combines to show that adsorption-induced conformational changes occur. Moreover, these changes appear to be nearly always irreversible; that is, even if a protein is desorbed from the interface, it cannot recover its original conformational state.

When considering the structure of a protein-based interfacial layer, there are other factors to be considered, namely the possibility that multilayers, rather than monolayers, are formed and the possibility that specific proteins may exhibit variable behavior depending on the conditions. Caseins are capable of this; for example, it is possible to prepare stable emulsions containing 20% (w/w) of soya oil, with as little as 0.3% casein, and in these, the surface coverage has been measured to be slightly less than 1 mg/m^2 . The hydrodynamic thickness of the adsorbed monolayer in these emulsions is about 5 nm. In emulsions prepared with larger amounts of casein (1–2%), the surface coverage increases to $2\text{--}3 \text{ mg/m}^2$ and the thickness of the adsorbed monolayer is about 10 nm (i.e., about twice that of the layer at lower surface coverage) (94). It has been suggested that this is a result of the adsorbed casein molecules adopting two different conformations: one at low coverage, where the proteins have to cover a maximum area of surface (about 48 nm^2 per molecule), and one at high coverage, where the molecules are more closely packed (about 13 nm^2 per molecule). The addition of more protein to the aqueous phase of emulsions made with low concentrations of caseinate results in the adsorption of some of the added protein and an increase in the thickness of the adsorbed layers. This is true, even if the added protein is not casein, and illustrates that, for caseins at least,

the proteins on the surface possess sufficient mobility to be moved as other proteins adsorb.

So far, we have considered monolayers. However, caseins and other proteins can form multilayers; this has been demonstrated for adsorption to planar interfaces, where large surface excesses are easily generated and multilayers are formed (80). There is less evidence for this in emulsions, although some high surface coverages (up to about 10 mg/m^2) have been measured (141), which can only arise from the presence of more than a single layer on the oil–water interface because it would be impossible to pack this amount of protein into a monomolecular layer. It is not clear why monolayers in some cases and multilayers in other cases are formed, although it is likely that the physical conditions of homogenization may be important, as well as there being a need for high concentrations of protein. Also, differences in the methods of preparing the caseins may be relevant; at neutral pH values, highly purified caseins have not generally been associated with multilayer formation, which seems generally to be associated with the use of commercial sodium caseinates.

Multiple layers seem to be more easily formed in emulsions containing whey proteins than with caseins. Because the whey proteins project less into solution than do the caseins, they may be less effective than caseins at sterically preventing the approach of additional molecules that go to form the multilayers. Finally, because they change conformation when they adsorb, they may offer new possibilities for interaction with incoming whey proteins from solution. There is evidence for multiple layers of whey proteins from both planar interfaces and emulsion droplets (11,142). However, although these multiple layers exist, there is no definite evidence that links them to changes in the functional properties of the emulsions. Nor is it well determined how stable the multiple layers are, compared with a monolayer. It is very difficult, or perhaps impossible, to simply wash adsorbed proteins from adsorbed monolayers formed on the interfaces of oil droplets (143). However, the outer portion of multilayers may be more readily displaced because it is held in place by protein–protein interactions only, which may be weaker than the forces which lead to adsorption. Generally, however, the properties of the outer parts of multilayers have been little studied.

C. Emulsions Stabilized by Particles

As a final degree of complexity, food emulsions may be stabilized by particles. Perhaps the most common are the protein “granules” from egg yolk, which play a role in the stabilization of mayonnaise (89), and casein micelles in products such as homogenized milk and in ice creams. Both of these

emulsifiers are known to be adsorbed to the oil–water interface as complex particles, which do not dissociate completely to their individual proteins either during or after adsorption (144,145). During the homogenization of milk, casein micelles are partially disrupted at the oil–water interface so that they adsorb either whole or in fragments. Indeed, once a micelle has adsorbed, it appears to be able to spread over an area of the interface (105,146,147). Thus, the fat droplets in homogenized milk are surrounded by a membrane that must contain some of the original fat globule membrane [phospholipid and protein (148)] but is primarily constituted of semi-intact casein micelles. If the milk has been heated before or after homogenization, whey proteins also form part of the layer surrounding the fat globules (39,149). Likewise, the oil–water interface in mayonnaise is partly coated by the granular particles formed from the phosphoprotein and lipoprotein constituents of egg yolk (150). In this high-lipid product, the granules also may act to keep the oil droplets well separated and prevent coalescence.

Natural fat globule membrane was mentioned earlier as a possible emulsifying agent (151). In its most native state (i.e., prepared in the laboratory from unheated milk), this membrane is an effective emulsifier (152), although little is known of its structure as it resurrounds oil droplets. However, heating at temperatures greater than about 65°C is sufficient to denature the proteins of the membrane. This appears to greatly diminish the efficacy of the membrane material as an emulsifying agent (153).

Emulsion formation by means of these aggregates of protein is generally less efficient than by the proteins when they are present in the molecular state, simply because the efficient formation of the emulsion depends on rapid coverage of the newly formed oil surface in the homogenizer. A particle containing many molecules of protein will encounter a fat surface less frequently than an equivalent amount of molecular protein. Thus, although it is possible to prepare homogenized milk with the proportions of casein and fat which occur naturally in milk (a ratio of about 1:1.5 w/w), it is not possible to use 1% w/w of micellar casein to stabilize an emulsion containing 20% oil (154). On the other hand, 1% casein in a molecular form (sodium caseinate) is quite sufficient to form a finely dispersed, stable emulsion with 20% oil. Therefore, unless the micelles are expected to confer some specific advantage on the functional properties of the emulsion or unless there are specific legislative reasons, it is generally more effective to use caseinate than casein micelles to stabilize an emulsion. With egg granules, the situation is different, inasmuch as the individual proteins from the egg granules are not readily available in a purified form analogous to caseinate. In this case, the choice between particulate and molecular forms of the protein does not arise.

VII. MODIFICATION OF THE INTERFACIAL LAYER AFTER EMULSION FORMATION

In many food emulsions, more than one surfactant is present, so that mixtures of proteins, small-molecule surfactants (oil soluble and water soluble), and lecithins may be on the interface or in the continuous phase. Under these circumstances, the interfacial layer will contain more than one type of molecule. The properties of the emulsion (the sizes of the droplets, the functionality, and the stability) will, in turn, depend on which types of molecule in the formulation are actually on the interface and what effect external factors have on the conformations of the adsorbed materials (Fig. 3).

A. Interfaces Containing Mixtures of Proteins

It has been shown that in mixtures of proteins in emulsions formed at neutral pH and moderate temperatures, there is generally no competition for the interface. For example, there is no preferential adsorption between the proteins when a mixture of α -lactalbumin and β -lactoglobulin is homogenized with oil; the amounts of protein adsorbed are in proportion to their concentrations (155). The same is true even when a mixture of sodium caseinate and whey protein is used as the surfactant in an emulsion (11). The only case where competitive adsorption has been truly observed is when

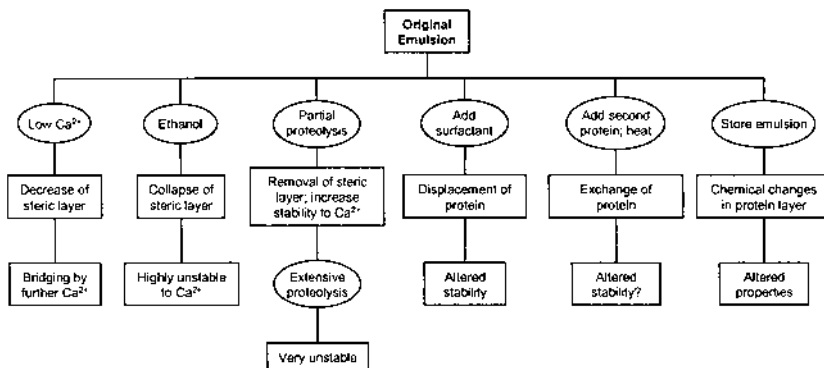


Figure 3 Examples of the potential modification of the adsorbed layer of protein during storage or processing of an emulsion stabilized by a layer of sodium caseinate. Various treatments (see text for details) can give rise to a number of modifications of the surface, which, in turn, affect the stability properties of the emulsion. The list of modifications is not exhaustive.

β -casein is used to displace adsorbed α_{s1} -casein, and vice versa, so that there is a possibility that these two proteins adsorb according to thermodynamic equilibrium (12). Even this observation is complicated, however, because it appears to apply only to mixtures of highly purified caseins; the displacement reactions with commercial sodium caseinate (where a similar result would *a priori* be expected), give much less clear results (16,156).

Rather than forming an emulsion in the presence of mixed surfactants, it is possible to form an emulsion using one protein and then to attempt to displace that protein from the interface with another. It is a general finding, however, that usually the protein which is first on the interface resists displacement (157). Because of its high surface activity and flexibility, β -casein appears to be the best displacing agent, but it is not always capable of displacing an already adsorbed protein. It can displace α_{s1} -casein or α -lactalbumin from an interface (12,158), but the process is more complex with adsorbed β -lactoglobulin (159), especially if the emulsion containing the β -lactoglobulin has been allowed to age before the β -casein is added.

The difficulty of replacing one protein with another is perhaps not surprising, because proteins are adsorbed to the interface by many independent points of contact (because they have several hydrophobic regions capable of binding to an interface). For all of these contacts to become desorbed at once is extremely unlikely, and so the spontaneous desorption of a protein molecule is very rare; this is why it is difficult to wash proteins from an oil-water interface (143). Replacement of an adsorbed protein molecule by one from solution must presumably require a concerted movement of the two molecules; as parts of one are displaced, they are replaced by parts of the other, until, finally, one of the two proteins is liberated into the bulk solution. Even this process, although more likely than spontaneous desorption, is not certain to succeed, especially if the adsorbed protein has been on the interface for some time and has been able to make bonds with neighboring molecules. Moreover, given the very high concentration of protein in the adsorbed layer (see earlier text), it may even be difficult for a second type of protein to penetrate the adsorbed layer to initiate the displacement process. Therefore, although thermodynamic considerations may favor one protein over another, kinetic factors militate against rapid exchange. Nonetheless, there do seem to be factors that influence the competition between proteins. As has been suggested earlier hydrophobicity and flexibility may be important criteria (because β -casein can be an effective displacing agent). Especially, whatever increases flexibility may lead to increasing competitiveness. The most obvious example of such a change is α -lactalbumin; in its native state, this protein has a globular structure partly maintained by the presence of one bound calcium ion (160). Removal of this Ca^{2+} leads to the protein adopting a "molten globule" state, whose tertiary structure is

altered (161), and this leads to increased flexibility and competitiveness at the interface (162). The removal of the Ca^{2+} can be achieved by chelation or by reducing the pH, and under these conditions, α -lactalbumin out-competes β -lactoglobulin for adsorption to the interface (102,104,162). To some extent, the competition can be reversed by reneutralizing in the presence of Ca^{2+} , so that in this case, there is dynamic competition between the proteins for the interface, not simply preferential adsorption during emulsion formation (104).

It should be noted that competition between proteins need not occur. For example, lysozyme (being positively charged at neutral pH) forms complexes with other egg-white proteins (negatively charged) on air–water interfaces. The complex may adsorb to the interface or the lysozyme may bind to already adsorbed proteins (163). This coadsorption is, however, not general, because it requires two proteins to be of opposite charge, which is relatively rare.

B. Addition of Small-Molecule Emulsifiers to a Protein-Stabilized Emulsion

Competition between adsorbed and free proteins can be considerably enhanced by the presence of small surfactant molecules (164). In such cases, there is competition between the proteins and small molecules as well as between the proteins themselves. However, in such a case, instead of the desorption of a protein requiring the inefficient process of simultaneous detachment at all points, or the slow creeping displacement of one protein molecule by another, it is possible for a number of small molecules to displace a protein by separately replacing the individual points of attachment. It is known that small-molecule surfactants are capable of efficiently displacing adsorbed proteins, although the details of the reactions depend on the type of surfactant and whether it is oil or water soluble (165–168). Water-soluble surfactants are capable of removing all of the adsorbed protein from the oil–water interface, although they may require a molecular ratio of about 30:1 surfactant:protein (164). At lower ratios, some, but not all, of the protein is displaced (Fig. 4). This displacement occurs either when the small-molecule emulsifier is present at the moment of homogenization or it is added later. Oil-soluble surfactants (low HLB numbers) are less effective at completely displacing protein or of preventing protein adsorption (16,168,169). For solubility reasons, these surfactants cannot be added to the emulsion after it has been formed, but must be incorporated during the homogenization step. In addition to competing with proteins for adsorption to the oil–water interface, both during formation of the emulsion and its subsequent storage, some small-molecule surfactants also facilitate the exchange

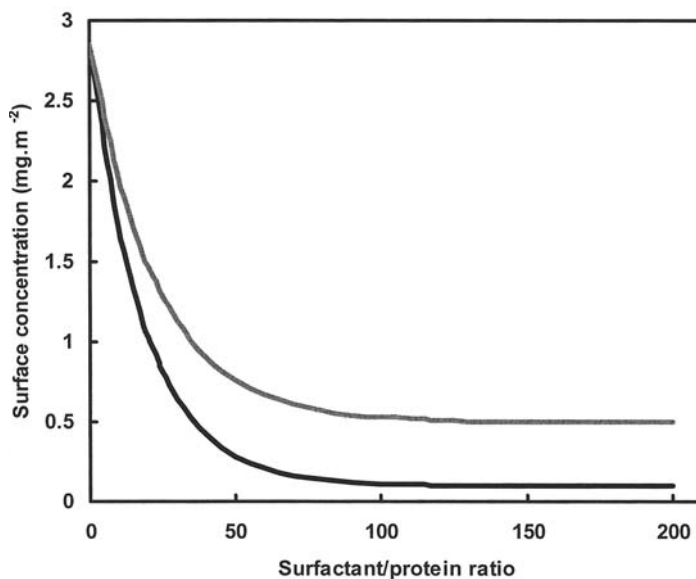


Figure 4 The displacement of caseins from an emulsion by the incorporation of the water-soluble surfactant Tween-20 (lower line) or the oil-soluble surfactant Span-20 (upper line). The water-soluble material can be added at any time before or after the emulsion is formed and can give almost complete displacement of the proteins. The oil-soluble surfactant must be present dispersed in the oil phase before emulsion formation takes place.

reactions of the proteins themselves. For example, although α -lactalbumin and β -lactoglobulin do not compete well with each other under normal circumstances at neutral pH (155), the presence of Tween causes the adsorption of α -lactalbumin to be favored over β -lactoglobulin (164). Presumably, the presence of surfactant enables a more thermodynamic equilibrium to be established, rather than the extremely slow kinetically determined exchange which normally occurs (if it occurs at all) between the two proteins. Alternatively, if the surfactant actually binds to the protein, its conformation may change so that it becomes more surface active, as was shown for the “molten globule” conformation of α -lactalbumin. Similarly, the presence of surfactants can alter the exchange between β -casein and β -lactoglobulin on an oil–water interface. Of the two proteins, β -casein is displaced first by both oil-soluble and water-soluble surfactants (18,170).

The displacement of proteins by small-molecule surfactants has been studied in some detail, using the technique of atomic force microscopy (AFM) which allows the detailed visualization of adsorbed films on a

planar interface. A series of reactions has been shown to occur when proteins are displaced by Tween. Rather than the protein molecules being displaced one by one, it is found that the surfactant pushes the protein aside from parts of the interface (171); in effect, a two-dimensional phase separation occurs. As this occurs, protein does not leave the surface, but forms multilayers over restricted areas of the interface (18). This “orogenic” displacement reaction explains some anomalous research results on the apparent thickness of adsorbed layers (17) and also offers the interesting possibility that the inhomogeneous structure of the interface may lead to areas of different reactivity. The results using AFM have been confirmed by studies using neutron reflectivity (172), which showed that the removal of the protein (β -lactoglobulin) by the surfactant is not a single continuous process. Modeling of the displacement reaction has been able to reproduce some aspects of the exchange behavior, using a fairly simple model (173,174). What must be critical to the behavior is the respective influence of interprotein and protein–solvent interactions. Because in practice the protein is displaced from the interface in an aggregated form, the changes in the protein structures and properties arising from adsorption and desorption can be qualitatively understood.

These observations lead to the question of whether the same type of behavior occurs when two proteins are present on an interface together. Here, the situation is not clear. Studies have been made on mixed proteins at air–water interfaces, and whereas in one case a slow phase-separation behavior has been seen over the course of some days (175,176), in another study by a different group, no such separation could be seen (18). It will be necessary to await further developments in this field before coming to a decision. Neither of the studies used emulsion droplets, which are not susceptible to the techniques, but it is intriguing to contemplate the possibility of producing controlled multifunctional surfaces by mixing appropriate proteins.

Lecithins represent a different type of small-molecule emulsifier. Although these molecules possess surfactant properties, they do not behave like other small-molecule emulsifiers. For example, they do not appear to displace proteins efficiently from the interface, even though the lecithins may themselves become adsorbed (8). They certainly have the capability to alter the conformation of adsorbed layers of caseins, although the way in which they do this is not fully clear; it is possibly because they can “fill in” gaps between adsorbed protein molecules (177). In actual food emulsions, the lecithins in many cases contain impurities, and the role of these (which may also be surfactants) may confuse the way that lecithin acts (178). It is possible also for the phospholipids to interact with the protein present to form vesicles composed of protein and lecithin, independently of

the oil droplets in the emulsion. The existence of such vesicles has been demonstrated (179), but their functional properties await elucidation.

C. Chemical Modification of the Interfacial Layer

Once a protein-stabilized emulsion has been formed, it is possible to modify the interfacial layer by chemical reactions. In fact, spontaneous reactions may occur during processing and storage of an emulsion, which change the structure and the properties of the interfacial layer. Both β -casein and β -lactoglobulin can suffer change in stored emulsions with soy oil (4,180). This may be attributed to the oxidation of the unsaturated fatty acid chains of the oil giving rise to enal molecules, which subsequently react with lysine or arginine residues of the proteins.

Changes in the conformations of adsorbed proteins can be induced by changes in the properties of the aqueous phase, especially for the caseins. Increases in ionic strength, or the presence of Ca^{2+} , cause the thickness of the adsorbed layers to decrease, because of smaller repulsive interactions between the charges of the protein molecules (43,181). Similarly, the addition of a poor solvent, such as ethanol, causes the adsorbed layer to collapse and lose its steric stabilizing properties (182). It is this effect that makes cream liqueurs so susceptible to the presence of Ca^{2+} (183).

The description in the previous section of the only moderate exchange between adsorbed and free proteins refers to results at room temperature, which is where nearly all of the detailed studies have been made. However, it appears that the exchange is temperature dependent. It has been demonstrated recently that whey proteins (especially β -lactoglobulin) can displace α_{s1} - and β -caseins from an oil-water interface during heating (this does not occur at room temperature) (129). If whey protein isolate is added to an emulsion prepared using oil and sodium caseinate and the mixture is heated to a temperature in excess of about 50°C, the whey proteins rapidly become adsorbed (Fig. 5), and as they do so, the caseins are desorbed, so the surface coverage by protein remains approximately constant (184). Only the major caseins are desorbed, however, with the α_{s2} - and κ -caseins remaining on the emulsion droplets. This behavior has been insufficiently studied to be fully understood. Interestingly, it is the whey protein which displaces β -casein; this is similar to the effect of surfactants described in the previous section. It is not known why the minor caseins resist displacement; the obvious possibility, that disulfide bonds are formed between these caseins and the whey proteins, does not seem to occur (185). It seems evident, however, that the exchange of proteins may occur more readily than was previously thought, especially in food preparations where an emulsion is added to a solution containing other proteins and the mixture undergoes a heat treatment.

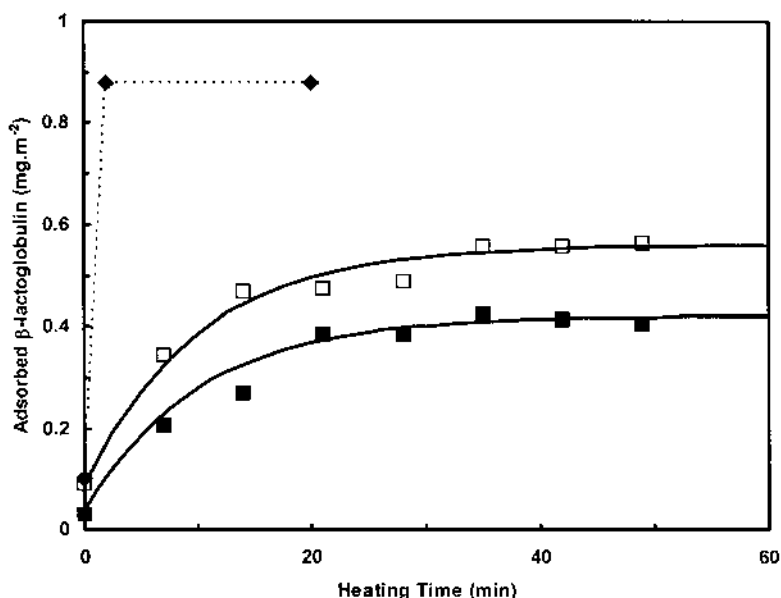


Figure 5 Kinetics of the exchange of whey protein with caseins at an emulsion interface. The figure shows the time-dependent adsorption of β -lactoglobulin from a whey protein isolate solution added to an emulsion originally made with sodium caseinate. Curves for the removal of the caseins from the surface are analogous. The results shown are for 45°C (■), 50°C (□), and 80°C (◆). The results show that not only is the rate of exchange temperature dependent, but so is the extent of replacement of one protein by another. The transfer at 80°C is too rapid to measure by the techniques employed in the research.

Mention has already been made of the disulfide-mediated polymerization of whey proteins (24). Evidently, the conformational changes produced as a result of adsorption allow the single sulfhydryl group of the protein to become accessible for reaction; normally, it is buried in the structure of the protein. The details of the reaction are not elucidated; evidently, the “activated” lactoglobulin molecules can react not only with one another but with α -lactalbumin as well, if it is present (74). It is even possible that the reactive adsorbed molecules can pull in molecules from the aqueous phase and that disulfide bonds can be formed between proteins on different particles. However, the free-sulfhydryl groups are not universally accessible, because β -lactoglobulin bound to an emulsion was not capable of reacting with κ -casein from caseinates added after the emulsion was formed, or from pure κ -casein added subsequently (184,185).

The sulfhydryl–disulfide exchange is a spontaneous phenomenon. It is also possible, however, to use cross-linking enzymes, such as transglutaminase, to polymerize the interfacial proteins (26). This polymerization, as may be expected, produces strong, rigid, interfacial layers (186), as long as the extent of cross-linking is not too large; these layers protect against coalescence and promote ethanol stability (187). Similar to the disulfide-induced polymerization, the cross-linking can be carried to an extent that causes the emulsions to destabilize (aggregate), presumably because cross-links begin to form between protein molecules adsorbed to different particles.

Finally, in this section, we mention the effects of ultra high pressure on systems containing emulsions. It seems probable that high pressure has an effect on the behavior of the proteins in emulsions and, consequently, the exchange between them. Thus, unlike the effect of heat, where β -lactoglobulin was shown to displace the major caseins, the application of pressure in such mixed-protein emulsion systems favors the adsorption of caseins (188), possibly because the high pressure denatures the β -lactoglobulin which is in solution, causes it to aggregate, and renders it incapable of adsorbing efficiently. Similar effects are found if a small-molecule emulsifier is mixed with the β -lactoglobulin-stabilized emulsion before pressure is applied. Further evidence of the effect of pressure-induced changes in β -lactoglobulin emulsions comes from the increased interaction of the protein with pectin as a result of the high-pressure treatment. Even at neutral pH, an interaction is observed (189). Clearly, the effect of pressure as a denaturing agent may influence the behavior even of adsorbed species.

It is worth noting that the structures of denatured proteins are different, depending on how they are denatured—whether by heat, by pressure, or by adsorption. The effects of combinations of these factors on the structures and reactivities of proteins are largely unknown; in fact, the effects of processing on emulsions are only now beginning to be studied in realistic systems, a trend which is much to be encouraged.

VIII. CONCLUDING REMARKS

The object of making food emulsions is to provide a stable and controllable source of food, whose texture, taste, and nutritional and storage properties are acceptable to the consumer. Although the number of possible ingredients is limited by the constraints of healthy nutrition, it is nevertheless evident that within the available range, there is a great deal of opportunity for variation in the properties of the emulsions—for instance, the particle size and the composition of the stabilizing layer of the interface, which, in

turn, influence the stability and functional behavior of the emulsion. On the other hand, many emulsions used in foods have their roots in established formulations, and an understanding of why certain emulsions behave as they do is still not established in a number of cases.

In the manufacture of many real food emulsions, the path followed is critical, emphasizing once again that emulsions, like many other food systems, are not in equilibrium states and that two products may be very different although they have the same overall composition. On this point, our knowledge is insufficient and needs to be extended. For example, the heat or high-pressure treatment of ingredient proteins either before or after the formation of an emulsion may critically affect the behavior of the emulsion. As foods containing emulsified material become more complex or sophisticated in their ingredients, the level of understanding required to control their formation and properties is increased. The challenge for the future is to be able to describe and control some of the most complex emulsions so as to enable greater functional stability for these food systems.

A further aspect, which is becoming of ever-increasing importance in the public mind, is that of the nutritional function of food emulsions. Reduced-fat formulations of traditional products are demanded, which, nevertheless, are required to possess textural and organoleptic properties as close as possible to those of the traditional material. This in itself provides a challenge to the emulsion technologist—to reproduce the properties while reducing the amount of “active” constituent. The demand for the incorporation of nutritionally beneficial lipid materials (phospholipids, specific fatty acids) also produces a challenge; the incorporation of these materials into foods, complete with antioxidants and other necessary ingredients, will require increased ingenuity on the part of the emulsion technologist. In addition, there is discussion of targeting the materials contained in a food. No longer is it sufficient simply to provide nutrition; ideally, it is necessary to define in which portion of the digestive tract the components of the food are to be liberated. Already there are encapsulated materials available whose coatings are designed for this purpose. With emulsions of specific oils being part of the “functional food” system, we may expect to see increased demand for emulsions which are controlled not only during manufacture but during consumption as well. This represents a real challenge for the emulsion technologist of the future.

REFERENCES

1. H. D. Goff, *J. Dairy Sci.* 80, 2620–2630 (1997).
2. H. D. Goff, *Int. Dairy J.* 7, 363–373 (1997).

3. J. M. Aguilera and H. G. Kessler, *J. Food Sci.* 54, 1213–1221 (1989).
4. E. M. Stevenson, D. S. Horne and J. Leaver, *Food Hydrocolloids* 11, 3–6 (1997).
5. H. D. Goff, M. Liboff, W. K. Jordan, and J. Kinsella, *Food Microstruct.* 6, 193–198, (1987).
6. D. F. Darling, *J. Dairy Res.* 49, 695–712 (1982).
7. B. E. Brooker, *Food Struct.* 9, 223–230 (1990).
8. J.-L. Courthaudon, E. Dickinson, and W. W. Christie, *J. Agric. Food Chem.* 3, 1365–1368 (1991).
9. S. O. Agboola, H. Singh, P. A. Munro, D. G. Dalgleish, and A. M. Singh, *J. Agric. Food Chem.* 46, 1814–1819 (1998).
10. D. G. Dalgleish, *Trends Food Sci. Technol.* 8, 1–6 (1997).
11. J. A. Hunt and D. G. Dalgleish, *Food Hydrocolloids* 8, 175–187 (1994).
12. E. Dickinson, S. E. Rolfe, and D. G. Dalgleish, *Food Hydrocolloids* 2, 397–405 (1988).
13. H. S. Rollema, in *Advanced Dairy Chemistry, I. Proteins* (P. F. Fox, ed.) Elsevier Science, Barking, UK, 1992, p. 111–140.
14. M. Srinivasan, H. Singh, and P. A. Munro, *Int. Dairy J.* 9, 337–341, 1999.
15. J. Chen and E. Dickinson, *J. Sci. Food Agric.* 62, 283–289 (1993).
16. S. E. Euston, H. Singh, D. G. Dalgleish, and P. A. Munro, *J. Food Sci.*, 60, 1124–1131 (1995).
17. D. G. Dalgleish, M. Srinivasan, and H. Singh, *J. Agric. Food Chem.*, 43, 2351–2355 (1995).
18. A. R. Mackie, A. P. Gunning, M. Ridout, P. Wilde, and V. J. Morris, *Langmuir* 17, 6593–6598 (2001).
19. P. W. J. R. Caessens, S. Visser, H. Gruppen, G. A. van Aken, and A. G. J. Voragen, *Int. Dairy J.* 9, 347–351 (1999).
20. P. W. J. R. Caessens, H. Gruppen, C. J. Slangen, S. Visser, and A. G. J. Voragen, *J. Agric. Food Chem.* 47, 1856–1862 (1999).
21. X. L. Huang, G. L. Catignani, and H. E. Swaisgood, *J. Agric. Food Chem.* 44, 3437–3443 (1996).
22. W. U. Wu, N. S. Hettiarachchy, and M. Qi, *J. Am. Oil Chem. Soc.* 75, 845–850 (1998).
23. M. Qi, N. S. Hettiarachchy, and U. Kalapathy, *J. Food Sci.* 62, 1110–1115 (1997).
24. E. Dickinson and Y. Matsumura, *Int. J. Biol. Macromol.* 13, 26–30 (1991).
25. S. Roth, B. S. Murray, and E. Dickinson, *J. Agric. Food Chem.* 48, 1491–1497 (2000).
26. M. Færgemand and B. S. Murray, *J. Agric. Food Chem.* 46, 884–890 (1998).
27. D. G. Dalgleish, *Colloids Surfaces B* 1, 1–8, (1993).
28. T. Nylander and M. Wahlgren, *J. Colloid Interf. Sci.* 162, 151–162 (1994).
29. T. Nylander, F. Tiberg, and M. Wahlgren, *Int. Dairy J.* 9, 313–317 (1999).
30. E. Dickinson, D. S. Horne, J. Phipps, and R. Richardson, *Langmuir* 9, 242–248 (1993).
31. F. A. Husband, M. J. Garrood, A. R. Mackie, G. R. Burnett, and P. J. Wilde, *J. Agric. Food Chem.* 49, 859–866 (2001).

32. A. L. de Roos and P. Walstra, *Colloids Surfaces B* 6, 201–208 (1996).
33. M. Corredig and D. G. Dalgleish, *Colloids Surfaces B* 4, 411–422 (1995).
34. Y. Fang and D. G. Dalgleish, *J. Colloid Interf. Sci.* 196, 292–298 (1998).
35. S. O. Agboola and D. G. Dalgleish, *J. Agric. Food Chem.* 44, 3637–3642 (1996).
36. T. van Vliet, *Colloid Polym. Sci.* 266, 518–524 (1988).
37. C. K. Reiffers-Magnani, J.-L. Cuq, and H. J. Watzke, *Food Hydrocolloids* 14, 521–530 (2000).
38. R. Jost, F. Dannenberg, and J. Rosset, *Food Microstruct.* 8, 23–28 (1989).
39. S. K. Sharma and D. G. Dalgleish, *J. Dairy Res.* 61, 375–384 (1994).
40. H. Casanova and E. Dickinson, *J. Agric. Food Chem.* 46, 72–76 (1998).
41. E. Dickenson and E. Davies, *Colloids Surfaces B* 12, 203–212 (1999).
42. E. P. Schokker and D. G. Dalgleish, *J. Agric. Food Chem.* 48, 198–203 (2000).
43. D. V. Brooksbank, C. M. Davidson, D. S. Horne, and J. Leaver, *J. Chem. Soc. Faraday Trans.* 89, 3419–3425 (1993).
44. E. Dickinson, M. I. Goller, and D. J. Wedlock, *J. Colloid Interf. Sci.* 172, 192–202 (1995).
45. E. Dickinson and M. Golding, *Food Hydrocolloids* 11, 13–18 (1997).
46. D. Reichman and N. Garti in *Food Polymers, Gels and Colloids* (E. Dickinson, ed.), Royal Society of Chemistry, Cambridge, 1991, pp. 549–556.
47. D. M. W. Anderson, in *Gums and Stabilisers for the Food Industry 3* (G. O. Phillips, D. J. Wedlock, and P. A. Williams eds.), Elsevier Applied Sciences, Barking, UK, 1986, 79–86.
48. B. F. M. Namee, E. D. O’Riordan, and M. O’Sullivan, *J. Agric. Food Chem.* 46, 4551–4555 (1998).
49. Y. Matsumura, C. Satake, M. Egami, and T. Mori, *Biosci. Biotechnol. Biochem.* 64, 1827–1835 (2000).
50. E. Dickinson and V. B. Galazka, *Food Hydrocolloids* 5, 281–296 (1991).
51. M. Darewicz and J. Dziuba, *Nahrung* 45, 15–20 (2001).
52. D. G. Dalgleish and A.-L. Hollocou, in *Food Colloids—Proteins, Lipids and Polysaccharides* (E. Dickenson and B. Bergenstahl, eds.), Royal Society of Chemistry, Cambridge, 1997, pp. 236–244.
53. E. Dickinson, M. G. Semenova, A. S. Antipova, and E. G. Pelan, *Food Hydrocolloids*, 12, 425–432 (1998).
54. D. F. Darling and R. J. Birkett, in *Food Emulsions and Foams* (E. Dickinson, ed.), Royal Society of Chemistry, Cambridge, 1987, pp. 1–29.
55. N. Krog, in *Microemulsions and Emulsions in Foods* (M. El-Nokaly and D. Cornell eds.), American Chemical Society, Washington, DC, 1991, pp. 139–145.
56. E. Li-Chan and S. Nakai, in *Food Proteins* (J. E. Kinsella and W. G. Soucie, eds.), American Oil Chemists’ Society, Champaign, IL, 1989, pp. 232–251.
57. E. Dickinson, D. J. Pogson, E. W. Robson, and G. Stainsby, *Colloids Surfaces* 14, 135–141 (1985).
58. A. Kato, N. Tsutsui, N. Matsudomi, K. Kobayashi, and S. Nakai, *Agric. Biol. Chem.* 45, 2755–2760 (1981).

59. E. Dickinson, J. A. Hunt, and D. G. Dalgleish, *Food Hydrocolloids* 4, 403–414 (1991).
60. A. Kato, S. Miyazaki, A. Kawamoto, and K. Kobayashi, *Agric. Biol. Chem.* 51, 2989–2994 (1987).
61. E. Dickinson, V. J. Pinfield, and D. S. Horne, *J. Colloid Interf. Sci.* 187, 539–541 (1997).
62. S. Damodaran and S. Xu, *J. Colloid Interf. Sci.* 178, 426–435 (1996).
63. B. M. Byrne, A. D. van het Schip, J. A. M. van de Klundert, A. C. Arnberg, M. Gruber, and G. Ab, *Biochemistry* 23, 4275–4279 (1984).
64. E. Keshavarz and S. Nakai, *Biochim. Biophys. Acta* 576, 269–279 (1979).
65. S. Nakai, *J. Agric. Food Chem.* 31, 676–683 (1983).
66. A. Kato and S. Nakai, *Biochim. Biophys. Acta* 624, 13–20 (1980).
67. F. MacRitchie and N. F. Owens, *J. Colloid Interf. Sci.* 29, 66–71 (1969).
68. C. A. Haynes and W. Norde, *Colloids Surfaces B* 2, 517–566 (1994).
69. W. Norde, F. MacRitchie, G. Nowicka, and J. Lyklema, *J. Colloid Interf. Sci.* 112, 447–456 (1986).
70. R. J. Green, I. Hopkinson, and R. A. L. Jones in *Food Emulsions and Foams* (E. Dickinson and J. M. Rodriguez Patino, eds.), Royal Society of Chemistry, Cambridge, 1999, pp. 285–295.
71. Y. Fang and D. G. Dalgleish, *Food Hydrocolloids* 12, 121–126 (1998).
72. W. Norde and J. P. Favier, *Colloids Surfaces* 64, 87–93 (1992).
73. M. C. L. Maste, E. H. W. Pape, A. van Hoek, W. Norde, and A. J. W. G. Visser, *J. Colloid Interf. Sci.*, 180, 632–633 (1996).
74. S. Damodaran and K. Anand, *J. Agric. Food Chem.* 45, 3813–3820 (1997).
75. E. A. Foegeding, in *Food Proteins* (J. E. Kinsella and W. G. Soucie, eds.), American Oil Chemists' Society, Champaign, IL, 1989, pp. 185–194.
76. K. D. Caldwell, J. Li, J.-T. Li, and D. G. Dalgleish, *J. Chromatogr.* 604, 63–71 (1992).
77. C. A. Haynes, E. Sliwinsky, and W. Norde, *J. Colloid Interf. Sci.* 164, 394–409 (1994).
78. C. Holt and L. Sawyer, *Protein Eng.*, 2, 251–259 (1988).
79. H. E. Swaisgood, in *Advanced Dairy Chemistry, 1. Proteins* (P. F. Fox, ed.), Elsevier Science, Barking, UK, 1992, pp. 63–110.
80. D. E. Graham and M. C. Phillips, *J. Colloid Interf. Sci.* 70, 415–426 (1979).
81. M. C. Phillips, *Chem. Ind.* 170–176 (1977).
82. D. E. Graham and M. C. Phillips, *J. Colloid Interf. Sci.* 70, 427–439 (1979).
83. D. G. Dalgleish and J. Leaver, in *Food Polymers. Gels and Colloids* (E. Dickinson, ed.), Royal Society of Chemistry, Cambridge, 1991, pp. 113–122.
84. S. G. Hambling, A. S. M. Alpine, and L. Sawyer, in *Advanced Dairy Chemistry, 1. Proteins* (P. F. Fox, ed.), Elsevier Science, Barking, UK, 1992, pp. 141–190.
85. R. D. Bee, J. Hoogland, and R. H. Ottewill, in *Food Colloids and Polymers, Stability and Mechanical Properties* (E. Dickinson and P. Walstra, eds.), Royal Society of Chemistry, Cambridge, 1993, pp. 341–353.
86. Y. Kamata, K. Ochiai, and F. Yamauchi, *Agric. Biol. Chem.* 48, 1147–1152 (1984).

87. P. Plietz, G. Damaschun, J. J. Müller, and K.-D. Schwenke. *Eur. J. Biochem.* 130, 315–320 (1983).
88. D. Causeret, E. Matringe, and D. Lorient, *J. Food Sci.* 56, 1532–1536 (1991).
89. L. D. Ford, R. Borwankar, R. W. Martin, Jr., and N. Holcomb, in *Food Emulsions* 3rd ed. (K. Larson and S. E. Friberg, eds.), Marcel Dekker, New York, 1997, pp. 361–412.
90. P. Walstra, in *Food Structure and Behavior* (J. M. V. Blanshard and P. Lillford, eds.), Academic Press, London, 1987, pp. 87–106.
91. P. Walstra, in *Encyclopedia of Emulsion Technology* (P. Becher, ed.), Marcel Dekker, New York, 1983, pp. 57–128.
92. L. Taisne, P. Walstra, and B. Cabane, *J. Colloid Interf. Sci.* 184, 378–390 (1996).
93. O. Robin, N. Remillard, and P. Paquin. *Colloids Surfaces A*, 80, 211–222 (1993).
94. Y. Fang and D. G. Dalgleish, *J. Colloid Interf. Sci.* 156, 329–334 (1993).
95. E. Dickinson, F. O. Flint, and J. A. Hunt, *Food Hydrocolloids* 3, 389–397 (1989).
96. L. V. Ogdén, P. Walstra, and H. A. Morris, *J. Dairy Sci.* 59, 1727–1737 (1976).
97. C. Holt, *Adv. Protein Chem.* 43, 63–151 (1992).
98. H. Oortwijn, P. Walstra, and H. Mulder, *Netherlands Milk Dairy J.* 31, 134–147 (1977).
99. P. Walstra, *Netherlands Milk Dairy J.* 34, 181–190 (1980).
100. S. R. Euston and R. L. Hirst, *J. Food Sci.* 65, 934–940 (2000).
101. H. Pessen, J. M. Purcell, and H. M. Farrell, *Biochim. Biophys. Acta* 828, 1–12 (1985).
102. J. A. Hunt and D. G. Dalgleish, *J. Agric. Food Chem.* 42, 2131–2135 (1994).
103. S. L. Turgeon, C. Sanchez, S. F. Gauthier, and P. Paquin, *Int. Dairy J.* 6, 645–608 (1996).
104. J. A. Hunt and D. G. Dalgleish, *Food Hydrocolloids* 10, 159–165 (1996).
105. W. Buchheim and P. Dejmek, in *Food Emulsions*, 3rd ed., (K. Larsson and S. E. Friberg, eds.), Marcel Dekker, New York, 1997, pp. 235–278.
106. T. Gershank, S. Benzeno, and S. Benita, *Pharmaceut. Res.* 15, 863–868 (1998).
107. K. N. Pearce and J. E. Kinsella, *J. Agric. Food Chem.* 26, 716–723 (1978).
108. P. Walstra, *J. Colloid Interf. Sci.* 27, 493–500 (1968).
109. K. Strawbridge and F. R. Hallett, *Macromolecules* 27, 2283–2290 (1994).
110. K. Strawbridge and J. Watton, *Can. J. Spectrosc.* 36, 53–60 (1991).
111. K. Strawbridge and F. R. Hallett, *Can. J. Phys.* 70, 401–406 (1992).
112. J.-L. Gelin, L. Poyen, J.-L. Courthaudon, M. Le Meste, and D. Lorient, *Food Hydrocolloids* 8, 299–308 (1991).
113. D. G. Dalgleish and F. R. Hallett, *Food Res. Int.* 28, 181–193 (1995).
114. F. R. Hallett, T. Craig, J. Marsh, and B. Nickel, *Can. J. Spectrosc.* 34, 63–70 (1989).
115. C. Urban and P. Schurtenberger, *J. Colloid Interf. Sci.* 207, 150–158 (1998).
116. C. Urban and P. Schurtenberger, *Phys. Chem. Chem. Phys.* 1, 3911–3915 (1999).

117. D. S. Horne and C. Davidson, *Colloids Surfaces A* 77, 1–8 (1993).
118. D. G. Dalgleish and D. S. Horne, *Milchwissenschaft* 46, 417–422 (1991).
119. A. Lips, T. Westbury, P. M. Hart, I. D. Evans, and I. J. Campbell, in *Food Colloids and Polymers, Stability and Mechanical Properties* (E. Dickinson and P. Walstra, eds.), Royal Society of Chemistry, Cambridge, 1993, pp. 31–44.
120. D. J. McClements, *Langmuir* 12, 3454–3461 (1996).
121. D. J. McClements and J. N. Coupland, *Colloids Surfaces A* 117, 161–170 (1996).
122. J. N. Coupland and D. J. McClements, *J. Food Eng.* 50, 117–120 (2001).
123. J. N. Coupland and D. J. McClements, *J. Am. Oil Chem. Soc.* 74, 1559–1564 (1997).
124. A. S. Dukhin and P. S. Goetz, *Colloids Surfaces A* 144, 49–58 (1998).
125. T. Wade and J. K. Beattie, *Colloids Surfaces B*, 10, 73–85 (1995).
126. L. Kong, J. K. Beattie, and R. J. Hunter, *J. Colloid Interf. Sci.* 238, 70–79 (2001).
127. J. M. M. Westerbeek and A. Prins, in *Microemulsions and Emulsions in Foods* (M. El-Nokaly and D. Cornell, eds.), American Chemical Society, Washington, DC, 1991, pp. 146–160.
128. A. Kabalnov, T. Tarara, R. Arlauskas, and J. Weers, *J. Colloid Interf. Sci.* 184, 227–235 (1996).
129. J. M. Brun and D. G. Dalgleish, *Int. Dairy J.* 9, 323–327 (1999).
130. F. MacRitchie, *Colloids Surfaces A* 76, 159–166 (1993).
131. J. Leaver and D. G. Dalgleish, *Biochim. Biophys. Acta* 1041, 217–222 (1990).
132. J. Leaver and D. G. Dalgleish, *J. Colloid Interf. Sci.* 149, 49–55 (1992).
133. D. G. Dalgleish, *Colloids Surfaces* 46, 141–155 (1990).
134. A. R. Mackie, J. Mingins, and A. N. North, *J. Chem. Soc. Faraday Trans.* 87, 3043–3049 (1991).
135. D. G. Dalgleish and J. Leaver, *J. Colloid Interf. Sci.* 141, 288–294 (1991).
136. M. Shimizu, A. Ametani, S. Kaminogawa, and K. Yamauchi, *Biochim. Biophys. Acta* 869, 259–264 (1986).
137. A. R. Mackie, J. Mingins, and R. Dann, in *Food Polymers, Gels and Colloids* (E. Dickinson, ed.), Royal Society of Chemistry, Cambridge, 1991, pp. 96–111.
138. F. A. M. Leermakers, P. J. Atkinson, E. Dickinson, and D. S. Horne, *J. Colloid Interf. Sci.* 178, 681–693 (1996).
139. E. Dickinson, D. S. Horne, V. J. Pinfield, and F. A. M. Leermakers, *J. Chem. Soc. Faraday Trans.* 93, 425–432 (1997).
140. E. Dickinson, V. J. Pinfield, D. S. Horne, and F. A. M. Leermakers, *J. Chem. Soc. Faraday Trans.* 93, 1785–1790 (1997).
141. M. Britten and H. J. Giroux, *J. Agric. Food Chem.* 41, 1187–1191 (1993).
142. M. Rosenberg and S. L. Lee, *Food Struct.* 12, 267–274 (1993).
143. F. MacRitchie, *J. Colloid Interf. Sci.* 105, 119–123 (1985).
144. D. G. Dalgleish and E. W. Robson, *J. Dairy Res.* 52, 539–546 (1985).
145. H. Oortwijn and P. Walstra, *Netherlands Milk Dairy J.* 33, 134–154 (1979).
146. P. Walstra and H. Oortwijn, *Netherlands Milk Dairy J.* 36, 103–113 (1982).

147. D. G. Dalgleish, S. Tosh, and S. West, *Netherlands Milk Dairy J.* 50, 135–148 (1996).
148. A. V. McPherson and B. J. Kitchen, *J. Dairy Res.* 50, 107–133 (1983).
149. M. E. Cano-Ruiz and R. L. Righter, *J. Dairy Sci.* 80, 2732–2739 (1997).
150. M. A. Tung and L. J. Jones, *Scanning Electron Microsc.* 3, 523–530 (1981).
151. C. Kanno, Y. Shimomura, and E. Takano, *J. Food Sci.* 56, 1219–1223 (1991).
152. M. Corredig and D. G. Dalgleish, *J. Agric. Food Chem.* 46, 2533–2540 (1998).
153. M. Corredig and D. G. Dalgleish, *J. Dairy Res.* 65, 465–477 (1988).
154. J. A. Hunt and D. G. Dalgleish, unpublished results.
155. E. Dickinson, S. E. Rolfe, and D. G. Dalgleish, *Food Hydrocolloids* 3, 193–203 (1989).
156. E. W. Robson and D. G. Dalgleish, *J. Food Sci.* 52, 1694–1698 (1987).
157. E. Dickinson, *J. Food Eng.* 22, 59–74 (1994).
158. E. Dickinson, S. E. Rolfe, and D. G. Dalgleish, *Int. J. Biol. Macromol.* 12, 189–194 (1990).
159. D. G. Dalgleish, S. E. Euston, J. A. Hunt, and E. Dickinson, in *Food Polymers, Gels and Colloids* (E. Dickinson, ed.), Royal Society of Chemistry, Cambridge, 1991, pp. 485–489.
160. M. Ikeguchi, K. Kuwajima, M. Mitani, and S. Sugai, *Biochemistry* 25, 6965–6972 (1986).
161. O. B. Ptitsyn, in *Protein Folding* (T. E. Creighton, eds.), W. H. Freeman, New York, 1992, pp. 243.
162. E. Dickinson and Y. Matsumura, *Colloids Surfaces B* 3, 1–17 (1994).
163. S. Damodaran, K. Anand, and L. Razumovsky, *J. Agric. Food Chem.* 46, 872–876 (1998).
164. J.-L. Courthaudon, E. Dickinson, Y. Matsumura, and A. Williams, *Food Struct.* 10, 109–115 (1991).
165. J.-L. Courthaudon, E. Dickinson, and D. G. Dalgleish, *J. Colloid Interf. Sci.* 145, 390–395 (1991).
166. J.-L. Courthaudon, E. Dickinson, Y. Matsumura, and D. C. Clark, *Colloids Surfaces* 56, 293–300 (1991).
167. J. A. de Feijter, J. Benjamins, and M. Tamboer, *Colloids Surfaces* 27, 243–266 (1987).
168. E. Dickinson and S. Tanai, *J. Agric. Food Chem.* 40, 179–183 (1992).
169. E. Dickinson, R. K. Owusu, S. Tan, and A. Williams, *J. Food Sci.* 58, 295–298 (1993).
170. M. Cornec, P. J. Wilde, P. A. Gunning, A. R. Mackie, F. A. Husband, M. L. Parker, and D. C. Clark, *J. Food Sci.* 63, 39–43 (1998).
171. A. P. Gunning, A. R. Mackie, A. R. Kirby, and V. J. Morris, *Langmuir* 17, 2013–2018 (2000).
172. D. S. Horne, P. J. Atkinson, E. Dickinson, V. J. Pinfield, and R. M. Richardson, *Int. Dairy J.* 8, 73–77 (1998).
173. C. M. Wijmans and E. Dickinson, *Phys. Chem. Chem. Phys.* 1, 2141–2147 (1999).
174. C. M. Wijmans and E. Dickinson, *Langmuir* 15, 8344–8348 (1999).

175. L. Razumovsky and S. Damodaran, *J. Agric. Food Chem.* 49, 3080–3086 (2001).
176. T. Sengupta and S. Damodaran, *J. Agric. Food Chem.* 49, 3087–3091 (2001).
177. Y. Fang and D. G. Dalgleish, *Colloids Surfaces B*, 1, 357–364 (1993).
178. C. H. McCrae and D. D. Muir, *J. Dairy Res.* 59, 177–185 (1992).
179. Y. Fang and D. G. Dalgleish, *Langmuir* 11, 75–79 (1995).
180. J. Leaver, A. J. R. Law, E. Y. Brechany, and C. H. McCrae, *Int. J. Food Sci. Technol.* 34, 503–508 (1999).
181. E. Dickinson, J. A. Hunt, and D. S. Horne, *Food Hydrocolloids* 6, 359–370 (1992).
182. D. S. Horne, *Biopolymers* 23, 989–993 (1984).
183. D. S. Horne and D. D. Muir, *J. Dairy Sci.* 73, 3613–3626 (1990).
184. D. G. Dalgleish, H. D. Goff, J. M. Brun, and B. Luan, *Food Hydrocolloids* 16, 303–311 (2002).
185. D. G. Dalgleish, H. D. Goff, and B. Luan, *Food Hydrocolloids* 16, 295–302 (2002).
186. M. Faergemand, B. S. Murray, and E. Dickinson, *J. Agric. Food Chem.* 45, 2514–2519 (1997).
187. M. Faergemand, J. Otte, and K. B. Qvist, *Int. Dairy J.* 8, 715–723 (1998).
188. E. Dickinson and J. D. James, *J. Agric. Food Chem.* 47, 25–30 (1999).
189. E. Dickinson and J. D. James, *Food Hydrocolloids* 14, 365–376 (2000).

2

Food Emulsifiers: Their Chemical and Physical Properties

Niels J. Krog and Flemming Vang Sparsø

Danisco, Brabrand, Denmark

I. INTRODUCTION

Foods are very complex colloidal systems and modern industrial production requires surface-active lipids such as emulsifiers as processing aids and to secure a uniform quality, improved texture, and long shelf life.

An emulsifier is defined as a substance that reduce surface tension between oil–water or air–water, thus enhancing emulsification and increasing emulsion stability. Many native polar lipids and proteins comply with this definition. Food emulsifiers, on the other hand, do not affect the emulsification process significantly, but have other functions which are related to interfacial properties and affect emulsion stability or destabilization of whippable emulsions. In addition, food emulsifiers have other functions in foods, such as the modification of fat crystallization, interactions with carbohydrate components, or act as film forming substances, controlling oxygen or humidity transport, and such applications are not related to the classical definition of an emulsifier.

The main goal of this chapter is to describe the relationship between the chemical structure and composition of the emulsifiers and their function in foods. The crystalline properties, interfacial adsorption, and interactions with food ingredients, such as fats, proteins, carbohydrates, and water, are playing important roles in the function of emulsifiers in food products.

II. CHEMICAL COMPOSITION AND PHYSICAL PROPERTIES

A. Monoglycerides

An overview of food emulsifiers and their identification numbers is presented in Table 1. The use of mono-diglycerides dates back to the 1930s, when they were first used in margarine production.

Table 1 Food Emulsifiers and Their Legal Status

Chemical name	Abbreviation	ADI value ^a	EU No.	US FDA 21 CFR
Lecithin	—	Not limited	E322	§184.1400 ^b
Mono-diglycerides (distilled monoglycerides)	MAG	Not limited	E471	§184.1505 ^b
Acetic acid esters of monoglycerides	ACETEM	Not limited	E472a	§172.828
Lactic acid esters of mono-diglycerides	LACTEM	Not limited	E472b	§172.852
Citric acid esters of mono-diglycerides	CITREM	Not limited	E472c	§172.832
Diacetyl tartaric acid esters of monoglycerides	DATEM	0–50	E472e	§184.1101 ^b
Succinic acid esters of monoglycerides	SMG	—	—	§172.830
Salts of fatty acids (Na, K, Ca)	—	Not limited	E470a	§172.863
Polyglycerol esters of fatty acids	PGE	0–25	E475	§172.854
Polyglycerol polyricinoleate	PGPR	0–7.5	E476	—
Propylene glycol esters of fatty acids	PGMS	0–25 ^c	E477	§172.856
Sodium stearyl-lactylate	SSL	0–20	E482	§172.844
Calcium stearyl-lactylate	CSL	0–20	E481	§172.846
Sucrose esters of fatty acids	—	0–10	E473	§172.859
Sorbitan monostearate	SMS	0–25	E491	§172.842
Sorbitan tristearate	STS	0–15	E492	— ^d
Polysorbate 60	PS 60	0–25	E435	§172.836
Polysorbate 65	PS 65	0–25	E436	§172.838
Polysorbate 80	PS 80	0–25	E433	§172.840

^aAcceptable daily intake in mg/kg body weight per day.

^bGenerally recognized as safe (GRAS).

^cCalculated as propylene glycol.

^dPetition filed and accepted.

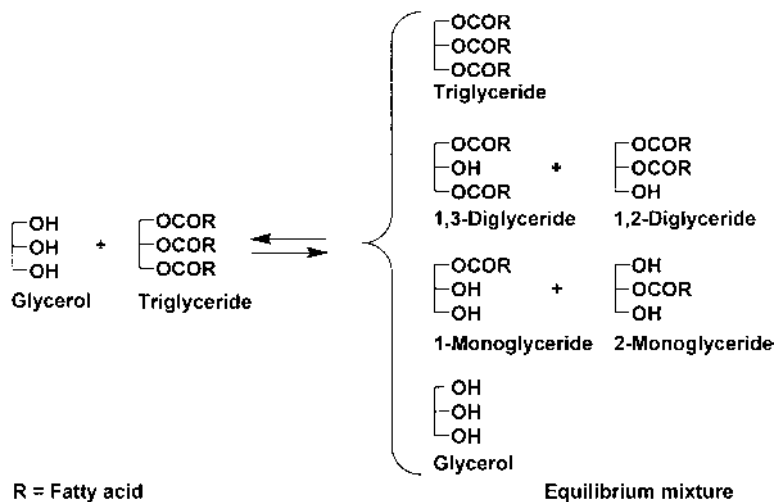


Figure 1 Reaction scheme of interesterification (glycerolysis) of triglycerides and glycerol. R₁, R₂, and R₃ are fatty acids.

Table 2 Composition of Glycerolysis Equilibrium Mixtures

Amount of glycerol added to triglyceride (% w/w)	Equilibrium mixture		
	Triglycerides (% w/w)	Diglycerides (% w/w)	Monoglycerides (% w/w)
0	100	—	—
7	35	50	15
14	15	45	40
16	11	43	46
20	8	39	53
24	5	35	60

Source: Adapted from Ref. 1.

Monoglycerides are produced industrially by interesterification (glycerolysis) of edible fats or oils with glycerol, the reaction of the components takes place at high temperature (200–260°C) under alkaline catalysis. The reaction scheme is shown in Fig. 1, and has been described in detail by Feuge and Bailey (1) and Sonntag (2). Table 2 shows the calculated composition of the fat-phase mixture from the glycerolysis of fat with different concentrations of glycerol. The so-called monodiglycerides produced by

Table 3 Equilibrium Reaction Mixtures of 1- and 2-Monoglycerides

Temperature (°C)	1-Monoglycerides (%)	2-Monoglycerides (%)
20	95	5
80	91	9
200	82	18

glycerolysis contain from 40% to a maximum of 60% monoglycerides with the balance being diglycerides and triglycerides. High-diglyceride-containing products can also be made by glycerolysis using 6 to 8 parts of glycerol to 100 parts of fat. This ratio yields a blend containing 15% monoglycerides, 50% diglycerides, and 35% triglycerides.

Concentrated monoglycerides are produced by a high-vacuum thinfilm molecular distillation process yielding products containing typically 95% monoglycerides, 3–4% diglycerides, 0.5–1% free glycerol, and 0.5–1% free fatty acids.

Freshly distilled monoglycerides contain an equilibrium of 1-monoglycerides and 2-monoglycerides. The ratio between the two isomers at different temperatures is shown in Table 3. The composition varies considerably with temperature. The rate constant of the equilibrium reaction is very low at room temperature and depends on fatty acid composition, crystal form, and traces of basic catalysts present (3). The content of 1-monoglycerides in commercial distilled monoglycerides is usually from 90% to about 95%.

Enzymatic synthesis of monoglycerides and other emulsifiers has been reported (7–9) as a method to produce stereospecific emulsifiers. However, isolation of the desired products from the reaction mixture is a problem for large-scale production, and commercial production of emulsifiers by biochemical methods is not commonly used.

Because the 1-monoglyceride isomer content can vary according to the temperature history of the product, the most reliable method for the determination of the monoglyceride content in commercial products is using gas–liquid chromatography (GLC) combined with a derivatization of the monoglycerides with, for example, trimethyl silylether (4). Figure 2 shows a gas chromatogram of distilled monoglycerides based on fully hydrogenated tallow fat.

Monoglycerides are polymorphic like triglycerides and can exist in different crystal forms depending on temperature conditions. Furthermore, as shown in Fig. 3, monoglycerides and diglycerides have a higher melting point than the corresponding triglycerides. For saturated

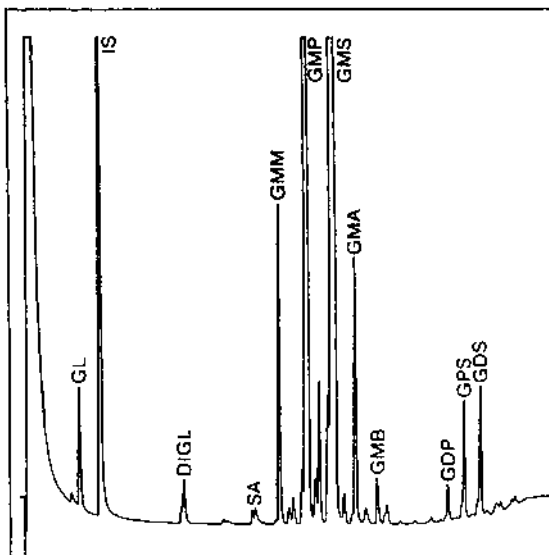


Figure 2 Gas-liquid chromatogram of trimethyl-silylether derivatives of distilled monoglycerides. GL = glycerol, IS = internal standard, DIGL = diglycerol, SA = stearic acid, GMM = glycerol monomyristate, GMP = glycerol monopalmitate, GMS = glycerol monostearate, GMA = glycerol monoarachidate, GMB = glycerol monobehenate, GDP = glycerol dipalmitate, GPS = glycerol palmitate-stearate, GDS = glycerol distearate.

monoglycerides of palmitic and stearic acid, the increase in melting point compared to the corresponding triglycerides is 10–12°C. For unsaturated glycerides, like mono-olein and triolein, the difference is as high as about 30°C.

The melting points of the polymorphs of pure monoglycerides with fatty acid chain length from C₁₀ to C₁₈ are shown in Fig. 4.

When cooled from melt, monoglycerides crystallize in a metastable α -form. On further cooling, a solid-state transition from an α -form to a sub- α -form takes place at a lower temperature. When stored at ambient temperature, transition to the stable β crystal form will take place. The polymorphism of monoglycerides thus follows the pattern of triglycerides that has been reviewed by Larsson (5).

All lipids form crystal structures with the hydrocarbon chains arranged in layers with a parallel chain axis. In lipids with polar head groups, such as surfactants, the molecule is always arranged in layers, with the polar head group in discrete layers separated by the fatty acid hydrocarbon chains, forming a lipid bilayer, which is an important feature

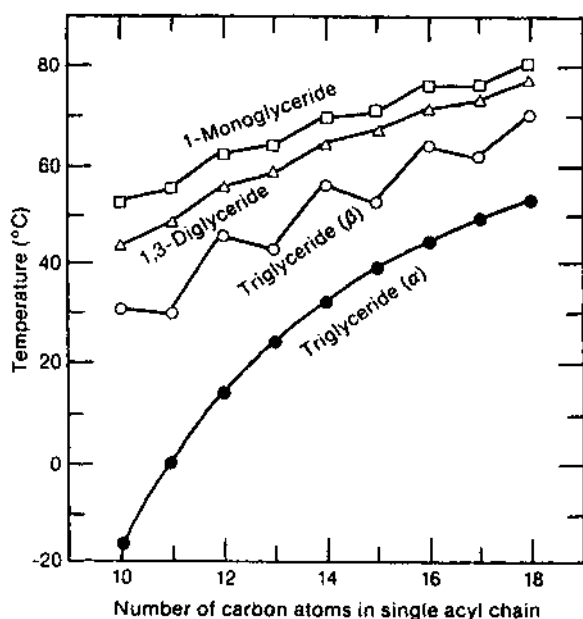


Figure 3 Melting points of monoglycerides and diglycerides compared to corresponding triglycerides with fatty acid chain length from C₁₀ to C₁₈. (From Ref. 2.)

of polar lipids. Figure 5 shows the molecular orientation in crystals of polar lipids with double-chain-length packing (DCL) and single-chain-length packing mode (SCL) schematically, where the hydrocarbon chains of two adjacent layers penetrate each other. The crystal forms of monoglycerides and diglycerides as well as of distilled monoglycerides are the same as those in triglycerides except that the β'-form is not usually found in commercial monoglycerides.

X-ray diffraction patterns of commercial monoglycerides show a strong short spacing at 4.2 Å for the α-form (hexagonal subcell), as seen in Table 4 showing crystallographic data and melting points of distilled monoglycerides based on single fatty acids with minimum 90% purity or hydrogenated vegetable fats.

When the α-form is cooled, it transforms into a sub-α crystal form at approximately 35°C; the sub-α-form is characterized by a strong spacing near 4.3 Å, and several spacings from 3.9 to 3.7 Å, with medium intensity.

The stable, high-melting β-form is characterized by a strong short spacing at 4.6 Å, combined with several spacings in the region 3.9–3.6 Å or lower, with medium intensity.

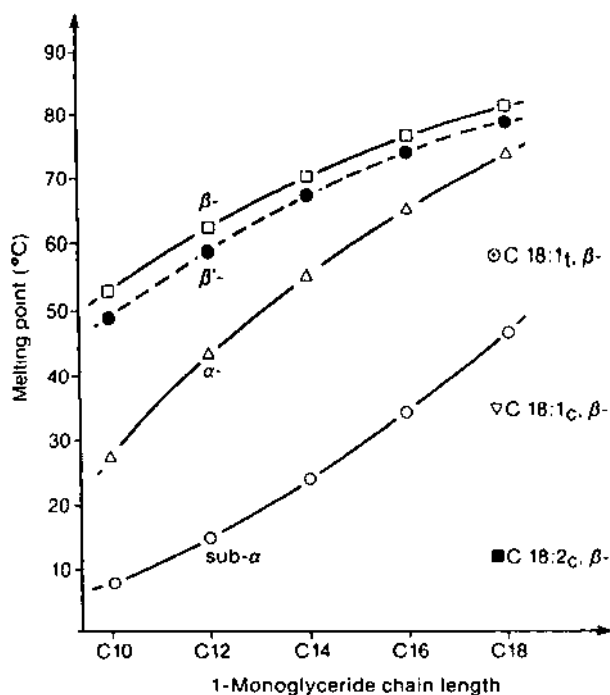


Figure 4 Melting points of crystal polymorphs of pure monoglycerides with chain length from C₁₀ to C₁₈. C₁₈:1_t = 1-monoelaidin, C₁₈:1_c = 1-mono-olein, C₁₈:2_c = 1-monolinolein.

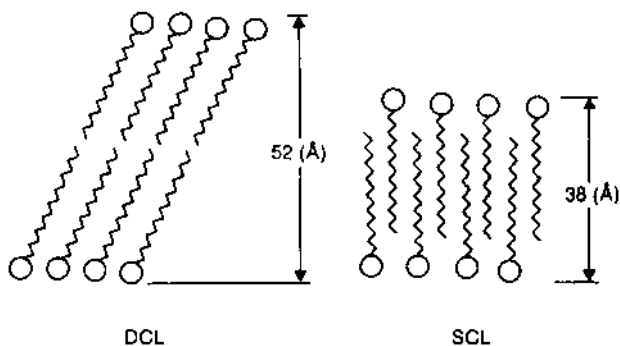


Figure 5 Schematic models of the molecular packing of polar lipids. DCL = double-chain-length structure, SCL = single-chain-length structure. Typical x-ray diffraction long spacings of the lipid bilayers are shown.

Table 4 Melting Points and X-Ray Diffraction Data of Mixed Fatty Acid Distilled Monoglycerides

Monoglyceride	Melting points ^a (°C)			Long spacings (Å)		Main short spacings (Å)	
	Sub- α	α	β	α	β	α	β
Monolaurin, 90% C ₁₂	16	45	61	—	37.3	4.15	4.57-4.32-4.00-3.84-3.71-2.44
Monomyristin, 90% C ₁₄	25	56	67	41.0	40.6	4.15	4.55-4.33-3.91-3.81-3.71-2.44
Monopalmitin, 90% C ₁₆	35	66	73	47.0	44.7	4.15	4.51-3.91-3.84-3.67-2.43
Mono-olein, 90% C _{18:1}	—	30	34	—	48.5	—	4.60-4.38-4.31-4.04
Monobehenin, 90% C ₂₂	56	82	85	57.3	57.5	4.15	4.50-3.94-3.84-3.74-2.43
Saturated monoglycerides ^{b,1} (hydrogenated soybean oil)	37	71	75	54.0	51.4	4.13	4.55-3.94-3.86-3.78-2.43
Saturated monoglycerides ^{b,2} (from hydrogenated lard)	20	66	72	53.2	49.8	4.15	4.52-4.35-3.93-3.84-2.43
Saturated monoglycerides ^{b,3} (hydrogenated palm oil)	16	68	72	51.6	47.0	4.15	4.55-4.33-3.89-2.43
Unsaturated monoglycerides ^{b,4} (palm oil)	8	(48)	60	—	46.5	—	4.55-4.31-4.03-3.86

^aDifferential scanning calorimetry (DSC) peak temperatures.

^bDanisco ingredients products: ¹DIMODAN[®] HS, ²DIMODAN[®] HL, ³DIMODAN[®] HP, ⁴DIMODAN[®] P/M.

Long spacings of C_{16/18} saturated monoglycerides are in the order of 50 Å, corresponding to the DCL packing mode. Above the melting point, monoglycerides show a diffuse x-ray diffraction line in the long spacing region corresponding to 30 Å. This means that monoglycerides maintain an ordered structure in the melt due to hydrogen-bonding between the polar groups.

Diglycerides are usually only present in monodiglycerides in minor quantities and are not considered to be the main components. However, it is possible to produce a high-diglyceride product containing 50–60% diglycerides by glycerolysis. Such products have found some applications due to the specific crystallization properties of 1,2-diglycerides. Diglycerides exist in two isomeric forms: 1,2- and 1,3-diglycerides (see Fig. 1) in a relative ratio of 40:60. The 1,2-diglycerides crystallize from melt in a metastable α -form, which transforms to a stable β' -form. They can, therefore, be used to stabilize β' crystals in fat blends, which otherwise show a tendency of growing β crystals, giving rise to textural problems (e.g., in margarine or low-calorie spreads).

B. Organic Acid Esters of Monoglycerides

The free hydroxyl groups in monoglycerides can be esterified with organic acids such as acetic, lactic, diacetyltartaric, citric, and succinic acids, and thus form more lipophilic or hydrophilic derivatives of monoglycerides. The esters are normally produced by reacting monoglycerides with the organic acid directly or with its anhydride.

The crystalline behavior, melting point, and polar properties of the organic acid esters are very different from that of the corresponding monoglycerides. Acetic and lactic acid esters are low-polar, lipophilic emulsifiers, whereas diacetyl tartaric acid esters or citric acid esters are anionic, hydrophilic emulsifiers. Therefore, such organic acid esters have different functional properties than monoglycerides and are used in many new applications in foods.

A common feature of the monoglyceride derivatives is that they are all monomorphic and crystallize from melt in an α -crystal form. The melting points and crystallographic data of organic acid esters are shown in Table 5. Some of the monoacyl esters crystallize with SCL packing mode, and these emulsifiers have the strongest decrease in melting point compared to monoglycerides (see Table 4).

The melting points shown in Table 5 are typical for monoglyceride derivatives based on blends of saturated palmitic and stearic acids. It should be noted that among commercial products, some variation in melting points

Table 5 Melting Points and X-Ray Diffraction Data of Organic Acid Esters of Monoglycerides (C_{16}/C_{18} ratio, 35:65)

Organic acid esters of monoglycerides	Melting point (°C)	Long spacings (Å)	Chain packing mode	Short spacings (Å)	Crystal form
Acetic acid esters (monoacetylated)	39	32.9	SCL	4.10	α
Lactic acid esters (LACTEM)	42	39.5	SCL	4.13	α
Diacetyl-tartaric acid esters (DATEM)	43	41.0	SCL	4.11	α
1.2-Dipalmitin-DATE ^a (synthetic)	—	54.6	DCL	4.21–3.76	—
Citric acid esters (CITREM)	60	60.3	DCL	4.11	α

^aDiacetyl-tartaric acid ester of pure 1.2-dipalmitin.

could occur. This is due to variations in chemical composition and fatty acid profile.

C. Acetic Acid Esters (ACETEM)

By reacting one or both of the free hydroxyl groups in distilled monoglycerides with acetic acid anhydrid and removing the surplus of free acetic acid by distillation, a more lipophilic product is formed. Acetylation may be partial or complete depending on the ratio of the acetic acid anhydrid and monoglyceride used. Normally, products with 50%, 70%, or 90% acetylation of free hydroxyl groups are used in foods, depending on application.

The melting point of ACETEM is about 20–30°C lower than that of the monoglycerides used in production and varies from 35°C to 40°C depending on the degree of acetylation and type of monoglyceride. Acetylation of unsaturated monoglycerides with iodine values higher than 40 yields a product that is liquid at room temperature (melting point approximately 10°C).

The crystallization behavior of monoglycerides is changed considerably by acetylation, as ACETEM is monomorphic and stable in its α crystal form. Chemically pure 1-aceto-3-stearin shows the following polymorphic transitions when chilled from melt to below 0°C: sub- $\alpha_1 \rightarrow 3.5^\circ\text{C} \rightarrow$ sub- $\alpha_2 \rightarrow 12.5^\circ\text{C} \rightarrow \alpha \rightarrow 45^\circ\text{C} \rightarrow \beta' \rightarrow 48.5^\circ\text{C} \rightarrow$ melt (6).

Acetylated, saturated monoglycerides of C_{16}/C_{18} fatty acids form flexible films that can be stretched up to eight times their length before they break, and they are therefore used as coatings on fruits, nuts, and meat products (7). Due to its α -tending properties, ACETEM is also used in fats (shortenings) in aerated foods such as cakes and toppings.

D. Lactic Acid Esters (LACTEM)

Production of LACTEM is normally based on a reaction between lactic acid and monoglycerides based on fully hydrogenated vegetable or animal fats. An alternative production method is esterification of glycerol, lactic acid, and fatty acids in a mole-to-mole ratio. Lactic acid esters may contain from 15% to 35% esterified lactic acid distributed on a number of isomeric compounds. Some of the most typical components are shown in Fig. 6.

For LACTEM based on a C_{16} – C_{18} chain length, saturated monoglycerides has a melting point of about 45°C. From melt, it crystallizes into a stable α crystal form. X-ray diffraction of LACTEM often shows two long spacings at 38 Å and about 55 Å, indicating that some of the LACTEM components crystallize in a SCL form (long spacing 38 Å) and other components crystallize in a DCL form (long spacing 55 Å).

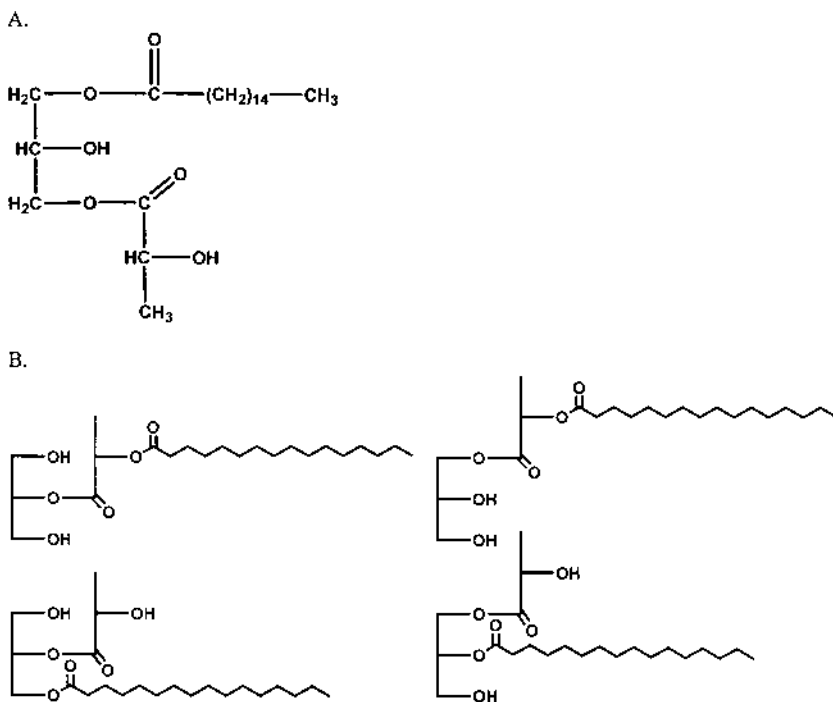


Figure 6 Chemical formulas of (A) lactic acid ester of monoglycerides (LACTEM) and (B) possible positional isomers of esters of lactic acid, palmitic acid, and glycerol.

Generally speaking, LACTEMs are nonionic emulsifiers, soluble in oils and fats, and only slightly water dispersible. LACTEMs are often less surface active than their corresponding monoglycerides, depending on the composition.

The LACTEMs are used mainly in foods such as cake shortenings and fats for toppings or imitation creams and often in combinations with saturated monoglycerides in order to make a product that is stable in the α crystalline form.

E. Diacetyl Tartaric Acid Esters (DATEM)

The anion-active and very hydrophilic DATEM products are produced by reacting diacetylated tartaric acid anhydride with monoglycerides. The diacetylated tartaric acid anhydride is produced from refined, natural tartaric acid from the wine industry by reaction with acetic acid anhydride. The chemistry of DATEM production is described in detail by Schuster and

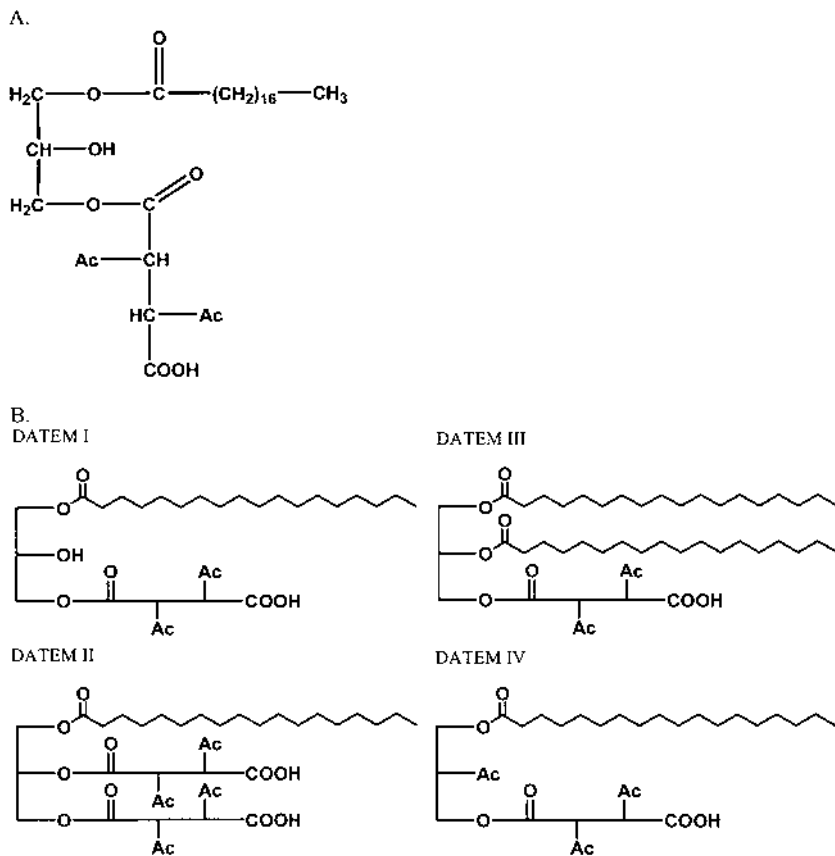


Figure 7 Chemical formulas of (A) diacetyl tartaric acid ester of 1-glycrol monostearate (DATEM) and (B) positional isomers referred to as DATEM I, II, III, and IV.

Adams (8). The main components of DATEMs are referred to as DATEM I, II, III, and IV, and their schematic molecular formula is shown in Fig. 7. Depending on the type of monoglycerides used as raw material, a DATEM can be crystallized in block, flake, or powder form or it can be semiliquid.

A DATEM of saturated, C_{16}/C_{18} monoglycerides is stable in an α crystal form with a melting point usually about 45°C . X-ray-diffraction long spacings are in agreement with a SCL packing of the hydrocarbon chains. It forms dispersions in water with low pH (2–3) due to its free-carboxyl group, and the solubility is increased if the pH value is adjusted to above 4–5 (see Section III). A DATEM is only partially soluble in oils

and fats. Compared to monoglycerides, a DATEM is very surface active and has a number of applications in food emulsions. However, its main application is as a dough conditioner in yeast-raised bakery products.

According to the Food Chemical Codex in the United States, a DATEM may contain 17–20% by weight of esterified tartaric acid and 14–17% esterified acetic acid. In Europe, the EU regulation prescribes a wider variation in composition, allowing 10–40% esterified tartaric acid and 8–32% acetic acid.

F. Citric Acid Esters (CITREM)

A CITREM is manufactured by esterification of monoglycerides with citric acid in an amount 12–20% by weight of the finished product, which is often neutralized partially, forming sodium salts of CITREM. CITREM manufactured on the basis of saturated monoglycerides crystallize from melt in an α -like crystal form, and the melting point is between 55°C and 60°C.

All esters of dicarboxylic or tricarboxylic acids and monoglycerides show a high degree of long-range order in the melted state, a phenomenon well known from soaps, called thermotropic mesomorphism. Low-angle x-ray diffraction of such materials shows one or several sharp lines in the long spacing region at temperatures above the melting point. Citric acid esters exhibit this behavior, especially due to strong molecular interactions between the polar groups in the melt.

A CITREM is an extremely hydrophilic, anionic emulsifier. It forms a milky dispersion in water and is only partially soluble in oils and fats. Its main application in foods is as antispattering agent in margarine or as emulsifier in meat or beverage emulsions. CITREM based on unsaturated monoglycerides is used to reduce the yield value and plastic viscosity of a chocolate mix.

G. Succinic Acid Esters (SMG)

Succinic acid esters are produced by a reaction of succinic anhydride with monoglycerides. A SMG is an anionic emulsifier, due to its free-carboxyl group, as it appears from its chemical formula shown in [Fig. 8](#).

A SMG based on saturated monoglycerides has a melting point of 55–60°C. When cooled from melt, it goes through a thermotropic liquid-crystalline state before crystallizing in an α -form with SCL chain packing (x-ray long spacing 38 Å). The α -form transforms to a stable β -form on storage at room temperature. The β -form has a DCL chain packing as found with monoglycerides.

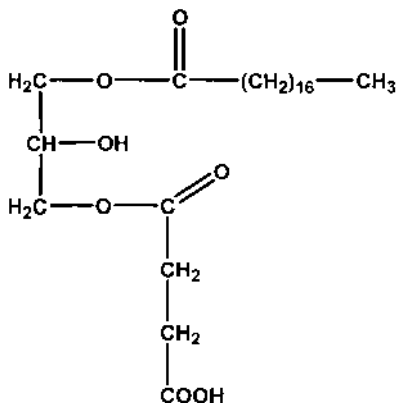


Figure 8 Chemical formula of succinic acid ester of glycerol monostearate.

Like a DATEM, a SMG is used mainly as a dough strengthener for yeast-raised baking products. However, its use in foods is limited to the United States, as EU regulations do not permit it.

H. Polyglycerol Esters of Fatty Acids (PGE)

Glycerol may be polymerised by dehydration and, by this reaction, a series of polyglycerol compounds is obtained. They can be esterified with edible fatty acids, usually palmitic stearic acid blends, forming polyglycerol esters. A structure formula of triglycerol monostearate is shown in Fig. 9. Commercial PGE products may vary considerably in composition, depending on the degree of polymerization and degree of esterification. According to EU regulations, the polyglycerol moiety should mainly be diglycerol, triglycerol, and tetraglycerol with a maximum of 10% of polyglycerols equal to or higher than heptaglycerol. In the United States, however, the U.S. FDA (Food and Drug Administration) regulation permits a polymerization degree up to decaglycerol. The composition of PGE products is very complex, with a high number of positional isomers.

A PGE with a low degree of polymerization (e.g., mainly triglycerol and tetraglycerol esters of C_{16}/C_{18} fatty acids) melts at approximately 55°C and crystallizes in a stable α -form. PGE is generally more hydrophilic than monoglycerides, but its dispersibility in water depends on polyol condensation composition and degree of esterification. PGEs are used in a number of food emulsions, ranging from margarine and dessert products to cakes and other bakery products.

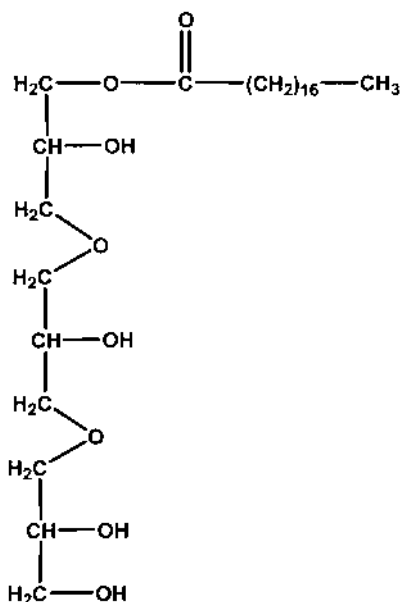


Figure 9 Chemical formula of a polyglycerol fatty acid ester [triglycerol monostearate (PGE)].

Table 6 Melting Points and X-Ray Diffraction Data of Fatty Acid Esters of Polyols and Lactic Acid (C₁₆/C₁₈ ratio, 50:50)

Product	Melting point (°C)	Long spacings (Å)	Chain packing mode	Short spacings (Å)	Crystal form
Polyglycerol monostearate	56	64.2	DCL	4.13	α
Propylene glycol monostearate	39	50.7	DCL	4.15–(3.99)	α
Sorbitan monodistearate	54	54.5	DCL	4.11	α
Sorbitan monostearate	—	33.8	SCL	4.11	α
Sorbitan tristearate	56	49.8	DCL	4.13	α
Sodium stearyl lactylate	38	37.6 (49.7)	SCL (DCL)	4.10	α

Table 6 presents the crystallographic data and melting point of polyol fatty acid esters.

Purified diglycerol fatty acid esters can be manufactured by esterification of diglycerol with edible fatty acids. The monoacyl fatty acid esters are

concentrated by a molecular distillation process. The diglycerol mono fatty acid esters are more hydrophilic than corresponding monoglycerides (9). On the contrary, polyglycerol polyricinoleate (PGPR) is primarily used to stabilize low-fat water-in-oil (w/o) emulsions (spreads) or to reduce yield value in chocolate mix.

I. Stearoyl-lactylates (SSL, CSL)

Esterification of stearic acid with lactic acid in the presence of sodium or calcium hydroxides yields a mixture of stearoyl-lactylates (sodium or calcium salts), fatty acid salts, and free fatty acids. The main component of stearoyl-lactylates is shown in Fig. 10. Esters of trilactic and polylactic acids are also present in commercial products, making the composition quite complex.

The Na stearoyl-lactylates (SSL) are normally present in an α -form with a melting point of about 45°C. This form is obtained by spray-cooling the melt into a powdered or beaded product. The α -form has a single short spacing at 4.1 Å and long spacings at about 38 Å, showing the SCL packing mode with penetrating hydrocarbon chains.

The SSL is water dispersible at neutral pH. At a pH value below 4–5, solubility is limited due to the content of 15–20% free fatty acids in SSL. The CSL is less water dispersible, but more oil soluble than SSL. Both SSL and CSL are used mainly in the baking industry as dough strengtheners. SSL is also used in many emulsions such as imitation creams, coffee whiteners, filling creams, and icings.

J. Propylene Glycol Esters of Fatty Acids (PGMS)

Propylene glycol esters can be manufactured by esterifying propylene glycol with edible fatty acids under alkaline catalysis at about 200°C under

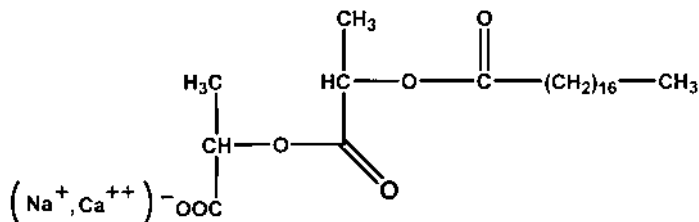


Figure 10 Chemical formula for stearoyl-lactoyl lactic acid sodium or calcium salt (SSL, CSL).

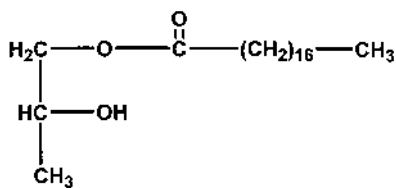


Figure 11 Chemical formula of propylene glycol monostearate (PGMS).

vacuum. After removal of excess propylene glycol, the reaction blend contains approximately 55% propylene glycol monoester and 45% diester. Structural formula is shown in Fig. 11. An alternative method is interesterification of triglycerides and propylene glycol, yielding a reaction mixture containing the propylene glycol monoesters and diesters, together with 10–15% monoglycerides and a minor amount of diglycerides as well as triglycerides. The propylene glycol monoester can be concentrated by a molecular distillation process as described for monoglycerides. Distilled PGMS contains a minimum of 90% monoesters and is normally based on saturated C₁₆/C₁₈ chain length fatty acids.

Commercial propylene glycol monostearate is stable in an α -like form, as shown in Table 6. However, pure 1-propylene glycol monostearate exists in four different crystal forms (10).

The PGMS are only slightly water dispersible, but completely soluble in oils and fats. Therefore, it is used only in combinations with fats of as an α -tending emulsifier in combination with monoglycerides or other emulsifiers. PGMS is mainly used in cake shortenings and fats for whippable emulsions, toppings, and so forth.

K. Sorbitan Esters of Fatty Acids

1. Sorbitan Esters of Fatty Acids (SMS, STS)

Sorbitan is derived from sorbitol by dehydration and then esterified with fatty acids and described for PGMS, and depending on the amount of fatty acids used for the esterification, sorbitan monoesters (SMS) or triesters (STS) are produced. The chemical formulas of SMS and STS are shown in Fig. 12.

All sorbitan esters are stable in the α crystal form, but their x-ray long spacings indicate a different molecular packing depending on the degree of esterification, as shown in Table 6. Commercial sorbitan monodistearate or sorbitan tristearate crystallize with a DCL chain packing mode, whereas a concentrated sorbitan monostearate with a mono-acyl content of 80% has a long spacing of about 34 Å, corresponding to SCL chain packing.

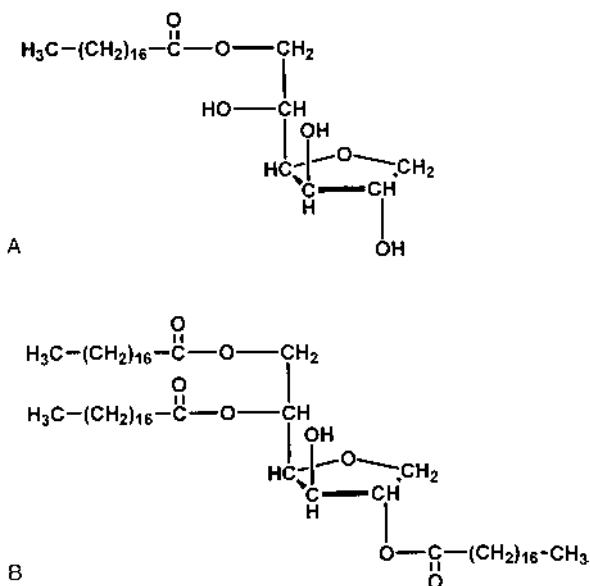


Figure 12 Chemical formula of sorbitan fatty acid esters: (A) sorbitan monostearate [6-stearoyl-1,4-anhydro-D-glucitol (SMS)] and (B) sorbitan tristearate (STS).

Sorbitan tristearate (STS) is very lipophilic and its main application is as a crystal modifier in fat-based foods (margarine, spreads, chocolate products). STSs are used to control crystallization of fats, where they stabilize the β' crystal form, preventing formation of the higher melting β crystal form. The β crystals tends to grow very large and cause a grainy texture in margarine or spreads. In chocolate products, similar fat crystal transitions are the reason for the development of a fault referred to as “bloom,” which appears as grayish spots on the surface.

Sorbitan monostearate (SMS) is dispersible in warm water and soluble in oils and fats, whereas STS is soluble in oils and fats only.

Sorbitan monostearate is used in many food products, primarily emulsions, and often in combination with the ethoxylated sorbitan esters (polysorbates).

2. Polyoxyethylene Sorbitan Esters

The hydrophilic properties of sorbitan esters can be strongly increased by ethoxylating the free-hydroxyl groups, yielding an ethoxylated sorbitan

ester. Such products are referred to as polysorbates and are plastic or liquid products, completely soluble in water, where they form micelles. Their production and properties are described in detail by Benson (11).

Polysorbates are highly surface active and are used in many technical emulsions, but their application in foods is somewhat limited due to their low acceptable daily intake (ADI) value.

L. Sucrose Esters of Fatty Acids

Sucrose esters have been known for more than 30 years as esterification products of fatty acids and sucrose and other sugars, or as mixtures of partial glycerides and sucrose esters made by trans-esterification of sugars and glycerides. A great number of components from monoesters to octaesters can exist in sucrose esters, depending on the degree of esterification.

There are several ways of producing sucrose esters (11,12) using different solvents or without solvent systems. The production may include solvent extraction for separation of esters with different hydrophilic-lipophilic characteristics. Sucrose monostearate is highly water soluble and can be used as an o/w emulsifier. Sucrose esters are generally accepted in Japan, but in other countries, the use of sucrose esters is limited in food systems.

M. Lecithin

Plant-seed lecithins are used in many foods, and lecithins from egg yolk have been used in margarine for many decades. The most common commercial lecithins today stem from soybean oil. The trade name lecithin is used commonly, although the product consists of a blend of different phospholipids.

Soybean lecithin is normally marketed as a solution of phosphatides in soybean oil containing between 60% and 70% phosphatides. Soybean lecithin can be fractionated in different ways (e.g., with acetone to remove most of the triglycerides present).

The composition of acetone-precipitated soybean phospholipids is approximately 41% phosphatidyl choline, 34% phosphatidyl ethanolamine, 19% phosphatidyl inositol, and 6% other phospholipids.

The isolated phosphatides may be further fractionated by ethyl alcohol or other short-chain alcohols, giving an alcohol-insoluble part consisting mainly of phosphatidyl choline. Lecithin may be hydrolyzed by enzyme treatment or reacted with hydrogen peroxide to make it more hydrophilic. A synthetic phosphatide for use in the chocolate industry, "Emulsifier YN," is manufactured by the reaction of a diglyceride with phosphorus pentoxide and neutralizing the reaction product partly with ammonia.

A comprehensive review of industrially produced lecithins and their applications are given by Szuhaj and List (13).

N. Structural Parameters of Emulsifiers

Long spacings obtained by x-ray diffraction analysis of homolog series of emulsifiers based on single fatty acids with varying chain lengths can give information about the molecular packing conditions in the crystalline state (14). Such data have been reported for monoglycerides, DATEMs and sorbitan esters (15). The size of the polar group in the crystalline lattice is of special interest, and for distilled monoglycerides, a value of 5.3 Å was found. This is quite similar to the polar group size of pure 1-monopalmitin (5.5 Å). The polar head group of DATEMs was found to be 9.3 Å, which is in the same range as pure 1,2-dimyristyl phosphatidyl choline (10.4 Å), as reported by Small (16). Sorbitan esters were found to have a polar head group size of 5.4 Å, quite similar to the dimension of glycerol in monoglycerides. Furthermore, the x-ray data indicate that in sorbitan tristerate crystals, the sorbitan group is oriented in the middle of the lipid bilayer, with one acyl group extended to one side and the two other acyl groups to the other. This indicates a similar structure to triacylglycerides and may explain why sorbitan tristearate is an effective crystal modifier in fat-based foods (17).

III. LYOTROPIC MESOMORPHISM

Humans have used aqueous liquid-crystalline phases in soap preparations for more than 2000 years. However, liquid crystals were first mentioned in 1904 by Lehman (18), and the structure of such polar lipid–water systems has been known only for about 50 years. Until about 1960, it was believed that both the so-called “neat” and “middle” soap phases had a lamellar-type structure. One of the first important attempts to clarify liquid crystalline structures was done by Luzzati and his co-workers in 1960 (19) when they demonstrated how to analyze lipid–water structures by low-angle x-ray diffraction. After that, numerous articles on mesomorphic lipid–water phases, their structure, phase behavior, and occurrence in biological systems have been published. Especially, soap systems and phospholipid–water systems have been studied extensively. A comprehensive review of surfactant–water liquid crystals has been given by Tiddy (20), and the phase behavior of phospholipids has been reviewed by Hauser (21); finally, the contribution by Small (16) gives the most detailed review on lipid–water interactions. Based on this background, only a brief description of lyotropic mesophases formed

by polar lipids will be given here, together with a survey of the mesomorphic properties of food emulsifiers.

The molecular orientations of polar lipids in their crystalline state and a lamellar liquid-crystalline phase are shown in Fig. 13a. In their crystalline state, the lipids are orientated in bilayers with the polar groups “head to head,” separated by layers of solid hydrocarbon chains usually packed in a DCL mode. Lipids with large polar groups may form crystals with penetration of hydrocarbon chains in a SCL mode as described earlier. When water is present and the temperature is above the Krafft point, T_c , water will penetrate through the polar region of the crystals. At the same time, transition from solid state to liquid state takes place in the hydrocarbon chain region, resulting in the formation of a liquid-crystalline phase. Such behavior is called lyotropic mesomorphism.

When a polar lipid in a stable crystalline form (e.g., β crystals) is mixed with water and heated to form a liquid-crystalline phase, less energy is required per mole of lipid than heating it in the absence of water to form a melt. This is demonstrated in Table 7, showing the transition enthalpy (ΔH) for β crystal transition to melt and β crystal + water transition to a liquid crystal of pure 1-monopalmitin (1-GMP) and of distilled, saturated monoglycerides ($C_{16}:C_{18}$ ratio = 35:65). The experimental value of ΔH are measured by differential scanning calorimetry (DSC).

It appears from Table 7 that the enthalpy values for the 1-monopalmitin transitions are higher than the corresponding values for distilled

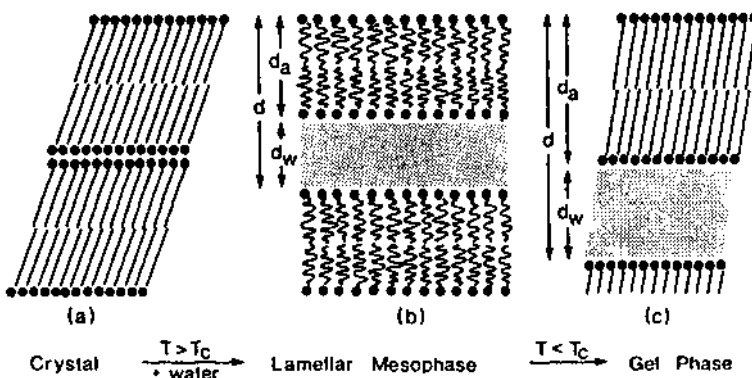


Figure 13 Structure models showing (a) the orientation of emulsifier molecules in the DCL structure in the crystalline state, (b) the formation of a lamellar, liquid-crystalline phase above the Krafft point (T_c) in water, and (c) the formation of an α -gel phase at a temperature (T) below T_c . The structure parameters d , d_a , and d_w can be measured by x-ray diffraction analysis.

Table 7 Transition Energies (ΔH) of Monoglycerides Compared to Monoglyceride–Water Systems

Transition scheme	Pure 1-monopalmitin		Distilled monoglycerides	
	Temp. (°C)	ΔH (J/g)	Temp. (°C)	ΔH (J/g)
Bulk lipid	75.9	210	70.0	172
β Crystals \rightarrow melt				
Melt \rightarrow α crystal	65.2	-113 ^a	65.0	-105
$\alpha \rightarrow$ Sub- α	37.7	-43	19.0	-17
Sub- $\alpha \rightarrow$ β crystal ^b	—	-54	—	-50
Monoglycerides + water systems	60.3	203	55.0	133
β Crystals + water				
\rightarrow lamellar lipid crystal				
Lamellar liquid crystal				
\rightarrow α -gel phase	47.7	-84	55.0	-63
α -Gel \rightarrow β crystals + water ^b	—	-119	—	-70

^aNegative ΔH values = exothermic transition.

^bCalculated values.

monoglycerides with a mixed fatty acid composition. This is probably due to a higher entropy in the distilled monoglycerides than in the pure 1-monopalmitin.

The latent heat of crystallization dissipated when the α -gel phase transforms to β crystals + water is a measure of the instability of the α -gel phase.

A. Lamellar Phase

The structure of the lamellar phase is shown in Fig. 13b and consists of bimolecular lipid layers separated by layers of water between the polar groups. The hydrocarbon chains are in a liquidlike state with a higher degree of motional freedom than in the corresponding anhydrous melt. The molecules in the lipid bilayer of the liquid-crystalline phases undergo several kinds of motion such as lateral diffusion, rotation, and the so-called flip-flop, which is a change in position from one side of the bilayer to another.

Figure 13b shows the structure parameters d , d_a , and d_w of the lamellar phase, which can be measured by low-angle x-ray diffraction methods.

The swelling of the lamellar phase can vary from 10 to 20 Å for the water layer thickness in pure 1-monoglyceride–water systems (22) to water

layers of several hundred angstroms in commercial monoglyceride–water systems containing small amounts of ionised free fatty acids (23).

B. Phase Behavior of Monoglyceride–Water Systems

The mesomorphic behavior of emulsifiers in water depends on a number of factors:

1. *Wedge shape of the surfactant molecule* (i.e., the relative size of the polar head group to the length and degree of unsaturation of the hydrocarbon chain)
2. *Temperature* and ratio of surfactant to water
3. Degree of *ionisation* of ionic surfactants (pH). *Ion concentration* in the aqueous phase

In general, a blend of surface-active lipids (polar and nonpolar) may behave like one component, with the average polar characteristics like that of the blend. The phase behavior of surfactants in water can, therefore, be controlled by adjusting the average polarity by the addition of polar surfactants to less polar ones and vice versa.

Distilled monoglycerides, with approximately 95% 1-monoglyceride content, form similar mesomorphic phases in water as do pure 1-monoglycerides, but show different swelling properties. When saturated, distilled monoglycerides in their β -crystalline form are mixed with water and the suspension is heated to a certain temperature (Krafft point); when the melting point of the hydrocarbon chain bilayer is reached, then water will penetrate through the planes of the polar groups and a lamellar mesophase is formed with water layers alternating with lipid bilayers (see Fig. 13b).

The degree of swelling (i.e., the thickness of the water layer) may vary considerably, depending on a number of factors. The hydration force or osmotic repulsion will induce swelling of monoglycerides to a water layer thickness of about 16 Å. At this interplanar distance of bilayers, there is a balance of long-range van der Waals forces that keep the bilayers together and the hydration force. With pure monoglycerides, swelling is therefore limited to a level corresponding to a water layer thickness of 16–20 Å (22).

Electrostatic repulsions may further increase the swelling process, so the water layer thickness may increase to several hundred angstroms. This can be obtained by the incorporation of ionic polar lipids in the lipid bilayers. Swelling may then increase continuously in proportion to the water content of the system (23).

Binary phase diagrams of distilled, saturated, and unsaturated monoglycerides, pure glycerol monoelaidate, and pure glycerol mono-oleate are shown in Fig. 14. The distilled, saturated monoglycerides are based on fully

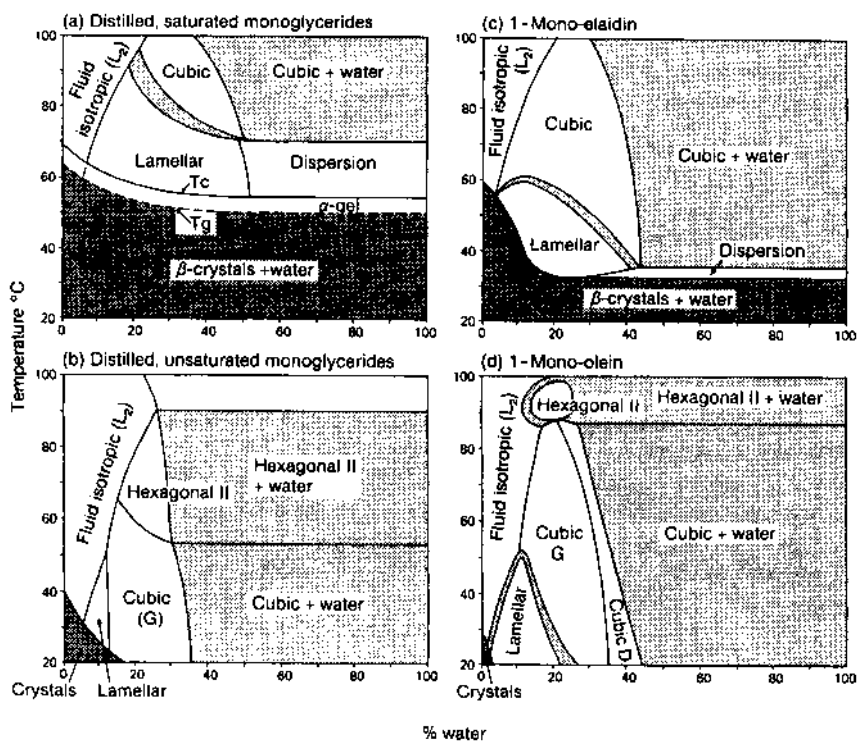


Figure 14 Binary phase diagrams of (a) distilled, saturated monoglycerides with fatty acid chain length C_{16}/C_{18} (35:65, DIMODAN HA, Danisco, Denmark), (b) distilled, unsaturated monoglycerides based on sunflower oil (DIMODAN U, Danisco, Denmark), (c) pure 1-monoelaidin, and (d) pure 1-mono-olein. Abbreviations: T_c = Krafft temperature; T_g = transition temperature for β crystal + water to α -gel; L = lamellar; G = gyroidal structure; D = diamond structure. (Modified from Refs. 24 and 25.)

hydrogenated animal fat (lard or tallow), a commercial product (Dimodan PM, from Danisco, Denmark). This product contains mainly C_{16}/C_{18} fatty acids and will be referred to as DGMS.

Studies of DGMS–water systems by means of a temperature-programmed x-ray diffraction method have shown that the phase transition from crystal + water to the lamellar phase takes place via formation of an α -gel phase. The α -gel phase exists in a temperature region of about 5°C below the region of the lamellar phase or dispersion state at high water contents. Such behavior is not found with pure monoglycerides. The phase diagram of pure 1-monopalmitin–water (22) shows a direct transition

from the β -crystalline state to a lamellar phase. The formation of the α -gel phase in DGMS–water systems may be due to the mixture of different fatty acid chain lengths and the presence of a minor content of free fatty acids and free glycerol (usually below 0.5%). Apart from the formation of an α -gel phase, the DGMS–water phase diagram is quite similar to that of pure 1-monopalmitin.

The distilled, unsaturated monoglycerides referred to in Fig. 14b are made from sunflower oil. The fatty acid composition is 22% oleic acid, 64% linoleic acid, and 13% saturated C₁₆ and C₁₈ fatty acids. The pure 1-monoelaidate and 1-mono-oleate were made synthetically from 99% pure elaidic and oleic acid.

The phase behavior of distilled unsaturated monoglycerides is dominated by the viscous, isotropic cubic phase, which is formed at room temperature at water contents above 20%. The cubic phase is of the gyroidal type and can accommodate up to approximately 35% water (26). At higher water contents, a two-phase system of the cubic phase + water exists. At higher temperatures, from 55°C to 65°C, the cubic phase transforms to a hexagonal II phase; above 90°C, a fluid isotropic L2 phase exists with excess free water at water contents above 30%.

Monoglycerides of elaidic and oleic acids are commonly present in commercial monoglycerides based on partially hydrogenated vegetable oils. Therefore, their phase diagrams in water are shown in Figs. 14c and 14d. It can be seen from Fig. 14c that 1-monoelaidin forms a lamellar phase at 33°C and has a very narrow temperature range for the dispersion state at high water contents. The dominating mesophase in the 1-mono-olein–water system is the cubic gyroidal phase, which exists at a temperature range from below 20°C to 90°C at water contents above 20%. Two types of cubic phase are shown: the gyroidal (G) phase, which exists at water contents from 10% to about 35%, and the diamond (D) phase, which exists at higher water contents than 35% (24).

The phase behavior in water of industrial distilled monoglycerides from different manufacturers may vary slightly due to small changes in composition. It is important that the product be completely free of triglycerides, because minor quantities thereof will change the phase behavior markedly. A minor content of diglycerides (3–5%) is normally always present in distilled products and does not affect the formation of mesophases.

Saturated, distilled monoglycerides are often used in food processing as an aqueous mixture to obtain good distribution of the monoglycerides in the product. This happens particularly in cases where monoglycerides cannot be added to the product via a suitable carrier, such as fats or oils.

When DGMS–water systems were first studied (25), it was discovered that a neutral pH and a low electrolyte concentration in the water was of great importance for the formation and stability of diluted dispersions of DGMS in water. When very dilute dispersions containing 5–10% DGMS were buffered to pH 7, a clear homogeneous dispersion was obtained, and when cooled down, a stable gel could be formed. If the pH value was as low as 5–6, the dispersion was not clear, but milky, and the gel transformed quickly into a coagel (β crystals + water). In this connection, the presence of small quantities of free fatty acids plays an important role. It was later demonstrated (23) that the neutralization of the free fatty acids in DGMS increases in the swelling capacity of the lamellar phase to an optimum level.

Figure 15 shows x-ray spacings of lamellar phase of distilled monoglycerides made from fully hydrogenated fat (C_{16}/C_{18} : 30/65) in water at 60°C (23). Curve a represents system with neutralized free fatty acids (pH 7.0), and curve b represents systems with distilled water (pH 4.0), where the amount of free fatty acids (0.5%) in monoglycerides is not neutralized. There is a great difference in the swelling properties of the two system.

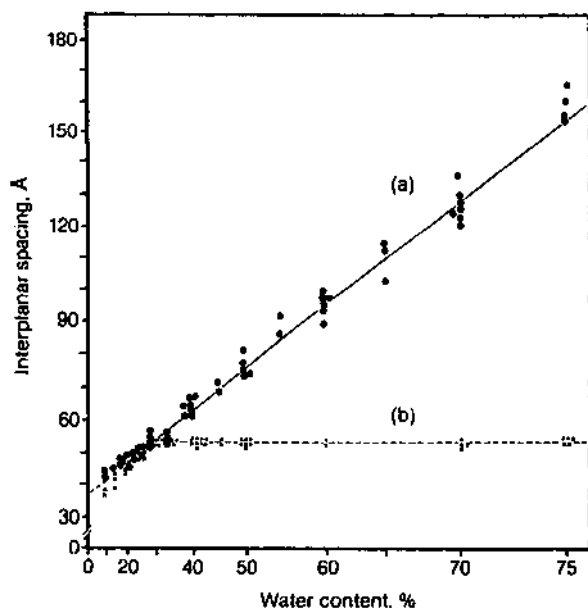


Figure 15 Swelling behavior of distilled, saturated monoglycerides (DIMODAN HA) in water at 60°C (a) with neutralization of 0.2% free fatty acids and (b) without neutralization. The interplanar spacing corresponds to the structure parameter d in Fig. 13b.

In the neutralized system (a), and d spacings increase in a linear relationship to the water content, showing continuous swelling behavior. Because $d_w = d - d_a$ and $d_a = 38 \text{ \AA}$, it means that at a water content of 75%, the water layer thickness (d_w) is about 120 \AA . The swelling of such neutralized monoglyceride–water systems continues with higher water contents, but no x-ray data are available for such diluted systems.

Contrary to the swelling behavior in neutralized water systems (pH 7.0), monoglycerides show a limited degree of swelling in distilled water with a pH below 4.0. Curve b in Fig. 15 shows a maximum d value of 54 \AA , at a water content of 30%, corresponding to a water layer thickness of 16 \AA . At higher water contents, no further increase in the d value is found, showing the same limited swelling behavior as found in pure 1-monoglycerides. The effect of introducing ionised amphiphilic molecules in the lipid bilayer is an increased swelling due to electric repulsion between charged groups in opposite bilayers. This repulsion effect will be reduced if the ion concentration of the water phase (e.g., $\text{Na}^+ \text{Cl}^-$) is increased. At concentrations above 0.3% sodium chloride in water, the effect of adding ionic active emulsifiers to the lamellar phase is inhibited (23).

C. Dispersion State and Crystalline Hydrates

All saturated monoglycerides form a dispersion as defined by Larsson (22) within the temperature region of the lamellar phase, when the water content of the system is higher than that corresponding to the lamellar phase. It is assumed that the dispersion consists of lamellar aggregates of monoglycerides in equilibrium with water.

The thickness of the water layer in the dispersion aggregates may vary considerably depending on the conditions with regard to pH, ion concentration, and purity of the monoglycerides. The dispersion state does not exist at temperatures above the transition point of lamellar phase to cubic phase. When the temperature of the dispersion is increased above that point, a two-phase mixture consisting of cubic phase + water is formed. Therefore, in diluted aqueous dispersions of monoglycerides, the temperature should always be carefully controlled in order to avoid formation of the cubic phase. Crystallization from a dispersion of monocraprin can be seen in Fig. 16, where a fragment of a β crystal is visible in the lower left corner. It can also be seen that a number of dispersion aggregates are in contact with the crystal surface. On the basis of similar observations, a specific mode of crystallization has been suggested which will lead to the formation of β crystals with unusual properties (27). It is proposed that the bimolecular lipid leaflets unfold from the dispersion aggregate into the surface of the crystal, which will then grow with discrete layers in a direction perpendicular

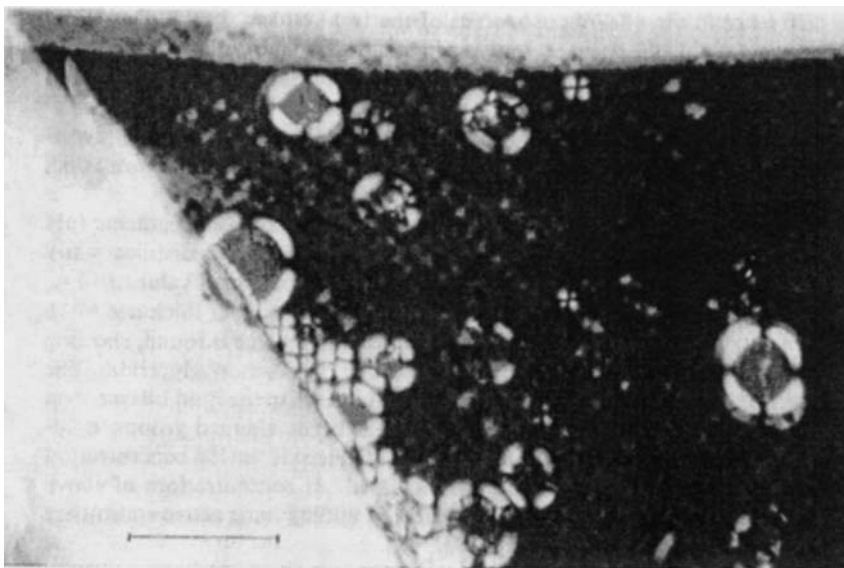


Figure 16 Photomicrograph of a dispersion of monocaprin in water, showing spherical dispersion aggregates with internal lamellar structure. A fraction of a β crystal of monocaprin is seen in the lower left corner. Bar: 30 μm , polarized light.

to the surface plane. This direction of growth can, in fact, be seen directly under the microscope in a dispersion, as shown in Fig. 16. The result of such a crystallization process will be surface consisting of the polar groups of the monoglycerides. Normally, the crystal surface consists of the lipophilic methyl end groups when crystallization takes place from the melt or from solvents. The polar surface formed when crystallized from an aqueous phase is responsible for a great water-binding capability. For example, 10 parts of monoglycerides by weight can absorb 90 parts of water; such a mixture has an ointment like consistency. Industrial products of 20–25% distilled, saturated monoglycerides in the form of β crystals suspended in water (so-called hydrates) are commercially available and are used to a great extent in the baking industry as crumb-softening or antistaling agents in bread.

The rate of crystallization initiated by cooling of the dispersion to a temperature below T_c depends on various factors such as the chain length of the monoglycerides and pH. Monoglycerides with short chain length, like monocaprin or monolaurin, recrystallize relatively quickly, compared to palmitic and stearic fatty acid monoglycerides. Pure 1-monoglycerides with chain lengths shorter than monomyristin transform directly from the lamellar phase to a β crystal + water mixture (22). At a low pH, the

addition of salts and mechanical agitation will promote the formation of β crystals, and this is used in the production of monoglyceride hydrates on a commercial scale.

D. Mesomorphic Phases of Other Food Emulsifiers

In general, the phase diagrams of the commercial food emulsifiers described in this sub-section will show the typical mesomorphic phase behavior of these products without going into detail about multiphase regions that may exist.

1. Polyglycerol Esters

The composition of commercial polyglycerol esters is very complex due to variation in both the degree of polymerization and degree of esterification. This results in products containing many different components. Therefore, when polyglycerol esters of C_{16}/C_{18} fatty acids are mixed with water above their melting point, they form reversed hexagonal phases. The hexagonal phase swells up to a content of 40% water, and at higher water concentrations a two-phase mix of emulsifier and water is obtained. The reversed hexagonal phase is common, with polar lipids containing a mix of polar and nonpolar components. Monodiglycerides with a mono ester content below approximately 60% form hexagonal phases in water (22).

The dispersibility in water of such lipophilic emulsifiers can be improved by adding high-polar coemulsifiers (e.g., sodium stearate). Commercial polyglycerol esters may contain up to 6% sodium stearate; this solubilizes the hexagonal phase, making it possible to produce aqueous dispersions or gels to be used as aerating agents in food products. The emulsifier is mixed with water at a temperature above its melting point (Krafft point) until total swelling is obtained; then, the mix is cooled to ambient temperature, forming a plastic gel. Such gels are used in the baking industry to facilitate aeration of cakes of various types. The phase behavior of triglycerol and octaglycerol esters have been described elsewhere (28).

Distilled diglycerol monoacyl fatty acid esters have a unique phase behavior in water. All diglycerol esters with chain lengths from C_{12} to C_{18} form lamellar phases above their Krafft point, and in contrast to the phase behavior of monoglyceride–water systems, no other liquid-crystalline phases have been observed. Even the unsaturated diglycerol mono-olein forms a lamellar phase only in the temperature region examined. The Krafft point of distilled diglycerol esters with fatty acid chain lengths from C_{12} and C_{18} is shown in Fig. 17.

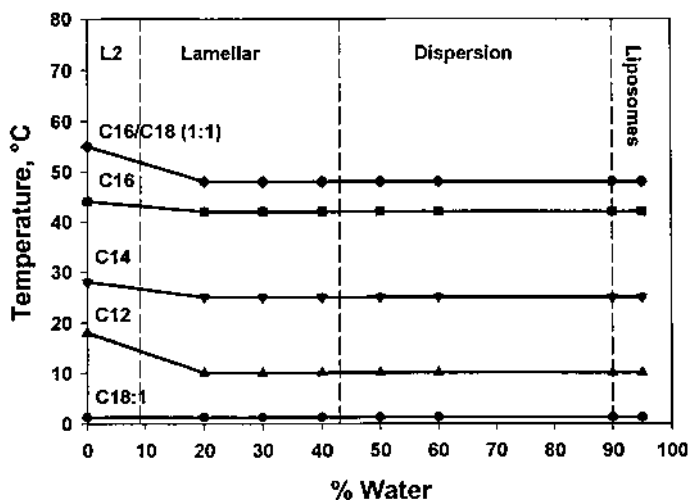


Figure 17 Krafft point lines of distilled, diglycerol fatty acid esters with fatty acid chain lengths from C_{12} to C_{18} . The formation of lamellar liquid-crystalline phases and dispersion of vesicles above the Krafft point of the emulsifiers as a function of the water content are indicated.

The swelling capacity of diglycerol esters in water is limited, and above a lipid : water ratio of 60 : 40, a stable dispersion of multilamellar vesicles is formed. The water layer thickness in the vesicles is 22–30 Å (15), corresponding to the swelling behavior of diacyl phosphatidyl choline (16). The addition of anionic coemulsifiers (e.g., sodium stearate) increases the swelling properties of diglycerol esters in a fashion similar to that of monoglycerides containing fatty acid sodium salts.

Distilled diglycerol esters of stearic or oleic acid are capable of forming liquid-crystalline films around oil droplets in o/w emulsions and can be used to stabilize protein-free emulsions (9).

2. Organic Acid Esters

The esters of dicarboxylic acids such as diacetyl tartaric acid or succinic acid and saturated monoglycerides (DATEM, SMG) contain a free-carboxyl group. Neutralization of the free-carboxyl group, by forming a sodium salt of DATEM or SMG, increases its swelling ability in water. X-ray data of the lamellar phase formed by DATEMs at 60°C show a similar swelling behavior to that of the neutralized DGMS–water systems. A schematic phase diagram of neutralized DATEMs in water is shown in Fig. 18.

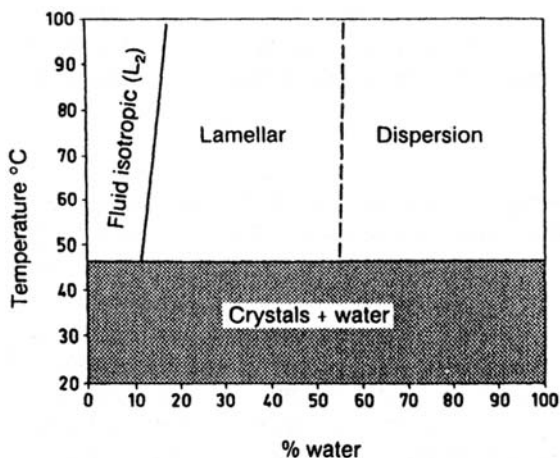


Figure 18 Schematic phase diagram of diacetyl tartaric acid ester of saturated monoglycerides (DATEMs) in water, pH 5.

A dispersion of 5% DATEMs in water has a pH value of 1–2, and at this low pH, very little, if any, swelling of DATEMs in water takes place.

An increase in pH, by adding sodium hydroxide to the water until a pH of 4.6 is reached, will give total swelling in water. The DATEMs based on saturated monoglyceride form lamellar phases above a temperature of 45°C. The DATEMs based on an unsaturated monoglyceride, such as mono-olein, form a lamellar phase at 20°C, which is stable up to above 80°C. Once the DATEM has swelled in water, it remains in its liquid, crystalline state, even when cooled below the temperature where the lamellar phase was formed. The hydrocarbon chains have little tendency to crystallize and form a gel. The DATEM esters are used mainly in the bakery industry in yeast-raised doughs, where their interactions with flour components improve the volume and texture of the finished product. The anionic emulsifiers (e.g., DATEM, SSL) are used in various o/w-type emulsions in order to increase stability towards coalescence, due to their interaction with interfacial bound proteins.

3. Stearoyl Lactylates

Sodium stearoyl lactylates (SSLs) are not neutralized completely. They have an acid value from 60 to 80, and the pH of an aqueous dispersion of SSL is therefore about 4–5. The phase behavior of SSL in water is strongly dependent on its degree of neutralization. At low pH conditions, a hexagonal II mesophase is formed at temperatures above 45°C, and this phase may

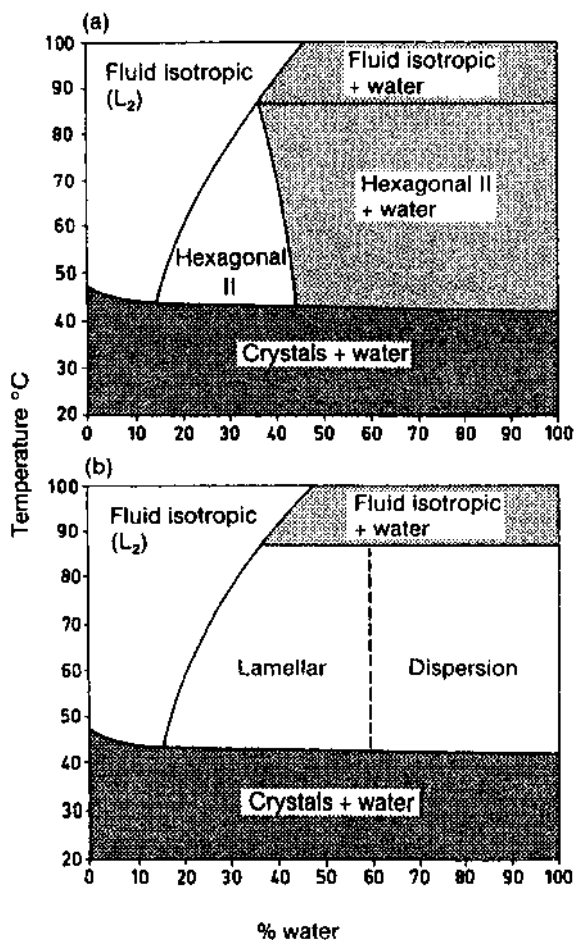


Figure 19 Schematic phase diagram of sodium stearyl lactylate (SSL) in water (a) with partial neutralization to pH 5.0 and (b) after neutralization to pH 7.0. The figure shows an increased swelling into a lamellar phase or a dispersion of vesicles at pH 7.0.

contain 20–40% water as shown in Fig. 19a. If more water is present, the excess water will separate from the mesophase. X-ray data concerning such a hexagonal II mesophase of SSL–water systems at 60°C and pH 4.5 have shown that the diameter d_w of the water cylinders increases from 24 Å at 20% water to 40 Å at 42% water and that the specific surface in contact with water (S) increases from 25 Å² to 43 Å³ with increasing water content from 20% to 42%. The structural parameters S , d_a , and d_w are very similar to

data reported by Reiss Husson (29) for egg phosphatidyl ethanolamine, which also forms a hexagonal II mesophase in water. When SSL is neutralized, its phase behavior is changed, and a lamellar phase is formed, instead of the hexagonal II phase, as shown in the phase diagram in Fig. 19b. The lamellar phase of the neutralized SSL can be diluted with water to dispersion. The gel formed from the lamellar phase on cooling is very stable, and SSL may be used together with other emulsifiers (i.e., monoglycerides in order to stabilize gel phase, which are used in food processing. Due to its hydrophilic nature, SSL is used in many o/w emulsions. Both SSL and the corresponding calcium salt (CSL) are effective starch-complexing agents and are used mainly in the bakery and starch industries.

4. Lecithin

Lecithin is a natural emulsifier that has been used in foods for centuries. The phase behavior of lecithins in water was been reviewed in detail (16,21), so only a brief description of their phase behavior will be given here. Pure phosphatidyl choline forms a lamellar mesophase in water at temperatures from ambient to 100°C. The swelling of the lamellar phase is limited to a 40% water content, corresponding to a water layer thickness of about 30 Å. At higher concentrations of water, a dispersion of spherical aggregates with internal lamellar structure in the excess water (liposomes) is formed. Phosphatidyl ethanolamine (cephalin) is reported to form both lamellar and hexagonal II phases in water (29), whereas egg yolk lysolecithin exhibits a different lyotropic behavior than that of the other egg yolk phosphatides. Due to its more hydrophilic character, it forms hexagonal I phases in water in concentrations of up to about 55% water at temperature above 37°C. Commercial lecithins from soybean or rapeseed are mixtures of phospholipids with different phase behaviors in water. Mixtures of phosphatidylcholine and phosphatidylinositol form only lamellar phases, whereas the more lipophilic phosphatidylethanolamine forms reversed hexagonal phases in water. Consequently, the phase behavior of oil seed lecithins may vary with their composition.

5. Polysorbates

When fat derivatives such as monoglycerides or sorbitan esters are reacted with ethylene oxide, the resulting products become more hydrophilic in character, and their ability to form micelles in water is greatly increased. Polyoxyethylene (20) sorbitan monoleate (POESMO) forms a mesomorphic phase in water of the hexagonal I type with lipid cylinders surrounded by water, at temperatures up to 30°C, and with water contents from 30% up to 60%. POESM-stearate also produces this phase with the same amount of

water, but at temperatures about 20°C higher (i.e., from 38°C to 50°C). At higher temperatures, an isotropic solution is formed. X-ray data of aqueous systems of these products (23) have shown that the specific surface S per molecule in contact with water is 145 \AA^2 , which is four times higher than the specific surface of monoglycerides in the lamellar phase, as shown in Table 8. The hexagonal I mesophase (middle) can solubilize triglycerides in small quantities. On further addition of triglycerides, a lamellar phase is formed.

Sorbitan monostearate has, in general, a similar phase behavior in water to that of glycerol monostearate, but it has not been studied in detail. It forms a lamellar phase, and when excess water is added, a liquid-crystalline dispersion is made. Sorbitan tristearate, however, does not form any mesomorphic phases in water. The use of polysorbates and sorbitan esters in emulsions of various types is reviewed by Benson (11).

E. The α -Crystalline Gel State

The term “gel” used in this context originates from the soap industry many decades ago. It was used then to describe certain soap–water systems with a clear gellike appearance. The term should not be confused with gels formed by other substances, such as starch, or hydrocolloids such as gelatin or pectin.

The gel is a crystalline state of the emulsifier with layers of water between the polar groups, as shown in Fig. 13c. The structure of the gel is similar to the lamellar phase. The difference is that the hydrocarbon chains are no longer in a liquidlike state, but are solid and orientated parallel to each other in an α -crystalline mode of packing. Consequently, the gel is characterized by a single strong x-ray diffraction line at 4.15 \AA in the short spacing region, and several long spacings with an interrelation of $1 : 1/2 : 1/3 : 1/4$, indicating a lamellar system. The angle of tilt of the hydrocarbon chains toward the water layer in a gel is 54° , and the lateral packing of the chains can be described by a hexagonal subcell, where the chains have rotational freedom (22). The gel is a metastable state, and the water layer between the polar groups will be reduced in time. When all the water is expelled, a suspension of crystals + water (coagel) is formed. The so-called hydrate form of monoglycerides is a coagel. Polymorphic emulsifiers such as monoglycerides will transform into the most stable crystal form, the β -form, because an anhydrous α -form does not exist in the presence of water. Emulsifiers that are nonpolymorphic and stable in the α -crystalline form may form gels with water that are very stable. This is the case with gels of sodium stearyl lactylates, tetraglycerol monostearates, SMG, DATEMs, and polysorbates. The stability of monoglyceride gels depends on their composition, because monoglycerides with fatty acid chain lengths of from C_{16} to C_{20} are more stable in the gel form than monoglycerides with

Table 8 X-ray Data of Lamellar Mesophases and Corresponding Gel Phases of Monoglyceride-in-Water Systems Compared to Other Emulsifier-in-Water Mesophases

Emulsifier-in-water system	X-ray spacings d (Å)	Lipid bilayer thickness d_a (Å)	Water layer thickness d_w (Å)	Specific surface in contact with water S (Å ²)
Monoglycerides				
Lamellar phase, 40% water, 60°C	63.8	38.1	25.7	32.0
Gel phase, 40% water, 25°C	93.9	54.9	39.0	22.0
Lamellar phase, 75% water, 60°C	154	38.0	116	32.0
Gel phase, 75% water, 25°C	230	55.0	175	22.0
Polysorbate-60				
Hexagonal I phase, 60% water, 45°C	90.0	59.8	30.2	145
Na-stearoyl lactylate				
Hexagonal II phase, 41% water, 60°C	59.5	19.2	40.3	42.6

shorter chain lengths. The swelling capacity and stability of industrial distilled monoglyceride gels are strongly influenced by the presence of ionic active emulsifiers and salt concentration in water (23,30).

When cooled the neutralized DGMS–water mixtures shown in Fig. 15 form gels with water contents up to about 75%, and the x-ray spacings increase in direct proportion to the water content up to about 230 Å at 75% water (30). No spacing were ever found in the region between 64 Å and 90 Å, corresponding to water contents between 20% and 40% in the neutralized system. A similar phenomenon has been described for soap–water systems by Skoulios (31), who suggested that the reason for this behavior was that certain water layer thickness cannot exist in a gel phase. When the d spacings of the DGMS–distilled water gels are increased up to 64 Å, corresponding to a water concentration of 20%, the d values remain constant at 64 Å, independent of the water concentration. The thickness of the bimolecular lipid layer d_a was calculated by analysis of the neutralized DGMS–water systems to be 55 Å (22). The value of d_a of the DGMS–distilled water systems was found to be only approximately 50 Å. The differences in thickness of the lipid bilayers may be due to a different angle of tilt of the hydrocarbon chains toward the water layer in the two systems. The d_a value of 55 Å in the neutralized systems is identical to the long spacing of the anhydrous α -form of DGMS. The water layer thickness, d_w , is 175 Å in mixtures containing 75% water. Undoubtedly, the swelling continues with a higher water content. The optical texture of neutralized DGMS gels containing 95% water indicates a lamellar structure, and such gels may have water layers of several hundred angstroms.

The microstructure of an α -gel phase and the corresponding β -crystalline coagel (hydrate) is demonstrated in Fig. 20. The α -gel has a typical lamellar structure with lipid bilayers alternating with water layers having a thickness of about 200 Å. The coagel is a tridimensional network of β -crystalline platelets suspended in water.

When a lamellar phase-of monoglyceridests cooled and a gel phase is formed, the x-ray spacings (d) increase, although the proportion between the water content and the lipid phase is kept constant. This phenomenon is due to the crystallization of the hydrocarbon chains in the lipid bilayer, which results in a decrease in the specific surface area (S) of the monoglyceride molecules in contact with the water, as shown in Table 5. The thickness of the lipid layer d_a increases from 38 Å in the lamellar phases to 55 Å in the gel phases, due to the crystallization process, whereby the hydrocarbon chains are stretched out and aligned parallel to each other. At the same time, the specific surface area S decreases from 32 Å² in the lamellar phase to 22 Å² in the gel phases. The crystallization of the hydrocarbon chains cannot alone account for the increase in interplanar spacings that occur on transition

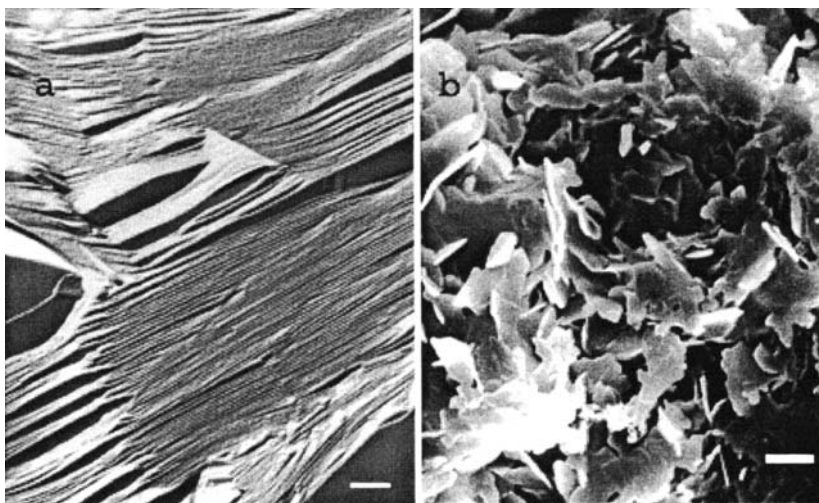


Figure 20 Microstructure of (a) an α -gel phase of distilled, saturated monoglycerides in water (25:75) by freeze-fracture transmission electron microscopy (bar = 0.2 μm) and (b) the corresponding coagel phases (hydrate) by scanning electron microscopy (bar = 2 μm). The water layer thickness of the gel phase was measured to approximately 200 \AA by x-ray diffraction analysis. The phase (b) is a network of β -crystalline platelets of monoglycerides in water. (Courtesy of Dr. W. Buchheim, Kiel, and Danisco, Denmark.)

from the lamellar phase to the gel state. It can be seen from [Table 5](#) that the water layer thickness increases during the formation of a gel, although the total water content is kept constant. The main reason for this extension of the water layer is the decrease in specific surface, S , of the monoglycerides in contact with the water, which is, in turn, caused by a lateral contraction of the lipid molecules. The rearrangement of the molecules during the transition from the lamellar phase to the gel phase is illustrated schematically in [Fig. 13](#), where the relative distances for d , d_a , and d_w are shown for a lamellar phase and a gel phase containing 40% water.

Sodium salts of stearic acid added directly to DGMS increase the swelling capacity of the gel phase to the same extent found when neutralizing the free fatty acids with sodium hydroxide. The minimum concentration of soaps needed to obtain the maximum degree of swelling is about 0.5% of the DGMS. The effect of sodium and calcium soaps on the gel phase is quite different. Sodium stearate gives a high degree of swelling, whereas calcium stearate inhibits the swelling of a gel (23). The ionic active emulsifiers shown in [Table 9](#) also increase the swelling and stability of monoglyceride gels, whereas the nonionic emulsifiers do not have this effect. Finally, it should be

Table 9 Influence of Various Additives on Swelling Capacity of DGMS and Distilled Water Systems Containing 70% Distilled Water

	Percent of additives by weight of DGMS	pH of aqueous mixtures	Lamellar phase (60°C)		Gel phase (25°C)	
			Spacings d (Å)	Water layer thickness d_w (Å)	Spacings d (Å)	Water layer thickness ^a d_w (Å)
Nonionic additives						
Tetraglycerol monostearate	4	4.7	54.1	16.0	62.3	12.3
Ethoxylated monoglycerides	4	4.6	54.6	16.5	79.1	29.1
Polyoxyethylene-(20)-sorbitan monostearate	4	4.2	61.7	23.6	67.0	17.0
Polyoxyethylene stearate	4	4.3	54.6	16.5	67.0	17.0
Lauryl alcohol polyglycol ether	1	4.3	55.1	17.0	61.7	11.7
Anionic active additives						
Succinylated monoglycerides (sodium salt)	4	5.4	123.2	85.1	156.0	101.1
Sodium stearyl-2-lactylate	4	4.7	128.4	90.3	163.0	128.1
Sodium lauryl sulfate	1	6.3	131.2	93.1	198.0	143.1
Sodium stearate	1	6.9	131.0	92.9	184.0	129.1
Calcium stearate	1	—	130.0	91.9	62.3	12.3
Cation active additives						
Cetyl pyridinium bromide	1	4.6	131.0	92.9	192.0	137.1
Benzotonium chloride (Hyamin 1622)	1	4.6	128.0	89.9	60.5	10.5
Control						
DGMS + distilled water	—	5.0	54.1	16.0	64.0	14.0

^aCalculations based on $d_a = 54.9 \text{ \AA}$ for systems with ionic additives and $d_a = 50 \text{ \AA}$ for system with non-ionic additives.

Source: From Ref. 23.

mentioned that the stability of the gel phase is very sensitive to the ion concentration in the water. The addition of 0.04% sodium chloride to the lamellar phase of monoglycerides in water inhibits the formation of a totally swollen gel at a high water content.

The stability of the monoglyceride gel structure or other emulsifiers in aqueous systems is an important factor in preventing changes in the functional effect of emulsifiers when gels are used as aerating agents.

Lipophilic, α -tending emulsifiers, such as ACETEM, LACTEM, or PGMS, and glycerol mono-olein (GMO) can swell in their crystalline state in the presence of water and form α -crystalline gel structures (32,33). This gel formation can be shown by x-ray diffraction analysis, as shown in Table 10. The emulsifiers, PGMS or GMO, are dissolved in coconut oil (Melting point = 31°C) and poured over a water phase in a beaker and then cooled to 5°C for several hours. Samples of the interfacial layer and upper bulk phase free of water are taken for x-ray analysis.

The x-ray data on the water-free bulk phase show two sets of long spacings representing (A) the PGMS or GMO and (B) the coconut oil. This shows that the emulsifiers do not cocrystallize with the coconut oil but form crystalline aggregates separately from the coconut oil crystals.

The interfacial layer also exhibits two sets of long spacings. The values of 56.1 Å and 66.0 Å represent long spacings of PGMS water gel and GMO water gel respectively, and the values of 35.4–36.1 Å represent long spacings of the coconut oil.

An interesting feature is the increase in the long spacings of the emulsifier phase (A) from the bulk system to the interfacial layer. For PGMS, the increase is about 7 Å, and for GMO, the increase is 17 Å. The changes in long spacings induced by the contact with water can only be due to water

Table 10 X-ray Diffraction of Interfacial Layers from Coconut Oil–Emulsifier–Water System at 5°C

Sample preparation	Long spacings d (Å)		Short spacings d (Å)
	A Emulsifier	B Coconut oil	
Interfacial layer			
Coconut oil–PGMS–water	56.1	35.4	4.18–3.83
Coconut oil–GMO–water	66.0	36.1	
Bulk phase			
Coconut oil–emulsifier (1 : 1) (melt, cooled to 5°C)	48.9	36.3	4.29–4.16–3.97–3.82–3.65

penetration through the polar regions of the emulsifier crystals driven by a hydration force, forming an α -gel structure. The hydration of GMO at ambient temperature or even lower temperatures is in good agreement with its phase diagram.

The α -gel formation is of great importance in whippable emulsions (creams, toppings), and the hydration of unsaturated monoglycerides at low temperature can be used to make powdered monoglyceride blends that are dispersible in water and used as cake emulsifiers.

F. Liquid Crystals and Emulsion Stability

Liquid crystals in emulsions were observed in 1969 by Friberg and his co-workers (34), and in 1971 (35), they demonstrated that liquid-crystalline phases may form on the surface of oil droplets in o/w emulsions and provide stability against coalescence.

The presence of liquid-crystalline mesophases in food systems is not a common feature partly due to a low concentration of polar emulsifiers and partly due to lack of stability of emulsifier–water mesophases, which may be negatively affected by other food ingredients, such as fats, proteins, carbohydrates, salts, and so forth.

An example of o/w emulsions where liquid crystals have been found by polarized microscopy is salad dressings made with egg yolk lecithins. A micrograph of such an emulsion is shown in Fig. 21. The strong birefringent layers around the oil droplets are present due to a formation of liquid-crystalline layers. Similar observations have been made with other types of emulsions (36,39).

The existence of lamellar, interfacial multilayers has been shown to provide stability to emulsions of sunflower oil in water by Pilpel and Rabbani (37,38). The emulsifiers used were sorbitan monopalmitate (Span-40) in combination with Polysorbate 40. The optimal ratio of the two emulsifiers for emulsion stability was found to be 5 mol of Span-40 to 1 mol of Polysorbate 40. With this ratio of the lipophilic Span-40 and the hydrophilic Polysorbate 40, ideal conditions for the formation of liquid-crystalline lamellar structure at the o/w interface exist. The formation of such lamellar structures around oil droplets was shown by electron microscopy.

G. Polar Lipid–Water Phases of Natural Origin

Plants contain polar and nonpolar lipids, and the polar lipids may exist in the form of liquid-crystalline phases containing water. This is the case in cereals (e.g., wheat flour), which contains about 2.5% total lipid on dry

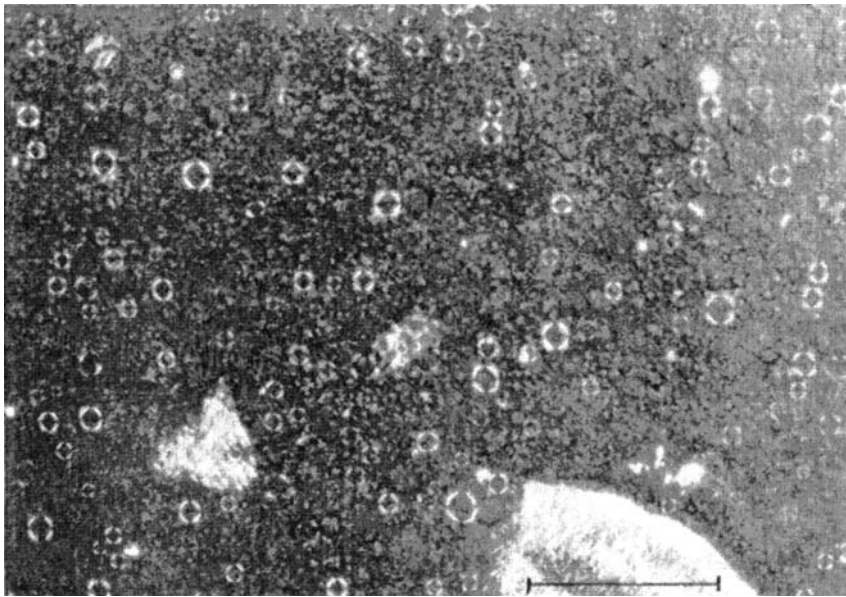


Figure 21 Commercial salad dressing made with egg yolk lecithin. The oil droplets are seen as dark spheres surrounded by liquid-crystalline layers of phospholipids, showing a strong birefringence in polarized light microscopy. Bar = 100 μm .

basis. The polar lipids in wheat flour are glycolipids, phospholipids, free fatty acids, and monoglycerides, which amount to approximately 45% of the total wheat lipids.

Carlson et al. (40) demonstrated that both lamellar and hexagonal II liquid-crystalline phases exist in ternary systems of nonpolar and polar wheat flour lipids and water. The amount of lamellar lipid water phases was found essential for the bread-baking quality of the flour. Liquid-crystalline phases of polar lipids and water have also been found in mature wheat endosperm by freeze-fracture electron microscopy (41).

IV. FUNCTIONAL PROPERTIES OF EMULSIFIERS IN FOODS

A. Emulsification and Emulsion Stability

The manufacture of o/w food emulsions often involves a homogenization process under turbulent flow conditions. The relative contribution to droplet disruption by energy input (e.g., homogenisation pressure) and the effect of emulsifiers on reduction of interfacial tension between oil and

water is approximately 100 : 1. The emulsification process and final particle distribution of the emulsion are thus mainly controlled by the energy input, and the influence of emulsifiers is negligible.

In the case w/o emulsions (e.g., margarine, spreads), which is made under low-energy impeller emulsification methods, the addition of emulsifiers has a significant effect on reducing the water droplet size.

B. Interfacial Emulsifier–Protein Interactions in Emulsions

Many food emulsions contain milk proteins or proteins from plants or animal origin. The main function of emulsifiers in such emulsions is either to increase stability toward coalescence or creaming/precipitation during long-term storage (e.g., recombined milk, coffee whiteners, salad dressings, etc.) or to induce destabilization and increase whippability of emulsions to be aerated (e.g. ice cream mix, cream, toppings, etc.).

Interfacial interactions between emulsifiers and proteins in emulsions play a vital role for the physical properties of emulsions. A cooperative emulsifier–protein adsorption at the surface of fat globules may improve the surface film strength and coherence, increasing emulsion stability (17). This is found with anionic emulsifiers (DATEM, SSL) that bind proteins to the surface of fat or oil droplets via a complex formation (42). Anionic emulsifiers are therefore very effective in emulsions, where long-term stability is important.

In contrast, nonionic emulsifiers (polysorbates, monoglycerides, LACTEM, or PGMS) compete with proteins for interfacial adsorption and may displace the proteins more or less from the interface. The displacement of protein from fat globule surfaces is part of the destabilization of whippable emulsions. Other important functions of emulsifiers in the destabilization process is to enhance crystallization of the fat phase and to reduce the coherence and viscoelastic properties of the surface film, making the fat globules more sensitive to shear (43,44), increasing flocculation and partial coalescence. The formation of fat globule aggregates during whipping is enhancing the foam formation and stabilizes the foam structure of aerated emulsions (17,33,45,46).

C. Interaction with Starch Components

Food emulsifiers are used in many starch-based foods such as bakery products, processed potatoes, breakfast cereals, pasta foods, and so forth. The primary function of emulsifiers such as monoglycerides, SSLs, CSLs, and others is to form a water-insoluble complex with the starch component

amylose. The amylose is present in most starches in an amount of 17–25% and is the source of textural problems (stickiness, firmness) in starch-containing foods. By formation of a lipid–amylose complex, the texture of reconstituted potato products and pasta foods is improved. Monoglycerides in wheat bread are used to reduce crumb firmness and delay the staling process. Saturated monoglycerides are the most effective amylose-complexing agents and are used in bread in the form of the β -crystalline hydrates (47), or dispersible fine powders. Stearoyl lactylates (SSLs, CSLs) are also used as starch-complex agents in many products, primarily bread.

The amylose-complex formation in wheat bread may also affect the retrogradation of amylopectin, the major starch component. At low use levels of monoglycerides (e.g., 0.3–0.5% based on flour weight), the monoglyceride mainly interacts with the amylose fraction. At higher concentrations of monoglyceride (1–2%), they seem to interact directly with the amylopectin fraction, reducing the rate of retrogradation, which is partly responsible for the bread-firming process during storage (47).

D. Dough-Strengthening Effects of Emulsifiers

Hydrophilic emulsifiers such as DATEMs, SMGs, SSLs, CSLs, and polysorbates are used in yeast-raised doughs to increase shock-resistance fermentation stability and enhance volume of baked products such as speciality bread, fiber bread, rolls, and buns. The emulsifier function mechanism in doughs is not completely understood, although many emulsifier action models have been proposed. A relation to the physical properties of natural flour lipids may be relevant because it is known that the polar flour lipids are very important for the baking quality of flour (48). The polar flour lipids form liquid-crystalline phases in water and—especially the lamellar phase formed by polar flour lipids, such as galactolipids and phospholipids—are considered important for the baking quality of flour. Polar-lipid bilayer structures may associate with hydrated gliadin proteins at gas cell–water interfaces and improve the gas-retention capacity of the dough during fermentation.

All effective dough-strengthening emulsifiers (DATEMs, SSLs, polysorbates, and lecithins) form lamellar liquid-crystalline phases in water under conditions similar to dough mixing. They may thus combine with the polar lipids in flour into biomembrane like structures and support the function of the native, polar lipids in flour. The role of lipids in bread making is extensively discussed by Eliasson and Larsson (49).

E. Legal Aspects

Before a food emulsifier is permitted for use in foods, it has to be tested in a number of toxicological studies including short- and long-term feeding trials on several animal species together with studies on metabolism.

The evaluation of emulsifiers is done by the Joint Expert Committee on Food Additives (JECFA) of the Food and Agriculture Organization World Health Organization (FAO/WHO), by the commission of the European Communities' Scientific Committee for Food (SCF), and in the United States by a department of the Food and Drug Administration (FDA).

The results of the scientific, independent toxicological evaluations are used by national health authorities for food regulations.

The acceptable daily intake (ADI) values and regulatory identification numbers for the emulsifiers dealt with here are shown in [Table 1](#). All emulsifiers approved by local health authorities should be considered as safe food ingredients when used within their limits of the ADI values, which are given in the reports of the Joint FAO/WHO Expert Committee on Food Additives (50).

V. CONCLUDING REMARKS

The aim of this chapter is to present a general review of the most commonly used emulsifiers in the food industry. Food emulsifiers should be considered polar lipids with specific properties and functions. Their chemical composition determines their physical properties, which is of importance for their different functions in foods. Most interactions between emulsifiers and other food ingredients take place in surface monolayers or at mixed lipid-protein interfacial structures. Such interactions takes place in emulsions, resulting in increased stability of some types of emulsions and partial destabilization of others.

The capability of lipid emulsifiers to form association structures with water in form of lamellar dispersions or vesicles enhance molecular interactions of emulsifiers with water soluble food components (e.g., starch components). Furthermore, specific lipophilic emulsifiers may be incorporated in the crystal lattice of fats, thus controlling crystallization and texture of the product.

The molecular behavior of emulsifiers in all states or order, in bulk phases and at interfaces in emulsions, foams, and colloidal systems is very important to understand in order to be able to predict functional properties of emulsifiers in foods.

REFERENCES

1. R. O. Feuge and A. E. Bailey, *Oil Soap* 23, 259 (1946).
2. N. O. V. Sonntag, in *Bailey's Industrial Oil and Fat Products* (P. Swern, ed.), Wiley, New York, 1982, Vol. 2, p. 99.
3. J. P. Brandner and R. L. Brikmeier, *J. Am. Oil Chem. Soc.* 37, 390 (1960).
4. J. B. S e, *Fette, Seifen, Anstrichmittel* 85, 72 (1983).
5. K. Larsson, in *Lipids—Molecular Organization, Physical Functions and Technical Applications*, Oily Press, Dundee, Scotland, 1994, p. 27.
6. J. B. Martin and E. S. Lutton, *J. Am. Oil Chem. Soc.* 49, 683 (1972).
7. R. O. Feuge, E. J. Vicknoir, and N. V. Loogren, *J. Am. Oil Chem. Soc.* 29, 11 (1952).
8. G. Schuster and W. Adams, *Seifen,  le, Fette, Wachse* 3, 61 (1981).
9. J. Holstborg, B. V. Pedersen, N. Krog, and S. K. Olesen, *Colloids Surfaces B: Biointerf.* 12, 383 (1999).
10. E. S. Lutton, C. B. Stewart, and J. B. Martin, *J. Am. Oil Chem. Soc.* 49, 186 (1972).
11. F. R. Benson, in *Nonionic Surfactants* (M. J. Schick, ed.), Marcel Dekker, New York, 1987, p. 247.
12. L.I. Osipow and W. Rosenblatt, *J. Am. Oil Chem. Soc.* 44, 307 (1967).
13. B. F. Szuhaj and G. R. List, eds., *Lecithins*, American Oil Chemical Society, Champaign, IL, 1985.
14. D. M. Small, in *The Physical Chemistry of Lipids* (D. M. Small, ed.), Plenum, New York, 1986, p. 386.
15. N. Krog, in *Crystallisation Processes in Fats and Lipid Systems* (N. Garli and K. Sato, eds.), Marcel Dekker, New York, 2001, p. 505.
16. D. M. Small, in *The Physical Chemistry of Lipids* (D. M. Small, ed.), Plenum, New York, 1986, p. 475.
17. N. Krog, in *Ingredient Interactions—Effects in Food Quality*, 2nd ed. (A. G. Gaonkar, ed.), Marcel Dekker, New York, in press.
18. O. Lehman, *Fl ussige Kristalle*, Engelmann, Leipzig, 1904.
19. V. Luzzati, H. Mustacchi, A. Skoulios, and F. Husson, *Acta Crystallogr.* 13, 660 (1960).
20. G. J. T. Tiddy, *Phys. Rep.* 57, 1 (1980).
21. H. Hauser, in *Proc. Eur. Sci. Found. Workshop, 4th* (P. L. Luisi and B. E. Straub, eds.), 1984, p. 37.
22. K. Larsson, *Zeit. Phys. Chem. Neue Folge* 56, 173 (1967).
23. N. Krog and A. P. Borup, *J. Sci. Food Agric.* 24, 691 (1973).
24. S. T. Hyde, S. Andersson, B. Ericsson, and K. Larsson, *Z. Kristallogr.* 168, 213 (1984).
25. N. Krog and K. Larsson, *Chem. Phys. Lipids* 2, 129 (1968).
26. B. Ericsson, Interactions between globular protein and polar lipids, Thesis, Lund University, Sweden, 1986, p. 20.
27. K. Larsson, British patent No. 1,174,672, 1967.
28. W. Hemker, *J. Am. Oil Chem. Soc.* 58, 114 (1981).

29. F. Reiss Husson, *J. Mol. Biol.* 25, 363 (1967).
30. K. Larsson and N. Krog, *Chem. Phys. Lipids* 10, 177 (1973).
31. A. Skoulios, *Adv. Colloid Interf. Sci.* 1, 79 (1967).
32. J. M. M. Westerbeek and A. Prins, in *Food Polymers, Gels and Colloids* (E. Dickinson ed.), Royal Society of Chemistry, Cambridge, 1991, p. 147.
33. N. Krog, in *Emulsions—A Fundamental and Practical Approach* (J. Sjöblom ed.), Kluwer, Dordrecht, 1992, p. 61.
34. S. Friberg, L. Mandell, and M. Larsson, *J. Colloid Interf. Sci.* 29, 155 (1969).
35. S. Friberg and L. Rydhag, *Kolloid-Z. Z. Polym.* 244, 233 (1971).
36. K. Shinoda and S. Friberg, *Emulsions and Solubilization*, Wiley, New York, 1986, p. 159.
37. N. Pilpel and M. E. Rabbani, *J. Colloid Interf. Sci.* 119, 550 (1987).
38. N. Pilpel and M. E. Rabbani, *J. Colloid Interf. Sci.* 122, 266 (1988).
39. S. Hamden, K. Anuar, and G. R. Michell, *J. Am. Oil Chem. Soc.* 72, 109 (1995).
40. T. L.-G. Carlson, K. Larsson, Y. Miezi, and S. Poovarodom, *Cereal Chem.* 56, 417 (1979).
41. A. Al Saleh, D. Marion, and D. J. Gallant, *Food Microstruct.* 5, 131 (1986).
42. E. Dickinson and Soon-Taek Hong, *J. Agric. Food Chem.* 42, 1602 (1994).
43. E. Davies, E. Dickinson, and R. D. Bee, *Ind. Dairy J.* 11, 827 (2001).
44. E. Dickinson, R. K. Owusu, and A. Williams, *J. Chem. Soc. Faraday Trans.* 89, 865 (1993).
45. N. Krog, N. M. Barfod, and W. Buchheim, in *Food Emulsions and Foams* (E. Dickinson, ed.), Royal Society of Chemistry, London, 1987, p. 144.
46. H. D. Goff, in *Lipid Technologies and Applications* (F. D. Gunstone and F. B. Padley, eds.), Marcel Dekker, New York, 1997, p. 329.
47. N. Krog, S. K. Olesen, H. Toernaes, and T. Joensson, *Cereal Food World* 34, 281 (1989).
48. F. MacRithchie, *J. Sci. Food Agric.* 28, 53 (1977).
49. A.-C. Eliasson and K. Larsson, *Cereals in Bread Making*, Marcel Dekker, New York, 1993.
50. World Health Organization, Technical Report Series Nos. 539 Toxicological evaluation of certain food additives with a review of general principles and of specifications (1974), 653 Evaluation of certain food additives (1980), and 683 Evaluation of certain food additives and contaminants (1982), Geneva, 1978.

3

Molecular Organization in Lipids and Emulsions

Kåre Larsson

Camurus Lipid Research, Lund, Sweden

I. INTRODUCTION

Important knowledge on the lipid structure in emulsions is based on studies of simple systems containing only a few components, such as a ternary system consisting of a polar lipid, a triglyceride oil, and water. Structures and phase equilibria in such model system provide information on emulsion-stabilizing mechanisms which can be translated into the behavior of complex food emulsions. The structures in the different states of order of lipid and lipid–water phases will be summarized with special regard to emulsions. Additional information on the chemistry and physics of emulsions are found in Ref. (1).

Lipids are unique in their ability to form a wide variety of structures, ranging from micellar solutions to liquid-crystalline phases and different crystalline forms (polymorphism). An important factor behind the molecular organizations they exhibit is the amphiphilic character of the molecule—the possibility to orient hydrophilic groups toward polar regions, such as water, and hydrophobic groups separated into nonpolar regions.

II. THE SOLID STATE

In crystals, it is possible to obtain exact and detailed information on the molecular conformation as well as the lateral molecular packing.

Knowledge about lipid crystal structures is therefore of fundamental importance for discussions of the structure in disordered states, such as liquid-crystalline lipid–water phases. Furthermore, there is a close resemblance between crystal structures and the structures of lipid monolayers at interfaces (e.g., on a water surface). A remarkable property of lipid crystalline phases that should be mentioned in this connection is that complex mixtures like natural fats can form solid solution with wide variations in molecular size.

A. Experimental Methods

When single crystals are available, it is possible to perform a complete structure determination by the x-ray diffraction technique. Even if single crystals are not available, a considerable amount of information on solid-state packing can be obtained by powder diffraction. It is thus possible to obtain a so-called long spacing from which the main features of the arrangement of the molecules in layers can be obtained, such as the number of molecular layers in the repetitive unit layer and the angle of tilt of the molecules within each layer. In the wide-angle region of the diffraction pattern, it is possible to identify dominating so-called short-spacing lines, which, in many cases, are sufficient for identification of the hydrocarbon chain packing.

X-ray diffraction is by far the most powerful method used to determine the structures in the solid state, even if important complementary information has been obtained by other methods (e.g., by infrared spectroscopy) (1).

B. Molecular Orientation in Lipid Crystals

The characteristic feature of lipid crystal structures is the arrangement of molecules in layers with the polar groups at the surface of the layer, as shown in Fig. 1. The molecular layers usually form unit layers of double molecular length, lipid bilayers, in order to permit polar interaction between the molecular layers (Fig. 1a). This means that there are only relatively weak van der Waals attractive forces between these bilayers separated by the methyl end-group gap. This explains the crystal morphology; the crystals form very thin plates parallel to these planes, with a pronounced tendency for cleavage at the methyl gap interface.

In cases with very weak attractive forces between the polar head groups or when the polar groups are not end groups, a head-to-tail arrangement as shown in Fig. 1b can be adopted. An example is ethyl stearate (2), in which the polar group is too far from the end of the linear molecule to give dimerization. Methyl stearate (3), on the other hand, forms the usual head-to-head structure.

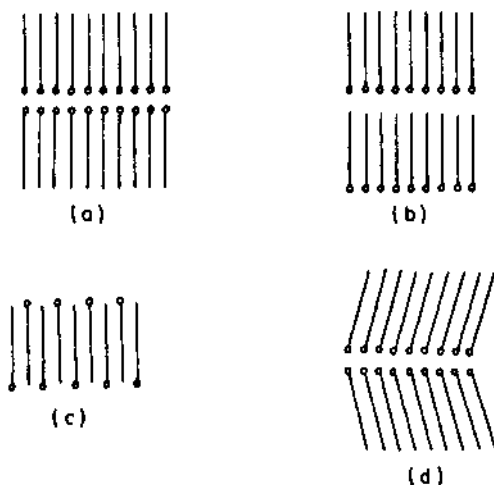


Figure 1 Schematic of the major types of molecular orientation in layers: (a) head-to-head arrangement, all molecules directed in the same way within each layer; (b) head-to-tail arrangement, all molecules directed in the same way within each layer; (c) head-to-tail arrangement within each layer; (d) tilted molecules within monomolecular layers (alternating directions of the tilt, as shown here, or nonalternating).

A head-to-tail arrangement within each layer, as shown in Fig. 1c, has been observed in cases with very bulky polar head groups. By means of such a structure, the polar groups obtain a cross-sectional area twice as large as the hydrocarbon chains.

In cases where the molecules are tilted, they are usually all parallel. The tilt results in an increased space for the polar head group (see Section II. F). In some structures, however, the angle of tilt alternates between opposite directions in successive layer, as indicated in Fig. 1d. Such an arrangement possesses particular advantages in cases of solid-state phase transitions, as translations along the methyl end-group planes can be avoided. Finally, it should be mentioned that structures with two chain directions within each molecular layer have been observed in cases where the forces between the polar head groups are of dominating importance (e.g., in amides) (4).

C. Hydrocarbon Chain Packing

The hydrocarbon chains are always in the extended planar zigzag conformation in lipid crystal forms. There are a few alternative close-packing arrangements of such chains, which can be best described by the corresponding

subcell (the smallest repetition unit within the layer). All chain packing alternatives that have been observed are summarized in Fig. 2. The triclinic packing, *T parallel*, and the orthorhombic one, *O perpendicular*, represent the most efficient packing from an energetic point of view, and they are

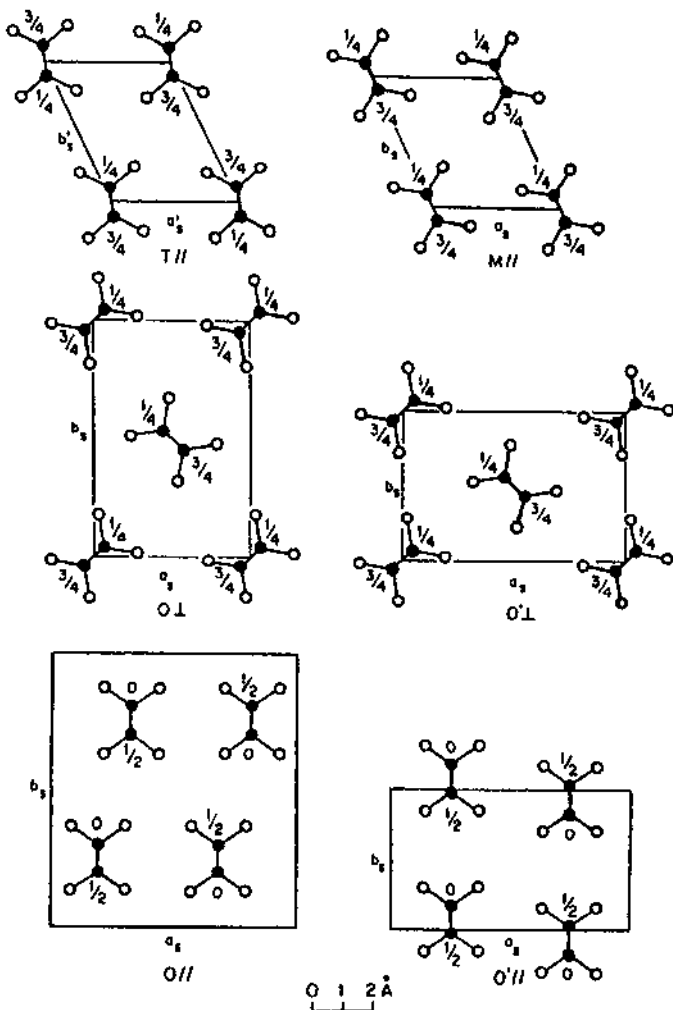


Figure 2 Hydrocarbon chain packing alternatives as defined by the corresponding subcell. One zigzag period is seen in the direction of the hydrocarbon chains with the atomic positions in the chain direction given by their fractional coordinates. Open circles represent hydrogen atoms and filled circles represent carbon atoms.

observed in *n*-paraffins, for example. All chain planes are parallel in the triclinic packing, whereas every second chain plane is perpendicular to the rest in the orthorhombic packing. The monoclinic packing, *M parallel*, has been observed in racemic 1-monoglycerides (5). An orthorhombic subcell, *O' perpendicular*, closely related to the common one, *O perpendicular*, was found in a branched fatty acid (6). In other structures with disturbances in the hydrocarbon chain region, two more orthorhombic chain packing types have been observed: *O parallel* and *O' parallel*, both with all chain planes parallel (7,8).

An interesting disordered crystal form, usually termed the alpha form (9), is observed near the melting point of many lipids. Its x-ray single-crystal data are in agreement with a hexagonal lateral symmetry of the hydrocarbon chains with rotational freedom (10). Due to the rotation of the molecules and its physical properties, this form is in fact a plastic crystal. In some lipids, however, the chains are anchored at the polar groups (e.g., in triglyceride), and it is obvious that only oscillation movements of the chains are possible. Finally, it should be mentioned that this hydrocarbon chain arrangement occurs in lipid–water phases and even in emulsions.

D. Polymorphism

The multiple melting phenomena exhibited by triglycerides was first explained by Malkin (11) as due to the occurrence of an alternative crystal form: polymorphism. One possibility for polymorphism is the arrangement of the different hydrocarbon chain close-packing types described earlier. The most common reason for polymorphism, however, is the possibility for variations in the angle of tilt of the hydrocarbon chains. The chains are successively displaced one or more whole zigzag periods in relation to adjacent chains so that the angle of tilt toward the end group plane is increased or decreased and the hydrocarbon chain region will not be changed.

Most lipids exhibit polymorphism. This can be illustrated by fatty acids. An even *n*-fatty acid in the chain-length range C₁₂ to C₁₈ can be obtained in three different crystal forms: the A, B and C forms. The crystal forms B and C have the same packing (*O perpendicular*) with different angles of tilt, whereas the A form shows another chain packing (*T parallel*).

E. Fatty Acids

The structure shown in [Fig. 1a](#) is characteristic for fatty acids with normal and saturated hydrocarbon chains. Branches can be accommodated into the

hydrocarbon chain region by relative displacements of adjacent chains or by changes in the tilt direction at the branch position (12).

When there are double bonds in the hydrocarbon chain, they will affect the chain packing differently according to the bond configuration. In oleic acid, where there is a *cis* double bond, there is a change in the chain direction at the double bond, whereas the corresponding *trans* isomer, elaidic acid, shows only one chain direction (8). The crystal structure of oleic acid is shown in Fig. 3.

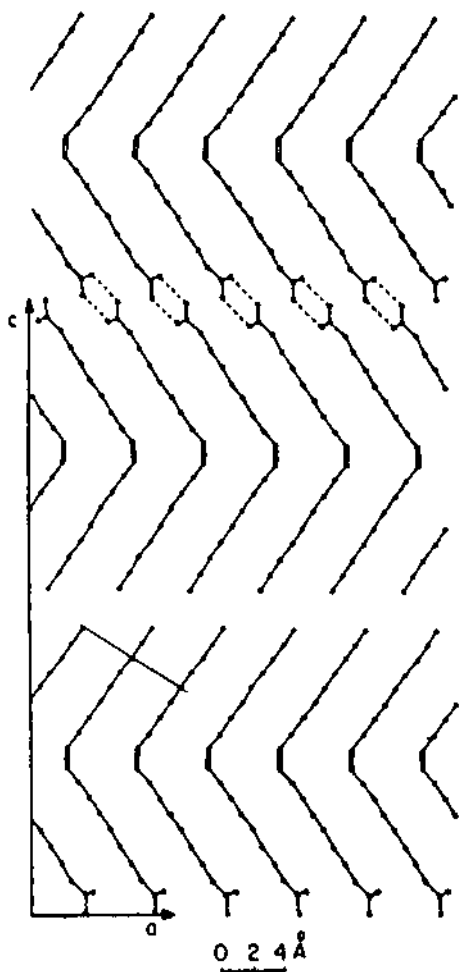


Figure 3 Crystal structure of oleic acid viewed along the *b* axis. (From Ref. 8.)

F. Monoglycerides and Emulsions Based on Crystalline Monoglycerides

Monoglycerides are most commonly used emulsifier in foods (see [Chapter 2](#)). An emulsification process, involving cooling through the crystallization of the monoglyceride solved in the oil, will result in the formation of a crystalline phase at the oil–water interface, as shown both from surface tension studies and phase identification (13). Organized lipid phases at the oil–water interface is a common emulsification-stabilizing mechanism in food emulsions; we will come back to this in connection with liquid crystals.

The crystal structure of a saturated 1-monoglyceride is shown in Fig. 4. There is a complex hydrogen-bond system linking the molecules together in two dimensions. When saturated monoglycerides are used as emulsifiers, a final emulsion product can be obtained stabilized by a crystalline monoglyceride film at the interface, with a methyl end group surface toward the oil phase and a monoglycerol head group surface toward water.

G. Diglycerides and Triglycerides

Crystal structure work has shown that there are two types of molecular conformation in diglyceride crystals. In one alternative, the two hydrocarbon

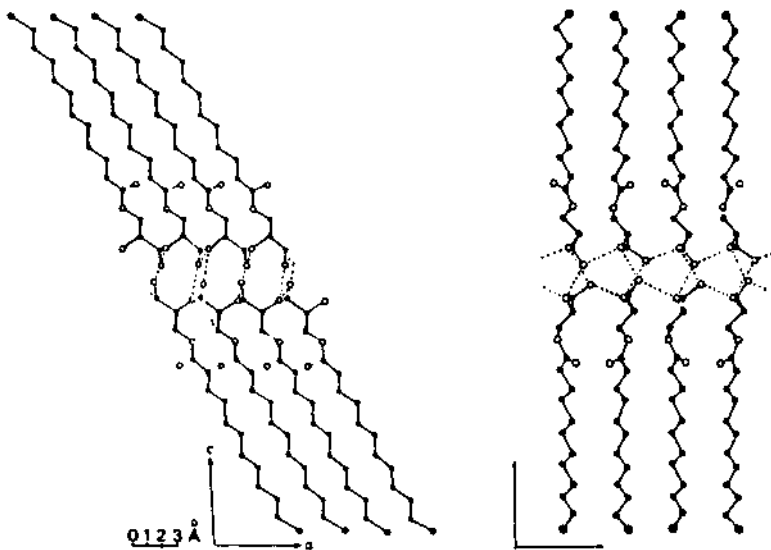


Figure 4 Crystal structure of a 1-monoglyceride viewed along two perpendicular directions. Also, 2-monoglyceride form similar to complex hydrogen bond networks linking the molecules in two dimensions. (From Ref. 5.)

chains have the same direction in relation to the head group, and then bilayers are formed just like the situation in monoglycerides. The other alternative is somewhat similar to triglyceride structures, with both chains pointing in opposite directions. Such a monolayer is then a unit layer in the crystal.

Simple saturated triglycerides crystallize in layers where extended molecules are arranged in the pairs as shown in Fig. 5. The acyl chains in the 1- and 3-position are extended, forming one chain, whereas the chain in the 2-position forms a branch. This is the characteristic molecular conformation of all triglycerides in the solid state. The presence of cis double bonds will result in a chain-sorting tendency so that unsaturated chains are localized in the same layer. This, in turn, will mean that sometimes the branching chain can be formed by the chain in the 1- or 3-position. Furthermore, the double-chain unit layer as shown in Fig. 5 cannot allow ideal chain sorting, and a triple-chain layer is instead the unit layer.

Simple triglycerides (all chains equal) show three polymorphic forms, and even complex triglycerides have a similar behavior although more forms may occur. The nomenclature now generally accepted to identify the polymorphic forms is based in x-ray diffraction with the following criteria:

Alpha form: One dominating diffraction line at 4.2 Å.

Beta prime form: Two diffraction lines at 4.2 and 3.8 Å dominate.

Beta form: Name for all other forms.

The crystal structure of the beta prime form and mechanisms involved in the polymorphic transitions have recently been determined by the pioneering work by Sato and co-workers (cf. Ref. 14).

The different polymorphic forms have different morphologies and this may influence emulsion stability. The beta prime form, for example, forms thin needles and they can sometimes extend through the oil-water interface and result in aggregation phenomena.

III. LIQUID-CRYSTALLINE PHASES

This term was introduced in order to describe structures with partial disorders like in liquids. Lipid-water phases form a wide variety of liquid-crystalline structures with technical significance, such as in food emulsions.

A requirement for the formation of liquid-crystalline phases is that the hydrocarbon chains are disordered, like in the liquid state of paraffin.

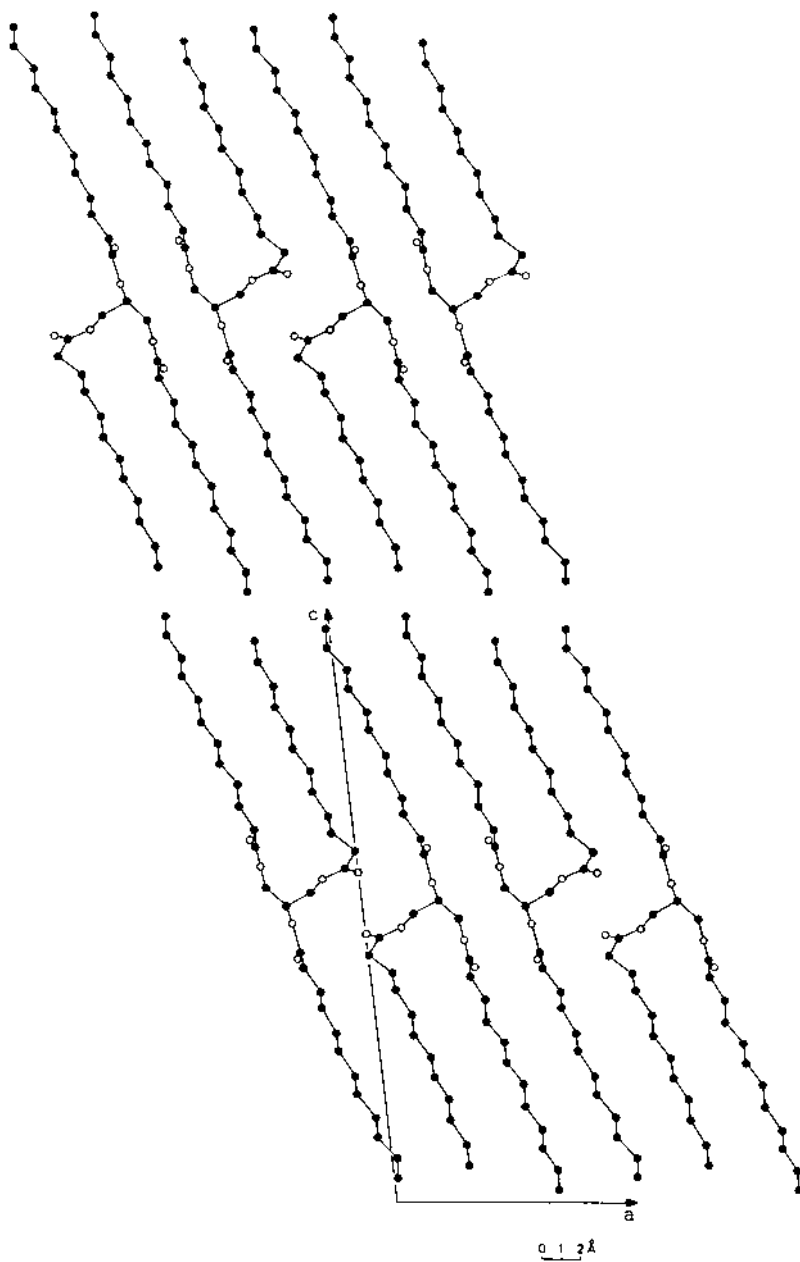


Figure 5 Molecular arrangement of trilaurin in the beta crystal form viewed along the shortest unit-cell axis. (From Ref. 5.)

The fundamental work in this field was reported more than four decades ago by Luzzati and co-workers (cf. Ref. 15). The different structures will be described and complementary information is found in [Chapter 4](#).

A. Methods

The most informative method is x-ray diffraction (or x-ray scattering). Due to the long unit periods in these phases, it is necessary to use small-angle diffraction/scattering equipment. The identification of liquid-crystalline phase is straightforward and based on the existence of sharp diffraction lines corresponding to long spacings in the structure combined with no diffraction lines in the small-angle region, only a diffuse line at 4.5 \AA . This line is due to the disordered chains, and the same line is obtained from a liquid triglyceride oil.

Spectroscopic methods, nuclear magnetic resonance (NMR) in particular, can also be used for phase identification and, in addition, provide important complementary information on dynamic properties.

Phase diagrams are useful tools in order to describe lipid–water system, and examples relevant to foods are shown in [Chapter 9](#). Samples with different water contents are equilibrated and single phases are analyzed by x-ray diffraction. First, inspections should be performed in the polarizing microscope, and the birefringence is an important feature of the liquid-crystalline phases. Only the cubic phases lack birefringence, but they are easy to detect because of their high viscosity.

B. Lamellar Liquid Crystals

This phase is characterized by a series of diffraction spacings in the ratio $1:2:3:4\dots$ corresponding to a one-dimensional repetition with the first-order spacing d equivalent to the thickness of the water layer and the bimolecular lipid layer. By simple geometry, the lipid bilayer thickness and the surface area per polar group can be calculated. The structure is shown in [Fig. 6](#).

A special structure related to the lamellar liquid-crystalline phase is the so-called gel phase. It also consists of water layers alternating with lipid bilayers, but the hydrocarbon chains are crystalline. This phase is often obtained as a meta-stable state when the lamellar liquid-crystalline phase is cooled below the transition point to crystalline chains. The chains in this phase are usually arranged according to the hexagonal symmetry, indicating rotational or oscillation movements around the chains axes.

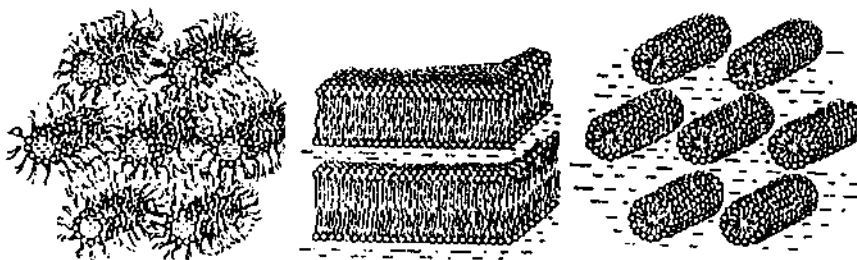


Figure 6 A fragment of the lamellar liquid-crystalline phase (in the middle), the hexagonal (to the right) and the reverse hexagonal (to the left) liquid-crystalline phases.

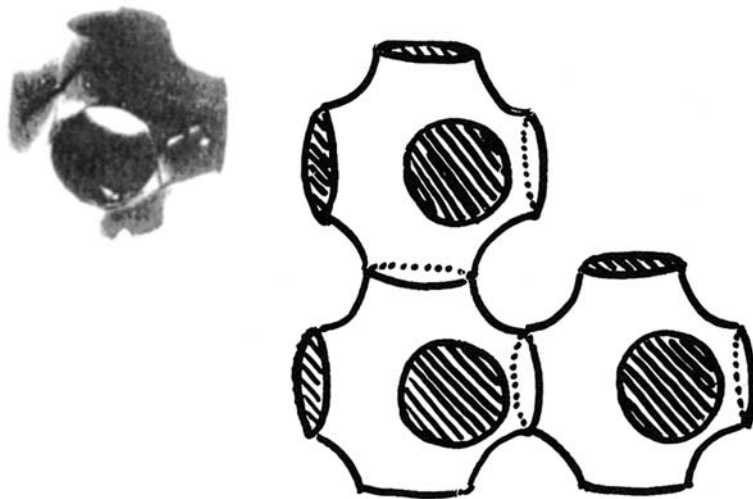
C. Hexagonal Liquid Crystals

A common aqueous lipid phase is often formed in lipids with a small hydrocarbon chain region at about equal amounts of water and lipid. It was called the middle phase in the earlier literature on soaps. This phase shows diffraction patterns with the square roots of the spacings in the ratios $1 : 3 : 4 : 7 : 12 \dots$, the condition of a two-dimensional hexagonal lattice. The swelling in water corresponds to an ideal two-dimensional swelling. The structure is shown in Fig. 6. Very polar lipids, such as lyso-phospholipids, form infinite cylinders with a liquid hydrocarbon chain core arranged in a hexagonal array and the polar heads facing the outside water. The space between the cylinders is taken up by water.

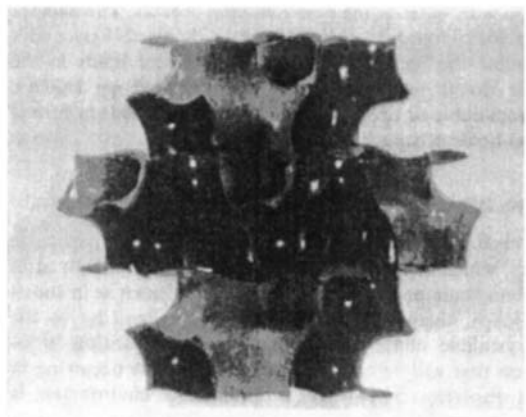
An alternative hexagonal structure of reversed type (i.e., water cylinders surrounded by lipid molecules) has been observed in many lipid systems with a relatively large hydrocarbon chain proportion. This phase, also shown in Fig. 6, is identified in the same way from x-ray diffraction pattern. By simple geometry, the diameter of the cylinders can be calculated from that the molecular length and the surface area per polar group. There is usually no problem in determining which is the true alternative of these two hexagonal structures, once the molecular dimensions have been calculated.

D. Cubic Liquid-Crystalline Phases

Cubic phases are the most complex of lipid–water phases and their bicontinuous structures have recently been revealed. Such a phase must show diffraction patterns where the square roots of the spacings form the ratios $1 : 2 : 3 : 4 : 5 : 6 : 8 : 9 : 10 : 11 : 12 \dots$. Absent lines are related to the actual symmetry (space group). The structure of one type of a cubic lipid–water



(a)



(b)

Figure 7 Structure of the simplest bicontinuous cubic lipid–water phase (space group $Im3m$) illustrated in (a) from the structure unit (plastic model) and the linkages of these bilayer units. Another phase (space group $Ia3d$) is shown in (b).

phase is shown in Fig. 7a. It has been shown that the lipid bilayer in such a phase follows an infinite, periodic, minimal surface (16). A minimal surface has zero average curvature in all points; that is, it is as convex as it is concave. The structure unit is illustrated in Fig. 7a, as well as the repetition of these units into an infinite three-dimensional surface. The lipid bilayer is centered on the surface, and on both sides, there is a water channel system.

Six water channels meet in the structure unit. The lipid bilayer is free from intersections and there is no connection between the two sides of the bilayer.

There are three different types of fundamental cubic minimal surface. They have different space groups, and x-ray data corresponding to all of them have been observed (16). All three have, in fact, been seen in the food-grade emulsifier monoolein. A second type of structure is shown in Fig. 7b, with three water channels joined into a structure unit. Finally, there is a structure with four channels joined in tetrahedral geometry.

E. Liquid-Crystalline Dispersions of the Lamellar Phase and Emulsions

The lamellar liquid-crystalline neat phase can swell only up to a particular water-layer thickness, which depends on the nature of the lipid. The situation that will be considered here is the one occurring in most lipids, when a dispersion of particles in an aqueous environment is formed when water is added above the swelling limit of the lamellar phase. The lamellar phase in neutral lipids swells up to a water-layer thickness of about 20 Å. The particles always have a closed structure with concentric bimolecular layers alternating with water layers. Such particles (termed liposomes) can encapsulate oil.

Friberg and co-workers more than three decades ago were the first to realize the significance of the lamellar liquid-crystalline phase in emulsion stabilization as demonstrated in the first edition of *Food Emulsions*. This stability criterion can easily be defined from phase equilibria; the oil phase and the water phase are in equilibrium with a lamellar liquid-crystalline phase.

A phase transition mechanism might also be utilized for destabilization purposes. If heating of the lamellar phase, for example, results in the formation of a reverse phase, this transition at the surface of the emulsion droplets will result in flocculation and coalescence.

Colloidal dispersions of cubic phases, cubosomes, can be prepared from food-grade components and may have applications in foods (cf. Ref. 17). In this connection, it should be mentioned that food additives that induce formation of a cubic phase with water has applications in order to obtain aggregation of fat globules (e.g., in artificial cream products).

REFERENCES

1. D. Gunstone, J. L. Harwood, and F. B. Padley eds., *The Lipid Handbook*, 2nd ed., Chapman & Hall, London, 1992.

2. S. Aleby, *Acta Chem Scand.* 17, 221 (1968).
3. S. Aleby and E. von Sydow, *Acta Crystallogr.* 13, 487 (1960).
4. J. D. Turner and E. C., Lingafelter, *Acta Crystallogr.* 16, 404 (1963).
5. K. Larsson, *Arkiv Kemi* 23, 29 (1964).
6. S. Abrahamsson, *Acta Crystallogr.* 12, 304 (1959).
7. E. von Sydow, *Acta Chem. Scand.* 12, 777 (1958).
8. S. Abrahamsson and I. Ryderstedt-Nahringbauer, *Acta Crystallogr.* 15, 1261 (1962).
9. K. Larsson, *Acta Chem. Scand.* 20, 2255 (1966).
10. K. Larsson, *Nature* 213, 383 (1967).
11. T. Malkin, *Progress in the Chemistry of Fats and Other Lipids*, Pergamon Press, London, 1954, Vol. 2, p. 1.
12. S. Abrahamsson, *Arkiv Kemi* 14, 65 (1959).
13. N. Krog and K. Larsson, *Fat Sci. Technol.* 94, 55 (1992).
14. K. Sato, M. Goto, J. Yano, K. Honda, D. R. Kodali, and D. M. Small, *J. Lipid Res.* 42, 338 (2001).
15. V. Luzzati, H. Mustacchi, A. Skoulios, and F. Husson, *Acta Crystallogr.* 13, 660 (1960).
16. K. Larsson, *J. Phys. Chem.* 93, 7304 (1989).
17. K. Larsson, *Curr. Opin. Colloid. Interf. Sci.* 5, 64 (2000).

4

Interactions Between Proteins and Polar Lipids

Tommy Nylander

Lund University, Lund, Sweden

I. INTRODUCTION

Proteins and polar lipids coexist in biological systems, sometimes unassociated with each other, but also as composite structures with specific actions (e.g., cell membranes and blood lipoproteins). They have a very important physical property in common—an inherent amphiphilic nature, which provides the driving force for formation of associated structures of lipids as well as for the folding of a polypeptide chain to form the unique conformation of a native protein. An important consequence of this dualistic character is that the molecules will orient at an interface. Composite biological structures are formed in this way, such as cell membranes, which separate one microenvironment from another. Therefore, it is not surprising that the major concern of the vast number of publications dealing with protein–lipid interactions have been focused on biological membranes. The main concern has been to gain a better understanding of biomembrane function, fusion, and other membrane processes, which has evoked a number of studies of these complex lipid–protein “supramolecular” systems. There are a number of reviews on this expanding area of research, such as Refs. 1–5 and the book edited by Watts (6). The classic technique for studying protein–lipid interactions in this context has been to study the properties of lipid or mixed lipid–protein monolayers at the air–aqueous interface by the surface film balance by itself or in combination with techniques such as surface rheology measurements and imaging techniques (4,7–14).

Many proteins have also the biological role of transporting molecules with hydrophobic properties, which bind to hydrophobic pockets in the protein. One such protein is the major whey protein in milk, β -lactoglobulin—a lipocalin type of protein. The biological role of β -lactoglobulin is thought to be to transport retinol (or possibly other hydrophobic ligands) (15–19). Several studies have clearly demonstrated that this protein has a high-affinity binding site for a range of ligands like phospholipids, fatty acids, cholesterol, and triglycerides (19–26). This has implications for the processing of milk and dairy products in terms of, for instance, thermal stability, as discussed by Sawyer et al. (27).

Water-soluble polar lipids and synthetic analogs (surfactants) are widely used in many technical and analytical applications. As we will discuss in the following, the interaction between proteins and polar lipids can lead both to stabilization of the protein structure and to unfolding. An example of the latter is the unfolding induced by sodium dodecylsulfate (SDS), used for analytical purpose in the SDS–polyacrylamide gel electrophoretic (SDS–PAGE) determination of molecular weights (28,29).

Proteins and lipids, separately as well as in mutual interaction, contribute significantly to the physical properties of many systems of technological interest (e.g., emulsions and foams). Further, protein structure, and thereby function and properties, are affected in various ways by polar lipids. The intention of the review is to discuss the diverse nature of (polar) lipid–protein interactions and how it can affect the physicochemical properties of lipid–protein systems. We will mainly focus on aspects relevant for the properties of emulsions and foams. However, it must be pointed out that lipid–protein interactions at interfaces are of fundamental importance also in many biological processes. One such example is the pulmonary surfactants system, consisting of a complex mixture of proteins and lipids, which is essential for the function of the lungs (30–32). Obviously, the function of the lungs involves the formation of lipid–protein film at the air–aqueous interface. Recently, the alveolar surface has been suggested to be lined by a liquid-crystalline phase (33–35), rather than a monolayer, which so far has been the traditional view as presented by Clements in the 1950s (36). Lipase-catalyzed lipolyses is another interfacial process that is of large physiological importance (37). In addition, lipase-catalyzed lipolyses has come to large industrial importance in many technical applications, including detergency and food processing (38). Because the lipases are water soluble and most of the natural lipids have low aqueous solubility, lipolyses takes place at the aqueous–lipid interface and therefore one often speaks of “interfacial activation” in connection with lipase activity (39,40).

The structure of lipids in aqueous systems is discussed in [Chapters 3](#) and [4](#). General information of proteins and protein conformation can be found in most textbooks on biochemistry. There are also publications dedicated to protein structure, like the excellent book by Creighton (41) or quite a number of good reviews (42–45). Here, we will highlight only the structural and physicochemical properties of importance for the understanding of polar lipid–protein interactions.

II. LIPIDS

Lipids can be divided into two major groups: polar and nonpolar lipids. The nonpolar lipids, primarily the triglycerides, have small polar groups and, hence, show only limited interaction with aqueous systems. The polar lipids, however, with large charged or uncharged polar groups, giving these lipids an amphiphilic nature, associate in aqueous systems. The common feature for the self-assembly of the polar lipids in aqueous environment is the formation of a polar interface, which separates the hydrocarbon and water regions. The hydrocarbon chains can exist either in a fluid state, as in liquid-crystalline phases, or in a solid state, as in the lipid gel phases (46). Generally, the melting of the chains in an aqueous environment occurs at a much lower temperature compared to the melting of the pure lipid.

Polar lipids can be divided further into two classes on the basis of their interaction with water:

1. Lipids and synthetic analogs that are water soluble in monomeric and micellar form (i.e., surfactants)
2. Lipids with very low water solubility, but with the ability to swell into liquid-crystalline phases

The water-soluble polar lipids (e.g., ionized fatty acids, bile salts, and synthetic surfactants, charged or uncharged) have monomeric solubility in the millimolar range and form micelles at higher concentrations. The critical micelle concentration (cmc) is considered to be a narrow concentration range, within which aggregates start to form by a strong cooperative process (47). The driving force for micelle formation is the hydrophobic interaction (cf. Ref. 48). The cmc for single-chain amphiphiles decreases with increasing chain length; for ionic amphiphiles, cmc also depends on the ionic strength, because the addition of salt reduces the electrostatic repulsion between the charged head groups. Increased temperature has, however, only a moderate influence on cmc, once the temperature has exceeded the critical temperature, where the monomer

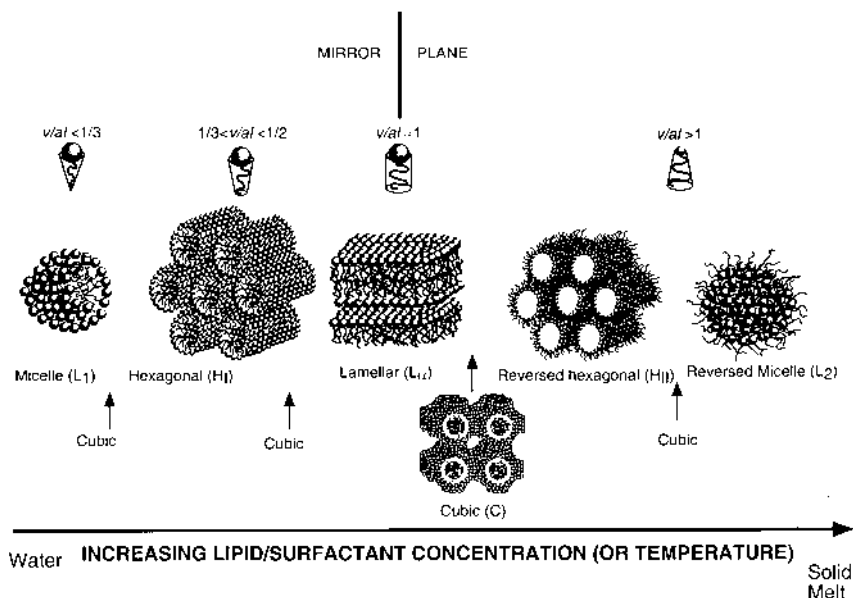


Figure 1 Commonly formed association structures by polar lipids. Phase transitions can be induced by changes in water content, temperature, or by interaction with other solution components, like proteins. The lamellar liquid-crystalline phase (L_{α}) can be regarded as the mirror plane, where the aggregates are of the “oil-in-water” type on the water-rich side and of “water-in-oil” type on the water-poor side (49). On both, the water-rich and water-poor sides of the L_{α} , there are two possible locations for cubic phases. Other “intermediate phases” may also occur. The formation of a particular phase can, in many cases, be understood by looking at the geometric packing properties of the amphiphilic molecule in the particular environment (50,51). This property can be expressed by the so-called packing parameter (v/ai), which is defined as the ratio between the volume of the hydrophobic chain (v) and the product of the head group area (a) and the chain length (l).

solubility is equal to the cmc (Krafft temperature). At low water content, an inverse micellar structure, the L_2 phase, is formed, in which the hydrocarbon chains form the continuous medium and the aqueous medium is present within the micelles.

A common feature of the two classes of polar lipids is the tendency to form lyotropic liquid-crystalline phases. A summary of some of the different liquid-crystalline phases that can occur is given in Fig. 1. With decreasing water content, the phase behavior of polar lipids often follows the sequence hexagonal phase (H_1) \rightarrow lamellar phase (L_{α}) for water soluble lipids and

lamellar phase (L_α) \rightarrow reversed hexagonal phase (H_{II}) for lipids with low water solubility. Cubic liquid-crystalline phases (Q) often occur in between these. Phase transitions can also occur with changes in temperature; with increasing temperature, the sequence of thermal transitions is usually the same as with decreased water content. In many cases, the formation of a particular phase can be understood by looking at the geometric packing properties of the amphiphilic molecule in the particular environment (50,51), which is the cross-section area of the polar head group in relation to that of the acyl chain. This property can be expressed by the so-called packing parameter (v/al), which is defined as the ratio between the volume of the hydrophobic chain (v) and the product of the head group area (a) and the chain length (l). The packing parameter for a particular environment will determine the curvature of the interface and, thus, the particular phase. Generally speaking (see Fig. 1), a value of the packing parameter lower than unity (cone-shaped amphiphile) facilitates the formation of structures where the polar interface is curved toward the hydrocarbon phase (i.e., structures of “oil-in-water” type (L_1 , H_I)). On the other hand, a value larger than unity (reversed cone-shaped amphiphile) will give the reverse curvature and favor “water-in-oil” structures like H_{II} and L_2 . When the packing parameter is changed, for instance, by the change of ionic strength or temperature or the addition of other molecules like proteins, phase transitions will ultimately arise. Increased temperature, for example, will increase chain mobility and thereby increase the volume of the lipophilic part of the molecules, explaining the often seen thermally induced transition $L_\alpha \rightarrow H_{II}$. Decreased hydration will decrease the head-group repulsion, resulting in a decreased interface area and, thus, in an increase of the packing parameter.

In nature and in many technical applications, the lipid aggregates consist of a mixture of different lipids, which either exist in a homogenous mixture or separate into domains. As discussed in the review by Raudino (52), the lateral distribution in these mixed aggregates is influenced by a number of factors like ionic strength, presence of polymers/proteins, as well as the composition of the lipids, and it is thus hard to give any general rules to predict when phase separation will occur.

Luzzati and co-workers determined the main features of the most commonly found mesophases in the early 1960s by x-ray diffraction [reviewed by Luzzati in 1968 (53); see also Chapter 3 of this book].

Results from spectroscopy studies have increased the understanding of the dynamic nature of these phases. The lamellar phase (L_α) consists of stacked infinite lipid bilayers separated by water layers, whereas the hexagonal phases consists of infinite cylinders, having either a hydrocarbon core (H_I) or a water core (H_{II}). As shown in Fig. 1, the cubic phases (Q) can exist in several locations in the phase diagram. The cubic phases have

been shown to exist in a number of lipid systems (54,55). They are isotropic and highly viscoelastic. Different structures of the cubic phases, depending on the particular lipid system, have been suggested (49,55–59). One type of cubic structure, consisting of rodlike aggregates connected three and three at each end, has been proposed by Luzzati et al. (56). The two polar rodlike networks formed in this way gives two continuous and unconnected systems of fluid hydrocarbon chains. We will, however, mainly focus on the other main type of cubic phase, which has been observed in aqueous dispersions of polar lipids with low aqueous solubility like monoglycerides, phospholipids, and glyceroglucolipids (46,54,57), as well as for water-soluble surfactants like ethoxylated fatty alcohols (60). This type of cubic phase is bicontinuous and based on curved nonintersecting lipid bilayers (cf. Fig. 10) that are organized to form two unconnected continuous systems of water channels (cf. Refs. 55,57, and 61 and Chapter 11 of this book). The two principal radii of curvature, R_1 and R_2 , can be used to describe the curvature of any surface. The average curvature $1/2(1/R_1 + 1/R_2)$ is by definition zero at any point for a minimal surface. Thus, at all points, the surface is as concave as it is convex. If an interface is placed in the gap between the methyl end groups of the lipid in the bicontinuous bilayer type of cubic phase, it will form a plane that can be described as a minimal surface (57,62). A minimal surface exhibiting periodicity, like in the cubic lipid–aqueous phase, is termed an *infinite periodic minimal surface* (IPMS). It has been shown by Hyde that the packing parameter for a lipid in such a curved bilayer is larger than unity and can be related to the Gaussian curvature $[1/(R_1 R_2)]$ of the IPMS. Three types of IPMS, described by different cubic space groups, have been shown to be important in lipid systems (57,59,62):

- The primitive lattice ($Pn3m$) which corresponds to the diamond (D) type of IPMS
- The body-centered lattice ($Ia3d$) which corresponds to the gyroid (G) type of IPMS
- The body-centered lattice ($Im3m$) which corresponds to the primitive (P) type of IPMS.

The occurrence of micellar cubic phase, C_{mic} , space group $Fd3m$, where disjointed reversed micelles embedded in a three-dimensional hydrocarbon matrix are organized in a cubic symmetry has been reported by Luzzati and co-workers (64). The formation of this type of C_{mic} phase has previously been reported for aqueous systems containing monoolein and oleic acid (64–67), for aqueous mixtures of sodium oleate and oleic acid (68), and, consequently, also during lipase-catalysed lipolysis of monoolein in aqueous dispersions under neutral/alkaline conditions (69,70).

Today cubic lipid–aqueous phases are recognized as important in biological systems (34,46,55,57,58,59,66,71–75). Some of these reports suggest that cubic lipid–aqueous phases can occur during the fusion of biological membranes. There are vast amount of studies of membrane fusion [cf. the comprehensive reviews by Kinnunen and Holopainen (2)], which is impossible to cover here. It is however worth mentioning that early studies on the fusion process for biological membranes reported that lipidic particles were discovered during the fusion event (76), indicating that additional liquid-crystalline phases occur during the fusion process. The nature of these intermediate phases during fusion is unclear, although the formation of interbilayer structures as inverted micelles have been proposed (77). In addition, the fusion rate is increased in systems which have a lamellar phase → inverted hexagonal phase transition (76,78,79). As will be discussed further, such a phase transition can be affected by proteins and polypeptides and there are also several reports on the promotion of fusion by proteins and polypeptides (52).

The liquid-crystalline lipid–aqueous phases can exist in excess of aqueous solution. One example of such lipid dispersions is unilamellar or multilamellar vesicles,* which are formed from lamellar (L_α), phases. The stability, size, and shape of vesicles can vary, depending on the composition of lipids and aqueous phase (for reviews, see Refs. 80–83). In analogy with liposomes, dispersions of a cubic lipid–aqueous phases, cubosomes, which were first discovered by Larsson et al. (57,75,84) are also formed with an excess of water. The stability of cubosomes, formed in MO–H₂O-based systems, and the corresponding dispersed H_{II} phase (hexosomes) in the MO–TO–H₂O system was found to increase in the presence of an amphiphilic block copolymer (polyoxamer) (84–86).

III. PROTEINS

An important consequence of protein–lipid interaction is the effect on the stability of the protein in solution as well as its behavior at interfaces. When discussing the stability of proteins, we may distinguish between the conformational stability of proteins and aggregation/precipitation phenomena due to reduced solubility at pH close to the isoelectric point, at high ionic strength (salting out), and/or caused by specific binding of ions (e.g., the formation of calcium bridges) or lipids. Although the two phenomena

*The term *liposomes* are, according to IUPAC recommendation, synonymous to lipid vesicles, but are sometimes used for multilamellar vesicles.

usually are connected, aggregation/precipitation can occur without major conformational changes of the protein (87). The conformational stability of a protein, which, of course, has no meaning for proteins lacking secondary structure, can be estimated by circular dichroism (cf. Ref. 41), compressibility measurement (cf. Ref. 88), and calorimetry (cf. Refs. 89–91). The stabilization of the protein structure have been extensively reviewed by a number of authors (cf. Refs. 43,44, and 89–92), and we will only focus on some aspects of significance in emulsion systems.

The native protein structure is a consequence of a delicate balance of forces, including electrostatic forces, hydrogen-bonding, van der Waals forces, conformational entropy, and so-called hydrophobic interactions (cf. Refs. 43 and 91–94). The amino acid sequence of the polypeptide chain (the primary structure) will determine the folding into structural units (the secondary structure), and the association of structural units into domains, tertiary and quaternary structures, gives each protein the unique conformation connected with its action and specificity. Naturally, cross-links, such as disulfide bridges, increase the stability of a protein.

The interior of a globular protein is very densely packed, having a quite constant mean packing density (0.74), a value also found for crystals of small organic molecules (94). Thus, van der Waals forces and hydrogen-bonding, which are short-range interactions, play an important role for the stability of folded proteins (91). As first pointed out by Kauzmann (95), it is clear that the so-called hydrophobic interactions play an important role in stabilizing the protein structure. The nonpolar amino acid residues will provide a strong driving force for folding, leading to an accumulation of hydrophobic residues in the core of the protein molecule. The polar amino acid residues (uncharged and charged) will have a high affinity for aqueous solvent and will, consequently, be located on the outside of the protein. The nature of hydrophobic interactions in this context is not yet fully understood (cf. Refs. 43,91, and 92), because it still is difficult to analyze them separately from other forces contributing to the stabilization of the protein structure (91).

It is important to bear in mind that proteins are only marginally stable at room temperature. This means that the exchange of only one amino acid residue, by, for instance, genetic engineering, might destabilize or stabilize the protein considerably. In the following, it will be demonstrated that the binding of lipids to the protein also can have the same effects. In many systems involving proteins and lipids, the protein–lipid interaction takes place at an interface. As discussed extensively by Norde et al. (96–98), the delicate balance between forces that stabilize and destabilize the protein might be shifted in the proximity of an interface, leading to unfolding upon adsorption. The loss of entropy upon protein folding is the main

force counteracting the stabilization of the protein structure (43). Thus, unfolding upon adsorption is an entropically favored process (96–98). Furthermore, at an interface, the unfolded hydrophobic domains might be oriented in such a way that their exposure to the aqueous environment is minimized. In fact, Norde argues that the entropy gained by the unfolding of the protein upon adsorption can be a significant driving force for adsorption (96–98). However, they also observed that adsorption of protein on apolar surfaces might lead to an increase order of the protein secondary structure as observed for enzymes like α -chymotrypsin and serine proteinase savinase on Teflon (98–100).

The folding and unfolding of proteins have been shown, under certain conditions, to occur via an intermediate state, the molten globule state (101–106). This state, which is somewhere between the native and completely unfolded state, is characterized by a retained secondary structure, but with a fluctuating tertiary structure. The protein molecule is also more expanded and exposes more hydrophobic domains. The molten globule state is hard to detect by calorimetric measurements, because the unfolding of the molten globule is accompanied with little or no heat absorption (104). As discussed by Dickinson and Matsumura (106), the molten globule state can be achieved in a number of ways, as pH changes, increase of temperature, the use of denaturation agents, breaking of disulfide bridges, and removal of ligands or cofactors bound to the protein. It is also suggested that the protein can adopt a molten globule state when interacting with an interface. In fact, it was found that α -lactalbumin was more surface active under conditions where it exists in the molten globule state. It has been proposed that the molten globule state of the protein may be required for the translocation of proteins across biological membranes (107,108).

It should be noted that although it is possible to classify proteins as globular, unordered (lacking secondary structure), and fibrous, there are marked differences between proteins belonging to the same class, due to their complex and intriguing design. Thus, it is much harder for proteins than for polar lipids to follow rules of thumb for their behavior. Protein properties such as conformation, charge distribution, association, and activity are also strongly influenced by environmental condition (e.g., pH, ionic strength, type of ion, and temperature). In this context, it is important to point out the effect of type, valence, and ionic strength of an added electrolyte. This can have a profound effect on interactions involving proteins and other polyelectrolytes, in particular under physiologically relevant conditions as discussed by Ninham et al. (109–111). They argue that the present theory is not sufficient to distinguish between van der Waals interactions and electrostatic interactions. In addition, as part of their biological role,

some proteins have specific binding sites for lipids. These binding sites can even be specific for a certain class of lipids. Thus, it is important to consider protein–lipid interactions in relation to the features of each individual protein.

IV. INTERACTION BETWEEN GLOBULAR PROTEINS AND WATER-SOLUBLE POLAR LIPIDS

A. In Solution

Ionic surfactants interact with most proteins. A high surfactant concentration will generally lead to unfolding of the protein structure. The interaction between nonionic surfactants are weaker and seldom affect the structure of proteins. Several reviews concerning the interaction between water-soluble polar lipids and protein are focused on the interaction between ionic surfactants [e.g., sodium dodecyl sulfate (SDS) and globular proteins at low and intermediate temperatures] (11,112–118). Because vast amounts of the surfactant–protein work is devoted SDS, we will use this system as an example, and at the end of this subsection, we will discuss some exceptions.

We can distinguish between two types of binding of water-soluble lipids to proteins:

1. A high-affinity type of binding that occurs at low lipid concentration
2. Nonspecific cooperative interaction taking place at higher concentrations (115,116).

An example of a binding isotherm, where the two types of binding occur, is given in [Fig. 2](#). In this isotherm, for the binding of SDS to lysozyme, the regions of high-affinity noncooperative binding, at low surfactant concentration, is well separated from the cooperative binding observed at a higher concentration. For comparison, an example of a binding isotherm for the binding of a nonionic surfactant, *n*-octyl- β -glucoside, to the same protein is also inserted. In this case, only nonspecific cooperative binding occurs.

The specific binding is mediated by ionic and hydrophobic interactions and usually occurs below the cmc of the surfactant (115,119–122).

The nonspecific interaction occurs close to or above the cmc and usually leads to a destabilization of the native conformation. The cmc of the surfactant is thus an important parameter and conditions that affect cmc will generally affect the binding (cf. Refs. 116 and 123). The saturation of all of the binding sites generally corresponds to 1–2 g of surfactant per gram of protein (115,116,124). The extent of interaction and unfolding depend

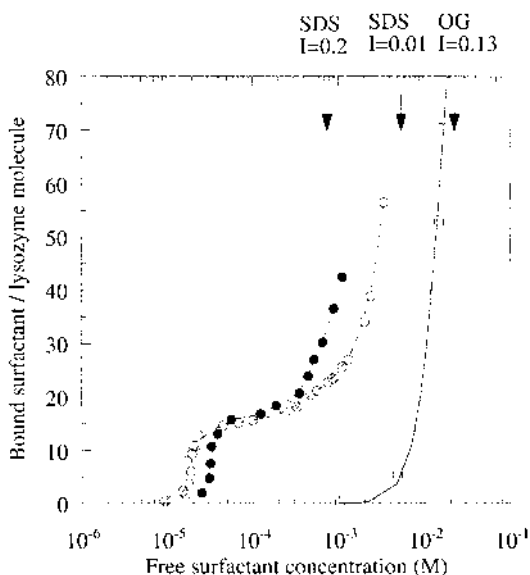


Figure 2 Binding isotherms for binding of surfactants to lysozyme in aqueous solution at 25°C. The isotherms (○, ●) for SDS have regions of both high-affinity noncooperative binding, at low surfactant concentration, and cooperative binding at high concentration. The influence of ionic strength on the binding isotherm is shown: ○, ionic strength (I) = 0.0119 M and ●, ionic strength = 0.2119 M at pH 3.2. For comparison, an example of a binding isotherm where only nonspecific cooperative binding occurs is also inserted. This isotherm, describing the binding of the nonionic *n*-octyl- β -glucoside (OG) to lysozyme (□) was measured at pH 6.4 and ionic strength of 0.132 M . The protein concentration was 0.13% (w/v). The arrows indicate the cmc for the different surfactants and ionic strengths. The data are adopted from Ref. 115 and the experimental details are given in Refs. 160 and 115 for SDS and OG, respectively.

mainly on the nature of the surfactant hydrophilic group, surfactant chain length, ionic strength, pH, temperature, and organic additives as well as on the protein itself (116). Organic additives include the presence of impurities in proteins as well as in the lipids. For instance, it has been demonstrated by Lunkenheimer and co-workers that commercial SDS samples usually contains a substantial amount of decanol, which actually is more surface active than SDS in itself (125–127). Similarly, it has been shown by Clark et al. that β -lactoglobulin contain bound fatty acids, which may alter the binding of other surface-active compounds (128). Clearly, the presence of amphiphilic impurities may give anomalous effects on the binding of other surfactants.

1. Anionic

The effect of surfactant protein interaction on the structural stability of proteins depends strongly on the mode of interaction. In fact, as shown in Fig. 3, the same surfactant can act to both stabilize and destabilize, depending on surfactant concentration as well as other solution conditions. At low surfactant-to-protein ratios, a high-affinity interaction between certain proteins and surfactants occurs. This interaction stabilizes the protein structure against thermally induced unfolding; thus, the thermally induced transition is shifted toward a higher temperature, as illustrated in Fig. 3 and previously reported by Hegg (129) for SDS and β -lactoglobulin. Similar findings have also been reported for other protein-surfactant complexes such as between fatty acids or SDS and bovine serum albumin (130) as well as between palmitic acid and β -lactoglobulin (131). As discussed earlier,

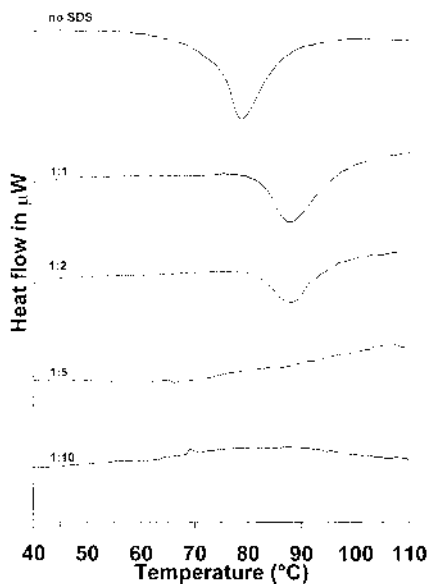


Figure 3 The thermograms from top to bottom shows the thermally induced unfolding of β -lactoglobulin (1.4 mM in 60 mM NaCl, pH 6) when increasing the protein/SDS molar ratio. The cmc of SDS is 0.47 mM at 25°C and \sim 1 mM at 90°C, when taking into account the ionic strength of the protein solution. Assuming that one SDS molecule is bound per β -lactoglobulin monomer, 3 mM SDS has to be added to reach the cmc of the surfactant at 90°C. The data are adopted from Ref. 123, where the experimental details are given also.

increasing the free-surfactant concentration to the cmc gives rise to non-specific cooperative binding, which, in turn, can lead to unfolding of the protein, as illustrated in Fig. 3 (123). This is in agreement with earlier reports, in which a surfactant ratio above 10 mol of SDS per mole of serum albumin or 1 mol of SDS per mole of β -lactoglobulin monomer was observed to cause unfolding of the protein (129,130).

Surfactant like alkylsulfates or alkylethersulfates interacting with proteins with opposite net charge (e.g., lysozyme or gelatine) might cause precipitation of the protein-surfactant complex due to neutralization of the net charge (119,132-137). Although the protein is precipitated, only small changes in the secondary structure occur. At an increased surfactant concentration, the complex is dissolved and the protein starts to be unfolded. Generally, denaturation of proteins by long-chain alkyl sulfates such as SDS results in a structure with large fractions of the polypeptide chain in an α -helical conformation (48,138,139). As a simple rule, proteins with a low content of α -helix in their native form, such as concanavalin A, β -lactoglobulin, and ovalbumin, will increase in α -helix content upon interacting with SDS. The reverse is observed for proteins with a high α -helix content in their native form (e.g., myoglobin and serum albumin) (138). The structure resulting from the interaction is thought to consist of helical segments with flexible joints and with most of the hydrophobic side chains exposed to the surfactant. The successive binding of SDS opens up the molecules, due to the increased electrostatic repulsion, and unveils new hydrophobic domains, which can bind additional surfactants. This association stabilizes α -helical folding at the expense of nonrepetitive structure. The free energy gained by this process in most cases by far exceeds the unfavorable free-energy change of disrupting the native conformation (48). Light-scattering studies confirm the expansion of the hydrodynamic radius of the protein upon interaction with SDS (140). Several models of the structure of complexes between SDS and proteins at high surfactant concentration, like the correlated necklace, rodlike structure, and flexible helix, have been considered (cf. Refs. 116 and 141). However, small-angle neutron-scattering data strongly indicates a structure resembling a necklace (141,142), where the polypeptide chain with high flexibility is decorated with SDS micelles (138,141), as shown in Fig. 4. This interaction is reported to take place via the monomeric form of the surfactant (116,138).

It should also be kept in mind that not all proteins are fully unfolded by SDS. For instance, it has been shown that the activities of glucose oxidase, papain, pepsin, and bacterial catalase were not affected by high concentration of SDS, correlated to the low binding of SDS (143,144).

Thus far, we have mainly addressed the interaction at low protein concentrations. Morén and Khan (136) investigated the phase behavior of

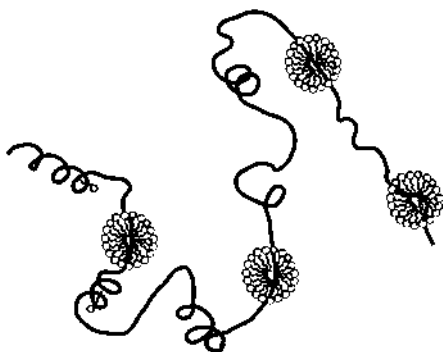


Figure 4 Schematic representation of the so-called necklace model for the interaction between SDS and proteins. The solid line represents the unfolded polypeptide chain, which still contains secondary structure. Micellelike clusters are cooperatively formed on the polypeptide chain.

the anionic SDS, positively charged lysozyme, and water over a wide concentration range and one of the phase diagrams they determined is given in [Fig. 5a](#). Stenstam et al. later investigated in detail the stoichiometry of the formed complex and their findings are summarized in [Fig. 5b](#) (137). Small amounts of SDS, at a ratio to lysozyme corresponding to charge neutralization of the protein, were found to give precipitation. A net attractive force exists between the surfactant–protein complexes and hydrophobic interactions dominate ([Fig. 5b](#)). Further addition of SDS lead to a redissolution of the precipitate, which was complete when the number of SDS molecules was equal to the number of positive charges on the protein (19). At this ratio between SDS and lysozyme, a narrow strip of a bluish gel phase occurred when the protein concentration was between 7% and 20% (w/w). At a higher ratio between SDS and lysozyme, the interaction between the surfactant protein complexes is net repulsive and electrostatic interactions dominate ([Fig. 5b](#)). Consequently, an isotropic solution is formed. Morén and Khan also investigated the effect of varying alkyl chain length, $C_{12}SO_4$, $C_{10}SO_4$, C_8SO_4 , and C_6SO_4 on the lysozyme–sodium alkyl sulfate–water ternary systems (145). The surfactant with shortest hydrophobic tail (C_6SO_4) forms the largest solution region with lysozyme prior to precipitation, and the extension of the solution region decreases with increasing surfactant chain length. The extension of the precipitation region toward higher surfactant concentrations increases with decreasing surfactant chain length. The surfactant concentration required to redissolve the precipitate at dilute protein concentrations therefore seems to follow the cmc for the surfactant in water, which also increases with decreasing surfactant chain

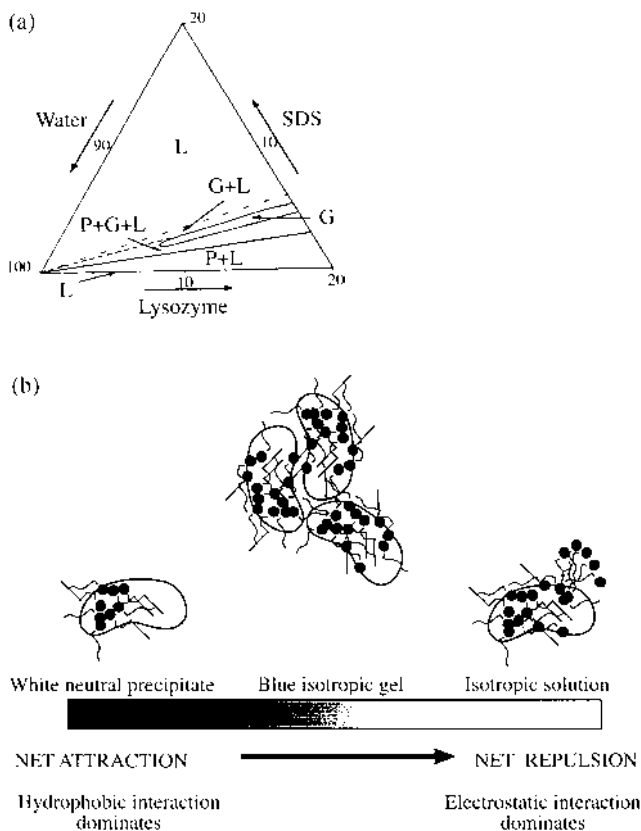


Figure 5 (a) Phase diagram of the lysozyme–SDS–water ternary system, where L indicates solution, G gel, and P precipitate. (Adapted from Ref. 136, where experimental details are given.) (b) Schematic representation of the interaction between protein surfactant complexes in the lysozyme–SDS–water system. (Adapted from Ref. 137, where the experimental details are given.)

length. A single gel phase was only observed for the $C_{12}SO_4$ and $C_{10}SO_4$ systems and not in the presence of C_8SO_4 and C_6SO_4 . A similar type of gel phase is expected to occur in more food-relevant surfactant–lipid and protein–aqueous ternary system and therefore offer potentially very interesting possibilities to vary the functional properties of foods and food ingredients.

Within the type of surfactant, the binding is dependent on the nature of the polar head group; for example, for an anionic surfactant, the

interaction decreases in the order alkyl sulfates > alkyl sulfonates > alkyl benzene sulfonates > carboxylates \approx alcohols (146,147).

2. Nonionic

The interaction between nonionic surfactants and proteins is generally weak (118,146,148–151). In the case of ionic surfactants, the specific ionic interaction, absent for a nonionic surfactant (Fig. 2), occurs in addition to the hydrophobic interaction, leading to more severe effects on the protein structure. For instance, each β -lactoglobulin monomer binds only one Tween-20 (152), or one sucrose ester (153), or one Triton X-100 (149). Generally, minor changes of the structure upon interaction are observed (148,150). An unordered, flexible protein, β -casein, was found to bind less than one sucrose ester per protein molecule, possibly due to incorporation of the surfactant in β -casein micelles (153). The reason for the weaker interaction between proteins and nonionic surfactants has been assigned to the lower cmc, which gives a too low monomer concentration to attain cooperative binding to the protein (148). The cmc is increased when the chain length is decreased, which may change this situation; The binding of octyl glucoside to various proteins was found to occur in a cooperative manner at surfactant/protein molar ratio of 100 and more, without any evidence of protein denaturation (150).

Also, the nature of the nonionic polar head groups will affect the interaction. For a series of Triton X surfactants, increasing the hydrophilic oxyethylene chain length was found to decrease the strength of interaction with bovine serum albumin (BSA), due to steric hindrance (151). The calorimetric data indicated that some conformational changes of BSA occurred during the saturation of the low-affinity, noncooperative binding sites (151).

Some studies have also been carried out with the zwitterionic surfactant lysophosphatidylcholine (LPC), which was found to bind cooperatively to puuroindoline, a lipid-binding protein isolated from wheat flour, at a molar ratio of 5–1 (154). One LPC molecule was also found to bind with less affinity to β -lactoglobulin than Tween-20 (21). The binding of Tween-20, as opposed to LPC, had a much more disruptive effect on the interfacial film of the protein, attributed to the bulkier head group of Tween-20. This implies that also a nonionic surfactant can disrupt the structure of a protein, provided that the binding is strong enough and the hydrophilic head group large enough to sterically induce conformational changes.

3. Cationic

Cationic surfactants generally seem to exhibit an intermediate action on water-soluble proteins. Reports in the literature indicate a cooperative

interaction with proteins, but with less affinity and, thus, with less perturbation of the folded state, compared to the effect of the anionic ones (123, 155–159). If the binding is governed both by electrostatic and hydrophobic interactions, anionic and cationic surfactants will obviously occupy different sites. Nozaki et al. have suggested that the lower affinity of many proteins for cationic compared to anionic surfactants can be explained by the fact that the cationic arginine and lysine side chains contribute more CH_2 groups than anionic aspartate and glutamate side chains (157). This implies that the combined electrostatic and hydrophobic interactions will be more favorable for anionic surfactants. As a consequence, the cooperative binding step will start at a higher concentration for cationic relative to anionic surfactants (116).

4. Effect of Solution Conditions

Increased ionic strength affects the interaction between protein and ionic surfactants by reducing the electrostatic attraction between surfactants and amino acid residues with opposite net charges. Generally, the high-affinity noncooperative binding is strongly influenced by the electrostatic interaction between surfactant and protein. Thus, this part of the binding isotherm will be shifted toward higher surfactant concentration upon the addition of salt, as observed for lysozyme and SDS (Fig. 2) (115,160). Increasing the ionic strength will, on the other hand, favor the cooperative binding by screening the repulsion between the charged surfactant head groups. This part of the surfactant-binding isotherm will therefore be shifted toward lower surfactant concentrations, parallel to the decrease of surfactant cmc. Here, it is important to point out that the presence of highly charged proteins as a polyelectrolyte as well as temperature will affect the formation of micelles. This has been amply demonstrated by Waninge et al. who studied thermally induced unfolding of β -lactoglobulin at a concentration of 1.4 mM in 60 mM NaCl, pH 6, in the presence of various molar ratio SDS, and their main findings are illustrated by the thermograms in Fig. 3 (123). From Fig. 3, we note that the peak corresponding to the thermal unfolding disappears when the protein/SDS molar ratio increases above 1:2. This corresponds to a SDS concentration of about 3 mM. The cmc for SDS is about 8.1–8.2 mM in water (161,162). However, the cmc for ionic surfactants decreases with ionic strength and increases with temperature (161–164). Taking account to these effects for the presence of β -lactoglobulin, which has a net charge of -5 , at a concentration of 1.4 mM in 60 mM NaCl, the cmc of SDS is expected to be 0.47 mM at 25°C and ~ 1 mM at 90°C. When taking into the specific binding of one SDS molecule per β -lactoglobulin monomer, 3 mM SDS

has to be added to reach the cmc of the SDS at 90°C. Thus, any effect of nonspecific cooperative interaction between the surfactant and the protein is expected to take place at this SDS concentration. In Fig. 3, we observe an apparent loss of protein structure. The unfolding of the protein structure at low temperature, which is observed in the presence of most anionic surfactants such as SDS at high concentration, is expected to be maintained at increased temperature. However, because the cmc generally increases with temperature, we might arrive at the situation where the cooperative binding ceases to exist at the high temperature, maybe even below the temperature at which thermally induced unfolding take place. Interestingly, Waninge et al. observed that the conformational changes invoked by the nonspecific cooperative binding of SDS at 25°C could be reversed by extensive dialysis (123). Referring to the discussion of the molten globule state earlier, it is tempting to compare it with the structure obtained by surfactant unfolding.

Although cationic surfactants seem to cause less unfolding of globular proteins at low temperature than anionic, some reports indicate that they can destabilize globular proteins at increased temperature (158,165). However, these reports also indicate that the unfolding process at the same time becomes considerably more reversible. The heat denaturation of ovalbumin, which in practice is completely irreversible, was found to be completely reversible in the presence of high concentrations of cationic surfactants (165). This was explained by decreased intermolecular and intramolecular interactions at high temperature, due to the interaction between the unfolded protein and surfactant, which facilitates the reformation of the native complex on cooling.

As a rule of thumb, an increase in pH will shift the binding of anionic surfactants to higher concentrations (166). A decrease of pH will have the same effect on the binding of cationic surfactants (167). At low surfactant concentrations (i.e., well below the cmc), cationic amphiphiles increase the solubility of proteins on the acidic side of the isoelectric point (pI), whereas precipitation can occur on the alkaline side of the pI . Anionic amphiphiles will affect solubility in the opposite direction. The solubilising effect is also observed at high temperatures.

We conclude that because the binding generally is thought to occur via monomers, any change affecting the cmc will also affect the cooperative binding at concentrations close to and above the cmc. Under some conditions, the formation of surfactant micelles will be energetically favored before binding to the protein. If the cmc is of the same order of magnitude as the concentration necessary for binding to occur, the lowering of the cmc caused by increasing ionic strength might even prevent binding.

B. At Interfaces

The stabilization of food emulsions and foams can be achieved by proteins, polar lipids, or mixtures of them. However, the mechanisms by which they stabilize emulsions and foams can be quite different. Here, we refer to the work of Clark and his colleagues (168), which have, based on results such as those from fluorescence recovery after photobleaching experiments, suggested a mechanism for stabilization of foams and emulsions. Generally, polar lipids are capable of reducing the interfacial tension more than proteins, whereas the protein molecules can be anchored at multiple sites at the interface. Therefore, many proteins stabilize foams and emulsions by forming intermolecular interactions between the adsorbed protein molecules, which encapsulates the dispersed phase. Such a mechanically rigid layer immobilizes the proteins and prevents perturbations, droplet coalescence, or flocculation. In contrast, lipids usually stabilize the dispersed droplet or bubble by forming a densely packed and much less rigid monolayer with high mobility. Any disturbance of the interface, such as expansion of the interface, will induce a (temporary) surface-tension gradient. This is, of course, unfavorable and the system tries to restore an even distribution of the surface free energy. During the lateral diffusion, or adsorption from the bulk, of the surface-active components, a flow counteracts the disturbance. This dynamic process is usually called the Gibbs–Marangoni effect (169). Thus, the rate of exchange of polar lipids at the interface is much higher than for proteins. The addition of polar lipids/surfactants to a protein film can, if the concentration becomes too high, destroy the integrity of the film by disrupting protein–protein interactions and, consequently, destabilize the foam or the emulsion. This points at another important reason to study the interaction between proteins and polar lipids in the adsorbed layer as well as during the competitive adsorption of the individual components. The surfactant-to-protein ratios as well as the properties of the components and the interface will determine the composition of the film.

In several investigations, surface-tension measurements have been used to study protein–lipid interactions (cf. Refs. 10,12,13,170, and 171). However, it must be kept in mind that any impurity with a higher surface activity than the studied components will accumulate at the interface, giving a lowering of the surface tension (125–127) and thus affecting the interpretation of the data. The presence of impurities (e.g., fatty acids) bound to β -lactoglobulin did have a profound effect on the interfacial behavior of mixtures with Tween-20, as judged from surface elasticity measurements at the air–aqueous interface (128). It was observed that the film containing purified β -lactoglobulin could maintain a more rigid film, at a much higher concentration of Tween-20 as compared to the sample containing impurities.

We will discuss some experimental data on the basis of possible factors that influence the way mixtures of proteins and polar lipids behave at an interface. These can be summarized as follows:

1. The surface activity of the individual components
 - (a) Competitive adsorption. The lipids and proteins compete for the interface, where the most surface-active and/or abundant molecule wins, depending on the ratio between surfactants and proteins in solution.
 - (b) Displacement. The polar lipids may, due to their higher surface activity, displace the proteins from the interface. This displacement can be hampered by a strong interaction between the protein and the interface and/or protein–protein interactions.
2. Protein–lipid interactions
 - (a) Increased surface activity of the lipid–protein complex
 - (i) The binding will cause unfolding and/or increase hydrophobicity of the protein that will lead to an increased affinity to the surface.
 - (ii) The binding (of ionic amphiphiles) will cause precipitation at the interface due to charge neutralization.
 - (b) Decreased surface activity of the lipid–protein complex
 - (i) The binding will make the protein more soluble and hence lower the affinity for the interface.
 - (ii) The binding will lead to precipitation of protein–lipid complex in the bulk, which will cause loss of surface-active material.
 - (c) Protein–lipid interactions at the interface
 - (i) The interaction will give more efficient packing at the interface and thus give a higher total surface concentration.
 - (ii) The interaction will disrupt the protein–protein interaction in the interfacial film.

We will use some of our surface-tension data on protein–surfactant mixtures to demonstrate the effect of different modes of interaction. Different modes of interaction are observed for the same system depending on the lipid/protein ratio. The data will also serve as the basis for the discussion according to the above factors. The interaction between a protein

(ovalbumin) and three types of surfactant [an anionic (SDS), a nonionic (1-monocaproin) and a cationic (hexadecylpyridinium chloride)] as observed from surface-tension isotherms is illustrated in Fig. 6 [the experimental procedure is given elsewhere (171)]. The protein concentration used was $21 \mu\text{M}$. To avoid precipitation, the measurements were carried out at pH 5.6 and 4.0 for SDS and hexadecylpyridinium chloride, respectively [i.e., below and above the isoelectric point (4.5–4.9) of ovalbumin]. The interaction between ovalbumin and ionic surfactants is considered to be nonspecific. Serum albumin has, however, specific binding sites for the surfactants (114) and, for comparison, the data for the surface tension of BSA ($13 \mu\text{M}$, 0.05 M phosphate buffer, pH 5.6) and SDS are also inserted in Fig. 6b. The surface-tension isotherms of the pure surfactants are shifted according to the differences in cmc although they have a similar shape. Hence, it is useful to discuss data in terms of the ratio between added number of surfactant monomers and protein molecules.

1. Competitive Adsorption

No synergistic effect is observed for the mixture of the nonionic surfactant, monocaproin, and ovalbumin (Fig. 6a). The component giving the lowest surface tension displaces the other at the interface. No molecular interactions seem to take place in either the bulk solution or at the interface. Also, for the cationic and anionic surfactants, the surface tension at high enough surfactant concentration is dominated by the contribution from surfactants. Thus, it is generally observed for a range of surfactant–protein systems that the protein dominates at low surfactant concentration, whereas the surfactant dominates at high surfactant concentration, as they generally give a lower surface tension [13].

The effect of interfacial properties of a solid surface on the competitive adsorption among a protein, fibrinogen, and a nonionic surfactant, pentaethyleneglycol mono *n*-dodecyl ether (C_{12}E_5), was investigated by using a wettability gradient silica surface (172). Fibrinogen was preferentially adsorbed on the hydrophilic surface at all concentrations, whereas the surfactant dominated at the hydrophobic and intermediate part of the gradient at surfactant concentrations close to the cmc and above. The preferential adsorption of the surfactant extended to a wider range of the gradient if the temperature was increased to a value close to the cloud point of the surfactant.

2. Displacement

Mackie et al. have, based on extensive studies using atomic force microscopy (AFM), Brewster-angle microscopy (BAM), fluorescence microscopy,

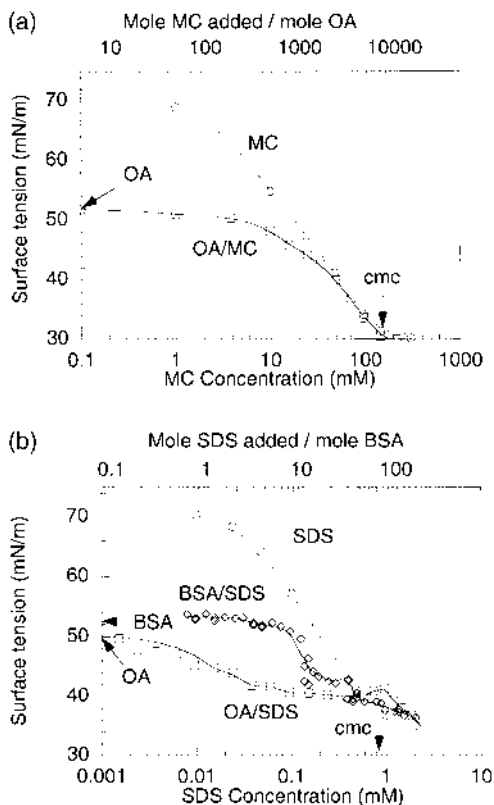


Figure 6 (a) Surface-tension isotherms of $21 \mu\text{M}$ ovalbumin (OA) (\square) in the presence of the nonionic monocaprin (MC) in water adjusted to pH 5.6, where the surface tension of the pure protein is marked with an arrow on the ordinate. Surface tension of pure MC is also shown (\circ) and the cmc is marked with an arrow on the abscissa. The surface-tension measurements were performed according to the drop-volume method as a function of time. The surface-tension value after 2000 s has been used for the isotherms. Further details are given elsewhere (171). (b) Surface-tension isotherms of $21 \mu\text{M}$ ovalbumin (OA) (\square) and $13 \mu\text{M}$ BSA (\diamond) in the presence of the anionic SDS in 0.05 M phosphate buffer, pH 5.6. The surface tension of the pure proteins are marked with arrows on the ordinate. The surface tension of pure SDS is also shown (\circ) and the cmc is marked with an arrow on the abscissa. Other conditions are the same as given for part (a). (c) Surface-tension isotherms of $21 \mu\text{M}$ ovalbumin (OA) (\square) in the presence of the cationic hexadecylpyridinium chloride (HPC) in water adjusted to pH 4.0. The surface tension of the pure protein is marked with an arrow on the ordinate. The surface tension of pure HPC is also shown (\circ) and the cmc is marked with an arrow on the abscissa. Other conditions are the same as given in part (a).

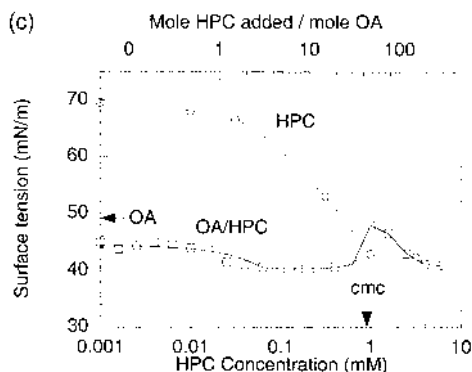


Figure 6 Continued.

and surface rheological techniques, developed an “orogenic” displacement model (173–175). This model is based on the adsorption of the displacing surfactant/lipid into localized defects in the heterogeneous protein network. These nucleation sites then grows, which leads to a compression of the protein network. During this initial stage, the protein film seems to be denser but not thicker. However, above a certain critical density, the film thickness starts to increase with the expanding surfactant domains while maintaining the protein film volume. Eventually, a protein network cannot withstand the high surface pressure, but it will collapse and the protein will be released and desorb from the interface. This model points at the importance of protein–protein and protein–interface interactions in relation to the interaction of the surfactant with defects in the protein network as well as with the interface.

Indirectly, the neutron reflectivity study on the binding of SDS onto preadsorbed layers of BSA at the hydrophilic silicon oxide–water interface by Lu et al. confirm the “orogenic” displacement model (176). Their results show a uniform layer distribution of SDS at low surfactant concentrations, whereas the distributions become unsymmetrical as the SDS concentration increases. The binding of SDS results in an expansion of the preadsorbed BSA layer from 35 Å in the absence of SDS to some 80 Å at $3 \times 10^{-4} M$ SDS, which Lu et al. interpreted as a considerable structural deformation of the protein. They based this interpretation on the close agreement between the volume ratio of SDS to BSA in the mixed layer of 0.45 and the literature value for the binding of SDS onto denatured protein in the bulk reported by Tanner et al. (140). The specular neutron reflection is sensitive to the density profile normal to the interface, but it does not give any lateral resolution. Therefore, the observations by Lu et al. (176) can also be explained by the “orogenic” displacement model (173–175).

The effect of the interfacial protein film age on the displacement of the protein from the surface of emulsion drops by nonionic water-soluble surfactants [Tween-20 and octaethylene glycol *n*-dodecyl ether ($C_{12}E_8$)] showed that β -lactoglobulin is harder to replace the longer the residence time was (177,178). Apart from the possible conformational changes that occur during the adsorption process, which can hamper displacement, it has been reported that β -lactoglobulin might polymerize through disulfide exchange at the oil-water interface (179). Consequently, the displacement of β -casein, which is a flexible and unordered protein without sulfhydryl groups, did not depend on the age of the film. Furthermore, it was observed that it was harder to replace β -lactoglobulin from a emulsion prepared close to the *pI* of the protein than at neutral pH, whereas the replacement from emulsions prepared at pH 3 was easier and no time effects was observed. Mackie et al. also studied displacement of β -lactoglobulin and β -casein by Tween-20, but from the air-water interface (173). They also found that β -casein was more easily displaced (i.e., β -lactoglobulin films breaks at higher surface pressures). Furthermore, stress invoked by penetration of the surfactant was found to propagate homogeneously through the β -casein film, which, in turn, resulted in the growth of circular surfactant domains at the interface. β -Lactoglobulin, on the other hand, was found to form elastic (gellike) networks at the air-water interface and the penetration of the surfactant therefore resulted in the growth of irregular (fractal) surfactant domains. Interestingly, Tween-20 preferentially displaced β -casein before β -lactoglobulin from a mixed β -casein/ β -lactoglobulin film at the air-water interface (174).

The effect of altering the protein conformational stability on the displacement of adsorbed protein layers by surfactants was also visualized at the solid-liquid interface by McGuire et al. (180). They found that the removal of wild-type and structural stability mutants of bacteriophage T4 lysozyme from hydrophobic and hydrophilic silica surfaces by a cationic detergent, decyltrimethylammonium bromide (DTAB), generally increased with the stability of the mutants.

Wahlgren and Arnebrant (181) investigated the effect of the surface properties on the displacement of adsorbed β -lactoglobulin (negative net charge) and lysozyme (positive net charge) by the cationic surfactant cetyltrimethyl ammonium bromide (CTAB) and the anionic SDS. They used hydrophobic (hydrophobised silica), negative (hydrophilic silica), neutral (chromium oxide), as well as positively charged (nickel oxide) surfaces and found four types of behavior for surfactant concentrations well above the cmc:

1. Surfactant binds to the protein and the complex desorbs on dilution. This was observed for SDS and β -lactoglobulin as well as

lysozyme on a negative silica surface and can be explained by simple electrostatic considerations. No adsorption from SDS–protein mixtures occurred.

2. The surfactant replaces the protein at the interfaces. This requires that the surfactant interacts more strongly with the surface than the protein, as was observed for CTAB with negative silica and SDS and CTAB with the hydrophobic surface when the adsorbed layer consisted of β -lactoglobulin.
3. The surfactant adsorbs reversibly on top of the protein layer. The protein–surface interaction is the stronger one and the surfactant is thus unable to solubilize the protein from the interface. This was observed for CTAB interacting with both proteins at the chromium oxide surface and SDS interacting with β -lactoglobulin at the nickel oxide surface.
4. Partial removal of the protein. This can be explained as due to the presence of multiple binding sites for the protein, which will give a combination of mechanism 1 and 2.

Others have made similar observations. For instance, Green et al. also studied the interaction between SDS and preadsorbed lysozyme at the hydrophilic silicon oxide–water interface by neutron reflectivity measurements (182). SDS binds cooperatively to the preadsorbed protein layer at intermediate surfactant concentrations, with no desorption of lysozyme from the interface. The protein was partly removed when the SDS concentration was increased to above 0.5 mM, whereas a surfactant concentration of 2 mM was required to completely remove both protein and surfactant from the interface in accordance with the type 1 behavior discussed.

3. Increased Surface Activity of the Lipid–Protein Complex

When comparing the data for the interaction between SDS and ovalbumin and the corresponding data for BSA, we clearly observe the different mode of interaction (Fig. 6b). The gradual decrease in surface tension with increasing surfactant concentration observed for ovalbumin and SDS mixtures can be explained by more efficient packing at the interface as discussed here. In addition, it has been argued that the electrostatic interaction between surfactant and protein might increase the hydrophobicity of the protein and, hence, its surface activity. The specific binding of SDS to BSA does not affect the surface tension until the concentration corresponding to saturation of the high-affinity binding sites is reached (i.e., 9–10 mol SDS per mole protein) (114), where a sharp decrease in surface tension is observed. This arises probably from an increase in the free-monomer concentration of SDS. The second plateau, indicating constant surfactant

monomer concentration, which is observed at increased surfactant concentration, is likely to be connected with saturation of the cooperative binding sites. As the surfactant concentration further increases, the surface-tension isotherms for the two protein–surfactant mixtures coincide. The second plateau observed in surface tension isotherms for ovalbumin and hexadecylpyridinium chloride (HPC) mixtures just below cmc of HPC (Fig. 6c) can be related to the electrostatic interaction between HPC and globular proteins that has been observed below the cmc in bulk solution (158). It is noteworthy that the surface tension is slightly lower than for pure HPC, suggesting that the complex is more surface active. Green et al. used specular neutron reflection and surface-tension measurements to study the adsorption of lysozyme and SDS at the air–water interface (183). Their results show that the lysozyme–SDS complexes are much more surface active than the unbound species as the surface excesses for both lysozyme and SDS increases and surface tension decreases upon addition of SDS (region A). Interestingly, the molar ratio of SDS to lysozyme was found to remain constant at about 7, although the total surface excesses increase with SDS concentration up to a surfactant concentration of $2.5 \times 10^{-4} M$. This indicates that the complex that adsorbed on the interface had a rather well-defined stoichiometric composition.

A further increase in SDS concentration beyond $2.5 \times 10^{-4} M$ led to a sharp decrease in the total surface excess, whereas the molar ratio of SDS to lysozyme increased. Eventually, as more SDS was added, the mixed protein–surfactant layer was replaced by a pure SDS monolayer.

The surface activity of the complex depends also on the properties of the interface, as shown by Wilde and Clark (152) for liquid interfaces. They found that the complex between Tween-20 and β -lactoglobulin was more surface active at the oil–water interface than at the air–water interface, where the same surface activity as for the nonbound protein was observed. The complexes adsorbed at both type of interfaces was, however, displaced by Tween-20 at the same surfactant-to-protein ratio. Here, we need to emphasize the difference in nature between the two types of liquid interface, the liquid–air and the one between two condensed media, which explains the experimental observations. The oil–water interface allows hydrophobic residues to become dissolved in and interact favorably with the oil phase, which is not possible at the air–water interface. We have also previously discussed that the unfolding of protein induced by the action of surfactants or by the presence of an interface generally leads to exposure of hydrophobic residues; that is, the unfolded protein can be substantially more “oil soluble” than the native one. This relates to the following section, dealing with molecular interactions, where it will be demonstrated that changes in oil-phase composition and hence solvent

properties also can lead to changes in the structure of the adsorbed protein film. At the hydrophobized silica–aqueous interface, it was found that the complex between β -lactoglobulin and SDS, formed at a high surfactant–protein ratio, but still below cmc of SDS, was more surface active than pure β -lactoglobulin (184).

4. Decreased Surface Activity of the Lipid–Protein Complex

The maxima in the surface-tension isotherm at HPC concentrations between 0.8 and 2.5 mM probably reflects an increased HPC–ovalbumin interaction in bulk solution (Fig. 6c). The formed highly charged complex is less surface active and an increase in surface tension is thus observed. The surface-tension maximum has been found to depend on ovalbumin concentration and is shifted toward higher HPC concentration at increased ovalbumin concentration (corresponds to 30 mol HPC per mole ovalbumin, independent of protein concentration) (185). The adsorption from mixtures of human serum albumin (HSA) and nonionic surfactant, decyl-dimethyl-phosphine-oxide (C_{10} DMPO) at the air-water interface was reported by Miller et al. (186). They reported an anomalous surface-tension increase for the mixtures at low surfactant concentrations to values higher than for the protein at the same concentration without the surfactant. Thus, it seemed that the surfactant–protein complex was less surface active. The likely explanation is that the nonionic surfactant is associated with HSA via hydrophobic interaction and thus makes the protein more hydrophilic and hence less surface active. Miller et al. also observed that the concentration range, where the coverage of protein and surfactant are comparable in the mixed surface layer was quite narrow (186).

The precipitation of protein in the bulk solution due to neutralization by added surfactant can also cause a decrease in surface concentration due to loss of surface-active material. Garcia Dominguez et al. (187) have shown that the surface-tension reduction of lysozyme and insulin at pH 3.5 (i.e., below pI) decreased when an anionic surfactant (SDS) was added, due to precipitation of the protein.

5. Protein–Lipid Interactions at the Interface

A synergistic effect on surface tension is seen for mixtures of proteins with both the anionic and cationic surfactants (Fig. 6b and 6c). For ovalbumin and SDS mixtures (Fig. 6b), a gradual decrease of the surface tension with increasing surfactant concentration is observed. This might be assigned to the more efficient packing in the formed mixed surfactant–protein layer compared to the one formed by the individual components at this concentration (171). Even at the lowest concentration of cationic surfactant

(0.05 mol HPC per mole ovalbumin), where the pure surfactant has the same surface tension as water, a decrease in surface tension for the protein–surfactant mixture, compared to pure ovalbumin, is observed (Fig. 6c). It is unlikely that any bulk interaction will affect the interfacial behavior at this low HPC-to-ovalbumin ratio. Therefore, the lowering in the surface tension probably arises from molecular interactions in the adsorbed surface film, giving a more condensed surface layer. Buckingham et al. (188) found a strong synergistic lowering of the surface tension of a mixed solution of SDS and poly-L-lysine at conditions at which no precipitation, micelle, or complex formation take place in the bulk solution. A similar behavior was observed for mixtures of low-molecular-weight surfactants of opposite charges (189). This effect has been assigned to the formation of electro-neutral complexes in the interfacial film.

Not only the composition of the interfacial layer but also the mechanical properties (e.g., the dilational viscosity) of the layer are important for the stability of emulsions and foams (8,11,14,190). In particular, both surface and bulk rheology as well as the disjoining pressure of the thin lamellae determine the stability of foams (14,191). Hence, in technical applications, thickeners are often added. The mechanical properties of interfacial films can, to a large extent, be controlled by the intermolecular interactions. This means that the protein stabilization of a foam is mainly due to protein–protein interaction and the destabilization is thought of as a disruption of these interactions. Sarker et al. (21) discussed the effect of the surfactant properties on the stability of interfacial films in foams. The addition of small amount of lysophosphatidylcholine (LPC) was found to increase the foam stability of β -lactoglobulin foams (21). A further increase of the surfactant concentration led to a decrease of the foam stability. The surface tension versus molar ratio of LPC and β -lactoglobulin shows an inflection point close to a molar ratio of unity, corresponding to the binding of the surfactant to the protein. No increase of foam stability was, however, observed for mixtures of Tween-20 and β -lactoglobulin, instead, the stability decreased with increasing surfactant concentration (192). The same observations were made for the stability of an oil-in-water emulsion, where it was found that small amount of Tween-20 increased the rate of shear-induced coalescence of β -lactoglobulin-stabilized emulsion droplets (178). The marked reduction in surface shear viscosity even at low surfactant-to-protein ratios confirmed that loosening of the protein layer occurred. The protein–surfactant complex is thought of being less surface active and a further increase of the surfactant concentration will lead to replacement of protein and protein–surfactant complexes with the surfactant at the interface (192,193). The mobility of the protein in a protein-stabilized thin liquid film, as measured with the fluorescence recovery after photobleaching technique (FRAP),

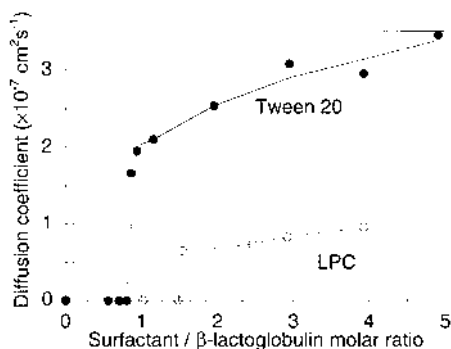


Figure 7 The effect of surfactant addition on the lateral diffusion in the adsorbed mixed layer of surfactant and β -lactoglobulin, measured with the FRAP technique. The diffusion coefficients of the fluorescent probe 5-*N*-(octadecanoyl)aminofluorescein and fluorescein isothiocyanate isomer 1 labeled β -lactoglobulin measured in the presence of L- α -lysophosphatidylcholine (○) and Tween-20 (●), respectively, are shown as a function of the molar ratio between surfactant and β -lactoglobulin. The data are adopted from the work of Sarker et al. (21) and Coke et al. (192), respectively, in which the experimental details also are given.

increases at lower surfactant-to-protein ratio for Tween-20 than for LPC (Fig. 7). This was attributed to the stronger binding of Tween-20, compared with LPC, to β -lactoglobulin (21) and will also explain why the foam becomes unstable at a lower surfactant concentration when Tween-20 is used. The foaming properties of puroindoline from wheat was found to be improved by the addition of LPC to protein molar ratio of 1–10 (154). This was assigned to the forming of a complex, which prevents the interfacial aggregation of the protein. Once the surfactant concentration becomes large enough, the protein–protein interactions within the surface film will be prevented, the mobility increased, and, thus, the foam stability decreased.

An ionic surfactant can also induce flocculation of protein-stabilized emulsions and this is dependent on the nature of the protein–lipid interaction, as discussed by Chen and Dickinson (134,135,194). An anionic surfactant, sodium lauryl ether sulfate (SLES), at sufficient concentration has been found to flocculate gelatine-stabilized oil-in-water emulsion (134). A further increase in surfactant concentration was found to lead to a restabilization of the flocculated emulsion. In bulk solution, the anionic surfactant will, at high enough concentrations, cause precipitation of the positively charged gelatine. At a further increased surfactant concentration, the precipitate was redispersed. Gelatine was initially displaced by SLES from the interface (194), but an increase of the surfactant concentration led to an increase of gelatine concentration at the interface and the

surface charge became partly neutralized (135), causing flocculation. A further increase of the surfactant concentration led to a decrease of the gelatine surface concentration (194) and a restabilization of the emulsion (134). It was also observed that the addition of SLES to a β -lactoglobulin-stabilized emulsion not did cause any flocculation, although some kind of complex was formed in bulk solution. It should be kept in mind that β -lactoglobulin was negatively charged under the experimental conditions used. This confirms the electrostatic nature of the observed SLES-induced flocculation of the emulsions stabilized by the positively charged gelatine. Flocculation of β -lactoglobulin-stabilized emulsions was, however, observed in the presence of gelatine and SLES. Because it only occurred above the cmc of the surfactant, it was suggested to depend on cross-linking of the emulsion droplets by surfactant micelles (134).

V. INTERACTIONS BETWEEN PROTEINS AND WATER-INSOLUBLE LIPIDS

In this section, we will discuss interactions involving lipids with low solubility, where the lipids exist as dispersed particles, liposomes or vesicles, liquid crystalline phases, as well as monolayers at interfaces. Many of the principles discussed in the earlier sections also apply for protein–lipid interactions in condensed systems. Polar lipids, which normally are water insoluble, associate into a variety of structures in aqueous solution. This process will have an impact on interactions with proteins. For water-soluble surfactants, the association with proteins mainly involves a surfactant in the monomeric state, whereas for insoluble lipids, the association structures also have to be considered. We also note that even polar lipids that are considered water insoluble have a certain monomer solubility, which, although small (about 10^{-7} for mono-olein and about 10^{-10} – 10^{-12} M for phospholipids), makes it possible for them to interact with proteins in the monomeric form—in particular, if the protein has a high-affinity binding site for the lipids. This is demonstrated in Fig. 8, which shows the thermograms from differential scanning calorimetry (DSC) measurements of β -lactoglobulin, distearoylphosphatidic acid (DSPA), and β -lactoglobulin + an aqueous dispersion of DSPA. We note that the peak corresponding to the thermally induced unfolding transition of β -lactoglobulin in the presence of DSPA is shifted toward a higher temperature compared to the one recorded for the pure protein. This confirms the presence of a specific interaction between phosphatidic acid and β -lactoglobulin that thermally stabilize the protein. This was also observed in the presence of dipalmitoylphosphatidic acid (DPPA), but no such interaction was observed

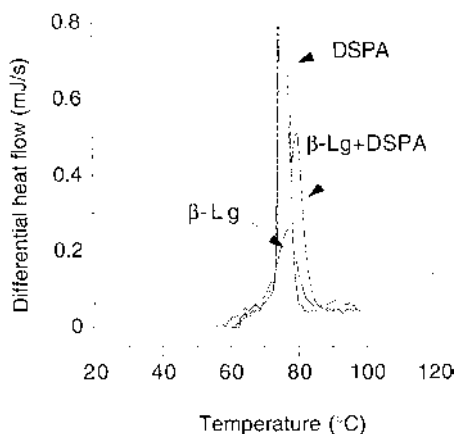


Figure 8 The interaction between DSPA and β -lactoglobulin (β -Lg) is demonstrated by the results from differential scanning calorimetry, where the thermogram of the protein-lipid mixture is compared with those of the pure components. Thermograms of DSPA, 5% (w/v) (—), β -Lg 5% (w/v) (- - -), and a mixture of β -Lg 5% and DSPA 5% (w/v) (- · - ·) in 1% sodium chloride at pH 7. A scanning rate of 10°C/min was used. (Data from Ref. 22, where the experimental details are given.)

when the protein was mixed with phosphatidylcholine, phosphatidylethanolamine, or phosphatidylglycerol (22). Neither could any interaction be observed if the lipid contained unsaturated fatty acid residues. Thus, the results show that the interactions between β -lactoglobulin and phospholipids are strongly dependent on the acyl chain as well as the head group. A small negatively charged head group is needed for the interaction to take place. Such an interaction can have important implication for the functional properties of the protein. We discussed earlier that fatty acids bound to β -lactoglobulin could affect the interfacial behavior of the protein (128). Kurihara and Katsuragi (277) reported that a lipid-protein complex formed between β -lactoglobulin and phosphatidic acid could mask a bitter taste. This property was suggested to be specific for phosphatidic acid, as no effect was observed for mixtures of β -lactoglobulin and phosphatidylcholine, triacylglycerol, or diacylglycerol.

The large number of studies using lipid monolayers at the air-aqueous interface and spread or adsorbed proteins have given us the basic knowledge of the interaction between proteins and polar lipids with low aqueous solubility. Therefore, we will start to discuss some of the main conclusions that can be drawn from such studies. The following subsections will address the interaction with oil-aqueous interface, vesicles, and liquid-crystalline phases.

A. Lipid Monolayers at the Air–Aqueous Interface

1. Driving Force for Lipid–Protein Interactions

Electrostatics. Phospholipid– β -lactoglobulin interactions at the air–aqueous interface has been investigated by Bos and Nylander (195) using the surface film balance. Some of their findings are summarized in Fig. 9, where

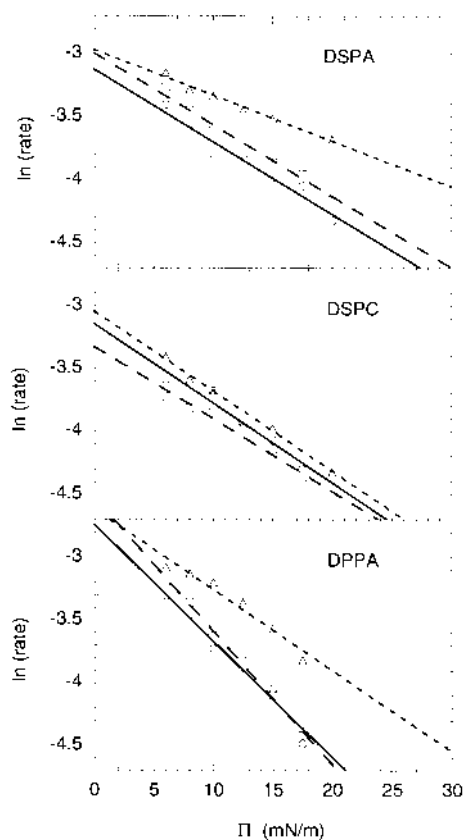


Figure 9 The rate of incorporation of β -lactoglobulin into monolayers of DSPA, DSPC, and DPPA versus surface pressure (Π). The data were recorded at constant surface pressure by measuring the area increase of the lipid monolayer spread on a protein solution contain 1.15 mg/L in 10 mM phosphate buffer of pH 7, with 0 mM ($\text{---}\circ\text{---}$), 50 mM ($\text{---}\square\text{---}$), or 150 mM ($\text{---}\triangle\text{---}$) sodium chloride. The rate (in mg/m^2) was calculated from the area increase by using the Π -area isotherm of spread monolayers of β -lactoglobulin. Data from Ref. 195, where the experimental details are given.

the rate of incorporation of β -lactoglobulin into monolayers of DSPA, distearoylphosphatidylcholine (DSPC) and DPPA is shown versus surface pressure (Π) at pH 7. The rate was calculated using a simple first-order kinetics model (8), where only the surface pressure barrier is taken into account. The highest rate of adsorption of β -lactoglobulin into a phospholipid monolayer was observed for anionic DSPA. The incorporation of the protein take also place at a higher surface pressure into a DSPA monolayer than into a monolayers of the other lipids. Because the β -lactoglobulin, with a zero net charge at pH \approx 5.2 (196), has a positive net charge at pH 4, a larger rate of adsorption into the negatively charged phosphatidic acid monolayers would be expected under acidic conditions. However, almost the same rates were found (195). As discussed earlier, anionic lipids seems to interact more strongly with proteins (i.e., to its cationic amino acid residues) compared to lipids with no or positive net charge. The incorporation into the zwitterionic DSPC monolayers is as expected less salt dependent than what was observed for the phosphatidic acid monolayers, where the rate increases with increasing ionic strength of the subphase. Probably, this is a consequence of a decreased repulsion within the phosphatidic acid protein monolayer at a higher ionic strength. The findings by Bos and Nylander (195) is somewhat contradictory to the findings of Cornell and Patterson, who studied the adsorption β -lactoglobulin to a negatively charged lipid monolayer, composed of a mixture of palmitoyloleoylphosphatidylcholine (POPC) and palmitoyloleoylphosphatidylglycerol (POPG) (65/35 mol%). They only observed a substantial binding of β -lactoglobulin at pH 4.4, which is when the protein carries a net positive charge, but not at higher pH (pH 7) (197). The differences probably arises from the different lipids and methodology used by Cornell et al. (197–199). Cornell et al. measured the amounts of protein adsorbed to the lipid layer by transferring the layer to a solid support. During the transfer, the surface pressure was kept at 30–35 mN/m, thus preventing insertion of portions of the protein in the lipid monolayer (199). Only protein molecules that interact strongly with the lipid head groups are transferred to the solid supported. Another difference is that their surface pressure data of the protein penetration is recorded under constant area, not at constant pressure, as in our study. In addition, Cornell et al. used lipids with their chains in the liquid state, which, as will be discussed, can influence the interaction. Cornell (198) also observed a specific interaction between β -lactoglobulin and egg yolk phosphatidic acid (e-PA) in spread mixed films at low pH (1.3 and 4) where β -lactoglobulin carries a positive net charge. No interaction was observed for e-PA in the neutral pH range or for egg yolk phosphatidylcholine (e-PC). Similar observations was made for the interaction between α -lactalbumin or BSA with mixed monolayers of POPC and POPG, where adsorption was

observed below the isoelectric point of the protein, where the lipid layer and the protein carry opposite net charge, but less was adsorbed around and almost nothing above the isoelectric point (199). The interaction was reduced in the presence of calcium as well as at increased ionic strength. Cornell et al. thus concluded that the interaction is of an electrostatic origin.

The work of Quinn and Dawson concerning the interaction between cytochrome-*c* (positive net charge below pH 10) and phospholipids from egg yolk also stresses the importance of the electrostatic interaction, although conformational changes of the protein are of importance (200,201). They measured the pressure increase caused by the penetration/adsorption of the protein to the lipid monolayers as well as the amount adsorbed by using ^{14}C -labeled protein. Their results show that the limiting pressure for penetration is 20 and 24 mN/m for phosphatidylcholine and phosphatidylethanolamine, respectively, whereas penetration into the phosphatidic acid and diphosphatidylglycerol (cardiolipin) monolayers occurred up to pressures close to the collapse pressure of the film (<40 mN/m). Furthermore, the penetration into the e-PC monolayers was not affected by increasing the sodium chloride concentration to 1 *M*. Cytochrome-*c* bound to the e-PC monolayers could not be removed by increasing the ionic strength. This is in contrast to the cardiolipin and e-PA monolayers, where the penetration was reduced when the sodium chloride content was increased to 1 *M*. It was also possible to partly desorb some cytochrome-*c* from e-PA monolayers. However, the pH dependence of the interaction was found to be quite complex, which suggests that subtle changes in the protein conformation also affect the interaction.

The importance of the electrostatic interaction with the phospholipid head group has also been shown by the work of Malmsten et al. (202,203), who studied the interaction of human serum albumin, IgG, and fibronectin from human plasma with phospholipid layers spin-coated onto methylated silica surfaces. Generally, he found no interaction between the proteins and lipids with no net charge or with shielded charges (e.g., phosphatidylcholine, phosphatidylethanolamine, sphingomyelin, and phosphatidylinositol), whereas interaction was observed with the surfaces containing unprotected charges (e.g., phosphatidic acid, diphosphatidylglycerol, and phosphatidylserine).

Hydrophobic Interactions. As observed in Fig. 8, the rate of adsorption of β -lactoglobulin into DPPA monolayers was significantly lower than into the monolayers, where the corresponding lipid had a longer chain length. This points to the importance of hydrophobic interactions for the incorporation. It was also observed that the incorporation was much faster

into the lipid monolayer than into its own proteinous layer, being less “oil-like” than the lipid layer (195). In addition, repulsive steric and electrostatic forces might contribute the lower rate of incorporation. Quinn and Dawson (201) found that the threshold surface pressure, above which no penetration of cytochrome-*c* took place in phosphatidylcholine monolayers, was considerably lower when DPPA was used instead of hydrogenated e-PC. The latter lipid contained fatty acid with a longer chain length, about 60% C₁₈ and 30% C₁₆. Du et al. (204) studied the influence of the alkyl chain length of glucolipids (dialkyl glycerylether- β -D-glucosides and dialkyl glycerylether- β -D-maltosides) on the interaction between lipid monolayers and glucose oxidase. The interaction, as shown by an increase in surface pressure, was found to increase with increasing lipid chain lengths for both types of lipid. These results suggest that the hydrophobic interaction is the predominant force. Furthermore, it is interesting to note that the interactions were not so strong with the lipids having the more bulky head group (i.e., the dialkyl glycerylether- β -D-maltosides), although the Π -*A* isotherms for the corresponding dialkyl glycerylether- β -D-glucosides were similar. This illustrates that a bulky head group can sterically hamper the protein-lipid (hydrophobic) interaction.

Effect of Lipid Fluidity. The complete hydrogenation of e-PC was found not to affect the surface pressure threshold for penetration of cytochrome-*c* compared to the native e-PC (201). However, the change in surface pressure due to the penetration of the protein versus initial surface pressure was less steep for the saturated one. A similar trend was observed for the e-PE samples (200). The conclusion was that the limiting pressure for penetration to take place is likely to be determined by the work necessary for the penetration, that is $\int \Pi dA$, where an area, *A*, of the interface has to be created for the protein to penetrate. Once the penetration is feasible, the magnitude will depend on the space between the molecules, and, thus, the degree of penetration is expected to be lower for the hydrogenated sample (201). The surface pressure threshold below which penetration of cytochrome-*c* into the anionic diphosphatidylglycerol (cardiolipin) monolayer took place was also found to decrease when the lipid was fully hydrogenated (201). Ibdah and Phillips found the same trend in their study of the effect of lipid composition and packing on the penetration of apolipoprotein A-I into lipid monolayers (205). In the biological system, this protein interacts with the phospholipid membrane of the serum high-density lipoprotein (HDL) particles (see Section V.B). Their results show that this protein adsorption occurs, to a larger extent, on expanded monolayers than on condensed monolayers (i.e., protein adsorption decrease in the order e-PC > egg sphingomyelin > DSPC). Furthermore, it was found that

protein adsorption generally decreased with an increasing amount of cholesterol in the lipid monolayer. It was suggested this was due to the condensing effect of cholesterol.

Effect of Protein Structure. Evidence of the importance of the protein structure was provided by Hanssens and Van Cauwelaert (206), who studied the penetration of α -lactalbumin in monolayers of DPPC and cardiolipin at physiological pH (pH 7.4) and at pH 4.6 with and without calcium. Reports have indicated that the protein is transferred to an intermediate, partially unfolded (molten globule) state at low pH and by depletion of calcium (101,103,104), which would expect to facilitate the penetration of α -lactalbumin into the monolayer. Furthermore, it has been reported that the calcium-free form of α -lactalbumin is more hydrophobic (207). Indeed, penetration occurred at low pH and was prevented if the protein was adsorbed from a calcium solution (206).

It is not easy to in situ monitor the structural changes of the protein on binding to a lipid monolayer. However, they can be monitored indirectly by recording the circular dichroism (CD) spectra of the mixed protein–lipid film transferred to a quartz plate. This technique was used to recorded CD spectra for β -lactoglobulin, α -lactalbumin, or BSA bound to mixed monolayers of POPC and POPG (197,199). The spectra show that the protein bound to the lipid monolayer was similar to the one recorded in solution, indicating that the conformation of the protein did not change significantly when interacting with the lipid monolayer.

2. Structure of the Interfacial Film

Even from the study of the penetration of protein versus surface pressure, it is also possible get some hints about the structure of the mixed layer. Cornell et al. (197,199) observed penetration of β -lactoglobulin, α -lactalbumin, or BSA into mixed monolayers of POPC and POPG at such high surface pressure that it is unlikely that the proteins could penetrate into a protein layer. Thus, they concluded that the formation of pure protein patches is unlikely and that portions of the protein is suggested to be intercalated into the lipid monolayer. Bos and Nylander made similar observation for the interaction between β -lactoglobulin and DSPC and DSPA monolayers (195).

Fluorescence microscopy and Brewster-angle microscopy (BAM) can be used to in situ image the structure of the film at the air–aqueous interface, although the lateral resolution is limited by the resolution of the optical microscope. Fluorescence microscopy together with the surface film balance technique was used by Heckl et al. to study the structure of

mixed phospholipid–cytochrome-*c* and cytochrome-*b* films (208). They found that proteins primarily were located in the fluid membrane phase, which coexisted with solid lipid domains without protein. The penetration into the lipid monolayer was reduced with increasing pressure. Cytochrome-*c* (positively charged) was found to interact with dimyristoylphosphatidic acid (DMPA) monolayers but not with dipalmitoylphosphatidylcholine (DPPC) layers, showing the electrostatic nature of the interaction. Schönhoff et al. concluded from their study of the incorporation of membrane proteins into DPPA/DOPA monolayers that incorporation mainly takes place in the fluid phases of the matrix (209). Zhao et al. used BAM to image the kinetics of β -lactoglobulin penetration into DPPC monolayers at the air–aqueous interface from a 500-nM solution in 10 mM phosphate buffer, pH 7 (210). For instance, at an initial surface pressure of 7.8 mN/m, it took 0.17 min until domains, with similar morphology as those appearing during the compression of a pure DPPC monolayer, appeared. These domains were found to consist only of the lipid, as confirmed by grazing incidence x-ray diffraction, and β -lactoglobulin penetration was found to occur without any specific interaction with DPPC. β -Lactoglobulin was not able to penetrate into a condensed DPPC monolayer (i.e., above a surface pressure of about 20 mN/m).

The lateral organization in mixed protein–lipid films at the air–aqueous interface can be studied by spectroscopic techniques and high-resolution imaging techniques such as electron microscopy and atomic force microscopy (AFM), after transferring the films to a solid support. Using electron microscopy, Cornell and Carroll found that only lipids with the chains in liquid state (e-PA, dioleoylphosphatidylcholine, and dioleoylphosphatidylethanolamine) formed homogenous films with β -lactoglobulin, whereas DPPA and DSPC formed heterogeneous layers (211). The use of AFM as powerful technique for studying the lateral organization in mixed films of proteins and soluble surfactants has already been demonstrated with the development of the “orogenic” displacement model (173–175). Diederich et al. studied the interaction between bacterial surface layer proteins (S-layer proteins) and phosphatidylethanolamine (DMPE and DPPE) monolayers using dual-label fluorescence microscopy, Fourier transform infrared (FTIR) spectroscopy, and electron microscopy (212). When the monolayer is in the two-phase region, with one isotropic and one anisotropic fluid phase, the S-layer protein adsorbed preferentially to the isotropic phase. However, two-dimensional crystallization could be nucleated in the boundaries between the two phases, but proceeded mainly underneath the anisotropic phase. The FTIR measurements clearly indicate that the protein crystallization leads to an increased order of the lipid acyl chains.

3. Monolayer Stability

One might expect that monolayer made up of lipids with a very low aqueous solubility would be stable. However, this is far from general. The metastability of monolayers can be caused by processes such as rearrangement within the layer, dissolution into the subphase, and transformation to a three-dimensional phase, which can occur at pressures above the equilibrium spreading pressure (213,214). Furthermore, the stability of the monolayers can be affected by the spreading solvent and the techniques used for spreading the lipid (215,216). The stability of the monolayer can also be considerably changed by the ion composition of the aqueous subphase. For instance, the stability of an arachidic (*n*-eicosanoic, C_{20:0}) acid monolayer was found to increase in the order H⁺ < Li⁺ < Na⁺ < Ca²⁺ < Mg²⁺ (213). There are several examples of proteins that are thought to have the role to stabilize a lipid monolayer or bilayer. One such example is the milk fat globule membrane that has been suggested to consist of the monolayer of polar lipids, which covers the fat globule surface, and an outer lipid-based bilayer (217,218). The milk fat globule membrane is expected to be inhomogeneous, with a significant amount of proteins in the membrane. An aqueous layer containing different proteins, like xanthine oxidase, is present between the monolayer and bilayer. One of the roles that have been assigned to xanthine oxidase is to stabilize the milk fat globule membrane (218). Interestingly, Kristensen et al. found that the presence of a xanthine oxidase can increase the stability of a monolayer composed of sphingomyelin from the milk fat globule membrane (219). They investigated the interaction between one of the major proteins, xanthine oxidase, and the major lipids, sphingomyelin and phosphatidylcholine, in the milk fat globule membrane at the air–aqueous interface by using the monolayer technique. Both lipids have a similar phosphorylcholine head group, which is zwitterionic in the neutral pH range, although the belt regions linking the phosphorylcholine group with the acyl chains are different. The Π–A isotherms of sphingomyelin and phosphatidylcholine are shown in Figs. 10a and 10b, respectively. The isotherms for sphingomyelin monolayers spread on pure buffer and a xanthine oxidase solution are shown. The slope of isotherm and the area of the compressed monolayer for pure sphingomyelin (Fig. 10a) are smaller than expected for these types of lipid. In addition, the large hysteresis and the dependence on the compression speed, not observed for distearoylphosphatidylcholine, confirms that the sphingomyelin monolayer is metastable. The difference in stability of monolayers formed by two different lipids can probably be related to the different conformations of choline groups in the two types of lipid, where intramolecular hydrogen-bonding is possible between the phosphate group and the amide and hydroxyl groups

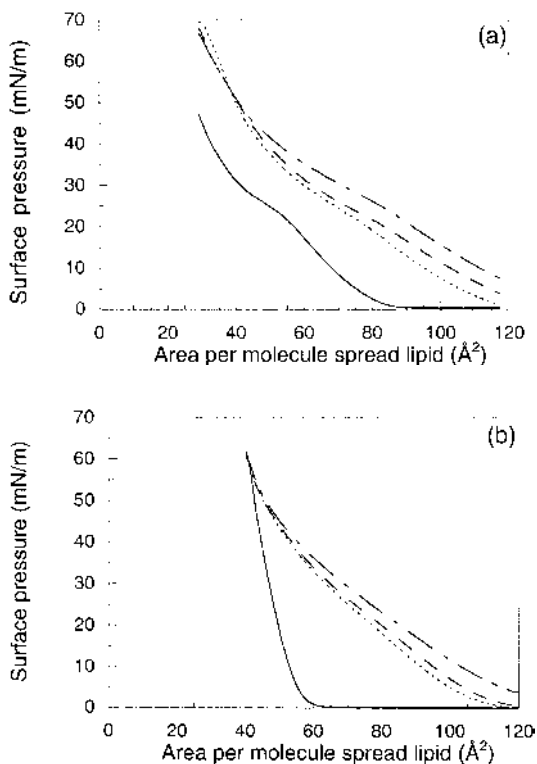


Figure 10 Dynamic surface pressure (Π) as a function of the molecular area of the spread amount lipid for compression of (a) sphingomyelin and (b) DSPC monolayers on a phosphate-buffered subphase (40 mM phosphate containing 0.1 M sodium chloride, pH = 7.4) with or without xanthine oxidase (5 mg/mL). The isotherms recorded for the lipid spread on pure buffer (—) and at 5 (- - -), 10 (- · -), and 20 (· · ·) min elapsed between spreading and compression. The lipid (25 μ g) was spread from a chloroform/methanol (2:1, v/v) solution on a maximum area of 50 \times 450 mm² and a compression speed of 12.5 mm/min was used. (Data from Ref. 219, where the experimental details are given.)

in the belt region of sphingomyelin (220). An increase in Π at maximum compression of the sphingomyelin monolayer, which reflects an increase in the monolayer stability, was observed in the presence of sphingomyelin. Furthermore, the area per sphingomyelin molecule increases in the presence of xanthine oxidase even at high Π values. This is in contrast to the results from the parallel study of the phosphatidylcholine monolayers with and without xanthin oxidase, where the interacting protein could be completely

squeezed out from the lipid monolayer at high enough surface pressures without affecting the collapse pressure. This indicates that the interaction between xanthine oxidase and sphingomyelin is much stronger than that between the protein and phosphatidylcholine.

B. Protein-Lipid Interactions at the Oil–Aqueous Interface

Most studies of protein–lipid interactions at the oil–aqueous interface has been carried out using model emulsions. The purity of polar lipid and the way it is added (e.g., to the oil or the water phase) are bound to affect the interactions with proteins, which, in turn, affect the emulsion stability. Yamamoto and Araki (221) studied this by comparing the interfacial behavior of β -lactoglobulin, in the presence of lecithin (PC) in the water or in the oil phase, with the stability of corresponding emulsions. In the presence of protein, crude lecithin was found to increase the stability of emulsion and lower the interfacial tension more effectively than a pure lecithin preparation. When crude lecithin was added to the oil phase, the interfacial tension was found to decrease and the emulsion stability increased compared to when the lecithin was dispersed in the aqueous phase. One might speculate whether these findings can be related to the presence of fatty acid and/or charged phospholipids in the crude lecithin. Aynié et al. studied the interaction between nitroxide homologs of fatty acids and milk proteins by following the mobility of the nitroxide radicals using electron spin resonance (222). At pH 7, the importance of the lipid–protein interaction was not determined by the structure of the protein, but positively correlated with the number of positive charges on the protein. Thus, it was observed that the importance of the interaction in the emulsions decreased in the order α_{s1} -casein > β -lactoglobulin > β -casein, suggesting that the interaction was of an electrostatic nature. The different proteins also affect the organization of the lipid monolayer, where α_{s1} -casein, in contrast to β -lactoglobulin and β -casein, induce, an ordering of a monolayer of nitroxide fatty acids on the surface of an emulsion droplet (222). This can probably be assigned to the stronger interaction of α_{s1} -casein with lipids compared to the other proteins.

Bylaite et al. studied the stability and droplet size of β -lactoglobulin- and lecithin [phosphatidylcholine from soybean (sb-PC)]-stabilized emulsions of caraway essential oil as well as the amount of protein on the emulsion droplets (223). It should be noted that sb-PC was dispersed in the oil phase. Some of their data are given in Fig. 11, where the amount of β -lactoglobulin adsorbed on the oil–aqueous interface is shown versus amount added of s-PC. These data show that sb-PC is likely to replace some of the protein at the oil–aqueous interface, although it is unable to completely replace the protein. The maximum reduction in the amount of

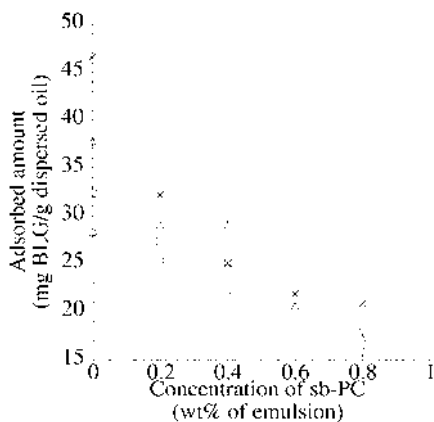


Figure 11 Adsorbed amount of protein at the caraway essential oil–water (Δ , \times) and olive oil–water (\circ , \square) interfaces in emulsions stabilized by 1 (Δ , \circ) and 2 (\times , \square) wt% β -lactoglobulin and variable amount of soybean-PC. Emulsions were prepared from 15 wt% oil in a 60 mM phosphate buffer of pH 6.7. (Data Ref. 223 where the experimental details are given.)

β -lactoglobulin adsorbed is by a factor of 3 for the caraway oil. These findings are in agreement with other studies, where lecithin was found to be less efficient in displacing milk proteins from the oil–water interface compared to other surfactants (224,225). Bylaite et al. found that emulsions with triglyceride oil generally proved to be more stable compared to those made with caraway essential oil as the dispersed phase (223). However, the stability of the emulsions could be improved considerably by adding sb-PC. An increase in the protein concentration also promoted emulsion stability. Fang and Dalgeish arrived at a somewhat different conclusion for casein-stabilized emulsions (226). They found that the presence of DOPC destabilized casein-stabilized emulsions of soybean oil in 20 mM imidazole/HCl at pH 7.0. This seemed to be independent on whether DOPC was present during emulsification or if it was added to the emulsion as dispersed aggregates. At a high concentration of casein, the emulsions were stable, and the decrease in surface load was a direct indication of the removal of casein from the interface by the presence of DOPC. The higher the DOPC concentration, the greater was the effect on emulsion stability and surface load. DPPC and egg PC either enhanced or did not affect the stability of the emulsion.

Bylaite et al. applied ellipsometry to study the adsorption of the lipid from the oil and the protein from the aqueous phase at the oil–water interface (223). Independently of the used concentration, close to monolayer coverage

of sb-PC was observed at the caraway oil–aqueous interface. On the other hand, at the olive oil–aqueous interface, the presence of only a small amount of sb-PC led to an exponential increase of the layer thickness with time beyond monolayer coverage. This interesting observation was assigned to the formation of a multilamellar layer of sb-PC at the olive oil–aqueous interface, when sb-PC reached the solubility limit in the olive oil.

The displacement of caseinate from the interface of emulsion droplets by monoglycerides, mono-oleoylglycerol, and monostearoylglycerol dissolved in the oil phase was found to correlate with the adsorption of the monoglycerides at the oil–water interface (227). The amount of mono-oleoylglycerol increased gradually with concentration and reached a plateau when approaching an oil-phase concentration of 1 wt%. Under these conditions, all of the caseinate was displaced from the interface. The saturated lipid, monostearoylglycerol, was much more efficient in displacing the protein. Already, at a concentration in the oil phase of between 0.2 and 0.3 wt%, the adsorbed amount of monostearoylglycerol increased sharply and reached much higher surface concentrations than mono-oleoylglycerol. At 0.3 wt%, all of the caseinate was removed from the interface.

C. Protein Interactions with Lipid Vesicles

The mechanisms that determine the stability, size, and shape of vesicles are complex and widely discussed (for reviews, see, e.g., Refs. 80–83). The spherical shape is generally the most stable shape for equal distribution of molecules between the two monolayers constituting the bilayer (81). These spherical vesicles can be large multilamellar vesicles (MLV) and large (LUV) and small (SUV) unilamellar vesicles (81). The bending of the lipid bilayer to form a vesicle imposes a strain on a symmetric bilayer, as the inner monolayer has a negative curvature, whereas the outer has a positive curvature. The magnitude of this curvature energy can be difficult to estimate, but it is thought to be significant enough in many cases to make the vesicles inherently unstable and energy has to be added to form them (81–83). The result of the tension can be a nonspherical vesicle (228). A mixture of phospholipids, which corresponds to the composition in the milk fat globule membrane, gives both spherical vesicles and tubular structures (229). In particular compositions (e.g., 80% DOPE, 12% DOPC, and 8% sphingomyelin) that at high lipid content give liquid-crystalline phases at the boundary of lamellar to reversed hexagonal phase tend to give microtubular structures at high water content rather than vesicles. A larger proportion of multilamellar vesicles were observed in buffer and divalent salts than in pure water. A small increase in the interlayer spacing

of the multilamellar vesicle was observed in the presence of β -lactoglobulin and β -casein.

1. Driving Force for the Protein–Vesicle Interaction

The driving mechanism for the interaction of proteins with the lipid bilayer of the vesicles are basically as for the interaction a lipid monolayer at the air–aqueous interface. In parallel to the Quinn and Dawson study discussed earlier (200,201), Rytömaa et al. (230) found a strong electrostatic contribution when cytochrome-*c* binds to cardiolipin–phosphatidylcholine liposomes. This interaction did not take place if the negatively charge lipid cardiolipin was absent in the membrane. Furthermore, the protein was dissociated from the vesicle in the presence of 2 mM MgCl_2 and 80 mM NaCl at pH 7. The apparent affinity of cytochrome-*c* to the vesicles also increased when the pH was dropped to 4. The interaction was found to be completely reversible for pH changes; that is, if the pH was increased to 7, the protein could be dissociated from the vesicle by adding salt.

Price et al. studied the adsorption of fibrinogen to neutral liposomes, composed mainly of phosphatidylcholine (PC) and cholesterol and negative liposomes, composed mainly of phosphatidic acid (PA) and cholesterol, as well as to the corresponding liposomes in which a polyethylene glycol (PEG)-modified phosphatidylethanolamine had been introduced (231). They found that negatively charge liposomes adsorbed more fibrinogen than the corresponding neutral liposomes. PEG modification was found to have no effect on neutral liposomes in terms of fibrinogen adsorption. However, PEG modification, which sterically stabilizes the liposome, markedly reduced the adsorption to the negative liposomes.

Brooksbank et al. conducted an extensive study on the interaction of β -casein, κ -casein, α_{s1} -casein, and β -lactoglobulin with negatively charged e-PG and zwitterionic e-PC vesicles using photon correlation spectroscopy (232). Their data on the adsorption of β -casein are shown in Fig. 12. All of the studied proteins were found to give a thicker layer on the negatively charged vesicles, although they all carried a negative net charge under the conditions used (160 mM sodium chloride at pH 6.2). Brooksbank et al. (232) suggested that binding to the vesicle surface takes place mainly through hydrophobic interactions and the differences in thickness of the adsorbed layers on the two types of vesicles were explained in terms of the protein charge distribution. For instance, the hydrophilic, N-terminal, part of β -casein has a net charge of -12 , whereas the remainder of the molecule carries almost no net charge. Thus, on the negatively charge vesicle surface, the molecules adopt a more extended configuration, as the N-terminal part is likely to be pushed away from the surface by means of

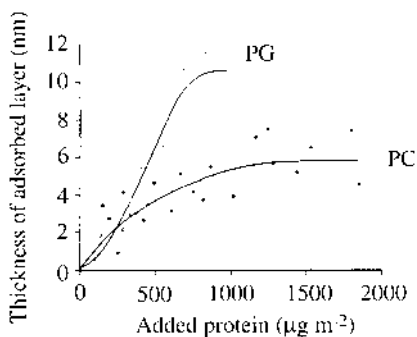


Figure 12 Thickness of adsorbed layer on β -casein on negatively charged e-PG and zwitterionic e-PC vesicles as a function added protein expressed as microgram of protein per square meter of available liposome surface. The liposomes were dispersed in 160 mM and the pH was about 6.2. The data are taken from a photon correlation spectroscopy study by Brooksbank et al, where further experimental details are given (232).

electrostatic repulsion. This explains the thicker layers on this surface as shown in Fig. 12. A similar reasoning can be applied for κ -casein. The apparently very thick adsorbed layer of α_{s1} -casein was explained by bridging flocculation of the vesicles mediated by the protein. The middle section of α_{s1} -casein carries a negative net charge, whereas the two ends have no net charge. One of the uncharged ends protrudes into the vesicle bilayer and the middle section is repelled from the vesicle surface, leaving the other uncharged end of the peptide chain free to interact with another vesicle. The charge distribution on β -lactoglobulin is more even and the interpretation of the results was not as straightforward.

As discussed by Kinnunen, the introduction of the H_{II} -forming double-chain lipid (a lipid with packing parameter > 1 ; see Fig. 1) in a lamellar membrane imposes a considerable stress on the membrane (1). This frustrated membrane is said to be in the L_e state according to the Kinnunen terminology (1). Free energy can be gained by allowing some of the lipids in the frustrated membrane to adopt the so-called extended or splayed chain conformation, where one of the acyl chains extends out from the bilayer, whereas the other chain remains in the membrane. Such an extend chain can also be accommodated within a proper (hydrophobic) cavity of protein interacting with the membrane (1). This is an interesting alternative explanation for the hydrophobic interaction between peripheral proteins and membranes that has been discussed in this review. The splayed chain conformation has also been suggest to be one mechanism for membrane fusion (2). This and other implications of

the splayed chain confirmation has recently been discussed by Corkery (233).

2. Influence of the Protein Structure on the Vesicle Interaction

Kim and Kim studied the interaction between α -lactalbumin and phosphatidylserine–phosphatidylethanolamine vesicles (1:1 molar ratio) versus pH (234). They found that the interaction, which almost did not exist at neutral pH, increased with decreasing pH (Fig. 13). What is interesting to note (Fig. 13) is that vesicle fusion, as estimated from the increase of the initial rate of Tb fluorescence increase, correlates with the binding of the protein to the vesicles. The binding was suggested to be due to hydrophobic interaction via protein segments penetrating into the lipid bilayer, as it was impossible to dissociate it by increasing the pH. This was further confirmed by using proteolytic enzymes, which were found to cut off both ends of the polypeptide chain, leaving only the segment that penetrates into the bilayer. This penetration protein loop was also believed to induce fusion of the vesicles.

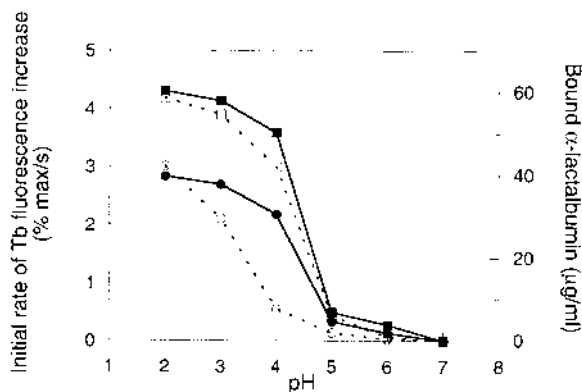


Figure 13 The initial rate of Tb fluorescence increase (---○---, ---□---) upon α -lactalbumin induced fusion of phosphatidylserine–phosphatidylcholine (1:1 molar ratio) vesicles is shown as a function of pH. The pH-dependent binding of α -lactalbumin is shown as the amount of protein bound per milliliter of vesicle suspension (—●—, —■—), which contained 1 mM lipid molecules (determined from the phosphor content) per milliliter of suspension. The results for initial protein concentrations of 50 (○, ●) and 100 (□, ■) μ g/mL are presented. As the curves for the fusion process represents kinetic data and the binding studies represent equilibrium data when the fusion process is over, only a qualitative comparison is possible. (Data Ref. 234, where the experimental details are given.)

The importance of the protein conformation on the interaction with vesicles was also shown in the study of Brown et al. (235). They found no interaction between native β -lactoglobulin and DPPC vesicles, but β -lactoglobulin, modified by exposing it to a 2:1 mixture of chloroform and methanol, did interact with the vesicles. Moreover, the lipid-protein complex formed had an α -helix content of at least 25–30% larger than for the native protein. The interaction was found to lead to aggregation of the vesicles at pH 7.2, whereas no aggregates were observed at pH 3.7. This was explained by the larger net charge at pH 3.7 (+20) compared to pH 7.2 (–10). These results imply that protein modification, either during processing or by special treatment, can increase the helix content, which, in turn can be boosted by lipid interaction. The lipid-protein complexes formed have been suggested as a way to improve the emulsification processes (236,237).

3. Lateral Phase Separation in Vesicle Bilayers

Raudino and Castelli reported that the presence of lysozyme could induced lateral phase separation in vesicle bilayers composed of a mixture of phosphatidic acid and phosphatidylcholine (238). Their differential scanning calorimetry study of the lipid chain melting transition showed good mixing in the absence of the protein and the single peak was shifted toward higher temperatures as the phosphatidic acid content increased. In the presence of lysozyme however, lateral phase separation did occur as the chain melting transition peak was split into two peaks. In addition, they found that the temperature of protein unfolding increased with the fraction of phosphatidic acid, suggesting a stabilization of the protein due to the interaction with phosphatidic acid.

It is important to bear in mind that microheterogeneity of the bilayer not only occurs for mixtures of different lipids but also close to the gel-to-fluid phase transition of the lipid. Hønger et al. studied the relation between phospholipase A_2 -catalyzed hydrolysis of one-component phosphatidylcholine vesicles and the microheterogeneity of the lipid bilayer (239). They varied the microheterogeneity by changing the temperature in the vicinity of the gel-to-fluid phase transition as well as using lipid chain lengths between C_{14} and C_{18} and found a strong correlation between the maximal lipase-lipid interaction and the maxima in the interfacial area between gel and fluid domains.

D. Protein Interaction with Liquid-Crystalline Phases/Gel Phases

As discussed previously, the interaction between water-soluble lipids and proteins usually takes place via monomers, and the associated surfactant

structures is generally formed in the same range, or higher, of surfactant monomer concentration as needed for the interaction to take place. For lipids with low aqueous solubility, on the other hand, the association structures, different lyotropic mesophases, are generally already present when mixed with the protein and have thus a profound impact on the protein–lipid interaction. It is therefore important to be familiar with the phase behavior of the particular lipid used because often seemingly conflicting results can be derived from differences in the phase structure of the lipids. For instance, we have observed that the interaction between β -lactoglobulin and phosphatidic acid only occurred when the lipids were present as a dispersion, but not when they were mixed in the gel state with the protein (22).

Even if no specific interaction occurs, proteins can have an impact on the liquid-crystalline phase or gel phase due to the limited space of the aqueous cavity. This was demonstrated by Minami et al., who investigated the incorporation of lysozyme, β -lactoglobulin, and α -lactalbumin in a sphingomyelin gel phase containing 0.6 wt% sodium palmitate and 80 wt% aqueous solution (240). The dimension of the aqueous layer in the gel phase was suggested to limit the amount of protein that could be incorporated. Above this limit, phase separation will occur with a gel phase and an “outside” protein-rich solution. The protein will, at high enough concentration, probably also compete for the water in the interlamellar spacing, which will eventually lead to a reduction of the aqueous layer thickness. This effect was demonstrated for high-molecular-weight polymers in equilibrium with the phosphatidylcholine lamellar phase (241). The polymer was unable to enter the aqueous layer, but still exerted an osmotic stress that was large enough to compress the lamellar lattice, as shown by x-ray diffraction data. This method has been used to measure the interaction between the lipid bilayers (241,242).

Proteins are, of course, also able to enter into the aqueous layer of a lamellar phase and thereby affect the swelling. This was shown by Rand (243), who studied the penetration of bovine serum between negatively charged lecithin/cardioliipin bilayers at pH 3.3, where the protein has a positive netcharge. BSA is also likely to adopt a more expanded structure at this pH, thus exposing more hydrophobic segments. He found that the interlamellar spacing of the lamellar phase, decreased with an increasing cardioliipin/bovine serum albumin ratio. This was related to a reduction of the negative charge of the lipid layer as the amount of bound protein increases.

We will start our discussion by giving some example of the interplay between the lipid structures and protein in terms of the effect on the curvature of the lipid–aqueous interface, because curvature has an important role

in condensed matter, as discussed in the book by Hyde et al. (59). McCallum and Epand found that changing the curvature of biological membranes could modify membrane-bound insulin receptor autophosphorylation and signaling (244). This was demonstrated by adding compounds that raised the bilayer to the reverse hexagonal (H_{II}) transition temperature of model membranes. This promoted a decrease of curvature and inhibited the insulin stimulation of the receptor phosphorylation.

The next part will focus on a specific structure, the bicontinuous cubic liquid-crystalline phase, where the interaction with the lipid bilayer as well as the physical entrapment within the cubic phase takes place. Finally, we will briefly discuss the effect of enzyme interactions, namely lipase action, on liquid crystalline phases.

1. Protein Interactions That Increase the Curvature of the Lipid–Aqueous Interfaces

Proteins or peptides that penetrate into the hydrophobic domain of the lipid bilayer generally provoke an increase of curvature of the lipid–aqueous interface (i.e., becomes more concave toward the aqueous space). Quite a few of the membrane-bound peptides have these properties, such as Gramicidin A, a hydrophobic polypeptide, which forms channels for monovalent cations in phospholipid membranes (245). This peptide was found to favor the transition lamellar phase \rightarrow reversed hexagonal (H_{II}) phase in dioleoylphosphatidylcholine (DOPC) and dioleoylphosphatidylethanolamine (DOPE) systems in an excess of water, as observed by nuclear magnetic resonance (NMR) studies (246).

Not only can proteins or peptides that penetrate into the lipid bilayer induce phase transitions, but also proteins that are certain to interact with the head groups of the phospholipid bilayer can give rise to similar effects. This has been demonstrated for cytochrome-*c*, which has a positive netcharge and has been shown to interact with negatively charged phospholipids (247). The binding of cytochrome-*c* to anionic cardiolipin liposomes induced the formation to an inverted hexagonal, H_{II} , structure (247). No interaction and, hence, no phase transition was observed in the presence of liposomes composed of neutral zwitterionic lipids like PC and phosphatidyl ethanolamine (PE). A phase transition to the H_{II} -phase was observed if a sufficient fraction of these lipids was replaced for cardiolipin. Interestingly, the protein was found to interact with liposomes with the anionic lipid phosphatidylserine (PS), but did not induce any phase transition. The interaction between cardiolipin and cytochrome-*c* was also studied by Spooner and Watts, using deuterium and phosphorus-31 NMR measurements (248). Likewise, they found that the interaction can, depending

on the lipid stoichiometry, cause a transition from a lamellar to a non-bilayer structure. The binding of the protein with the liquid-crystalline bilayers of cardiolipin was also found to cause extensive derangement of the cytochrome-*c* secondary structure (248,249).

Studies of the interaction between cytochrome-*c* and suspensions of DMPG or admixtures of dioleoylglycerol (DOG) or DOPC with DOPG also showed that binding of cytochrome-*c* could promote an increase in surface curvature of the lipid aggregates from a bilayer structure (250). This is deduced from NMR data where an isotropic peak occurs in the presence of cytochrome-*c*, indicating cubic lipid phases, small spherical vesicles, or extended bilayers with high local curvature. The structure of cytochrome-*c* was found to change on binding to the lipid, and two forms, depending on the lipid composition, were identified with resonance Raman measurements:

- I. Close to the native conformation in solution
- II. Unfolded with the heme crevice opened

The changes in protein structure could be correlated with the curvature of the lipid bilayer, as illustrated in Fig. 14, as the ratio between the unfolded (II) and native (I) cytochrome-*c* (cyt *c*) in DOPC/DOG dispersions versus DOG mol%. The presence of DOG was found to induce spontaneous curvature in the DOPG lipid bilayer in the pure lipid system, which at a DOG content of ~50%, leads to the transition to a reversed hexagonal (H_{II})

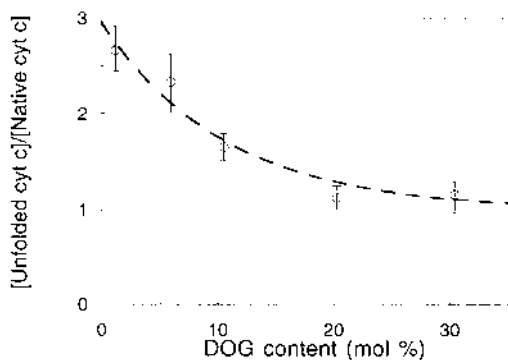


Figure 14 Concentration of unfolded (II) and native (I) cytochrome-*c* (cyt *c*) in DOPC / DOG dispersions versus DOG mol% determined from Raman resonance spectra. The concentrations of lipid and cytochrome-*c* were 300 and 20 μ M, respectively, in an aqueous buffer (1 mM HEPES, 1 mM EDTA) of pH 7.5. (Data Ref. 250, where the experimental details are given.)

phase. In the absence of DOG (i.e., a strict bilayer structure), the binding of the more unfolded form (II) of cytochrome is favored, whereas the fraction of the more native globular protein structure (I) increases with the amount of DOG (Fig. 14) and thus with curvature of the surface. The physical state of the lipid was also found to affect the proportions of the two structural forms of cytochrome-*c*. In the fluid state of pure DMPG, the fraction of the more unfolded form (II) was larger (85%) than when the lipid was in the gel state (80%). It is noteworthy that they found that the bound fraction of the more unfolded form (II) to the fluid DOPG bilayer structure was substantially lower (75%), indicating that not only the fluidity of the bilayer matters but also the type of lipid.

The interaction between cytochrome-*c* and mono-olein in the cubic phase was studied by Razumas et al. by differential scanning calorimetry (DSC) and optical microscopy (251). In line with the above-reported studies, they also found that the presence of cytochrome-*c* at high enough concentrations favored lipid aggregates with a larger curvature. Thus, they observed that the phase transition cubic \rightarrow H_{II} \rightarrow L₂ in the mono-olein–cytochrome-*c*–water system took place at a lower temperature than in the binary mono-olein–water system (251). Similar effects were observed when glucose oxidase was included into mono-olein–aqueous cubic phase (252). The temperature of the phase transition cubic \rightarrow H_{II} in the mono-olein–glucose oxidase aqueous system decreases with the increase in glucose oxidase concentration.

2. Protein Interactions That Decrease the Curvature of the Lipid–Aqueous Interfaces

Fraser et al. investigated the ability of a range of basic proteins and polylysine to convert a reversed hexagonal (H_{II}) phase, consisting of DOPE and mixtures of DOPE and PS, to stable lamellar (L_α) phases at pH 9, where DOPE is anionic, and at pH 7, when it is zwitterionic (253). The proteins investigated were all capable of binding to the H_{II} phase at pH 9, but only myelin basic protein and polylysine did induce transition to the L_α phase. Lysozyme formed a new H_{II} phase in which the protein was included. A lowering of the pH seemed to release the proteins, except for mellittin, which also seemed to penetrate into the hydrophobic core of the lipid aggregates. The presence of PS in the H_{II} phase at pH 7 increased the protein binding, but only interaction with myelin basic protein gave a lamellar phase. Based on earlier studies, Fraser et al. suggested that the myelin basic protein stabilized the lamellar phase by interacting with the DOPE headgroup and thereby increasing its effective size (253). They concluded that the properties of myelin basic protein in terms of stabilizing the lamellar

structure could be related to the role of the protein to stabilize the myelin sheath multilayers.

3. Cubic Lipid–Protein Aqueous Phases

Lipid bilayers can be folded into such intriguing structures as cubic liquid-crystalline lipid–aqueous phases. In these structures not only the surface properties and the curvature but also the dimensions of the aqueous space affect protein–lipid interactions. The main features of the bicontinuous cubic phase is illustrated in Fig. 15. The mono-olein–aqueous system is a thoroughly studied example of such a system, where two types of cubic phase have been observed on the water-rich side of the lamellar phase (84,254–257). We have already discussed the biological implications of lipid-cubic phases. Here, we will highlight some of the main features that are of importance for the functionality of lipid cubic phases. First, it is the bicontinuity of the cubic phase. This is illustrated Figs. 16a and 16b, where the mobility of glucose solubilized in the aqueous channels and vitamin K solubilized in the lipid bilayer, respectively is illustrated. Figure 16a shows the concentration profiles of glucose in the cubic mono-olein–aqueous phase equilibrated against water as determined by holographic laser interferometry (258). These profiles could be fitted to Ficks second law, which gave a diffusion coefficient four times lower than the value in the aqueous solution. The mobility of the molecules in the aqueous channels of the cubic phase is certain to be affected by the dimensions of the channels and the size of the solute. Thus, electrochemical studies of the transport of cytochrome-*c* in the mono-olein–aqueous cubic phase gave values of diffusion coefficients that were about 70 times lower than the bulk values (251). Figure 16b shows the mobility of mono-olein and vitamin K₁ dispersed in the lipid bilayer as the NMR self-diffusion coefficients plotted versus lipid volume fraction in the cubic phases. It is noteworthy that the mobility of the introduced vitamin K₁ follows that of mono-olein, indicating complete dispersion of vitamin K₁.

The dimensions of the water channels in the bicontinuous cubic phases, which depend on the degree of swelling and type of cubic phase are in the same range as the size of proteins (cf. Ref. 252). Furthermore, as liquid-crystalline phases they are quite flexible structures. These features have triggered a number of studies, which have shown that a large range of hydrophilic proteins with molecular weights up to 590 kDa can be entrapped in the aqueous cavity of the mono-olein–aqueous cubic phases (251,252,259–262). The entrapped proteins have been found to be protected in the cubic phase, with retained native confirmation (260,262–265). Enzymes can be kept for a very long time (months, in

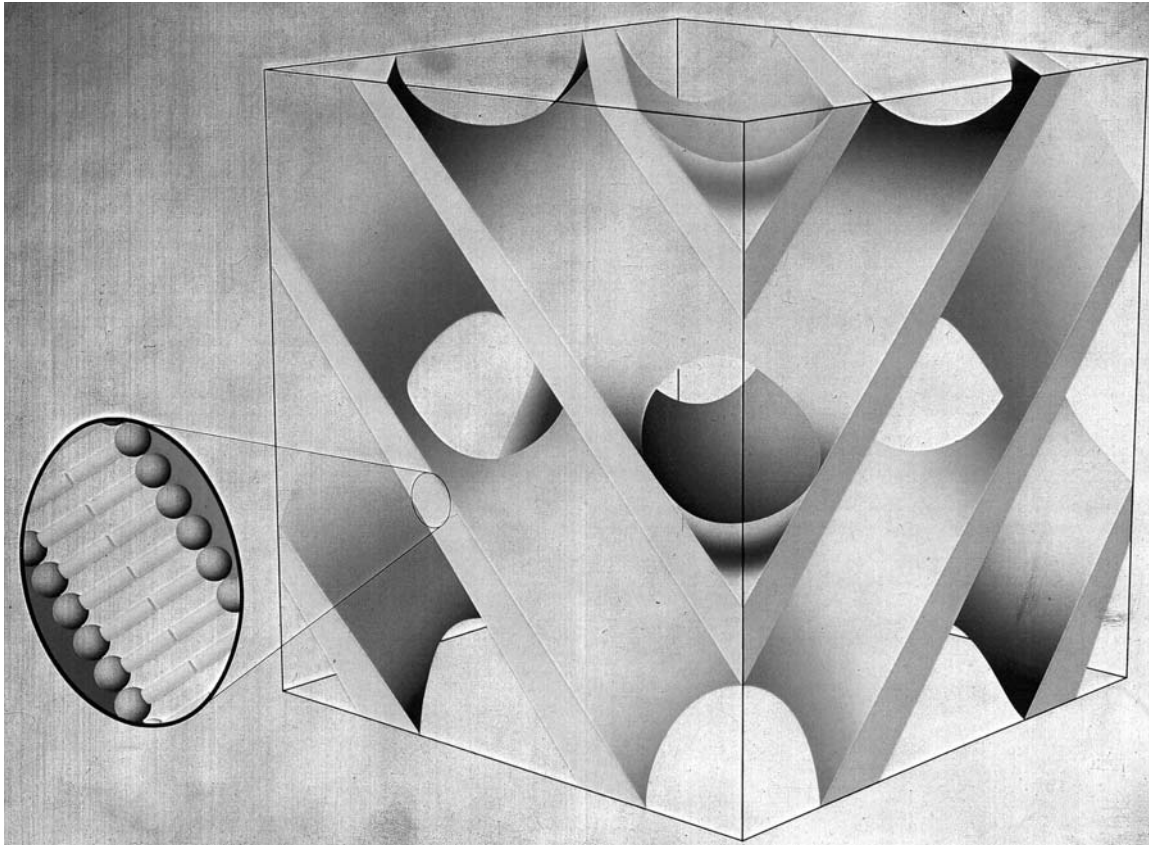


Figure 15 Schematic of the cubic phase, showing the two unconnected water channel systems. The location of the lipid bilayer is also indicated. The type of cubic phase shown can be described as a diamond of an infinite periodic minimal surface (IPMS) corresponding to a primitive cubic lattice ($Pn3m$).

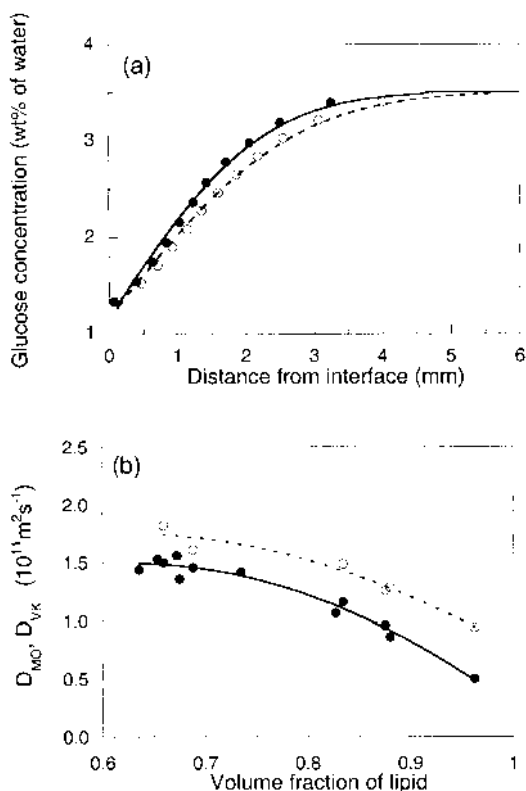


Figure 16 (a) Glucose concentration profiles in a mono-olein–aqueous cubic phase (62:38 wt%), where the aqueous solution initially contained 3.5 wt% glucose, after 3 h (●) and 4 h (○) equilibration against pure water. The concentration is given as the wt% glucose in the aqueous solution of the cubic phase. The solid and broken lines represent the best theoretical fit of Fick's law, giving diffusion coefficients of $1.39 \times 10^{-10} \text{ m}^2/\text{s}$ and $1.47 \times 10^{-10} \text{ m}^2/\text{s}$ after 3 and 4 h, respectively. The corresponding bulk value is $6.7 \times 10^{-10} \text{ m}^2/\text{s}$. The data, obtained by holographic laser interferometry, are from Refs. 258 and 261, where the experimental details are given. (b) NMR self-diffusion coefficients at 25°C in mono-olein–aqueous cubic phases containing 0–5 wt% vitamin K₁ are shown as a function of the lipid volume fraction (including vitamin K₁). The self-diffusion coefficients were measured in the cubic (both gyroid and diamond type) and in the reversed micelle, L₂, phases. Self-diffusion coefficients of mono-olein (D_{MO}) (●) and vitamin K₁ (D_{VK}) (○) are shown. The lines are arbitrary fits to demonstrate the similar trends. The data are from Ref. 271, where the experimental details are given.

some cases), with retained activity, which is not possible in the aqueous solution (259,261).

Spectroscopic data have revealed changes in the molecular organization of the lipids evoked by the presence of the protein. FTIR measurements on the mono-olein–cytochrome-*c* aqueous system showed that the presence of cytochrome-*c* increased the conformational order of the mono-olein acyl chain and caused structural rearrangements in the polar-head-group region (251). These observations are in agreement with the decrease of the mono-olein packing parameter upon incorporation of cytochrome-*c*, which was deduced from the increase in unit-cell dimension of the cubic phase as determined by small-angle x-ray diffraction. The Raman scattering studies on the mono-olein–lysozyme–aqueous system demonstrated an increase in the number of hydrogen-bond C=O groups of mono-olein, but no increase in the acyl chain order relative to the binary lipid–aqueous system (260). A similar increase in the hydrogen-bonding, caused by the presence of a protein, was observed in the mono-olein–hemoglobin–aqueous system using FTIR spectroscopy (262). However, in this case, the protein incorporation also caused a decrease in the acylchain order.

The cubic monoglyceride phases have also the ability to solubilize lipophilic proteins like A-gliadin from wheat (266) and bacteriorhodopsin (267), as well as relatively large amounts of membrane lipids (260,261,268–270) and other hydrophobic compounds of biological relevance (268,271,272). These compounds are most probably dispersed in the lipid bilayer region of the cubic phase.

Apart from the biological significance of cubic lipid–aqueous phases, Razumas et al. demonstrated that cubic mono-olein–aqueous phases, containing enzymes, could be used as the biocatalytic layer in amperometric and potentiometric biosensors (259). Their results for biosensors, based on a variety of enzymes, show that the long-term stability decreases in the order lactate oxidase > creatinine deiminase > glucose oxidase > urease, (i.e.; is basically in the order of increasing molecular weight). Also, the cubic phases of other amphiphiles like ethoxylated fatty alcohols can be used to entrap glucose oxidase, to construct a simple glucose monitor (60). The bicontinuous cubic structures have, by virtue of their well-defined porosity, also a large potential in drug delivery systems (46). Stable particles of lipid–aqueous cubic phases, cubosomes, can also be produced for this purpose (46,56,75,84–86). Landau and Rosenbusch demonstrated that the bicontinuous phases based on mono-olein and monopalmitolein could provide matrices for the crystallization of membrane proteins like bacteriorhodopsin (267). They pointed out that the use of these types of cubic phase is advantageous as they provide nucleation sites, and the membrane proteins can be dissolved in the lipid bilayer. In addition, they support

growth by allowing lateral diffusion of the protein molecules in the membrane.

4. Lipase Action on Liquid-Crystalline Phases

Another food application, in which cubic lipid phases are believed to play an important role, is in the degradation of lipids. This is also an example of protein–lipid interaction. However, lipases act at such a low concentration that their presence as protein does not significantly affect the global lipid self-assembly structure. It is rather their catalytic activity that has an impact on the lipid self-assembly structure. It is also important to remember that the action of lipases only decreases the time taken to reach the equilibrium and does not affect the equilibrium composition as such. Thus, the changes in structure and composition would have occurred even without the lipase if given enough time. In a simple experiment, Wallin and Arnebrant demonstrated that a cubic phase was much faster decomposed by the action of lipase from *Thermomyces* (former *Humicola*) *lanuginosa* than the reference sample consisting of triolein and the aqueous phase (273). This was attributed to the much larger interfacial area in the cubic phase. In an in vitro study of lipolysis of triglycerides in a intestine-like environment, Patton and Carey observed (37), apart from the initially occurring crystalline phase, a viscous isotropic phase composed of monoglycerides and fatty acids, which is identical to the one formed in monoglyceride systems. In excess of bile salts, the lipolysis products are rapidly solubilized in mixed micelles. However, the bile acid amounts in vivo are not sufficient to solubilize all lipids after a meal rich in fats, which implies that the liquid-crystalline phases exist in vivo (274). Lipase and water must be free to diffuse through the phases formed by the lipolysis products, surrounding the diminishing fat droplet. Thus, the bicontinuity as well as the incorporation properties of the cubic monoglyceride phases are thought to be important features for the lipolysis process (275). Recently, Borné et al., in a series of studies, have investigated the effect of lipase action on the liquid-crystalline phase as well as other self-assembled structures such as vesicles and cubosomes (69,70,276). Some of their findings are summarized in Fig. 17, which shows a schematic representation of the change in structure of the different liquid crystalline phases as a function of time after adding *Thermomyces lanuginosa* lipase. The observed changes in self-assembled structures could be predicted from either the mono-olein–oleic acid–aqueous ternary phase diagram, where the lipolysis give rise to a transition of cubic → reversed hexagonal → micellar cubic → reversed micellar phase + dispersion or mono-olein–sodium oleate–aqueous ternary phase diagram, where the corresponding sequence is lamellar → normal hexagonal. These difference in

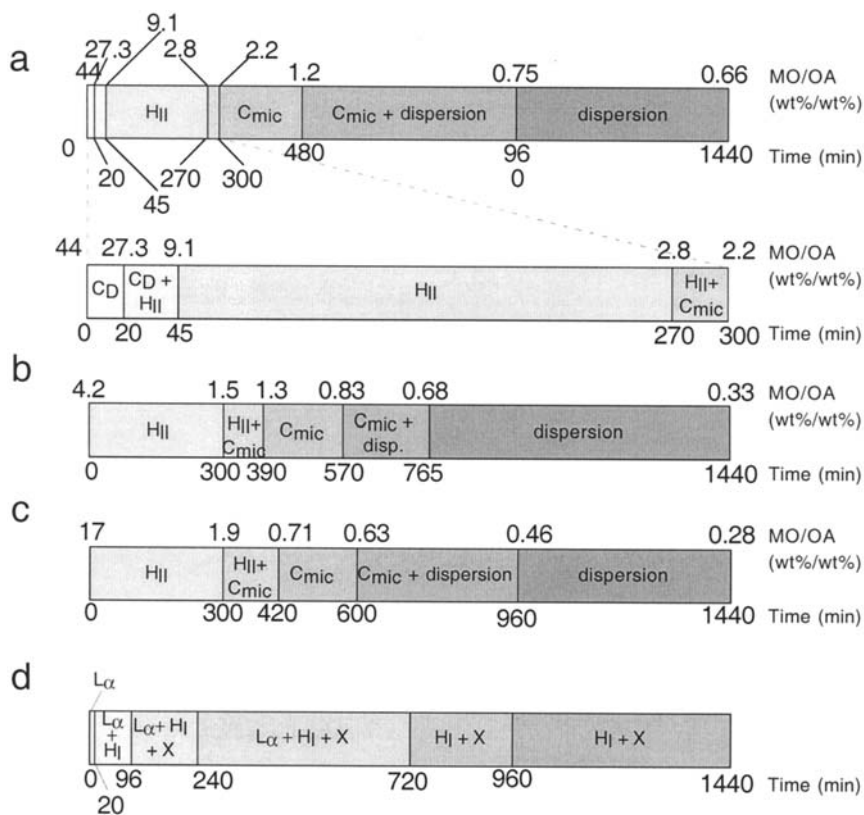


Figure 17 Schematic representation of the change in structure during lipolysis of mono-olein (MO) (or diolein DO) in different liquid-crystalline phases: (a) C_D phase (63 wt% MO, 37 wt% 2H_2O), (b) oleic acid (OA)– H_{II} phase (65.4 wt% MO, 15.6 wt% OA, 19 wt% 2H_2O), (c) DO– H_{II} phase (68 wt% MO, 18 wt% DO, 14 wt% 2H_2O), and (d) L_α phase [10 wt% MO, 5 wt% sodium oleate (NaO), 85 wt% 2H_2O]. The main liquid-crystalline phases as determined by small-angle X-ray diffraction (SAXD), are indicated in the figure as a diamond type of bicontinuous cubic phase, space group $Pn3m$ (C_D), reversed hexagonal phase (H_{II}), normal hexagonal phase (H_I), lamellar phase (L_α), and micellar cubic phase, space group $Fd3m$ (C_{mic}). These may exist in excess of water or in the presence of minor amounts of other phases. Some of the observed reflections in the diffractograms, obtained by SAXD, could not be unambiguously assigned to a structure. This unidentified structure is denoted by X. (Adapted from Ref. 70, where details are given.)

reaction sequences could be rationalized in terms of differences in degree of protonation of the fatty acid (70). The initially lamellar phase had a high pH (about 10), (i.e., a low degree of protonation) and thus the degradation as expected follows the mono-olein–sodium oleate–aqueous ternary phase diagram. The initially cubic and hexagonal phase had a low pH (4–7), (i.e., a high degree of protonation) and thus the degradation as expected follows mono-olein –oleic acid–aqueous ternary phase diagram. Adding *Thermomyces lanuginose* lipase to aqueous dispersions of cubic phases (cubosomes) and lamellar dispersions (vesicles) at high water content and gave the corresponding morphological changes as for the liquid-crystalline phases (276). The phase diagrams of the relevant systems can thus be used as maps to navigate through the changes in the self-assembly structure of the substrate and the product. Borné et al found similar specific activity of *Thermomyces lanuginose* lipase on the cubic as on the reversed hexagonal mono-olein-based liquid-crystalline phases, which was somewhat unexpected (70).

ACKNOWLEDGMENTS

The fruitful discussions and collaboration with Bodil Ericsson, Kåre Larsson, Barry Ninham, Valdemaras Razumas, Thomas Arnebrant, Björn Lindman, Ali Khan, Maura Monduzzi, Francesca Caboi, Helena Ljusberg, Marie Paulsson, Johanna Borné, Justas Barauskas, Anna Stenstam, Marie Wahlgren, Fredrik Tiberg, Alan Svendsen, Karl Hult, and others are greatly acknowledged. This work has benefited from the financial support from the Swedish Research Council.

REFERENCES

1. P. K. J. Kinnunen, *Chem. Phys. Lipids* 81, 151–166 (1996).
2. P. K. J. Kinnunen and J. M. Halopainen, *Biosci. Rep.* 20, 465–482 (2000).
3. Y. Barenholz and G. Cevc, in *Physical Chemistry of Biological Interfaces* (A. Baszkin and W. Norde, eds.), Marcel Dekker, New York, 2000, pp. 171–241.
4. H. Ringsdorf, in *Physical Chemistry of Biological Interfaces* (A. Baszkin and W. Norde, eds.), Marcel Dekker, New York, 2000, pp. 243–282.
5. L. Saiz, S. Bandyopadhyay, and M. L. Klein, *Biosci. Rep.* 22, 151–173 (2002).
6. E. Watts, (ed.) *Protein–Lipid Interactions*, Elsevier, Amsterdam, 1993.
7. R. Verger and F. Pattus, *Chem. Phys. Lipids* 30, 189–227 (1982).
8. F. MacRitchie, *Chemistry at Interfaces*, Academic Press, San Diego, CA, (1990).
9. M. Ahlers, W. Müller, A. Reichert, H. Ringsdorf, and J. Venzmer, *Angew. Chem. Int. Ed. Engl.* 29, 1269–1285 (1990).

10. V. B. Fainerman, E. H. Lucassen-Reynders, and R. Miller, *Colloids Surfaces A: Physicochem. Eng. Aspects* 143, 141–165 (1998).
11. E. Dickinson, *Colloids Surfaces B: Biointerf.* 15, 161–176 (1999).
12. D. Vollhardt and V. B. Fainerman, *Adv. Colloid Interf. Sci.* 86, 103–151 (2000).
13. R. Miller, V. B. Fainerman, A. V. Makievski, J. Krägel, D. O. Grigoriev, V. N. Kazakov, and O. V. Sinyachenko, *Adv. Colloid Interf. Sci.* 86, 39–82 (2000).
14. M. A. Bos and T. van Vliet, *Adv. Colloid Interf. Sci.* 91, 437–471 (2001).
15. M. J. Papiz, L. Sawyer, E. E. Eliopoulos, A. C. T. North, B. C. Findlay, R. Sivaprasadarao, T. A. Jones, M. E. Newcomer, and P. J. Kraulis, *Nature* 324, 383–385 (1986).
16. L. Sawyer, *Nature* 327, 659 (1987).
17. A. C. T. North, *Int. J. Biol. Macromol.* 81, 56–58 (1989).
18. S. Brownlow, J. H. Morais Cabral, R. Cooper, D. R. Flower, S. J. Yewdall, I. Polikarpov, A. C. T. North, and L. Sawyer, *Structure* 5, 481–495 (1997).
19. L. Sawyer, S. Brownlow, I. Polikarpov, and S.-Y. Wu, *Int. Dairy J.* 8, 65–72 (1998).
20. M. C. Diaz de Villegas, R. Oria, F. J. Salva, and M. Calvo, *Milchwissenschaft* 42, 357–358 (1987).
21. D. K. Sarker, P. J. Wilde, and D. C. Clark, *Colloids Surfaces B: Biointerf.* 3, 349–356 (1995).
22. A. Kristensen, T. Nylander, M. Paulsson, and A. Carlsson, *Int. Dairy J.* 7, 87–92 (1995).
23. B. Y. Qin, L. K. Creamer, E. N. Baker, and G. B. Jameson, *FEBS Lett.* 438, 272–278 (1998).
24. S.-Y. Wu, M. D. Perez, P. Puyol, and L. Sawyer, *J. Biol. Chem.* 274, 170–174 (1999).
25. L. Ragona, F. Fogolari, L. Zetta, D. M. Perez, P. Puyol, K. De Kruif, F. Lohr, H. Ruterjans, and H. Molinari, *Protein Sci.* 9, 13478–1356 (2000).
26. L. Sawyer and G. Kontopidis, *Biochim. Biophys. Acta* 1482, 136–148 (2000).
27. L. Sawyer, P. N. Barlow, M. J. Boland, L. K. Creamer, H. Denton, P. J. B. Edwards, C. Holt, G. B. Jameson, G. Kontopidis, G. E. Norris, S. Uhrinová, and S.-Y. Wu, *Int. Dairy J.* 12, 299–310 (2002).
28. A. L. Shapiro, E. Vinuela, and J. V. Maizel, *Biochem. Biophys. Res. Commun.* 28, 815–820 (1967).
29. K. Weber and M. Osborn, *J. Biol. Chem.* 244, 4406–4412 (1969).
30. J. Goerke, *Biochim. Biophys. Acta*, 1408, 79–89 (1998).
31. I. Frerking, A. Günther, W. Seeger, and U. Pison, *Intens. Care Med.* 27, 1699–1717 (2001).
32. J. Pérez-Gil, *Biol. Neonate* 81(Suppl. 1), 6–15 (2002).
33. M. Larsson, K. Larsson, S. Andersson, J. Kakhar, T. Nylander, B. Ninham, and P. Wollmer, *J. Dispers. Sci. Technol.* 20, 1–12 (1999).
34. M. Larsson, K. Larsson, and P. Wollmer, *Prog. Colloid Polym. Sci.* 120, 28–34 (2002).
35. M. Larsson, J. J. Haitzma, B. Lachmann, K. Larsson, T. Nylander, and P. Wollmer, *Clin. Physiol. Functional Imaging* 22, 39–48 (2002).

36. J. A. Clements, *Proc. Soc. Exp. Biol. Med.* 95, 170–172 (1957).
37. J. S. Patton and M. C. Carey, *Science* 204, 145–148 (1979).
38. A. Svendsen, *Biochim. Biophys. Acta* 1543, 223–238 (2000).
39. R. Verger, *Trends Biotechnol.* 15, 32–38 (1997).
40. I. Panaiotov and R. Verger, *Physical Chemistry of Biological Interfaces* (A. Baszkin and W. Norde, eds.), Marcel Dekker, New York, 2000, pp. 359–400.
41. T. E. Creighton, *Proteins—Structure and Molecular Properties*, 2nd ed., W. H. Freeman, New York, 1993.
42. J. S. Richardson, *Adv. Protein Chem.* 34, 167–339 (1981).
43. K. A. Dill, *Biochemistry* 29, 7133–7155 (1990).
44. T. E. Creighton, *Biochem. J.* 270, 1–16 (1990).
45. W. R. Taylor, A. C. W. May, N. P. Brown, and A. Aszodi, *Rep. Prog. Phys.*, 64, 517–590 (2001).
46. K. Larsson, *Lipids—Molecular Organization, Physical Functions and Technical Applications*, Oily Press, Dundee, 1994.
47. B. Lindman and H. Wennerström, *Topics Curr. Chem.* 87, 1–83 (1980).
48. C. Tanford, *The Hydrophobic Effect: Formation of Micelles and Biological Membranes*, 2nd ed., Wiley, New York, 1980.
49. K. Fontell, *Adv. Colloid Interf. Sci.* 41, 127–147 (1992).
50. J. N. Israelachvili, D. J. Mitchell, and B. W. Ninham, *J. Chem. Soc. Faraday Trans. II* 72, 1525–1568 (1976).
51. D. J. Mitchell and B. W. Ninham, *J. Chem. Soc. Faraday Trans. 2* 77, 601–629 (1981).
52. A. Raudino, *Adv. Colloid Interf. Sci.* 57, 229–285 (1995).
53. V. Luzzati, *Biological Membranes* (D. Chapman, ed.), Academic Press, New York, 1968, pp. 77–123.
54. K. Fontell, *Colloid Polym. Sci.* 268, 264–285 (1990).
55. R. H. Templer, *Curr. Opin. Colloid Interf. Sci.* 3, 255–263 (1998).
56. V. Luzzati, A. Tardieu, T. Gulik-Krzywicki, E. Rivas, and F. Reiss-Husson, *Nature* 220, 485–488 (1968).
57. K. Larsson, *J. Phys. Chem.* 93, 7304–7314 (1989).
58. G. Lindblom and L. Rilfors, *Biochim. Biophys. Acta* 988, 221–256 (1989).
59. S. T. Hyde, A. S., L. K., Z. Blum, T. Landh, S. Lidin, and B. W. Ninham, *The Language of Shape. The Role of Curvature in Condensed Matter: Physics, Chemistry and Biology*, Elsevier, Amsterdam, 1997.
60. R. Wallin, S. Engström, and C. F. Mandenius, *Biocatalysis* 8, 73–80 (1993).
61. G. Lindblom, K. Larsson, L. Johansson, K. Fontell, and S. Forsén, *J. Am. Chem. Soc.* 101, 5465–5470 (1979).
62. S. Andersson, S. T. Hyde, K. Larsson, and S. Lidin, *Chem. Rev.* 88, 221–242 (1988).
63. S. T. Hyde, *J. Phys. Chem.* 93, 1458–1464 (1989).
64. V. Luzzati, R. Vargas, A. Gulik, P. Mariani, J. M. Seddon, and E. Rivas, *Biochemistry* 31, 279–285 (1992).
65. P. Mariani, E. Rivas, V. Luzzati, and H. Delacroix, *Biochemistry* 29, 6799–6810 (1990).

66. P. Mariani, V. Luzzati, and H. Delacroix, *J. Mol. Biol.* 204, 165–189 (1988).
67. J. Borné, T. Nylander, and A. Khan, *Langmuir* 17, 7742–7751 (2001).
68. J. M. Seddon, E. A. Bartle, and J. Miggins, *J. Phys. Condens. Matter* 2, SA285–SA290 (1990).
69. F. Caboi, J. Borné, T. Nylander, A. Khan, A. Svendsen, and S. Patkar, *Colloids Surfaces B: Biointerf.* 26, 159–171 (2002).
70. J. Borné, T. Nylander, and A. Khan, *Langmuir* 18, 8972–8981 (2002).
71. J. M. Seddon, *Biochim. Biophys. Acta* 1031, 1–69 (1990).
72. T. Landh, *FEBS Lett.* 369, 13–17 (1995).
73. V. Luzzati, *Curr. Opin. Struct. Biol.* 7, 661–668 (1997).
74. B. De Kruijff, *Curr. Opin. Colloid Interf. Sci.* 1, 564–569 (1997).
75. K. Larsson, *Curr. Opin. Colloid Interf. Sci.* 5, 64–69 (2000).
76. A. J. Verkleij, C. Mommers, W. J. Gerritsen, L. Leunissen-Bijvelt, and P. R. Cullis, *Biochim. Biophys. Acta* 555, 358–361 (1979).
77. D. P. Siegel, *Biophys. J.* 45, 399–420 (1984).
78. J. G. Mandersloot, W. J. Gerritsen, L. Leunissen-Bijvelt, A. Van Echteld, P. C. Noordam, and J. De Gier, *Biochim. Biophys. Acta* 640, 106–113 (1981).
79. M. J. Hope and P. R. Cullis, *Biochim. Biophys. Acta* 640, 82–90 (1981).
80. W. Helfrich, *Liquid Crystallogr.* 5, 1647–1658 (1989).
81. D. D. Lasic, *Liposomes—From Physics to Applications*, Elsevier, Amsterdam, 1993.
82. S. Komura, in *Vesicles* (M. Rosoff, ed.), Marcel Dekker, New York, 1996, pp. 198–236.
83. D. D. Lasic, R. Joannic, B. C. Keller, P. M. Frederik, and L. Auvray, *Adv. Colloid Interf. Sci.* 89–90, 337–349 (2001).
84. T. Landh, *J. Phys. Chem.* 98, 8453–8467 (1994).
85. J. Gustafsson, H. Ljusberg-Wahren, M. Almgren, and K. Larsson, *Langmuir* 12, 4611 (1996).
86. J. Gustafsson, H. Ljusberg-Wahren, M. Almgren, and K. Larsson, *Langmuir* 13, 6964 (1997).
87. C. Tanford, *Physical Chemistry of Macromolecules*, Wiley, New York, 1967.
88. K. Gekko and Y. Hasegawa, *Biochemistry* 25, 6563–6571 (1986).
89. P. L. Privalov, *Adv. Protein Chem.* 33, 167–241 (1979).
90. P. L. Privalov, *Adv. Protein Chem.* 35, 1–104 (1982).
91. P. L. Privalov and S. J. Gill, *Adv. Protein Chem.* 39, 191–234 (1988).
92. P. K. Ponnuswamy, *Prog. Biophys. Mol. Biol.* 59, 57–103 (1993).
93. C. N. Pace, L. M. Fisher, and J. F. Cupo, *Acta Biol. Med. Germ.* 40, 1385–1392 (1981).
94. F. M. Richards, *Annu. Rev. Biophys. Bioeng.* 6, 151–176 (1977).
95. W. Kauzmann, *Adv. Protein Chem.* 14, 1–63 (1959).
96. W. Norde, *Adv. Colloid Interf. Sci.* 25, 267–340 (1986).
97. C. A. Haynes and W. Norde, *Colloids Surfaces B: Biointerf.* 2, 517–566 (1994).
98. W. Norde, *Physical Chemistry of Biological Interfaces* (A. Baszkin and W. Norde, eds.), Marcel Dekker, New York, 2000, pp. 115–135.

99. M. C. L. Maste, W. Norde, and A. J. W. G. Visser, *J. Colloid Interf. Sci.* 196, 224–230 (1997).
100. T. Zoungrana, G. H. Findenegg, and W. Norde, *J. Colloid Interf. Sci.* 190, 437–448 (1997).
101. D. A. Dolgikh, R. I. Gilmanshin, E. V. Brazhnikov, V. E. Bychkova, G. V. Semisotnov, S. Y. Venyaminov, and O. B. Ptitsyn, *FEBS Lett.* 136, 311–315 (1981).
102. M. Ohgushi and A. Wada, *FEBS Lett.* 164, 21–24 (1983).
103. D. A. Dolgikh, L. V. Abaturov, I. A. Bolotina, E. V. Brazhnikov, V. E. Bychkova, R. I. Gilmanshin, Y. O. Lebedev, G. V. Semisotnov, E. I. Tiktopulo, and O. B. Ptitsyn, *Eur. Biophys. J.* 13, 109–121 (1985).
104. K. Kuwajima, *Proteins: Struct. Funct. Genet.* 6, 87–103 (1989).
105. O. B. Ptitsyn, R. H. Pain, G. V. Semisotnov, E. Zerovnik, and O. I. Razgulyaev, *FEBS Lett.* 262, 20–24 (1990).
106. E. Dickinson and Y. Matsumura, *Colloids Surfaces B: Biointerf.* 3, 1–17 (1994).
107. V. E. Bychkova, R. H. Pain, and O. B. Ptitsyn, *FEBS Lett.* 238, 231–234 (1988).
108. F. G. van der Goot, J. M. González-Mañas, J. H. Lakey, and F. Pattus, *Nature* 354, 408–410 (1991).
109. M. Boström, D. R. M. Williams, and B. W. Ninham, *Phys. Rev. Lett.* 87, 168103 (2001).
110. M. Boström, D. R. M. Williams, and B. Ninham, *Langmuir* 18, 8609–8615 (2002).
111. B. W. Ninham, *Progr. Colloid Polym. Sci.* 120, 1–12 (2002).
112. J. Steinhardt and J. A. Reynolds, *Multiple Equilibria in Proteins*, Academic Press, New York, 1969.
113. S. Lapanje, *Physicochemical Aspects of Protein Denaturation*, Wiley, New York, 1978.
114. S. Makino, *Adv. Biophys.* 12, 131–184 (1979).
115. M. N. Jones and A. Brass, *Food, Polymers, Gels, and Colloids* (E. Dickinson, ed.), Royal Society of Chemistry, Cambridge, 1991, pp. 65–80.
116. K. P. Ananthapadmanabhan, *Interactions of Surfactants with Polymers and Proteins* (K. P. Ananthapadmanabhan and G. E. D., eds.), CRC Press, Boca Raton, FL, 1993, pp. 319–366.
117. E. Dickinson, *Interactions of Surfactants with Polymers and Proteins* (K. P. Ananthapadmanabhan and G. E. D., eds.), CRC Press, Boca Raton, FL, 1993, pp. 295–317.
118. M. Bos, T. Nylander, T. Arnebrant, and D. C. Clark, *Food Emulsifiers and Their Applications* (G. L. Hasenhuettl and R. W. Hartel, eds.), Chapman & Hall, New York, 1997, pp. 95–146.
119. M. N. Jones and P. Manley, *J. Chem. Soc. Faraday Trans. 1* 75, 1736–1744 (1979).
120. M. N. Jones and P. Manley, *J. Chem. Soc. Faraday Trans. 1* 76, 654–664 (1980).

121. A. Yonath, A. Podjarny, H. B., A. Sielecki, and W. Traub, *Biochemistry* 16, 1418–1424 (1977).
122. A. Yonath, A. Sielecki, J. Moulton, A. Podjarny, and W. Traub, *Biochemistry* 16, 1413–1417 (1977).
123. R. Waninge, M. Paulsson, T. Nylander, B. Ninham, and P. Sellers, *Int. Dairy J.* 8, 141–148 (1998).
124. J. A. Reynolds and C. Tanford, *Proc. Natl. Acad. Sci. USA* 66, 1002–1007 (1970).
125. R. Miller and K. Lunkenheimer, *Colloid Polym. Sci.* 264, 273–276 (1986).
126. K. Lunkenheimer and R. Miller, *J. Colloid Interf. Sci.* 120, 176–183 (1987).
127. K. Lunkenheimer and G. Czichocki, *J. Colloid Interf. Sci.* 160, 509–510 (1993).
128. D. C. Clark, F. Husband, P. J. Wilde, M. Cornec, R. Miller, J. Krägel, and R. Wüstneck, *J. Chem. Soc. Faraday Trans.* 91, 1991–1996 (1995).
129. P.-O. Hegg, *Acta Agric. Scand.* 30, 401–404 (1980).
130. S. Gumpen, P.-O. Hegg, and H. Martens, *Biochim. Biophys. Acta* 574, 189–196 (1979).
131. P. Puyol, M. D. Perez, J. M. Peiro, and M. Calvo, *J. Dairy Sci.* 77, 1494–1502 (1994).
132. K. Fukushima, Y. Murata, N. Nishikido, G. Sugihara, and M. Tanaka, *Bull. Chem. Soc. Jpn.* 54, 3122–3127 (1981).
133. K. Fukushima, Y. Murata, G. Sugihara, and M. Tanaka, *Bull. Chem. Soc. Jpn.* 55, 1376–1378 (1982).
134. J. Chen and E. Dickinson, *Colloids Surfaces A: Physicochem. Eng. Aspects* 100, 255–265 (1995).
135. J. Chen and E. Dickinson, *Colloids Surfaces A: Physicochem. Eng. Aspects* 100, 267–277 (1995).
136. A. K. Morén and A. Khan, *Langmuir* 11, 3636–3643 (1995).
137. A. Stenstam, A. Khan, and H. Wennerström, *Langmuir* 17, 7513–7520 (2001).
138. W. L. Mattice, J. M. Riser, and D. S. Clark, *Biochemistry* 15, 4264–4272 (1976).
139. B. Jirgensons, *Biochim. Biophys. Acta* 434, 58–68 (1976).
140. R. E. Tanner, B. Herpigny, S. H. Chen, and C. K. Rha, *J. Chem. Phys.* 76, 3866–3872 (1982).
141. X. H. Guo and S. H. Chen, *Chem. Phys.* 149, 129–139 (1990).
142. X. H. Guo, N. M. Zhao, S. H. Chen, and J. Teixeira, *Biopolymers* 29, 335–346 (1990).
143. C. A. Nelson, *J. Biol. Chem.* 246, 3895–3901 (1971).
144. M. N. Jones, P. Manley, P. J. W. Midgley, and A. E. Wilkinson, *Biopolymers* 21, 1435–1450 (1982).
145. A. K. Morén and A. Khan, *Langmuir* 14, 6818–6826 (1998).
146. J. Reynolds, S. Herbert, and J. Steinhardt, *Biochemistry* 7, 1357–1361 (1968).
147. H. M. Rendall, *J. Chem. Soc. Faraday Trans. 1*, 72, 481–484 (1976).
148. S. Makino, J. A. Reynolds, and C. Tanford, *J. Biol. Chem.* 248, 4926–4932 (1973).
149. F. A. Green, *J. Colloid Interf. Sci.* 35, 481–485 (1971).

150. J. Cordoba, M. D. Reboiras, and M. N. Jones, *Int. J. Biol. Macromol.* 10, 270–276 (1988).
151. W. W. Sukow, H. E. Sandberg, E. A. Lewis, D. J. Eatough, and L. D. Hansen, *Biochemistry* 19, 912–917 (1980).
152. P. J. Wilde and D. C. Clark, *J. Colloid Interf. Sci.* 155, 48–54 (1993).
153. D. C. Clark, P. J. Wilde, D. R. Wilson, and R. Wustneck, *Food Hydrocolloids* 6, 173–186 (1992).
154. P. J. Wilde, D. C. Clark, and D. Marion, *J. Agric. Food Chem.* 41, 1570–1576 (1993).
155. C. Tanford and Epstein, *J. Am. Chem. Soc.* 76, 2163–2169 (1954).
156. S. Kaneshina, M. Tanaka, T. Kondo, T. Mizuno, and K. Aoki, *Bull. Chem. Soc. Jpn.* 46, 2735–2738 (1973).
157. Y. Nozaki, J. A. Reynolds, and C. Tanford, *J. Biol. Chem.* 249, 4452–4459 (1974).
158. B. Ericsson, P.-O. Hegg, and K. Mårtensson, *J. Dispers. Sci. Technol.* 8, 271–287 (1987).
159. B. Ericsson, P.-O. Hegg, and K. Mårtensson, *J. Dispers. Sci. Technol.* 8, 289–301 (1987).
160. M. N. Jones, P. Manley, and A. Holt, *Int. J. Biol. Macromol.* 6, 65–68 (1984).
161. R. J. Williams, J. N. Phillips, and K. J. Mysels, *Trans. Faraday Soc.* 51, 728–737 (1955).
162. B. D. Flockhart, *J. Colloid Interf. Sci.* 16, 484–492 (1961).
163. D. F. Evans, D. J. Mitchell, and B. W. Ninham, *J. Phys. Chem.* 88, 6344–6348 (1984).
164. D. F. Evans, M. Allen, B. W. Ninham, and A. Fouda, *J. Solution Chem.* 13, 87–101 (1984).
165. B. Ericsson, P.-O. Hegg, and K. Mårtensson, *J. Food Technol.* 18, 11–19 (1983).
166. J. A. Reynolds, J. P. Gallagher, and J. Steinhardt, *Biochemistry* 9, 1232–1238 (1970).
167. M. Subramanian, B. S. Sheshadri, and M. P. Venkatappa, *J. Biochem. (Tokyo)* 95, 413–421 (1984).
168. D. C. Clark, M. Coke, P. J. Wilde, and D. R. Wilson, *Food, Polymers, Gels and Colloids* (E. Dickinson, ed.), Royal Society of Chemistry, London, 1991, pp. 272–278.
169. W. E. Ewers and K. L. Sutherland, *Austr. J. Sci. Res. Ser. A5*, 697–710 (1952).
170. N. Nishikido, T. Takahara, H. Kobayashi, and M. Tanaka, *Bull. Chem. Soc. Jpn.* 55, 3085–3088 (1982).
171. B. Ericsson and P.-O. Hegg, *Prog. Colloid Polym. Sci.* 70, 92–95 (1985).
172. M. Wahlgren, S. Welin-Klintström, T. Arnebrant, A. Askendal, and H. Elwing, *Colloids Surfaces B: Biointerf.* 4, 23–31 (1995).
173. A. R. Mackie, A. P. Gunning, P. J. Wilde, and V. J. Morris, *J. Colloid Interf. Sci.* 210, 157–166 (1999).
174. A. R. Mackie, A. P. Gunning, M. J. Ridout, P. J. Wilde, and V. J. Morris, *Langmuir* 17, 6593–6598 (2001).

175. A. R. Mackie, A. P. Gunning, M. J. Ridout, P. J. Wilde, and J. Rodriguez Patino, *Biomacromolecules* 2, 1001–1006 (2001).
176. J. R. Lu, T. J. Su, and R. K. Thomas, *J. Phys. Chem. B* 102, 10,307–10,315 (1998).
177. J. Chen and E. Dickinson, *J. Sci. Food Agric.* 62, 283–289 (1993).
178. J. Chen, E. Dickinson, and G. Iveson, *Food Struct.* 12, 135–146 (1993).
179. E. Dickinson and Y. Matsumura, *Int. J. Biol. Macromol.* 13, 26–30 (1991).
180. J. McGuire, M. C. Wahlgren, and T. Arnebrant, *J. Colloid Interf. Sci.* 170, 182–192 (1995).
181. M. C. Wahlgren and T. Arnebrant, *J. Colloid Interf. Sci.* 142, 503–511 (1991).
182. R. J. Green, T. J. Su, J. R. Lu, and J. Penfold, *J. Phys. Chem. B* 105, 1594–1602 (2001).
183. R. J. Green, T. J. Su, H. Joy, and J. R. Lu, *Langmuir* 16, 5797–5805 (2000).
184. M. C. Wahlgren and T. Arnebrant, *J. Colloid Interf. Sci.* 148, 201–206 (1992).
185. B. Ericsson, *Interactions Between Globular Proteins and Lipids*, PhD Thesis, University of Lund, Lund, Sweden, 1986.
186. R. Miller, V. B. Fainerman, A. V. Makievski, J. Krägel, and R. Wüstneck, *Colloids Surfaces A: Physicochem. Eng. Aspects* 161, 151–157 (2000).
187. J. J. Garcia Dominguez, R. Infante, P. Erra, and R. Juliá, *Tenside Detergents* 18, 310–313 (1981).
188. J. H. Buckingham, J. Lucassen, and D. Giles, *J. Colloid Interf. Sci.* 67, 423–431 (1978).
189. E. H. Lucassen-Reynders, J. Lucassen, and D. Giles, *J. Colloid Interf. Sci.* 81, 150–157 (1981).
190. A. Prins and D. J. M. Bergink-Martens, *Food Colloids and Polymers: Stability and Mechanical Properties* (E. Dickinson and P. Walstra, eds.), The Royal Society of Chemistry, Cambridge, 1992, pp. 291–300.
191. E. Dickinson and G. Stainsby, *Colloids in Food*, Applied Science Publishers, London, 1982.
192. M. Coke, P. J. Wilde, E. J. Russell, and D. C. Clark, *J. Colloid Interf. Sci.* 138, 489–504 (1990).
193. J. Krägel, R. Wüstneck, D. Clark, P. Wilde, and R. Miller, *Colloids Surfaces A: Physicochem. Eng. Aspects* 98, 127–135 (1995).
194. J. Chen and E. Dickinson, *Colloids Surfaces A: Physicochem. Eng. Aspects* 101, 77–85 (1995).
195. M. A. Bos and T. Nylander, 12, 2791–2797 (1996).
196. S. G. Hambling, A. S. McAlpine, and L. Sawyer, *Advanced Dairy Chemistry. Vol. 1: Proteins* (P. Fox, ed.), Elsevier Applied Science, London, 1992, pp. 141–190.
197. D. G. Cornell and D. L. Patterson, *J. Agric. Food Chem.* 37, 1455–1459 (1989).
198. D. G. Cornell, *J. Colloid Interf. Sci.* 88, 536–545 (1982).

199. D. G. Cornell, D. L. Patterson, and N. Hoban, *J. Colloid Interf. Sci.* 140, 428–435 (1990).
200. P. J. Quinn and R. M. C. Dawson, *Biochem. J.* 113, 791–803 (1969).
201. P. J. Quinn and R. M. C. Dawson, *Biochem. J.* 115, 65–75 (1969).
202. M. Malmsten, P. Claesson, and G. Siegel, *Langmuir* 10, 1274–1280 (1994).
203. M. Malmsten, *J. Colloid Interf. Sci.* 172, 106–115 (1995).
204. Y. K. Du, J. Y. An, J. Tang, Y. Li, and L. Jiang, *Colloid Surfaces B: Biointerf.* 7, 129–133 (1996).
205. J. A. Ibdah and M. C. Phillips, *Biochemistry* 27, 7155–7162 (1988).
206. I. Hanssens and F. H. Van Cauwelaert, *Biochem. Biophys. Res. Commun.* 84, 1088–1096 (1978).
207. L. Lindahl and H. J. Vogel, *Anal. Biochem.* 140, 394 (1984).
208. W. M. Heckl, B. N. Zaba, and H. Möhwald, *Biochim. Biophys. Acta* 903, 166–176 (1987).
209. M. Schönhoff, M. Lösche, M. Meyer, and C. Wilhelm, *Prog. Colloid Polym. Sci.* 89, 243–248 (1992).
210. J. Zhao, D. Vollhardt, G. Brezesinski, S. Siegel, J. Wu, J. B. Li, and R. Miller, *Colloids Surfaces A: Physicochem. Eng. Aspects* 171, 175–184 (2000).
211. D. G. Cornell and R. J. Carroll, *J. Colloid Interf. Sci.* 108, 226–233 (1985).
212. A. Diederich, C. Sponer, D. Pum, U. B. Sleytr, and M. Lösche, *Colloids Surfaces B: Biointerf.* 6, 335–346 (1996).
213. D. Vollhardt, *Adv. Colloid Interf. Sci.* 47, 1–23 (1993).
214. D. Vollhardt, T. Kato, and M. Kawano, *J. Phys. Chem.* 100, 4141–4147 (1996).
215. A. Gericke, J. Simon-Kutscher, and H. Hühnerfuss, *Langmuir* 9, 2119–2127 (1993).
216. A. Carlsson, M. Bergqvist, R. Nilsson, and T. Nylander, *Program Drug Delivery Systems* 5, 105–115 (1995).
217. S. Danithine, C. Blecker, M. Paquot, N. Innocente, and C. Deroanne, *Lait* 80, 209–222 (2000).
218. I. H. Mather, *J. Dairy Sci.* 83, 203–247 (2000).
219. D. Kristensen, T. Nylander, J. T. Rasmussen, M. Paulsson, and A. Carlsson, *Langmuir* 12, 5856–5862 (1996).
220. D. J. Siminovitich and K. R. Jeffrey, *Biochim. Biophys. Acta* 645, 270–278 (1981).
221. Y. Yamamoto and M. Araki, *Biosci. Biotech. Biochem.* 61, 1791–1795 (1997).
222. S. Aynié, M. Le Meste, B. Colas, and D. Lorient, *J. Food Sci.* 57, 883–887 (1992).
223. E. Bylaite, T. Nylander, R. Venskutonis, and B. Jönsson, *Colloids Surfaces B: Biointerf.* 20, 327–340 (2001).
224. J. L. Courthaudon, E. Dickinson, and W. W. Christie, *J. Agric. Food Chem.* 39, 1365–1368 (1991).
225. E. Dickinson and G. Iveson, *Food Hydrocolloids* 6, 533–541 (1993).
226. Y. Fang and D. G. Dalgleish, *J. Am. Oil Chem. Soc.* 73, 437–442 (1996).
227. I. Heertje, J. Nederlof, H. A. C. M. Hendrickx, and E. H. Lucassen-Reynders, *Food Struct.* 9, 305–316 (1990).

228. U. Seifert, K. Berndl, and R. Lipowsky, *Phys. Rev. A* 44, 1182–1202 (1991).
229. R. Waninge, T. Nylander, M. Paulsson, and B. Bergenståhl, *Colloids Surfaces B: Biointerf.* in press (2003).
230. M. Rytömaa, P. Mustonen, and P. K. J. Kinnunen, *J. Biol. Chem.* 267, 22,243–22,248 (1992).
231. M. E. Price, R. M. Cornelius, and J. L. Brash, *Biochim. Biophys. Acta* 1512, 191–205 (2001).
232. D. V. Brooksbank, J. Leaver, and D. S. Horne, *J. Colloid Interf. Sci.* 161, 38–42 (1993).
233. R. W. Corkery, *Colloids Surfaces B: Biointerf.* 26, 3–20 (2002).
234. J. Kim and H. Kim, *Biochemistry* 25, 7867–7874 (1986).
235. E. M. Brown, R. J. Carroll, P. E. Pfeffer, and J. Sampugna, *Lipids* 18, 111–118 (1983).
236. E. M. Brown, *J. Dairy Sci.* 67, 713–722 (1984).
237. J. N. de Wit, *Developments in Dairy Chemistry—4* (P. F. Fox, ed.), Elsevier Applied Science, London, 1989, pp. 285–322.
238. A. Raudino and F. Castelli, *Colloid Polym. Sci.* 270, 1116–1123 (1992).
239. T. Hønger, K. Jørgensen, R. L. Biltonen, and O. G. Mouritsen, *Biochemistry* 35, 9003–9006 (1996).
240. H. Minami, T. Nylander, and A. Carlsson, *Phys. Chem. Lipids*, submitted (1995).
241. D. M. LeNeveu, R. P. Rand, and V. A. Parsegian, *Biophys. J.* 18, 209–230 (1977).
242. A. C. Cowley, N. L. Fuller, R. P. Rand, and V. A. Parsegian, *Biochemistry* 17, 3163–3168 (1978).
243. R. P. Rand, *Biochim. Biophys. Acta* 241, 823–834 (1971).
244. C. D. McCallum and R. M. Epand, *Biochemistry* 34, 1815–1824 (1995).
245. B. A. Wallis, *Biophys. J.* 49, 295–306 (1986).
246. V. Chupin, J. A. Killian, and B. De Kruijff, *Biophys. J.* 51, 395–405 (1987).
247. B. De Kruijff and P. R. Cullis, *Biochim. Biophys. Acta* 602, 477–490 (1980).
248. P. J. R. Spooner and A. Watts, *Biochemistry* 30, 3880–3885 (1991).
249. P. J. R. Spooner and A. Watts, *Biochemistry* 30, 3871–3879 (1991).
250. T. Heimburg, P. Hildebrandt, and D. Marsh, *Biochemistry* 30, 9084–9089 (1991).
251. V. Razumas, K. Larsson, Y. Miezes, and T. Nylander, *J. Phys. Chem.* 100, 11,766–11,774 (1996).
252. J. Barauskas, V. Razumas, and T. Nylander, *Prog. Colloid Polym. Sci.* 116, 16–20 (2000).
253. P. E. Fraser, R. P. Rand, and C. M. Deber, *Biochim. Biophys. Acta* 983, 23–29 (1989).
254. K. Larsson, *Nature* 304, 664 (1983).
255. S. T. Hyde, S. Andersson, B. Ericsson, and K. Larsson, *Z. Kristallogr.* 168, 213–219 (1984).
256. J. Briggs, H. Chung, and M. Caffrey, *J. Phys. II France* 6, 723–751 (1996).
257. H. Qui and M. Caffrey, *Biomaterials* 21, 223–234 (2000).

258. C. Mattisson, T. Nylander, A. Axelsson, and G. Zacchi, *Chem. Phys. Lipids* 84, 1–12 (1996).
259. V. Razumas, J. Kanapienienė, T. Nylander, S. Engström, and K. Larsson, *Anal. Chim. Acta* 289, 155–162 (1994).
260. V. Razumas, Z. Talaikytė, J. Barauskas, K. Larsson, Y. Mieziš, and T. Nylander, *Chem. Phys. Lipids* 84, 123–138 (1996).
261. T. Nylander, C. Mattisson, V. Razumas, Y. Mieziš, and B. Håkansson, *Colloids Surfaces A: Physicochem. Eng. Aspects* 114, 311–320 (1996).
262. S. B. Leslie, S. Puvvada, B. R. Ratna, and A. S. Rudolph, *Biochim. Biophys. Acta* 1285, 246–254 (1996).
263. B. Ericsson, K. Larsson, and K. Fontell, *Biochim. Biophys. Acta* 729, 23–27 (1983).
264. M. Portmann, E. M. Landau, and P. L. Luisi, *J. Phys. Chem.* 95, 8437–8440 (1991).
265. E. M. Landau and P. L. Luisi, *J. Am. Chem. Soc.* 115, 2102–2106 (1993).
266. K. Larsson and G. Lindblom, *J. Dispers. Sci. Technol.* 3, 61–66 (1982).
267. E. M. Landau and J. P. Rosenbusch, *Proc. Natl. Acad. Sci. USA* 93, 14532–14535 (1996).
268. J. Baruskas, V. Razumas, and T. Nylander, *Chem. Phys. Lipids* 97, 167–179 (1999).
269. H. Gutman, G. Arvidson, K. Fontell, and G. Lindblom, *Surfactants in Solution* (K. L. Mittal and B. Lindman, eds.), Plenum, New York, 1984, pp. 143–152.
270. J. Engblom, Y. Mieziš, T. Nylander, V. Razumas, and K. Larsson, *Prog. Colloid Polym. Sci.* 116, 9–15 (2000).
271. F. Caboi, T. Nylander, V. Razumas, Z. Talaikytė, M. Monduzzi, and K. Larsson, *Langmuir*, 13, 5476–5483.
272. F. Caboi, G. S. Amico, P. Pitzalis, M. Monduzzi, T. Nylander, and K. Larsson, *Chem. Phys. Lipids* 109, 47–62 (2001).
273. R. Wallin and T. Arnebrant, *J. Colloid Interf. Sci.* 164, 16–20 (1994).
274. M. Lindström, H. Ljusberg-Wahren, K. Larsson, and B. Borgström, *Lipids* 16, 749–754 (1981).
275. J. S. Patton, R. D. Vetter, M. Hamosh, B. Borgström, M. Lindström, and M. C. Carey, *Food Microstruct.* 4, 29–41 (1985).
276. J. Borné, T. Nylander, and A. Khan, *J. Phys. Chem. B* 106, 10,492–10,500 (2002).
277. K. Kurihara and Y. Katsuragi, *Nature* 365, 213–214 (1993)

5

Droplet Flocculation and Coalescence in Dilute Oil-in-Water Emulsions

Øystein Sæther and Johan Sjöblom

Norwegian University of Science and Technology, Trondheim, Norway

Stanislav S. Dukhin

New Jersey Institute of Technology, Newark, New Jersey, U.S.A.

I. INTRODUCTION

Emulsions are common in the food industry. They are presented to the consumer as finished products or they appear during the preparation of food from the mixing and treatment of suitable constituents. The emulsion has a certain texture which influences the perception of the food aesthetics and which to the consumer is the most important feature. At the basis lies emulsion stability, which represents the scientific point of view. The texture can be interpreted as a function of the physicochemical properties of the emulsion—the dispersed concentration, droplet size and interactions, bulk and interfacial rheology, and so on—properties that also control droplet aggregation (flocculation or coagulation) and rupture of the membrane between aggregated droplets (coalescence).

Emulsions are thermodynamically unstable (unlike microemulsions), and stability is achieved kinetically. The notion of stability includes both retardation of sedimentation or creaming (driven by the density difference between droplets and the surrounding fluid, and greatly dependent on the viscosity of the last and droplet size), reduction of coagulation [irreversible droplet aggregation, countered (e.g., by repulsion arising from the

adsorbed layer)], and stabilization of the interface in order to retard coalescence (linked to the viscoelastic properties of the interfacial layer).

Food emulsions include milk, butter, ice cream, mayonnaise, margarine, and many more. Milk, cream, and mayonnaise are oil-in-water emulsions, stabilized from coalescence by interfacially adsorbed surfactants indigenous to the raw material.

The next example illustrates how the processes of destabilization are countered. The homogenization of milk induces droplet breakup by passing the liquid through a high-pressure-drop mixing valve, resulting in droplet sizes down to about 250 nm (1). A droplet size of 250 nm is so small that the creaming rate is extremely low and Brownian diffusion will dominate droplet motion. The newly formed interface is stabilized by adsorbed casein (and relatives) and phospholipids, expectedly forming a complex film of monomers, aggregates, and even particles (2). Adsorbed species at the interface give rise to a repulsive contribution to the droplet–droplet interaction potential (electrostatic and/or steric), reducing the *collision efficiency* (the ratio of collisions leading to coalescence to the total number of collisions). The film formed by the species can, to some system-specific degree, resist rupture upon collision, as elastic film properties will restore the film as collision energy is dissipated. These separate factors work to decrease the rate of separation and give milk a certain lifetime. Figure 1 shows snapshots of

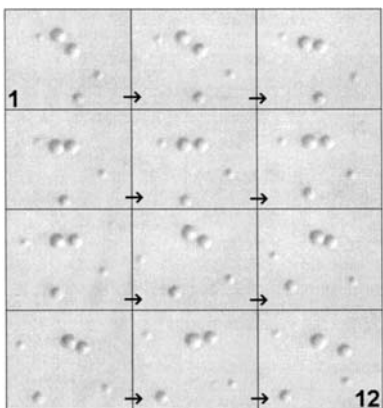


Figure 1 Image series (from frame 1 at the upper left to frame 12 at the lower right) showing oil droplets in milk interacting, and the formation and fragmentation of a short-lived doublet. The milk (“1.5% fat”) was centrifuged to reduce the droplet numerical concentration in the prepared sample. The largest droplet is about 3 μm , the time between images 0.5 s.

droplets interacting in a milk sample in which the majority of droplets have been centrifuged off to isolate droplet pair effects.

In the following, the authors attempt to describe the interplay of mechanisms that influence the breakdown of kinetically stabilized emulsions, namely droplet aggregation (flocculation or coagulation), droplet aggregate fragmentation and coalescence.

A. Kinetic and Thermodynamic Stability in Macroemulsions and Miniemulsions

The majority of emulsion technology problems relate to the stabilization and destabilization of emulsions (3–9). Despite the existence of many fundamental studies related to the stability of emulsions, the extreme variability and complexity of the systems involved in any specific application often pushes the industry to achieve technologically applicable results without developing a detailed understanding of the fundamental processes. Nevertheless, because in most cases, technological success requires the design of emulsions with a very delicate equilibrium between stability and instability, a better understanding of the mechanisms of stabilization and destabilization might lead to significant breakthroughs in technology.

Notwithstanding their thermodynamic instability, many emulsions are kinetically stable and do not change appreciably for a prolonged period. These systems exist in the metastable state (10–17). The fundamentals of emulsion stability (destabilization) comprise emulsion surface chemistry and physicochemical kinetics.

In contrast to the large success in industrial applications of emulsion surface chemistry, the potential of physicochemical kinetics as basis for emulsion dynamics modeling is almost never used in emulsion technology. This situation has started to change during the last decade. Although the coupling of the subprocesses in emulsion dynamics modeling (EDM) continues to represent a large problem yet to be solved, models are elaborated for (a) macroemulsions (12,18–24) and (b) miniemulsions (25–32) for long and short lifetimes of thin emulsion films.

- (a) For large droplets (larger than 10–30 μm) in macroemulsions, the rate of thinning of the emulsion film formed between two approaching droplets is rather low and, correspondingly, the entire lifetime of an emulsion need not be short, even without surfactant stabilization of the film. For this case, the notion of *kinetic stability* is introduced (12,18–21) to denote the resistance of the film against *rupture during thinning*. Droplet deformation

and flattening of the interface is the cause of this strong resistance, described by the Reynolds equation (33,34). According to theory, the role of deformation (35–37) decreases rapidly with decreasing droplet dimension.

- (b) For small droplets (smaller than 5–10 μm) in miniemulsions, droplet deformation can be neglected, because the Reynolds drainage rate increases as (12,38) (R_d = the Reynolds film radius) and because the smaller the droplets, the smaller is the deformation (35–37).

In distinction from macroemulsions, where the kinetic stability is the manifestation of droplet–droplet hydrodynamic interaction and droplet deformation, in miniemulsions the kinetic stability is the manifestation of the interplay between surface forces and Brownian movement (25). As the molecular forces of attraction decrease linearly with decreasing droplet dimension (viz. approximately 10 times at the transition from macroemulsions to miniemulsions) the potential minimum of droplet–droplet interaction (the secondary minimum) decreases, and for miniemulsions, this depth can be evaluated as 1–5 kT (14,39). At such low energy, Brownian movement causes disaggregation of droplet doublets after a short time (the doublet fragmentation time, τ_d). If this time is shorter than the lifetime of the thin film, a rapid decrease in the total droplet concentration (t.d.c) is prevented (restricted by the coalescence time, τ_c); that is, stability is achieved due to this kinetic mechanism (25).

B. Current State of Emulsion Stability Science

A large misbalance exists between knowledge concerning kinetic stability and thermodynamic stability. Attention has been paid primarily to *kinetic stability* for both macroemulsions (18–24) and miniemulsions (25–32). As a result, the droplet–droplet interaction and the collective processes in dilute emulsions are quantified (40,41) and important experimental investigations have been made (29,30,42). Some models are elaborated for the entire process of coalescence in concentrated emulsions as well (43,44). Given thermodynamic stability, a thin interdroplet film can be metastable.

In contrast to the large achievements in the investigations of kinetic stability, modest attention has been paid to the fundamentals of the thermodynamic stability in emulsions, especially regarding the surfactant adsorption layer's influence on the coalescence time. There are several investigations devoted to the surface chemistry of adsorption related to

emulsification and demulsification. However, the link among the chemical nature of an adsorption layer, its structure and the coalescence time is not yet quantified.

A premise for such quantification is the theory of a foam bilayer lifetime (45). The main notions of this theory is similar to theory of Derjaguin et al. (46,47). However, the theory (45) is specified for amphiphile foam films, it is elaborated in detail, and it is proven by experiment with water-soluble amphiphiles, such as sodium dodecyl sulfate (48). Because as the dependence of the rupture of the emulsion film on surfactant concentration is similar to that of a foam film, modification of the theory with respect to emulsions may be possible. Although this modification is desirable, the specification of theory for a given surfactant will not be trivial, because the parameters in the equation for the lifetime (47) are unknown and their determination is not trivial. As the theory (45,49) is proposed for amphiphiles and a wider class of chemical compounds can stabilize emulsions, the film rupture mechanism (46) is not universal regarding emulsions.

In contrast to the quantification of kinetic stability, the empirical approach continues to predominate regarding thermodynamic stability. Meanwhile, thermodynamic stability provides greater opportunity for long-term stabilization of emulsions than does kinetic stability. This means that the experimental characterization of thermodynamic stability (i.e., the measurement of coalescence time) is of major importance.

C. Specificity of Emulsion Characterization

Generalized emulsion characterization (i.e., measurement of droplet size distribution, electrokinetic potential, Hamaker constant, etc.) is not always sufficient. Thermodynamic stability with respect to bilayer rupture cannot be quantified with such a characterization procedure alone. Consequently, measurement of the coalescence time τ_c is of major importance for an evaluation of emulsion stability; it is an important and specific parameter of emulsion characterization.

The current state of miniemulsion characterization neglects the importance of τ_c measurement. The practice of τ_c measurement is practically absent with the exception of only a few articles considered in this chapter. Meanwhile, many articles devoted to issues more or less related to emulsion stability do not discuss τ_c measurement. One reason for this scientifically and technologically unfavorable situation in which emulsions are incompletely characterized might originate from a lack of devices enabling τ_c measurement.

D. Scope of the Chapter

This chapter is focused on kinetic stability in miniemulsions, with emphasis on the coupled destabilizing subprocesses. In general, there are three coupled subprocesses which will influence the rate of destabilization and phase separation in emulsions. These are aggregation, coalescence, and floc fragmentation. Often, irreversible aggregation is called coagulation and the term *flocculation* is used for reversible aggregation (45,50). Ostwald ripening (51,52) coupled (26) with aggregation and fragmentation is a separate topic and will be not considered here.

A simplified theory is available for the coupling of coalescence and flocculation in emulsions void of larger flocs. This theory is considered in Section II and will assist in the consideration of the more complicated theory of coupling of coalescence and coagulation (Sec. III). The experimental investigations are described in parallel. Section IV is devoted to the theory of doublet fragmentation time and its measurement, as this characterizes an emulsion regarding fragmentation and because its measurement is an important source of information about surface forces and the pair interaction potential. The discrimination between conditions for coupling of coalescence with coagulation or with flocculation is considered in Section V. The quantification of kinetic stability creates new opportunities for the long-term prediction of miniemulsion stability, for stability optimization, and for characterization with standardization of τ_c and τ_d measurements. This forms the base for emulsion dynamics modeling (Sec. VI).

II. COUPLING OF COALESCENCE AND FLOCCULATION

A. Singlet–Doublet Quasiequilibrium

Each process among the three processes under consideration is characterized by a characteristic time, namely τ_{Sm} , τ_d , and τ_c . The Smoluchowski time (53), τ_{Sm} , gives the average time between droplet collisions. If the time between two collisions is shorter than τ_d , a doublet can transform into a triplet before it spontaneously disrupts. In the opposite case—at

$$\tau_{Sm} \gg \tau_d \tag{1}$$

—the probability for a doublet to transform into a triplet is very low because the disruption of the doublet occurs much earlier than its collision

with a singlet. The rate of multiplet formation is very low for

$$\text{Rev} = \frac{\tau_d}{\tau_{\text{Sm}}} \ll 1 \quad (2)$$

where we introduce the notation Rev for small values of the ratio corresponding to the reversibility of aggregation and a singlet–doublet quasiequilibrium.

The kinetic equation for reversible flocculation in a dilute mono-disperse oil-in-water (o/w) emulsion when neglecting coalescence is (54–56)

$$\frac{dn_2}{dt} = \frac{n_1^2}{\tau_{\text{Sm}}} - \frac{n_2}{\tau_d} \quad (3)$$

where n_1 and n_2 are the dimensionless concentrations of doublets and singlets and $n_1 = N_1/N_{10}$ and $n_2 = N_2/N_{10}$, where N_1 and N_2 are the concentrations of singlets and doublets, respectively, and N_{10} is the initial concentration, and

$$\tau_{\text{Sm}} = \left(\frac{4kT}{3\eta} N_{10} \right)^{-1} = (K_f N_{10})^{-1} \quad (4)$$

where k is the Boltzmann constant, T is the absolute temperature, and η is the viscosity of water. For aqueous dispersions at 25°C, $K_f = (4kT/3\eta) = 6 \times 10^{-18} \text{ m}^3/\text{s}$. The singlet concentration decreases with time due to doublet formation, whereas the doublet concentration increases. As a result, the rates of aggregation and floc fragmentation will approach each other. Correspondingly, the change in the number of doublets $dn_2/dt = 0$. Thus, a dynamic singlet–doublet equilibrium (s.d.e.) is established:

$$n_{2\text{eq}} = \frac{\tau_d}{\tau_{\text{Sm}}} n_{1\text{eq}}^2 \quad (5)$$

At condition (2), it follows from Eq. (5) that

$$n_{1\text{eq}} \cong 1, \quad N_{1\text{eq}} = N_{10} \quad (6)$$

$$N_2 = (\text{Rev})N_{10} \quad \text{or} \quad n_2 \ll 1 \quad (7)$$

Thus, at small values of Rev, the s.d.e. is established with only small deviations in the singlet equilibrium concentration from the initial concentration [Eq. (6)]. The doublet concentration is very low compared to the singlet concentration, and the multiplet concentration is very low compared to the doublet concentration. The last statement follows from a comparison

of the production rates of doublets and triplets. The doublets appear due to singlet–singlet collisions, whereas the triplets appear due to singlet–doublet collisions. The latter rate is lower due to the low doublet concentration. The ratio of the number of singlet–doublet collisions to the number of singlet–singlet collisions is proportional to Rev.

B. Kinetic Equation for Coupling of Flocculation and Intradoublet Coalescence in Monodisperse Emulsions

Both the rate of doublet disaggregation and the rate of intradoublet coalescence are proportional to the momentary doublet concentration. This leads (25,31) to a generalization of Eq. (3):

$$\frac{dn_2}{dt} = \frac{n_1^2}{\tau_{Sm}} - n_2 \left(\frac{1}{\tau_d} + \frac{1}{\tau_c} \right) \quad (8)$$

There are two unknown functions in Eq. (8), so an additional equation is needed. This equation describes the decrease in the droplet concentration caused by coalescence:

$$\frac{d}{dt}(n_1 + 2n_2) = -\frac{n_2}{\tau_c} \quad (9)$$

The initial conditions are

$$n_2|_{t=0} = 0 \quad (10)$$

$$\left. \frac{dn_2}{dt} \right|_{t=0} = \frac{n_{10}}{\tau_{Sm}} \quad (11)$$

Condition (11) follows from Eqs. (8) and (9). The solution of the set of Eqs. (8) and (9) taking into account boundary conditions (10) and (11) is a superposition of two exponents (25,31). In the case

$$\tau_c \gg \tau_d \quad (12)$$

the solution simplifies (25,31) to

$$n_2(t) = \frac{\tau_d}{\tau_{Sm}} \left[\exp\left(-\frac{2\tau_d t}{\tau_{Sm}\tau_c}\right) - \exp\left(-\frac{t}{\tau_d}\right) \right] \quad (13)$$

Equation (13), as compared to Eqs. (5) and (6), corresponds to the s.d.e. if the expression in the second set of brackets equals 1. In the time interval

$$\tau_d < t < \tau \quad (14)$$

where

$$\tau = \tau_c \frac{\tau_{Sm}}{2\tau_d} \quad (15)$$

the first term in the second set of brackets approximately equals 1, whereas the second term decreases from 1 to a very small value. Thus, the s.d.e. is established during the time τ_d and preserves during the longer time interval [according to Eq. (14)].

For times longer than τ , there is no reason to apply Eq. (13) because the condition to linearize Eq. (8) is no longer valid with the concentration decrease. At the beginning of the process, the doublet concentration increases, whereas later in the process, coalescence predominates and the doublet concentration decreases. Thus, the function in Eq. (13) has a maximum (25,31).

C. Coalescence in a Singlet–Doublet System at Quasiequilibrium

After a time t_{max} , a slow decrease in the doublet concentration takes place simultaneously with the more rapid processes of aggregation and disaggregation. Naturally, an exact singlet–doublet equilibrium is not valid due to the continuous decrease in the doublet concentration. However, the slower the coalescence, the smaller is the deviation from the momentary dynamic equilibrium with respect to the aggregation–disaggregation processes.

It is reasonable to neglect the deviation from the momentary doublet–singlet equilibrium with the condition

$$\frac{dn_2}{dt} \ll \frac{n_2}{\tau_d} \quad (16)$$

Indeed, for this condition, the derivative in Eq. (3) can be omitted, which corresponds to s.d.e. characterized by Eq. (5).

It turns out (25,29–31) that the deviation from s.d.e. is negligible because the condition (15) is valid [i.e., for conditions (2) and (12)]. For these conditions, the fragmentation of flocs influences the coalescence kinetics, which can be represented as a three-stage process, as illustrated in Fig. 2. During a rather short time τ_d , the approach to s.d.e. takes place

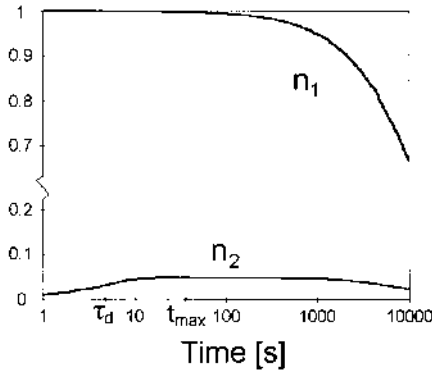


Figure 2 Three stages in the coupling of aggregation, fragmentation, and coalescence at the condition $\tau_d \ll \tau_{Sm} \ll \tau_c$. Initially, the doublet concentration n_2 is very low and the rates of doublet fragmentation and of coalescence are correspondingly low compared to the rate of aggregation (first stage, no coupling). Due to increasing n_2 , the fragmentation rate increases and equals the aggregation rate at t_{max} (exact singlet–doublet equilibrium). The growth in n_2 stops at t_{max} (second stage, coupling of aggregation and fragmentation). Intradoublet coalescence causes a slight deviation from exact s.d.e. to arise at $t > t_{max}$, and the singlet concentration n_1 and the doublet concentration decrease due to intradoublet coalescence (third stage, coupling of aggregation, fragmentation, and coalescence). n_1 and n_2 are dimensionless, ($n_1 = N_1/N_{10}$, $n_2 = N_2/N_{10}$, N_{10} is the initial singlet concentration). (From Ref. 25.)

[i.e., a rather rapid increase in the doublet concentration (stage 1)]. During the next time interval, $\tau_d < t < t_{max}$, the same process continues. However, the rate of doublet formation declines due to coalescence (stage 2). The exact equilibrium between the doublet formation and their disappearance due to coalescence takes place at the time t_{max} when the doublet concentration reaches its maximum value, $n_2(t_{max})$. During the third stage, when $t > t_{max}$, the rate of doublet fragmentation is lower than the rate of formation, because of the coalescence within doublets. This causes a slow monotonous decrease in the concentration. Taking into account the s.d.e. [Eqs. (5) and (7)], Eq. (9) can be expressed as

$$\frac{dn_1}{dt} = -\frac{\tau_d}{\tau_{Sm} \tau_c} n_1^2 \quad (17)$$

The result of the integration of Eq. (17) can be simplified to

$$n_1(t) = \frac{n_1(t_{max})}{1 + n_1(t_{max})t/2\tau} \cong \left(1 + \frac{t}{2\tau}\right)^{-1} \quad (18)$$

with a small deviation in $n_1(t_{\max})$ from 1. Differing from the preceding stages when the decrease in the droplet concentration caused by coalescence is small, a large decrease is now possible during the third stage. Thus, this is the most important stage of the coalescence kinetics.

D. Reduced Role of Fragmentation with Decreasing τ_c

With decreasing τ_c , condition (12) is violated and new qualitative features of the destabilization process not discussed in Refs. 29–31 arise. As the ratio τ_c/τ_d diminishes and

$$\tau_c < \tau_d \quad (19)$$

the s.d.e. is violated because a larger part of the doublets disappears due to coalescence. Correspondingly, the smaller the ratio τ_c/τ_d , the smaller is the fragmentation rate in comparison with the aggregation rate (i.e., the larger the deviation from s.d.e.). In the extreme case

$$\tau_c \ll \tau_d \quad (20)$$

the fragmentation role in s.d.e. can be neglected. This means that almost any act of aggregation is accompanied by coalescence after a short doublet lifetime. Neglecting this time in comparison with τ_{Sm} in agreement with condition (1), one concludes that any act of aggregation is accompanied by the disappearance of one singlet:

$$\frac{dn_1}{dt} = -\frac{n_1^2}{\tau_{Sm}} \quad (21)$$

This leads to a decrease in the singlet concentration described by an equation similar to the Smoluchowski equation for rapid coagulation:

$$n_1(t) = \left(1 + \frac{t}{\tau_{Sm}}\right)^{-1} \quad (22)$$

The Smoluchowski equation describing the singlet time evolution does not coincide with Eq. (22). The peculiarity of Eq. (22) is that it describes the kinetics of coupled aggregation and coalescence with a negligible fragmentation rate. Due to fragmentation, doublet transformation into multiplets is almost impossible at condition (1).

The coupling of aggregation, fragmentation, and coalescence in the more general case described by condition (19) leads to

$$n_1(t) = \frac{n_1(t_{\max})}{1 + n_1(t_{\max})t/2\tau_g} \cong \left(1 + \frac{t}{2\tau_g}\right)^{-1} \quad (t > \tau_d + \tau_c) \quad (23)$$

with a small deviation of $n_1(t_{\max})$ from 1 and

$$\tau_g = \frac{\tau_{\text{Sm}}(\tau_d + \tau_c)}{2\tau_d} \quad (24)$$

At conditions (1) and (12) $\tau_g \approx \tau$ and Eq. (23) transforms into Eq. (18). At conditions (1) and (20) $\tau_g \approx \tau_{\text{Sm}}$ and Eq. (23) transforms into Eq. (22). Equation (24) demonstrates the reduction of the role of fragmentation with decreasing τ_c . It is seen that at the transition from condition (19) to condition (20), τ_d cancels in Eq. (21) (i.e., the fragmentation role diminishes).

E. Experimental

1. Video-Enhanced Microscopy (Microslide Preparative Technique) for Investigation of Singlet–Doublet Equilibrium and Intradoublet Coalescence (29–31)

Direct observation of doublets in the emulsion bulk is difficult due to doublets tending to move away from the focal plane during the time of observation. The microslide preparative technique can, however, be successfully applied, providing pseudobulk conditions. A microslide is a plane-parallel glass capillary of rectangular cross section. The bottom and top walls of the capillary are horizontal, and the gravity-induced formation of a sediment or cream on one of the inner normal surfaces is rapidly completed due to the modest inner diameter of the slide (typically 50–100 μm). If both the volume fraction of droplets in an emulsion and the slide inner diameter are small, the droplet coverage along the inside surface amounts to no more than a few percent, and the analysis of results is rather simple. It can be seen through the microscope that the droplets which have sedimented (or for the case of oil droplets, creamed) toward the capillary surface participate in chaotic motion along the surface. This indicates that a thin layer of water separating the surface of the microslide from the droplets is preventing the main portion of droplets from adhering to the microslide surface—an action which would stop their Brownian motion.

During diffusion along the microslide ceiling, the oil droplets collide. Some collisions lead to the formation of doublets. Direct visual observation enables evaluation of the doublet fragmentation time, which varies in a broad range (27). Another approach to doublet fragmentation time determination is based on the evaluation of the average concentration of singlets and doublets and using the above-outlined theory.

The application of the microslide preparative technique combined with video microscopy is promising and has enabled the measurement of the coupling of reversible flocculation and coalescence (29,31). However, some experimental difficulties were encountered. A modest number of droplets could sometimes be seen sticking to the glass surface of the microslide—an effect that corresponded to electrolyte-induced reduction of electrostatic stabilization by adsorbed surfactant. According to theory, increased salt concentration would increase the number of droplets adhering to the surface, reducing the span of electrolyte concentrations that could be used.

2. Improving the Experimental Technique with the Use of Low-Density Contrast Emulsions (30)

The sticking of droplets indicates a droplet–wall attraction and the existence of a secondary potential pit as that for the droplet–droplet attraction in a doublet. The droplet concentration within the pit is proportional to the concentration on its boundary. The latter decreases with a decrease in the density contrast (i.e., the density difference between the droplet and continuous phases). The higher the contrast, the greater the gravity promoted adhesion of droplets to the wall. The electrostatic barrier between the potential pit and the wall retards the rate of sticking. The lower the droplet flux through this barrier, the lower is the potential pit occupancy by droplets. Thus, an essential decrease in the rate of sticking is possible with decreasing density contrast.

Oil-in-water emulsions were prepared (30) by mixing dichlorodecane (DCD, volume fraction 1%) into a 5×10^{-5} M sodium dodecyl sulfate (SDS) solution with a Silverson homogenizer. The oil phase was a 70:1 mixture of DCD, which is characterized by an extremely low-density contrast to water, and decane.

The droplet distribution along and across the slide was uniform (30). This indicates that there was no gravity-induced rolling either. One slide among four was examined for 2 weeks without any sticking being observed (30). The absence of the rolling and sticking phenomena allowed acquisition of rather accurate data concerning the time dependence of the droplet size distribution.

3. Measurement of Coalescence Time and Doublet Fragmentation Time

The doublet fragmentation time was measured by direct real-time on-screen observation of the doublets and by analysis of series of images acquired with 1–3-min time intervals (47). The formation and disruption/coalescence of a doublet could thus be determined.

The general form of the concentration dependence agrees with the theory. At $C \sim 3 \times 10^{-3}$ M, both theory and experiment yield times of about 1 min; at $C = 9 \times 10^{-3}$ M, these times exceed 10 min. For the calculation of the doublet fragmentation time, the electrokinetic potential was measured (31,48).

In experiments with different droplet concentrations, it was established that the higher the initial droplet concentration, the higher the doublet concentration. This corresponds to the notion of singlet–doublet equilibrium. However, if the initial droplet concentration exceeds 200–300 per observed section of the microslide, multiplets predominate. Both the initial droplet concentration and size affect the rate of decrease in the droplet concentration. The larger the droplets, the smaller the concentration sufficient for the measurement of the rate of decrease in the droplet concentration. This agrees with the theory of doublet fragmentation time, which increases with droplet dimension. Correspondingly, the probability for coalescence increases. These first series of experiments (29,31) were accomplished using toluene-in-water emulsions without the addition of a surfactant and decane-in-water emulsions stabilized by SDS. The obtained data concerning the influence of the electrolyte concentration and surface charge density were in agreement with the existing notions about the mechanism of coalescence. With increasing SDS concentration and correspondingly increasing *surface potential*, the rate of decrease in the droplet concentration is reduced.

Two methods were used for the measurement of the coalescence time (30,31). Measurement of the time dependence for the concentrations of singlets and doublets and a comparison with Eq. (9) enables an evaluation of the coalescence time. Further, information about the time dependence for singlets and the doublet fragmentation time may be used as well. These results in combination with Eqs. (18) and (15) determine the coalescence time. The good agreement between results obtained by these very different methods indicates that the exactness of the theory and experiments is not low.

In recent years, several research groups have improved significantly the theoretical understanding of coalescence of droplet or bubbles. The new results (55–59) together with results of earlier investigations (60–64)

have clarified the role of double-layer interaction in the elementary act of coalescence.

Derjaguin-Landau-Verwey-Overbeek (DLVO) theory was applied (65,66) for the description of “spontaneous” and “forced” thinning of the liquid film separating the droplets. These experimental results and DLVO theory were used (65) for the interpretation of the reported visual study of coalescence of oil droplets 70–140 μm in diameter in water over a wide pH interval. A comparison based on DLVO theory and these experimental data led the authors to conclude (65) that “if the total interaction energy is close to zero or has a positive slope in the critical thickness range, i.e. between 30 and 50 nm, the oil drops should be expected to coalesce.” In the second article (66), in which both ionic strength and pH effects were studied, coalescence was observed at constant pH values of 5.7 and 10.9, when the Debye thickness was less than 5 nm. The main trend in our experiments and in Refs. 65 and 66 are in accordance, because it was difficult to establish the decrease in total droplet concentration (t.d.c.) at NaCl concentrations lower than 5×10^{-3} M (i.e., DL thicknesses larger than 5 nm). An almost quantitative coincidence in the double-layer influence on coalescence established in our work for micrometer-sized droplets and in Refs. 65 and 66 for almost 100 times larger droplets is important for the general knowledge about coalescence.

F. Perspective for Generalization of the Theory for Coupling of Coalescence and Flocculation

The proposed theory for coupling of coalescence and flocculation at s.d.e. enables the proposal of some important applications (Sec. VI). At the same time, generalized theory is necessary, because the role of multiplets increases after some time or with a higher initial concentration. At least two approaches to this difficult task are seen.

According to our video-microscopic observations, there are large peculiarities in the structure and behavior of multiplets arising at conditions close to s.d.e. These peculiarities can be interpreted as the manifestation of quasiequilibrium, comprising singlets, doublets, and multiplets. Similar to doublets, the lifetime of triplets, tetraplets, and so forth can be short due to fragmentation and coalescence. This can be valid for multiplets with an “open” structure, in distinction from another structure which can be called “closed.” In “open” multiplets, any droplet has no more than one or two contacts with other droplets, which corresponds to a linear chainlike structure. This causes easy fragmentation, especially for the outermost droplets within a chain. The “closed” aggregates have a denser and more

isometric structure, in which droplets may have more than two contacts with neighboring droplets. As result, fragmentation is more difficult and the frequency is lower.

The recent progress in theory of aggregation with fragmentation (67–71) for a suspension creates a premise for a theoretical extension toward emulsions. However, the necessity in accounting for coalescence makes this task a difficult one.

III. COUPLING OF COALESCENCE AND COAGULATION

A. General

For emulsion characterization, the notation n_1 represents the number density of single droplets and n_i represents the number density of aggregates comprising i droplets ($i=2, 3, \dots$). The total number density of single droplets and all kinds of aggregates is given by

$$n = \sum_{i=1}^{\infty} n_i \quad (25)$$

This characterization corresponds to Smoluchowski's theory (53). To characterize coalescence, the total number of individual droplets moving freely plus the number of droplets included in all kinds of aggregates, n_T ,

$$n_T = \sum_{i=1}^{\infty} i n_i \quad (26)$$

is introduced as well.

In distinction from Smoluchowski's theory for suspensions, which predicts the time dependence of the concentration of all kinds of aggregates, the time dependence for the total droplet number can be predicted at the current state of emulsion dynamics theory.

The quantification of coagulation within the theory of coupled coagulation and coalescence (CCC theory) is based on the Smoluchowski theory of perikinetic coagulation. Correspondingly, all restrictions inherent to the Smoluchowski theory of Brownian coagulation are preserved in the CCC theory. This means that creaming and gravitational coagulation are taken into account. A variant of Smoluchowski's theory specified with regard for gravitational coagulation is well known (72). However, its application is very difficult because the rate constant of collisions induced by gravity depends on droplet dimension (14). Due to the weak particle (aggregate) dimension dependence of the rate constants for Brownian collisions, Smoluchowski's theory is valid for polydisperse suspensions

and remains valid as polydisperse aggregates arise. Unfortunately, this advantage of the Smoluchowski theory can almost disappear when combined with the coalescence theory, because the coalescence rate coefficients are sensitive to droplet dimension. Thus, droplet and aggregate polydispersity does not strongly decrease the exactness of the description of coagulation in the CCC theory, whereas the exactness of the coalescence description can be severely reduced.

Although the coalescence influence on the Brownian coagulation rate coefficient can be neglected, its influence on the final equations of the Smoluchowski theory remains. It can be shown that Smoluchowski's equation for the total number of particles,

$$n(t) = \left(1 + \frac{t}{\tau_{\text{Sm}}}\right)^{-1} \quad (27)$$

remains valid, whereas, in parallel, the equations for the singlet and aggregate concentrations cannot be used to account for coalescence. Regarding coupled coagulation and coalescence, the Smoluchowski equation for $n_1(t)$ is not exact because it does not take into account the singlet formation caused by coalescence within doublets.

The coalescence within an aggregate consisting of i droplet is accompanied by the aggregate transforming into an aggregate consisting of $i - 1$ droplets. Because coalescence changes the aggregate type only, the total quantity of aggregates and singlets does not change. This means that the Smoluchowski function $n(t)$ does not change during coalescence, because Smoluchowski defined the total quantity of particles as consisting of aggregates and singlets.

B. Average Models

Average models do not assign rate constants to each possibility for coalescence within the aggregates; they deal with certain averaged characteristics of the process. The models in Refs. 40 and 73 introduce the average number of drops in an aggregate m , because the number of films in an aggregate n_f and m are interconnected. For a linear aggregate,

$$n_f = m - 1 \quad (28)$$

As the coalescence rate for one film is characterized by τ_c^{-1} , the decrease in the average droplet quantity in an aggregate is n_f times larger. This is taken into account in the model of van den Tempel for simultaneous droplet quantity increase due to aggregation and decrease due to coalescence.

Van den Tempel formulates the equation which describes the time dependence for the average number of droplets in an aggregate as

$$\frac{dm}{dt} = K_f N_{10} - \tau_c^{-1}(m - 1) \quad (29)$$

where the first term is derived using Smoluchowski's theory.

The total number of droplets n_T is the sum of single droplets $n_1(t)$ and the droplets within aggregates,

$$n_T(t) = n_1(t) + n_v(t)m(t) \quad (30)$$

where n_v is the aggregate number. The latter can be expressed as

$$n_v(t) = n(t) - n_1(t) \quad (31)$$

Both terms are expressed by Smoluchowski's theory. The integration of Eq. (29) and the substitution of the result into Eq. (30) yields the time dependence $n_T(t)$ according to the van den Tempel model.

1. The Model of Borwankar et al.

In Ref. 40, the van den Tempel model is criticized and improved through the elimination of Eq. (29). The authors point out that the "incoming" aggregates which cause the increase in m have themselves undergone coalescence. This is not taken into account in the first term on the right-hand side of Eq. (29). Instead of taking a balance on each aggregate (as van den Tempel did), Borwankar et al. took an overall balance on all particles in the emulsion. For linear aggregates, the total number of films in the emulsion is given by

$$n_f n_v = (m - 1)n_v \quad (32)$$

Thus, instead of Eq. (29), the differential equation for n_T follows:

$$-\frac{dn_T}{dt} = \tau_c^{-1}(m - 1)n_v \quad (33)$$

where m can be expressed through n_T using Eq. (30). The advantage of this equation in comparison with Eq. (29) is obvious. However, there is a common disadvantage of both theories, caused by the use of the Smoluchowski equation for $n_1(t)$. Coalescence does not change the total

particle concentration $n(t)$, but it changes $n_1(t)$ and, correspondingly, $n_v(t)$, according to Eq. (31).

The application of Smoluchowski's theory in the quantification of the coupling of coalescence and coagulation has to be restricted with the use of the total particle concentration $n(t)$ only. The average models of van den Tempel and Borwankar et al. do not meet this demand.

The theory of Danov et al. (41) does not contradict this demand, which makes it more correct than the preceding theories. Among the Smoluchowski results, the function $n(t)$ only is present in the final equations of this theory. Although the exactness of averaged models is reduced due to the violation of the restriction in the use of the Smoluchowski theory, results for some limiting cases are not erroneous.

2. Limiting Cases of Fast and Slow Coalescence

Two limiting cases can be distinguished:

The rate of coalescence is much greater than that of flocculation (rapid coalescence):

$$\tau_c^{-1} \gg \tau_{Sm}^{-1} \quad (34)$$

The rate of flocculation is much greater than that of coalescence (slow coalescence):

$$\tau_c^{-1} \ll \tau_{Sm}^{-1} \quad (35)$$

According to general regularities of physicochemical kinetics, the slowest process is rate controlling. If the coagulation step is rate controlling [viz. when condition (34) is valid], then the coalescence is rapid and the general equation of the theory in Ref. 40 is reduced to second order kinetics [i.e., to Smoluchowski's equation (27)]. Flocs composed of three, four, and more droplets cannot be formed because of rapid coalescence within the floc. In this case, the structure of the flocs becomes irrelevant.

At first glance, the coagulation rate has not manifested itself in the entire destabilization process in the case of slow coalescence [condition (35)]. At any given moment, the decrease in the total droplet concentration is proportional to the momentary total droplet concentration (first-order kinetics), which causes an exponential decrease with time:

$$n = \exp\left(-\frac{t}{\tau_c}\right) \quad (36)$$

However, this equation cannot be valid for an initial short period of time, because at the initial moment, there are no aggregates and their quantity continues to be low during a short time. This means that the coagulation is limiting during an initial time at any slow coalescence rate. This example illustrates the necessity of a more exact approach than that which uses average models. This was done by Danov et al. (41).

C. The DIGB Model for Simultaneous Coagulation and Coalescence

This kinetic model proposed by Danov, Ivanov, Gurkov, and Borwankar is called the DIGB model here for the sake of brevity. Danov et al. (41) generalized the Smoluchowski scheme (Fig. 3a) to account for droplet coalescence within flocs. Any aggregate (floc) composed of k particles can partially coalesce to become an aggregate of i particles ($1 < i < k$), with the rate constant being $K_c^{k,i}$ (Fig. 3b). This aggregate is further involved in the flocculation scheme, which makes the flocculation and coalescence processes interdependent. Therefore, the system exhibiting both flocculation and coalescence is described by a combination of schemes 1 and 2:

$$\frac{dn_k}{dt} = \sum_{i=1}^{k-1} K_f^{i,k-i} n_i n_{k-i} - 2 \sum_{i=1}^{\infty} K_f^{k,i} n_k n_i + \sum_{i=k+1}^{\infty} K_c^{i,k} n_i - \sum_{i=1}^{k-1} K_c^{k,i} n_k \quad (37)$$

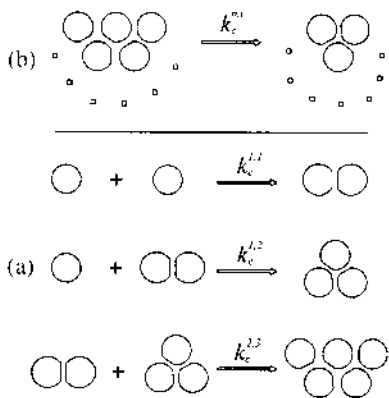


Figure 3 (a) Model of flocculation according to the Smoluchowski scheme (41). (b) Coalescence in an aggregate of k particles to become an aggregate of i particles, with a rate constant $K_c^{k,i}$, $1 < i < k$ (41).

Equation (37) is multiplied by k and summed up for all k , which yields the equation for n_T , which is expressed through double sums. The change of the operation sequence in these sums leads to the important and convenient equation

$$\frac{dn_T}{dt} = \sum_{k=1}^{\infty} k \sum_{i=k+1}^{\infty} K_c^{i,k} n_i - \sum_{i=2}^{\infty} k \sum_{i=1}^{k-1} K_c^{k,i} n_k \quad (38)$$

Afterward, a total rate coefficient referring to complete coalescence of the i th aggregate

$$K_{c,T}^i = \sum_{k=1}^{i-1} (i-k) K_c^{i,k}, \quad i = 2, 3, \dots \quad (39)$$

is introduced. For linearly built aggregates

$$K_{c,T}^i = K_c^{2,1}(i-1) \quad (40)$$

is derived. With this expression for $K_{c,T}^i$, using also Eqs. (25) and (26), Eq. (40) is transformed into

$$\frac{dn_T}{dt} = -K_c^{2,1}(n_T - n) \quad (41)$$

The integration result of this first-order linear differential equation is well known and is represented in general form without specification of $n(t)$ (Eq. (18) in Ref. 41). An interesting peculiarity of this important derivation is the disappearance of terms, related to coagulation at the transition from the equation set (37) to the main equation (38). This corresponds to the fact that the total quantity of droplets does not change due to coagulation; it decreases due to coalescence only.

The coagulation regularity manifests itself in the $n(t)$ dependence, arising in Eq. (41). It creates the illusion that Eq. (41) can be specified for any $n(t)$ function corresponding to any subprocess affecting the droplet aggregate distribution. For example, the gravitational coagulation theory leads to a function $n_g(t)$ (72), but it does not create the opportunity to describe the gravitational coagulation coupling with coalescence by means of substituting $n_g(t)$ into the integral of Eq. (41). Because the coalescence influences the gravitational coagulation, another function has to be substituted into Eq. (41) instead of $n_g(t)$. This function has to be derived to

account for the coupling of coalescence and coagulation. One concludes that Eq. (41) cannot be used, because its derivation assumes that the coupling of gravitational coagulation (or another process) and coalescence is already quantified.

A useful exception is Brownian coagulation and its modeling by Smoluchowski with the coagulation rate coefficients, of which sensitivity to aggregate structure and coalescence is low. The substitution of function (27) into the integral of Eq. (41) yields the equation, characterizing the coupling of coalescence and Brownian coagulation (41).

In fractal theory (74), it is established that diffusion-limited aggregates and diffusion-limited cluster–cluster aggregates are built up linearly. This can simplify the application of the DIGB model. However, the diffusivity of fractal aggregates (75) cannot be described by simple equations and the Smoluchowski theory. This will cause coagulation rate coefficient dependence on aggregate structure, decreasing the exactness of Eq. (41) when applied to fractal aggregates. However, there is no alternative to the DIGB model, which can be used as a crude but useful approximation in this case as well. In the absence of an alternative, the DIGB model can be recommended for evaluation in the case of gravitational coagulation.

Danov et al. compares their theory with the predictions of averaged models for identical conditions. It turns out that if coalescence is much faster than flocculation, the predictions of the different models coincide. Conversely, for slow coalescence, the results of the averaged models deviate considerably from the exact solution. These two results of the comparison are in agreement with the qualitative considerations in Section III.B.

Data for the relative change in the total number of droplets as a function of time are presented in Fig. 4 (41). Figures 4a–4c refer to $K_F N_{10} = 0.1 \text{ s}^{-1}$ and the coalescence constant $K_c^{2,1}$ varies between 0.1 s^{-1} (Fig. 4a) and 0.001 s^{-1} (Fig. 4c). It is seen that the agreement between the Danov et al. and Borwankar et al. models is better the faster the coalescence, as was explained qualitatively earlier. The van den Tempel curves deviate considerably from the other two solutions.

For very long times and irrespective of the values of the kinetic parameters, the model of Borwankar et al. (40) is close to the numerical solution. This is probably because the longer the time, the smaller the concentration of single droplets. In this extreme case, the error caused in the average models due to the influence of coalescence on the singlet concentration [not taken into account in the equation for $n(t)$] is negligible.

The shortcomings of the averaged models (40,73) and the advantages of the DIGB model are demonstrated in Ref. 41. However, the range of applicability of this model is restricted by many simplifications and the

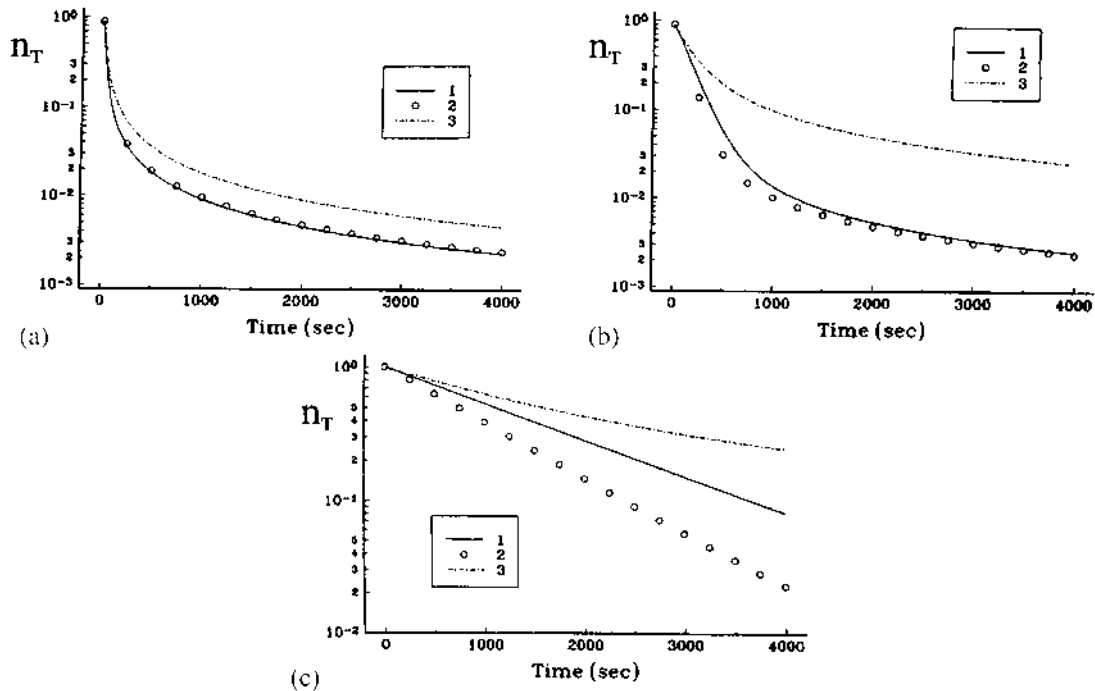


Figure 4 Relative change in the total number of droplets versus time: initial number of primary particles $N_{10} = 1 \times 10^{10} \text{ cm}^{-3}$; flocculation rate constant $K_f = 1 \times 10^{-11} \text{ cm}^3/\text{s}$; curve 1, the numerical solution of the set (37); curve 2, the model of Borwankar et al. (40) for diluted emulsions; curve 3, the model of van den Tempel (73). (a) Coalescence rate constant $K_c^{2,1} = 1 \times 10^{-1} \text{ s}^{-1}$; (b) $K_c^{2,1} = 1 \times 10^{-2} \text{ s}^{-1}$; (c) $K_c^{2,1} = 1 \times 10^{-3} \text{ s}^{-1}$. (From Ref. 41.)

neglect of other subprocesses (see Sec. III.A). An efficient analytical approach was made possible due to the neglect of the coalescence rate coefficient's dependence on the dimensions of both interacting droplets.

The model of Borwankar et al. was examined experimentally in Ref. 42. The emulsions were oil-in-water, with soybean oil as the dispersed phase, volume fraction 30%, and number concentration 10^7 – 10^{10} cm⁻³. The emulsions were gently stirred to prevent creaming during the aging study. A sample was placed on a glass slide, all aggregates were broken up, and the size of the individual droplets was measured. A rather good agreement with the theory was established. However, the fitting of the experimental data was accomplished using two model parameters, namely the coalescence and coagulation rate coefficients. For the last coefficient, the optimal values (different for two emulsions) were obtained, strongly exceeding the Smoluchowski theory value (Sec. II.A). An interpretation is that orthokinetic and perikinetic coagulation took place simultaneously due to stirring. Several experiments are known (discussed in Ref. 56) which demonstrate better agreement with the value for the coagulation constant predicted in the Smoluchowski theory.

IV. DOUBLET FRAGMENTATION TIME

A. Theory of Doublet Fragmentation Time

A doublet fragmentation was described by Chandrasekhar (76) by the diffusion of its droplets from the potential minimum, characterizing their attraction. The time scale for this process takes the form (77)

$$\tau_d = \frac{6\pi\eta a^3}{\kappa T} \exp\left(\frac{-U_{\min}}{\kappa T}\right) \quad (42)$$

where U_{\min} is the depth of the potential minimum.

To derive the formula for the average lifetime of doublets, Muller (78) considered the equilibrium in a system of doublets and singlets; that is, the number of doublets decomposing and forming are equal. Both processes are described by the standard diffusion flux J of particles in the force field of the particle that is regarded as central.

Each doublet is represented as an immovable particle with the second singlet “spread” around the central one over a spherical layer, which corresponds to the region of the potential well. The diffusion flux J of “escaping” particles is described by equations used in the Fuchs theory of slow coagulation. The first boundary condition corresponds to the assumption that the escaping particles do not interact with other singlets.

The second condition reflects the fact that the potential well contains exactly one particle.

At a small separation between the droplets in a doublet, the droplet diffusivity reduces because of the increasing hydrodynamic resistance during the droplet approach. A convenient interpolation formula was used (78) for the description of the influence of hydrodynamic interaction on the mutual diffusivity. The difference between the more exact Muller equation and Eq. (42) is caused mainly because of this hydrodynamic interaction.

B. Doublet Fragmentation Time of Uncharged Droplets

In this subsection, we consider a doublet consisting of droplets with a nonionic adsorption layer. The closest separation between two droplets surfaces h_0 exceeds the double thickness of the adsorption layer ($2h_a$). As a crude approximation, h_0 can be identified with $2h_a$. In the case of small surfactant molecules, $2h_a \approx 2$ nm.

In this case, the potential well has a sharp and deep minimum. This means that the vicinity of this minimum determines the value of the integral (42). For examination of this assumption, Eq. (42) was calculated numerically and according to the approximate equation (28)

$$\int_{\alpha}^{\beta} \varphi(t) \exp[f(t)] dt = \left[\frac{2\pi}{f''(t_m)} \right]^{1/2} \varphi(t_m) \exp[f(t_m)] \quad (43)$$

where t_m corresponds to the potential well minimum.

The difference in results was small and enabled application of Eq. (43) for the calculation and substitution of the asymptotic expression (13,16):

$$U(h) = -\frac{A a}{12 h} \quad (44)$$

which is valid at small distances to the surface. The result of calculations according to Eqs. (43) and (44) (the Hamaker constant $A = 1.3 \times 10^{-20}$ J) are shown in Fig. 5. The chosen value of the Hamaker constant is consistent with those reported elsewhere (79,80). In addition to the value of $A = 1.3 \times 10^{-20}$ J, we mention other values of the Hamaker constant employed elsewhere. For example, in food emulsions (80), the Hamaker

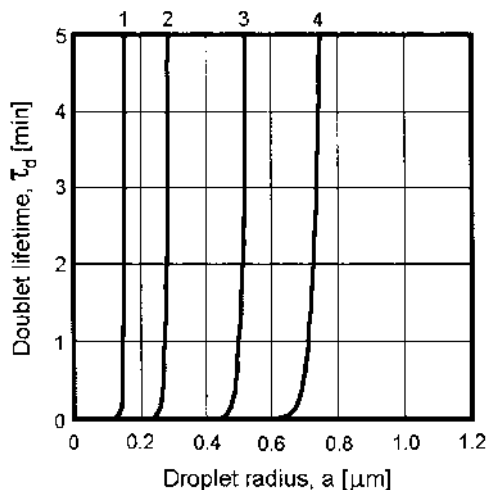


Figure 5 Dependence of doublet lifetime on droplet dimension at different values of the Hamaker constant A : curve 1: $A = A_1 = 1.33 \times 10^{-20}$ J; curve 2: $A = 0.5A_1$; curve 3: $A = 0.35A_1$; curve 4: $A = 0.25A_1$; curve 5: $A = 0.1A_1$. The shortest interdroplet distance is 2 nm. (From Ref. 28.)

constant lies within the range of 3×10^{-21} J to 10^{-20} J. The results of calculations for smaller Hamaker constants are also presented in Fig. 5.

The influence of the adsorption layer thickness on doublet lifetime is shown in Fig. 6 for one value of the Hamaker constant. There is high specificity in the thickness of a polymer adsorption layer. β -Casein adsorbed onto polystyrene latex causes an increase in the radius of the particle of 10–15 nm (81). A layer of β -lactoglobulin appears to be in the order of 1–2 nm thick, as compared to 10 nm for the caseins (82).

When adsorbed layers of hydrophilic nature are present, the repulsive hydration forces must be taken into account. At low ionic strengths, the repulsion follows the expected exponential form for double-layer interaction:

$$U(h) = K_s e^{-(h/h_s)} \quad (45)$$

In Ref. 83, the authors emphasize that the surface charge in food emulsions is low, electrolyte concentrations are high, and, hence, the DL is not responsible for emulsion stability. The stabilization can be caused by the hydration forces. However, the flocculation to the secondary minimum remains. Meanwhile, this conclusion must be specified with account for droplet dimension.

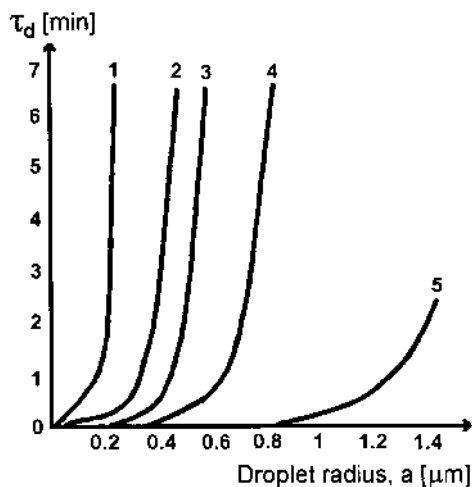


Figure 6 The adsorption layer thickness influence on the droplet lifetime of an uncharged droplet. Adsorption layer thickness: curve 1: $h_0 = 1$ nm; curve 2: $h_0 = 2$ nm; curve 3: $h_0 = 4$ nm; curve 4: $h_0 = 6$ nm. $A = 1.33 \times 10^{-20}$ J. (From Ref. 28.)

C. Lifetime of a Doublet of Charged Droplets and Coagulation/Flocculation

As seen in Fig. 1 of Ref. 39, the coordinates of the secondary minimum corresponds to $\kappa h_{\min} = 5\text{--}12$ nm. Due to this rather large distance, the frequency dependence of the Hamaker constant may be of importance, and the Hamaker function $A(h)$ characterizing molecular interaction should be introduced.

In Ref. 84, the distance-independent interaction at zero frequency and interaction at nonzero frequency is considered separately:

$$A(h) = A_0 + [A(h) - A_0] \quad (46)$$

The result from 36 systems in Ref. 84 are in a rather good accordance with the calculations of other papers. According to Churaev, the system polystyrene–water–polystyrene can be used to estimate the Hamaker function for oil–water systems. However, with increasing droplet separation, the importance of A_0 is increasing because of $A(h) - A_0$. The component A_0 is screened in electrolyte concentrations, because of dielectric dispersion (85–87). At a distance of $\kappa h_{\min} \approx 3\text{--}5$ nm, the authors (86) found that molecular interaction

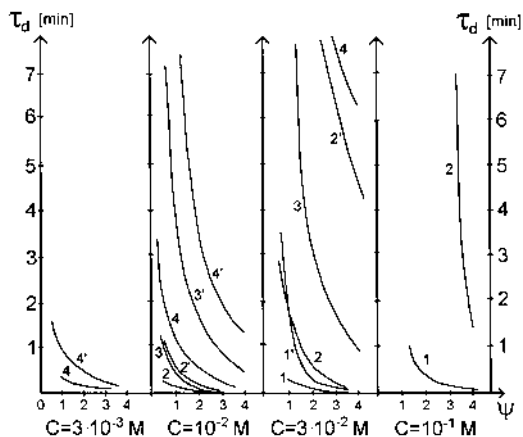


Figure 7 The dependence of doublet lifetime on the Stern potential for different electrolyte concentrations and droplet dimensions. Numbers near the curves correspond to droplet radius. Curves 1–4 without account for retardation of molecular forces of attraction, $\Psi = e\psi/kT$. Curves 1'–4' with account for retardation. (From Ref. 28.)

disappeared at zero frequency. Experimental evidence concerning this statement is discussed in Ref. 16. When evaluating the secondary minimum coagulation, A_0 can be omitted, as illustrated in Ref. 87.

For illustration of the influence of electrolyte concentration, Stern potential, and particle dimension, some calculations of doublet lifetime are made and their results are presented in Fig. 7. The potential well depth increases and, in parallel, doublet lifetime increases with increasing particle dimension and electrolyte concentration and decreasing surface potential.

V. COALESCENCE COUPLED WITH EITHER COAGULATION OR FLOCCULATION IN DILUTE EMULSIONS

Limited attention is paid to the role of fragmentation in emulsion science. A comparison of the prediction of coalescence with and without accounting for fragmentation (Secs. II and III) enables evaluation of the significance of fragmentation. This comparison will be done in Section V.A.

The theories of Refs. 41 and 25 have different areas of applicability (not specified in the articles) and are complementary. Naturally, this

complicates the choice between these theories with respect to concrete conditions of the experiments. An approximate evaluation of the aforesaid areas of applicability is given in Section V.B.

A. Fragmentation of Primary Flocs in Emulsions and the Subsequent Reduction of Coalescence

Floc fragmentation reduces the quantity of interdroplet films and, correspondingly, retards the entire coalescence process. This retardation can be characterized by the comparison of Eq. (18) with the theory of Ref. 41, which neglects fragmentation. The longer the time, the greater the retardation, which enables the use of the simpler theory of Ref. 40 for comparison. The results for longer times coincide with the predictions of the more exact theory of Ref. 41.

The results of the theory of Ref. 41 concerning slow coalescence are illustrated by curve 1 in Fig. 3c in Ref. 41, which is redrawn here as Fig. 8a. It can be seen that for a low value of the coalescence rate constant, the semilogarithmic plot is linear, indicating that the process follows a coalescence rate-controlled mechanism according to Eq. (36). Differing from the simple exponential time dependence in Eq. (36), second-order kinetics dominate at rapid doublet fragmentation, even if coalescence is very slow. The physical reason becomes clear when considering how Eq. (18) is derived. As seen from Eq. (17), the rate of decline in the droplet concentration is proportional to the doublet concentration. The latter is proportional to the square of the singlet concentration at s.d.e., which causes second-order kinetics. Thus, at slow coalescence, the disaggregation drastically changes the kinetic law of the coalescence (i.e., from the exponential law to second-order kinetics).

In the second stage, coagulation becomes the rate-controlling process because of the decrease in the collision rate accompanying the decrease in the droplet concentration. Thus, at sufficiently long times, second-order kinetics characterizes both reversible and irreversible aggregation. Nevertheless, a large difference exists even when identical functions describe the time dependence, as the characteristic times are expressed through different equations for irreversible and reversible aggregation. In the first case, it is the Smoluchowski time; in the second case, it is the combination of three characteristic times [i.e., Eq. (18)].

Let us now try to quantitatively characterize the reduction in coalescence caused by doublet disintegration. For this purpose, the calculations are performed according to Eq. (6) at $\tau_{sm} = 10$ s and $\tau_c = 10^3$ s (Fig. 8a), 10^2 s (Fig. 8b), and 10 s (Fig. 8c). For all figures, the same value of the ratio

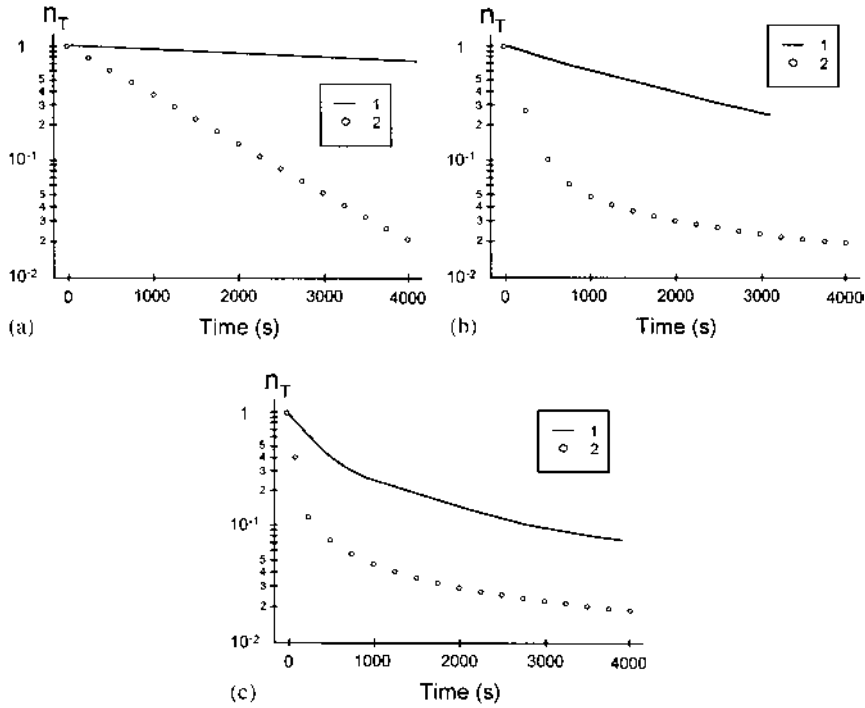


Figure 8 Relative change in the total number of droplets versus time; initial number of droplets $N_{10} = 1 \times 10^{10} \text{ cm}^{-3}$; flocculation rate constant $K_f = 1 \times 10^{-11} \text{ cm}^3/\text{s}$; curve 1—calculations according to Eq. (18); curve 2—the model of Borwankar et al. (40) for dilute emulsions coalescence rate constants: (a) $K_c^{2,1} = 1 \times 10^{-1} \text{ s}^{-1}$; (b) $K_c^{2,1} = 1 \times 10^{-2} \text{ s}^{-1}$; (c) $K_c^{2,1} = 1 \times 10^{-3} \text{ s}^{-1}$. Coalescence times: (a) $\tau_c = 10^3 \text{ s}$; (b) $\tau_c = 10^2 \text{ s}$; (c) $\tau_c = 10 \text{ s}$. Smoluchowski time $\tau_{\text{Sm}} = 10 \text{ s}$. Doublet lifetime $\tau_d = 0.5 \text{ s}$. n_T is the dimensionless total droplet concentration, $n_T = N_T/N_{10}$. (From Ref. 25.)

$2\tau_d/\tau_{\text{Sm}} = 0.1$ is accepted, satisfying condition (2). In all of these figures, the calculations according to Eq. (18) are illustrated by curve 2.

The comparison of curves 1 and 2 characterizes the reduction of coalescence caused by doublet disintegration; the lower the Rev values, the stronger the reduction. The simple curve 1 in Fig. 8a can be used also for higher τ_c values, because then the condition (12) is even better satisfied. Thus, if τ_{c1} and t_1 correspond to the data of Fig. 8a and $\tau_{c2} = m\tau_{c1}$ with $m \gg 1$, the identity

$$\tau_{c2}t_2 = \tau_{c1}m\frac{t_1}{m} \quad (47)$$

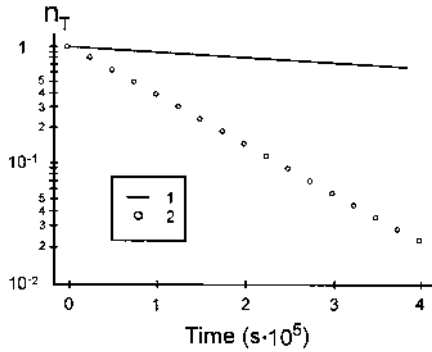


Figure 9 Similar to Fig. 8, with other values for the characteristic times. Coalescence time $\tau_c = 10^5$ s; the Smoluchowski time $\tau_{sm} = 10^3$ s; Doublet fragmentation lifetime $\tau_d = 50$ s. (From Ref. 25.)

is useful. This means that

$$\frac{n_T}{n_0} \left(\tau_{c1} m, \frac{t_1}{m} \right) = \frac{n_T}{n_0} (\tau_{c1}, t_1) \quad (48)$$

[i.e., $t_2 = t_1/m$, where the right-hand side of Eq. (48) is drawn in Fig. 9]. For example, Fig. 9 is similar to Fig. 8a and can be used for 100 fold longer time, shown on the abscissa axis. The increase in τ_c enables us to increase τ_{sm} without violating condition (35) and with Eq. (36) valid. Thus, $\tau_{sm} = 1000$ s or lower can be chosen as condition for Fig. 9. Curve 2, characterizing the rate of doublet disintegration, preserves as well if the value of $2\tau_d/\tau_{sm} = 0.1$ remains; now, it corresponds to a higher τ_d value of 5 s.

B. Domains of Coalescence Coupled Either with Coagulation or with Flocculation

The condition

$$\text{Rev} \gg 1 \quad (49)$$

corresponds to coagulation. A theory for the intermediate case

$$\text{Rev} \sim 1 \quad (50)$$

when part of the droplets participate in flocculation and another coagulate is absent. To specify the conditions (2) and (49), the doublet lifetime must be

expressed through surface force characteristics (viz. through the surface electric potential and the Hamaker function) and droplet dimension, as was described in Section IV.

In the equation for the Smoluchowski time [Eq. (4)], the droplet numerical concentration N_{10} can easily be expressed through the droplet volume fraction φ and the average droplet radius a (we replace a polydisperse emulsion by an “equivalent” monodisperse emulsion). The resulting analysis respective to a and φ is easier than relating to N_{10} because the boundary of application of different regularities are usually formulated respective to a and φ . The Smoluchowski time is

$$\tau_{\text{Sm}} = \kappa_F^{-1} \varphi^{-1} \frac{4}{3} \pi a^3 \quad (51)$$

We exclude from consideration a special case of extremely dilute emulsions. Comparing Fig. 7 and the results of calculations according to Eq. (51), one concludes that condition (49) is mainly satisfied. It can be violated if simultaneously the droplet volume fraction and the droplet dimension are very small. This occurs if $\varphi < 10^{-2}$ and $a < 0.2\text{--}0.3 \mu\text{m}$. Discussing this case, we exclude from consideration the situation when $a \leq 0.1 \mu\text{m}$, corresponding to microemulsions and $\varphi \ll 10^{-2}$. With this exception, one concludes that for uncharged droplets, flocculation is almost impossible because condition (2) cannot be satisfied. A second conclusion is that at

$$a < 0.2\text{--}0.3 \mu\text{m} \quad (52)$$

the theory in Ref. 41 cannot be applied without some corrections made necessary by the partially reversible character of the aggregation. The main conclusion is that when

$$a > 0.2 \mu\text{m} \quad \text{and} \quad \varphi > 10^{-2} \quad (53)$$

the theory in Ref. 41 does not need corrections respective to the reversibility of flocculation. However, this conclusion will change at the transition to a thicker adsorption layer. As described in Section IV, the thicker the adsorption layer, the shorter is the doublet fragmentation time.

The electrostatic repulsion decreases the depth of the potential well and, correspondingly, decreases the doublet lifetime. As result, flocculation becomes possible for submicrometer droplets as well as for micrometer-sized droplets if the electrolyte concentration is not too high, the surface potential

is rather high, and the droplet volume fraction is not too high. This is seen from Fig. 7.

The reversibility criterion depends on many parameters in the case of charged droplets. To discriminate and to quantify the conditions of coagulation and flocculation, let us consider Rev values lower than 0.3 as low and values higher than 3 as high. In other words, coagulation takes place when $Rev > 3$, whereas at $Rev < 0.3$, there is flocculation; that is, the conditions

$$Rev = \frac{\tau_d(c_0, \varphi, a)}{\tau_{Sm}(a, \varphi)} > 3 \quad (54)$$

$$Rev < 0.3 \quad (55)$$

determine the boundaries for the domains of coagulation and flocculation. These domains are characterized by Fig. 10 and correspond to fixed values of the droplet volume fraction. In addition, a definite and rather large droplet dimension $2a = 4 \mu\text{m}$ is fixed. After fixation of the values of

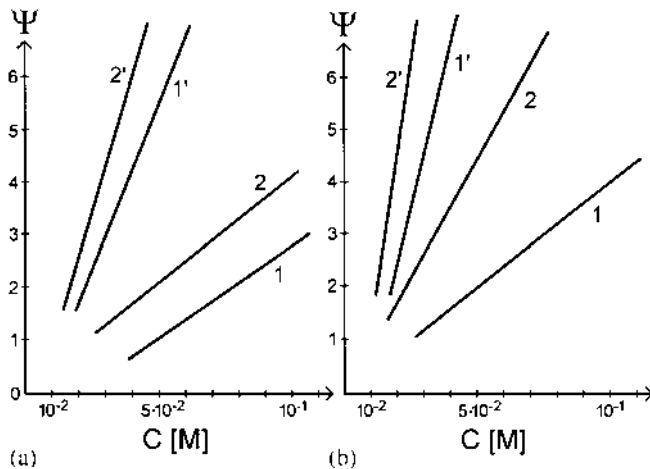


Figure 10 Domains of coagulation and flocculation. Curves 1 and 2 are calculated with the Rabinovich–Churaev Hamaker function; a twice higher value is used for the calculation of curves 1' and 2'. The domain of flocculation is located above curve 1, while the domain of coagulation is located beneath curve 2. Volume fractions: $\varphi = 0.01$ (Fig. 10a) and $\varphi = 0.1$ (Fig. 10b); particle dimension $2a = 4 \mu\text{m}$. (From Ref. 28.)

volume fraction and droplet dimension, the domains are characterized in coordinates Ψ and C .

In Fig. 10, the domain of flocculation is located above and to the left of curve 2; the domain of coagulation is located beneath and to the right of curve 1. To indicate the sensitivity of the domain boundaries to the Hamaker function value, curves 1' and 2' are calculated using values two times higher than those of curves 1 and 2.

In distinction from uncharged droplets, flocculation in the range of micrometer-sized droplets is possible. As seen in Fig. 10, even rather large droplets (4 μm) aggregate reversibly if the electrolyte concentration is lower than $(1-5) \times 10^{-2} \text{ M}$ and the Stern potential is higher than 25 mV. For smaller droplets, the domain of flocculation will extend while the domain of coagulation shrinks. For submicrometer droplets, flocculation takes place even at high electrolyte concentrations (0.1 M).

C. Hydration Forces Initiate Flocculation

Due to the similar dependence on the distance h of hydration forces and electrostatic interaction, the decrease of doublet lifetime caused by hydration forces of repulsion can be calculated because of this similarity. It is sufficient to use the substitution h_s for κ^{-1} and K_s for

$$16\epsilon \left(\frac{kT}{e}\right)^2 \tanh\left(\frac{e\psi}{kT}\right)^2 \quad (56)$$

where k is the Boltzmann constant, T is absolute temperature, and e is the elementary charge. The doublet lifetime can be determined with the use of the results presented in Fig. 7. For the sake of brevity, a similar figure with K_s given on the ordinate axis and h_s on the abscissa axis is not shown. It turns out that the decrease in τ_d caused by hydration forces leads to flocculation of submicrometer droplets. As for micrometer-sized droplets, coagulation takes place with the exception for the case when both h_s and K_s are rather large.

VI. APPLICATIONS

The restrictions in Eqs. (1) and (15) corresponding to strong retardation of the rate of multiplet formation and slow intradoublet coalescence are not frequently satisfied. Nevertheless, these conditions are important because they correspond to the case of very stable emulsions. Because the kinetics of retarded destabilization of rather stable emulsions are of interest, attention

has to be paid to provide these conditions and, thus, the problem of coupled coalescence and flocculation arises.

There are large qualitative distinctions in the destabilization processes for the coupling of coalescence and coagulation, and coalescence and flocculation. In the first case, rapid aggregation causes rapid creaming and further coalescence within aggregates. In the second case, the creaming is hampered due to the low concentration of multiplets, and coalescence takes place both before and after creaming. Before creaming, singlets predominate for a rather long period of gradual growth of droplet dimensions due to coalescence within doublets. The discrimination of conditions for coupling of coalescence with either flocculation or coagulation is accomplished in Ref. 28.

The creaming time is much shorter in the case of coagulation and, correspondingly, the equation describing the coupling of coalescence and flocculation preserves its physical sense for a longer time than is the case for coagulation. One concludes that the theory of the coupling of coalescence and flocculation provides a new opportunity for the long-term prediction of emulsion stability, although creaming restricts the application of this theory as well. Note that this restriction weakens in emulsions of low-density contrast and in water-in-oil (w/o) emulsions with a high-viscosity continuum.

Long-term prediction is a two-step procedure. The first step is the determination of whether an emulsion exhibits coagulation or flocculation. It means that the characteristic time τ_d must be measured and compared with τ_{Sm} , the value of which is easily evaluated taking into account the measured concentration using Eq. (4). A comparison of these times enables the choice between condition (1) and the opposite condition ($\tau_{Sm} \ll \tau_d$). The second step is the prediction of the evolution in time for the t.d.c. If condition (1) is valid, Eq. (18) has to be used for the prediction [τ in Eq. (18) has to be specified in accordance with Eq. (15)]. In the opposite case, DIGB theory must be used.

A. Long-Term Prediction of Emulsion Stability

It is possible, in principle, to give a long-term prediction of emulsion stability based on the first indications of aggregation and coalescence. The next example clarifies the principal difficulty in a reliable long-term prediction if a dynamic model of the emulsion is not available.

The first signs of aggregation and coalescence can always be characterized by a linear dependence if the investigation time t is short compared with a characteristic time τ for the evolution of the total droplet

concentration $n(t)$:

$$n(t) = n_0 \left(1 - \frac{t}{\tau}\right) \quad (57)$$

This short-time asymptotic corresponds to many functions [e.g., to Eq. (18) or to Eq. (36)]. The first can arise in the case of coalescence coupled with coagulation (41), whereas the second can arise for coalescence coupled with flocculation (31). The discrimination between irreversible and reversible aggregation is only one component of emulsion dynamics modeling (EDM) and it is seen that without this discrimination, the difference in the prediction of the time necessary for a droplet concentration decrease (e.g., 1000 times) can be 7τ and 1000τ .

B. Refinement of Methods for Emulsion Stabilization (Destabilization) by Means of the Effect on Both Coalescence and Flocculation

Emulsion stability (or, for that matter, instability) can be described from the viewpoint of the coupling of coalescence and flocculation. However, for emulsifiers (or demulsifiers), only their influence on the elementary act of coalescence is primarily taken into account. The coupling of coalescence and flocculation is reflected in Eq. (15) and one concludes that it follows the multiplicativity rule and not the additivity rule. This means that the total result of the application of a stabilizer (destabilizer) depends very much on both flocculation and fragmentation. The development of a more efficient technology for emulsion stabilization (destabilization) is possible by taking into account the joint effect on both the coalescence and the aggregation (disaggregation) processes.

1. Combining Surfactants and Polymers in Emulsion Stabilization

The coalescence rate depends mainly on the thin-film (black) stability and correspondingly on the short-range forces, whereas flocculation depends on the long-range surface forces. Due to this important difference, synergism in the dependence of these processes on the different factors can be absent. The use of a single surfactant only may not provide, at the same time, both the optimal fragmentation and optimal stability of an emulsion film. Probably the use of a binary surfactant mixture with one component which provides the film stability and a second one which prevents the flocculation may provide optimal emulsion stabilization. Naturally, coadsorption of the

two is necessary. For such an investigation, a measurement method for both the doublet fragmentation time and the coalescence time is necessary.

2. There Is a Strong Influence of Low Concentrations of Ionic Surfactant on Doublet Fragmentation Time and Coalescence Time

Let us consider the situation when an emulsion is stabilized against coalescence by means of an adsorption layer of nonionic surfactant and is strongly coagulated because of the subcritical value of the Stern potential that is usual for inorganic electrolytes (48) at moderate pH. In a large floc, any droplet has many neighbors, meaning a rather high number of interdroplet films per droplet. The coalescence rate is proportional to the total number of films and can be rather high. It can be strongly decreased by adding even a low concentration of an ionic surfactant. This can be sufficient to provide a supercritical Stern potential value that will be accompanied by a drastic decrease in the doublet lifetime compared to that of weakly charged droplets.

At shorter doublet lifetimes, flocculation can become reversible and it can stop at the stage of singlet–doublet equilibrium. It will provide a strong decrease in the coalescence rate because coalescence occurs within doublets only and their concentration can be very low.

Thus, a modest addition of an ionic surfactant to an amount of a nonionic surfactant sufficient to provide an almost saturated adsorption layer can make the overall emulsion stabilization more efficient. The nonionic surfactant suppresses coalescence but cannot prevent flocculation, whereas the ionic surfactant retards the development of flocculation.

We can give an example when both coalescence and flocculation are affected by an ionic surfactant (SDS). In Ref. 88, it is established that coalescence is suppressed at SDS concentrations exceeding 6×10^{-5} M. Meanwhile, the CCC is 2×10^{-2} M NaCl at 10^{-6} M SDS. Thus, SDS concentrations slightly above 10^{-6} M are sufficient to retard flocculation. In this example, it is essential that the concentrations needed to retard flocculation are very low compared to those needed to prevent coalescence.

It is noteworthy that low concentrations of an ionic surfactant can increase emulsion stability due to the simultaneous manifestation of three mechanisms. First, the depth of the secondary potential minimum decreases due to the electrostatic repulsion that is accompanied by a τ_d decrease. Second, the transition from the secondary minimum through an electrostatic barrier and into the primary minimum extends the

coalescence time. Third, the time of true coalescence (i.e., the time necessary for thin-film rupture) increases due to electrostatic repulsion as well (29,65).

C. Standardization of the Measurement of τ_c and τ_d

Direct investigation of the coalescence subprocess in emulsions is difficult. Instead, the entire destabilization process is usually investigated. Meanwhile, the rate of the destabilization process depends on the rates of both flocculation and disaggregation and on the floc structure as well. All these characteristics vary in a broad range. Given an unknown value for the time of the elementary act of coalescence, τ_c , the different times can be measured for the integrated process and different evaluations of τ_c are then possible.

The rate of coalescence in an aggregate essentially depends on the number of droplets within it and the packing type (i.e., on the number of films between the droplets). This complication is absent when considering the case of the s.d.e.

The possible advantage of τ_c measurement at s.d.e. is in avoiding the difficulty caused by polydispersity of droplets appearing during preceding coalescence within large flocs. At s.d.e., the initial stage of the entire coalescence process can be investigated when the narrow size distribution of an emulsion is preserved.

At s.d.e., determination of the time dependence of the t.d.c. is sufficient for the investigation of coalescence. In Refs. 29 and 30, this was accomplished through direct visual observation. By using video-enhanced microscopy and computerized image analysis, the determination of the t.d.c. can be automated. Such automated determination of total droplet number in a dilute DCD-in-water emulsion at the s.d.e. can be recommended as a standard method for the characterization of the elementary act of coalescence.

In parallel, the second important characteristic (viz. the doublet fragmentation time) is determined by the substitution of τ_c , τ_{Sm} , and measured τ_d into Eq. (18).

D. Experimental–Theoretical Approach to Emulsion Dynamics Modeling

1. General

To predict the evolution of the droplet (floc) size distribution is the central problem concerning emulsion stability. It is possible, in principle, to predict

the time dependence of the distribution of droplets (flocs) if information regarding the main subprocesses (flocculation, floc fragmentation, coalescence, creaming), constituting the whole phenomenon, is available. This prediction is based on consideration of the population balance equation (PBE).

The PBE concept was proposed by Smoluchowski. He specified this concept for suspensions and did not take into account the possibility of floc fragmentation. Even with this restriction, he succeeded in the analytical solution neglecting gravitational coagulation and creaming, and he obtained the analytical time dependence for a number of aggregates n_i comprising i particles ($i = 2, 3, \dots$).

In the most general case, the equation for the evolution of the total droplet number takes into account the role of aggregation, fragmentation, creaming, and coalescence. There is no attempt to propose an algorithm even for a numerical solution to such a problem.

The usual approach in the modeling of an extremely complicated process is the consideration of some extreme cases with further synthesis of the obtained results. The next three main simplifications are inherent to the current state of emulsion dynamics modeling: the neglect of the influence of the gravitational field (i.e., neglect of creaming/sedimentation); in a first approximation, it is possible to consider either coagulation or flocculation; finally, neglect of the rate constant dependence on droplet dimension.

2. Combined Approach in Investigations of Dilute and Concentrated Emulsions

The modeling of collective processes in concentrated emulsions is extremely complicated. Recently, the efficiency of computer simulation in the systematic study of aggregates, gels, and creams has been demonstrated (50). Monte Carlo and Brownian dynamics are particularly suited to the simulation of concentrated emulsions. However, information about droplet–droplet interaction is necessary. The reliability of this information is very important to provide reasonable results concerning concentrated emulsions. In other words, the assumption concerning pairwise additive potentials for droplet–droplet interaction and the thin-emulsion-film stability must be experimentally confirmed. The extraction of this information from experiments with concentrated emulsions is very difficult. On the other hand, measurement of the doublet fragmentation time in dilute emulsions is a convenient method to obtain information about pairwise additive potentials. Information about pair potentials and the elementary act of coalescence obtained in experiments with dilute emulsions *preserves its significance for concentrated emulsions as well.*

One concludes that modeling of concentrated emulsions becomes possible by combining experimental investigation of the simplest emulsion model system with computer simulation accounting for the characteristics of a concentrated emulsion (high droplet volume fraction, etc.).

3. In the Transformation of PBE into an Efficient Tool for EDM, the Determination of Kernels Is the Main Task

The levels of knowledge concerning kernels describing different subprocesses differ strongly. There exists a possibility for quantification of kernels related to aggregation and fragmentation (14,39,78). On the other hand, the current state of knowledge is not sufficient for prediction of the thin-film breakdown time.

The deficit in knowledge about thin-film stability currently makes purely theoretical modeling of emulsion dynamics impossible. As a result, a complex semitheoretical approach to EDM is necessary. The PBE is the main component of both the experimental and the theoretical stages of this approach. In the experimental stage, the PBE simplified for s.d.e. provides the background for the determination of the coalescence kernels with the use of experimental data (29,30).

For the determination of the coalescence kernels, the more complicated reverse task must be solved—namely their determination based on the comparison of experimental data about the emulsion evolution in time with solution of the PBE. In the absence of an analytical solution, the reverse task is usually very difficult. The most efficient way to overcome this difficulty is an experimental realization with the use of the universally simplest conditions for emulsion time evolution, which can be described analytically.

4. The Simplest Emulsion State for Which Investigation Can Provide Information About Coalescence Is at Singlet–Doublet Quasiequilibrium with Slow Coalescence Within the Doublets

The simplest singlet–doublet emulsion can exist at singlet–doublet quasiequilibrium given slow coalescence within doublets. Its simplicity results in a very simple kinetic law for the entire kinetics of coupled flocculation and coalescence, [viz. Eq. (18)]. Thus, s.d.e. provides the most convenient conditions for investigations of the elementary act of coalescence and the doublet fragmentation time.

The main simplification in all existing models for emulsion dynamics (25,41) is the neglect of the coalescence time dependence on droplet

dimensions. This simplification is not justified and reduces severely the value of the prediction, which can now be made with use of the PBE. For elimination of this unjustified simplification, it is necessary to determine the coalescence time for emulsion films between droplets of different dimensions i and j (viz. τ_{cij} , similar to the existing analytical expressions for the doublet fragmentation time, τ_{dij}) (14). The determination of a large set of τ_{cij} values by means of a comparison of experimental data obtained for an emulsion consisting of different multiplets and the PBE numerical solutions for it is impossible. On the other hand, this paramount experimental–theoretical task can be solved for a dilute emulsion at s.d.e. and slow intradoublet coalescence.

5. Substitution of the Coalescence Kernels Makes the PBE Equation Definite and Ready for the Prediction of Emulsion Time Evolution (With the Restriction of Low-Density Contrast and Without Accounting for Gravitational Creaming and Coagulation)

With application of the scaling procedure for the representation of the kinetic rate constants for creaming and gravitational coagulation, the PBE is solved analytically in Ref. 89. This scaling theory creates a perspective for the incorporation of creaming in the emulsion dynamics model in parallel with coalescence, aggregation, and fragmentation.

VII. SUMMARY

The mechanisms of kinetic stability in macroemulsions and miniemulsions are completely different. Strong droplet deformation and flattening of the interface in a macroemulsion cause the Reynolds mode of drainage, which prolongs the life of the emulsion. This mechanism is not important for miniemulsion droplet interaction, because either the deformation and flattening are weak (charged droplets) or the Reynolds drainage is rapid due to the small dimension of the interdroplet film (uncharged droplets). Kinetic stability in a miniemulsion can result from floc fragmentation if the electrokinetic potential is not too low and the electrolyte concentration is not too high, corresponding to a degree of electrostatic repulsion.

The potential strength of physicochemical kinetics with respect to emulsions is the PBE, enabling prediction of the time evolution of the droplet size distribution (d.s.d.) when the subprocesses [including droplet aggregation, aggregate fragmentation, droplet coalescence and droplet (floc) creaming] are quantified. The subprocesses are characterized in the PBE by

the kinetic coefficients. The coupling of the four subprocesses, the droplet polydispersity, and the immense variety of droplet aggregate configurations causes extreme difficulty in EDM. The three processes of aggregation, fragmentation, and creaming can be quantified. In contrast, only the experimental approach is now available for efficient accumulation of information concerning emulsion film stability and coalescence kernel quantification.

Correspondingly, EDM may be accomplished by combining experiment and theory: (a) the determination of coalescence and fragmentation kernels with the use of emulsion stability experiments at low-density contrast (l.d.c.) and s.d.e., because this allows for the omission of creaming and gravitational terms in PBE, simplifying the equation and enabling kernel determination; (b) the prediction of the droplet size evolution as function of time by means of solution of the PBE, specified for the determined coalescence and fragmentation kernels. This mathematical model has to be based on the PBE supplemented by terms accounting for the role of creaming and gravitational coagulation in the aggregation kinetics.

Emulsion dynamics modeling with experiments using l.d.c. emulsions and s.d.e. may result in the following: (a) The quantification of emulsion film stability [viz. the establishment of the coalescence time dependence on the physicochemical specificity of the adsorption layer of a specific surfactant (polymer), its structure, and the droplet dimensions]. Such quantification can form a basis for optimized selection and synthesis of emulsifiers and demulsifiers for a broad variety of technological applications of emulsions, replacing the current empirical approach dominating this area. (b) The elaboration of a commercial device for coalescence time measurement, in combination with EDM, will represent a useful approach to the optimization of emulsion technology with respect to stabilization and destabilization.

ACKNOWLEDGMENT

The technology program FLUCHA, financed by industry and the Norwegian Research Council, is acknowledged for financial support.

REFERENCES

1. D. G. Dalgleish, in *Emulsions and Emulsion Stability* (J. Sjöblom, ed.), Marcel Dekker, New York, 1996, pp. 287–325.
2. D. G. Dalgleish, in *Encyclopedic Handbook of Emulsion Technology* (J. Sjöblom, ed.), Marcel Dekker, New York, 2001, pp. 207–232.

3. P. Becher (ed.), *Encyclopedia of Emulsion Technology, Volume 1*, Marcel Dekker, New York, 1983.
4. P. Becher (ed.), *Encyclopedia of Emulsion Technology, Volume 2*, Marcel Dekker, New York, 1985.
5. J. Sjöblom (ed.), *Emulsions—A Fundamental and Practical Approach*, Kluwer Academic, Dordrecht, 1992, p. 1.
6. R. A. Mohammed, A. I. Bailey, P. F. Luckham, and S. E. Taylor, *Colloids Surfaces* 80, 223 (1993); 80, 237 (1993); 83, 261 (1994).
7. C. I. Chitewelu, V. Hornof, G. H. Neale, and A. E. George, *Can. J. Chem. Eng.* 72, 534 (1994).
8. L. Bertero, A. DiLullo, A. Lentini, and L. Terzi, in Proceedings of the SPE Annual Technical Conference and Exhibition (Part 2) (SPE 28543) Society of Petroleum Engineers, New Orleans, 1994, p. 283–295.
9. J. F. McCafferty and G. G. McClafin, in Proceedings of the SPE Annual Technical Conference, SPE 24850, Society of Petroleum Engineers, 1992, pp. 857–868.
10. J. A. Kitchener and P. R. Musselwhite, in *Emulsion Science* (I. P. Sherman, ed.), Academic Press, New York, 1968.
11. J. Sjöblom (ed.), *Emulsions and Emulsion Stability*, Marcel Dekker, New York, 1996.
12. I. B. Ivanov and P. A. Kralchevsky, *Colloids Surfaces* 128, 155 (1997).
13. B. V. Derjaguin, *Theory of Stability of Colloids and Thin Films*, Plenum Press, New York, 1989.
14. S. S. Dukhin and J. Sjöblom, in *Emulsions and Emulsion Stability* (J. Sjöblom, ed.), Marcel Dekker, New York, 1996, p. 41.
15. I. Gregory, *Crit. Rev. Environ. Control.* 19, 185 (1989).
16. J. N. Israelachvili, *Intermolecular and Surface Forces*, Academic Press, London, 1991.
17. J. Lyklema, *Fundamentals of Interface and Colloid Science*, Academic Press, London, 1993, Vol. 1.
18. P. A. Kralchevsky, K. D. Danov, and N. D. Denkov, in *Handbook of Surface and Colloid Chemistry* (K. S. Birdi, ed.), CRC Press, London, 1996.
19. Reference deleted.
20. R. K. Prud'homme (ed.), *Foams: Theory, Measurement and Applications*, Marcel Dekker, New York, 1995.
21. P. A. Kralchevsky, K. D. Danov, and I. B. Ivanov, in *Foams: Theory, Measurement and Applications* (R. K. Prud'homme, ed.), Marcel Dekker, New York, 1995.
22. S. A. K. Jeelani and S. Hartland, *J. Colloid Interf. Sci.* 164, 296 (1994).
23. P. D. I. Fletcher, in *Drops and Bubbles in Interface Research* (D. Mobius and R. Miller, eds.), Elsevier, New York, 1998, Vol. 6.
24. P. J. Breen, D. T. Wasan, Y. H. Kim, A. D. Nikolov, and C. S. Shetty, in *Emulsions and Emulsion Stability* (J. Sjöblom, ed.), Marcel Dekker, New York, 1996.
25. S. S. Dukhin and J. Sjöblom, *J. Dispers. Sci. Technol.* 19, 311 (1998).
26. Ø. Holt, Ø. Sæther, J. Sjöblom, S. S. Dukhin, and N. A. Mishchuk, *Colloids Surfaces* 123–124, 195 (1997).

27. Ø. Sæther, S. S. Dukhin, J. Sjöblom, and Ø. Holt, *Colloid J.* 57, 836 (1995).
28. S. S. Dukhin, J. Sjöblom, D. T. Wasan, and Ø. Sæther, *Colloids Surfaces* 180, 223 (2001).
29. Ø. Sæther, J. Sjöblom, S. V. Verbich, N. A. Mishchuk, and S. S. Dukhin, *Colloids Surfaces* 142, 189 (1998).
30. Ø. Sæther, J. Sjöblom, S. V. Verbich, and S. S. Dukhin, *J. Dispers. Sci. Technol.* 20, 295 (1999).
31. Ø. Holt, Ø. Sæther, J. Sjöblom, S. S. Dukhin, and N. A. Mishchuk, *Colloids Surfaces* 141, 269 (1998).
32. S. S. Dukhin, Ø. Sæther, J. Sjöblom, *Proc. Special Symposium in honor of D.T. Wasan on Emulsions, Foams, Thin Films and Interfacial Rheology* as part of 72nd ACS Colloid and Surface Science Conference, 1998.
33. O. Reynolds, *Phil. Trans. R. Soc. (London)* A 177, 157 (1886).
34. A. Scheludko, *Adv. Colloid. Interface Sci.* 1, 391 (1967).
35. K. D. Danov, D. N. Petsev, N. D. Denkov, and R. Borwankar, *J. Chem. Phys.* 99, 7179 (1993).
36. K. D. Danov, N. D. Denkov, D. N. Petsev, and R. Borwankar, *Langmuir* 9, 1731 (1993).
37. D. N. Petsev, N. D. Denkov, and P. A. Kralchevsky, *J. Colloid Interf. Sci.* 176, 201 (1995).
38. I. B. Ivanov and D. S. Dimitrov, in *Thin Liquid Films* (I. B. Ivanov, ed.), Marcel Dekker, New York, 1998.
39. N. A. Mishchuk, J. Sjöblom, and S. S. Dukhin, *Colloid J.* 57, 785 (1995).
40. R. P. Borwankar, L. A. Lobo, and D. T. Wasan, *Colloids Surfaces* 69, 135 (1992).
41. K. D. Danov, I. B. Ivanov, T. D. Gurkov, and R. P. Borwankar, *J. Colloid Interf. Sci.* 167, 8 (1994).
42. L. A. Lobo, D. T. Wasan, and M. Ivanova, in *Surfactants in Solution* (K. L. Mittal and D. O. Shah, eds.), Plenum Press, New York, 1992, Vol. 11, p. 395.
43. L. Lobo, I. Ivanov, and D. Wasan, *Mater. Interf. Electrochem. Phenomena* 39, 322 (1993).
44. G. Narsimhan and E. Ruckenstein, in *Foams: Theory, Measurement and Applications* (R. K. Prud'homme, ed.), Marcel Dekker, New York, 1995.
45. D. Exerova, D. Kashchiev, and D. Platikanov, *Adv. Colloid Interf. Sci.* 40, 201 (1992).
46. B. V. Derjaguin and Yu. V. Gutop, *Kolloid. Zh.* 24, 431 (1962).
47. A. V. Prokhorov and B. V. Derjaguin, *J. Colloid Interf. Sci.* 125, 111 (1988).
48. S. V. Verbich, S. S. Dukhin, A. Tarovsky, Ø. Holt, Ø. Sæther, and J. Sjöblom, *Colloids Surfaces* 23, 209 (1997).
49. D. Kashchiev and D. Exerova, *J. Colloid Interf. Sci.* 203, 146 (1998).
50. E. Dickinson and S. R. Euston, *Adv. Colloid Interf. Sci.* 42, 89 (1992).
51. P. Taylor, *Adv. Colloid Interf. Sci.* 75, 107 (1998).
52. H. W. Yarranton and Y. H. Masliyah, *J. Colloid Interf. Sci.* 196, 157 (1997).
53. M. Smoluchowski, *Phys. Z.* 17, 557 (1916).
54. G. A. Martynov and V. M. Muller, *Kolloidn. Zh.* 36, 687 (1974).
55. V. M. Muller, *Kolloidn. Zh.* 40, 885 (1978).

56. H. Sonntag and K. Strenge, *Coagulation Kinetics and Structure Formation*, VEB Deutscher Verlag der Wissenschaften, Berlin, 1987.
57. J. D. Chan, P. S. Hahn, and J. C. Slattery, *AIChE J.* 34, 140 (1988).
58. S. A. K. Jeelani and S. Hartland, *J. Colloid Interf. Sci.* 156, 467 (1993).
59. R. W. Aul and W. I. Olbriht, *J. Colloid Interf. Sci.* 115, 478 (1991).
60. A. Scheludko and D. Exerova, *Colloid J.* 168, 24 (1960).
61. A. Scheludko, *Proc. K. Ned. Akad. Wet. Ser. B* 65, 87 (1962).
62. D. Platikanov and E. Manev, in *Proceedings, 4th International Congress of Surface Active Substances*, Plenum, New York, 1964, p. 1189.
63. K. A. Burrill and D. R. Woods, *J. Colloid Interf. Sci.* 42, 15 (1973).
64. K. A. Burrill and D. R. Woods, *J. Colloid Interf. Sci.* 42, 35 (1973).
65. S. R. Deshikan and K. D. Papadopoulos, *J. Colloid Interf. Sci.* 174, 302 (1995).
66. S. R. Deshikan and K. D. Papadopoulos, *J. Colloid Interf. Sci.* 174, 313 (1995).
67. M. E. Costas, M. Moreau, and L. Vicente, *J. Phys. A: Math. Gen.* 28, 2981 (1995).
68. F. Le Berre, G. Chauveteau, and E. Pefferkorn, *J. Colloid Interf. Sci.* 199, 1 (1998).
69. B. J. McCoy and G. Madras, *J. Colloid Interf. Sci.* 201, 200 (1998).
70. J. Widmaier and E. Pefferkorn, *J. Colloid Interf. Sci.* 203, 402 (1998).
71. I. M. Elminyawi, S. Gangopadhyay, and C. M. Sorensen, *J. Colloid Interf. Sci.* 144, 315 (1991).
72. M. von Smoluchowski, *Phys. Chem.* 92, 129 (1917).
73. M. van den Tempel, *Rec. Trav. Chim.* 72, 419 (1953); 72, 433 (1953).
74. P. Meakin, *Adv. Colloid Interf. Sci.* 28, 249 (1988).
75. R. Nakamura, Y. Kitada, and T. Mukai, *Planet. Space Sci.* 42, 721 (1994).
76. S. Chandrasekhar, *Rev. Mod. Phys.* 15, 1 (1943).
77. W. B. Russel, D. A. Saville, and W. R. Schowalter, *Colloidal Dispersions*, Cambridge University Press, New York, 1989.
78. V. M. Muller, *Colloid J.* 58, 598 (1996).
79. Ia. I. Rabinovich and A. A. Baran, *Colloids Surfaces* 59, 47 (1991).
80. P. Walstra, in *Gums and Stabilizers for the Food Industry* (G. O. Philips, P. A. Williams, and D. J. Wedlock, eds.), IRL, Oxford, 1988, Vol. 4, p. 233.
81. D. G. Dalgleish, *Colloids Surfaces* 46, 14 (1990).
82. D. G. Dalgleish and Y. Fang, *J. Colloid Interf. Sci.* 156, 329 (1993).
83. B. Bergenstahl and P. M. Claesson, in *Food Emulsions* (K. Larson and S. Friberg, eds.), Marcel Dekker, New York, 1989, p. 41.
84. Ya. I. Rabinovich and N. V. Churaev, *Kolloidn. Zh.* 46, 69 (1984); 52, 309 (1990).
85. D. J. Mitchell and P. Richmond, *J. Colloid Interf. Sci.* 46, 128 (1974).
86. V. N. Gorelkin and V. P. Smilga, *Kolloidn. Zh.* 34, 685 (1972).
87. V. N. Gorelkin and V. P. Smilga, in *Poverkhnostnye Sily v Tonkikh Plenkakh i Ustoichivost Kolloidov* (B. V. Derjaguin, ed.), Nauka, Moscow, 1974, p. 206.
88. S. Usui, Y. Imamura, and E. Barough, *J. Dispers. Sci. Technol.* 8, 359 (1987).
89. S. B. Grant, C. Poor, and S. Relle, *Colloids Surfaces* 107, 155 (1996).

6

Structure and Stability of Aerated Food Emulsions

D. T. Wasan, W. Xu, A. Dutta, and A. Nikolov

Illinois Institute of Technology, Chicago, Illinois, U.S.A.

I. INTRODUCTION

The development of a stable structure and a suitable product texture in food emulsions and foam-based food products depends on the interactions between the fat globules and between fat globules and air bubbles (1). An important factor influencing the stability of food emulsions and foams is the developed fat particle structure. The fat particle structure variation and destabilization during the shearing process are very complex. Many factors such as shear rate, shear time, temperature, the composition of the surfactant mixture, and the ratio of liquid to solid content inside a fat globule can greatly affect the fat particle structure of the final product. Researchers have investigated some of these factors in relationship to emulsions.

Long-term stability of whipped foams is thought to result from the formation of a three-dimensional fat particle network structure (2,3). The presence of solid fat (to promote fat globule rupture) and of liquid fat (to promote clumping) might be necessary for the formation of a stable whipped foam. Darling (4) obtained similar results. He found that a prerequisite for effective whipping was that the solid part of the fat and the whipping time were directly related to the proportion of solid fat. Brooker and his colleagues (5,6) found that the development of a stable structure in a whipped foam depends on the interactions between the fat globules and between fat globules and air bubbles. The stabilization of air was a two-step process involving the selective adsorption of proteins and emulsions to the air-bubble surface, followed by the attachment of fat globules to the

air–water interface under shear stress. The attached globules stayed at the air–water interface in such a way that part of the fat became exposed to the air and slightly protruded into it. In the final product, bubbles were stabilized predominantly by the fat globules, but the remains of the initial protein-adsorbed interface persisted between the globules. In the aqueous phase, the fat particles form a three-dimensional network structure connecting different bubbles, which decreases the mobility of the bubbles and, hence, mechanically stabilizes the whipped product.

However, most information about the stability of whipped foams or foam-based products has come from studies utilizing simplified solutions that neglected the effect of the dispersed phase or from empirical studies providing information that was not easily translated quantitatively. The lack of detailed information from actual whipped foams stems from the lack of methods or tools to measure the component functional properties in systems as complex as whipped foams, which has prevented a further understanding of the relationship between component interactions (structure and conformation) and the stability of whipped foams. We have successfully applied the backlight-scattering technique to quantitatively measure the fat particle structure inside the food systems in a noninvasive way (7).

It has been generally accepted that interfacial properties such as surface and interfacial tension, diffusion, and adsorption–desorption properties of surfactants and proteins are of paramount importance to the stability of foam-based food products (4,8–13). Researchers have expended much effort in determining the static and dynamic interfacial properties, and a number of methods exist to study that. However, all of these methods are based on the concept that the foam or emulsion stability is controlled by the interfacial properties of a single interface in isolation. However, several of the interfaces are in close proximity to the surfaces in these aerated emulsion systems, with a film of only a few nanometers to almost a few micrometers in thickness. Under these conditions, there are interactions occurring across the film that can be significant. Toward this end, we have recently developed a new noninvasive method to measure the static and dynamic properties of the foam and emulsion films (14–18).

Dispersed air may degrade in many ways; for example, it may degrade through aggregation, creaming, coalescence, or Ostwald ripening and gas diffusion (19). Ostwald ripening is the process by which larger bubbles grow at the expense of the smaller ones because of differences in their chemical potential. The growth occurs by the diffusion of the dispersed phase through the continuous phase. Liftshitz and Slezov (20) and, independently, Wagner (21) developed an analytical solution for the Ostwald ripening process for a dilute dispersed phase. Gas diffuses out of the system in an open system where the dispersed phase is gas, and it results in a decrease in the bubble

size and overrun. De Vries (22,23) and Princen et al. (24,25) have provided the basic framework for studying gas diffusion to the atmosphere. Prins (26) showed the effect of the viscoelasticity of the bubble surface on the rate of gas diffusion. Recent studies (27–29) have been done to understand the effect of bulk rheology on bubble dissolution. However, very little work has been done to understand the effects of gas diffusion and Ostwald ripening on the stability of aerated food emulsions.

The purpose of this chapter is to provide quantitative descriptions of the fat particle structure variation during the whipping process using the backlight-scattering technique and to relate this structure to the stability of the whipped products. This research also attempts to interpret the dynamic film tension, film elasticity, and film thickness stability of foam-based products and to understand the effects of Ostwald ripening and gas-diffusion mechanisms on the long-term stability of aerated food products.

II. MATERIALS AND METHODS

A. Emulsion Preparation and Whipping

The emulsion preparation is as follows: Sodium caseinate, emulsifiers (poly-sorbate 60 and sorbitan monostearate), and gums (xanthan and guar) were dispersed in water. Partially hydrogenated vegetable oil, syrups, and flavors were then added to make a preemulsion, which was then pasteurized and homogenized in a two-stage homogenizer. The resulting emulsion was cooled to 1–3°C and aged for 45 min in a tank at about 5°C to produce the final emulsion samples used in this study. Air was injected into the aged emulsion under pressure, and the mixture was whipped under high stress for 15 min. The final whipped foam was produced after equilibrium was reached inside contherm 1 and contherm 2 (Fig. 1). Two food emulsion samples were prepared by this method. The fat concentrations in these two samples are 12 wt% and 20 wt%, respectively.

The sizes of the fat particles inside the food emulsion samples were measured using a Horiba LA-900 particle size distribution analyzer (Horiba Instruments Incorporated, Irvine, CA). The fat particle sizes in these two food emulsion samples were nearly the same (mean particle size around 0.4 μm).

B. Mesophase Preparation

The aerated mesophase was chosen as a model system to study the role of gas diffusion and Ostwald ripening on the stability of an aerated food system. The mesophase consisted of 2 wt% surfactant,

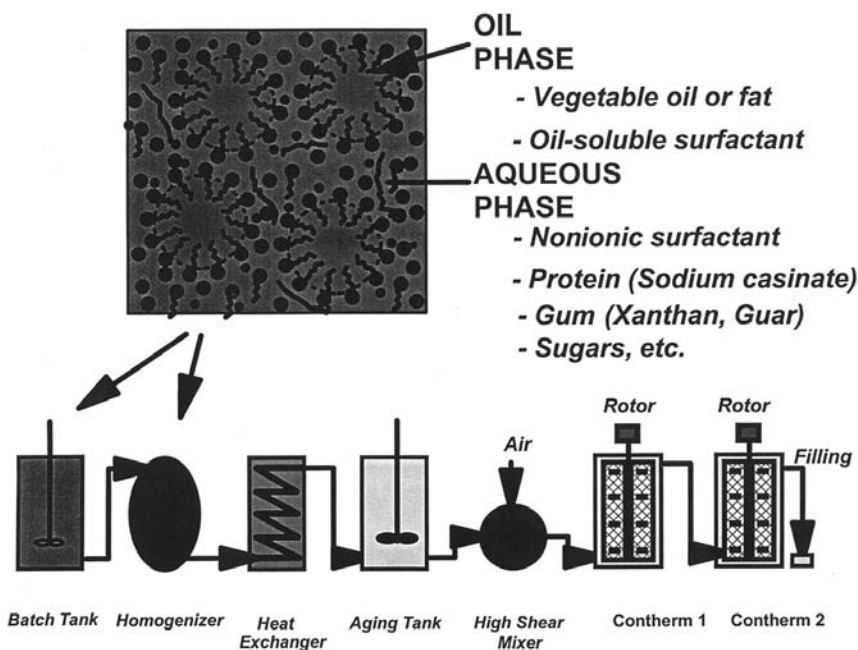


Figure 1 Sketch of typical food emulsion and foam process.

33 wt% sugar, and 65 wt% water. We chose propylene glycol stearate [hydrophile-lipophile balance (HLB): 1.8; molecular weight (MW): 387] and triglycerol stearate (HLB: 7.2; MW: 568) as low-HLB surfactants and sucrose stearate (HLB: 15; MW: 652) as a high-HLB surfactant. A low-HLB surfactant is dry mixed with sucrose stearate in the desired proportions (i.e., a high-HLB to low-HLB surfactant molar ratio was kept as 0.56) and added, under vigorous stirring, to water maintained at a temperature of 80°C. The total surfactant concentration was kept at 6 wt%. The surfactants were mixed for about 15 min in order to ensure the complete dissolution of the surfactants in the solution. The mesophase was refrigerated overnight prior to use. At the time of the experiment, the mesophase was mixed with equal weights of sugar and water. The mesophase was whipped using a Hobart (N-50) whipping machine. Whipping was done for 1 min at low speed followed by a high speed of aeration for 2 min at room temperature (22–25°C). The aerated mesophase was stored at room temperature and in refrigerated conditions. We measured the bubble size distribution and overrun as a function of time in order to describe the destabilization process quantitatively.

C. Backlight-Scattering Experiment

The nondestructive backlight-scattering technique has been successfully applied to obtain the information of the particle structure and interparticle interactions inside colloidal dispersions in our previous research (7,30). In this research, the backlight-scattering technique was used to obtain the information about the particle structure variation under and after the shear stress. Figure 2 illustrates the experimental setup: a collimated green light beam (50 μm in diameter, wavelength 543 nm) produced by a 0.5-mW He-Ne laser (Model 155A, Spectra-Physics Laser Products, Mountain View, CA) was scattered by colloidal particles inside the sample under a controlled temperature and produced a scattering image on the surface of a glass vial. The image intensity was then recorded by a vertically polarized coupled-charge device (CCD) digital camera (Lynxx 2000 Frame 336*244FT, Spectra Source Instruments, Westlake Village, CA) and downloaded to a

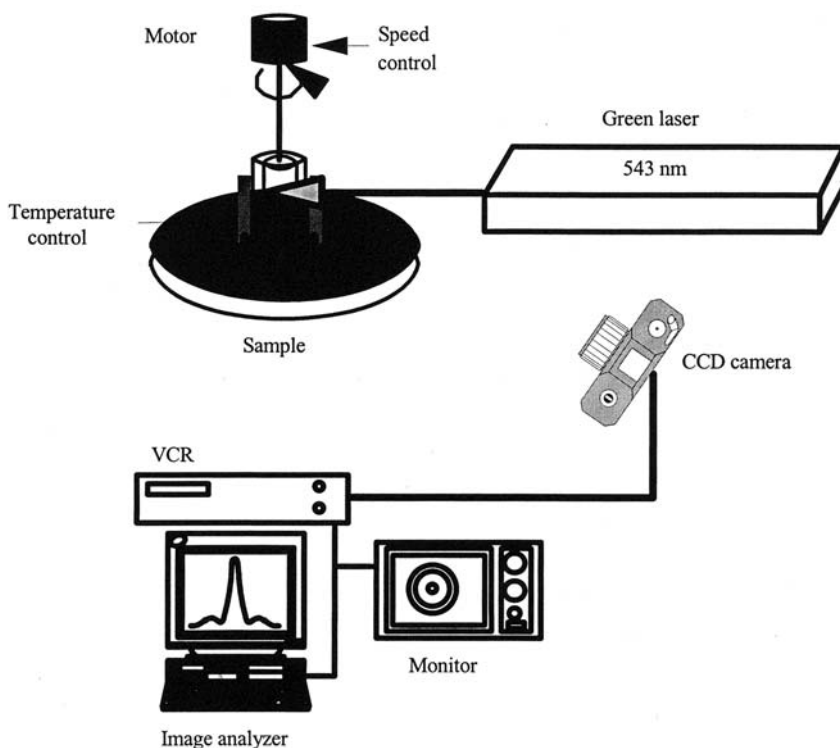


Figure 2 Backlight-scattering experimental setup.

computer (IBM-compatible PC Pentium/120 MHz). The recorded image was transformed into an intensity profile by image-analyzing software (Lynxx 2000, Version 3.04b, Spectra Source Instrument, Westlake, CA). According to our previous research (7), the value of the normalized structure factor $S(Q)$ [which is defined as the structure factor $S(Q)_{\max}$ at the first maximum point divided by the structure factor $S(Q)_{\min}$ at the first minimum point] can be used to quantify the fat particle structure inside food emulsions due to the decreased oscillatory behavior of the structure factor against the scattering vector. Larger values of $S(Q)$ yield more ordered structures inside colloidal dispersions.

D. Film Rheology and Film Thickness Stability

When the bubbles or droplets interact in a foam or emulsion system, a film is formed from the continuous phase between the bubbles or drops. The stability of any foam or emulsion depends on the response of the thin liquid film and the Plateau borders during shear and dilatation. In real polydispersed foam and emulsion systems, thin liquid films formed between bubbles or drops are not flat, but have a spherical curved shape. We developed a dynamic film tensiometer (Fig. 3) to study the film's rheological properties and thickness stability (14–18, 30,31). A small drop of emulsion (15–20 μm in size) is placed at the tip of a glass capillary (0.6 mm of inner diameter and 0.05 mm of wall thickness) and a drop with a double meniscus is formed. The capillary is connected to a feed syringe with a piston having a fine screw. A curved, spherical, cap-shaped film is formed with its meniscus adhering to the capillary drop by expelling the emulsion using air (Fig. 3). The diameter of the film for the foam lamella is slightly larger than the capillary diameter. Because the inner and the outer parts of the foam are air, the surface of the foam lamella is a part of a sphere. A sensitive pressure transducer (with sensitivity of $\pm 0.25 \text{ dyn/cm}^2$) was used to measure the capillary pressure versus time. The output of the pressure transducer is fed into a computer using a data acquisition card. The size of the film is controlled (i.e., expanded or contracted) by the feed syringe.

The interfacial film tension (f) is related by the Young–Laplace equation to the film radius (R_f) and capillary pressure (P_c) as

$$P_c = \frac{2f}{R_f} \quad (1)$$

The film tension is equal to the two times the single interfacial tension because the film consists of two single interfaces.

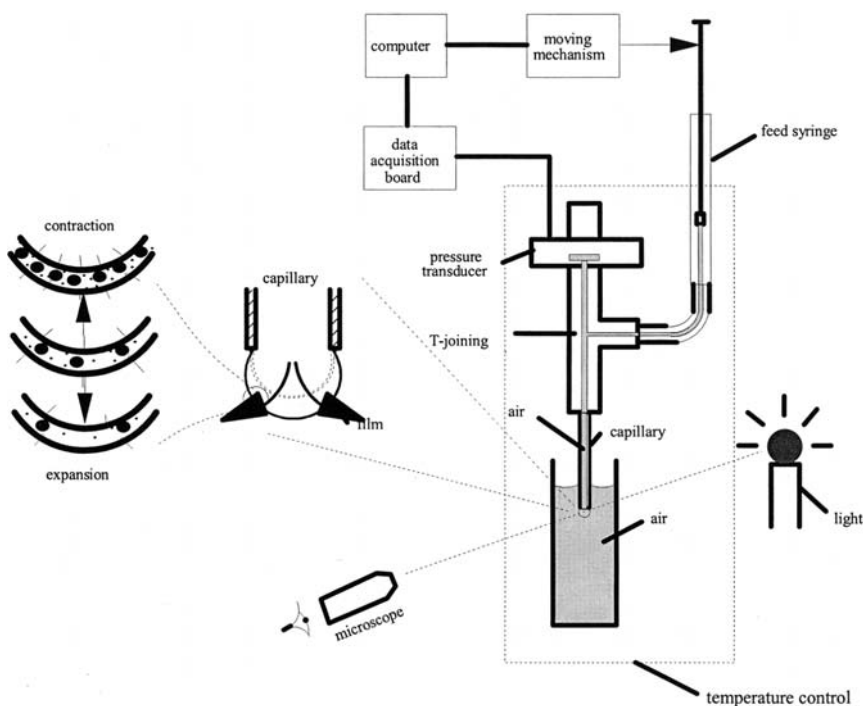


Figure 3 Diagram of the film rheometer.

Dynamic experiments are usually conducted by either expanding or contracting the film area. In the film stress–relaxation experiments, the film is quickly expanded or contracted, and then the relaxation of the film tension (capillary pressure) is measured. During this process, the film area is kept constant. When the film area expands, the surfactant concentration on the film surfaces drops. The film tension and the capillary pressure jump from the equilibrium value of the surface tension to the value corresponding to the new area per surfactant molecule on the film surfaces. The surfactants in the meniscus and in the film start to adsorb to restore equilibrium and, thus, the capillary pressure and film tension decreases as time progresses and finally approach an equilibrium value. The initial film tension (f_i) versus the logarithm of the relative film expansion area provides information about Gibbs film elasticity as follows:

$$E_f = \frac{df_i}{d \ln(A/A_0)} \quad (2)$$

where A_0 is the initial film area.

Our film rheometric technique also allows for the study of the dynamic film thickness stability of curved films. Due to the decreased surfactant concentration on the film expansion surface, critical film expansion ratio exists, and after that, the films will rupture.

E. Foam Film Air Permeability

The stability of foam-based food products depends on the air permeability throughout the foam lamella (32). In order to measure the foam film air permeability, a curved, spherical, cap-shaped foam film was formed at the tip of a glass capillary (0.6 mm inner diameter and 0.05 mm wall thickness), and the foam bubble diameter and capillary pressure were monitored versus time. The temperature was kept constant at 5°C during the measurement. Foam film permeability can be calculated by using the air flow rate, capillary pressure, foam lamella area, viscosity, and foam lamella thickness. The foam film tension measurement by the film rheometer provides simultaneous information about the capillary pressure, gas flow rate, and foam lamella area as a function of time. The gas flow rate (q) throughout the foam lamella is related by the Darcy equation to the film area (A), the capillary pressure (P_c), viscosity μ , foam lamella thickness (h), and permeability (k) (33):

$$q = k \left(\frac{AP_c}{\mu h} \right) \quad (3)$$

When the foam lamella is formed on the tip of capillary, the lamella thins. During that time, the air diffuses throughout the foam lamella and the foam cell shrinks. The foam lamella increases its thickness due to the viscosity effect during the shrinking. The rate of the foam cell shrinking process is modeled assuming that the film thinning rate (V_f) follows Reynolds law:

$$V_f = \frac{2h^3 F}{3\pi\mu r_1^4} \quad (4)$$

where r_1 is the film radius of the curved film, h is the film thickness, and F is the capillary force. As the film drains, the thickness decreases from the initial thickness h_1 to thickness h_2 . The time that the film thickness decreases from h_1 to h_2 is given by the Reynolds equation:

$$t_{12} = \frac{3\pi\mu r_1^4}{4F} \left(\frac{1}{h_2^2} - \frac{1}{h_1^2} \right) \quad (5)$$

Assuming that the total film volume is constant during foam cell shrinking (i.e., high film viscosity as in food emulsions samples), then

$$h_2 = \frac{R_1 L_1 h_1}{R_2 L_2} \quad (6)$$

where R_1 is the foam cell radius before shrinking, R_2 is the foam film radius after shrinking, L_1 is the foam cell height before shrinking, and L_2 is the foam cell height after shrinking.

Combining Eqs. (5) and (6), the film thickness of the shrinking foam film as a function of time can be derived as

$$h_2 = h_{2,\text{drainage}} + h_{2,\text{shrinkage}} - h_1 \quad (7)$$

where

$$h_{2,\text{shrinkage}} = \frac{R_1 L_1 h_1}{R_2 L_2} \quad (8)$$

and

$$h_{2,\text{drainage}} = \left(\frac{1}{h_1^2} + \frac{4\Delta t_{12} P_c A_f}{3\pi\mu r_1^4} \right)^{-1/2} \quad (9)$$

F. Measurement of Overrun and Bubble Size

Overrun of the mesophase is defined by the percentage of incorporated air with respect to the initial mesophase volume. Incorporated air reduces the density of the mesophase. The amount of incorporated air can be estimated by measuring the change in the density of the mesophase. Measurement error was estimated to be about 5–10% in this method. However, this is an absolute error (i.e., if the overrun is 1000%, then the confidence interval is 990–1010%). Bubble size distributions were measured from the video frames using a transmitted light microscope and VCR, and diameter measurements were taken using ImagePro Software (images from the videotape can be captured by this software). These captured images can be analyzed automatically or manually. Bubbles are clearly seen in this image. We used the manual mode to measure the diameter of the bubbles; one can accurately measure bubbles having a diameter of 1 μm or more. (The presence of smaller bubbles can be observed visually.) Aerated samples were sandwiched between a glass slide and a thin glass plate. The thin glass plate was very light and probably did not affect the bubble shape as only a very small number of distorted bubbles were observed. This is probably the result of

the high elasticity of the mesophase, which could sustain the weight of the thin glass. As an additional measure, we measured the diameters of bubbles that appear distorted and took the average. We then focused on a single plane of the mesophase. The bubbles from the other planes are out of focus and cannot be seen very clearly. We did not measure the bubbles that were out of focus. A substantial number of bubbles (100–150) were counted in each frame. In order to obtain statistical estimates of bubble size distribution, 6–10 frames (containing a total of about 800–900 bubbles) were used.

G. Measurement of Gas Diffusion

The rate of air loss from a single bubble is measured to quantify the gas loss (decrease in overrun) from the system. A bubble is formed inside the liquid (i.e., mesophase) and the diameter of the bubble is measured as a function of time. This would give an idea of the permeability of the surfactant film to air and permeability of air through the liquid medium. The pressure difference between the bubble and the atmosphere is the main cause for gas transfer from the bubble to the atmosphere. The rate of gas loss depends on the size of bubble, the surface tension of the liquid, the permeability of the liquid film, and the distance from the free gas–liquid surface. Air bubbles are either at the gas–liquid interface or in the bulk liquid. In order to simulate an aerated mesophase, we decided to study two cases: (I) gas diffusion from a bubble when the bubble is at the gas–liquid interface and (II) gas diffusion from a bubble when the bubble is inside the bulk liquid. The bubble shrinks over time when the bubble is formed at the gas–liquid interface. Let us imagine that a bubble of radius r is formed at the gas–liquid interface. The pressure difference between the bubble and the atmosphere will be

$$\Delta P = \frac{2\sigma}{r} \quad (10)$$

where σ is the surface tension.

Now, the concentration difference can be expressed in terms of the pressure difference. If we combine the above equation with the ideal gas law and Fick's law of diffusion, the following equation (24) can be obtained:

$$r^2 = r_0^2 - 4\alpha \left(\frac{D\sigma}{hP_0} \right) t \quad (11)$$

where r is the radius at the instant time t , r_0 is the initial radius, P_0 is the atmospheric pressure, D is the diffusivity of the film, h is the thickness of the film, σ is the surface tension, and α is the dimensionless factor (24). α is a measure of the area of the bubble that is exposed to the air directly above

the plane of contact with the liquid. This equation relates the radius of a shrinking bubble with time. Almost all of the gas diffuses through the film area when the bubble is at the gas–liquid interface (directly exposed to the atmosphere). The rate of gas diffusion depends on the area of the film, the thickness of the film, and the film structure (molecular packing in the film).

The physics of the problem remains the same when the bubble is inside the bulk liquid. Let us imagine that a bubble of radius r is placed inside the liquid at a distance h from the gas–liquid interface. If we neglect the pressure exerted by the liquid height h , the pressure difference between the bubble and the atmosphere can be expressed by Eq. (10). The concentration difference can be expressed in terms of the pressure difference using Henry’s law. By combining Eqs. (10) and (11) with the ideal gas law and Henry’s law, we obtain

$$r^2 = r_0^2 - 4 \left(\frac{RT}{P_0} \right) \left(\frac{DS\sigma}{h} \right) t \quad (12)$$

Equation (12) relates the radius of a shrinking bubble with time when the bubble is inside the liquid; S is the solubility of the dispersed phase (air) at the interface.

A bubble is formed inside the mesophase using the setup described in Fig. 4 in order to measure the gas diffusion from a bubble inside the mesophase. The bubble is kept at a fixed distance from the air–mesophase interface using a thin glass plate. The distance of the bubble from the air–mesophase interface was approximately 250 μm . The diameter of the bubble is measured as a function of time to determine the rate of air loss from a single bubble.

III. RESULTS AND DISCUSSION

A. Fat Particle Structure Variation During Homogenization

Homogenization is responsible for the formation of food emulsions. The structure factor was measured immediately after homogenization for three emulsions containing 5 wt%, 12 wt%, and 20 wt% fat. Figure 5 shows that the structure factor for all the samples was approximately 1, indicating that a very poor fat-particle-packing structure was produced after homogenization; therefore, all of the food emulsions were unstable.

The temperature is very high after homogenization (around 72.5°C). Xu et al. (7) observed that a food emulsion become less stable with an increase in temperature. Figure 5 also reveals that the fat-particle-ordering structure was better (more than 1) for an emulsion containing 20 wt% fat.

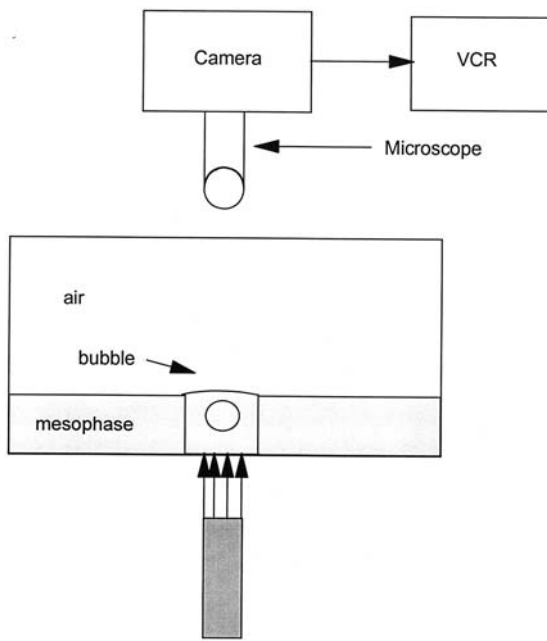


Figure 4 Experimental setup for the single-bubble experiment.

The fat particle concentration inside a 20-wt% fat emulsion was much higher than that of other two samples and the increased fat particle concentration probably resulted in improved fat particle structure.

B. Fat Particle Structure During Cooling

The emulsions were cooled to nearly 5°C to prevent fat particle aggregation or coalescence after homogenization. The fat particle structuring factor greatly improved after cooling the three samples when compared with the particle size distribution after homogenization. It was found that the particle size distribution remained unchanged in all three samples. The normalized structure factor for an emulsion containing 20 wt% fat is shown in [Fig. 6](#). Increased fat particle structuring suggests that the food emulsions should be cooled down immediately after homogenization to avoid fat particle aggregation or coalescence. The particle size distribution for all three samples remained unchanged. Starch particles were added after cooling and before aging. The fat particle structure becomes less ordered due to the addition of large starch particles for the 5-wt% fat whipped foam. The effect of starch particles and fat destabilization has been systematically

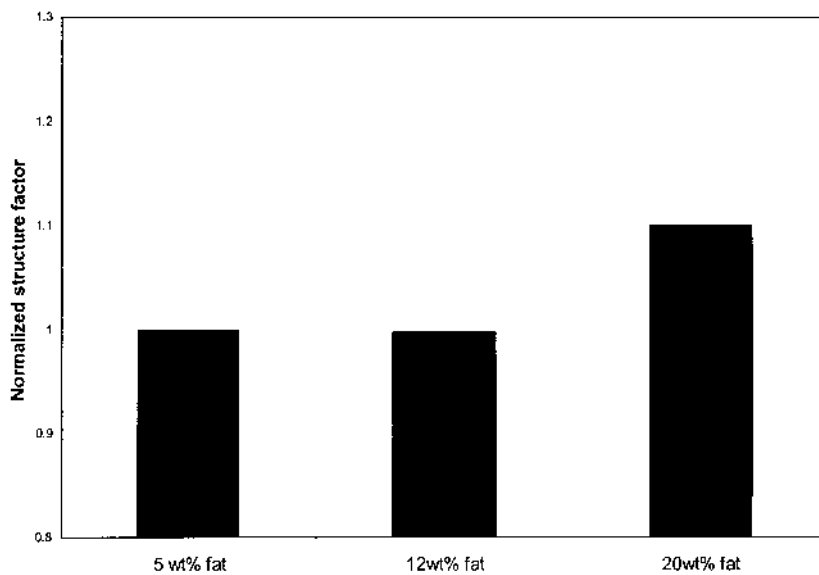


Figure 5 Normalized structure factor after homogenization.

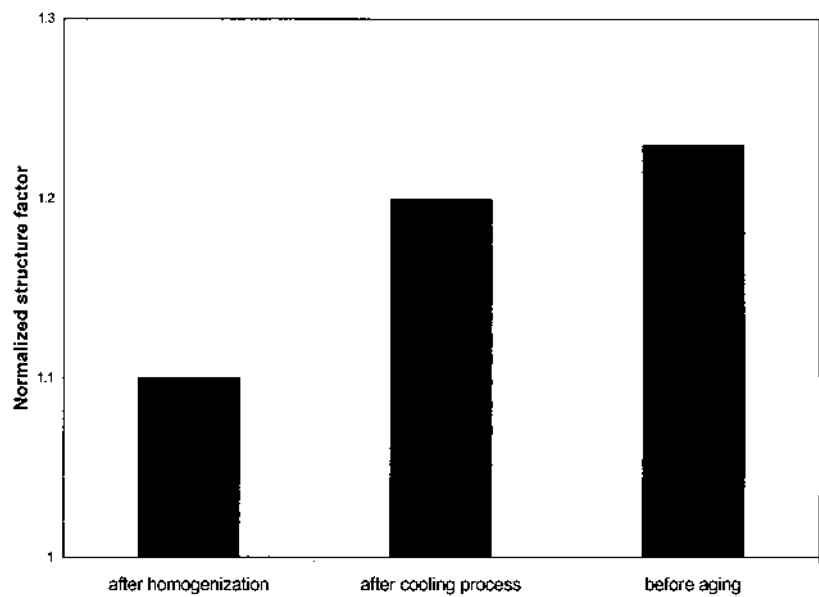


Figure 6 Normalized structure factor after cooling for an emulsion containing 20 wt% fat.

studied by Xu et al. (7). It was found that the effect of starch on the fat particles was similar to that of particle polydispersity. Increased particle polydispersity decreased the particle ordering (7), and the stability of the food emulsion decreases.

The fat particle structure for the 12-wt% fat and 20-wt% fat whipped foams are slightly greater than the other sample and benefited from the adsorption of surfactants and proteins on the fat particle structure. However, the increase in the fat particle structuring was small, implying that most of the adsorption of surfactants and protein on the fat particle surface was completed before aging.

C. Fat Particle Structure During Aging

It was observed that the fat particle structure for emulsions containing 5-wt% and 12-wt% fat did not change with aging time. For an emulsion containing 20 wt% fat, a small and gradual increase was observed (Fig. 7). No significant change was observed in the fat particle size distribution during the aging process. Some studies (4,34) have concluded that one

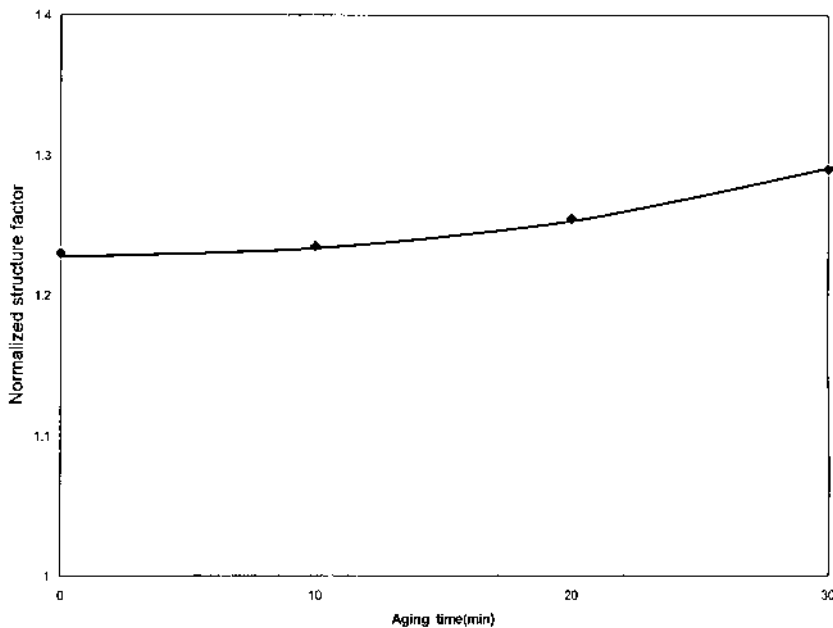


Figure 7 Fat particle structure variation during aging for an emulsion containing 20 wt% fat.

important role of aging was to provide the necessary time to achieve the complete coverage of fat globules with adsorbed molecules and competitive adsorption between surfactant and proteins. However, our results suggest that most of the adsorption of surfactant and proteins was completed before the aging process. Based on our observations and the results of the other studies (4,34), the role of aging can be summarized as follows:

1. The polysaccharide stabilizers, such as gums, require time for full hydration; therefore, the bulk viscosity increases with the aging time.
2. The crystallization of fat particles occurs during the aging process. According to Darling and Goff (34), the existence of crystalline fat inside fat particles was important to the whippability of food emulsions. They found that without the crystalline phase, the undesired coalescence of fat droplets occurs during the whipping process, and the resulting whipped foams are unstable.

D. Fat Particle Structure During Aeration

It was observed that the fat particle structure inside the low-fat emulsions (5 wt% and 12 wt%) did not change during the aeration process. However, the fat particle structure inside the high-fat product (20% fat) decreased. This is probably the result of the increased collision between the fat particles at high fat concentrations due to high mechanical agitation. Increased fat particle collisions resulted in flocculation and clustering, which, in turn, reduced the fat-particle-ordering structure.

E. Fat Particle Structure During the Whipping Process

It was observed that the fat particle structuring was greatly improved (Figs. 8–10) during the whipping process, indicating a well-developed fat particle structuring in the bulk phases. It is worth noting that the normalized structure factor after whipping in our samples is found to be the same as the sequence of stability of whipped foam products (i.e., 20 wt% fat whipped foam > 5 wt% fat whipped foam > 12 wt% fat whipped foam), indicating that many factors, such as fat particle attachment at the air–water interface and the formation of a three-dimensional fat particle network structure between neighboring air bubbles, can influence the stability of whipped foams. The developed fat particle structure in the bulk phase after whipping is one of the most important factors in determining the stability of whipped foams.

The data shown in Figs. 8–10 also indicate that in a stable whipped foam, most of the fat particles in the bulk phase remain in a single particle

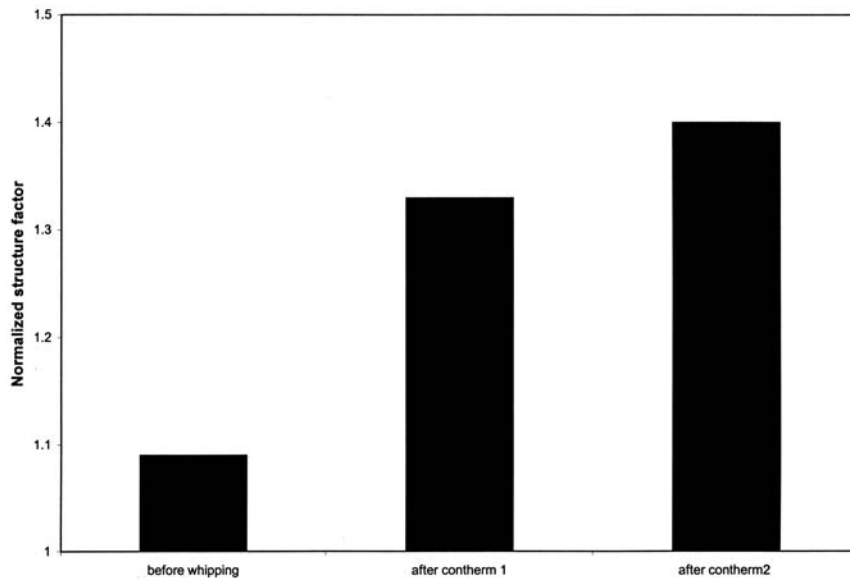


Figure 8 Fat particle structure variation during whipping process (for an emulsion containing 5 wt% fat).

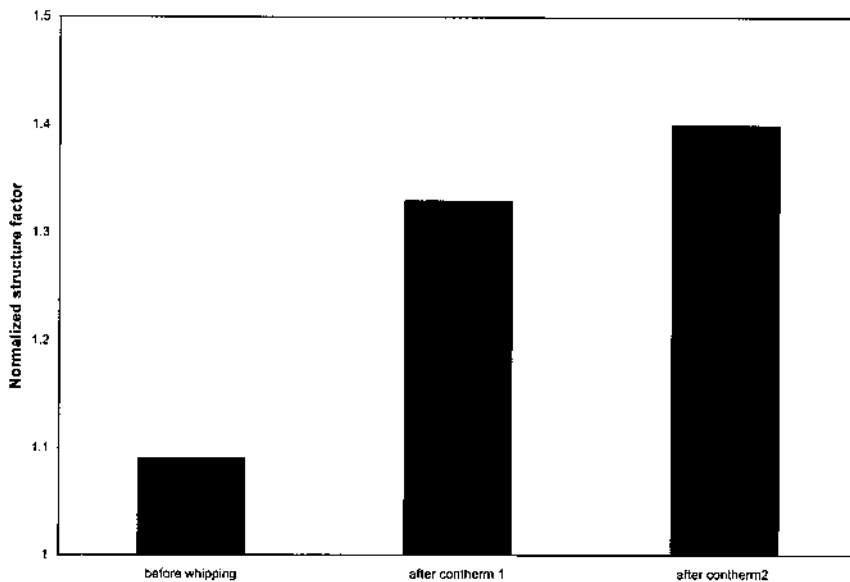


Figure 9 Fat particle structure variation during whipping process (for an emulsion containing 12 wt% fat).

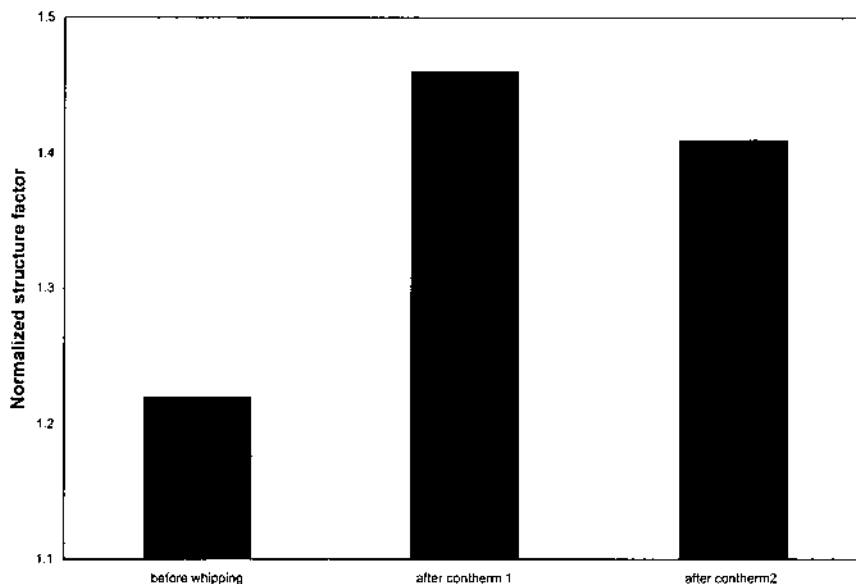


Figure 10 Fat particle structure variation during whipping process (for an emulsion containing 20 wt% fat).

state and are well distributed in space, rather than being flocculated, clustered, clumped, or even coalesced to form large particles. The effect of fat particle floccules, clusters, clumps, or coalesced fat particles on the fat particle structure is similar to the addition of particle polydispersity. When fat particle aggregation occurs, the fat particle structure should become less ordered (7). Other researchers reached a similar conclusion using various techniques (2,3,5,6,11). They found that the outline of the individual fat globules and clusters in a stable whipped foam were clearly observable; in the unstable dairy foam, the fusion/coalescence of fat particles was observed.

Controlled fat particle destabilization is necessary in order to produce stable whipped foams. For example, before fat particles can attach to the air-water interface or the three-dimensional fat particle network structure can form between neighboring air bubbles, the fat particles have to be ruptured or destabilized (clustered or clumps). The fat particle destabilization during the whipping process should be optimally controlled to produce a stable whipped foam. The fat particle structure decreased with the increasing fat particle concentration in the second whipping stage (contherm 2). In fact, the fat particle structure decreased for the 20-wt% fat whipped foam, indicating that too many fat particles were destabilized and overwhipping

occurred. In this case, only one whipping stage is necessary for high-fat products.

The stability of the whipped foams depends on the interactions between the fat globules and air bubbles. This leads to the buildup of a matrix in which air bubbles are stabilized. The initial stage of the whipping process involves the adsorption of protein and surfactants onto the air–water interface. This gives an initial stabilizing effect on the foams. Subsequent phases of the whipping process involve a progressive increase in the extent to which the fat particles are whipped to attach at the air–water interface, the formation of a fat particle structure in the bulk phase, the buildup of a three-dimensional network structure between neighboring air bubbles, and changes in the number and the size of the air bubbles. The periphery of each air cell in fully whipped foams is composed primarily of fat globules (5), but there is also a variable amount of original protein adsorbed at the air–water interface. The rigidity of the foam structure is provided by bridges of clustered fat particles connected to adjoining air cells and by the formation of a well-developed fat particle structure in the bulk phase.

F. Film Tension, Elasticity, and Thickness Stability

The film elasticity and dynamic film stability of two types of fat-in-water emulsions were investigated: a 12-wt% fat-in-water emulsion and a 20-wt% fat-in-water emulsion. Figures 11 and 12 show the data of foam film stress relaxation with a relative film area expansion of 26%, 46%, and 66% for the 20-wt% fat-in-water emulsion and the 12-wt% fat-in-water emulsion, respectively. Initially, the film was expanded very quickly; the surfactant concentration on the film surface suddenly decreased due to the increased film area. As a consequence, the film tension jumped from its equilibrium value to the maximum value. After that, because the concentration of surfactants in the meniscus was higher than that of in the film, the surfactants diffused from the meniscus to the inside of the film, and from the inside of the film to the film surface; as a consequence, the film tension decreased and finally reached the equilibrium film tension (in approximately 15 min). Figures 11 and 12 show that the equilibrium values of the foam film tension of 20 wt% and 12 wt% fat-in-water emulsions are both approximately 91 dyn/cm. However, the initial value of the film tension right after the expansion and the value of the initial slope of the curved film tension versus time were different (Figs. 11 and 12). These data are presented in Table 1. Based on the data, the film elasticity was calculated for the 20-wt% fat and 12-wt% fat foam films formed from the corresponding emulsions (Fig. 13). The film elasticity data show that the 20-wt% fat foam film had a

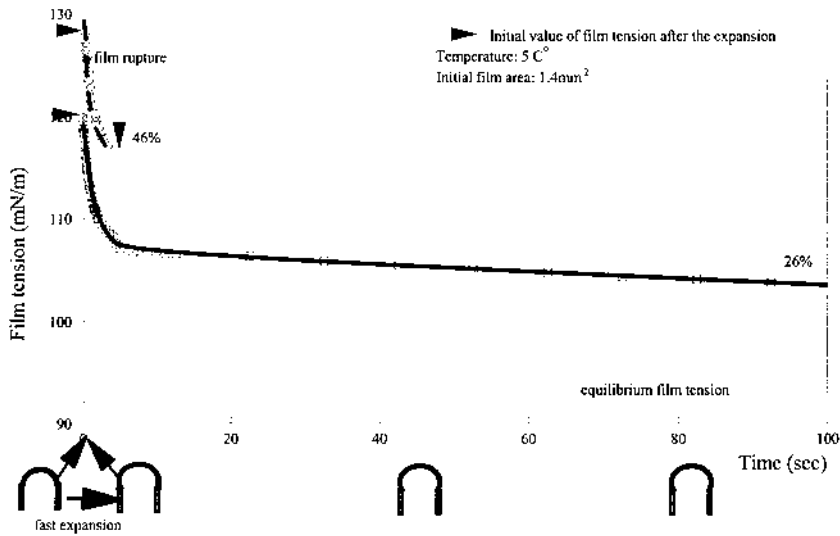


Figure 11 Foam film stress relaxation with relative film expansion area: 26% and 46% for fat-in-water emulsion (fat concentration: 12 wt%).

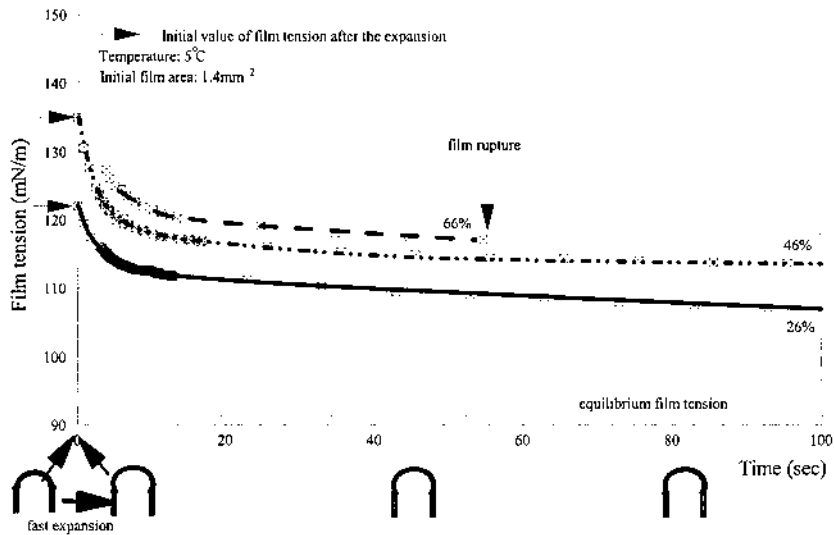
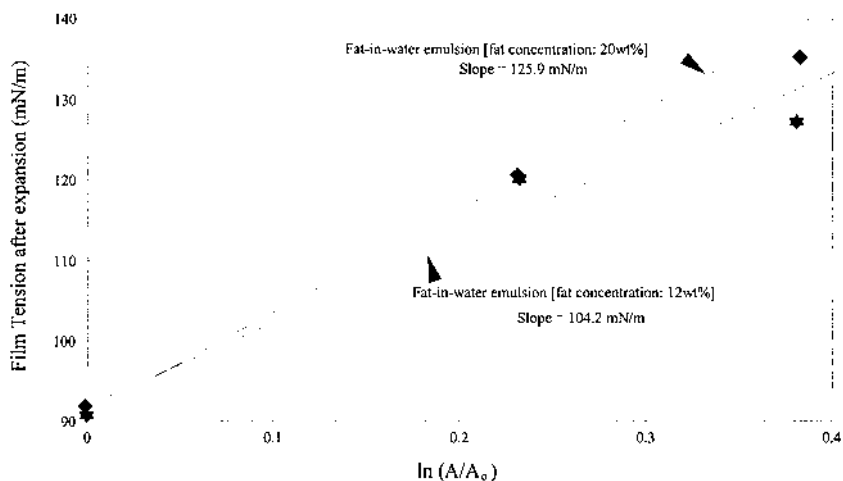


Figure 12 Foam film stress relaxation with relative film expansion area: 26%, 46%, and 66% for fat-in-water emulsion (fat concentration: 20%).

Table 1 Foam Film Rheological Properties

Sample	Equilibrium film tension (mN/m)	Initial slope of the curved film tension versus time (26% expansion) (mN/m s)	Gibbs film elasticity (mN/m)
20 wt% Fat-in-water emulsion	91	-12.7	125.9
12 wt% Fat-in-water emulsion	92	-25.0	104.2

**Figure 13** Foam film elasticity for fat-in-water emulsions.

higher film elasticity, indicating that the 20-wt% fat foam film should have a higher dynamic film stability. This showed a good correlation with the stability sequence of whipped foams produced from the corresponding food emulsions (i.e., 20 wt% fat whipped foam > 12 wt% whipped foam).

It is also found that the initial slope of the curves shown in Figs. 11 and 12 for the 12-wt% fat-in-water emulsion was higher than the slope for the 20-wt% fat-in-water emulsion, indicating that the diffusion rate of surfactants (polysorbate 60) in a 20-wt% fat-in-water emulsion was slower than that of the 12-wt% fat-in-water emulsion. The Marangoni–Gibbs effect on the stability of foam films was more pronounced for the 20-wt%

fat-in-water emulsion sample, and the foam film produced from 20-wt% fat-in-water emulsion should be more stable. This shows a good correlation with the stability sequence of whipped foams produced from the corresponding food emulsions.

Additionally, the film expansion ratios that the two systems could tolerate without rupturing were different. No rupture for the 20-wt% fat system was observed in the course of the experiments for the expansion ratios of 26% and 46%; the 12-wt% fat system was stable and ruptured only at 26% expansion. This film ruptured in about 3 s at a 46% expansion ratio. The 20-wt% fat system withstood a 66% expansion ratio for 57 s. In this experiment, the initial foam film area was 1.4 mm² for all samples. The data show the same conclusion as the elasticity measurement that the foam film produced from the 20-wt% fat-in-water emulsion—it had a higher dynamic stability than that produced from the 12-wt% fat-in-water emulsion.

We have observed a similar correlation between the foam film elasticity and the stability of the whipped dairy cream emulsion using polyglycerin fatty acid ester and sucrose ester as emulsifiers (35). It was found that at the same mole of emulsifiers (3.3×10^{-4} M) the emulsion containing 30 wt% fat and polyglycerin fatty acid ester had a film elasticity of 57.8 dyn/cm compared to 46.5 dyn/cm for the emulsion containing sucrose ester, thereby demonstrating that greater stability results from a higher film elasticity.

G. Foam Film Air Permeability

The stability of aerated emulsions also depends on the air permeability throughout the foam (32). Figure 14 presents the experimental foam bubble diameter as a function of time for the 20-wt% fat-in-water emulsion and the 12-wt% fat-in-water emulsion. The initial foam bubble diameter was 1 mm for both samples. The rate of bubble shrinkage for foam lamella formed from the 12-wt% fat-in-water emulsion was about 1.5 times faster than that of lamella formed from the 20-wt% fat-in-water emulsion. Similar observations were made when the experimental capillary pressure, foam film surface area, and foam volume were plotted as a function of time.

The calculated foam lamella permeability/film thickness for the fat-in-water emulsion systems is presented in Fig. 15. The value of the foam lamella permeability/film thickness for the 12-wt% fat-in-water emulsion has a maximum (15×10^6 darcy/cm) at 150 min. The data for the 20-wt% fat-in-water emulsion are almost in a straight line. At a film thickness of 200 nm, the foam lamella formed from the 12-wt% fat-in-water emulsion at 150 min has an air permeability of about 50 darcy; under the same conditions, the foam lamella formed from the 20-wt% fat-in-water emulsion has a permeability of about 5 darcy (10 times lower). One can conclude that

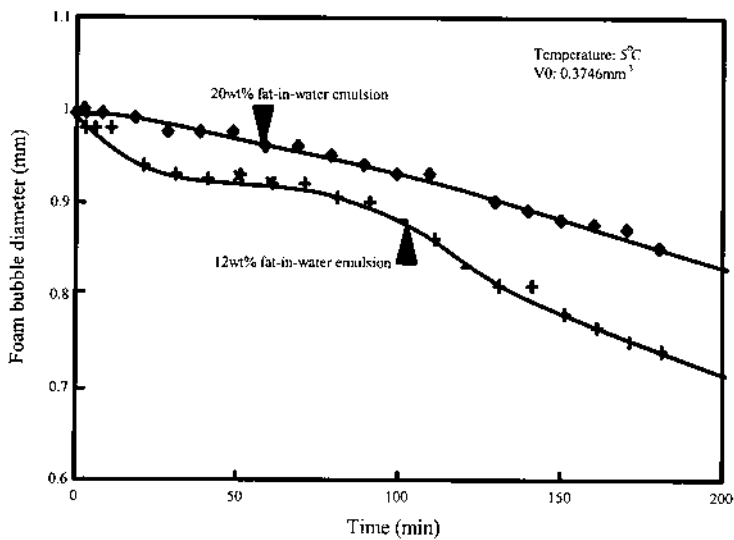


Figure 14 Experimental foam bubble diameter versus time for fat-in-water emulsions.

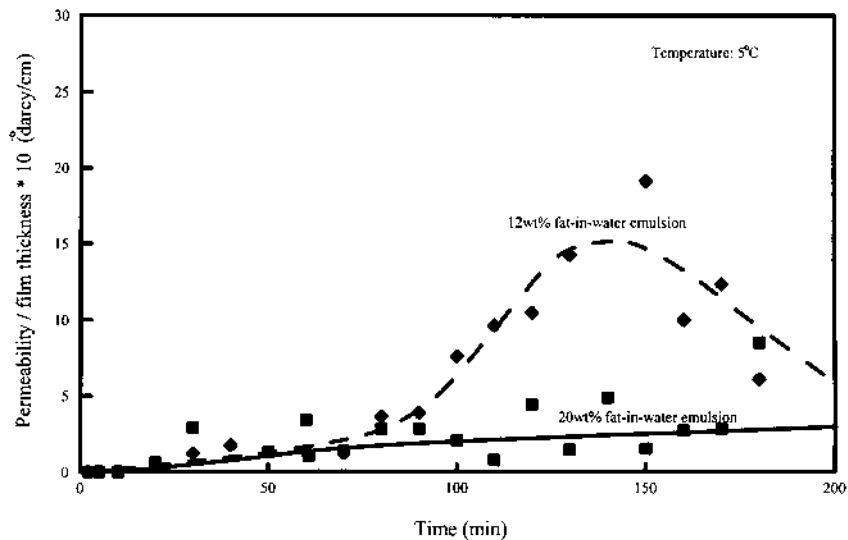


Figure 15 Foam lamella air permeability of fat-in-water emulsions.

smaller foam film permeability values result in greater stability in foam-based products.

H. Long-Term Stability of Model Aerated Food Emulsions

As discussed earlier, the dispersed air within the aerated food emulsions may degrade because of Ostwald ripening and the gas-diffusion process. The roles of these processes were studied using a model system (mesophase) before studying the effect of these processes on actual aerated food emulsion systems. In analyzing the long-term stability of the aerated mesophase, it is important to measure the change in the overrun and the change in the bubble size distribution over time. It must also be noted that the contribution of the large bubbles to the overrun is much more significant than the contribution from the small bubbles because the volume of air in a bubble of diameter d varies as d^3 . Therefore, it is more instructive to interpret the stability of the aerated mesophase using a plot of the volume distribution of bubbles rather than the number distribution. The bubble volume at each size for the samples after a period of 1 week was multiplied by the ratio of the final to initial overrun and is plotted for the propylene glycol stearate–sucrose stearate system and triglycerol stearate–sucrose stearate system (Figs. 16 and 17, respectively). In order to present the loss of air as a function of the bubble size distribution, the initial overrun was chosen as a benchmark. This kind of normalization accounts for the change in the overrun and brings all curves to the same basis (viz. the volume of the total system occupied by bubbles of different sizes). The volume distribution shifts to the large-size range and a significant fraction of the air is retained in bubbles in the size range of 70 μm or more for the propylene glycol stearate system (Figs. 16 and 17). Note that bubbles in this size range were absent to begin with; even after a period of 1 week, the bubbles of this size are small in number, but significant in their contribution to the gas volume. The practical implication of this effect is that this aerated mesophase will be less suitable for use in the food emulsion because the large bubble size will tend to phase separate under the effect of buoyancy. In comparison, the volume distribution of the triglycerol stearate system does not change as much with time (i.e., after 1 week) and the bulk of the air volume is retained in bubbles of nearly the same size range—as was the case initially. Second, it is to be noted that the change in the overrun over a period of 1 week is significantly more for the propylene glycol stearate system than it is for the triglycerol stearate system, implying that the former is less stable than the latter. Finally, it is of significance that the storage temperature does not affect the size distribution to a great extent, but affects the overrun. The change in the overrun is due to the diffusion of

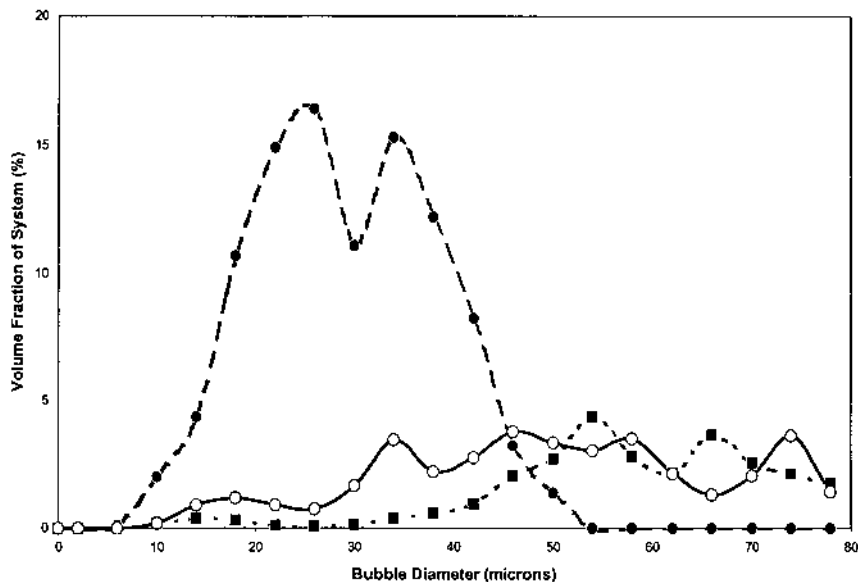


Figure 16 Long-term stability results for the propylene glycol surfactant system. The effect of temperature on volume distribution (corrected for overrun) of bubbles is shown. The solid circle (●) represents results just after whipping (overrun 1000%); the open circle (○) represents the results for the samples stored at 10°C for 1 week (overrun 320%) and the solid square (■) represents the results for samples stored at 25°C for 1 week (overrun 220%).

gas from the bubbles to the atmosphere. The rate of diffusion is greater at higher temperatures, resulting in the loss of more air from the aerated product and a lower overrun over a fixed period of time. The reason for the difference in the degree of air loss to the atmosphere between the two systems is due to the difference in the diffusivity of air in the two liquids.

1. Measurement of the Gas-Diffusion Rate

A bubble is formed inside the mesophase and the diameter of the bubble is measured as a function of time to determine the rate of air loss from a single bubble; this would give an idea about the rate of gas loss through the bulk liquid medium. The pressure difference between the bubble and the atmosphere is the main cause for gas transfer from the bubble to the atmosphere. The rate of gas loss depends on the size of the bubble, the surface tension of the liquid, the permeability of the liquid film, the distance

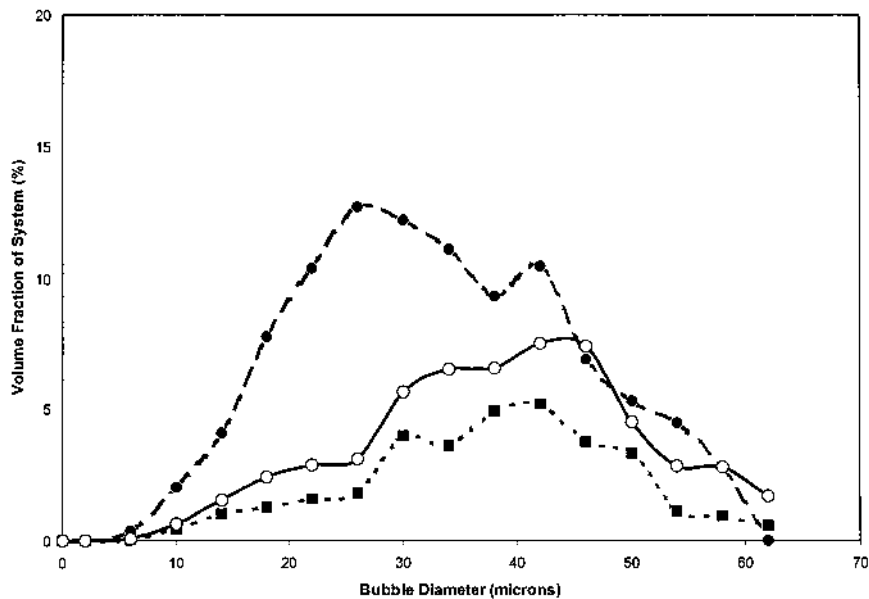


Figure 17 Long-term stability results for the triglycerol stearate surfactant system. The effect of temperature on volume distribution (corrected for overrun) of bubbles is shown. The solid circle (●) represents results just after whipping (overrun 820%). The open circle (○) represents the results for the samples stored at 10°C for 1 week (overrun 450%) and the solid square (■) represents the results for samples stored at 25°C for 1 week (overrun 270%).

from the free gas–liquid surface. Consider that a bubble of radius r_0 is placed inside the liquid at distance h from the gas–liquid interface. Pressure inside the bubble would be higher than the atmospheric pressure due to the capillary effect. This pressure difference would cause the gas to diffuse from the bubble to the atmosphere. De Vries (22,23) has modeled this phenomenon and related the radius of a shrinking bubble with time when the bubble is inside the liquid using the ideal gas law and Fick’s first law [Eq. (12)].

The slopes were 4.4 and 6.7 $\mu\text{m}^2/\text{min}$ for the triglycerol stearate–sucrose stearate system and the propylene glycol stearate–sucrose stearate system, respectively, when the square of the radius was plotted as a function of time and the bubble was formed at a distance 250 μm from the free surface. Results suggest that the diffusivity of the gas from the propylene glycol stearate–sucrose stearate system is one and half times greater than that of the triglycerol stearate–sucrose stearate system. This explains the higher overrun loss for the propylene glycol system.

2. Ostwald Ripening Model and the Gas-Diffusion Model

A schematic of a section of aerated mesophase is shown in Fig. 18. Air bubbles are assumed to be surrounded by a layer of continuous medium of thickness δ and at a distance h_i from the free surface (i.e., the aerated system is in contact with the atmosphere, which we can imagine as a bubble of infinite radius). ϕ_{mi} , ϕ_{si} , and ϕ_∞ are the volume fraction of the gas phase in a continuous medium, at the bubble surface, and at the free surface, respectively. The difference in the concentration of the gas phase is due to the capillary pressure and the effect of the surrounding bubbles. The gas phase concentration in the continuous medium (ϕ_{mi}) can be assumed to be always greater than that at the free surface (ϕ_∞). This difference would lead to the transfer of gas from the continuous medium to the free surface. De Vries (22,23) has modeled gas transfer from a single bubble through a continuous medium to a free surface. ϕ_{mi} would be greater than the ϕ_{si} for bubbles larger than the critical radius and less than the ϕ_{si} for bubbles smaller than the critical radius. [Yarranton and Masliyah (36) have modeled the similar phenomena for the emulsion system]. Thus, air would be transferred from the continuous medium to bubbles larger than the critical radius and air would diffuse out of the bubbles smaller than the critical radius. The exchange of gas among the bubbles is called Ostwald ripening.

a. Ostwald Ripening. The change in radius of a bubble due to Ostwald ripening can be described by the following equations (36):

$$\frac{dr}{dt} = \frac{r(r + \delta)D}{r^2\delta} (\phi_{mi} - \phi_{si}) \quad (13)$$

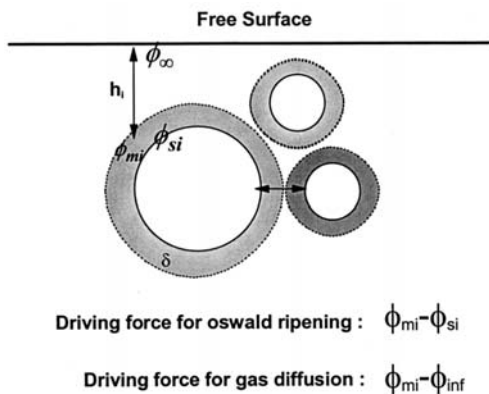


Figure 18 Schematic representation of the gas-diffusion and Ostwald ripening processes.

where D is the gas diffusion coefficient, r is the radius of the bubble, t is the time, and δ , ϕ_{mi} , ϕ_{si} are as defined earlier.

Yarranton and Masliyah (36) provided an expression for the dispersed-phase volume fraction in the continuous phase surrounding the droplet as a function of the droplet diameter and droplet size distribution:

$$\phi_{mi} = \phi_{si} + \frac{\alpha\phi_{\infty}\delta}{(r_i + \delta)} \left(\frac{1}{r_{10}} - \frac{1}{r_i} \right) \quad (14)$$

where r_{10} is the average bubble size (i.e., average radius of the bubbles) and α is defined as $\alpha = 2\sigma v_d / RT$, where σ is the interfacial tension between the two phases, v_d is the molar volume of the dispersed phase, R is a universal gas constant, and T is the temperature.

b. Gas Diffusion. Ostwald ripening does not predict any gas loss from the system. However, the overrun (i.e., amount of incorporated air) of the system decreases with time because of gas diffusion to the atmosphere. If Fick's first law is used to describe gas diffusion to the atmosphere from a bubble having radius r_i and at a distance h_i from the free surface, the following equation is obtained:

$$\frac{dN_A}{dt} = \frac{4\pi D(\delta + r_i)^2(\phi_{mi} - \phi_{\infty})}{h_i} \quad (15)$$

Now, because gas diffuses from the continuous medium surrounding the bubble, the dispersed phase volume will change:

$$\Delta\phi_{mi} = \frac{\Delta N_{Ai}}{\Delta V_i} \quad (16)$$

So, we can obtain

$$\frac{d\phi_{mi}}{dt} = \frac{3D(r_i + \delta)^2(\phi_{mi} - \phi_{\infty})}{h_i[3r_i\delta(\delta + r_i) + \delta^3]} \quad (17)$$

Using Eq. (14), we obtain

$$\frac{d\phi_{mi}}{dt} = \frac{d\phi_{si}}{dt} + \frac{d}{dt} \left[\frac{\alpha\phi_{\infty}\delta}{(r_i + \delta)} \left(\frac{1}{r_{10}} - \frac{1}{r_i} \right) \right] \quad (18)$$

$$\frac{d\phi_{mi}}{dt} = \frac{dr_i}{dt} \left[\frac{\alpha\phi_{\infty}}{r_i^2} - \frac{\alpha\phi_{\infty}\delta}{(r_i + \delta)^2} \left(\frac{2}{r_i} + \frac{\delta}{r_i^2} - \frac{1}{r_{10}} \right) \right] \quad (19)$$

Rearranging Eq. (19) and using Eq. (17), we can write

$$\frac{dr_i}{dt} = -g(\delta, \phi_\infty, r_i, r_{10}) \frac{3D(r_i + \delta)^2(\phi_{mi} + \phi_\infty)}{h_i[3r_i\delta(\delta + r_i) + \delta^3]} \quad (20)$$

where the function $g(\delta, \phi_\infty, r_i, r_{10})$ is defined as

$$\frac{1}{g(\delta, \phi_\infty, r_i, r_{10})} = \left[\frac{\alpha\phi_\infty}{r_1^2} - \frac{\alpha\phi_\infty\delta}{(r_i + \delta)^2} \left(\frac{2}{r_i} + \frac{\delta}{r_1^2} - \frac{1}{r_{10}} \right) \right] \quad (21)$$

Combining Eqs. (13) and (21), one can obtain the composite effect of Ostwald ripening and gas diffusion:

$$\frac{dr_i}{dt} = \frac{r(r + \delta)D}{r^2\delta}(\phi_{mi} - \phi_{si}) - g(\delta, \phi_\infty, r_i, r_{10}) \frac{3D(r_i + \delta)^2(\phi_{mi} - \phi_\infty)}{h_i[3r_i\delta(\delta + r_i) + \delta^3]} \quad (22)$$

3. Model Prediction

We observed that overrun decreases substantially over 1 week for both experimental systems. The bubble size distribution also changes significantly over the same period. Loss of gas could be attributed to the gas diffusion to the atmosphere. In order to obtain quantitative agreement, we simulated models for gas diffusion and the effect of Ostwald ripening. The simulation was conducted on 120,000 bubbles (with an initial size distribution that matches the experimental one) in a cylindrical vessel 12 cm in height. With this number of bubbles, the system volume that corresponds to an air volume overrun of 1000 vol% for propylene glycol system and 820 vol% for the triglycerol stearate system is a small fraction of the experimental system volume, although the simulation cell has the same height as the experimental system. This reduction in scale (i.e., smaller area) is necessary in order to keep the number of bubbles in the simulation manageable and it was found that this reduction in scale does not affect the results. For computational purposes, the cylinder was divided into 1200 layers. The thickness of a layer (100 μm) was chosen to accommodate the largest air bubble observed in the experiment.

a. Effect of Gas Diffusion on Overrun. The effect of gas diffusion on overrun (i.e., the long-term stability) was studied in two cases. In the first case, the De Vries model [Eq. (12)] was simulated for the bulk system. It was assumed that the radius of each bubble decreases with time as predicted by Eq. (12). The distance of each bubble from the free surface was known

because we had fixed the position of the each bubble in the vertical direction. The rate [slope of Eq. (12)] was obtained from the shrinking bubble experiments. The results of our simulations for the system are presented in Fig. 19. The De Vries (22,23) model predicts that the overrun of the triglycerol stearate–sucrose stearate system would decrease from 820% to 176% and the overrun of propylene glycol–sucrose stearate system would decrease from 1000% to 78%. However, for a finite dispersed-phase volume concentration, the gas-diffusion rate would be affected by the gas volume fraction and the bubble size distribution as described by Eq. (17). The simulation results are shown in Fig. 19. We did not see significant improvement when compared to the prediction of the De Vries (22,23) model. The results are understandable because our average bubble size was large (20 μm). When the bubble size is large, the contribution of the second term of Eq. (13) becomes negligible. This would make Eq. (17) the same as Eq. (12); both models predict almost the same decrease in the overrun for the system. When the average bubble size is small (as much as 5 μm), we observed a significant difference (as much as 50%) between the predictions of the De Vries model and Eq. (20).

b. Effect of Ostwald Ripening on Overrun. We observed the theoretical predictions were lower than the experimental observations when only the effect of gas diffusion was taken into account (overrun decreases from

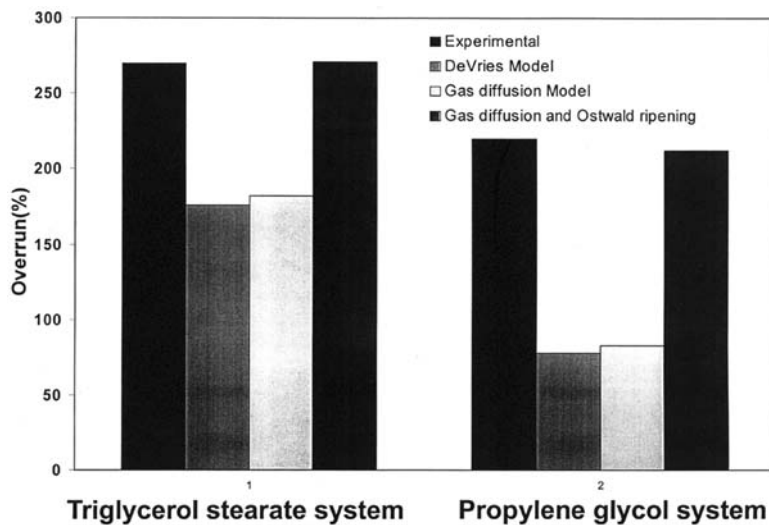


Figure 19 Comparison of experimental and model predicted overruns after 1 week storage at room temperature.

820% to 270% and 1000% to 220% for the triglycerol stearate and propylene glycol systems, respectively). The bubbles would transfer gas among themselves because of the capillary pressure difference. Large bubbles continue to grow at the expense of smaller bubbles. The system approaches a state where the capillary pressure (being inversely proportional to the radius) in most of the bubbles is much lower than it was initially. Thus, the driving force for the transfer of air to the atmosphere decreases with time, resulting in a lower rate of air loss. It must be also be noted that in a system such as the one we studied experimentally, the distance between bubbles is very small, thereby also reducing the diffusion path for Ostwald ripening. Thus, one can expect a reduction in the air loss from the system. We combined the effect of gas diffusion and Ostwald ripening in Eq. (22). The value of $D\phi_{\infty}\alpha$ is taken as $5 \times 10^{-4} \mu\text{m}^3/\text{s}$ and $8 \times 10^{-4} \mu\text{m}^3/\text{s}$ for the triglycerol stearate and propylene glycol systems, respectively. The estimated value of $D\phi_{\infty}\alpha$ for the nitrogen-in-water system is $2 \times 10^{-3} \mu\text{m}^3/\text{s}$. The value for $D\phi_{\infty}\alpha$ for the triglycerol system was chosen in order to match the final overrun. The value of $D\phi_{\infty}\alpha$ for the propylene glycol system was estimated by using the ratio of the gas-diffusion rate for these two systems [$8 \times 10^{-4} \approx 5 \times 10^{-4}$ (6.8/4.4)]. Figure 19 shows that when the effects of gas diffusion and the Ostwald ripening process are taken into account, the model predictions are in good agreement with the experimental results. Figure 20 depicts the effect of Ostwald ripening on the long-term stability of the aerated mesophase. It can be concluded that the Ostwald ripening process retards the gas-diffusion process by transferring the gas to larger bubbles (the gas-diffusion rate is inversely proportional to the bubble radius).

The bubble size distribution (measured independently) was also used to verify the model predictions. Figure 21 plots the experimental and model predictions of the volume of air distribution among bubbles of different sizes on a cumulative basis for the triglycerol stearate system. The data corresponding to 1 week of aging have been corrected to account for the loss of air from the system. The volume fraction of air in this case refers to the ratio of the volume of air to the initial volume of the system, in order to aid comparison with the initial data. There is a reasonable match between the model and experimental data for the bubble size distribution.

4. Application of Model in Predicting Long-Term Stability of an Aerated Emulsion System

The above model was used to predict the long-term stability of the two different aerated emulsion systems (one containing fatty acid ester as the emulsifier and the other having the sucrose ester as the emulsifier). The bubble size predicted using the model is compared with the experimentally

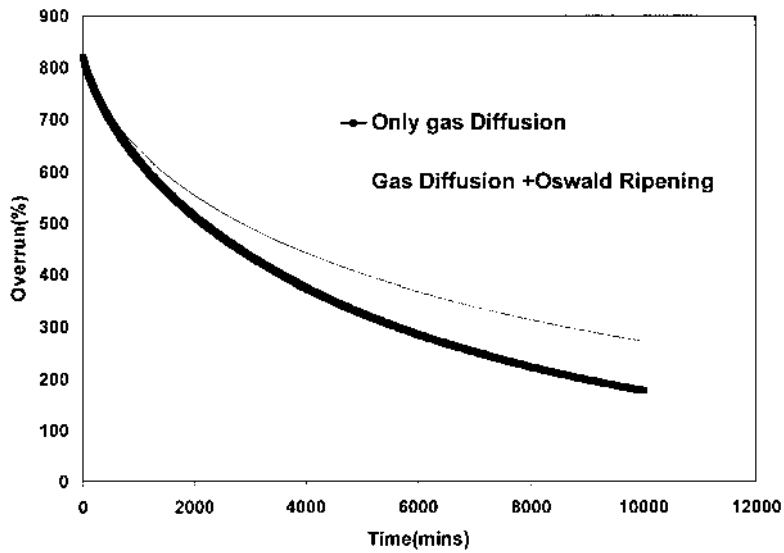


Figure 20 Effect of Ostwald ripening on gas diffusion.

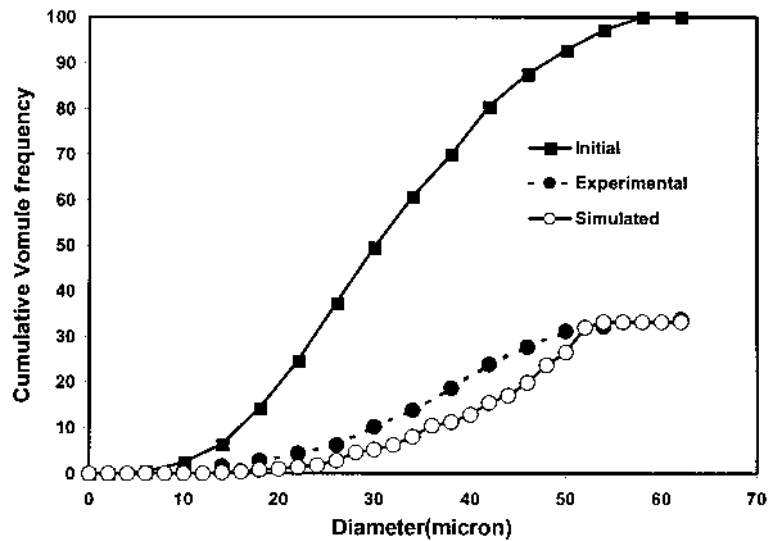


Figure 21 Comparison of experimental bubble size distribution with the model prediction for triglycerol stearate system.

observed bubble size after 1 week. After a period of 1 week, the mean bubble size increased for both emulsion systems. The mean bubble size increased from 41.2 μm to 60 μm in the case of the emulsion containing the fatty acid ester. This confirms our earlier observation about the effect of Ostwald ripening on the bubble size distribution (i.e., larger bubbles grow at the expense of smaller bubbles and this results in a higher mean bubble size). We also obtained good agreement between the experimentally observed bubble size and the model predicted bubble size for both systems (35).

IV. CONCLUSIONS

The study of fat particle structure during the whipping process such as homogenization, cooling, aging, aeration, and whipping revealed that a very poor fat particle structure was produced immediately after homogenization due to the very high temperature of the food emulsions. The fat particle structure improved greatly after cooling. It was observed that the fat particle structure inside low-fat products (5 wt% fat whipped foam and 12 wt% fat whipped foam) does not change with the aging time, whereas the fat particle structure is slightly improved for a high-fat product (20 wt% fat whipped foam), indicating that most of the adsorption of the surfactant and protein on the fat particle surface have been completed before aging. The fat particle structure improved greatly for all the products after whipping, indicating that a well-developed fat particle structure is formed in the bulk phase and stabilizes the foam products.

The foam film rheology and foam film thickness stability produced from fat-in-water emulsions have been investigated using a film rheometer. Several important physical properties, such as equilibrium film tension, dynamic film tension, foam film elasticity, and critical film expansion area, were obtained. A good correlation exists between the stability of foam-based products and the foam film rheological properties. A high foam film elasticity and critical film expansion area and a small value of the initial slope of the curved film tension versus time led to more stable foam-based products.

The stability of aerated emulsions also depends on the air permeability through the foam lamella. Smaller values for foam film permeability yield a higher stability in foam-based food products.

From numerical simulations and experimental studies of the destabilization of the aerated mesophase (overruns were 820% and 1000% for the triglycerol system and the propylene glycol system, respectively), we found that the predominant mechanisms of destabilization are gas diffusion to the atmosphere and Ostwald ripening. The overrun of the system decreases

(from 820% to 270% and from 1000% to 220% for the triglycerol system and propylene glycol system, respectively) with time because of the gas diffusion from the bubbles to the atmosphere. The rate of gas diffusion depends on the permeability of air through the adsorbed layer and mesophase and on the bubble size (driving force is inversely proportional to the bubble size).

Bubbles would transfer gas among themselves due to the capillary pressure difference (the Ostwald ripening phenomenon). Large bubbles continue to grow at the expense of smaller bubbles. Thus, the driving force (being inversely proportional to the radius) for the transfer of air to the atmosphere decreases with time, resulting in a lower rate of air loss. Ostwald ripening also affects the bubble size distribution. Bubbles smaller than the critical size shrink and may eventually disappear. A theoretical model was developed to predict the effects of gas diffusion and Ostwald ripening on the long-term stability of the aerated food products. The gas-diffusion rate was obtained from the shrinking bubble experiments. The model was verified with the experimental results of overrun and good agreement was observed. Model predictions for the bubble size distribution as a function of time are found to be in agreement with the experimentally observed bubble sizes, which were determined by conducting an independent set of experiments.

REFERENCES

1. W. Buchheim, N. M. Barlord, and N. Krog, Relation between microstructure destabilization phenomena and rheological properties of whippable emulsions, *Food Microstruct.* 4, 221–232 (1985).
2. E. C. Needs, Importance of milk proteins to the whippable properties of 38% fat cream, in *Food Colloids, The Proceedings of an International Symposium Organized by the Food Chemistry Group of the Royal Society of Chemistry*, 1988.
3. E. C. Needs and B. E. Brooker, Factors affecting the formation and stabilization of high fat foams, in *Food Polymers, Gels and Colloids, The Proceedings of an International Symposium Organized by the Food Chemistry Group of the Royal Society of Chemistry*, 1990, pp. 227–231.
4. D. F. Darling, Recent advances in the destabilization of dairy emulsions, *J. Dairy Res.* 49, 695–712 (1982).
5. B. E. Brooker, M. Anderson, and A. T. Andrews, The development of structure in whipped cream, *Food Microstruct.* 5, 277–285 (1986).
6. B. E. Brooker, The adsorption of crystalline fat to the air–water interface of whipped cream, *Food Struct.* 9, 223–229 (1990).
7. W. Xu, A. Nikolov, D. T. Wasan, A. Gonsalves, and R. P. Borwankar, Particle structure and stability of colloidal dispersions as probed by Kossel diffraction technique, *J. Colloid Interf. Sci.* 191, 471–481 (1997).

8. E. Dickenson, Food colloids—An overview, *Colloids Surfaces* 42, 191–204 (1989).
9. J. Courthandon, E. Dickinson, and D. G. Dalgleish, Competitive adsorption of β -casein and nonionic surfactants in oil-in-water emulsions, *J. Colloid Interfa. Sci.* 145(2), 391–395 (1991).
10. L. A. Lobo, Stability of emulsions and foams, PhD thesis, Illinois Institute of Technology, Chicago, 1991.
11. E. Dickinson, Interfacial interactions and the stability of oil-in-water emulsions, *Pure Appl. Chem.* 64(11), 1721–1724 (1992).
12. P. Richmond, Food technology and nutrition: Challenges for colloid and interface science, *Pure Appl. Chem.* 64(11), 1751–1755 (1992).
13. J. Chen, E. Dickinson, and G. Iveson, Interfacial interactions, competitive adsorption, and emulsion stability, *Food Struct.* 12, 135–146 (1993).
14. J. M. Soos, K. Koczo, E. Erdos, and D. T. Wasan, An automatic apparatus for measuring interfacial and film tension under static and dynamic conditions, *Rev. Sci. Instrum.* 65(11), 3555–3562 (1994).
15. Y. H. Kim, D. T. Wasan, and P. J. Breen, A study of dynamic interfacial mechanisms for demulsification of water-in-oil emulsions, *Colloids Surfaces* 95, 235–247 (1995).
16. Y. H. Kim, A. D. Nikolov, D. T. Wasan, H. Diaz-Arauzo, and C. S. Shetty, Demulsification of water-in-crude oil emulsions: Effects of film tension, elasticity, diffusive, and interfacial activity of demulsified individual components and their blends, *J. Dispers. Sci. Tech.* 17(1), 33–53 (1996).
17. Y. H. Kim and D. T. Wasan, Effect of demulsifier partitioning on the destabilization of water-in-oil emulsions, *Ind. Eng. Chem. Res.* 35(4), 1141–1149 (1996).
18. Y. H. Kim, K. Koczo, and D. T. Wasan, Dynamic film and interfacial tensions in emulsion and foam systems, *J. Colloid Interfa. Sci.* 187, 29–44 (1997).
19. B. Sood, Study of foam dynamics, texture and stability with application to aerated and foamed products, MS thesis, Illinois Institute of Technology, Chicago, pp. 2.1–2.12.
20. I. M. Lifshitz and V. V. Slyozov, The kinetics of precipitation from supersaturated solid solutions, *J. Phys. Chem. Solids* 19(1/2), 35 (1961).
21. C. Wagner, *Ber. Bunsenges. Phys. Chem.* 65, 581 (1961).
22. A. J. De Vries, Foam Stability Part I, *J. Recueil* 77, 81–91 (1958).
23. A. J. De Vries, Foam Stability Part II, *J. Recueil* 77, 209–223 (1958).
24. H. M. Princen and S. G. Mason, The permeability of soap films to gases. *J. Colloid Sci.* 20, 353–375 (1965).
25. H. M. Princen, J. T. G. Overbeek, and S. G. Mason, The permeability of soap films to gases. II. A simple mechanism to monolayer permeability. *J. Colloid Sci.* 24, 125–130 (1967).
26. A. Prins, Theory and practice of formation and stability of food foams, in *Food Emulsions and Foams* (E. Dickenson, ed.), Special Publication No. 58, The Royal Society of Chemistry, London, 1987, pp. 30–39.
27. A. Arefmanesh and S. G. Advani, *Rheol. Acta* 30, 274 (1991).
28. D. C. Venerus and N. Yala, *Aiche J.* 43, 2948 (1997).

29. D. C. Venerus, N. Yala, and B. Bernstein, *J. Non-Newtonian Fluid Mech.* 75, 55 (1998).
30. D. T. Wasan and A. D. Nikolov, Structure and stability of emulsions, in *Encyclopedic Handbook of Emulsion Technology* (J. Sjoblom, ed.), Marcel Dekker, New York, 2001, pp. 59–70.
31. R. Nagargan, K. Koczo, E. Erods, and D. T. Wasan, Controlled drop tensiometer for measuring dynamic interfacial tension and film tension, *AICE J.* 41(4), 915–923 (1995).
32. M. E. Wijnen and A. Prins, Disproportion in aerosol whipped cream, in *Food Macromolecules and Colloids*, (E. Dickenson and D. Lorient, eds.), Special Publication No. 156, The Royal Society of Chemistry, London, 1995, pp. 309–311.
33. F. Dullien, *Porous Media Fluid Transport and Pore Structure*, Academic Press, New York, 1979.
34. H. D. Goff, The role of chemical emulsifiers and dairy proteins in fat destabilization during the manufacture of ice cream, PhD thesis, Cornell University, Ithaca, NY, 1988.
35. S. Uchil, Structure and stability of imitation dairy cream emulsion, MS thesis, Illinois Institute of Technology, Chicago, 2001.
36. H. W. Yarranton and J. H. Masliyah, Numerical simulation of ripening in emulsions, *J. Colloid Interfa. Sci.* 196, 157–169 (1997).

7

Surface Forces and Emulsion Stability

Per M. Claesson, Eva Blomberg, and Evgeni Poptoshev

Royal Institute of Technology, Stockholm, Sweden

I. INTRODUCTION

Emulsions are dispersions of one liquid in another liquid, most commonly water-in-oil or oil-in-water. The total interfacial area in an emulsion is very large, and because the interfacial area is associated with a positive free energy (the interfacial tension), the emulsion system is thermodynamically unstable. Nevertheless, it is possible to make emulsions with an excellent long-term stability. This requires the use of emulsifiers that accumulate at the oil–water interface and create an energy barrier toward flocculation and coalescence. The emulsifiers can be ionic, zwitterionic, or nonionic surfactants, proteins, amphiphilic polymers, or combinations of polymers and surfactants. The structure of the adsorbed layer at the water–oil interface may be rather complex, involving several species adsorbed directly to the interface as well as other species adsorbing on top of the first layer.

The first question one may ask is if an oil-in-water emulsion or a water-in-oil emulsion is formed then the two solvents are dispersed into each other with the use of a given emulsifier. There are several empirical rules addressing this problem. The first is due to Bancroft (1), who stated that if the emulsifier is most soluble in the water phase, then an oil-in-water emulsion will be formed. A water-in-oil emulsion will be obtained when the reverse is true. The HLB (hydrophilic–lipophilic balance) concept is used for describing the nature of the surfactant. It was first introduced by Griffin (2) and later extended by Davies (3). Hydrophobic emulsifiers having a low HLB number, say below 6, are predicted to be suitable for forming

water-in-oil emulsions, whereas more hydrophilic emulsifiers with high HLB values, above about 10, are suggested to be suitable for forming oil-in-water emulsions. The HLB value can easily be calculated from the structure of the emulsifier (3). An HLB value has also been assigned for most common oils. It is defined as the HLB number of the emulsifier in a homologous series that produces the most stable oil-in-water emulsion. A nonpolar oil is found to have a lower HLB number than a polar oil. Hence, the choice of emulsifier has to be adjusted to the type of oil that is to be emulsified.

The use of an HLB value for nonionic emulsifiers of the oligo (ethylene oxide) type has its drawbacks because their properties are strongly temperature dependent. This is clearly seen in three-component oil–water–surfactant phase diagrams. At low temperatures, microemulsions of oil droplets in water (Winsor I) are formed. In a small temperature interval, bicontinuous microemulsions (Winsor III) are stable, followed at higher temperatures by a microemulsion consisting of water droplets in oil (Winsor II). These transitions are due to a change in the spontaneous monolayer curvature from positive at low temperatures to negative at high temperatures. This behavior is closely mimicked by the thermodynamically unstable (macro)emulsions, and it is common to describe these emulsions in terms of the phase-inversion temperature (PIT). Below the PIT, the emulsion is of the oil-in-water type, whereas above the PIT, it is of the water-in-oil type. Very close to the PIT, no stable (macro)emulsions can be formed. It has been argued that this change in behavior, as for the microemulsions, is due to the change in spontaneous curvature of such surfactant films at the oil–water interface, particularly the ease with which hole formation leading to coalescence occurs (4). Note that the PIT depends not only on the nature of the emulsifier but also on the type of oil used, which often can be explained by the degree of oil penetration into the emulsifier film.

When two droplets approach each other, they will interact with hydrodynamic forces and with surface forces of molecular origin. Finally, when the droplets are close enough, they may coalesce and form one larger droplet. An emulsion will have a long-term stability if the droplets are prevented from coming close to each other by strong repulsive forces and if they are prevented from coalescing even when they are close to each other. However, in this case also, a slow destabilization due to Ostwald ripening will occur.

II. INTERACTIONS AND HOLE FORMATION

In this section, we will give a short overview of hydrodynamic and surface forces as well as hole formation leading to coalescence. References will be provided for the reader who wants to delve further into these subjects.

A. Hydrodynamic Interactions

When liquid drains from the gap between two approaching spherical emulsion droplets of equal size, a hydrodynamic force resulting from viscous dissipation is produced. As long as the surfaces do not deform (i.e., small forces) and the liquid next to the surface is stationary (no slip condition, see next page) the hydrodynamic force is given by (5).

$$F = -\frac{3\pi\mu R^2}{2D} \frac{dD}{dt} \quad (1)$$

where R is the radius of the spheres, μ is the viscosity of the draining liquid, D is the separation between the spheres, and t is the time. This equation describes the hydrodynamic interaction when the droplets are far apart and do not interact with each other very strongly. However, as soon as the interaction between the surfaces is sufficiently large, the emulsion droplets will deform and Eq. (1) is no longer valid.

In concentrated emulsions, we meet another extreme case. A thin planar liquid film now separates the emulsion droplets, and they may change their shape from spherical to polyhedral (6). In this case, the liquid drains out of the flat part of the film owing to the capillary suction pressure. The outflow of liquid between rigid parallel disks was considered by Reynolds (7,8) who found that the pressure varied with the radial distance from the center of the disk as

$$P = P_0 + \frac{3\mu}{D^3}(r_0^2 - r^2)V_R \quad (2)$$

where P is the pressure at a distance r from the center, r_0 is the radius of the plate, P_0 is the hydrostatic pressure, which equals the total pressure at the edge of the contact, (i.e., at $r=r_0$, and V_R is the rate of approach (i.e., $-dD/dt$).

The repulsive hydrodynamic force acting on the plates is obtained by integrating over the plate area and subtracting the hydrostatic pressure contribution:

$$\begin{aligned} F &= 2\pi \int_0^{r_0} (P - P_0)r \, dr = 2\pi \int_0^{r_0} \left[\frac{3\mu}{D^3}(r_0^2 - r^2)V_R \right] r \, dr \\ &= \frac{3\pi r_0^4 \mu V_R}{2D^3} \end{aligned} \quad (3)$$

The average excess pressure (which equals the capillary pressure) between circular plates can be expressed as

$$\bar{P} = \frac{F}{\pi r_0^2} \quad (4)$$

Hence, we obtain the well-known Reynolds equation

$$V_R = -\frac{dD}{dt} = \frac{2D^3 \bar{P}}{3\mu r_0^2} \quad (5)$$

We immediately see that the film-thinning rate is reduced, and thus the emulsion stability increased, by an increase in bulk viscosity. In the case in which the liquid film is so thin that surface forces no longer can be neglected, the capillary pressure term in the Reynolds equation should be replaced by the total driving force (ΔP) for the thinning. This is equal to the difference between the capillary pressure and the disjoining pressure (Π) due to the surface forces acting between the emulsion droplet surfaces: $\Delta P = (\bar{P} - \Pi)$. Clearly, a positive disjoining pressure (i.e., a repulsive force) reduces the driving force for film thinning and thus the drainage rate.

Experimentally determined rates of thinning do not always agree with the predictions of the Reynolds model. For foam films stabilized by an anionic surfactant, sodium dodecyl sulfate (9,10), it has been shown that typical thinning rates exhibited a much weaker dependence on the film radius ($r^{-0.8-0.9}$) than the predicted r^{-2} dependence. To obtain an understanding for why the Reynolds theory of thinning does not always agree with experimental results, it is worthwhile to consider two assumptions made when arriving at Eq. (5). First the result is valid only under “no-slip” conditions (i.e., the velocity of the liquid at the film interface is assumed to be zero). This is the case when the drainage takes place between solid hydrophilic surfaces. In contrast, only the adsorbed emulsifier layer provides the surface rigidity in foam and emulsion films, and it is not obvious that the no-slip condition is fulfilled. The drainage rate would be larger than predicted by Eq. (5) if this condition was not valid. Jeelani and Hartland (11), who calculated the liquid velocity at the interfaces of emulsion films for numerous systems studied experimentally, addressed this point. They showed that even at a low surfactant concentration, the liquid mobility at the interface is dramatically reduced by the adsorbed surfactant. Hence, it is plausible that when the adsorption density of the emulsifier is large (nearly saturated monolayers), the surface viscosity is high enough to validate the no-slip condition. It has been pointed out that a nonzero liquid viscosity at the interface is not expected to have an influence on the functional dependence of the drainage rates on the film radius (9). Hence, the deviations found experimentally have to have another origin.

A second assumption made when arriving at Eq. (5) is that the drainage takes place between parallel surfaces. Experimental studies on liquid films (9,10) have shown that during the thinning process, it is common that nonuniform films are formed which have a thicker region, a dimple, in the center. For larger films, even more complicated, multidimpled profiles have been found. Calculating the drainage rate for interfaces with such a complex shape is far from easy. However, recently Manev et al. (9) proposed a model for the drainage between nonparallel, immobile surfaces. The following expression has been proposed for the rate of thinning:

$$V = \frac{8}{3\mu} \sqrt[5]{\frac{4D^{12}\Delta P^8}{\alpha_1^{12}\sigma^3 r^4}} \quad (6)$$

Here, α_1 is the first root of the first-order Bessel function of the first kind and σ is the surface tension. Note that in Eq. (6), the rate of thinning is inversely proportional to $r^{4/5}$. This is in good agreement with some experimental observations.

III. SURFACE FORCES

At sufficiently small droplet separations, say below 100 nm, surface forces have to be considered. These forces affect the drainage rate as well as the equilibrium interactions, particularly if flocculation occurs. The most commonly encountered forces are briefly described in this section. For a general reference to surface force, see the book by Israelachvili (12).

A. Van der Waals Forces

Van der Waals forces originate from the motion of negatively charged electrons around the positively charged atomic nucleus. For condensed materials (liquids or solids), this electron motion gives rise to a fluctuating electromagnetic field that extends beyond the surface of the material. Thus, when, for example, two particles or emulsion droplets are close together, the fluctuating fields associated with them will interact with each other. The energy of interaction per unit area (W_{vdw}) between two equal spheres with radius R a distance D apart is given by:

$$W_{\text{vdw}} = -\frac{A}{6} \left[\frac{2R^2}{D^2 + 4RD} + \frac{2R^2}{D^2 + 4RD + R^2} + \ln \left(\frac{D^2 + 4RD}{D^2 + 4RD + R^2} \right) \right] \quad (7)$$

where A is the nonretarded Hamaker constant. When the particle radius is much larger than the separation of the particles, Eq. (7) is reduced to

$$W_{\text{vdw}} = -\frac{AR}{12D} \quad (8)$$

The Hamaker constant depends on the dielectric properties of the two interacting particles and the intervening medium. When these properties are known, one can calculate the Hamaker constant. An approximate equation for two identical particles (subscript 1) interacting across a medium (subscript 2) is:

$$A = \frac{3kT}{4} \left(\frac{\varepsilon_1 - \varepsilon_2}{\varepsilon_1 + \varepsilon_2} \right)^2 + \frac{3h\nu}{16\sqrt{2}} \left(\frac{(n_1^2 - n_2^2)^2}{(n_1^2 + n_2^2)^{3/2}} \right) \quad (9)$$

where k is the Boltzmann constant, T is the absolute temperature, ν is the main absorption frequency in the ultraviolet (UV) region (often about 3×10^{15} Hz), h is Planck's constant, ε is the static dielectric constant, and n is the refractive index in visible light.

From Eqs. (8) and (9), it is clear that the van der Waals interaction between two identical particles or emulsion droplets is always attractive. One may also note that the Hamaker constant for two oil droplets interacting across water is identical to the Hamaker constant for two water droplets interacting across oil.

B. Electrostatic Double-Layer Forces

Electrostatic double-layer forces are always present between charged particles or emulsion droplets in electrolyte solutions. Counterions to the emulsion droplet (ions with opposite charges to that of the drop) are attracted to the surfaces and co-ions are repelled. Hence, outside the charged emulsion droplet, in the so-called diffuse layer, the concentration of ions will be different than that in bulk solution, and the charge in the diffuse layer balances the surface charge.

An electrostatic double-layer interaction arises when two charged droplets are so close together that their diffuse layers overlap. The electrostatic double-layer interaction, W_{dl} , for two identical charged drops with a small electrostatic surface potential and a radius large compared to their separation is approximately given by

$$W_{\text{dl}} = 2\pi R\varepsilon\varepsilon_0\Psi_0^2 \exp(-\kappa D) \quad (10)$$

where ε_0 is the permittivity of vacuum, ε is the static dielectric constant of the medium, Ψ^0 is the surface potential, and κ^{-1} is the Debye screening length given by:

$$\kappa^{-1} = \sqrt{\frac{\varepsilon_0 \varepsilon k T}{1000 N_A e^2 \sum_i c_i z_i^2}} \quad (11)$$

where e is the charge of the proton, N_A is Avogadro's number, c_i is the concentration of ion i expressed as mol/dm³, and z_i is the valency of ion i .

The double-layer interaction is repulsive and it decays exponentially with surface separation with a decay length equal to the Debye length. Further, the Debye length and, consequently, the range of the double-layer force decreases with increasing salt concentration and the valency of the ions present. The famous Derjaguin Landau Verwey Overbeek (DLVO) theory for colloidal stability (13,14) takes into account double-layer forces and van der Waals forces.

C. Hydration and Steric-Protrusion Forces

Hydration and steric-protrusion forces are repulsive forces that have been found to be present at rather short separations between hydrophilic surfaces such as surfactant head groups. At least two molecular reasons for these forces have been identified. First, when two polar surfaces are brought close together, the polar groups will be partly dehydrated, which gives rise to a repulsive force (15). Second, as two surfaces are brought close together, the molecules at the interface will have a decreased mobility perpendicular to the surface, which decreases the entropy of the system, and this gives rise to a steric type of repulsion (16). Empirically, it has been found that the hydration/steric repulsion between surfactant and lipid head groups decays roughly exponentially with distance:

$$W_{\text{hyd}} = W_{\text{hyd}}^0 \exp\left(-\frac{D}{\lambda}\right) \quad (12)$$

where λ is the decay length of the force, typically 0.2–0.3 nm.

D. Polymer-Induced Forces

The presence of polymers on surfaces gives rise to additional forces that can be repulsive or attractive. Under conditions when the polymer is firmly anchored to the surface and the surface coverage is large, a steric

repulsion is expected. As the surfaces are brought together, the segment density between them increases, which results in an increased number of segment–segment contacts and a loss of conformational entropy of the polymer chains. The conformational entropy loss always results in a repulsive force contribution that dominates at small separations. The increased number of segment–segment contacts may give rise to an attractive or a repulsive force contribution. This is often discussed in terms of the chi-parameter (χ -parameter) or in terms of the solvent quality. Under sufficiently poor solvent conditions ($\chi > 1/2$), when the segment–segment interaction is sufficiently favourable compared to the segment–solvent interaction, the long-range interaction can be attractive. Otherwise, it is repulsive. The steric force can be calculated by using lattice mean field theory (17) or scaling theory (18). The actual force encountered is highly dependent on the adsorption density, the surface affinity, the polymer architecture, and the solvency condition. Hence, no simple equation can describe all situations. However, a high-density polymer layer, a “brush” layer, in a good solvent, provides good steric stabilization. The scaling approach provides us with a simple formula that often describes the measured interactions under such conditions rather well (19). It states that the pressure $P(D)$ between two flat polymer-coated surfaces is given by

$$P(D) \approx \frac{kT}{s^3} \left[\left(\frac{D^*}{D} \right)^{9/4} - \left(\frac{D}{D^*} \right)^{3/4} \right] \quad (13)$$

where Eq. (13) is valid provided that the separation, D , is less than D^* (where D^* is twice the length of the polymer tail), and s is the linear distance between the anchored chains on the surface. For the interactions between two spheres with a radius significantly larger than their separation, this relation is modified to

$$\frac{F(D)}{R} \approx -\pi \int_{D^*}^D P(D') dD' \quad (14)$$

The parameters needed to calculate the force are the length of the extended polymer chain and the separation between the polymer chains on the surface. The latter parameter can be estimated from the adsorbed amount, whereas the length of the polymer chains enters as a fitting parameter. The formula predicts a repulsion that increases monotonically with decreasing separation.

E. Coalescence and Hole Formation

When studying drainage and equilibrium interactions in single-foam films above the critical micellar concentration (cmc) of the surfactant, it is often found that the film thickness undergoes sudden changes (20,21). This phenomenon is known as stratification. Below the cmc, one sudden change from a water-rich common black film to a very thin Newton black film may occur. This transition does not occur uniformly over the whole film area but initially in some small regions. The thinner regions are often called black spots because they appear darker than the rest of the film when viewed in reflected light. Once formed, the size of a black spot grows as the liquid drains out from the foam lamellae. Bergeron and co-workers noted that the viscous resistance to the flow in the thin film is large and that this leads to an increase in the local film thickness next to the black spot (22,23). The suggested shape of the thin liquid layer, which is supported by experimental observations and theoretical calculations (22,23) is illustrated in Fig. 1. In many cases, no or unstable Newton black films are formed. In these cases, the films rupture due to formation of a hole that rapidly grows as a result of surface-tension forces. Emulsion coalescence occurs in a similar manner.

The mechanism of black spot formation and rupture has been extensively studied (24). It is generally recognized that the liquid film is unstable in regions of the disjoining pressure (Π) isotherm (force curve) where the derivative with respect to film thickness (D) is larger than zero (i.e., $d\Pi/dD > 0$). Hence, close to a maximum in the disjoining pressure isotherm (see Fig. 2), a small disturbance causing a change in film thickness and/or capillary pressure may spontaneously grow and lead to significant change in film thickness (e.g., Newton black film formation or rupture).

The stability of foams and emulsions depends critically on whether formation of a stable Newton black film or a hole leading to coalescence is favored. Kabalnov and Wennerström (4) addressed this question by

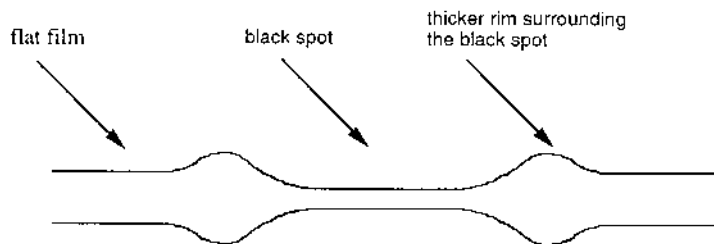


Figure 1 Illustration of shape of the thin liquid film around the position of a newly formed black spot.

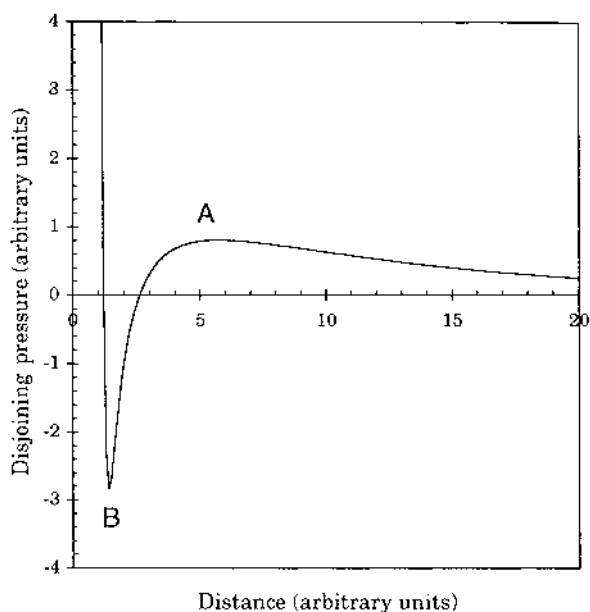


Figure 2 Typical disjoining pressure isotherm showing one maximum (A) and one minimum (B); the film is unstable between points A and B.

developing a temperature-induced hole nucleation model. They point out that the coalescence energy barrier is strongly affected by the spontaneous monolayer curvature. The authors consider a flat emulsion film, covered by a saturated surfactant monolayer, in thermodynamic equilibrium with a micellar bulk solution. The emulsion breaks if an induced hole grows along the film having a thickness $h = 2b$ (Fig. 3). The change in free energy occurring when a hole is formed is given as the difference in the interfacial tension integrals over the interface for a film with a hole compared to that for a planar film:

$$W = \int_{\text{(film with hole)}} \sigma(x, y, z) dA - \int_{\text{(flat film)}} \sigma(x, y, z) dA \quad (15)$$

The driving force for the formation of a hole is the reduction in free energy owing to a decrease in surface area of the planar part of the film, whereas it is counteracted by the increased free energy due to the surface area created around the hole. In general, the change in free energy goes through a maximum as the hole radius increases. One new feature of the Kabalnov–Wennerström model is that the surface tension at the hole edge is

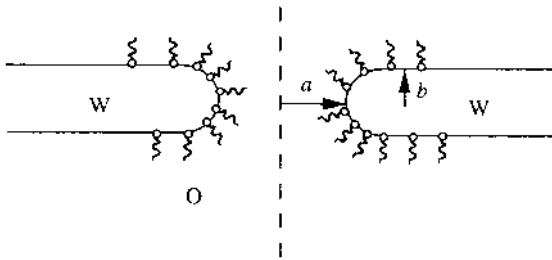


Figure 3 Geometry of the thin film just after a hole has been created. (Redrawn from Ref. 4, with permission.)

considered to be different than that at the planar film surface. The reason for this is that the curvature of the interface is different, leading to a difference in surfactant monolayer bending energy. This can be expressed as (4)

$$\sigma^{\text{curved}} = \sigma^{\text{planar}} + 2\kappa(H - H_0)^2 - 2\kappa H_0^2 \quad (16)$$

Here, H and H_0 are the mean and the spontaneous curvatures and κ is the bending modulus.

Clearly, the surface tension has a minimum when the spontaneous curvature of the surfactant film equals the mean curvature of the interface. The mean curvature for a flat interface is zero, larger than zero for an interface curving toward the oil (oil-in-water emulsions), and smaller than zero for a water-in-oil emulsion. Hence, a large positive spontaneous monolayer curvature, as for a strongly hydrophilic surfactant, favors oil-in-water emulsions and vice versa. The Kabalnov–Wennerström model also allows the thickness of the film to vary in order to minimize the free energy of hole formation (i.e., the mean curvature of the film close to the hole can approach the spontaneous monolayer curvature). The Kabalnov–Wennerström model has to be solved numerically in order to calculate the coalescence activation energy. However, a “big hole approach” where $a \gg b$ (see Fig. 3) gives surprisingly good results. In this model, the energy for creating a hole with radius a is given as

$$W = 2\pi a\gamma - 2\pi a^2\sigma \quad (17)$$

where $2\pi a$ is the circumference of the hole, γ is the line tension, πa^2 is the area of the hole at each interface, and σ is the surface tension. The second term is the free energy gain by reducing the flat area of the film, and the first term is the energy penalty of creating the inside of the hole. The value of the

line tension can be calculated when the spontaneous monolayer curvature and the monolayer bending modulus is known (4). The activation energy of coalescence (W^*) is obtained by finding the point where $dw/da=0$, which gives the final expression:

$$W^* = \frac{\pi\gamma^2}{2\sigma} \quad (18)$$

The particular feature with ethylene oxide-based surfactants is that their interaction with water is less favourable at higher temperatures. This leads to a decrease in the spontaneous monolayer curvature with temperature, explaining the transition from oil-in-water emulsions below the PIT to water-in-oil emulsion above the PIT. In the vicinity of the PIT, the energy barrier against coalescence (W^*) varies very strongly with temperature. For the system *n*-octane–C₁₂E₅–water, the following approximate relation was obtained in terms of $\Delta T = T - T_d$, where T_d is the PIT (4):

$$\frac{W^*}{kT} = 0.43 + 30.9|\Delta T| \quad (19)$$

The predicted very steep increase in the coalescence barrier away from the PIT is qualitatively in good agreement with the experimentally observed macroemulsion behavior (25).

IV. SURFACE FORCE TECHNIQUES

There are several methods available for measuring forces between two solid surfaces, two particles, or liquid interfaces (26). In this section, we briefly mention some of the features of the techniques that have been used in order to produce the results described in the later part of this chapter. The forces acting between two solid surfaces were measured either with the interferometric surface force apparatus (SFA) or with the MASIF (measurements and analysis of surface and interfacial forces). Interactions between fluid interfaces were determined using various versions of the thin-film pressure balance (TFB).

A. Interferometric Surface Force Apparatus

The forces acting between two molecularly smooth surfaces, normally mica or modified mica, can be measured as a function of their *absolute* separation with the interferometric SFA (Fig. 4) (27). This provides a convenient way to measure not only long-range forces but also the thickness of adsorbed

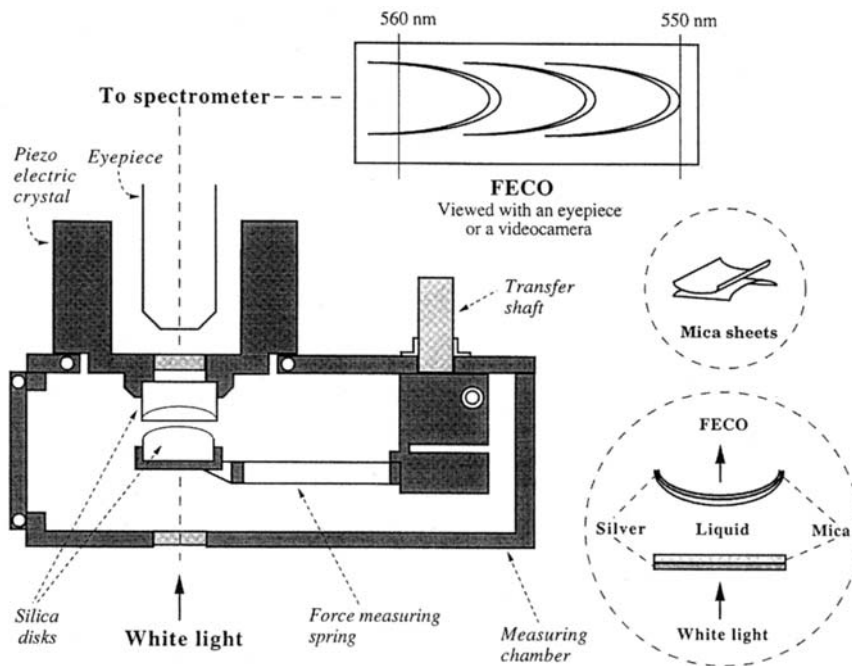


Figure 4 Schematic of a surface force apparatus (SFA). The measuring chamber is made from stainless steel. One of the surfaces is mounted on a piezoelectric tube that is used to change the surface separation; the other surface is mounted on the force measuring spring. (From Ref. 26, with permission.)

layers. The absolute separation is determined interferometrically to within 0.1–0.2 nm by using fringes of equal chromatic order. The surfaces are glued on optically polished silica disks and mounted in the SFA in a crossed cylinder configuration. The surface separation is controlled either by adjusting the voltage applied to a piezoelectric crystal rigidly attached to one of the surfaces or by a synchronous motor linked by a cantilever spring to the other surface. The deflection of the force-measuring spring is also determined interferometrically, and the force is calculated from Hooke's law. For further details, see Ref. 27.

When an attractive force component is present, the gradient of the force with respect to the surface separation, $\partial F/\partial D$, may at some distance become larger than the spring constant, k . The mechanical system then enters an unstable region causing the surfaces to jump to the next stable point (compare instabilities in free liquid films that occur when $d\Pi/dD > 0$). The adhesion force, $F(0)$, normalized by the local mean radius of curvature,

R , is determined by separating the surfaces from adhesive contact. The force is calculated from

$$\frac{F(0)}{R} = \frac{kD_j + F(D_j)}{R} \quad (20)$$

where $F(D_j)$ is the force at the distance (D_j) to which the surfaces jumped on separation, and R is the mean radius of the surfaces.

B. The Bimorph Surface Force Apparatus

The force as a function of the surface separation between glass substrate surfaces was measured with a MASIF instrument (28). This apparatus is based on a bimorph force sensor to which one of the surfaces is mounted (Fig. 5). The other surface is mounted on a piezoelectric tube. The bimorph (enclosed in a Teflon sheath) is mounted inside a small measuring chamber, which is clamped to a translation stage that serves to control the coarse position of the piezoelectric tube and the upper surface.

The voltage across the piezoelectric tube is varied continuously and the surfaces are first pushed together and then separated. The bimorph will deflect when a force is experienced and this generates a charge in proportion to the deflection. From the deflection and the spring constant, the force follows simply from Hooke's law. The motion of the piezo is measured during each force run with a linear displacement sensor. The signal together with the signal from the bimorph charge amplifier, the voltage applied to the piezoelectric tube, and the time are recorded by a computer. The speed of approach, the number of data points, and other experimental variables can easily be controlled with the computer software.

When the surfaces are in contact, the motion of the piezoelectric tube is transmitted directly to the force sensor. This results in a linear increase of the force sensor signal with the expansion of the piezoelectric tube. The sensitivity of the force sensor can be calibrated from this straight line, and this measuring procedure allows the determination of forces as a function of separation from a hard wall contact with a high precision (within 1–2 Å in distance resolution). Note, however, that the assumption of a “hard wall” contact is not always correct (29).

The MASIF instrument does not use interferometry to determine surface separations, which leads to the drawback that the layer thickness cannot be determined, but to the advantage that the instrument can be used with any type of hard, smooth surfaces. In most cases, spherical glass surfaces are used. They are prepared by melting a 2-mm-diameter glass rod until a molten droplet with a radius of 2 mm is formed.

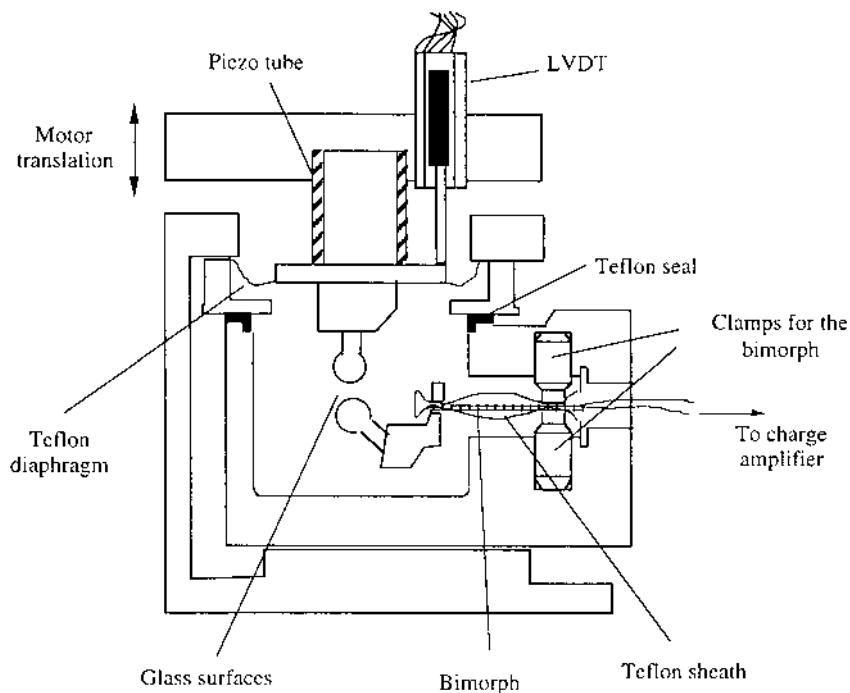


Figure 5 Schematic of the MASIF instrument. The upper surface is mounted on a piezoceramic actuator that is used for changing the surface separation; the hysteresis of the piezoexpansion/contraction cycle can be accounted for by using a linear variable displacement transducer (LVDT). The lower surface is mounted on a bimorph force sensor. (From Ref. 26, with permission.)

C. Derjaguin Approximation

The force measured between crossed cylinders (F_c), as in the SFA, and between spheres (F_s), as in the MASIF, a distance D apart is normalized by the local geometric mean radius (R). This quantity is related to the free energy of interaction per unit area between flat surfaces (W) according to the Derjaguin approximation (30):

$$\frac{F_c}{2\pi R} = \frac{F_s}{\pi R} = W \quad (21)$$

This approximation is valid when the radius (about 2 cm in the SFA and 2 mm in the MASIF) is much larger than the surface separation (typically 10^{-5} cm or less), a requirement fulfilled in these experiments. With the SFA,

the local radius is determined from the shape of the standing-wave pattern, whereas in the MASIF, we have used the assumption that the local radius is equal to the macroscopic radius, determined using a micrometer. The radius used in Eq. (21) is that of the undeformed surfaces. However, under the action of strongly repulsive or attractive forces, the surfaces will deform and flatten (31,32). This changes the local radius and invalidates Eq. (21) because R becomes a function of D .

D. Thin-Film Pressure Balance

Accurate information about the rate of thinning, the critical thickness of rupture, and the forces acting between two air–water interfaces, between two oil–water interfaces, and between one air–water and one oil–water interface can be gained by using thin-film pressure balance techniques. The thickness of the separating water film is determined by measuring the intensity of reflected white light from a small flat portion of the film (33). Due to interference of the light reflected from the upper and lower film surfaces, characteristic interference colors are observed during the thinning. These colors correspond to a shift in the wavelengths undergoing constructive and destructive interference. When such a process is recorded (normally as intensity of a given light wavelength versus time), a sequence of intensity minima and maxima appears. The equivalent water film thickness can be calculated from the following equation (33):

$$h_{\text{eq}} = \left(\frac{\lambda}{2\pi n_1} \right) \arcsin \left(\sqrt{\frac{\Delta}{1 + [4R(1 - \Delta)/(1 - R)^2]}} \right)$$

$$R = \left(\frac{n_1 - n_2}{n_1 + n_2} \right)^2 \quad (22)$$

$$\Delta = \left(\frac{I - I_{\text{min}}}{I_{\text{max}} - I_{\text{min}}} \right)$$

where λ is the wavelength and n_1 and n_2 are the bulk refractive indices of the continuous and the disperse phases respectively (in the case of foam films $n_2 = 1$); I_{max} and I_{min} are the intensity values of the interference maximum and minimum, and I is the instantaneous value of the light intensity. The above equation gives the equivalent film thickness, h_{eq} (i.e., the film thickness plus the thickness of the adsorbed layers calculated by assuming a constant value of the refractive index equal to n_1). A better approximation to the true film thickness can be obtained by correcting for the difference in

refractive index between the bulk film and the adsorbed layer. The corrected film thickness is (23)

$$h = h_{\text{eq}} - 2h_{\text{hc}} \left(\frac{n_{\text{hc}}^2 - n_1^2}{n_1^2 - n_2^2} \right) - 2h_{\text{pg}} \left(\frac{n_{\text{pg}}^2 - n_1^2}{n_1^2 - n_2^2} \right) \quad (23)$$

In Eq. (23), h_{hc} and h_{pg} are the thickness of the region occupied by the surfactant hydrocarbon chain and polar group, respectively. Similarly, n_{hc} and n_{pg} are the corresponding refractive indices. The thickness values needed in order to use Eq. (23) can be estimated from the volume of the two parts of the molecule together with values of the area per molecule at the interface obtained from adsorption data (e.g., the surface-tension isotherm). Finally, the thickness of the core layer (water in the case of foam films) can be calculated as

$$h_{\text{core}} = h - 2(h_{\text{hc}} + h_{\text{pg}}) \quad (24)$$

The apparatus used for studying thin liquid films is schematically depicted in Fig. 6. This device, commonly known as a thin-film pressure balance, allows drainage patterns of single foam, emulsion, or wetting films

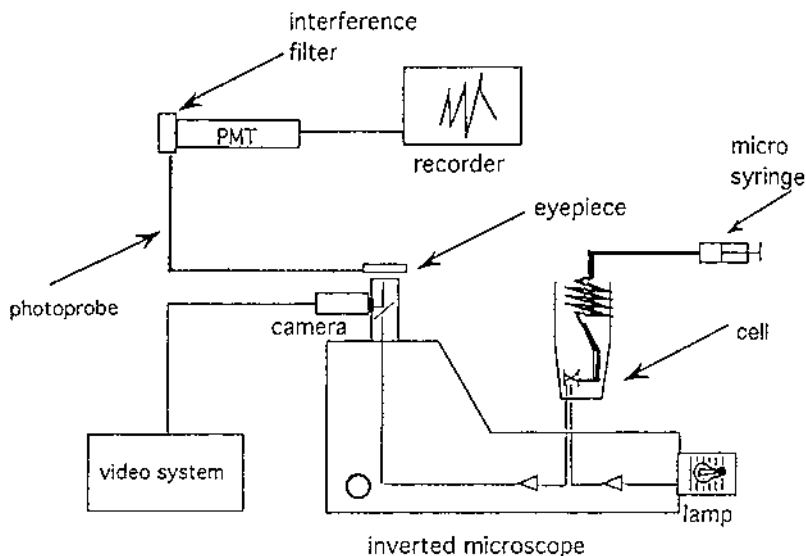


Figure 6 Schematic of the main components of a typical thin-film pressure balance.

to be recorded. The film is formed in a specially constructed cell that is placed on the stage of an inverted microscope. The reflected light from the film is split into two parts: one directed to a charge-coupled device (CCD) camera and another to a fiber-optic probe tip located in the microscope eyepiece. The radius of the tip is only about $20\ \mu\text{m}$, which allows light from a small portion of the film to be registered. The light signal is then passed through a monochromatic filter and, finally, directed on to a high-sensitivity photomultiplier. The output of the photomultiplier is connected to a chart recorder and the data are collected in the form of intensity (as a photocurrent) versus time. This graph is called an interferogram.

An essential part of the thin-film balance is the cell holding the thin film. The cell can be constructed in several ways depending on the type of measurement to be done and the systems under investigation. For, emulsion films, the type of cell proposed by Scheludko (33) is often used. The cell is illustrated in Fig. 7. The film is formed between the tips of the menisci of a biconcave drop held in a horizontal tube with radius 1.5–2 mm. The tube and the spiral capillary are filled with the aqueous phase and immersed in a cuvette (the lower part of the cell) containing the oil phase. A small suction pressure applied through the capillary controls the film radius. Recently, a cell that is similar to that of Scheludko, but miniaturized about 10-fold was used by Velev et al. (34). This allowed film sizes and capillary pressures found in real emulsion systems to be studied. Bergeron and Radke (35)

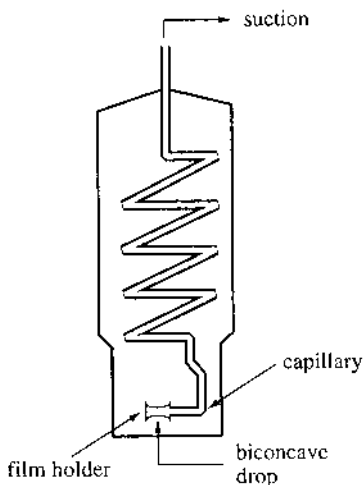


Figure 7 Illustration of the Scheludko cell used for investigation of single, horizontal foam and emulsion films.

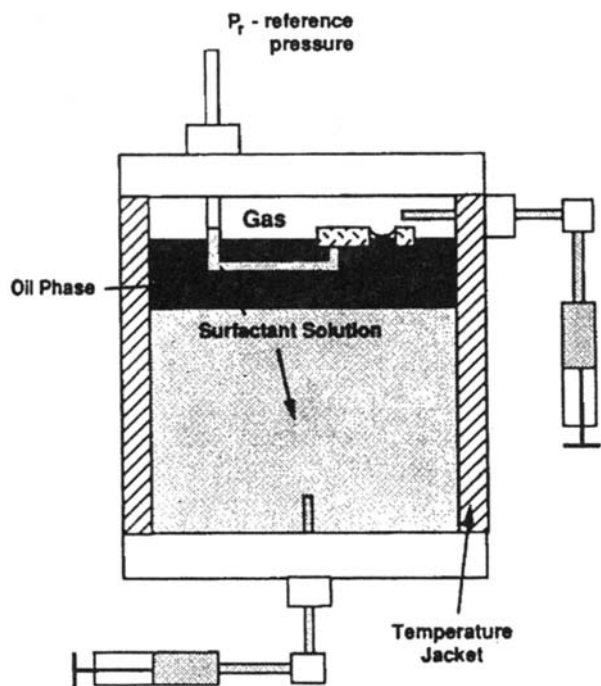


Figure 8 Modified porous-plate cell for investigation of pseudoemulsion films. (Ref. 35, with permission.)

used a cell with a porous frit holder as suggested by Mysels and Jones (36) for measuring equilibrium forces across foam and pseudoemulsion films. Their construction is shown in Fig. 8. The main advantage of this so-called porous-plate technique is that one can vary the pressure in the film by simply altering the gas pressure in the cell, and thus the stable part of the equilibrium disjoining pressure isotherm (where $d\Pi/dD < 0$) can be obtained.

V. RESULTS AND DISCUSSION

A. Ionic Surfactants on Hydrophobic Surfaces

Many oil-in-water emulsions are stabilized by an adsorbed layer of surfactants. One example is asphalt oil-in-water emulsions that often are stabilized by cationic surfactants (37). The surfactants fulfill two purposes. First, they generate long-range repulsive forces which prevent the emulsion droplets

from coming close to each other. Second, the surfactant layer acts as a barrier against coalescence if the emulsion droplets by chance come close to each other despite the long-range repulsive forces. The coalescence is hindered by a high spontaneous monolayer curvature, monolayer cohesive energy, surface elasticity, and surface viscosity, which increase the activation energy for hole formation and slow down the depletion of surfactants from the contact region. The importance of the cohesive energy for foam films stabilized by a homologous series of cationic surfactants was particularly clearly demonstrated by Bergeron (38). We note that an increased cohesive energy in the monolayer increases the bending modulus and thus the free energy cost for the surfactant film to have a curvature different than the spontaneous curvature.

Surface force measurements using a hydrophobic solid surface as a model for a fluid hydrocarbon–water interface provide a good picture of the long-range forces acting between emulsion droplets. However, the coalescence behavior of emulsions will not be accurately described from such measurements. One reason is that the fluid interface is much more prone to deformation than the solid surface (facilitating hole formation), and the surfactant chains can readily penetrate into the fluid oil phase but not into the solid hydrocarbon surface. Further, the mobility of the surfactants on a solid hydrophobic surface will be different than the mobility at a fluid interface.

The forces acting between two hydrophobic surfaces across dodecylammonium chloride surfactant solutions are illustrated in Fig. 9 (39). The long-range repulsion is due to the presence of an electrostatic double-layer force. This force is generated by the cationic surfactants that adsorb to the hydrophobic surface thereby generating a surface charge density. The range of the double-layer force decreases with increasing surfactant concentration, which is simply a result of the increased ionic strength of the aqueous media. On the other hand, the magnitude of the double-layer force at short separations increases with increasing surfactant concentrations. This is a consequence of the increased adsorption of the ionic surfactant that results in an increase in surface charge density and surface potential. The surfactant concentration will influence the long-range interactions between oil-in-water emulsions in the same way as observed for the model solid hydrophobic surfaces; that is, the range of the double-layer force will decrease and the magnitude of the force at short separations will increase. However, the adsorbed amount at a given surfactant concentration may not be the same on the emulsion surface as on the solid hydrophobic surface.

At low surfactant concentrations, it is observed that an attraction dominates at short separations. The attraction becomes important at separations below about 12 nm when the surfactant concentration is 0.01 mM, and

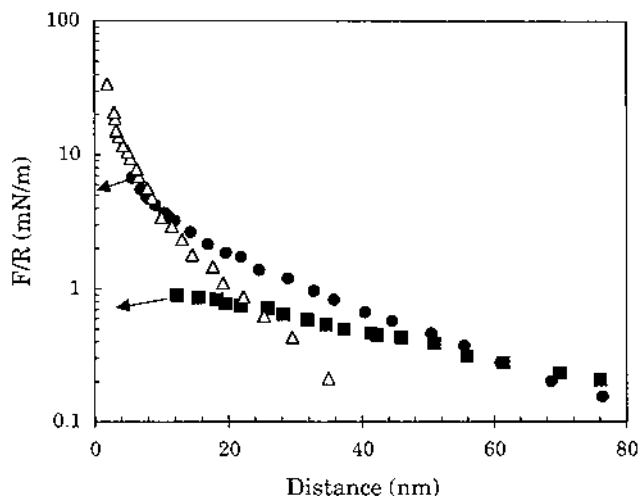


Figure 9 Force normalized by radius measured between two hydrophobized mica surfaces in crossed cylinder geometry across aqueous solutions of dodecylammonium chloride; the surfactant concentration was 0.01 mM (■), 0.1 mM (●), and 1 mM (Δ), respectively. The arrows indicate inward jumps occurring when the force barrier has been overcome. (Redrawn from Ref. 39, with permission.)

below about 6 nm when the concentration is increased to 0.1 mM. Once the force barrier has been overcome, the surfaces are pulled into direct contact between the hydrophobic surfaces at $D=0$, demonstrating that the surfactants leave the gap between the surfaces. The solid surfaces have been flocculated. However, at higher surfactant concentrations (1 mM) the surfactants remain on the surfaces even when the separation between the surfaces is small. The force is now purely repulsive and the surfaces are prevented from flocculating. Emulsion droplets interacting in the same way would coalesce at low surfactant concentrations once they have come close enough to overcome the repulsive barrier, but remain stable at higher surfactant concentrations. Note, however, that the surfactant concentration needed to prevent coalescence of emulsion droplets cannot be accurately determined from surface force measurements using solid surfaces.

For application purposes, it is often found that asphalt emulsions stabilized by cationic surfactants function better than such emulsions stabilized by anionic surfactants. One main reason is that the interaction between the emulsion droplet and the road material differs depending on the emulsifier used (37). When the asphalt emulsion is spread on the road surface, it should rapidly break and form a homogeneous layer. The stones on the road surface are often negatively charged and there will be an electrostatic

attraction between cationic emulsion droplets and the stones. This attraction facilitates the attachment and spreading of the emulsion. On the other hand, when the emulsion droplet is negatively charged, there will be an electrostatic repulsion between the stones and the emulsion droplets.

B. Nonionic Surfactants on Hydrophobic Surfaces

Nonionic ethylene oxide-based surfactants are commonly used as emulsifiers. Because these surfactants are uncharged, they are not able to generate stabilizing long-range electrostatic forces. Instead, they generate short-range hydration/protrusion forces that prevent the emulsion droplets from coming into direct contact with each other. The short-range forces acting between hydrophobic solid surfaces coated with such surfactants as a function of temperature are illustrated in Fig. 10 (40). The zero distance in the diagram is defined as the position of the hard wall (at a value of $F/R \approx 100$ mN/m).

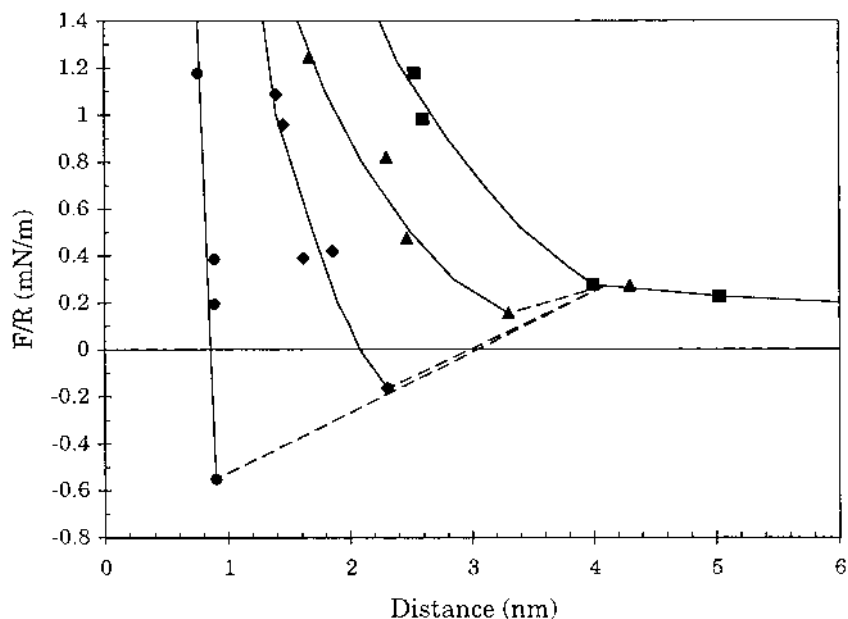


Figure 10 Force normalized by radius measured between hydrophobized mica surfaces in crossed cylinder geometry across a 6×10^{-5} M aqueous solution of penta(oxyethylene) dodecyl ether. The temperatures were 15°C (■), 20°C (▲), 30°C (◆), and 37°C (●). The lines are guides for the eye. (Redrawn from Ref. 40, with permission.)

The force present at distances above 4 nm is a weak double-layer force. It originates from remaining charges on the hydrophobic substrate surface. The force observed at smaller separations has a pronounced temperature dependence. It becomes less repulsive with increasing temperature. At the same time, the adsorbed layer thickness increases, demonstrating that the repulsion between the adsorbed molecules within one layer is also reduced at higher temperatures, facilitating an increased adsorption. The increase in layer thickness is not seen in Fig. 10 due to our definition of zero separation.

A decreasing interlayer and intralayer repulsion with increasing temperature is common for all surfactants and polymers containing oligo(ethylene oxide) groups. This shows that the interaction between ethylene oxide groups and water becomes less favorable at higher temperatures (i.e., the ethylene oxide chain becomes more hydrophobic). There are several theoretical attempts to explain this phenomenon, but it is outside the scope of this chapter to discuss them and the reader is referred to the original literature (41–48). The temperature dependence of the interaction between oligo(ethylene oxide) chains and water has several important consequences. The micellar size increases with temperature (49), and the micellar solution has a lower consolute temperature (i.e., a phase separation occurs on heating) (50). The cloud points for a range of micellar alkyl ethoxylate solutions are

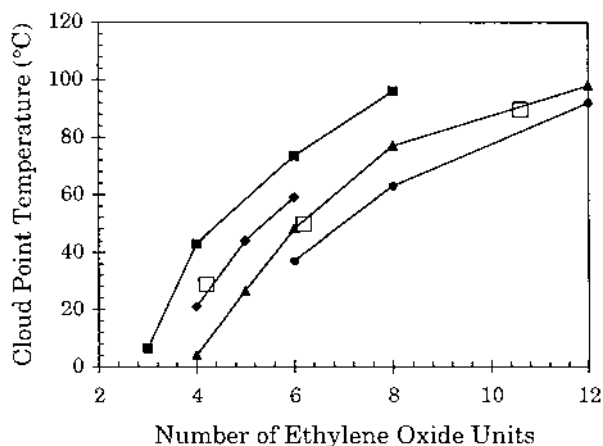


Figure 11 Cloud point temperature of micellar solutions as a function of the ethylene oxide chain length: the hydrophobic part is an alkyl chain with 8 (■), 10 (◆), 12 (▲), or 16 (●) carbon atoms. (Data from Ref. 51.) The symbols (□) represent the phase-inversion temperature for a 1:1 cyclohexane–water emulsion containing 5% commercial ethylene oxide-based emulsifiers having dodecylalkyl chains as a hydrophobic group. (Data from Ref. 54.)

provided in Fig. 11 (51). The cloud point increases with the number of ethylene oxide units. The reason is that a longer ethylene oxide chain gives rise to a longer-range intermicellar repulsion and a larger optimal area per head group (favoring smaller micelles). On the other hand, the cloud point decreases with the length of the hydrocarbon chain. By considering the geometry of the surfactant as described by the packing parameter (52), one realizes that the micellar size is expected to increase with the hydrocarbon chain length. It is also found that surfaces coated with (ethylene oxide containing) polymers often have good protein-repellent properties at low temperatures, whereas proteins adsorb more readily to such surfaces at higher temperatures (53).

For emulsions the most important aspect may be that the optimal area per head group in an adsorbed layer decreases with increasing temperature, which reduces the spontaneous monolayer curvature (4). This is the reason why emulsions stabilized by ethylene oxide-based surfactants may change from oil-in-water to water-in-oil when the temperature is increased. The temperature when this occurs is known as the phase-inversion temperature (PIT). The PIT depends on the length of the hydrocarbon chain and the ethylene oxide chain in a manner similar to the cloud point (54) (see Fig. 11). However, the PIT also depends on the type of oil used (55), which is partly due to differences in solubility of the ethylene oxide surfactants in the different oils and to differences in oil penetration in the surfactant layer. We also note that if the emulsifier concentration is high enough, a liquid-crystalline phase may accumulate at the oil-water interface. In such cases, emulsions which are very stable toward coalescence may be formed (56). This is a result of the decreased probability of hole formation (4). In this case, the type of oil used has a dramatic effect on the emulsion stability, which can be understood by considering the three-component phase diagram.

C. Nonionic Polymers on Hydrophobic Surfaces

Earlier, we discussed how the length of the oligo(ethylene oxide) chain influences the properties of emulsions stabilized by alkyl ethoxylates. When the ethylene oxide chain becomes sufficiently long, one normally refers to the substance as a diblock copolymer rather than as a surfactant. Of course, there is no clear distinction, but the properties vary in a continuous fashion with increasing ethylene oxide chain length. It is of interest to follow how the forces acting between two surfaces carrying adsorbed diblock copolymers vary with the length of the adsorbing (anchor) block and the nonadsorbing (buoy) block. A nice experimental work addressing this question is that of Belder et al (57). Fleer et al. give a thorough theoretical treatment in their book (17), where it was suggested that the most

efficient steric stabilization is obtained when the anchor block has a size that is 10–20% of that of the buoy block. The reason for this optimum is that when the anchor block is too small, the driving force for adsorption is weak and the adsorbed amount will be low. On the other hand, when the anchor block is too large, the area per adsorbed molecule will be large. As a consequence, the buoy block layer will be dilute and it will not extend very far out into the solution, leading to a not very pronounced steric force.

The forces acting between solid hydrophobic surfaces coated with different ethylene oxide-based diblock polymers are illustrated in Fig. 12. The forces acting between surfaces coated with penta(oxyethylene) dodecyl ether, $C_{12}E_5$, becomes significantly repulsive at distances below about 2 nm, calculated from the hard wall contact at $D=0$. Note that the surfactant layer remains between the surfaces, and the range of the force given is thus relative to the position of direct contact between the compressed adsorbed surfactant layers. The forces between hydrophobic surfaces coated with a diblock copolymer containing 8 butylene oxide units and 41 ethylene oxide units, B_8E_{41} , are significantly longer ranged. The interaction at distances above 4 nm from the “hard wall” is dominated by a weak electrostatic double-layer force originating from remaining charges on the silanated glass surface. However, at shorter distances, a steric force predominates.

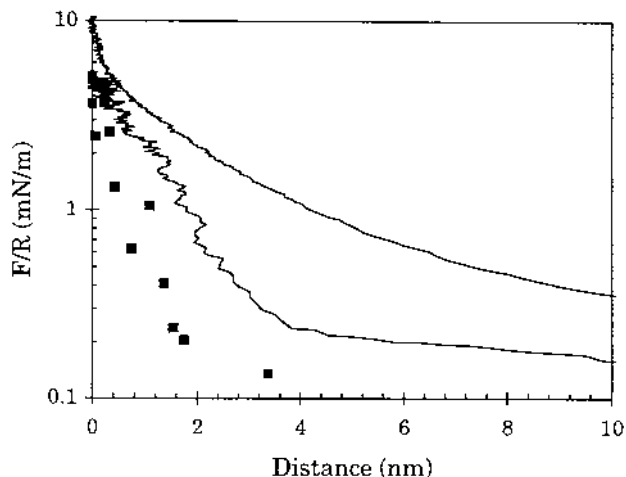


Figure 12 Force normalized by radius between hydrophobized mica or glass surfaces coated by penta(oxyethylene) dodecyl ether at 20°C (■), and copolymers of butylene oxide (B) and ethylene oxide (E) with compositions B_8E_{41} (lower line) and $B_{15}E_{200}$ (upper line). All data have been recalculated to spherical geometry.

Hence, the molecules with the longer ethylene oxide chains give rise to a longer-range force. Note that this is true even when the range is calculated from the position of the hard wall (i.e., without considering the difference in compressed layer thickness). A much longer-range force is observed in the case of B₁₅E₂₀₀, where the steric force extends to more than 10 nm away from the hard wall contact.

From the above, it is clear that rather large diblock copolymers are efficient in generating long-range repulsive steric forces, which is beneficial for increasing the stability of dispersed particles and emulsion droplets. An even higher stability may be obtained if a mixture of diblock copolymers and charged surfactants are used, thus providing both steric and electrostatic stabilization.

D. Polyelectrolytes on Surfaces

Both steric and electrostatic stabilization was utilized by Fäldt et al. (58) when making soybean oil emulsions. They first made the emulsion using a mixture of phosphatidylcholine and glycolic acid (bile salt) with a pK_a of 4.4. The emulsion droplets obtained a net negative surface charge due to dissociation of the glycolic acid. To improve the stability of the emulsion a weak cationic polyelectrolyte, chitosan, with a pK_a of 6.3–7 was added. The polyelectrolyte adsorbs to the negatively charged emulsion droplet surface, which becomes positively charged at low pH. It was found that the emulsion was stable at high and low pH but not at pH values around 7, where irreversible aggregation was observed. This clearly shows that the forces acting between the emulsion droplets change with pH. To shed light on this behavior, the forces acting between negatively charged solid surfaces coated by chitosan were measured as a function of pH (Fig. 13).

A repulsive double-layer force dominated the long-range interaction at pH values below 5. However, at distances below about 5 nm, the measured repulsive force is stronger than expected from DLVO theory due to the predominance of a steric force contribution. The layer thickness obtained under a high compressive force was 1 nm per surface. Hence, it is clear that positively charged chitosan adsorbs in a very flat conformation on strongly oppositely charged surfaces such as mica with only short loops and tails. When the pH is increased to 6.2, the mica–chitosan system becomes uncharged, because the charge density of the chitosan molecules has decreased. The decrease in charge density of the chitosan also results in a decrease in segment–segment repulsion and, therefore, an even more compact adsorbed layer. At this pH value, there is an attraction between the layers at a surface separation of about 2 nm. The steric repulsion is, in this

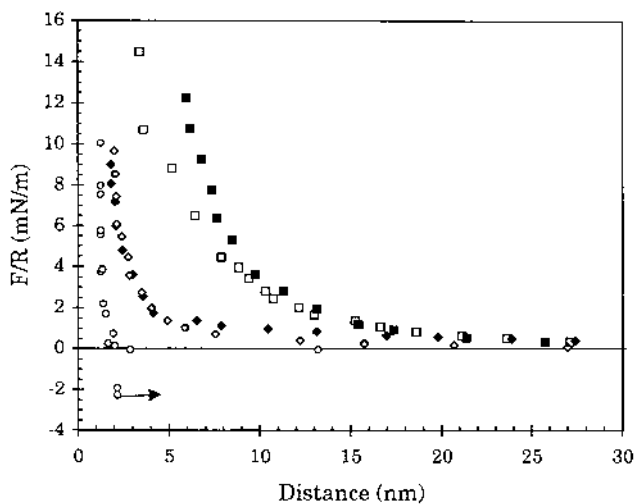


Figure 13 Force normalized by radius between negatively charged mica surfaces in crossed cylinder geometry precoated with a layer of chitosan, a cationic polyelectrolyte. The forces were recorded at pH 3.8 (◆), 4.9 (◇), 6.2 (○), 7.6 (□), and 9.1 (■); the arrow indicates an outward jump. (From Ref. 58, with permission.)

case, very short range (< 2 nm) and steep. A further increase in pH to 9.1 results in a recharging due to the fact that the charges on the polyelectrolyte no longer can compensate for all of the mica surface charges. Further, as the charge density of the polyelectrolyte is reduced, the range of the steric force increases again due to the lower affinity of the polyelectrolytes for the surface. Clearly, the mica–chitosan system is positively charged at low pH (i.e., the charges on the polyelectrolyte overcompensate for the charges on the mica surface), uncharged at pH 6.2, and negatively charged at high pH due to an undercompensation of the mica surface charge by the polyelectrolyte charges.

The flocculation behavior of the soybean emulsion can now be better understood. A stable emulsion is formed by a low pH owing to the electrostatic repulsion generated by the excess charges from the adsorbed chitosan. An intermediate pH values, the soybean emulsion is uncharged and the adsorbed chitosan layer is very flat. Hence, no long-range electrostatic force or long-range steric force is present that can stabilize the emulsion. At a high pH, the charges due to ionization of the glycolic acid are no longer compensated for by the high pH at nearly uncharged chitosan. Thus, stabilizing electrostatic forces are once again present. Further, the range of the stabilizing steric force is most likely also increased.

E. Proteins on Hydrophobic Surfaces

Amphiphilic proteins have properties similar to those of block copolymers and surfactants in the sense that they have clearly separated hydrophilic and hydrophobic domains that allow the formation of monodisperse aggregates or micelles in solution. For β -casein, the association process starts at a protein concentration of around 0.5 mg/mL at room temperature (59). Amphiphilic proteins adsorb strongly to nonpolar surfaces in contact with aqueous solutions, and they may generate stabilizing steric and electrostatic forces. In fact, caseins isolated from milk are widely used in different technical products ranging from food to paint and glue. One reason for this is that the caseins have excellent properties as emulsifiers and foaming agents, and emulsions stabilized by proteins constitute the most important class of food colloids. The caseins protect the oil droplets from coalescing and also provide long-term stability during storage and subsequent processing (60). β -Casein is more hydrophobic compared to the other caseins and the charged domain is clearly separated from the hydrophobic part, which makes the β -casein molecule, as whole, distinctly amphiphilic (61). At pH 7, the isolated β -casein molecule carries a net charge of about -12 (61).

Nylander and co-workers investigated the interactions between adsorbed layers of β -casein in order to clarify the mechanism responsible for the ability of β -casein to act as a protective colloid (62,63). The force as a function of surface separation between hydrophobic surfaces across a solution containing 0.1 mg/mL β -casein and 1 mM NaCl (pH = 7) is illustrated in Fig. 14. At separations down to about 25 nm, an electrostatic double-layer force dominates the interaction. The hydrophobic substrate surface was uncharged, so the charges responsible for this force had to come from the adsorbed protein. When the surfaces are compressed closer together, the repulsive force is overcome by an attraction at a separation of about 25 nm, and the protein-coated surfaces are sliding into contact about 8 nm out from the hydrophobized mica surface (Fig. 14, inset). This observation, as well as the adhesive force found on separation, was interpreted as being due to bridging of the hydrophilic tails that extend out into solution. Further compression does not significantly change the surface separation. The results indicate that the adsorbed β -casein layer consists of an inner compact part and a dilute outer region.

This conclusion compares favorably to what is known from studies of the adsorption of β -casein on to air-liquid, liquid-liquid, and solid-liquid interfaces using a range of other techniques. It has generally been found that the adsorbed amount of β -casein on hydrophobic surfaces is between 2 and 3 mg/m² over a wide range of bulk concentrations. This is the case for planar

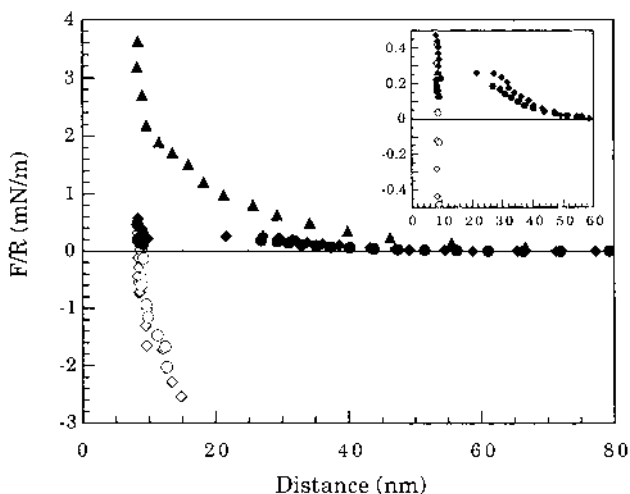


Figure 14 Normalized force measured between hydrophobized mica surfaces in crossed cylinder geometry coated with β -casein in a solution containing 0.1 mg β -casein/mL (pH = 7; 1 mM NaCl) (\blacklozenge , \diamond) and after dilution with 1 mM NaCl (\bullet , \circ). Filled and unfilled symbols represent the force measured on compression and decompression, respectively; \blacktriangle represents, the force measured between hydrophobized mica surfaces across a 0.1-mM NaCl solution at pH 5.6 containing 0.2 mg proteoheparan sulfate/mL. The inset shows the measured forces between adsorbed layers of β -casein before and after dilution with 1 mM NaCl on an expanded scale. (From Ref. 26, with permission.)

air–water and planar oil–water interfaces (59), for hydrocarbon oil–water interfaces in emulsions (64), and for interfaces between water and polystyrene latex particles (65–67) and hydrophobized silica (68). At the triglyceride–water interface, however, the adsorbed amount is somewhat lower (69).

Information about the adsorbed layer structure of β -casein at the hydrophobic surface can be obtained by employing neutron reflectivity, small-angle x-ray scattering (SAXS), and dynamic light scattering. It was found that the layer of β -casein adsorbed to a hydrocarbon oil–water interface or an air–water interface (70,71) consisted of a dense inner part, 2 nm thick, and a protein volume fraction of 0.96, immediately adjacent to the interface. Beyond that, a second dilute region with a protein volume fraction of 0.15 extended into the aqueous phase. A similar structure of β -casein adsorbed onto polystyrene latex particles was observed with SAXS (65). The electron density profile calculated from the SAXS data indicated that most of the protein resided within 2 nm from the surface. The profile

also showed a small amount of protein extending some 10 nm into the aqueous phase. Further, the hydrodynamic layer thickness estimated from the diffusion coefficient determined by dynamic light scattering of latex particles (67,72,73) and emulsion droplets (69) coated with β -casein was found to be 10–15 nm. The fact that different experimental techniques give a different value of the layer thickness is simply because they have a different sensitivity to the extending tails.

This type of layer structure, with a compact inner region and a dilute outer region, was also predicted by self-consistent field theory and by computer simulations. For instance, Monte Carlo simulations show that a dense layer (1–2 nm thick) is present close to the planar interface (74). This layer contained about 70% of the segments. Further out, a region of much lower density was found to extend about 10 nm into the aqueous phase. Similar results were obtained by self-consistent field calculations (75), which also showed that the most hydrophilic segments reside predominantly in the outer layer.

The properties of adsorbed β -casein layers can be changed by the action of enzymes. Leaver and Dalglish (69) have observed that the N-terminal end is more accessible to trypsinolysis than the rest of the adsorbed molecule, and that loss of the tail leads to a reduced layer thickness. A similar change was observed by Nylander and Wahlgren (68), who found that the addition of endoproteinase ASP-N to an adsorbed layer of β -casein reduced the adsorbed amount by approximately 20%. The removal of the extending tails will clearly reduce the range of the stabilizing steric force and thus reduce the emulsion stability against flocculation. We note that the forces generated by adsorbed β -casein are not very strongly repulsive (Fig. 14). Hence, the excellent stability of emulsion droplets coated by β -casein is most likely because the hole nucleation energy barrier is high.

Proteoglycan sulfate is an amphiphilic membrane glycoprotein. Like β -casein, it has one large hydrophobic region. Proteoglycan sulfate has three to four hydrophilic and strongly charged side chains, whereas β -casein has only one less charged tail. Proteoglycan sulfate is not used for stabilizing emulsions. However, it is nevertheless of interest to compare the forces generated by this protein with those generated by β -casein. The interaction between hydrophobic surfaces across a 1-mM NaCl solution containing 0.2 mg proteoglycan sulfate/mL is shown in Fig. 14 (62,76). The long-range interaction is dominated by a repulsive double-layer force, considerably stronger than that observed for β -casein. This is simply because proteoglycan sulfate is more strongly charged than β -casein. A steric force dominates the short-range interaction for both proteins.

F. Phospholipids on Polar Surfaces in Oil

We have seen earlier that surface force measurements provide important information about interactions between solid hydrophobic surfaces coated with surfactants and polymers, and that some of the information obtained is directly relevant for oil-in-water emulsions. However, the details of the interaction profiles are expected to be different for liquid hydrocarbon droplets coated with the same molecules as the model solid surfaces. In particular, the coalescence behavior of the emulsion droplets cannot be modeled. It is even more difficult to make a solid model surface that mimicks the behavior of water-in-oil emulsions. At present, the best one can do is to use a polar surface that attracts the polar part of the emulsifier. In this way, the orientation of the emulsifier on the model surface and at the water-in-oil emulsion surface will be the same. This will allow us to draw some conclusions about how polar solid surfaces coated with emulsifiers interact across oil, but care should be taken when using such results to draw conclusions about water-in-oil emulsions.

The forces between polar mica surfaces interacting across triolein containing 200 ppm of soybean phosphatidylethanolamine (PE) have been studied (77). Some results obtained at two different water activities are illustrated in Fig. 15. When the water activity is 0.47, a monolayer of PE is adsorbed on each surface. The orientation is such that the polar group is attached to the mica surface with the nonpolar part directed toward the oil phase. Thus, adsorption of the phospholipid renders the mica surface non-polar. No force is observed until the surfaces are about 6 nm apart. At this point, a very steep repulsion is experienced which is due to compression of the adsorbed layers. A weak attraction is measured on separation. The forces change significantly when the triolein is saturated with water (water activity = 1). The adsorbed layer becomes significantly thinner, and now only a rather weak compressive force is needed in order to merge the two adsorbed layers into one. The reason is that water molecules adsorb next to the polar mica surface and in the region of the zwitterionic lipid head group. This increases the mobility of the adsorbed phospholipid and decreases the force needed to merge the two adsorbed layers. Interestingly, it is not possible to remove the last adsorbed layer even by employing a very high compressive force.

From these observations, we can draw some conclusions that are relevant for water-in-oil emulsions. First, no long-range electrostatic forces are present in the nonpolar media. This is because the dissociation of surface groups is very unfavorable in low-polarity media. Hence, generally it is very difficult to utilize electrostatic forces for generating long-range stabilizing forces in oil. Surfactants like phospholipids or alkyl ethoxylates adsorbed

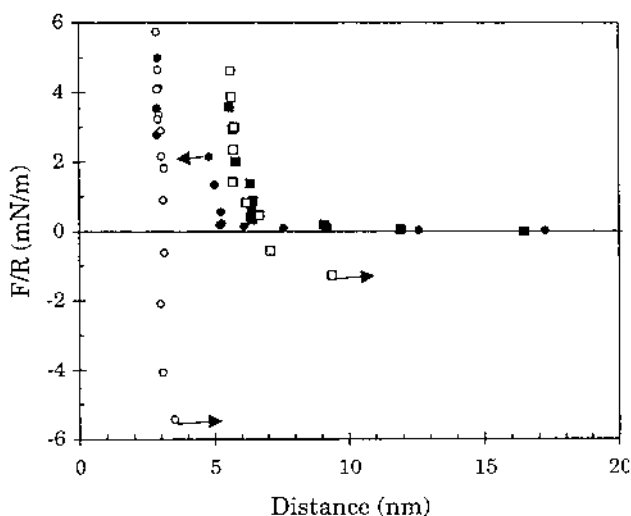


Figure 15 Force normalized by radius between mica surfaces in crossed cylinder geometry interacting across a triolein solution containing 200 ppm of soybean phosphatidylethanolamine. The forces of soybean were measured at water activities of 0.47 on approach (■) and separation (□), as well as at a water activity of 1 on approach (●) and separation (○); the arrows indicate inward and outward jumps. (From Ref. 77, with permission.)

in monolayers will only generate short-range repulsive forces due to compression of the hydrocarbon chains penetrating into the oil medium. These substances will be efficient in preventing coalescence of water-in-oil emulsions only when the adsorbed amount is high enough and the spontaneous monolayer curvature is sufficiently negative.

G. Polymers on Polar Surfaces in Oil

We saw earlier that surfactants adsorbed in monolayers only give rise to rather short-range forces in oil media. The range of the forces can be increased considerably if liquid-crystalline phases are accumulated at the interface, or if amphiphilic oil-soluble polymers are used instead of low-molecular-weight surfactants. An example of such a polymer is PGPR (polyglycerol polyricinoleate), which is a powerful water-in-oil emulsifier used in the food industry (78). PGPR has a complex branched structure as indicated in Fig. 16. This polymer was used for studying interactions between polar mica surfaces in triolein (79). The forces obtained at a polymer concentration of 200 ppm are shown in Fig. 17. In this system, repulsive steric forces are observed at distances below 15 nm. The magnitude of the

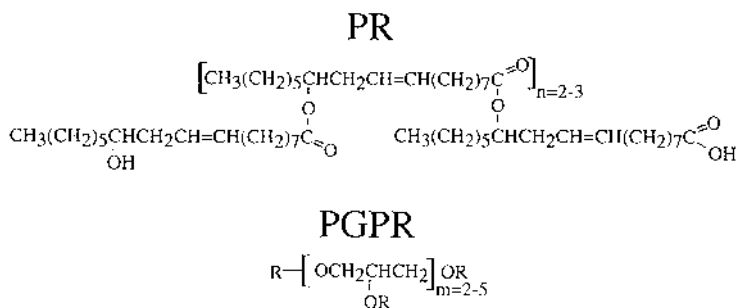


Figure 16 Illustration of the structural elements of PGPR. The upper structure is that of the polyricinoleate moiety; the lower structure shows the polyglycerol backbone. The R in the structure can be either hydrogen, a fatty acid residue, or a polyricinoleate residue. In PGPR, at least one of the side chains is polyricinoleate.

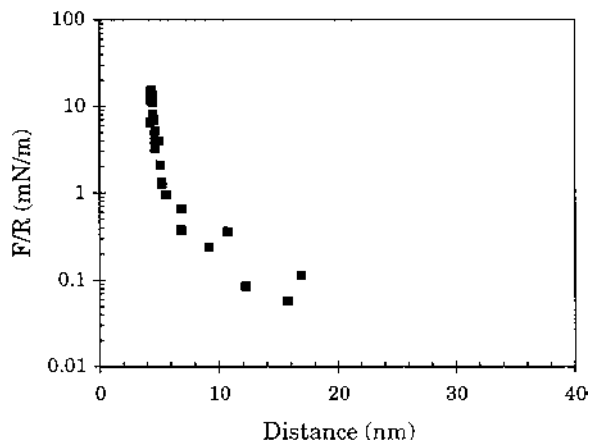


Figure 17 Force normalized by radius between mica surfaces interacting across a triolein solution containing 200 ppm of PGPR measured on approach.

force increases rather slowly with decreasing surface separation until the surfaces are about 5 nm apart. A further compression of the layers results in a steep increase of the steric force. The force profile indicates that the adsorbed layer consists of an inner dense region and an outer dilute region with some extended tails and loops. When dense polymer layers that generate long-range steric forces and have a high surface elasticity and viscosity are adsorbed at the interface of water-in-oil emulsions, one can expect that the emulsion stability against flocculation and coalescence will be good.

H. Forces Between Surfaces Across Emulsions

Emulsion droplets do not only break by coalescing with each other, but they may also break by attaching to a solid surface. Depending on the application, this may be wanted or unwanted. In order to study emulsion–surface interactions, a model oil-in-water emulsion was prepared from purified soybean oil (20 wt%) using fractionated egg phosphatides (1.2 wt%) as the emulsifier. The major components of the emulsifier were phosphatidylcholines and PEs. The mean diameter (D_Z average) of the emulsion was 320 nm, as determined with photon-correlation spectroscopy. A small amount of negatively charged lipids was also present, giving the emulsion droplets a net negative zeta potential of about -40 mV (80). This emulsion was then placed inside a SFA.

The forces acting between two glass surfaces across the 20% oil-in-water emulsion measured by using the MASIF are illustrated in Fig. 18 (81). A repulsive force dominates the interactions at separations below 200 nm.

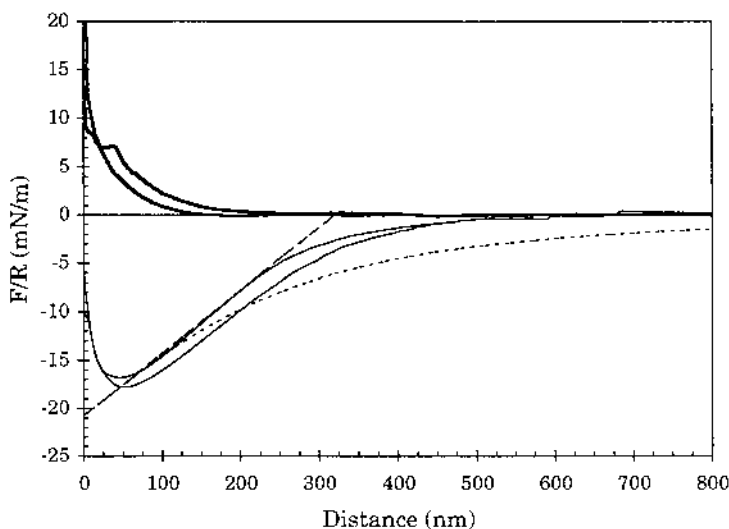


Figure 18 Force normalized by local geometric mean radius as a function of surface separation between glass across a concentrated emulsion solution (20 wt% oil and 1.2 wt% phospholipid). The thinner lines correspond to the force measured on separation, the dashed line represents the calculated force between two spherical surfaces connected by a capillary condensate in the full equilibrium case [Eq. (25)], and the dotted line represents the force between two spherical surfaces connected by a capillary condensate in the nonequilibrium case [Eq. (26)]. (From Ref. 81, with permission.)

The force increases strongly with decreasing distance. This illustrates that large aggregates, with a diameter of at least 100 nm, are associated with each surface and the repulsion between 40 and 200 nm is due to deformation and eventual breaking of these aggregates. The range of the repulsive force is consistent with the layer thickness obtained in a previous ellipsometric study by Malmsten et al. (80). They found that the thickness of a layer adsorbed from the emulsion on to a negatively charged silica surface was around 100 nm, independent of surface coverage.

In some force curves, one or two distinct steps are present. Figure 18 illustrates one such force curve where a clear step is seen at a separation of about 40 nm. At a separation of about 10 nm, another step, but less pronounced, is seen. These steps are interpreted as being due to coalescence of adsorbed emulsion droplets and/or due to materials that collectively leave the zone between the surfaces. On subsequent approaches of the surfaces on the same position, the range of the repulsion remains at about 200 nm. However, the steps in the force profile become less pronounced or disappear completely, indicating a change in the adsorbed layer when exposed to a high compressive force.

A strong and long-range force is observed when the surfaces are separated. It is plausible that this attraction is due to the formation of a capillary condensate of oil between the surfaces (Fig. 19). This capillary condensate originates from the emulsion droplets that have been destroyed when the surfaces are brought together. The forces between two spherical surfaces connected by a capillary condensate in the full equilibrium case are given by (82)

$$\frac{F}{R} = 2\pi(\sigma_{sc} - \sigma_{sb})\left(1 - \frac{D}{R_k}\right) \quad (25)$$

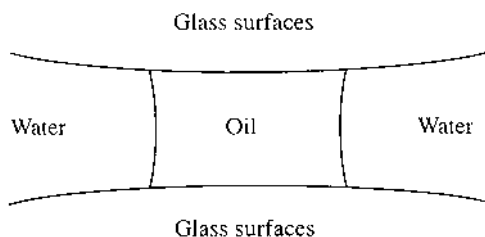


Figure 19 Schematic of the capillary condensate formed between glass surfaces due to breakdown of adsorbed emulsion droplets. The figure is not according to scale. (From Ref. 81, with permission.)

where σ is the interfacial tension and the subscript s , c , and b stand for surface, capillary condensate, and bulk, respectively; R_K is the Kelvin radius of the capillary condensate. In cases when the surfaces are separated too rapidly to allow the volume of the capillary to change with separation, one instead obtains (82)

$$\frac{F}{R} = 2\pi(\sigma_{sc} - \sigma_{sb}) \left[1 - \frac{1}{\sqrt{(1 + R_K^2/D^2)}} \right] \quad (26)$$

Two theoretical force curves calculated by using Eqs. (25) and (26) are shown in Fig. 18. In these calculations, we used a Kelvin radius of 320 nm and an interfacial tension difference of 3.3 mN/m. The measured force curves fall in between the extreme cases of full equilibrium, where the volume of the condensate is changing with distance to minimize the free energy, and the case of no change in condensate volume with separation. Long-range forces due to capillary condensation have been observed previously by Petrov et al., who found that a lamellar phase condensed between two surfaces immersed in an L_3 -phase (83). Capillary condensation of sparingly soluble surfactants between surfaces close to each other in surfactant solutions has also been reported (84).

It is worth pointing out that the functional form of the measured attraction shows that the volume of the capillary condensate decreases with increasing separation. However, this does not occur fast enough compared to the speed of the measurements (the attractive part took about 30 s to measure) to allow full equilibrium to be established. Also, the range of the measured repulsion on approach does not increase with the number of times the surfaces are brought into contact but rather the reverse. Both of these observations point to the fact that the material present in the capillary condensate is spontaneously reemulsified when the surfaces are separated.

In order to obtain information about whether a monolayer, a bilayer, or a multilayer was firmly attached to the surfaces, we employed the interferometric SFA and mica surfaces rather than glass surfaces (81). In these measurements, a drop of the emulsion was placed between the surfaces. The emulsion was very opaque and no interference fringes could be seen until the surfaces were close to contact. The force measured between mica surfaces across a concentrated emulsion were repulsive and long range (several hundred nanometers), which was in agreement with the results obtained using glass surfaces. Because the forces were so highly repulsive, no attempt was made to measure them accurately, but under a high compressive force, the

surfaces come to a separation 8.5 nm. This corresponded to a bilayer of phospholipid on each surface.

I. Forces Due to Stratification in Foam and Pseudoemulsion Films

The thinning of thin liquid films in micellar solution is found to occur in a stepwise fashion, known as stratification. Bergeron and Radke (35) set out to study the forces responsible for this phenomenon using the porous frit version of the thin-film pressure balance. They found that the equilibrium disjoining pressure curve (force curve) showed an oscillatory behavior both for foam and pseudoemulsion (i.e., asymmetric oil–water–gas) films stabilized by the anionic surfactant sodium dodecyl sulfate above the cmc (Fig. 20). The reason for this oscillatory force profile was the layering of micelles in the confined space in the thin aqueous film separating the two interfaces. The periodicity of the oscillations was the same for foam films and for pseudoemulsion films. The main difference between the two systems was found in the high-pressure region of the disjoining pressure isotherm. The pseudoemulsion films ruptured at much lower imposed pressures than the foam films. This was attributed to the action of the oil phase as a foam destabilizer.

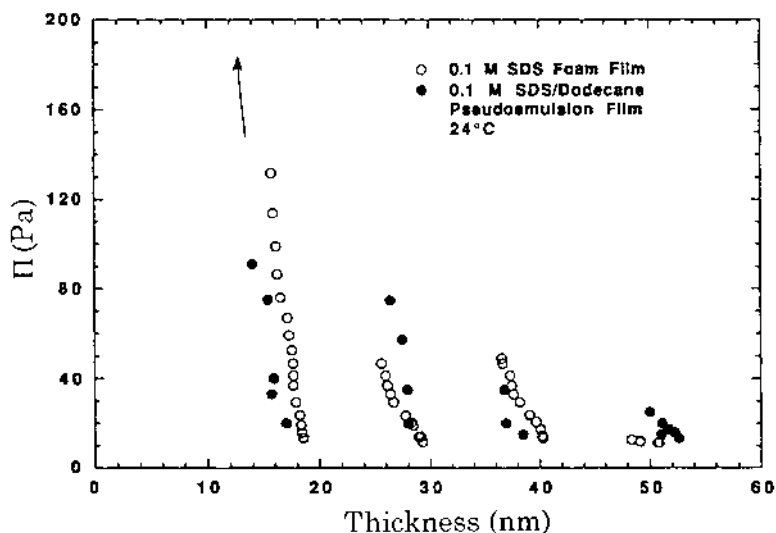


Figure 20 Low-pressure region of the disjoining pressure isotherm across a 0.1 M SDS solution in a single-foam lamella, and across a 0.1 M SDS solution separating a dodecane–solution interface from an air–solution interface. (Reproduced from Ref. 35, with permission.)

VI. SUMMARY

Several techniques are available for studying long-range interactions between solid surfaces and fluid interfaces. The forces generated by surfactants, polymers, and proteins have been determined. For oil-in-water emulsions, both steric and electrostatic stabilizing forces are of importance, whereas only steric forces are operative for the case of water-in-oil emulsions. These forces are well understood theoretically. The experimental techniques employed give very detailed information on the long-range forces, and in this respect, the results obtained for the model systems can be useful for understanding interactions in emulsion systems. However, the surface force techniques employed are not suitable for modeling the molecular events leading to coalescence of emulsion droplets once they have been brought in close proximity to each other. Some data illustrating the breakdown and reemulsification of emulsion droplets in the gap between two macroscopic solid surfaces were also presented. This is a new research topic and very little is known about how the surface properties and the type of emulsifier influence the stability of emulsion droplets at surfaces and in narrow gaps between surfaces.

ACKNOWLEDGMENT

This work was partly sponsored by the Competence Centre for Surfactants Based on Natural Products (SNAP).

REFERENCES

1. W. D. Bancroft, *J. Phys. Chem.* 19, 275 (1915).
2. W. C. Griffin, *J. Soc. Cosmet. Chem* 1, 311 (1949).
3. J. T. Davies, *Proc. 2nd Int. Congr. Surf. Activity 1957*, Vol. 1, 426.
4. A. Kabalnov and H. Wennerström, *Langmuir* 12, 276 (1996).
5. D. Y. C. Chan and R. G. Horn, *J. Chem. Phys.* 83, 5311 (1985).
6. J. Kizling and B. Kronberg, *Colloids Surfaces* 50, 131 (1990).
7. O. Reynolds, *Phi. Trans. R. Soc. London* 177, 157 (1886).
8. F. W. Cain and J. C. Lee, *J. Colloid Interf. Sci.* 106, 70 (1985).
9. E. D. Manev and R. Tsekov, and B. P. Radoev, *J. Dispers. Sci. Technol.* 18, 769 (1997).
10. B. P. Radoev, A. D. Scheludko, and E. D. Manev, *J. Colloid. Interf. Sci.* 95, 254 (1983).
11. S. A. K. Jeelani and S. Hartland, *J. Colloid Interf. Sci.* 164, 296 (1994).

12. J. N. Israelachvili, *Intermolecular and Surface Forces*, Academic Press, London, 1991.
13. E. J. N. Verwey and J. T. G. Overbeek, *Theory of Stability of Lyophobic Colloids*, Elsevier, Amsterdam, 1948.
14. B. V. Derjaguin and L. Landau, *Acta Physicochim. URSS* 14, 633 (1941).
15. V. A. Parsegian, N. Fuller, and R. P. Rand, *Proc. Natl. Acad. Sci. USA* 76, 2750 (1979).
16. J. N. Israelachvili and H. Wennerström, *J. Phys. Chem.* 96, 520 (1992).
17. G. J. Fleer, M. A. Cohen Stuart, J. M. H. M. Scheutjens, T. Cosgrove, and B. Vincent, *Polymers at Interfaces*, Chapman & Hall, London, 1993.
18. P.-G. de Gennes, *Scaling Concepts in Polymer Physics*, Cornell University Press, Ithaca, NY, 1979.
19. P.-G. de Gennes, *Adv. Colloid Interf. Sci.* 27, 189, (1987).
20. A. D. Nikolov and D. T. Wasan, *J. Colloid Interf. Sci.* 133, 1–12, (1989).
21. V. Bergeron and C. J. Radke, *Langmuir* 8, 3020 (1992).
22. V. Bergeron, A. J. Jiménez-Laguna, and C. J. Radke, *Langmuir* 8, 3027 (1992).
23. V. Bergeron, Forces and structure in surfactant-laden thin-liquid films, PhD thesis, University of California, Berkeley, 1993.
24. A. L. de Vries, *Rec. Trav. Chim. Pays-Bas* 77, 383 (1958).
25. K. Shinoda and H. Saito, *J. Colloid Interf. Sci.* 30, 258 (1969).
26. P. M. Claesson, T. Ederth, V. Bergeron, and M. W. Rutland, *Adv. Colloid Interf. Sci.* 67, 119 (1996).
27. J. N. Israelachvili, G. E. Adams, *J. Chem. Soc. Faraday Trans. I* 74, 975 (1978).
28. J. Parker, *Prog. Surf. Sci.* 47, 205 (1994).
29. K. Schillén, P. M. Claesson, M. Malmsten, P. Linse, and C. Booth, *J. Phys. Chem.* 101, 4238 (1997).
30. B. Derjaguin, *Kolloid Z.* 69, 1557 (1934).
31. R. G. Horn, J. N. Israelachvili, and F. Pribac, *J. Colloid Interf. Sci.* 115, 480 (1987).
32. P. Attard and I. L. Parker, *Phys. Rev. A* 46, 7959 (1992).
33. A. Scheludko, *Adv. Colloid Interf. Sci.* 1, 391 (1967).
34. O. D. Velev, G. N. Constantinides, D. G. Avraam, A. C. Paytakes, and R. P. Borwankar, *J. Colloid Interf. Sci.* 175, 68 (1995).
35. V. Bergeron and C. J. Radke, *Colloid Polym. Sci.* 273, 165 (1995).
36. K. J. Mysels and M. N. Jones, *Disc. Faraday Soc.* 42, 42 (1966).
37. R. L. Ferm, in *Emulsion and Emulsion Technology* (K. J. Lissant, ed.), Marcel Dekker, New York, 1974, Vol I p. 387.
38. V. Bergeron, *Langmuir* 13, 3474 (1997).
39. P. C. Herder, *J. Colloid Interf. Sci.* 134, 336 (1990).
40. P.M. Claesson, R. Kjellander, P. Stenius, and H. K. Christenson, *J. Chem. Soc. Faraday Trans. I* 82, 2735 (1986).
41. R. Kjellander, *J. Chem. Soc. Faraday Trans. II* 78, 2025 (1982).
42. R. E. Goldstein, *J. Chem. Phys.* 80, 5340 (1984).
43. G. Karlström, *J. Phys. Chem.* 89, 4962 (1985).
44. A. Matsuyama and F. Tanaka, *Phys. Rev. Lett.* 65, 341 (1990).

45. P.-G. de Gennes, *C.R. Acad. Sci. Paris* 313, 1117 (1991).
46. S. Bekiranov, R. Bruinsma, and P. Pincus, *Europhys. Lett.* 24, 183 (1993).
47. P. Linse and B. Björling, *Micromolecules* 24, 6700 (1991).
48. M. Björling, *Macromolecules* 25, 3956 (1992).
49. W. Brown, R. Johnsen, P. Stilbs, and B. Lindman, *J. Phys. Chem.* 87, 4548 (1983).
50. G. J. T. Tiddy, *Phys. Rep.* 57, 3 (1980).
51. D. J. Mitchell, G. J. T. Tiddy, L. Waring, T. Bostock, and M. P. McDonald, *J. Chem. Soc. Faraday Trans. I* 79, 975 (1983).
52. J. N. Israelachvili, D. J. Mitchell and B. W. Ninham, *J. Chem. Soc. Faraday Trans. II* 72, 1525 (1976).
53. S. I. Jeon and J. D. Andrade, *J. Colloid Interf. Sci.* 142, 159 (1991).
54. K. Shinoda and H. Takeda, *J. Colloid Interf. Sci.* 32, 642 (1970).
55. B. A. Bergenstahl and P. M. Claesson, in *Food Emulsions* (S. E. Friberg and K. Larsson, eds), Marcel Dekker, New York, 1997.
56. S. E. Friberg and C. Solans, *Langmuir* 2, 121 (1986).
57. G. F. Belder, Gten Brinke and G. Hadziioannou, *Langmuir* 13, 4102 (1997).
58. P. Fäldt, B Bergenstahl and P. M. Claesson, *Colloids Surfaces A* 71, 187 (1993).
59. D. G. Schmidt and T. A. J. Payens, *J. Colloid Interf. Sci.* 39, 655 (1972).
60. E. Dickinson, *J. Dairy Sci.* 80, 2607 (1997).
61. H. E. Swaisgood, *Development in Dairy chemistry— I*, Applied Science, London, 1982.
62. P. M. Claesson, E. Blomberg, J. C. Fröberg, T. Nylander, and T. Arnebrandt, *Adv. Colloid Interf. Sci.* 57, 161 (1995)
63. T. Nylander and N. M. Wahlgren, *Langmuir* 10, 1274 (1997).
64. J.-L. Courthaudon, E. Dickinson, and D. G. Dalgleish, *J. Colloid Interf. Sci.* 145, 390 (1991).
65. A. R. Mackie, J. Mingins, and A. N. North, *J. Chem. Soc. Faraday Trans.* 87, 3043 (1991).
66. J. R. Hunter, P. K. Kilpatrick, and R. G. Carbonell, *J. Colloid Interf. Sci.* 142, 429 (1991).
67. D. V. Brooksbank, C. M. Davidson, D. S. Horne, and J. Leaver, *J. Chem. Soc. Faraday Trans.* 89, 3419 (1993).
68. T. Nylander and N. M. Wahlgren, *J. Colloid Interf. Sci.* 162, 151 (1994).
69. J. Leaver and D.G. Dalgleish, *J. Colloid Interf. Sci.* 149, 49 (1992).
70. E. Dickinson, *J. Chem. Soc. Faraday Trans.* 88, 2973 (1992).
71. E. Dickinson, D. S. Horne, J. S. Phipps, and R. M. Richardson, *Langmuir* 9, 242 (1993).
72. D. G. Dalgeish, *Colloids Surfaces* 46, 141 (1990).
73. D. G. Dalgeish and J. Leaver, *J. Colloid Interf. Sci.* 141, 288 (1991).
74. E. Dickinson and S. R. Euston, *Adv. Colloid Interf. Sci.* 42, 89 (1992).
75. F A. M. Leermakers, P. J. Atkinson, E. Dickinsin, and D. S. Horne, *J. Colloid Interf. Sci.* 178, 681 (1996).
76. M. Malmsten, P. M. Claesson, and G. Siegel, *Langmuir* 10, 1274 (1994).
77. A. Dedinaite, P. M. Claesson, B, Campbell, and H. Mays. *Langmuir* 14, 5546 (1998).

78. R. Wilson, B. I. van Schie, and D. Howes, *Food Chem. Toxicol.* 36, 711 (1998).
79. A. Dedinaite, B. Campbell, *Langmuir* 16, 2248–2253 (2000).
80. M. Malmsten, A.-L. Lindström, and T. Wårnheim, *J. Colloid Interf. Sci.* 173, 297 (1995).
81. E. Blomberg, P. M. Claesson, and T. Wårnheim, *Colloids Surfaces A*, 159, 149–157 (1999).
82. D. F. Evans and H. Wennerström, *The Colloidal Domain*, 2nd ed., VCH, New York, 1998.
83. P. Petrov, U. Olsson, and H. Wennerström, *Langmuir* 13, 1000, (1979).
84. Å. Walthermo, P. M. Claesson, and I. Johansson, *J. Colloid Interf. Sci.* 183, 506 (1996).

8

Coalescence Mechanisms in Protein-Stabilized Emulsions

George A. van Aken

Wageningen Centre for Food Sciences, Wageningen, The Netherlands

I. INTRODUCTION

A. Importance of Coalescence in Food Emulsions

Coalescence of emulsified oil may be defined as any physical process that leads to the merging of the oil droplets into a larger droplet. Coalescence is desired in some cases—for example, during butter manufacture, where churning of cream leads to the separation of butter granules through a phase-inversion process that involves coalescence of milk fat globules (1). Another example is during whipping of cream (2), where coalescence leads to the formation of a network of partially coalesced fat globules, which stabilizes the air bubbles in the cream (1,3). A final example is a limited amount of coalescence in the mouth, which may lead to the release of some oil that may coat the oral tissues and provide oily lubricity (4) and enhance the release of fat-soluble flavours (5). However, usually coalescence is undesired, such as during emulsion formation by homogenisation, where the occurrence of coalescence of newly formed droplets reduces the efficiency of the homogenizer (6), and during storage, where coalescence leads to the formation of larger droplets with an increased creaming rate or even a visible oil layer on top of the emulsion.

B. Adsorbed Protein Layers

In food emulsions, stability against coalescence is obtained from an adsorbed layer at the surface of the oil droplets. The composition of this

layer is usually complex, often consisting primarily of protein and protein aggregates, in combination with polar lipids, such as lecithin, and a wide range of low-molecular-weight surfactants, such as monoglycerides and diglycerides, polysorbates, Tweens, Spans, and sucrose esters (7,8). The most commonly used proteins in food applications are the caseins and whey proteins derived from milk. Caseins are a group of proline-rich proteins with relatively little secondary structure and low solubility at pH 4.6 (2,9). In solution, they are often present in the form of micelles that solubilize calcium phosphate. Whey proteins are a group of globular proteins (2,9) which have in common a much more compact and ordered molecular structure, organized in tight conformations, such as α -helices and β -sheets, and stabilized by physical bonds (e.g., hydrogen bonds, hydrophobic bonds) and covalent bonds (mainly disulfide bridges).

After proteins have adsorbed to the oil–water interface of the emulsion droplets, they slowly change their conformation (“unfold”), adapting their molecular structure to the changed environment at the interface (10–13). It has been suggested that on adsorption, globular protein molecules largely retain their secondary structure of α -helices and β -sheets but that the organization of these elements (tertiary structure) changes. This reorganization leads to an increase of the binding energy of the protein to the interface and exposure of hydrophobic moieties and sulfhydryl groups at the aqueous side of the adsorbed protein layer (14,15). Intermolecular bonds are formed between the adsorbed molecules, largely hydrophobic bonds but, for many proteins, probably also intermolecular disulfide bonds (16). This leads to the formation of a cohesive layer of the adsorbed molecules, with strongly reduced lateral mobility of the molecules and the tendency of the adsorbed layer to fracture rather than flow when the adsorbed layer is deformed (17).

Some compounds bind to adsorbed protein layers. (e.g., polyphenols (tannins) and many polysaccharides, such as propylene glycol alginate, pectin and carrageenan). This was shown to enhance the elasticity of a mixed adsorbed layer of protein and low-molecular-weight surfactants and to reduce the rate of drainage of foams stabilized by such a mixed adsorbed layer (18).

The presence of coadsorbed surfactants and polar lipids often improves the overall performance of protein- or peptide-stabilized emulsions. These surfactants help to lower the surface tension during emulsification. Moreover, physical interactions occur between proteins and lipids and surfactants, forming molecular complexes (19). Investigation of mixed adsorbed layers of protein and surfactant has revealed that polar lipids and surfactants can displace proteins from the interface. If the protein is only partially displaced, the mixed adsorbed layer is often laterally

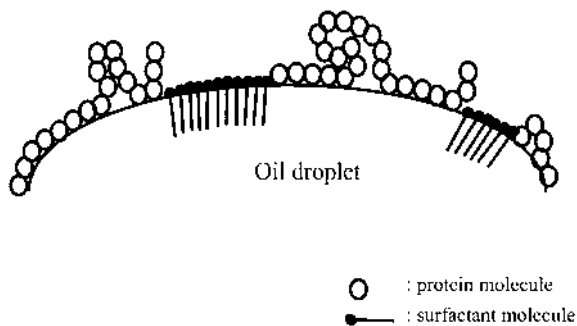


Figure 1 Sketch of an oil–water interface with an adsorbed layer of protein, to which a low-molecular-weight surfactant has been added, which displaces the adsorbed protein layer by the “orogenic” mechanism, leading to patchwise adsorption of protein and surfactant.

inhomogeneous, with a patchwise distribution of protein-rich and surfactant-rich regions. The displaced protein often remains attached to the interface as a wrinkled sheet in the protein-rich regions (“orogenic” displacement, illustrated in Fig. 1) (20,21).

Another important aspect is protein hydrolysis, which leads to the formation of protein fragments, peptides, and free amino acids. Protein hydrolysis usually occurs by proteolytic enzymes (e.g., during the preparation of fermented products such as yogurt and cheese). It may also be carried out to improve the solubility of the protein (e.g., in the preparation of soy protein isolates or for the formulation of low-allergenic infant food). The emulsifying and foaming properties of peptides obtained by hydrolysis are strongly dependent on the molecular mass and composition. Usually, the surface activity and the film-stabilizing properties become much lower with decreasing molecular masses. As a rule of thumb, good surface-active properties were obtained for amphipolar peptides with molecular masses exceeding 2000 Da and preferably containing disulfide-linked fragments (22,23).

C. Complexity of Processes Preceding Coalescence in Food Emulsions

In food emulsions, coalescence is usually not caused by a single process, but, instead, by a complex sequence of several processes preceding the final step of coalescence. These preceding processes strongly vary among different products and therefore cannot be generalized. However, some common tendencies can be distinguished.

An important aspect in the application of proteins as emulsion stabilizers is that the molecular structure and properties of the molecules in solution may change during processing. For example, the solubility is highly dependent on pH and, for most proteins, becomes very small in the vicinity of their isoelectric pH. In many food products, the pH is lowered to around 4–5 during manufacture, which is close to the isoelectric pH of many proteins. Another example is that microbial contamination is often reduced in the last stage of production by a heat treatment (sterilization or pasteurization). This may lead to irreversible denaturation of the proteins, which, as a result, often become insoluble. The denatured protein may precipitate as flocs and remain separate from the emulsion droplets or may precipitate onto the droplet surface, forming thick adsorbed layers or even encapsulating the droplets in the precipitate (2).

The sensitivity to coalescence often changes during storage due to ongoing chemical (e.g., oxidation), physical (e.g., creaming, crystallization of lactose or inorganic salts), and enzymatic (e.g., protease and lipase activity) transformations in the product. During handling, the emulsion is spread, stirred, mixed with other ingredients, acidified, heated, and exposed to air, all of which may lead to large structural and compositional changes in the emulsion, which may induce coalescence.

Finally, it is the complex behavior of the emulsion in the mouth that determines its perception by the consumer. Several processes change the structure of the emulsion and the release of flavor compounds (24), such as mixing with saliva, melting of the gelled continuous phase, hydrolysis of starch by amylases in saliva (25), and possibly also release of fat from the emulsion and its adherence to the mucosa (4).

D. Aim of This Work

The complexity of the composition and structure of food emulsions and foams complicates understanding and adequate control the behavior of these systems. The final step of coalescence can be caused by several mechanisms and, as consequence, may reveal itself in many different ways, such as a coarsening of the droplet size distribution (dressings), formation of oil lenses on top of the emulsion (soups), and clumping of fat (cream). Because of the inherent complexity of food products and their application, predictive tests to determine the stability of an emulsion to coalescence are often not very reliable. These tests accelerate only one specific mechanism, which is not necessarily the most important in the situation considered. For example, a centrifugation test (26) is not suitable to predict coalescence mediated by the surface of expanding gas bubbles (Section IV. B). Clearly, there is a gap of knowledge in the realm of coalescence mechanisms

in food emulsions. The aim of the present work is give a general overview of the multitude of physical mechanisms in food emulsions that are collectively referred to as “coalescence.”

The organization of the main part of this chapter is as follows. The role of the adsorbed layer in coalescence processes is discussed Section II. The structure and stability of thin films are related to the properties of the constituent adsorbed layers, making a comparison between surfactant- and protein-stabilized thin films. Section III describes homogeneous coalescence. The main consecutive steps, droplet encounter and initiation of film rupture, are distinguished, and for each step, various mechanisms will be discussed. Finally, Section IV will focus on mechanisms of heterogeneous coalescence, which involves the interaction with a third phase. Distinction will be made among coalescence intermediated by a solid and liquid surfaces, coalescence induced by shearing in confined spaces, and coalescence caused by puncturing of thin films by small particles.

II. ROLE OF THE ADSORBED LAYER IN COALESCENCE

A. Thin Films

Stability against coalescence is directly related to the properties of the protective coating of adsorbed material at the droplet surface. This is because adsorbed layers on adjacent droplets repel each other (“disjoining pressure”), in this way keeping the internal phases of these droplets separated. This repulsion is usually of electrostatic steric origin. If the droplets attract each other (e.g., by van der Waals forces) or are pushed together by an external force, a thin film is formed. The thickness of this thin film is determined by a balance of attractive and repulsive forces and mainly depends on the range of the repulsive interactions (Fig. 2). For adsorbed layers consisting of uncharged polar lipids, the repulsion is the short-range Born repulsion. The thin film then consists of a bilayer of adsorbed material and hardly contains free water in between the adsorbed layers. Such a thin film is called a Newton black film (NBF). For charged adsorbed layers or adsorbed layers with hydrophilic chains extending into the continuous liquid [an example of the latter is an adsorbed layer of β -casein in which charged and hydrophilic N-terminal chain segment protrude into the water (27)], the distance between the adsorbed layers remains larger and the thin films contain free water. Such a film is called a common black film (CBF).

Over the last decade, the understanding of thin films stabilized by proteins has substantially increased. At pH remote from the isoelectric pH, adsorbed protein layers are charged. If two droplets of a protein-stabilized emulsion are pushed together, the electrostatic repulsion between

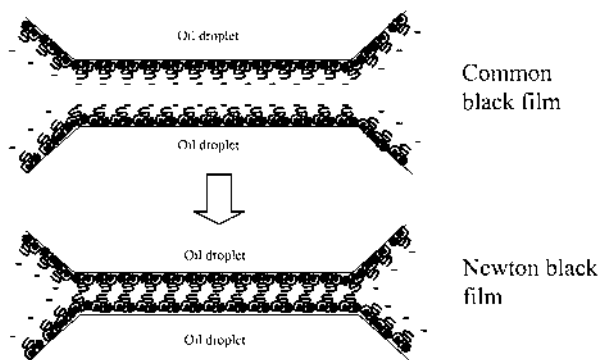


Figure 2 Transition between a common black film and a Newton black film, induced by increasing the normal pressure onto the thin film or by reducing the electrostatic repulsion between the films. Here, the thin films are stabilized by negatively charged layers of adsorbed protein molecules.

these layers keeps the adsorbed layers separated, thus forming a CBF. Increasing the concentration of 1:1 electrolytes reduces the Debye length, thereby decreasing the range of double-layer repulsion and the thickness of the CBF. This also increases the stability of the NBF state with respect to the CBF state and also reduces the energy barrier involved in the transition of CBF to NBF. High-valency cations (Ca^{2+} , Al^{3+}) are even more effective in this because they also lower the charge and surface potential by binding to the adsorbed protein molecules (28–30).

As described in Section I. A, proteins change their conformation after adsorption, leading to the formation of an elastic adsorbed film at the interface. At least for the whey proteins, this also leads to exposure of hydrophobic amino acid residues and free sulfhydryl groups to the water phase. When adsorbed layers on adjacent droplets are in contact, corresponding to the NBF state, hydrophobic and disulfide bonds will then also be formed between these layers, strongly increasing the attractive interaction between the adsorbed layers. The binding may become so strong that it becomes effectively irreversible (15,30,31).

In dilute protein-stabilized emulsions at pH remote from the isoelectric pH, the electrostatic repulsion between the adsorbed layers keeps the droplets separated. Increasing the concentration of 1:1 electrolytes and especially high-valency cations promotes droplet flocculation and stabilizes the NBF state with respect to the CBF state. Because the NBF state allows the formation of intermolecular bonds between adsorbed layers in contact, the binding between the adsorbed layers becomes enforced and droplet flocculation becomes irreversible (often referred to as “coagulation”).

In effect, on increasing the electrolyte concentration or approaching the isoelectric pH, the thin films between the flocculated droplets “jump” from the CBF state into an irreversible NBF state (32).

B. Rupture of Thin Films

Film rupture occurs when a hole is formed in the thin film, with a diameter larger than a critical size, so that the hole will grow spontaneously. The hole can be formed spontaneously or by mechanical forces pulling at the film. Film rupture related to spontaneous formation of a hole will be called “spontaneous film rupture.” Film rupture induced by mechanical forces will be called “induced film rupture.” Various mechanisms may initiate film rupture and the most important ones will be treated in Section III. A. The way by which adsorbed layers protect the thin film against coalescence depends on the molecular properties of the adsorbed layer. Based on the properties of adsorbed protein layers discussed in the previous subsections, we may expect large differences between the ways proteins and low-molecular-weight surfactants to stabilize thin films.

Low-molecular-weight surfactants form mobile adsorption layers. Thin film stability is mainly due to a fast hole-repair mechanism (33), in combination with a preferred curvature of the adsorbed layer that opposes the mean curvature of a neck of liquid connecting the liquid volumes on both sides of the thin film (34). If the surfactant is charged or exposes a hydrophilic chain into the solution, a relatively large distance is maintained between the two sides of the thin film due to electrostatic or steric repulsion, respectively, which improves the stability of the thin film.

Proteins, on the other hand, form thick, cohesive, and elastic adsorbed layers and the molecules in the adsorbed layer are relatively immobile (35). These properties afford a strong barrier against film rupture under quiescent conditions (36). However, on large deformation, the adsorbed layers may fracture (Section I.B) and this may have important consequences for the stability of the thin films (see Section III. A. 1). As discussed in the previous section, on close contact between adsorbed layers, strong hydrophobic and covalent bonds can be formed between the adsorbed layers, leading to coagulation of the droplets. The presence of these bonds makes the emulsion sensitive to a specific mechanism of coalescence that will be discussed in Section III.A.3.

III. HOMOGENEOUS COALESCENCE

Commonly, coalescence involves the process of merging of two emulsion droplets, dispersed in a continuous liquid. This process of coalescence

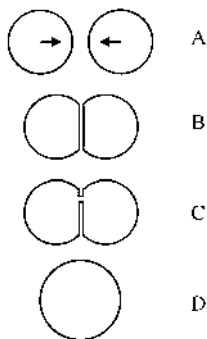


Figure 3 Basic coalescence process involving two droplets: (A) encounter of droplets; (B) thin-film formation; (C) thin-film rupture; (D) merging of droplets.

generally comprises two main consecutive steps: (1) encounter of droplet surfaces and the formation of a thin film and (2) initiation of thin-film rupture. The first step corresponds to the flocculation (reversible) and coagulation (irreversible) of the emulsion droplets (steps A and B in Fig. 3). The second step corresponds to the actual irreversible process of coalescence (steps C and D in Fig. 3). A detailed treatment on this subject in terms of the characteristic times for flocculation, coagulation, and film rupture has been given by Dukhin et al. (37). Which of the two main steps will be rate determining not only depends on the properties of the adsorbed layer but also on many other aspects, such as the droplet-size distribution, the volume fraction of droplets and the presence of liquid flow. These two main steps will be discussed in Sections III.A and III.B.

A. Initiation of Thin-Film Rupture

Film rupture is the final step of the coalescence process. It is initiated by the formation of a hole larger than a critical size in the thin film, leading to the merging of two droplets into one (Fig. 3, step C). Hole formation may have a number of causes, of which vacancies in the adsorbed layer, spontaneous passage formation and rupture by film stretching are the most important.

1. Rupture by the Presence of Vacancies

This mechanism prevails if the adsorption is below saturation adsorption, where part of the droplet surface remains uncovered by an adsorbed layer. If the adsorbed molecules attract each other, a two-dimensional phase separation between closed-packed molecules and empty regions (“vacancies”) will take place (Fig. 4). Film rupture is initiated if sufficiently large vacancies

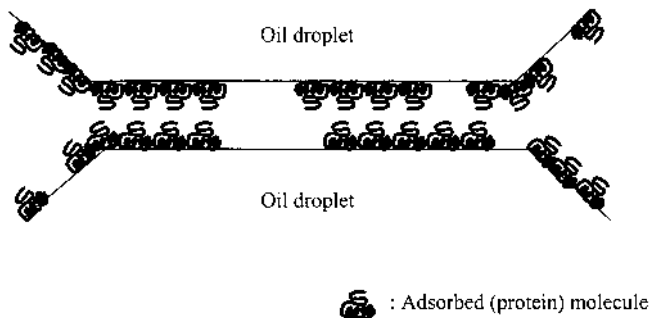


Figure 4 Sketch of a thin film between emulsion droplets, with vacancies in the adsorbed layer due to unsaturation of the adsorbed layers.

adjoin on both sides of the thin film. The lifetime of such a film then depends on nucleation and growth of these vacancies. This mechanism was modelled by Kashchiev and Exerova (38) and Exerova and Nikolova (39) to calculate the lifetime of surfactant bilayer films (which are equivalent to Newton black films).

Slightly below saturation adsorption of the surfactants in the adjacent monolayers, the model predicts a sharp transition toward very high stability of the bilayer. Also, for protein-stabilized films, a similar sharp transition in thin-film stability was found when the adsorption density reached saturation adsorption (40,41).

2. Rupture by Spontaneous Passage Formation

Here, a “passage” or “neck” is defined as a canal of the dispersed liquid passing through the sheet of thin film, in which the surface between the canal and the thin-film liquid is covered by an adsorbed layer. In this way, the surface of the passage forms a continuous bridge between the surfaces of the adjoining emulsion droplets (Fig. 5). Theories for the initiation of rupture by spontaneous passage formation have been developed mainly for surfactant-stabilized emulsions.

De Vries (42) described initiation of rupture of common black films by calculating the energy barrier related to the area increase needed to form a passage through the layer of liquid water. Related to this is a theoretical treatment by Harbich et al. (43) for the energy barrier involving passage formation in vesicles and lamellar phases. Later, Kozlov and Markin (44) extended this treatment by incorporating curvature components of the surface tension to describe the energy effect involved in the surface-topological transition of merging two droplets into one. Recently, Kabalnov and

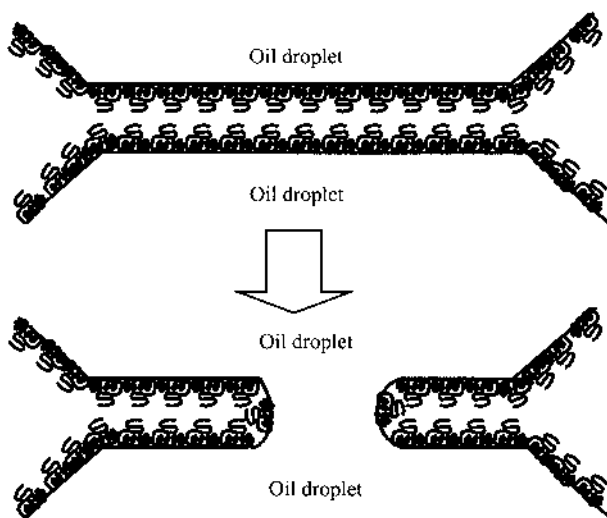


Figure 5 Sketch of rupture of a thin film between adjacent emulsion droplets, due to the formation of a passage through the thin film.

Wennerström (34) further developed this approach for the formation of a passage in thin films between emulsion droplets stabilized by low-molecular-weight surfactants for temperatures close to the phase-inversion temperature. In this “oriented-wedge theory,” the formation of a passage through a thin film of the continuous liquid is strongly inhibited if the surfactant tends to form micelles in the continuous phase (Fig. 6). This mechanism seems to be unimportant for emulsions stabilized by only protein, because of the thickness and hydrophilicity of the adsorbed layer (40).

3. Rupture by Film Stretching

Thin films may rupture when they are stretched at such a speed that the reduction of the adsorption density of the stabilizing surface-active material cannot be restored by adsorption from the bulk or by lateral mobility of adsorbed material. Stretching then leads to depletion of adsorbed material in the adsorbed layers, which may induce rupture by the presence of vacancies (Section III.A.1). This may occur for emulsion stabilizers that form relatively immobile films and are dissolved in the continuous liquid, which makes transport toward the middle of the thin film a slow process. These requirements are met for adsorbed protein layers (Section I.B). For thin films stabilized by cohesive layers of adsorbed

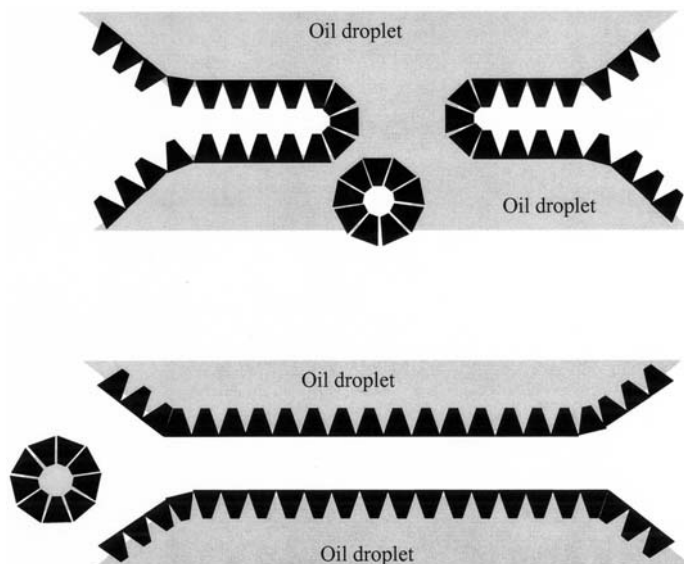


Figure 6 Oriented-wedge model for film-stabilizing properties of low-molecular-weight surfactants. The surfactant molecules are depicted as wedges, with the broader side oriented either to the oil phase (upper diagram) or the aqueous phase (lower diagram). The upper case corresponds to low-hydrophilic-lipophilic-balance (low-HLB) surfactants, which are able to form micelles in the oil phase and easily form a passage through an aqueous thin film, therefore not suited to stabilize oil-in-water emulsions. The lower diagram corresponds to high-HLB surfactants, which are able to form micelles in the aqueous phase and inhibit the formation of a passage through the aqueous film, therefore suited to stabilize oil-in-water emulsions.

protein molecules (Section I.B), we may also expect that initiation of rupture corresponds to fracturing of these adsorbed layers.

An additional requirement of this film rupturing mechanism is that external forces exerted on the emulsion lead to stretching of the thin films. This will only occur if external forces exerted on an emulsion are transferred onto the thin film in a direction parallel to the thin film. As a consequence, this mechanism will not be effective in relatively dilute, unaggregated emulsions under quiescent or gentle-flow conditions.

Rupture by film stretching was shown to occur in highly concentrated emulsions stabilized by protein (40,45–47). Emulsions are said to be highly concentrated whenever the volume fraction of the droplets exceeds the limit of close packing (Fig. 7). The starting point for explaining the experimental results is the hypothesis that film stretching occurs in these systems if externally applied stresses cannot relax sufficient by flow in the emulsion (46).

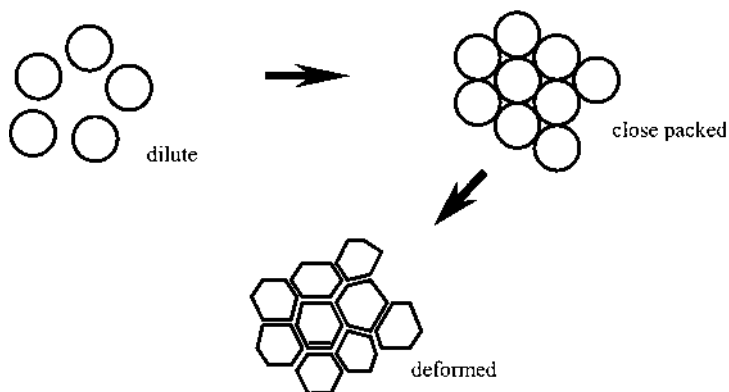


Figure 7 Formation of a highly concentrated emulsion by removal of the aqueous phase.

This occurs when slip between the droplet surfaces is inhibited by the presence of shear-resisting connections between the adsorbed layers of adjacent droplets (47). Van Aken et al. (46) suggested that the formation of shear-resisting connections is closely related to the transition of CBF to NBF that was discussed in the context of droplet aggregation in dilute emulsions stabilized by whey protein in Section II. B. Nuclear magnetic resonance (NMR) mobility measurements of water molecules pointed out that a state corresponding to a Newton black film (essentially no free water between the adsorbed layers forming the thin film) can indeed be obtained in a highly concentrated emulsion stabilized by β -lactoglobulin (48).

Similarly to the bonds formed in dilute emulsions stabilized by whey protein, the shear-resisting connections are probably formed by strongly attractive short-range forces such as hydrophobic interaction (47). They were shown to form between adsorbed protein layers of both β -lactoglobulin and β -casein when the droplet surfaces were pushed together with sufficiently large pressure (46). It was argued that this critical pressure is related to a pressure-induced jump over the kinetic barrier that is related to the transition of CBF to NBF. This was supported by kinetic measurements that showed that the rate of formation of shear-resisting connections increases as a function of the applied pressure and the ionic strength, and was strongly enhanced in the presence of calcium ions (47).

This mechanism was shown to be relevant also in a more dilute emulsion of irreversibly aggregated droplets, where deformation of droplet aggregates by shear stresses may cause coalescence of droplets within the aggregate (Fig. 8) (47).

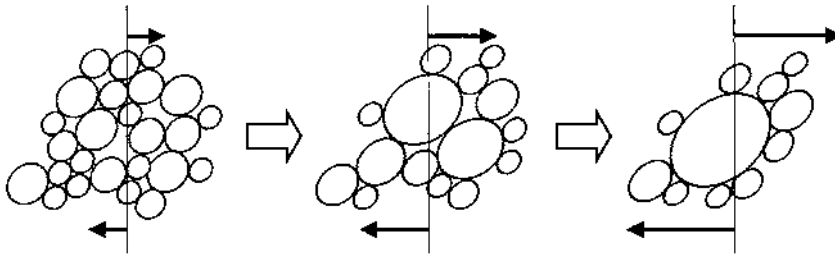


Figure 8 Deformation of a droplet aggregate by external forces, inducing coalescence by stretching of thin films between the droplets because slip between the adsorbed layers of the thin films is inhibited.

B. Encounter of Droplet Surfaces and the Formation of a Thin Film

Before a thin film is formed, two consecutive steps have to take place (Fig. 3). First, the emulsion droplets have to come close together on a colloidal scale-droplet encounter, step A in Fig. 3) and second, a thin film must be formed on a molecular scale (outflow of the continuous phase from the spacing between the droplet and thin-film formation, step B in Fig. 3).

1. Droplet Encounter Under Quiescent and Gentle-Flow Conditions

Droplet encounter may occur through diffusion (in analogy to fast perikinetic flocculation (49,50)) but is strongly accelerated by convection because this increases the encounter rate of the emulsion droplets (in analogy to fast orthokinetic flocculation (51)) and very weak repulsion between the droplet surfaces may be overcome by the shearing force.

The rate of droplet encounters is greatly increased by concentrating the emulsion either by an artificial procedure such as reverse osmosis or centrifugation or spontaneously by creaming (52). The ultimate situation is the previously discussed case of highly concentrated emulsions, in which the droplets are in continuous contact with each other (Fig. 7).

When the surfaces are sufficiently close together, they start to interact, first by hydrodynamic interaction, which retards the outflow of liquid (53–56), but at sufficiently short separation also by dispersion forces between the liquid interiors of the droplets and short-range forces between the adsorbed layers (57). The outflow of liquid becomes retarded if the hydrodynamic repulsion between the approaching droplets deforms the droplets, leading to the formation of a (dimpled) thin film (57). The retardation is enhanced by the elasticity of the adsorbed layers, because this resists the outflow of liquid by the coupling of liquid flow and surface flow (58).

This retardation is of importance mainly if the droplets are relatively large the surface tension is relatively low and under highly dynamic condition, such as during emulsification (58).

Finally, thin spots can form in the remaining liquid film by a spinodal thinning mechanism, described by Scheludko (59) and Vrij (60). This mechanism describes local thinning of a CBF caused by thermal undulations of the film thickness and is commonly accepted as one of the main steps in the process of spontaneous film rupture (61). This mechanism is retarded by increasing the viscosity of the continuous liquid and surface dilational elasticity of the adsorbed layers. Already at a very low surface elastic modulus ($\ll 1$ mN/m), the surface dilational elasticity strongly suppresses the spinodal thinning mechanism (62). This is the case for adsorbed protein layers, because the surface dilational elasticity is usually in the range 20–80 mN/m. Therefore, thinning of protein-stabilized films is strongly retarded and the spinodal thinning process is strongly damped, predicting that also the transition CBF to NBF is strongly retarded for protein-stabilized emulsions, as was indeed observed experimentally (35,63).

2. Droplet Encounter in Turbulent Flow

In turbulent flow, droplets bounce together by inertial forces, which may lead to large droplet deformation and to forces stretching the adsorbed layers and thin films between colliding droplets. Film rupture may then occur by similar mechanisms as described in Section III. A.3. As a first approach to describing homogeneous coalescence induced by turbulent flow, we will estimate the conditions needed for the occurrence of coalescence in highly turbulent flow. In turbulent flow, the outflow of the continuous phase from the spacing between the droplets may be greatly enhanced by the inertial between the droplets when they are bouncing against each other. Walstra and Smulders (64) estimated the magnitude of this pressure from Kolmogorov theory as

$$\Delta p = \varepsilon^{2/3} d^{2/3} \rho^{1/3} \quad (1)$$

where ε is the power density of the turbulent flow, d is the length-scale distance considered, for which we take the droplet diameter, and ρ is the density of the emulsion. The outflowing liquid exerts a shear force onto the adsorbed layers of the thin film, tending to stretch them. This may lead to film rupture by film stretching as described in Section III.A.3 (Fig. 9). This can be quantified by taking into account the surface tension gradient $\Delta\gamma$ along the surfaces of the thin film, which for immobile adsorbed layers

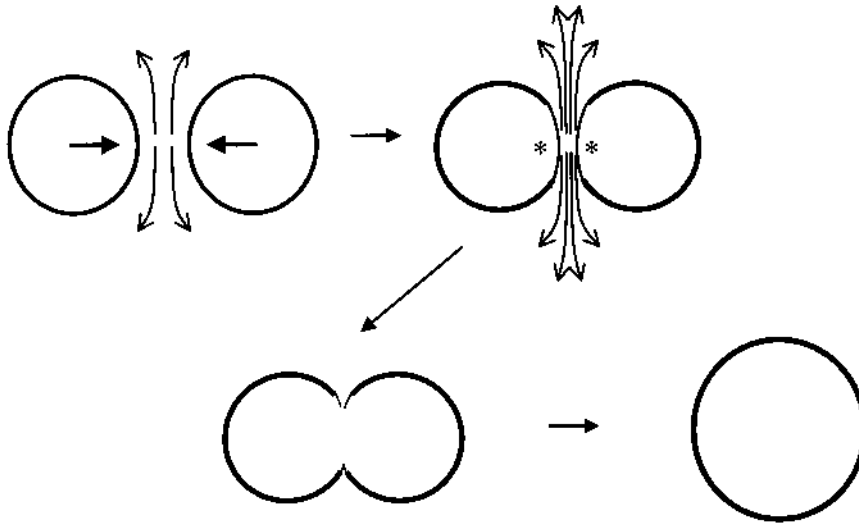


Figure 9 Coalescence induced by film stretching of droplets impacting in highly turbulent flow. The second drawing shows the outflow of continuous liquid from the spacing between the approaching droplets, as shown by flow lines, which drags along the adsorbed layers at the droplet interfaces. This produces a spot with high surface tension and low adsorption density in the thin film, as indicated by the asterisk, initiating film rupture and coalescence.

will be magnitude (64)

$$\Delta\gamma \approx \frac{1}{4}(\Delta p)d \quad (2)$$

Combination with Eq. (1) yields

$$\Delta\gamma = \frac{1}{4}\varepsilon^{2/3}d^{5/3}\rho^{2/3} \quad (3)$$

For $\rho = 1000 \text{ kg/m}^3$ and $d = 10^{-6} \text{ m}$, we find $\Delta\gamma = 2.5 \times 10^{-8} \varepsilon^{2/3}$. For adsorbed proteins, the maximum reduction of the equilibrium surface tension is limited to approximately 0.03 N/m , which is related to the occurrence of collapse of the adsorbed layer above this value. This value may therefore be taken as an estimate of $\Delta\gamma$, although for the very short time scale of droplet impact and the resulting film stretching, higher values may be attainable. Moreover, the actual rupture mechanism will probably be related to fracture of the adsorbed layer rather than collapse. Nevertheless, taking this

estimate for $\Delta\gamma$, coalescence is expected if $\varepsilon > 1.3 \times 10^9 \text{ W/m}^3$. This is much higher than highest value for the power density that can be obtained by a toothed colloid mill in highly viscous emulsions (for this situation, a maximum power density of approximately 10^7 W/m^3 was reported by Karbstein and Schubert (65)). According to Walstra and Smulders, an Ultra-Turrax type of machine and high-pressure homogenisers can produce power densities up to 10^{10} and 10^{12} W/m^3 , respectively (64), which should be sufficient for this coalescence mechanism.

Little experimental evidence on this coalescence mechanism can be found in the literature. One of the few studies on this subject was by Chen et al. (66), who showed an increased rate of coalescence under highly turbulent flow conditions. However, it cannot be excluded that coalescence was caused by the introduction of air (which may lead to air-intermediated coalescence, discussed in Section IV.B) or occurred at the surface of the impeller blade (which may lead to surface-intermediated coalescence, discussed in Section IV. A).

For surfactant-stabilized emulsions, surface-tension gradients may be suppressed by fast exchange of the surfactant from solution. However, in the thin-film region, supply of surfactant from the dispersed phase is much more efficient than from the continuous phase. Therefore, if the surfactant is preferentially dissolved in the dispersed phase, it is more difficult to induce surface-tension gradients and vacancies in the thin-film region, and film thinning will proceed faster than if the surfactant is preferentially dissolved in the continuous phase. However, if the preferential partitioning of the surfactant in the dispersed phase is caused by micelle formation in this phase, the oriented-wedge theory would predict fast film rupture by passage formation in this case (Section III. A. 2).

IV. SURFACE-INTERMEDIATED COALESCENCE

In some cases, a third phase intermediates in the coalescence of emulsion droplets. This class of coalescence mechanisms has received relatively little attention in the literature. Based on general considerations, the critical step must be the rupturing of a thin water film between the droplet and the third phase. The third phase may be solid (e.g., the wall of the processing equipment or the wall of the container in which the emulsion is stored, or a gas, such as the headspace in the container or air bubbles beaten in during pumping or whipping). A special, very important case is the situation where the third phase is formed by small solid particles. These cases will be treated in the following subsections.

A. Coalescence Intermediated by a Solid Surface

Although not much is known about this mechanism, we may expect that coalescence intermediated by a solid surface is related to spreading of the dispersed phase onto this surface (Fig. 10). A crucial requirement for this mechanism must be that the dispersed phase (partially) wets the surface; the contact angle should be lower than 90° or so. The kinetics of this mechanism will be determined by the rupture of the thin (aqueous) film between the droplet and the solid surface, which can be understood as the dewetting of the thin film of the continuous liquid at the solid surface. Dewetting has been described by spinodal dewetting (67) and by nucleation by nanoscale gas nuclei, as first suggested by Derjaguin and Gutop (68).

It has been suggested that coalescence intermediated by a solid surface may occur at the surface of the impeller blades in an agitated vessel, in the context of phase inversion of liquid dispersions (69). The process would be important if the dispersed liquid has a higher density than the continuous liquid, so that the drops are able to reach the impeller surface by inertial impaction, where they may spread at the impeller surface or not, depending on the wetting conditions. Also, for emulsification in a colloid mill, the spreading behavior of the dispersed phase onto the wall of the colloid mill was shown to be important for the efficiency of the emulsification process (70).

B. Coalescence Intermediated by a Liquid Interface

Coalescence intermediated by a liquid interface (the interface between a gas and a liquid or between two immiscible liquids) resembles that at a solid surface, but is different because interfacial flow and area dilations are possible (Fig. 11). A requirement is again that the dispersed phase must spread upon the liquid interface, which is the case for pure triglycerides at pure air–water interfaces. Under quiescent conditions, the liquid interface will be covered by an adsorbed layer of surface-active material supplied by the solution. Emulsion droplets that approach the interface will be repelled by this layer, and on close encounter, a thin film will be formed. The rate

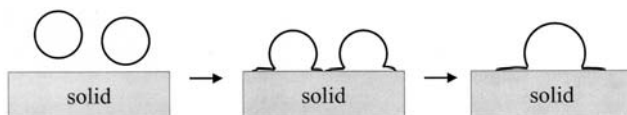


Figure 10 Coalescence intermediated by adsorption and (partial) wetting of droplets on the surface of a solid substrate.

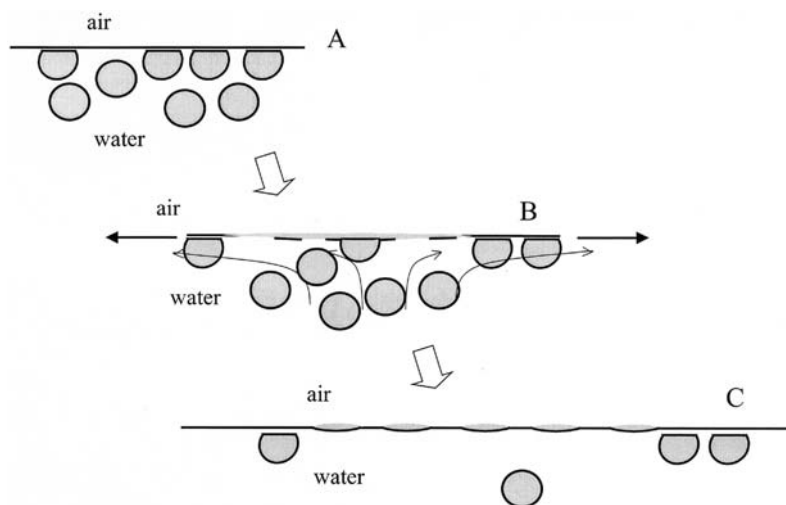


Figure 11 Coalescence intermediated by adsorption and spreading of the droplets at an expanding interface. (A) Droplets do not enter the air–water interface because of the kinetic stabilization by an air–water–oil thin film; (B) expansion of the air–water interface lowers the adsorption density at the air–water interface, leads to convective transport of droplets toward the air–water interface and increases the surface tension of the air–water interface to a value that enables spreading of the liquid oil onto this interface; (C) after spreading, the oil film contracts and breaks up into oil lenses.

of insertion and spreading of these droplets at the interface will then depend on the lifetime of this thin film. If the interface is expanded, the adsorption density at the interface will decrease by an amount that depends on the rate of adsorption of the surface-active material (Fig. 12). Higher expansion rates result in lower adsorption densities and higher surface tensions of the air–water interface. Moreover, if a cohesive adsorbed layer is formed, expansion of this layer may even result in the formation of bare cracks at the air–water interface by fracturing of this layer. In this way, expansion of the air–water interface will lower stability of the thin film between the expanding surface and the emulsion droplet, promoting droplet insertion.

Coalescence intermediated by air was studied at an expanding interface by Hotrum et al. (71) for emulsions stabilized by whey protein and β -lactoglobulin. It was shown that droplet spreading occurred if the air–water interface was expanded at such a rate that the surface tension of the interface exceeded a critical value. This critical value was shown to

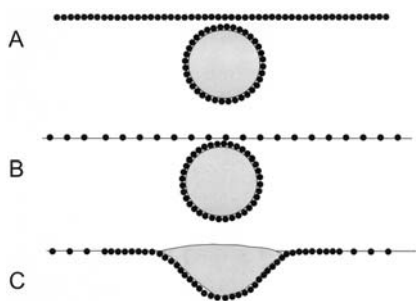


Figure 12 Coalescence intermediated by adsorption and spreading of the droplets at an expanding interface. Sketch showing how expansion of the air–water interface may reduce the stability of the air–water–oil thin film, promoting insertion of droplets at the air–water interface, which may initiate subsequent spreading of droplets. (A) quiescent air–water interface; (B) expanding air–water interface, with reduced adsorption density of surface-active material; (C) situation just after insertion: a lens is formed and surface-active material previously adsorbed on the droplet is transferred to the air–water interface.

correspond to the criterion of spreading of the oil at the air–water interface. Insertion of droplets without spreading should, in principle, be possible at lower expansion rates; however, this was not observed, probably because it is strongly suppressed by the high stability of the thin films between the emulsion droplets and the interface.

A self-amplifying mechanism for droplet spreading at the expanding interface was suggested by Hotrum et al (71). Spreading of oil at an air–water interface is a very fast process, with high expansion rates at the oil–water interface of the spreading emulsion droplet. The rapidly expanding oil–water interface may attract emulsion droplets from the underlying solution by convection, and if the spreading oil film is not sufficiently quickly covered by a protecting adsorbed layer, these droplets immediately coalesce with the spreading oil film. In this way, the spreading oil film is supplied with additional oil from emulsion droplets coalescing with the spreading film, amplifying the process.

After expansion, the spread oil film may be reintroduced into the emulsion in the form of droplets if the air–water interface disappears. In foamed emulsions, this may, for example, occur by coalescence or disproportionation of the gas bubbles. A well-known practical application of this process is the conventional process of butter manufacture by churning, where coalescence of milk fat globules and subsequent clumping to butter granules is intermediated by expanding and disappearing air–water interfaces (1).

Coalescence intermediated by a liquid interface may also be of great importance in several other situations. For example, during whipping of cream, dilating bubble surfaces may cause insertion and (partial) spreading of milk fat globules. When an emulsion is poured, the air–water interface with area A will expand. The expansion rate ($d \ln A/dt$) depends on the pouring rate and presence of surface-active material and will be on the order of 0.1 s^{-1} , similar to expansion rates measured in overflowing cylinders (72) or canals (73). During pumping, air bubbles may be beaten into the emulsion and be strongly deformed, leading to local high expansion rates of the bubble surfaces. On depressurizing or heating an emulsion, dissolved gas may be released as growing gas bubbles. The same may happen if gas is produced by (bio-)chemical reactions (e.g., the release of carbon dioxide during fermentation). In all cases, this may cause insertion and spreading of the emulsion droplets, by an extent that depends on the expansion rate of the interface and the rate of supply of film-stabilizing material from solution.

C. Coalescence by Shearing in Confined Spaces

Probably of great practical importance is the behavior of emulsions when confined to a thin layer between solid surfaces in relative motion to each other (Fig. 13). It is thought that such a situation occurs during oral processing, where the emulsion lubricates the movement between the tongue and palate (74). However, also during processing (e.g., homogenization in a colloid mill) and handling (e.g., spreading of a food emulsion with a knife), similar processes may occur. Obviously, conditions of high shear can easily be obtained in these configurations, but a special situation occurs when the distance between the shearing plates is the same order of magnitude as the droplet size or droplet size aggregates or is smaller than this. This is a largely unexplored field of thin-film tribological behavior, governed by large deformations and breakup of droplets and droplet

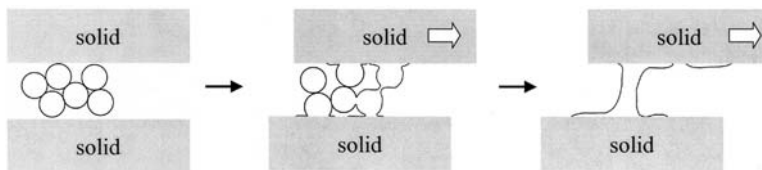


Figure 13 Coalescence induced by shearing in confined spaces. To illustrate possible processes, a combination of homogeneous and surface-intermediated coalescence is sketched for a droplet aggregate sheared between two closely spaced surfaces.

aggregates, droplet coalescence, and the interaction of the droplets with the solid surfaces (wetting, contact angles).

D. Rupture by Penetration of Particles

Film rupture by penetration of particles can be viewed as a special case of surface-intermediated coalescence (Fig. 14). It is a very commonly encountered mechanism. Particles that are fully wetted by either the dispersed liquid or the continuous liquid may puncture the thin film due to mechanical forces. However, often the particles are partially wetted by the other phase (finite contact angle at the oil–water interface), in which case the crystals have the tendency to reside at the oil–water interface and bridge the thin film. The particles may originate from the aqueous phase (e.g., calcium phosphate, lactose) or the oil phase (fat crystals).

Rupture by particles dispersed in the continuous liquid has been studied for foams in relation to antifoam agents (75), but much less for emulsions. De Gennes (76) has described a mechanism for coalescence caused by film rupture by penetration of particles. In this model, a single particle that remains emerged in the continuous phase may lead to a sequence of film ruptures that finally results in a few large droplets embedded in remaining uncoalesced droplets. An example of coalescence caused by penetration of thin films by water-soluble sodium nitrate crystals is shown in Fig. 15. Here, a highly concentrated emulsion, stabilized by whey protein isolate, was dried by exposure to the air. The emulsion was quickly destabilized and separated oil as soon as sodium nitrate, dissolved in the aqueous phase, started to crystallize.

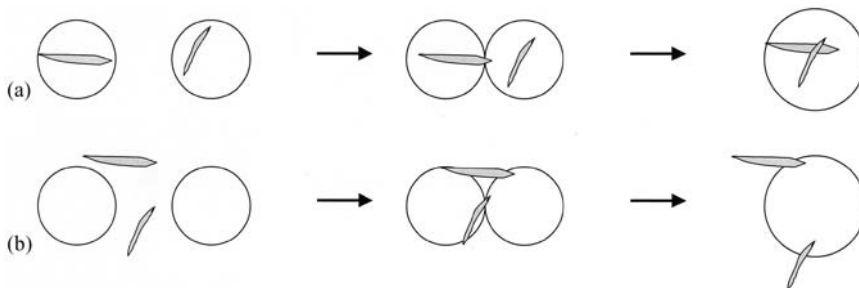


Figure 14 Coalescence intermediated by film penetration by particles suspended in (a) the dispersed oil and (b) the continuous water. The particles may or may not reside at the oil–water interface because of partial wetting by both liquids (as explained in the text).

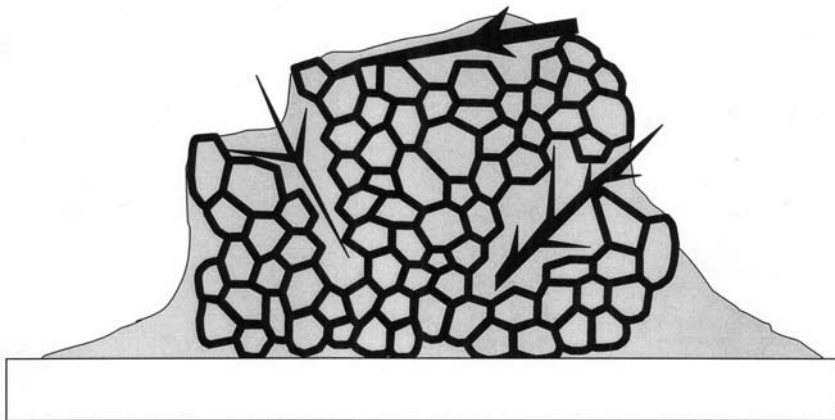
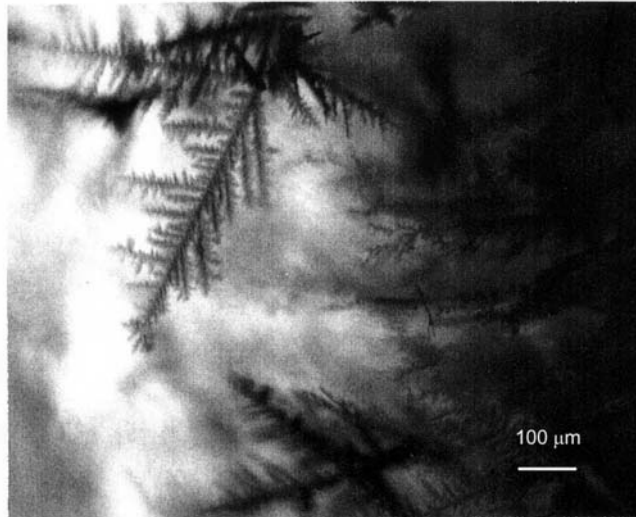


Figure 15 A highly concentrated oil-in-water emulsion (droplet diameter = 1 μm, volume fraction of oil = 0.9), stabilized by whey protein isolate and containing 0.1 *M* sodium nitrate dissolved in the aqueous phase. Visible are sodium nitrate crystals that were formed when the emulsion was dried by exposure to the air. The formation of these crystals lead to rapid separation of oil from the highly concentrated emulsion, which did not occur if a similar highly concentrated emulsion without sodium nitrate was dried. Individual emulsion droplets or separated oil cannot be observed because of the low optical contrast. The drawing shows a sketch of the situation.

An important example of rupture by particles embedded in the dispersed phase is the phenomenon of “partial coalescence,” which has been studied extensively for dairy-related emulsions (77,78). Here, the particles are fat crystals that are present in the oil droplets at the temperature of application. Dependent on the presence of surfactants or polar lipids and on the mobility of the fat crystals inside the droplet, these fat crystals may move to and reside at the oil–water interface, finally leading to rupture of the thin films. Partial coalescence of emulsions of partially crystallized fat leads to the formation of clumps of fat globules, which retain part of their original droplet structure because the fat crystals inhibit the flow of two spherical droplets into one (step D in Fig. 3). In this way, networks of clumped fat globules can be formed, which are important for structuring products such as whipped cream and ice cream.

V. CONCLUSIONS AND PERSPECTIVE

A large number of coalescence processes may be responsible for the coarsening of the droplets in a food emulsions. Fundamental knowledge of these processes is needed in order to distinguish them and to take adequate action to control them. The intention of this work was to give an overview of possible mechanisms, some of which are already known in the literature, but most of them are hardly studied. The present overview may initiate new research in this complex field of coalescence in food emulsions.

REFERENCES

1. H. Mulder and P. Walstra, *The Milk Fat Globule*, Pudoc, Wageningen, The Netherlands, 1974.
2. P. Walstra and R. Jenness, *Dairy Chemistry and Physics*, Wiley, New York, 1984.
3. G. A. van Aken, Aeration of emulsions by whipping, *Colloids Surfaces A* 190, 333–354 (2001).
4. A. Akashe, D. Das, and M. Miller (inventors), Mesophase-stabilized emulsions and dispersions for use in low-fat and fat-free food products, U.S. patent No. 6068876, 2001.
5. C. R. T. Brown, J. E. Homan, M. G. Jones, M. E. Malone, and I. T. Norton, (inventors), Non-frozen, low-fat food emulsions and processes thereof, U.S. patent No. 2001041207, 2001.
6. P. E. A. Smulders, Formation and stability of emulsions made with proteins and peptides, Thesis, Wageningen University, Wageningen, The Netherlands, 2000.
7. G. Schuster, *Emulgatoren für Lebensmittel*, Springer-Verlag, Berlin, 1985.

8. N. J. Krog, Food emulsifiers and their chemical and physical properties, in *Food Emulsions*, K. Larsson and S.E. Friberg,(eds.), K. Marcel Dekker, New York, 1990 pp.127–180.
9. K. D. Schwenke, Proteins: some principles of classification and structure, in *D. Proteins at Liquid Interfaces*, D. Möbius, and R. Miller, (eds.), Elsevier, Amsterdam, 1998, pp.1–50.
10. F. MacRitchie, Reversibility of protein adsorption, in *Proteins at Liquid Interfaces*, D. Möbius, and R. Miller, (eds.), Elsevier, Amsterdam, 1998, pp. 149–177.
11. M. Corredig and D. G. Dalgleish, A differential microcalorimetric study of whey proteins and their behaviour in oil-in-water emulsions, *Colloids Surfaces B* 4, 411–422 (1995).
12. Y. Fang and D. G. Dalgleish, Conformation of β -lactoglobulin studied by FTIR: Effect of pH, temperature, and adsorption to the oil-water interface, *J. Colloid Inter. Sci.*196, 292–298 (1997).
13. E. Dufour, M. Dalgarrondo, and L. Adam, Conformation of β -lactoglobulin at an oil/water interface as determined from proteolysis and spectroscopic methods, *J. Colloid Inter. Sci.* 207, 264–272 (1998).
14. E. Dickinson and Y. Matsumura, Time-dependent polymerisation of β -lactoglobulin through disulphide bonds at the oil–water interface in emulsions, *Int. J. Biol. Macromol.* 13, 26–32 (1991).
15. D. J. McClements, F. J. Monahan, and J. E. Kinsella, Disulfide bond formation affects stability of whey-protein isolate emulsions, *J. Food Sci.* 58, 1036–1039 (1993).
16. E. Dickinson and Y. Matsumura, Protein at liquid interfaces: role of the molten globule state, *Colloids Surfaces B* 3, 1–17(1993).
17. A. Martin, M. Bos, M. A. Cohen Stuart, and T. van Vliet, Stress–strain curves of adsorbed protein layers at the air/water interface measured with surface shear rheology, *Langmuir* 18, 1238–1243 (2002).
18. P. J. Wilde and D. K. Sarker, Enhancement of bubble surface elasticity by crosslinking agents and their effects on protein foam stability, in *Bubbles in Food*. (G. M. Campbell, C. Webb, S. S. Pandiella, and K. Niranjan eds.), American Association of Cereal Chemists, St. Paul, MN, 1999, pp.145–152.
19. B. Ericsson, Lipid–protein interactions, in *Food Emulsions* K. Larsson and S. E. Friberg, eds., Marcel Dekker, New York, 1990, pp. 181–201.
20. A. R. Mackie, P. A. Gunning, P. J. Wilde, and R. J. Morris, Competitive displacement of β -lactoglobulin from the air/water interface by sodium dodecyl sulfate, *Langmuir* 16, 8176–8181 (2000).
21. A. R. Mackie, P. A. Gunning, P. J. Wilde, and V. J. Morris, Orogenic displacement of protein from the oil/water interface, *Langmuir* 16, 2242–2247 (2000).
22. P. W. J. R. Caessens, S. Visser, H. Gruppen, G. A van Aken, and A. G. J. Voragen, Emulsion and foam properties of plasmin derived β -casein peptides, *Int. Dairy J.* 9, 347–351 (1999).
23. P. W. J. R. Caessens, W. F. Daamen, H. Gruppen, S. Visser, and A. G. J. Voragen, β -Lactoglobulin hydrolysis. 2. Peptide identification, SH/SS

- exchange, and functional properties of hydrolysate fractions formed by the action of plasmin, *J. Agric. Food Chem.* 47, 2980–2990 (1999).
24. S. Odake, J. P. Roozen, and J. J. Burger, Effect of saliva dilution on the release of diacetyl and 2-heptanone from cream style dressings, *Nahrung* 42, 385–391 (1998).
 25. L. M. Beidler, Saliva. Its functions and disorders, in *Handbook of Olfaction and Gustation* (R.L. Doty, ed.), Marcel Dekker, New York, 1995, pp. 503–519.
 26. R. D. Vold and R. C. Groot, An ultracentrifugal method for the quantitative determination of emulsion stability, *J. Phys. Chem. (Ithaca)* 66, 1969–1975 (1962).
 27. P. J. Atkinson, E. Dickinson, D. S. Horne, and R. M. Richardson, Neutron reflectivity of adsorbed beta-casein and beta-lactoglobulin at the air/water interface, *J. Chem. Soc. Faraday Trans.* 91, 2847–2854 (2001).
 28. A. Kulmyrzaev, R. Chanamai, and D. J. McClements, Influence of pH and CaCl₂ on the stability of dilute whey protein stabilized emulsions, *Food Res. Int.* 33, 15–20 (2000).
 29. S. P. F. M. Roefs and H. A. Peppelman, Aggregation and gelation of whey proteins: Specific effect of divalent cations? in *Food Colloids: Fundamentals of Formulation*, (E. Dickinson and R. Miller, eds.), Royal Society of Chemistry, Cambridge, 2001, pp. 358–368.
 30. O. D. Velev, B. E. Campbell, and R. P. Borwankar, Effect of calcium ions and environmental conditions on the properties of β -casein stabilized films and emulsions, *Langmuir* 14, 4122–4130 (1998).
 31. S. Damodaran and K. Anand, Sulfhydryl–disulfide interchange-induced interparticle protein polymerisation in whey protein-stabilized emulsions and its relation to emulsion stability, *J. Agric. Food Chem.* 45, 3813–3820 (1997).
 32. D. J. McClements, *Food Emulsions: Principles, Practice and Techniques*, CRC Press, Boca Raton, FL, 1999.
 33. D. C. Clark, R. Dann, A. R. Mackie, J. Mingins, A. C. Pinder, P. W. Purdy, E. J. Russell, L. J. Smith, and D. R. Wilson, Surface diffusion in sodium dodecyl sulfate-stabilized thin liquid films, *J. Colloid Interf. Sci.* 138, 195–206 (1990).
 34. A. Kabalnov and H. Wennerström, Macroemulsion stability: The oriented wedge theory revisited, *Langmuir* 12, 276–292 (1996).
 35. D. C. Clark, M. Coke, A. R. Mackie, A. C. Pinder, and B. Wilson, Molecular diffusion and thickness measurements of protein-stabilized thin liquid films, *J. Colloid Interf. Sci.* 138, 207–219 (1990).
 36. B. Biswas and D. A. Haydon, The coalescence of droplets stabilised by viscoelastic adsorbed films, *Kolloid Z.* 185, 31–38 (1962).
 37. S. S. Dukhin, J. Sjöblom, D. T. Wasan, and Ø. Sæther, Coalescence coupled with either coagulation or flocculation in dilute emulsions, *Colloids Surfaces A* 180, 223–234 (2001).
 38. D. Kaschiev and D. Exerova, Nucleation mechanism of rupture of Newtonian black films, *J. Colloid Interf. Sci.* 77, 501–511 (1980).
 39. D. Exerova and A. Nikolova, Short-range molecular interactions and stability of amphiphile bilayers, *J. Dispers. Sci. Technol.* 18, 683–697 (1997).

40. G. A. van Aken and F. D. Zoet, Coalescence in highly concentrated coarse emulsions, *Langmuir* 16, 7131–7138 (2000).
41. S. Tcholakova, N. D. Denkov, I. B. Ivanov, and B. Campbell, Coalescence in β -lactoglobulin stabilized emulsions: Effects of protein adsorption and drop size, *Langmuir* 18, 8960–8971 (2002).
42. A. J. de Vries, Foam stability, *Rec. Trav. Chim.* 77, 383–399 (1958).
43. W. Harbich, R. M. Servuss, and W. Helfrich, Passages in lecithin-water systems, *Z. Naturforsch.* 33a, 1013–1017 (1978).
44. M. M. Kozlov and V. S. Markin, *Biofizika* 28, 242 (1983).
45. G. A. van Aken and T. van Vliet, Mechanisms of coalescence in highly concentrated protein-stabilized emulsions, in *Food Colloids Fundamentals of Formulation* (E. Dickinson and R. Miller, eds.), The Royal Society of Chemistry, Cambridge, 2001, pp. 125–132.
46. G. A. van Aken, Flow-induced coalescence in protein-stabilized highly concentrated emulsions, *Langmuir* 18, 2549–2556 (2002).
47. G. A. van Aken and T. van Vliet, Flow-induced coalescence in protein-stabilized highly concentrated emulsions: role of shear resisting connections between the droplets, *Langmuir* 18, 7364–7370 (2002).
48. G. A. van Aken, F. D. Zoet, and J. Diederer, Composition of thin films between emulsion droplets stabilized by protein, as measured in highly concentrated emulsions, *Colloids Surfaces B* 26, 269–279 (2002).
49. M. von Smoluchowski, *Phys. Z* 17, 557–585 (1916).
50. M. von Smoluchowski, *Z. Phys. Chem.* 92, 129 (1917).
51. T. G. M. van de Ven, *Colloidal Hydrodynamics*, Academic Press, London, 1988.
52. S. Kumar, G. Narshimhan, and D. Ramkrishna, Coalescence in creaming emulsions. Existence of a pure coalescence zone, *Ind. Eng. Chem. Res.* 35, 3155–3162 (1996).
53. B. V. Derjaguin and V. M. Muller, *Dokl. Akad. Nauk. SSSR (Eng.)* 176, 738 (1967).
54. E. P. Honig, G. J. Roebertsen, and P.H. Wiersema, Effect of hydrodynamic interaction on the coagulation rate of hydrophobic colloids, *J. Colloid Interf. Sci.* 36, 97–109 (1971).
55. L. A. Spielman, Viscous interactions in Brownian coagulation, *J. Colloid Interf. Sci.* 33, 562–671 (1970).
56. S. Hartland, Coalescence in dense-packed dispersions, in *Thin Liquid Films* (I. B. Ivanov, eds.), Marcel Dekker, New York, 1988, pp 663–766.
57. O. D. Velev, K. D. Danov, and I. B. Ivanov, Stability of emulsions under static and dynamic conditions, *J. Dispers. Sci. Technol.* 18, 625–645 (1997).
58. P. Walstra and P. E. A. Smulders, Making emulsions and foams :an overview, in *Food Colloids; Proteins, Lipids and Polysaccharides* (E. Dickinson and B. Bergenståhl, eds.), The Royal Society of Chemistry, Cambridge 1997, pp. 367–381.
59. A. Scheludko, Thin liquid films, *Adv. Colloid Interf. Sci.* 1, 391–464 (1967).
60. A. Vrij, Possible mechanism for the spontaneous rupture of thin, free liquid films, *Discuss. Faraday Soc.* 42, 23–33 (1966).

61. I. B. Ivanov and D. S. Dimitrov, Thin film drainage, in *Thin Liquid Films: Fundamentals of Application* (I. B. Ivanov, ed.), Marcel Dekker, New York, 1988, pp. 379–496.
62. A. Vrij, F. T. Hesselink, J. Lucassen, and M. van den Tempel, Waves in thin liquid films. II. Symmetrical modes in very thin films and film rupture, *Proc. K. Ned. Acad. Wet. B* 73, 124–135 (1970).
63. M. Coke, P. J. Wilde, E. J. Russell, and D. C. Clark, The influence of surface composition and molecular diffusion on the stability of foams formed from protein/surfactant mixtures, *J. Colloid Interf. Sci.* 138, 489–504 (1990).
64. P. Walstra and P. E. A. Smulders, Emulsion formation, in *Modern Aspects of Emulsion Science* (B. P. Binks, eds.), The Royal Society of Chemistry, Cambridge, 1998, pp. 56–99.
65. H. Karbstein and H. Schubert, Developments in the continuous mechanical production of oil-in-water macro-emulsions, *Chem. Eng. Proc.* 34, 205–211 (1995)
66. J. Chen, E. Dickinson and G. Iveson, Interfacial interactions, competitive adsorption and emulsion stability, *Food Struct.* 12, 135–146 (1993).
67. H. J. Schulze, K. W. Stöckelhuber, and A. Wenger, The influence of acting forces on the rupture mechanics of wetting films–nucleation or capillary waves, *Colloids Surfaces A* 192, 61–72 (2001).
68. B. V. Derjaguin and Yu. V. Gutop, *Doklad. Akad. Nauk SSSR* 153, 859 (1963).
69. S. Kumar, R. Kumar, and K. S. Gandhi, Influence of the wetting characteristics of the impellor on phase inversion, *Chem. Eng. Sci.* 46, 2365–2367 (1991).
70. J. T. Davies, *Emulsions*, Academic Press, New York, 1964, pp. 129–167.
71. N. E. Hotrum, T. van Vliet, M. A. Cohen Stuart, and G. A. van Aken, Monitoring entering and spreading of emulsion droplets at an expanding air/water interface: a novel technique, *J. Colloid Interf. Sci.* 247, 125–131 (2002).
72. D. J. M. Bergink-Martens, H. J. Bos, and A. Prins, Surface dilation and fluid dynamical behaviour of newtonian liquids in an overflowing cylinder, II. Surfactant solutions, *J. Colloid Interf. Sci.* 165, 221–228 (1994).
73. C. G. J. Bisperink, The influence of spreading particles on the stability of thin liquid films, Thesis, Wageningen University, Wageningen, The Netherlands, 1997.
74. S. Giasson, J. Israelachvili, and H. Yoshizawa, Thin film morphology and tribology study of mayonnaise, *J. Food Sci.* 62, 640–646 (1997).
75. P. R. Garrett, Recent developments in the understanding of foam generation and stability, *Chem. Eng. Sci.*, 48, 367–392 (1993).
76. P. G. de Gennes, Two remarks on wetting and emulsions, *Colloids Surfaces A* 186, 7–10 (2001).
77. K. Boode and P. Walstra, Partial coalescence in oil-in-water emulsions. 1. Nature of the aggregation, *Colloids Surfaces A* 81, 121–137 (1993).
78. K. Boode, P. Walstra, and A. E. A. de Groot-Mostert, Partial coalescence in oil-in-water emulsions. 2. Influence of the properties of the fat, *Colloids Surfaces A* 81, 139–151 (1993).

9

Orthokinetic Stability of Food Emulsions

Siva A. Vanapalli

University of Michigan, Ann Arbor, Michigan, U.S.A.

John N. Coupland

The Pennsylvania State University, University Park, Pennsylvania, U.S.A.

I. INTRODUCTION

Many foods and food ingredients are oil-in-water emulsions. The functional properties of the emulsion depend on its microstructure, which is, in turn, controlled by the ingredients and processes used. Thus, it is useful to establish predictive links between (a) ingredients/process and microstructure and (b) microstructure and functionality. In the present context, our main concern is how shear, which is ubiquitous to almost all process operations, influences droplet aggregation (a microstructural feature) in emulsions.

There are very many mechanisms by which emulsions may break down, perhaps the most important are flocculation and, in the case of semicrystalline droplets, the related phenomenon of partial coalescence. Both mechanisms lead to the formation of extensive networks of droplets that can increase the viscosity of a product and lead to eventual coalescence and oiling-off (1). Flocculation can occur by a number of mechanisms and cause a wide range of changes in bulk functional properties, but in all cases, we can identify the fundamental event as two isolated droplets being held at a finite separation for a significant period of time. There must be a minimum in the interdroplet pair potential to hold the particles together, but to reach this separation, the droplets must first approach one

Table 1 Typical Shear Rates Encountered in Food Emulsions

Situation operation	Shear rate (s ⁻¹)
Creaming	10 ⁻⁶ –10 ⁻³
Pouring	10 ⁻² –10 ²
Chewing and swallowing	10 ¹ –10 ²
Mixing and stirring	10 ¹ –10 ³
Pumping	10 ⁰ –10 ³

Source: Adapted from Refs. 2 and 3.

another. It is here that applied shear forces have their greatest effect. Droplets encounter one another in a quiescent fluid through Brownian motion, but this rate may be increased by imposed movement in the fluid. Additionally, the kinetic energy of a particle may enable it to overcome local repulsion in the pair potential and allow droplets to aggregate, or the shear forces may rupture existing flocs. The relationships between applied flow and structure is further complicated by the fact that the structures formed and broken will, in turn, affect the emulsion viscosity and, hence, the rate of strain caused by an applied stress.

Despite the wide range of shear forces at all stages of food preparation and use (see Table 1) and their theoretical importance on emulsion stability, there have been very limited quantitative considerations of shear as a variable in the food science literature. This work is an attempt to summarize the basic theories of particle aggregation under shear in a format useful for food scientists and, second, to review some of the studies of the effects of shear on the stability of emulsions. Our major focus is on floc formation and fracture and we neglect the related topic of emulsion formation (see Ref. 4). We similarly neglect any treatment of the effects of emulsion structure on the shear properties of the bulk fluid [i.e., emulsion rheology (5)]. We begin by reviewing the fundamental Smoluchowski theory of colloidal aggregation and some of the more recent attempts to deal with its limitations. We next consider trajectory analysis, which is a complementary approach to Smoluchowski theory. Finally, we review some experimental studies on orthokinetic stability relevant to food emulsions.

II. THEORETICAL APPROACHES

The mechanism of aggregation involves two major steps: the *transport* step, leading to collision between two droplets, and the *attachment* step, in which the droplets stick to each other. Collisions occur due to local variations in

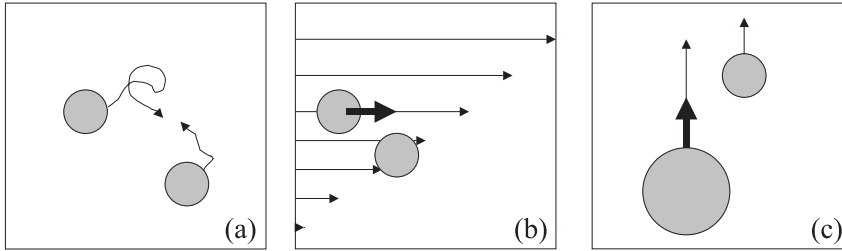


Figure 1 Various mechanisms of particle collision: (a) perikinetic, particles move by random Brownian motion and collide; (b) orthokinetic, particles move in a velocity gradient and the velocity difference between two particles leads to collision; (c) differential, particles cream at different rates because of their different sizes and the velocity gradient leads to a collision.

fluid/droplet velocities arising from (a) random thermal movement of droplets due to Brownian motion (*perikinetic* flocculation), (b) externally imposed velocity gradients from mixing (*orthokinetic* flocculation), and (c) differences in creaming velocities of individual droplets (*differential* flocculation) (Fig. 1). In general, for particle sizes $> 1 \mu\text{m}$, perikinetic aggregation becomes less significant and orthokinetic aggregation predominates (6). For particle sizes $> 10 \mu\text{m}$, differential flocculation becomes important (7).

The flux of particles through a collision surface is typically represented by the *collision frequency*. Because not all collisions lead to attachment, *collision efficiency* is used to describe the percentage of collisions that lead to aggregation. Collision efficiency is governed by the interdroplet potential arising from the sum of colloidal and hydrodynamic interactions. The rate of droplet flocculation (J) can be taken as the product of a collision rate and collision efficiency, so that

$$J_{ij} = \alpha \beta_{ij} n_i n_j \quad (1)$$

where α denotes the collision efficiency (whose value lies between 0 and 1) and β_{ij} is the collision frequency between droplets of size i and j and n_i and n_j are the number concentrations of droplets of sizes i and j , respectively. The product $\alpha \beta_{ij}$ represents the number of successful collisions leading to flocculation and is, therefore, sometimes referred to as *flocculation frequency*. The creation of an aggregate of a given size necessarily means the loss of one or two aggregates of another size, hence, the changing number in a given size class can be represented by a population balance equation:

$$\frac{dn_p}{dt} = \frac{1}{2} \sum_{i+j=p} \alpha_{ij} \beta_{ij} n_i n_j - \sum_{i=1}^{\infty} \alpha_{ip} \beta_{ip} n_i n_p \quad (2)$$

The first term on the right-hand side denotes the formation of particles of size p due to aggregation of particles of sizes i and j (e.g., a single particle, $i=1$, and an aggregate containing five particles, $j=5$, will form an aggregate composed of six particles, $p=6$). The factor of $\frac{1}{2}$ is to compensate for counting the same collisions twice. The second term represents the loss of particles of size p due to collision with other particles. Equation (2) summarizes the information we need to properly understand the kinetics of particle aggregation [i.e., $n_p(t)$], but, in practice, it is too complex to be of direct value. For each value of p in Eq. (2), there is a differential equation to be solved (assuming α_{ij} and β_{ij} are known). A realistic aggregate may contain several hundred particles, at which point the complexity is overwhelming. The useful theory arises from attempts to find a workable approximation to Eq. (2).

A. Smoluchowski Theory

The first attempt to describe the flocculation process in a population of particles was made by von Smoluchowski (8), who started by making several significant assumptions (listed in Table 2). Using these assumptions, Smoluchowski derived simple analytical expressions of collision frequency under perikinetic and orthokinetic conditions as shown in Eqs. (3) and (4), respectively:

$$\beta_{ij,\text{perikinetic}} = \frac{2kT}{3\mu} \quad (3)$$

$$\beta_{ij,\text{orthokinetic}} = \frac{4\gamma}{3} a^3 \quad (4)$$

where k is the Boltzmann constant, T is the temperature, μ is the viscosity of the continuous phase, a is the droplet diameter, and γ is the velocity

Table 2 Assumptions Used by von Smoluchowski in Deriving Particle Collision Rates

-
1. Particles are spherical after collision.
 2. All collisions lead to immediate and complete coalescence (i.e., collision efficiency α equals unity and no colloidal or hydrodynamic forces exist).
 3. There is no fracture of particles or aggregates.
 4. Fluid motion is exclusively either diffusional or exclusively laminar shear.
 5. Particles are of identical size.
 6. Only two-particle collisions occur.
-

Source: Ref. 8.

gradient in the fluid. From Eq. (3), it can be seen that the collision frequency for perikinetic flocculation is independent of droplet size. To the contrary, for orthokinetic flocculation, Eq. (4) dictates that the collision frequency should increase with the cubic power of droplet size. Therefore, for fine droplets, applying a shear field may cause little change in the collision rate, whereas for larger droplets, there will be a large increase in the rate. The *total* number concentration (n_t) of the particles at any time t under orthokinetic conditions is given by the solution of the population balance equation (taking into account assumptions in Table 2) as

$$n_t = n_0 \exp\left(-\frac{4\gamma\phi t}{\pi}\right) \quad (5)$$

where n_0 is the initial total concentration of the particles and ϕ is the volume fraction of the particles. Equation (5) predicts that if the assumptions of this model are correct, then the number of particles is predicted to decrease exponentially with time at a rate proportional to volume fraction and shear rate.

Although Smoluchowski theory remains the basis for understanding particle collision rates, there remain fundamental problems. Most of the assumptions listed in Table 2 are violated in real systems and so the collision efficiency term α becomes an adjustable parameter without any theoretical basis. Several approaches have been taken to avoid one or more of the assumptions and, in particular, the methods of trajectory analysis have proved as a useful complementary approach to Smoluchowski theory.

B. Assumptions of Smoluchowski Theory

Smoluchowski theory remains the basis for understanding collision rates in sheared and unsheared emulsions. Several authors have made modifications to the Smoluchowski theory to avoid some of the assumptions violated in real systems. To some extent, it is possible to correct for these assumptions either with an entirely empirical collision efficiency or by using a more rigorous approach such as trajectory analysis (see Section II.C).

In this subsection, we will take the approach of Thomas et al. (9) and reevaluate Smoluchowski's assumptions and how other workers have attempted to deal with violations.

1. Particles Are Spherical in Shape After Collision

Although liquid emulsion droplets are spherical, we are often more concerned with their flocculation rather than calescence and, hence, in the

formation and properties of extended flocs. The Smoluchowski derivation for the rate of aggregation assumes that the particles remain spherical after collision; that is, the volumes of the two particles are additive, so that for an aggregate of N particles each of volume v and radius r , the total volume of the aggregate, V_N , and its radius, R_N , is given as

$$V_N = Nv \quad (6)$$

$$R_N = N^{1/3}a \quad (7)$$

However, experiments on shear-induced aggregation of solid particles have shown that the aggregates are not spherical but rather have an irregular structure (10–12) frequently described using fractal analysis (13,14). For a fractal aggregate, Eq. (7) is written as

$$R_N = N^{1/D}a \quad (8)$$

where D is the mass fractal dimension. If $D=3$ (as assumed in the Smoluchowski approach), then the structure is completely space filling. If $3 > D > 1$, then the volume of the aggregated structure is greater than the summed volume of the parts and so the collision radius of a fractal aggregate is always greater than that for an equivalent spherical aggregate. The lower the fractal dimension, the more open (porous) the aggregate structure. If $D=1$, the aggregated structure is linear, implying an aggregate consisting of a string of particles. Torres et al. (12) obtained a fractal dimension of $D=1.8$ for rapid coagulation under laminar shear flow and have shown that the floc structure (fractal dimension) was independent of shear rate. In addition, their experiments reveal that the floc structure is similar for perikinetic and orthokinetic aggregation, but the growth kinetics are different. Oles (11) showed that the initial growth phase of aggregation can be characterized by a fractal dimension of 2.1 and that later stages of growth yield $D=2.5$.

The presence of fractal flocs has important consequences for particle collision frequencies and efficiencies, as both of them are functions of particle size. In general, a decrease in fractal dimension enhances particle collision rates (15) (due to a larger collision profile) and increases collision efficiency (due to reduced viscous resistance to fluid flow; see Section II.C) (16). For fractal flocs, the orthokinetic collision frequency is similar to the expression developed by Smoluchowski [Eq. (4)] but uses the fractal aggregate radius from Eq. (8):

$$\beta_{ij} = \frac{4\gamma}{3}a^3N^{3/D} \quad (9)$$

2. All Collisions Lead to Immediate and Complete Coalescence

The collision efficiency can take on a value less than 1 because of some repulsive interaction between the approaching particles. This may be due to colloidal forces or the hydrodynamic effects acting on the droplets. Colloidal forces are the result of the various noncovalent interactions that occur between particles. Each interaction decreases in magnitude in a specific manner with separation, and if particles move, they must do so either in response to or in opposition to the sum of forces acting at a given separation. This can be mapped as an interaction pair potential which describes the energy cost to move one particle from infinite separation to a given distance from a second, fixed particle and results from a summation of the various forces acting. One of the most commonly used pair potential is the DVLO potential (given as a sum of electrostatic repulsive and van der Waals attractive forces) and this is illustrated in Fig. 2.

At long separations, the interaction between the particles is effectively zero, but as they approach closer, the repulsive electrostatic interactions dominate over the attractive van der Waals forces and the particles are repulsed. At very close separations, the attractive forces dominate and the particles aggregate. (Note that for hard particles, there will be a very strong short-range steric repulsive force added to prevent coalescence.) The probability of two particles on a collision path approaching one another to the point of impact then depends on their kinetic energy and the potential energy surface over which they move. The important features of the inter-droplet potential are the depth of the close separation energy well and the

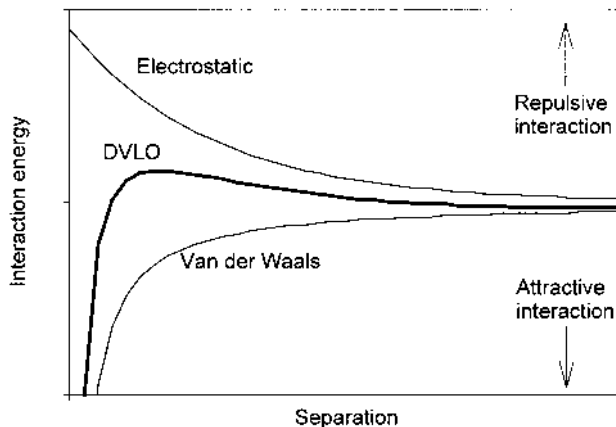


Figure 2 Diagrammatic representation of the DVLO interaction potential.

height of the intermediate separation barrier. Knowing these, it is possible to calculate a value for α under perikinetic conditions (17).

Hydrodynamic forces represent the energy required to make the fluid between the approaching particles to “get out of the way.” They will act against particle approach and are thus repulsive forces. The relative movement of the fluid will also tend to cause approaching particles to rotate and take on a curved trajectory and miss one another. (Trajectory analysis is covered in more depth in Section II.C). Consequently, the presence of hydrodynamic forces will always reduce the collision frequency, sometimes by up to five orders of magnitude, compared to rectilinear trajectories (18). It is possible to calculate the effects numerically (7,18) and it is notable that the most dramatic reduction is in the case of orthokinetic flocculation—particularly with a wide disparity in particle sizes.

The structure of the flocs can affect the colloidal forces acting between them:

- **Impermeable porous flocs.** In the case of impermeable porous flocs (i.e., no passage of fluid through the floc), the collision efficiency (obtained from trajectory analysis) can be corrected for the fact that the van der Waals force between porous flocs is smaller than that of solid particles. This is so because the attractive force between two flocs can be considered to be that between the nearest primary particles, because the other particles in the floc are separated by too large a distance (19). Using this hypothesis, Kusters et al. (16) showed that collision efficiency between impermeable flocs decreases more rapidly with increasing particle size than that for solid particles.
- **Permeable porous flocs.** For permeable porous flocs, the hydrodynamic forces are less pronounced, due to penetration of fluid flow, resulting in higher values of collision efficiencies. The Debye shielding ratio, ξ , defined as

$$\xi = \frac{R}{\sqrt{\kappa}} \quad (10)$$

denotes the extent of passage of fluid flow, where R is the outer radius of floc and κ is the floc permeability. Porous flocs can also be represented using a shell–core model, which has an impermeable core with a completely permeable outer shell. The outer collision radius represents the distance within which another floc must approach for aggregation to occur. The inner impermeable core radius describes the drag experienced by the floc and corresponds to the hydrodynamic radius (R_H). With the knowledge of

hydrodynamic functions for hard spheres (20), the trajectories of the two colliding impermeable flocs are calculated and the outer radius is used to determine the point of contact. In this way, the influence of fluid flow penetration is accommodated in the collision efficiencies that follow from trajectory analysis (see Section II. C). Colloidal forces have not yet been satisfactorily incorporated in this model of floc structure. Nevertheless, the existing shell–core model has been shown to be in good qualitative agreement with the experimental results for aggregate growth under turbulent flow conditions (12,21).

More recently, experiments have demonstrated a nonuniform internal structure of the floc, in contrast to the uniform porosity assumed in the shell–core model (22). Collision efficiency of fractal flocs can be predicted by performing trajectory analysis, using the shell–core model described earlier (16). The floc structure is incorporated into the shell–core model using the Debye-shielding ratio that depends on the outer collision radius (which is a function of fractal dimension).

3. There Is No Fracture of Particles or Aggregates

Although neglected in Smoluchowski theory, in most systems flocs can break under the applied shear forces and the actual size distribution at any given time must account for both formation and destruction rates. The breakup of flocs occurs at a critical shear rate, at which the hydrodynamic force exceeds the attractive forces holding the flocs together; that is,

$$\frac{3}{2}\pi\mu R^2\gamma \leq F_A \quad (11)$$

where R is the floc radius and F_A is the attractive force between the flocs (12). Two distinct modes of floc breakage have been reported in the literature under turbulent conditions: *floc erosion* and *floc fracture* (23). Floc erosion corresponds to the removal of primary particle from the surface of the floc and, in turbulent flow, predominates when floc size is smaller than the Kolmogorov scale. Floc fracture occurs in larger flocs and is due to the fluctuating motion of the fluid. Yeung and Pelton (24) showed experimentally that compact flocs are more susceptible to undergo surface erosion and less compact flocs are likely to fracture. Using a mean-field approach, Sonntag and Russel (25) developed a model for breakup that incorporates floc density in the form of fractal dimension. Their model was able to predict the shear-rate dependence of floc size, although their model neglected the rearrangement of flocs after breakup.

In practice, a flocculating system of particles, subjected to shear will eventually reach a steady state where the rate of floc fracture matches the rate of floc formation. The shear-rate dependence on the maximum stable floc size ($d_{F,\max}$) is given by (26,27):

$$d_{F,\max} = b\gamma^{-m} \quad (12)$$

where b and m are constants determined by the strength of the attractive forces and the internal floc structure, respectively. However, experimental results show that the effects of shear on maximum floc size could be quite complex. For example, restructuring of aggregates was observed at moderate shear rates ($40\text{--}80\text{ s}^{-1}$) but not at lower shear rates (28). Further, longer shearing times could lead to the formation of compact flocs (with higher fractal dimensions) due to restructuring (11,29). If the particle concentration is below a certain critical value, the maximum aggregate size depends only on shear rate, otherwise it is a function of both shear rate and concentration (30).

4. Fluid Motion Is Exclusively Laminar Shear

The approach taken by Smoluchowski was essentially a two-dimensional simplification of three-dimensional laminar flow. In most realistic cases, flow is three dimensional and it is more complex to define the motion of one particle relative to another. Camp and Stein (31) developed an alternative version of Eq. (4), replacing the velocity gradient with the root-mean-square velocity gradient (γ_{rms}), and although this approach is flawed (9), it retains considerable practical value. Root-mean-square velocity was related to the local rate of energy dissipation, ε , in laminar flow and the kinematic viscosity (ν) as

$$\gamma_{\text{rms}} = \sqrt{\frac{\varepsilon}{\nu}} \quad (13)$$

Camp and Stein further extended this idea to turbulent flow by defining a bulk root-mean-square velocity (γ_{rms}^*) in terms of the bulk rate of energy dissipation (ε^*). Incorporating the fractal dimensionality of realistic flocs, the collision rate is given as [see Eqs. (4) and (9)]

$$\beta_{ij} = 10.352 \left(\frac{\varepsilon^*}{\nu} \right)^{1/2} a^3 N^{3/D} \quad (14)$$

5. Particles Are of Identical Size

Although fine liquid droplets are necessarily spherical, real emulsions are rarely monodisperse. Even for a hypothetical monodisperse emulsion,

Smoluchowski's assumption would soon be violated as doublets and triplets formed early in the aggregation process start to take part in further reactions. Solving for all of the rate constants in Eq. (2) is impractical for a large range of sizes; some authors have made assumptions instead about the allowable particle sizes:

- The allowable particle size must follow a predefined mathematical series (e.g., geometric, $n = 1, 2, 4, 8, 16, \dots$). The loss of sensitivity is the cost for the reduced complexity of the calculations.
- The initial particle size distribution displays properties of self-preservation; that is, as the system aggregates, the entire distribution shifts to larger sizes but retains the same shape. In such instances, a correction factor can be introduced to collision efficiency to account for polydispersity (32).

6. Only Two-Particle Collisions Occur

As systems become progressively more concentrated, this assumption becomes less valid; however, the theoretical demands of multibody collisions have not yet been adequately incorporated into Smoluchowski theory.

Despite its limitations, Smoluchowski theory, particularly as modified by Camp and Stein [Eq. (13)], remains the basis for understanding droplet collision behavior. However, as we have seen, it has many limitations restricting its applicability and many of the approaches to deal with its assumptions are largely empirical. A more detailed and fundamental approach can be gained through trajectory analysis.

C. Trajectory Analysis

The limitations of Smoluchowski theory are typically addressed through the adjustable parameter α , the collision efficiency. This approach is broadly macroscopic and allows no detailed description of the nature of the interactions taking place. If we know all of the forces involved, it would be theoretically possible to simulate the aggregation process through computer simulation (Monte Carlo or colloidal dynamics). However, it is often preferred to consider only two-body interactions in more depth. Trajectory analysis is a powerful, although somewhat complex, tool to understand the motion of one particle relative to another, but it is only suitable for two-body interactions and, thus, is only quantitatively valid for very dilute suspensions ($\phi \ll 0.01$). We shall introduce some of the important conclusions from trajectory analysis in the following paragraphs, but for a more in

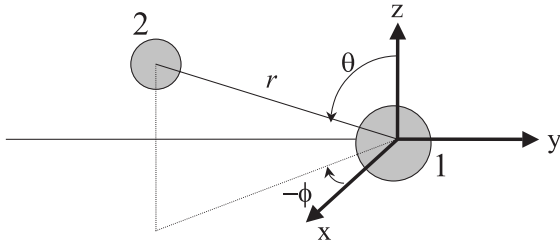


Figure 3 Diagram showing the axis system used for trajectory analysis of the interaction between a reference sphere (1) and a collision sphere (2). The flow direction is along y axis and the velocity gradient is along the x axis.

depth discussion, the reader is advised to refer to Van de Ven's book (33) and a recent review by Vanni and Baldi (34).

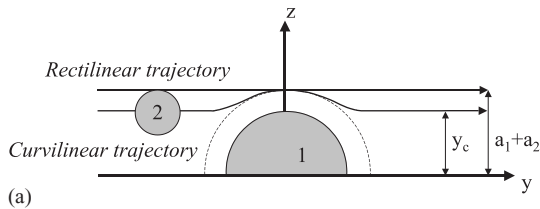
Trajectory analysis is a method to determine the path of interaction of two spheres in a fluid flow. It is assumed that one of the spheres is fixed at the origin (reference sphere) and the relative trajectory of the other sphere (collision sphere) is then calculated (Fig. 3). Another key assumption is that the interaction forces act along the line joining the centers of the two spheres and are balanced by the component of the hydrodynamic force in that direction. The equations governing the trajectories of the two particles in a *simple laminar shear flow* are given by Vanni and Baldi (34):

$$\frac{dr}{dt} = \gamma r(1 - A) \sin^2 \theta \sin \phi \cos \phi + \frac{CE_{\text{int}}}{6\pi\mu a_1} \quad (15)$$

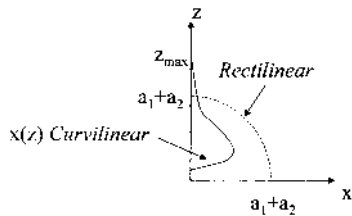
$$\frac{d\theta}{dt} = \gamma(1 - B) \sin \theta \cos \theta \sin \phi \cos \phi \quad (16)$$

$$\frac{d\phi}{dt} = \gamma \left(\cos^2 \phi - \frac{B}{2} \cos 2\phi \right) \quad (17)$$

where γ is the shear rate and the angles θ and ϕ , and the distance r represent the relative positions of the particles in radial coordinates (see Fig. 3). F_{int} is the interparticle pair potential, and A , B , and C are hydrodynamic mobility functions which depend on the dimensionless center distance $r^* = r/a_1$ and on the size ratio $\lambda = a_2/a$ where a is the particle radius and subscripts 1 and 2 refer to the reference and collision spheres, respectively. Approximate



(a)



(b)

Figure 4 (a) Limiting trajectories of the interaction of a collision sphere (2) with a reference sphere (1). The broken circle indicates the region through which sphere 2 must pass to collide with sphere 1. The rectilinear trajectory starts at the minimum distance from the origin for sphere 2 to miss sphere 1 using Smoluchowski assumptions (i.e., rectilinear trajectories). The curvilinear trajectory starts at the minimum distance from the origin for sphere 2 to miss sphere 1 when hydrodynamic forces are included (i.e., curvilinear trajectories). Note that $y_c < a_1 + a_2$ when hydrodynamic forces act, so fewer particles in the flux will collide. Again, the y - x plane is the flow-gradient plane. (b) Collision surfaces calculated from trajectory analysis. The surface marked rectilinear is that predicted from the Smoluchowski (i.e., no colloidal forces acting). The surface marked curvilinear is a sample result that may occur when colloidal and hydrodynamic forces are taken into account. (Adapted from Ref. 34.)

expressions for the hydrodynamic (34) and the interparticle pair potential functions (35) are available in the literature.

The trajectory of the collision sphere is determined by numerically integrating Eqs. (15–17) (Fig. 4a). The numerical integration requires knowledge of the initial position and velocity of the particle. The collision sphere is made to approach the reference sphere from an infinite distance (at least 10 particle separations) and can have 3 possible outcomes. It can undergo collision (i.e., primary coagulation: $r/a_1 < 1 + a_2/a_1 + \varepsilon$,

where ε is a predetermined parameter set in the numerical integration) or orbit around the reference sphere (i.e., secondary coagulation: $\phi > \pi/2$) or simply depart to infinity without contacting the reference sphere ($y/a_1 > 10$). The calculation is repeated from a number of starting positions and a collision surface is mapped.

A collision surface can be calculated as those starting positions for fluid flow that would result in particle collision (Fig. 4b). If interparticle forces and hydrodynamic forces are neglected, then the collision sphere would follow the stream lines of the simple shear flow (i.e., rectilinear trajectories). In such as case, a collision occurs for all particles that move toward the reference particle within the cylinder defined by $a_1 + a_2$. If the distance of approach is greater than this distance, the particles will miss each other. The collision surface in Smoluchowski theory is a circle, whose radius is defined by the distance of limiting trajectory from the origin (i.e., $a_1 + a_2$) (Fig. 4b).

The flux is given by

$$J = \int dJ = \int_s NvZ(s) ds \quad (18)$$

where N is the number of particles crossing the collision surface $Z(s)$ and v represents the particle velocity. Taking $Z(s)$ as a circle of radius $a_1 + a_2$, simple integration yields the Smoluchowski flux equation:

$$J_0 = \frac{4}{3}\gamma N(a_1 + a_2)^3 \quad (19)$$

[Note Eq. (19) is a general case of Eq. (4) for dissimilar particle sizes.] When only hydrodynamic forces are acting, then the trajectories become curvilinear (Fig. 4a) and the definition of the collision surface is no longer obvious (Fig. 4b). The hydrodynamic forces cause the collision particle to roll past the reference particle and miss even though it started within the $a_1 + a_2$ limit for collision if the path had been rectilinear (Fig. 4a; $y_c < a_1 + a_2$). Note that the trajectory is symmetric about the y axis; that is, the positions of the collision particle at the upstream and downstream region are mirror images of each other. The full problem of incorporating colloidal and hydrodynamic forces into trajectory analysis has been solved by various authors (36–39) to calculate the collision surface. The collision surface in this case could be quite irregular, as shown in Fig. 4b. In this case, the flux is given by

$$J = 4\gamma N \int_0^{z_{\max}} xz(x) dx \quad (20)$$

Note that in this case the trajectories are asymmetrical about the y axis, because the collision sphere spends a much longer time in the vicinity of the reference sphere due to the colloidal interaction force. In addition, the curvilinear trajectory in Fig. 4b extends beyond the Smoluchowski limit of $a_1 + a_2$, suggesting that some of the particles may stick in the downstream region after crossing the x - z plane.

The collision efficiency is then given by the ratio of Eqs. (19) and (20) (i.e., the ratio between actual collision rates incorporating all forces and the ideal collision rate with no forces acting):

$$\alpha = \frac{3}{(a_1 + a_2)^3} \int_0^{z_{\max}} xz(x) dx \quad (21)$$

By this method, it is possible to directly calculate the adjustable parameter, α , in Smoluchowski theory from known physical properties of the system. This formulation of trajectory analysis assumes diffusional mobility of the particles is insignificant compared to shear. For particle aggregation under shear flow, Swift and Friedlander (40) showed that the Brownian and bulk convective motion could be treated independent of each other and thus merely added to determine the combined effect; however van de Ven and Mason (41) showed that the additive assumption is incorrect when Brownian effects were large compared to shear forces [i.e., at very low Pe (the Peclet number)].

This analysis is strictly for solid droplets and there are some important differences for fluid particles, which can deform due to the forces acting. The hydrodynamic functions for interacting droplets depend not only on the size ratio of the two droplets and the dimensionless interdroplet distance but also on the droplet–medium viscosity ratio because the particles can deform somewhat to absorb the hydrodynamic stress (42,43).

III. EXPERIMENTS IN FOOD SYSTEMS

Finally, we shall consider some of the experimental studies on food emulsion stability that have considered shear as a variable. Most of the orthokinetic studies in food emulsions have been done in fairly concentrated emulsions (10–30 wt%) and will be reviewed first. Later, we will examine recent work by the Leeds group that has developed a particle capture technique to study interactions between two colloidal particles in a laminar shear field (44).

A. Orthokinetic Studies on Concentrated Emulsions

In experimental studies on shear-induced aggregation of concentrated food emulsions, the measured parameter almost always has been the change in droplet size distribution. The variation in droplet size distributions due to coalescence/flocculation is transformed into a coalescence rate constant or coalescence efficiency, to quantify the effect of shear. In some cases, viscosity is used as a proxy for particle aggregation. Typical results show a sigmoidal function for particle size in time for emulsion destabilization under shear (Fig. 5). In the first portion of the graph, there is no change because the primary droplets have a very low reactivity. However, once a few droplets do aggregate, then the rate of reaction increases with particle size (particularly important for fractal flocs). However, large flocs are eroded (or fractured) by the velocity gradient, and as the size increases, this process will match the rate of aggregation and reach an equilibrium value of particle size. This equilibrium may change if the shear rate is changed or stopped.

1. Emulsions Containing Liquid Droplets

Van Boekel and Walstra studied the effect of laminar Couette flow on the stability of paraffin oil-in-water emulsions stabilized by various surfactants. The experimental rate constant for coalescence (k_{exp}) was taken as the slope of a linear fit to a plot of droplet size with time (on a semilog scale). The theoretical rate constant of coalescence was derived from Smoluchowski rate equation

$$\frac{dn_t}{dt} = -k_{\text{theory}}n_t \quad (22)$$

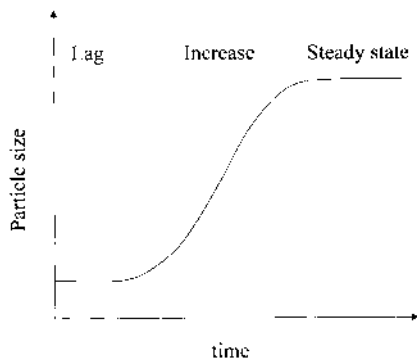


Figure 5 Schematic diagram showing typical changes in particle size for an emulsion undergoing orthokinetic flocculation.

which is obtained by differentiating Eq. 5, where

$$k_{\text{theory}} = \frac{4\gamma\varphi}{\pi} \quad (23)$$

They quantified the effect of shear in terms of coalescence efficiency defined as the ratio of k_{exp} to k_{theory} . The orthokinetic studies showed that emulsions that were stable at rest were also stable during Couette flow (45,46). In addition, they observed that in emulsions that were unstable at rest, Couette flow did not have any significant influence on the rate of coalescence. Increasing the shear rate would increase the frequency of collisions, but these authors argued that it would simultaneously decrease the duration of encounters (i.e., collision efficiency decreased with shear rate in Couette flow). Attempts were made by these authors to increase the orthokinetic collision efficiency through the addition of NaCl, but the emulsions remained resistant to shear-induced coalescence. This led them to suggest that the duration of an encounter is more important than the number of encounters *per se*. In addition, the authors performed trajectory analysis to calculate the collision efficiency for doublet formation, which was much higher than the measured value.

In contrast, under turbulent flow, a dramatic increase in aggregation rate after a few larger, more reactive particles were formed was seen by Dickinson and Williams (47) in a study of the orthokinetic stability of protein-stabilized emulsions. They observed that there was a sharp divergence in d_{32} after an initial lag phase and defined a characteristic destabilization time at the maximum rate of increase in the mean droplet diameter. They proposed the sudden destabilization in terms of an increasing reactivity of droplets with increasing droplet size (α is a strong function of particle diameter), similar to the critical phenomenon in a sol-gel transition (48) and used a two-parameter model to describe the process:

$$\frac{dn_t}{dt} = k_d n_t - k_c n_t^2 \quad (24)$$

where k_d and k_c are the rate constants for disruption and coalescence, respectively. The coalescence rate constant was assumed to depend on droplet size and fractal dimension [see Eq. (9)]. They further invoked a minimum droplet size breakup criterion [see Eq. (11)]. This model showed that a fractal dimension $D \sim 2$ was required to match the experimental data, which is in reasonable agreement with other orthokinetic studies. These and other workers argued that attractive colloidal forces make emulsions more vulnerable to shear-induced aggregation. For example, adjusting the

pH toward the pI of the protein-stabilizing layer (47) and adding calcium to a caseinate-stabilized system (49,50) have all been shown to increase the susceptibility to orthokinetic destabilization. Furthermore, adding a small amount of small-molecule surfactant to a protein-stabilized emulsion increased the orthokinetic destabilization rate without causing significant displacement (51,52). (It was argued that the increased membrane fluidity caused by adsorbed surfactant was responsible.) On the other hand, increased amounts of interfacial protein (presumably forming a thicker layer) decreased the susceptibility to orthokinetic destabilization (50).

As well as increasing the rate of orthokinetic aggregation, increased shear rates can limit the maximum (equilibrium particle size) achieved by increasing the rate of aggregate fracture. For example, Schokker and Dalgleish (50) showed that reciprocal maximum particle diameter was proportional to the shear rate used for a caseinate-stabilized emulsion [i.e., $m = -1$ in Eq. (11)]. Again, by increasing the magnitude of the attractive forces between aggregated particles, which oppose the shear-induced stresses on the floc [e.g., by adding calcium to a caseinate stabilized emulsion (49,50), the final floc size achieved can be increased].

2. Emulsions Containing Semicrystalline Droplets

For liquid-oil emulsions, aggregation is generally due to interactions between the surface layers and the oil composition itself has limited effect. However, in many emulsions of practical interest, the oil phase may be partially crystalline at usage temperatures (46). The crystals can form as spikes at the droplet interface and the crystalline droplets are more reactive toward other semisolid droplets (53). The fat crystals in one droplet induce instability by penetrating the thin film between two approaching droplets and allowing liquid oil to flow out around the interaction site to reinforce the link. This phenomenon is known as partial coalescence because although there is mixing of the oil from two droplets, the crystal network is sufficient to maintain the doublet shape. Completely solid or liquids cannot partially coalesce, as they lack the required liquid or solid fat fraction, respectively. Because partial coalescence requires direct droplet–droplet contact, it would be reasonably expected to be highly dependent on shear rate. Walstra (1) argued that the applied shear (a) increases the collision rate, (b) pushes the colliding droplets closer together so the protruding crystal size approaches the film thickness, and (c) the hydrodynamic forces between the droplets causes the droplets to roll around one another, increasing the probability that a suitable protruding crystal will be able to penetrate the interdroplet membrane.

Partial coalescence is particularly important in milk fat emulsions because butter oil has a wide melting range and under storage conditions ($\sim 5^{\circ}\text{C}$) is semisolid. Milk fat globules are quite stable to coalescence when at rest (except slow creaming). However, it has been shown that liquid milk fat globules are unstable under Couette flow (46), probably because the increased collision rate for the large droplets is sufficient to enhance the rate of partial coalescence. Van Boekel and Walstra (46) observed that the coalescence efficiency remained constant with increasing laminar shear rate, indicating that the rate of coalescence was proportional to the encounter frequency and not the product of frequency and duration, as suggested for liquid-oil emulsions (see above).

Minor components in the fat are very capable of affecting the orientation of crystals to the surface and hence the orthokinetic stability of the semicrystalline emulsion. Davies and others (54) studied the shear stability of partly crystalline triglyceride droplets stabilized with sodium caseinate. The emulsions were quiescently stable but had clear stress limits that, if exceeded, would quickly lead to emulsion destabilization. The magnitude of these stress limits decreased with increasing solid fat content and with increasing added monoglycerides. The monoglycerides were believed to both weaken the protein coat of the droplets and act as a template favoring crystal growth/accumulation at the surface (55). Hinrichs and Kessler (56) also noted the presence of a critical limit in the strain rate required to destabilize milk fat globules. The magnitude of this critical limit decreased linearly with fat volume fraction and increased with solid fat content.

B. Two-Particle Aggregation Under Shear

The macroscopic approaches used in the above-described studies, although practical, does not provide quantitative information regarding the interplay of colloidal and hydrodynamic forces. Recently, the role of such forces in food systems was studied by the Leeds Group using a colloidal particle scattering technique (57–60). In this technique, the capture of one droplet moving in a shear field by a second (fixed) droplet was observed. This microscopic approach yields trajectories of the moving droplet, which were then compared with computer simulations of the trajectories (similar to the trajectory analysis discussed in Section II. C) to obtain quantitative information about dynamic colloidal interactions. In addition, the capture efficiency (which is qualitatively similar to collision efficiency described in Section III. A) was determined, which was defined as the ratio of number of collisions leading to the formation of a doublet to the total number of trials.

The particles used in the particle-scattering technique were latex and emulsion droplets, coated with protein emulsifiers including sodium caseinate, β -casein, and α_{s1} -casein. They observed that in caseinate-stabilized emulsions, the capture efficiency was highest at the isoelectric point (pH = 4.7) (60), as expected from the macroscopic studies (e.g., Ref. 47). To achieve a good fit with the experimental data, it was necessary to develop a theory for the colloidal forces acting between the droplets [see Eq. (15)]. These workers initially used a DLVO potential (as shown in Fig. 2) with an additional DeGennes steric repulsive interaction but this agreed poorly with the data. Further, this model did not predict the observed upstream sticking of the mobile particle to the fixed particle. Only by incorporating a pH-dependent tangential interparticle force, which they hypothesized could arise from entanglement of the adsorbed polymer layers at the interface, were they able to successfully predict the variation of capture efficiency with pH. When ionic strength was included as an additional parameter, the behavior was complex. At lower pH (< 5.2), sticking probability was sensitive to lower values of ionic strengths ($< 0.2 M$), indicating the importance of charged interactions in shear-induced aggregation. At higher ionic strength ($= 0.5 M$), it was unclear as to why the capture efficiency would decrease dramatically.

IV. CONCLUSIONS

We are interested in the changing structure and functionality of food emulsions over long periods of quiescent storage and short periods of varying flow during manufacture and use. The forces acting on the droplets in each case and so the behavior of the emulsions can be very different. Although the basic Smoluchowski approach is often invalid in sheared systems because of the strong effect of hydrodynamic forces, it is possible to use modified theories, particularly in combination with trajectory analysis, to give good predictions of collision rates in dilute emulsions. However, as concentration is increased, the theoretical assumptions are violated and the theories may prove unreliable. Furthermore, the colloidal interaction potential needed for trajectory analysis are difficult to know precisely a priori for a realistic system and can easily become a hidden fitting parameter. The particle scattering approach taken by Dickinson and others (44,57–60) provides a more experimental approach to verify the behavior of pairs of particles, although the possibility of multibody interactions at higher concentrations cannot be considered.

Experimental study of emulsion destabilization in flow is also challenging. Modern rheometers are ideal for providing controlled flow rates

in a fluid, but the characterization of the response of the suspension is more complex. Increased viscosity is a sensitive measure of droplet flocculation (but not to coalescence) and is relatively easy to measure in situ if the rheometer is also used to generate the fluid flow (e.g., Ref. 54). However, although it is possible to infer aggregate structure from rheological measurements, this is an indirect approach. Removing samples from the flow for analysis by conventional light scattering (48) or microscopy (61–64) is possible, but this has the disadvantage of changing the balance of forces acting and possibly the structures present (65). Some authors have combined rheometers and light-scattering instruments to study aggregation under shear, but this is necessarily restricted to dilute systems (12,28,66). Other methods of particle sizing suited to concentrated emulsions, particularly ultrasonic spectroscopy, may be more suited to the study of suspension structure under shear (61,64). Hamberg and others (67) recently used several methods to study the changes in the structure of latex particles covered with whey protein in shear flow. First, by using fluid gelatine solution as the continuous phase, they were able to easily fix samples removed from the rheometer for optical microscopy. Second they used a four-roll mixer to generate a region of laminar shear flow between the rollers and imaged this flow using a confocal laser scanning microscope.

In conclusion, we can expect that the fluid flow to drastically effect emulsion structure and that studies on quiescent systems need not apply when the mixture is sheared. The effects can be both complex and unexpected.

REFERENCES

1. P. Walstra, Emulsion stability, in *Encyclopedia of Emulsion Technology* (P. Becher, ed.), Marcel Dekker, New York, 1996, Chap. 1.
2. H. A. Barnes, Rheology of emulsions—a review, *Colloids Surfaces A* 91, 89–95 (1994).
3. J. F. Steffe, *Rheological Methods in Food Process Engineering*, 2nd ed., Freeman Press, East Lansing, MI, 1996.
4. P. Walstra, Principles of emulsion formation, *Chem. Eng. Sci.* 48, 333–349 (1993).
5. E. Dickinson, Proteins at interfaces and in emulsions. Stability, rheology and interactions, *J. Chem. Soc. Faraday Trans.* 94, 1657–1667 (1998).
6. V. G. Levich, *Physicochemical Hydrodynamics*, Prentice-Hall, Englewood Cliffs, NJ, 1962.
7. M. Y. Han and D. F. Lawler, The (relative) insignificance of g in flocculation, *J. Am. Water Works Assoc.* 84, 79–91 (1992).

8. M. Smoluchowski, Verusch einer Mathematischen Theorie der Koagulationskinetik Kolloider Lösungen, *Z. Phys. Chem.* 92, 129–168 (1917).
9. D. N. Thomas, S. J. Judd, and N. Fawcett, Flocculation modeling: A review, *Water Res.* 33, 1579–1592 (1999).
10. R. C. Klimpe and R. Hogg, Effects of flocculation conditions on agglomerate structure, *J. Colloid Interf. Sci.* 113, 121–131 (1986).
11. V. Oles, Shear-induced aggregation and breakup of polystyrene latex particles, *J. Colloid Interf. Sci.* 154, 351–358 (1992).
12. F. E. Torres, W. B. Russel, and W. R. Schowalter, Flocc structure and growth kinetics for rapid shear coagulation of polystyrene colloids, *J. Colloid Interf. Sci.* 142, 554–574 (1991).
13. B. B. Mandelbrot, *The Fractal Geometry of Nature*, W. H. Freeman, San Francisco, 1982.
14. P. Meakin, Fractal aggregates, *Adv. Colloid Interf. Sci.* 28, 249–331 (1988).
15. Q. Jiang and B. E. Logan, Fractal dimensions of aggregates determined from steady state size distributions, *Environ. Sci. Technol.* 25, 2031 (1991).
16. K. A. Kusters, J. G. Wijers, and D. Thoenes, Aggregation kinetics of small particles in agitated vessels, *Chem. Eng. Sci.* 52, 107–121 (1997).
17. N. Fuchs. Über die stabilität und aufladung der aerosole, *Z. Phys.* 89, 736–743 (1934).
18. D. F. Lawler, Physical aspects of flocculation: From microscale to macroscale, *Water Res.* 27, 164–180 (1993).
19. B. A. Firth and R. J. Hunter, Flow properties of coagulated colloidal suspensions. I. Energy dissipation in the flow units, *Colloid Interf. Sci.* 57, 248–256 (1976).
20. P. M. Adler, Heterocoagulation in shear flow, *J. Colloid Interf. Sci.* 83, 106–115 (1981).
21. K. A. Kusters, The influence of turbulence on aggregation of small particles in agitated vessel, Ph. D. thesis, Eindhoven University of Technology, Eindhoven, 1991.
22. R. C. Sonntag and W. B. Russel, Structure and breakup of flocs subjected to fluid stresses 1. Shear experiments, *J. Colloid Interf. Sci.* 113, 399–413 (1986).
23. K. Muhle, Flocc stability in laminar and turbulent flow, in *Coagulation and Flocculation: Theory and Applications* (B. Dobias, ed.), Marcel Dekker, New York, 1993, pp. 355–390.
24. A. K. C. Yeung and R. Pelton, Micromechanics: A new approach to studying the strength and break-up of flocs, *J. Colloid Interf. Sci.* 184, 579–585 (1996).
25. R. C. Sonntag and W. B. Russel, Structure and breakup of flocs subjected to fluid stresses 2. Theory, *J. Colloid Interf. Sci.* 115, 378–389 (1986).
26. J. C. Flesch, P. T. Spicer, and S. E. Pratsinis, Laminar and turbulent shear-induced flocculation of fractal aggregates, *AIChE J.* 45, 1114–1124 (1999).
27. A. A. Potanin, On the mechanism of aggregation in the shear flow suspensions, *J. Colloid Interf. Sci.* 145, 140 (1991).

28. C. Selomulya, R. Amal, G. Bushell, and T. D. Waite, Evidence of shear rate dependence on restructuring and break-up of latex aggregates, *J. Colloid Interf. Sci.* 236, 67–77 (2001).
29. P. T. Spicer and S. E. Pratsinis, Shear-induced flocculations: The evolution of floc structure and the shape of the size distribution at steady state, *Water Res.* 30, 1049–1056 (1996).
30. T. Serra and X. Casamitjana, Effect of shear and volume fraction on the aggregation and breakup of particles, *AIChE J.* 44, 1724–1730 (1998).
31. T. R. Camp and P. C. Stein, Velocity gradients and internal work in fluid motion, *J. Boston Soc. Civil Eng.* 30, 219–237 (1943).
32. V. Mishra, S. M. Kresta, and J. H. Masliyah, Self-preservation of the drop size distribution function and variation in the stability ratio for rapid coalescence of a polydisperse emulsion in a simple shear field, *J. Colloid Interf. Sci.* 197, 57–67 (1998).
33. T. G. M. Van der Ven, *Colloidal Hydrodynamics*, Academic Press, London, 1989.
34. M. Vanni and G. Baldi, Coagulation efficiency of colloidal particles in shear flow, *Adv. Colloid Interf. Sci.* 97, 151–177 (2002).
35. J. N. Israelachvili, *Intermolecular and Surface Forces*, Academic Press, London, 1992.
36. D. L. Feke and W. R. Schowalter, The effect of Brownian diffusion on shear-induced coagulation of colloidal dispersions, *J. Fluid Mech.* 133, 17 (1983).
37. D. L. Feke and W. R. Schowalter, The influence of Brownian diffusion on binary flow-induced collision rates in colloidal dispersions, *J. Colloid Interf. Sci.* 106, 203 (1985).
38. T. G. M. Van der Ven and S. G. Mason, The microrheology of colloidal dispersions. VII. Orthokinetic doublet formation of spheres, *Colloid Polym. Sci.* 255, 468–479 (1977).
39. G. R. Zeichner and W. R. Schowalter, Use of trajectory analysis to study stability of colloidal dispersions, *AIChE J.* 23, 243–254 (1977).
40. D. L. Swift and S. K. Friedlander, The coagulation of hydrosols by Brownian motion and laminar shear flow, *J. Colloid Sci.* 19, 621–647 (1964).
41. T. G. M. Van der Ven and S. G. Mason, The microrheology of colloidal dispersions. VIII. Effect of shear on perikinetic doublet formation, *Colloid Polym. Sci.* 255, 794 (1977).
42. H. Wang, A. Z. Zinchenko and R. H. Davis, The collision rate of small drops in linear flow fields, *J. Fluid Mech.* 265, 161–188 (1994).
43. A. Z. Zinchenko and R. H. Davis, Collision rates of spherical drops of particles in a shear flow at arbitrary Peclet numbers, *Phys. Fluid* 7, 2310–2327 (1995).
44. B. S. Murray, E. Dickinson, J. M. McCarney, P. V. Nelson, M. Whittle, Observation of the dynamic colloidal interaction forces between casein-coated latex particles, *Langmuir* 14, 3466–3469 (1988).
45. M. A. J. S. van Boekel and P. Walstra, Effect of Couette flow on stability of oil-in-water emulsions, *Colloids Surfaces* 3, 99–107 (1981).

46. M. A. J. S. van Boekel and P. Walstra, Stability of oil-in-water emulsions with crystals in the disperse phase, *Colloids Surfaces* 3, 109–118 (1981).
47. E. Dickinson and A. Williams, Orthokinetic coalescence of protein-stabilized emulsions, *Colloids Surfaces A* 88, 317–326 (1994).
48. A. Lips, T. Weatbury, P. M. Hart, I. D. Evans, and I. J. Campbell, On the physics of shear-induced aggregation in concentrated food emulsions, in *Food Colloids and Polymers: Stability and Mechanical Properties* (P. Walstra, ed.), Royal Society of Chemistry, Cambridge, 1993, pp. 31–44.
49. E. Dickinson and E. Davies, Influence of ionic calcium on stability of sodium caseinate emulsions, *Colloids Surfaces B* 12, 203–212 (1999).
50. E. P. Schokker and D. G. Dalgleish, Orthokinetic flocculation of caseinate-stabilized emulsions: Influence of calcium concentration, shear rate and protein content, *J. Agric. Food Chem.* 48, 198–203 (2000).
51. E. Dickinson, G. Iverson, and J. Chen, Interfacial interactions, competitive adsorption and emulsion stability, *Food Struct.* 12, 135–146 (1993).
52. E. Dickinson, R. K. Owusu, and A. Williams, Orthokinetic destabilization of a protein stabilized emulsion by a water soluble surfactant, *J. Chem. Soc. Faraday Trans.* 89, 865 (1993).
53. D. Rousseau, Fat crystals and emulsion stability—a review, *Food Res. Int.* 33, 3–14 (2000).
54. E. Davies, E. Dickinson, and R. D. Bee, Shear stability of sodium caseinate emulsions containing monoglyceride and triglyceride crystals, *Food Hydrocolloids* 14, 145–153 (2000).
55. E. Davies, E. Dickinson, and R. D. Bee, Orthokinetic destabilization of emulsions by saturated and unsaturated monoglycerides, *Int. Dairy J.* 11, 827–836 (2001).
56. J. Hinrichs and H. G. Kessler, Fat content of milk and cream and effects on fat globule stability, *J. Food Sci.* 62, 992–995 (1997).
57. H. Casanova, J. Chen, E. Dickinson, B. S. Murray, P. V. Nelson, and M. Whittle, Dynamic colloidal interactions between protein-stabilized particles—experiment and simulation, *Phys. Chem. Chem. Phys.* 2, 3861–3869 (2000).
58. E. Dickinson, B. S. Murray, M. Whittle, and J. Chen, Dynamic interactions between adsorbed protein layers from colloidal particle scattering in shear flow, *Food Colloids: Fundamentals of Formulation* (R. Miller, ed.), Royal Society of Chemistry, Cambridge, 2000, pp. 37–51.
59. M. G. Semenova, J. Chen, E. Dickinson, B. S. Murray, and M. Whittle, Sticking of protein-coated particles in a shear field, *Colloid Surfaces B* 22, 237–244 (2001).
60. M. Whittle, B. S. Murray, J. Chen, and E. Dickinson, Simulation and experiments on colloidal particle capture in a shear field, *Langmuir* 16, 9784–9791 (2000).
61. R. Chanamai, N. Hermann, and D. J. McClements, Ultrasonic spectroscopy study of flocculation and shear-induced floc disruption in oil-in-water emulsion, *J. Colloid Interf. Sci.* 204, 268–276 (1998).

62. H. Mousa, W. Agterof, and J. Mellema, Experimental investigation of the orthokinetic coalescence efficiency of droplets in simple shear flow, *J. Colloid Interf. Sci.* 240, 340–348 (2001).
63. A. Nandi, D. V. Khakhar, and A. Mehra, Coalescence in surfactant-stabilized emulsions subjected to shear flow, *Langmuir* 17, 2647–2655 (2001).
64. S. A. Vanapalli and J. N. Coupland, Emulsions under shear—the formation and properties of partially coalesced lipid structures, *Food Hydrocolloids* 15, 507–512 (2001).
65. E. P. Schokker and D. G. Dalgleish, The shear-induced destabilization of oil-in-water emulsions using caseinate as emulsifier, *Colloids Surfaces A* 145, 61–69 (1988).
66. W. Xu, A. Nikolov, D. T. Wasan, A. Gonsalves, and R. P. Borwankar, Fat particle structure and stability of food emulsions, *J. Food Sci.* 63, 183–188 (1998).
67. L. Hamberg, P. Walkenstrom, M. Stading, and A. M. Hermansson, Aggregation, viscosity measurements and direct observation of protein coated latex particles under shear, *Food Hydrocolloids* 15, 139–151 (2001).

10

Recent Developments in Double Emulsions for Food Applications

Nissim Garti and Axel Benichou

The Hebrew University of Jerusalem, Jerusalem, Israel

I. OPENING REMARKS

Multiple emulsions are emulsion within emulsions. The major types are of water-in-oil-in-water (w/o/w) and oil-in-water-in-oil (o/w/o) double emulsions. These multicompartiment liquid dispersions, at least in theory, have a significant potential in many food applications because the internal droplets can serve as an entrapping reservoir for active ingredients that can be released by a controlled transport mechanism. In practice, double emulsions consist of large and polydispersed droplets which are thermodynamically unstable with a strong tendency for coalescence, flocculation, and creaming.

Efforts have been made to improve the two major drawbacks of these systems related to the thermodynamic emulsion's instability and the uncontrolled release of active matter. Almost any possible blends of low-molecular-weight emulsifiers, oils, cosolvents, and coemulsifiers have been tested. The nonviscous fluid double emulsions were always unstable and the release of the active matter from the inner phase to the outer continuous phase remained difficult to control. Only semisolid double-emulsion, gelled or thickened systems have a long shelf life with prolonged stability. Biopolymers, synthetic graft and comb copolymers, and polymerizable emulsifiers that impart steric or mechanical stabilization exhibited improved stability and better controlled release. Macromolecular surfactants, naturally occurring or synthetic polymeric amphiphiles, will increase the viscosity of each of the phases, will complex with the oil or the emulsifiers, and will

be able to form systems that will behave much like microcapsules, microspheres, and/or mesophasic liquid crystals.

The chapter will stress the most recent findings that can enhance the stability of the double emulsions and/or will reduce droplets sizes for potential food applications. The achievements include (1) choice of food-grade emulsifiers to enhance emulsion stability at both inner and outer interfaces, (2) droplet size reduction by forming microemulsions (or liposomes) as the vehicles for the active matter in the internal phase, (3) use of different preparation techniques to enhance the monodispersibility of the droplets, and (4) use of various additives (carriers, complexing agents, natural polymeric emulsifiers) to control and modify the reverse micellar transport phenomena.

Double emulsions were recently used as intermediate structures in the preparation of microcapsules capable of protecting entrapped addenda and assisting in controlling delivery. The literature is “flooded” with tens of new examples every year, demonstrating release patterns and control of active ingredients using double emulsions. However, practically no double-emulsion-based products exist in the marketplace.

The chapter will critically review the relevant literature and will bring some new emerging improvements involving the stability and the control issues. Mechanistic considerations will be discussed and alternative ways to deal with the double emulsions concerns related to food applications will be evaluated.

II. INTRODUCTION

Double emulsions are complex liquid dispersion systems known also as “emulsions of emulsions,” in which the droplets of one dispersed liquid are further dispersed in another liquid. The inner dispersed globule/droplet in the double emulsion is separated (compartmentalized) from the outer liquid phase by a layer of another phase (1–8).

Several types of double emulsion have been documented. Some consist of a single, internal compartment, whereas others have many internal droplets and are known as “multiple-compartment emulsions.” The most common double emulsions are w/o/w, but in some specific applications, o/w/o emulsions can also be prepared. The term “multiple emulsion” was coined historically because microscopically it appeared that a number (multiple) of phases were dispersed one into the others. In most cases, it was proven that, in practice, most systems are composed of double (or duplex) emulsions. Thus, more suitable and more accurate term for such systems should be “emulsified emulsions.” A schematic presentation of

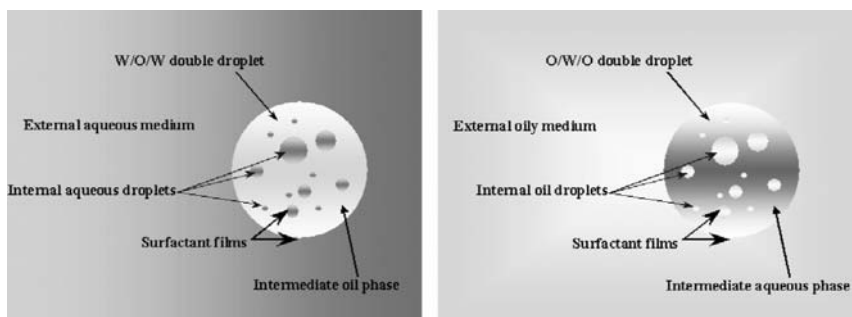


Figure 1 Schematic presentation of the two types of double-emulsion droplet. On the left is a typical w/o/w multiple droplet and on the right is a typical o/w/o multiple droplet.

the two types of double-emulsion droplets (w/o/w and o/w/o) is shown in Fig. 1.

Potential applications for double emulsions are well documented and many of these applications have been patented (9–15). In most cases, double emulsions are aimed for a slow and sustained release of active matter from an internal reservoir into the continuous phase (mostly water). In some applications, the double emulsions can serve also as an internal reservoir to entrap matter from the outer diluted continuous phase into the inner confined space. These applications are aimed at removing toxic matter. In other applications, double emulsions are reservoirs for improved dissolution or solubilization of insoluble materials. The materials will dissolve in part in the inner phase, in part at the internal interface, and occasionally at the external interface. Applications related to the protection of sensitive and active molecules from the external phase (antioxidation) have been recently mentioned (16–19). Many more applications are expected to emerge in the near future. Special attention must be paid to the most promising new application of double emulsions as intermediate systems in the preparation of solid or semisolid microcapsules (20–22).

III. PREPARATION ROUTES: THE EMULSIFIERS

Double emulsions consist of two different interfaces that require two sets of different types of emulsifier. In o/w/o double emulsions, the first set of emulsifiers, for the internal interface, must be hydrophilic and the second set of emulsifiers, for the external interface, must be hydrophobic. For w/o/w double emulsions, the order of the emulsifiers is the opposite;

the inner emulsifiers are hydrophobic and the outer ones are hydrophilic. In many cases, a blend of two or more emulsifiers in each set is recommended for better stabilization results. This review will discuss primarily w/o/w double emulsions, as most of the food applications require such emulsions. Some o/w/o emulsions applications are also given.

In early reports on the formation of double emulsions, only one set of emulsifiers and an inversion process were used. Such preparations were done in one step, but the stability was questionable in most cases. It was difficult to control the distribution of the emulsifiers within the two interfaces. There was fast migration of the emulsifiers between the phases that destabilized the emulsions. In most recent emulsion formulations, the emulsions are prepared in two steps. At first, a high-shear homogenization was applied on the water which was added to the solution of the oil and the hydrophobic emulsifiers, to obtain stable w/o emulsion. In the second step, the w/o emulsion is gently added with stirring (not homogenization) to the water and hydrophilic emulsifier solution (Fig. 2). The droplet size distribution of a typical classical double emulsion ranges from 10 to 50 μm .

Some more sophisticated preparation methods have been reported in the literature, of which two are interesting and worth being mentioned. The “lamellar-phase dispersion process” was reported by Vigie (23) (Fig. 3). The procedure is derived from the process employed to obtain liposomelike vesicles with nonionic emulsifiers. This process can be used only when the constituents form a lamellar phase by mixing with water in definite proportions. This procedure offers some advantage because it requires only a simple emulsification step. The mesophase formed by an ideal ratio of lipophilic emulsifiers in water is thermodynamically stable and can be obtained rapidly and easily. The method’s main limitation is derived from the fact that most emulsifiers do not form a lamellar phase. When the lamellar mesophase exists, the hydrophile-lipophile balance (HLB) of the blend of emulsifiers is often too high, which is disadvantageous for the stability of a multiple emulsion. In addition, the quantity of oil incorporated into the lamellar phase is always low, rarely higher than 10 wt%. Another drawback of this process is the weak control of the rate of encapsulation of the active substances.

Grossiord et al. (24) discussed an additional method termed the “oily isotropic dispersion process” by them. We prefer the more accurate term “emulsified microemulsions.” The idea is to disperse an oil phase within water by a surfactant and to form an L_2 phase (or water-in-oil microemulsion). This phase is further emulsified with water to form a double emulsion (Fig. 4). The problem is that there is no evidence that the formation of the microstructures by this method leads to multiple emulsions indeed. Moreover, there is no good evidence that the internal phase remains, after

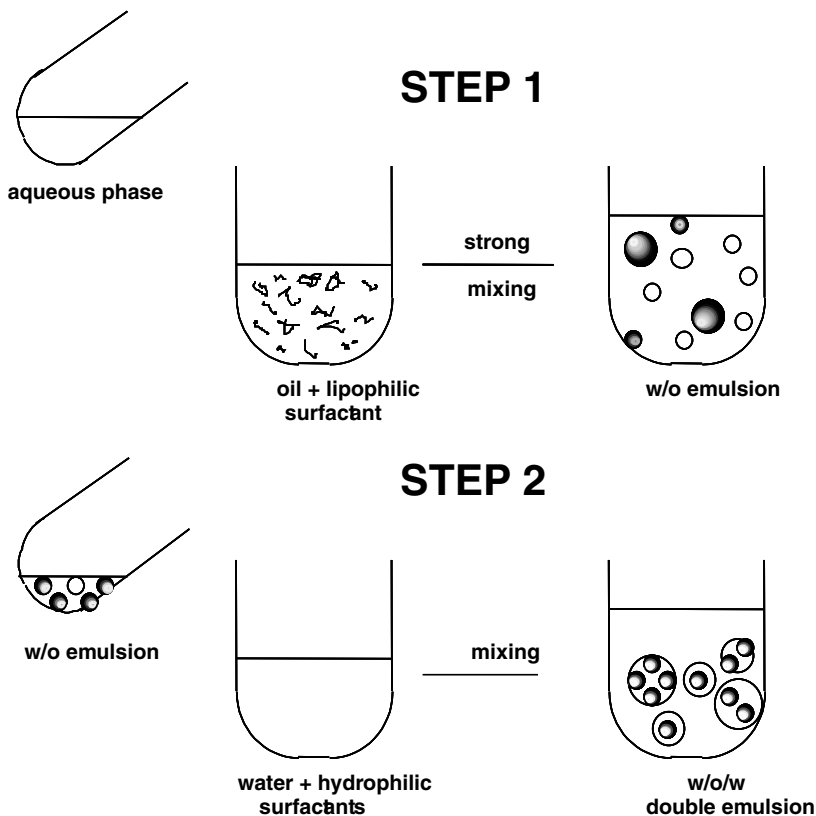


Figure 2 Schematic of a two-step process in the formation of a double emulsion.

the second emulsification process, a L_2 phase of a submicronal droplet in size. It seems that in some cases, the process is a well-characterized two-step emulsification that leads to relatively large double-emulsion droplets. The same concept of “emulsified microemulsion” was earlier reported by Pilman et al. (25) and also patented (10). This process is worth further investigation and should be more carefully evaluated. If one can prove that the internal compartmentalization is of a stable microemulsion, it might bring a breakthrough to this field because the sizes of the external droplets could be reduced to values below $1\ \mu\text{m}$. Such formulations will allow the formation of injectable double emulsions.

Gaonkar (10) claimed to have developed a completely new method in the preparation of double emulsions. This unique new type of preparation does not require any homogenization step and does not require the use of a

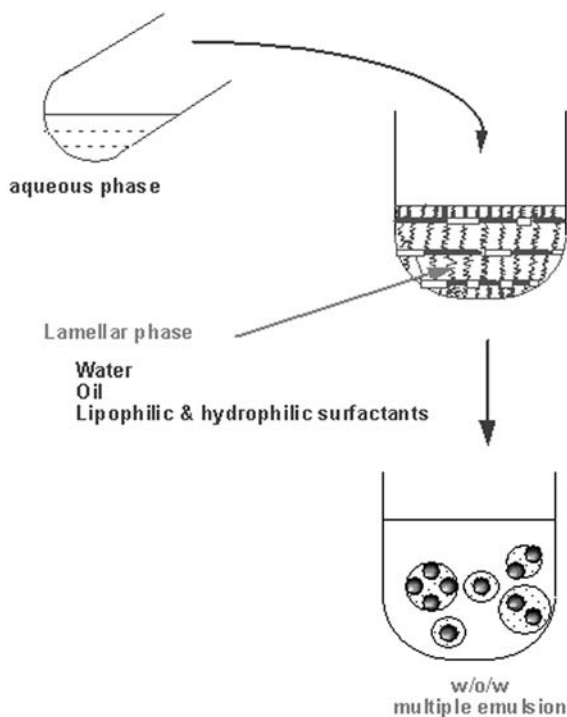


Figure 3 Preparation of water-in-oil-in-water multiple emulsion by lamellar-phase dispersion. (From Ref. 23.)

lipophilic emulsifier. In the method, a mixture of oil, water, a second alkyl containing a polar, protic solvent, such as methanol, ethanol, propanol, glycerol, propylene glycol, dodecanol, and their blend, and a hydrophilic emulsifier is prepared to form a o/w microemulsion. The o/w microemulsion is then diluted with sufficient water to cause destabilization of the microemulsion and to provide a w/o/w multiple emulsion.

Higashi et al. (26) described yet another new method of producing w/o/w multiple emulsions by a “membrane emulsification technique.” This method permits the formation of monodispersed liquid microdroplets containing aqueous microdroplets to form a w/o/w system. In this method, the aqueous internal phase is mixed with an oil phase containing lipophilic emulsifier. The mixture is sonicated to form a w/o emulsion, which is poured into the upper chamber of a special apparatus (Fig. 5). The external aqueous phase containing the hydrophilic emulsifier is continuously injected into the lower chamber to create a continuous flow. Nitrogen gas is fed into

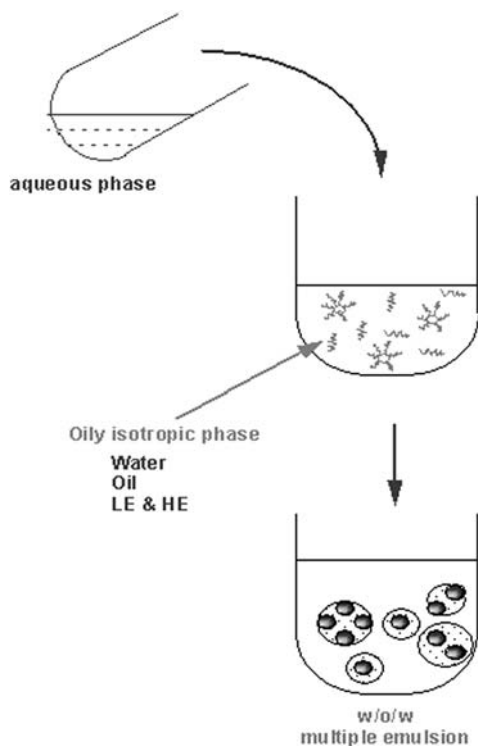


Figure 4 Preparation of water-in-oil-in-water multiple emulsion by “oily isotropic dispersion” (emulsified microemulsion). (From Ref. 24.)

the upper chamber, initiating a permeation of w/o through the controlled-pore glass membrane into the emulsifying chamber and forming a w/o/w multiple emulsion. The emulsion is progressively removed from the apparatus. This process was claimed to be used currently on an industrial scale.

It should be noted that low-molecular-weight emulsifiers migrate from the w/o interface to the oil phases and alter the required HLB of each of the phases. Most of the studies, in the years 1970–1985, searched for a proper monomeric emulsifier blend or combination (hydrophilic and hydrophobic) to be used at the two interfaces and the proper ratios between the two. Matsumoto and colleagues (1,27–33) established a minimum “magic” weight ratio of 10 of the internal hydrophobic to the external hydrophilic emulsifiers (Fig. 6). Garti and colleagues (34–39) proved that the free exchange between the internal and the external emulsifiers required a calculation of an “effective HLB value” of emulsifiers to optimize the stabilization of the emulsion. Complete parameterization work was done on almost

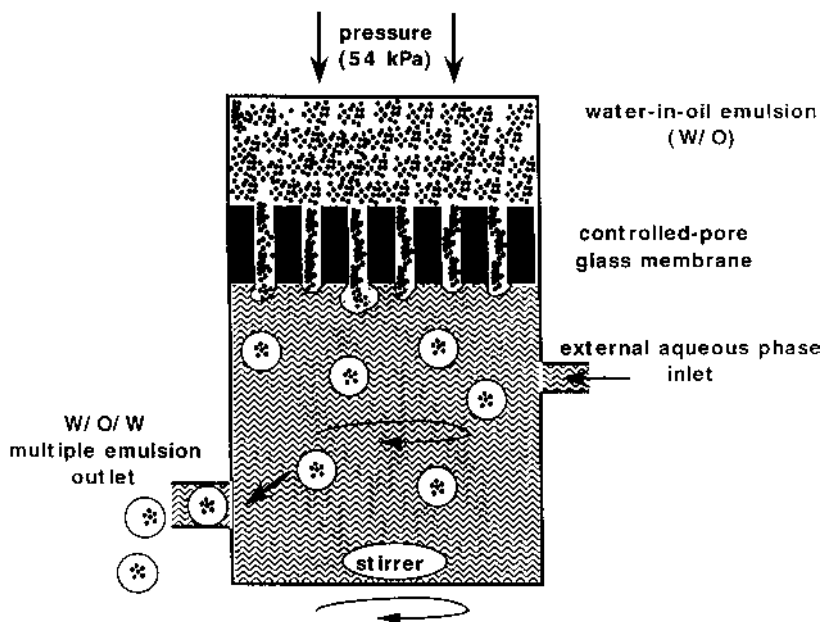


Figure 5 Preparation of water-in-oil-in-water multiple emulsion by a “membrane emulsification technique.” (From Ref. 26.)

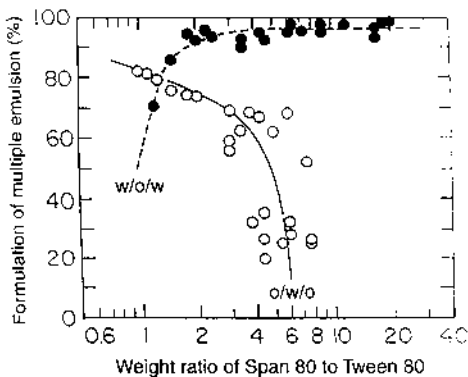


Figure 6 Yield of formation of double emulsions of w/o/w and o/w/o as a function of the weight/weight ratio of the internal hydrophobic emulsifier, Span 80, and the external hydrophilic emulsifier, Tween-80. (From Ref. 1.)

every possible variation in the ingredients and compositions (1–8). In most cases, the internal emulsifiers were used in great excess to the external emulsifiers. The nature of the emulsifiers also dictated the number of compartments and the internal volume that the inner phase occupies.

Many of the more recent studies explore various more sophisticated emulsifiers such as sphingomyelins (40), modified or purified phospholipids (41), cholates, and so forth. The principles for selecting the proper emulsifiers are similar to those known for classical emulsions. Some of the emulsions might have better stability than others, but the general trend remains unchanged. It should be stressed also that one must adjust the emulsifiers to the final application and must substitute one emulsifier by the other, depending on the total composition of the system.

It must be also recognized that “empty” double emulsions will behave differently from those containing active matter (electrolytes, biologically active materials, proteins, sugars, drugs, etc.) due to osmotic pressure gradients (caused by the additives) between the outer and the inner phases. In addition, many of the active ingredients have some hydrophobicity and surface properties. Such molecules (peptides, drugs, pesticides) will migrate from the inner bulk and will adsorb onto the interface, changing the delicate emulsifiers’ HLB. The emulsifiers around the water or the oil droplets will not cover the droplets fully and the stability will be reduced.

IV. THE OIL PHASE

In food applications, only a limited number of different “oil phases” (water-immiscible liquids) have been suggested and tried throughout years of research. In most applications, the oil phase is based on vegetable or animal unsaturated triglycerides such as soya oil, cotton, canola, sunflower, and others. It was also suggested to replace the long-chain triglycerides (LCT), which are “oxygen and hydrolysis sensitive” by medium-chain triglyceride (MCT), which are fully saturated and thus oxidation resistant. Moreover, the MCT is easier to emulsify and requires less shear.

In cosmetic applications, the freedom to use different oils is greater. Long-chain fatty acids, fatty alcohols, and simple esters such as isopropylmyristate (IPM), jojoba oil, and essential oils are only few examples. In addition, various waxes, sterols, and paraffin oils have been tried.

Several scientists tried to correlate the nature of the oil phase and its volume fraction to the stability of the double emulsions. No unusual or surprising findings were observed. Double-emulsion interfaces behave very much like simple emulsions except for the severe limitations on sizes of the droplets and the internal distribution of the emulsifiers.

V. STABILITY CONSIDERATIONS

Double emulsions made of low-molecular-weight emulsifiers (the so-called monomeric emulsifiers) are mostly unstable thermodynamically mainly because in the second stage of the emulsification, severe homogenization or shear are not recommended and, as a result, large droplets are obtained. During years of research, attempts have been made to find proper and more suitable combinations of emulsifiers to reduce droplets sizes and to improve the emulsion stability. Aggregation, flocculation, and coalescence (occurring in the inner phase and between the double-emulsion droplets) are major factors affecting the instability of the emulsions, resulting in rupture of droplets and separation of the phases.

Double emulsions are usually not empty. Water-soluble active materials are entrapped during the emulsification in the inner aqueous phase. It is well documented that because of the difference in osmotic pressure through a diffusion-controlled mechanism, the active matter tends to diffuse and migrate from the internal phase to the external interface, mostly through a mechanism known as “reverse micellar transport” (Fig. 7a). The dilemma that researchers were faced with was how to control the diffusion of water molecules as well as the emulsifier molecules and mostly the active matter from the internal phase to the outer phase. It seemed almost impossible to retain the active material within the water phase upon prolonged storage. Attempts to increase the HLB of the external emulsifier or to increase its concentration in order to improve the stability

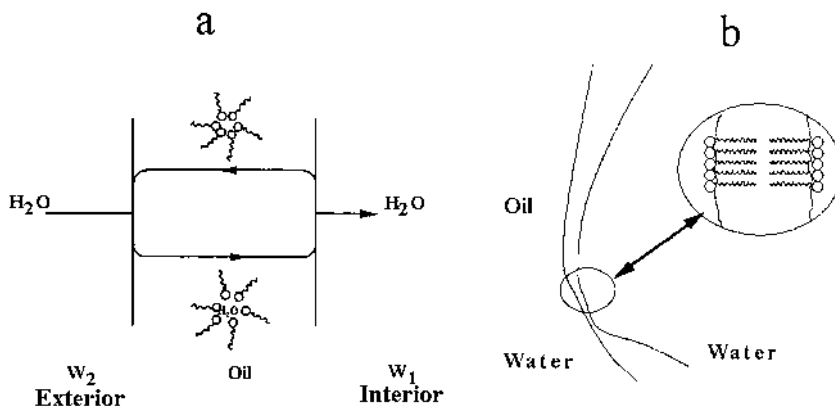


Figure 7 Schematic of two possible transport mechanisms: (a) reverse micellar and (b) lamellar thinning transport of a marker from the inner aqueous phase to the continuous aqueous phase.

of the emulsion worsens the situation and ended in a faster release of the drug or electrolytes.

Much work was devoted to establish the effects of osmotic pressure differences between the internal and the external phases on the stability of the emulsions and on the release rates of the markers from the internal phase, and the engulfment of the internal droplets by the flow of water from the outer continuous phase to the inner droplets. Single- and multiple-compartment emulsions were prepared and evaluated in view of the enormous potential that these low-viscosity liquid systems have in the slow delivery of water-soluble drugs.

Additional instability mechanisms and release pathways have been demonstrated and discussed in detail by various authors. These mechanisms include “transport through thinned lamella” (Fig. 7b), transport of adducts or complexes that are formed in the oil phase, and other variations of these mechanisms. It seems however, that the main instability and release mechanisms are parallel or simultaneously occurring phenomena of “reverse micellar transport” and coalescence.

All of the above mechanisms have been well established, but it seems that the stability and the release patterns of these complex double-emulsion systems depend on various parameters that simultaneously interplay and that a simplified or unique mechanism cannot explain all of the in-parallel pathways that take place in the double emulsions.

In a recent study, Ficheux et al. (42) identified two types of thermodynamic instability that are responsible for the evolution of double emulsions. Both mechanisms are in good agreement with the Bancroft rule (Fig. 8) but stress different aspects of the previously mentioned mechanisms. The mechanisms elucidated by the authors result in a different behavior of the entrapped matter in the double emulsion. The first is a “coalescence of the small inner droplets with the outer droplets interface” that is due to the rupture of the thin nonaqueous film that forms between the external continuous phase and the inner small water droplets. This instability irreversibly transforms a double droplet into a simple direct emulsion. Such a mechanism is suitable for delivery of entrapped water-soluble substances. The second mechanism was termed “coalescence between the small inner droplets within the oil globule.” The first type of instability leads to a complete delivery of the small inner droplets toward the external phase, whereas the second one does not. The second mechanism leads to an increase of the average diameter of the internal droplets and a decrease in their number. The authors worked both with anionic (SDS, sodium dodecyl sulfate) and cationic (TTAB, tetradecyltrimethylammonium bromide). It was demonstrated that the kinetics associated with the release of the small inner droplets due to the former instability is clearly related to the hydrophilic

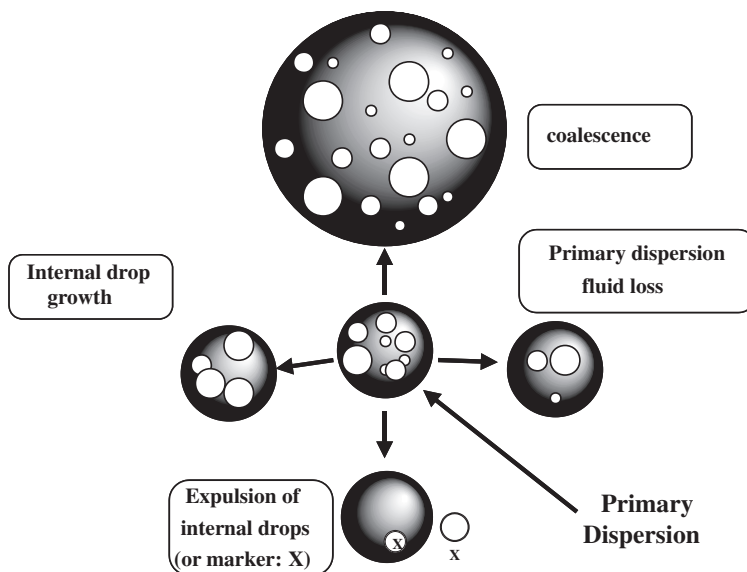


Figure 8 Schematic representation of the possible pathways for breakdown in multiple emulsions.

surfactant concentration in the external phase (Figs. 9a and 9b). Depending on the value of this concentration, double emulsions may be destabilized with a timescale ranging from several months to a few minutes.

Rosano et al. (43) explored the influence of “ripening and interfacial interactions” on the stability of the w/o/w double emulsions. The oil-insoluble solute was shown to stabilize both the first w/o emulsion (of the inner water droplets) and the external o/w interface. The authors provided a theoretical model and experimental results (video-microscope observations). It was shown that the presence of an electrolyte in the inner water phase is necessary for the stability of a multiple emulsion. The stability is achieved from the osmotic pressure equalization derived from the differences (excess) in the Laplace pressure. This effect stabilizes the inner w/o emulsion. It is possible also to determine the correct salt concentration necessary to balance the osmotic pressure between the two water phases. In a set of experiments (Tables 1 and 2), they show a total of 15 formulations in which both the oil phase and the W_2 phase are constant, and the only parameter varied is the NaCl concentration in the W_1 phase. The first six formulations were prepared with betaine, and the others were made with SDS. In the case of betaine, without any salt in the inner phase an unstable multiple emulsions is observed and both Ostwald ripening and

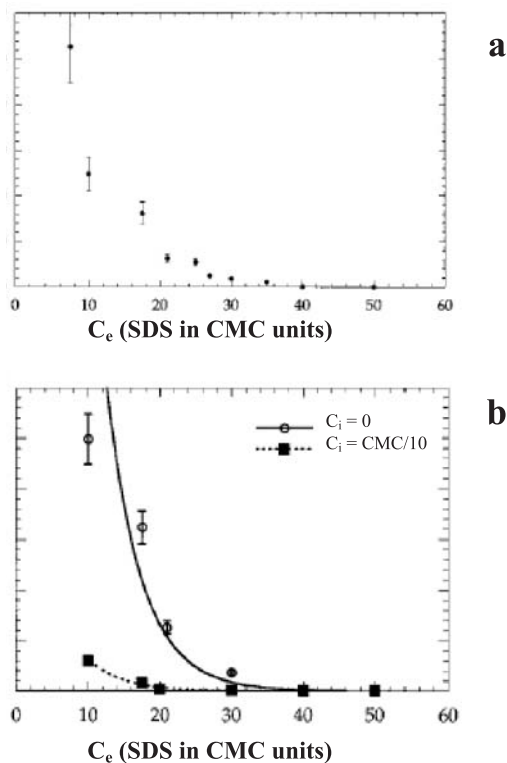


Figure 9 (a) Plot, at 20°C, of the lifetime τ , of internal droplets entrapped in the oil globules as a function of the external phase surfactant concentration C_e . The double emulsions are composed of 90% external phase and 10% double droplets. There is 10% water within the large double globules, 2% Span 80 was used within the oil, and SDS was used in the external water phase. (b) Influence of the internal surfactant concentration C_i on the $\tau = f(C_e)$ curve, at 20°C. System: Span 80/SDS as in (a). (After Ref. 42.)

release of the W_1 phase into the W_2 phase occur. As the concentration of the salt is increased in the W_1 phase, the systems do not separate, the structure is still multiple, and a large increase in viscosity is observed (9500 cP for 0.07 wt% to 27600 cP for 0.4 wt% NaCl). The authors conclude that one must consider that three possible factors influence the stability: the Laplace and osmotic pressure effects between the two aqueous phases, the interaction between the low- and high-HLB emulsifiers at the outer o/w interface, and the polymeric thickener–hydrophilic emulsifier interactions in the outer phase (W_2).

Table 1 The Role of the Concentration of Salt in the Inner W_1 Phase for Formation Made with Cocamidopropylbetaine

Formulation number	Composition (wt%)					
	1	2	3	4	5	6
W_1H_2O	27.5	27.43	27.35	27.2	27.1	27.2
NaCl	0	0.07	0.15	0.3	0.4	0.3
Light paraffin	21.5	21.5	21.5	21.5	21.5	21.5
Abil EM 90	1	1	1	1	1	1
W_2H_2O	48.9	48.9	48.9	48.9	48.9	48.9
Betaine	0.3	0.3	0.3	0.3	0.3	0.3
Carbapol 1342	0.1	0.1	0.1	0.1	0.1	0.05
Separation (%)	50 (20) ^a	0 (80)	0 (80)	0 (80)	0 (80)	0 (110)
Structure	Simple	Multiple	Multiple	Multiple	Multiple	Multiple

^aNumber of days.

The variations between the different suggested mechanisms are not dramatic. Some authors tend to stress certain mechanistic aspects and to neglect others, whereas other authors stress, in very specific formulations, the more relevant pathways. It seems that most suggested mechanisms are basically very similar.

VI. RELEASE CONSIDERATIONS

Several attempts have been made to explain the transport phenomena of addenda and water from the inner to the outer phase of w/o/w double-emulsion droplets. It was demonstrated that for un-ionized lipid-soluble material dissolved in the oil phase, the release obeys first-order kinetics and is diffusion controlled with excellent accordance to Fick's law. However, ionized and un-ionized water-soluble materials (dissolved in the aqueous inner phase) can also be transported. Matsumoto et al. (27,31) have suggested two possible mechanisms for the permeation through the oil phase; the first being via the "reverse micellar transport" (Fig. 7a) and the second by "diffusion across a very thin lamellae" of the surfactant phase formed in areas where the oil layer is very thin (Fig. 7b).

Our studies (37–39) on the release of electrolytes in the presence of monomeric emulsifiers, have indicated that the transport takes place even if the droplets are very stable to coalescence and even when the osmotic pressure of the two phases has been equilibrated. The Higuchi approach and

Table 2 The Role of the Concentration of Salt in the Inner W_1 Water Phase for Formulations Made with SDS

Formulation number	Composition (wt%)								
	7	8	9	10	11	12	13	14	15
W_1H_2O	27.43	27.4	27.36	27.2	27.1	25.95	26.9	26.6	27.2
NaCl	0.07	0.1	0.14	0.3	0.4	0.45	0.6	0.9	0.3
Light paraffin	21.5	21.5	21.5	21.5	21.5	21.5	21.5	21.5	21.5
Abil EM 90	1	1	1	1	1	1	1	1	1
W_2H_2O	48.9	48.9	48.9	48.9	48.9	50	48.9	48.9	48.9
Betaine	1	1	1	1	1	1	1	1	1
Carbapol 1342	0.1	0.1	0.1	0.1	0.1	0.1	0.1	0.1	0.2
Separation (%)	4 (40) ^a	3 (40)	17 (40)	38 (40)	9 (40)	16 (40)	52 (90)	40 (40)	0 (20)
Structure	Multiple	Multiple	Multiple	Multiple	Multiple	Multiple	Multiple	Multiple	Multiple

^aNumber of days.

model for the release of matter from polymeric matrices was adopted (44). A model was worked out and a modified release equation was offered and tested. The release factor B was plotted against the time, t , and reciprocal initial concentrations of the solute ($1/C_0$).

$$B = \frac{3}{2[1 - (1 - F)2/3]} - F = \frac{3D_e t}{r_0^2 C_0}$$

where D_e is the effective diffusion coefficient, r_0 is the radius of the outer phase droplets, F is the release fraction, and C_0 is the initial solute concentration.

The straight lines (with accordance with the above expression) and the excellent correlation coefficient obtained in these experiments indicate the existence of a “diffusion-controlled release mechanism.” It has been demonstrated that the water can flow into the inner w/o droplets if an osmotic pressure gradient is provided in the presence of hydrophobic emulsifiers present in the oil phase (32,33). It was also demonstrated that surfactant molecules, water molecules, and water-soluble addenda are transported at enhanced rates, even without the osmotic pressure gradient, in the presence of increasing concentrations of a lipophilic emulsifier added to the oil phase (37–39,44). Therefore, it has been concluded that the dominant diffusion-controlled mechanism is facilitated by the presence of reverse micelles formed at the oil phase. The mechanism was termed “diffusion-controlled release mechanism of reverse micellar transport.” Most of the release mechanistic studies in the literature involve double emulsions stabilized with synthetic polymeric amphiphiles and therefore, is of less interest for food applications. Nevertheless, these models of release patterns allow one to better understand the transport phenomena of entrapped addenda from the inner phase to the outer phase.

VII. STABILIZATION BY MACROMOLECULAR AMPHIPHILES

Macromolecules adsorb onto interfaces and facilitate more (or better) coverage than monomeric emulsifiers. The amphiphilic macromolecules form, in most cases, thick, flexible films which are strongly anchored into the dispersed and the dispersion phases. The adsorbed polymers are known to enhance steric stabilization mechanisms and were proved to be good emulsifiers in food colloids, primarily, in some food-grade oil-in-water emulsions. The use of macromolecular amphiphiles and stabilizers, such as proteins and polysaccharides, was long ago adopted by scientists exploring the stability of double emulsions. Gelatin (45,46), whey proteins

(47), bovine serum albumin (BSA) (48–51), human serum albumin (HSA), caseins, and other proteins were mentioned and evaluated. The proteins were used usually in combination with other monomeric emulsifiers (49). A significant improvement in the stability of the emulsions was shown when these macromolecules were encapsulated onto the external interface. In most cases, the macromolecule was used in low concentrations (maximum 0.2 wt%) and in combination with a large excess of nonionic monomeric emulsifiers. Furthermore, from the release curves, it seems that the marker transport is more controlled. Dickinson et al. (50–53) concluded that proteins or other macromolecular stabilizers are unlikely to completely replace lipophilic monomeric emulsifiers in double emulsions. However, proteins in combination with stabilizers do have the capacity to confer some enhanced degree of stability on a multiple-emulsion system and, therefore, the lipophilic emulsifier concentration is substantially reduced.

The authors of this review (49) have used BSA along with monomeric emulsifiers, both in the inner and the outer interfaces (in low concentrations of up to 0.2 wt%) and found significant improvement both in the stability and in the release of markers as compared to the use of the protein in the external phase only (Fig. 10). It was postulated that although BSA has no stability effect at the inner phase, it has a strong effect on the release of the markers (mechanical film barrier). On the other hand, BSA together with

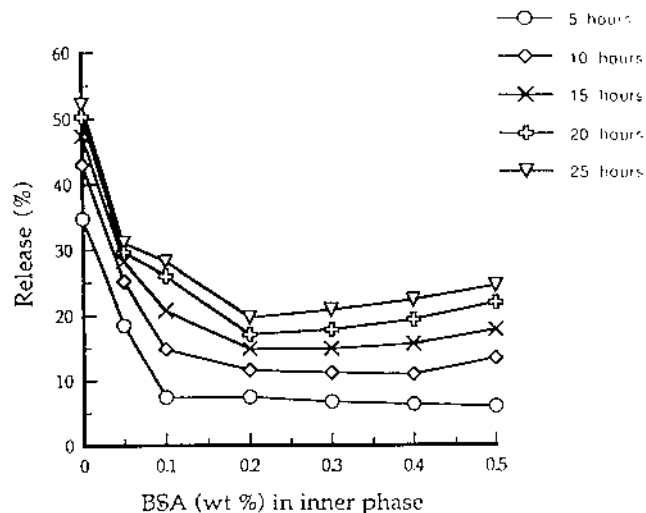


Figure 10 Percent release of NaCl with time from a double emulsion prepared with 10 wt% Span 80 and various BSA concentrations in the inner phase and 5 wt% Span 80 + Tween80 (1:9) in the outer aqueous phase. (From Ref. 49.)

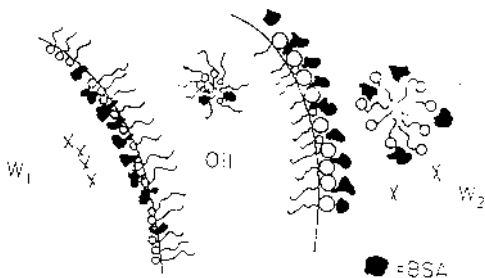


Figure 11 Schematic of a possible organization and stabilization mechanism of BSA and monomeric emulsifiers (Span 80) at the two interfaces of a double emulsion. (From Ref. 49.)

small amounts of monomeric emulsifiers (or hydrocolloids) serves as good steric stabilizers and improves stability and shelf life, and slows down the release of the markers. Therefore, BSA plays a double role in the emulsions: film former and barrier to the release of small molecules at the internal interface, and steric stabilizer at the external interface. The release mechanisms involving reverse micellar transport were also established (Fig. 11).

In more recent studies (54,55) the biopolymer chitosan was used as an emulsifier in food double emulsions. Chitosan has surface activity and seems to stabilize w/o/w emulsions. Chitosan reacts with anionic emulsifiers such as SDS at certain ratios to form a water-insoluble complex that has strong emulsification capabilities. Chitosan solution was used to form double emulsions of o/w/o as intermediates from which, by a simple procedure of stripping the water, the authors formed interesting porous spherical particles of chitosan (55).

Cyclodextrins (α , β , and γ) were shown to be potential stabilizers for o/w/o emulsions (56). The advantages of the cyclodextrins are their ability to complex with certain oil components at the oil–water interface resulting in no need for additional surfactant. It appears that the stabilizer efficacy depends on the nature of the oil and the type of the cyclodextrin ($\alpha > \beta > \gamma$). The presence of any active matter in the inner phase (such as benzophenone) destabilized the emulsion. Only the α -cyclodextrin yielded stable emulsions. The reason is an interfacial interaction between the components present at the interface, which changes the HLB and causes a destabilization effect. This elegant idea of interfacial complexation between the “oil components” and the surfactant cannot be a universal solution. The idea suffers from very severe intrinsic disadvantages once a different additive is included in the emulsion. For every additive at any concentration, an adjustment must be made and the given cyclodextrin or the complexing agent might be totally unfit.

VIII. STABILIZATION BY HYBRIDS OF BIOPOLYMERS

A. Protein–Polysaccharide Interactions in Aqueous Medium

Proteins, polysaccharides, and their blends, as examples of natural biopolymers, are surface-active materials. Under specific conditions (such as protein-to-polysaccharide ratio, pH, ionic strength, temperature, mixing processing), it has been stated that proteins and polysaccharides form hybrids (complexes) with enhanced functional properties in comparison to the proteins and polysaccharides alone. In the case of uncomplexed blends of biopolymers, competitive adsorption onto hydrophobic surfaces is generally reported. Conversely, electrostatic complexation between oppositely charged proteins and polysaccharides allows better anchoring of the newly formed macromolecular amphiphile onto oil–water interfaces (57).

Recently, the term “water-in-water emulsion” was employed to describe such dispersions when “protein-rich aqueous aggregates” are dispersed into a “polysaccharide-rich aqueous medium” (58). A mixture of gelatin and gum arabic solutions was reported (upon reducing the pH of the mixture) to separate in two phases (the upper phase very low in polymer content and the lower phase containing a highly concentrated precipitate of the two polymers). During the last century, many scientists developed models and theories to describe polymer interactions and phase separation (incompatibility) which occur when mixing two polymer solutions. The interactions between the polymers (protein–protein, protein–polysaccharide, or polysaccharide–polysaccharide) in solution and with the solvent (water in this case) will govern the solubility and cosolubility of the biopolymers, the viscoelastic properties of the final mixture, and even their behavior at different interfaces (solid–liquid or liquid–liquid).

Natural amphiphilic macromolecules or biopolymers are mainly based on proteins and polysaccharides. Attraction and repulsion are the two major types of interaction that occur between proteins and polysaccharides in solution and can result in complex formation or immiscibility of the two biopolymers (thermodynamic incompatibility). Owing to polyelectrolyte interactions in solution, these interactions and their consequences on the mixture will be strongly influenced by pH, ionic strength, conformation, charge density, and the concentration of the biopolymers.

In the aqueous solution, complex coacervation takes place between two oppositely charged polymers owing to electrostatic attraction. For instance, complexation between proteins and anionic polysaccharides occurs below the protein isoelectric point and at low ionic strengths (59). Factors that influence compatibility and complex formation are protein/polysaccharide ratio, pH, ionic strength (60–70), and the nature of the polymers (molecular weight, net charge, ternary structure, and flexibility

of chains) (70–75). Pretreatment of the polymer's solutions also enhances the complex formation. High-pressure (dynamic or hydrostatic) treatment as well as temperature have been reported to affect the stabilization of the newly formed complexes (64,76–79).

Phase diagrams could be built to describe the interactions for each biopolymer pair (Fig. 12, right). Two phase-separation phenomena can be observed, depending on the affinity between the biopolymers and the solvent. When the Flory–Huggins parameter, χ_{23} , which describes the protein–polysaccharide interactions, is positive, indicating a net repulsion between the two biopolymers, segregative phase separation (thermodynamic incompatibility) is generally observed. Solvent–biopolymer(s) interactions are favored to the detriment of biopolymer–biopolymer and solvent–solvent interactions, and the system demixes in two phases, each of which contains both of the two biopolymers. When the protein–protein or polysaccharide–polysaccharide interactions are sufficiently high in comparison to the polymer–solvent interactions (i.e., $\chi_{23} < 0$), congregative phase separation (or coacervation) is observed, leading to an upper solvent-rich phase and a lower biopolymer-rich phase forming the so-called “coacervate.” This is possible at a pH higher than the isoelectric point (IEP) of the protein, when both the protein and the polysaccharide carry the same charge (in the case of a negatively charged polysaccharide). By reducing the pH of the mixture below to the IEP of the protein, the interactions between the two oppositely charged biopolymers are favored ($\chi_{23} < 0$) and complexation takes place. The newly formed protein–polysaccharide complex could be soluble or can lead to an aggregative phase separation (region II, Fig. 12). The Flory–Huggins theory presents some limits to the protein–polysaccharide interactions in aqueous medium-modified models have been established to describe these systems in the case of globular proteins and colloidal protein particles (80,81).

Complexation between two charged biopolymers is usually a reversible process depending on pH and ionic strength. At high ionic strength (0.2–0.3) or at pH values above the protein IEP, the complex will dissociate. However, electrostatic interactions between anionic polysaccharides and positively charged proteins can occur at a pH above the IEP of the protein.

B. Protein–Polysaccharide Interactions in Emulsion

Protein–polysaccharide interactions play a significant role in the structure and stability of many processed foods. The control of these macromolecular interactions is a key factor in the development of novel food processes and products as well as in the formulation of fabricated products. Much was written on the possible interactions between proteins and hydrocolloids in

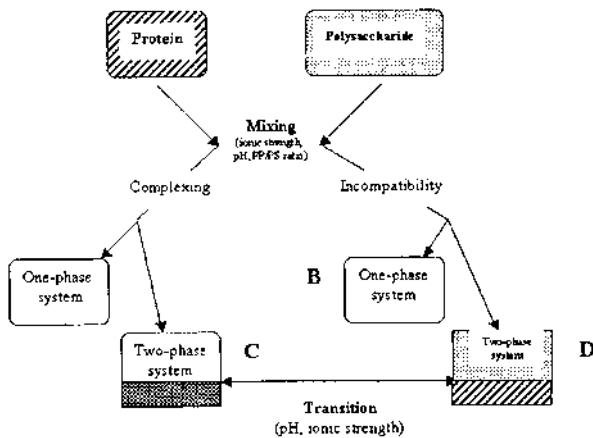
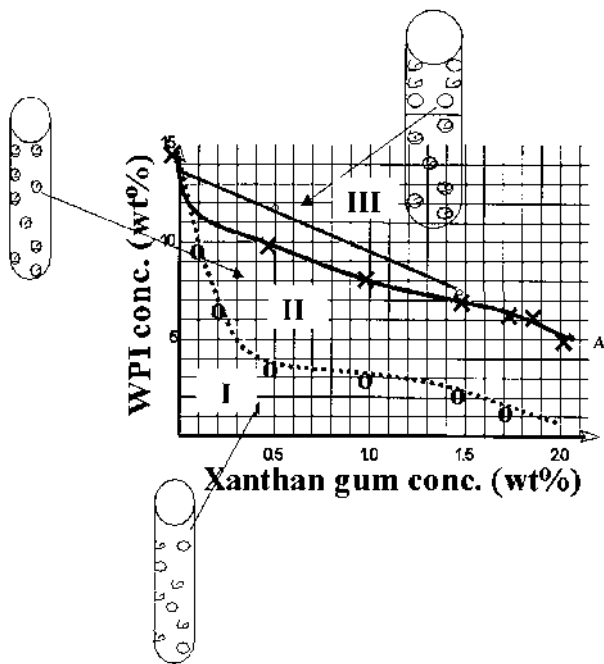


Figure 12 Phase diagram of water–whey protein isolate (WPI)–xanthan gum mixtures (top) which describes the different types of interaction between the protein and the polysaccharide in an aqueous medium (bottom). Binodal curves (solid line) delimit the boundaries between one phase region (below) and two separated phases region (above). Region II corresponds to protein–hydrocolloid hybrids formation.

model and real systems but very little advantage was provided by these studies in designing new amphiphilic molecules based on these hybrids. The chemically bound structures as well as the hydrogen-bound associates or even the ion–dipole or dipole–dipole associates form a well-balanced amphiphilic structures which can be utilized in fabricated emulsions and can replace the synthetic low-molecular-weight emulsifiers. These associates will not require any additional legislation (i.e., FDA) and will have textural and stability advantages. If one can add some nutritional or health benefits to it (and the hydrocolloids have shown such effects), the fabricated emulsions, food products, or food processes will become more attractive to the food producers.

Dickinson and colleagues claimed (82,83) that the best way to adsorb hydrocolloids onto interfaces is to link them to proteins. The proteins are surface-active materials consisting of flexible hydrophobic and hydrophilic moieties, preferentially adsorbing onto the interfaces and replacing the hydrocolloids from the surface. A hydrocolloid that is thermodynamically incompatible with an adsorbed protein (58,60) can be distributed at the interface only if it interacts somehow with the protein. Its distribution on the interface will depend on the nature of these interactions. Strong chemical bonds will cause a different surface distribution rather than weak associations between the two.

It was also recognized that polysaccharides could interact at the interface with other polymers (nonproteins, other polysaccharides) as well as with groups residing at the interface (protein–water, oil–water, or air–water) with the formation of an aqueous structured material with useful viscoelastic mechanical properties under conditions of low shear stress. Understanding the detailed chemistry of these polymer–polymer interactions and relating them to the observed rheology is a significant aspect of the study of hydrocolloids.

Complexation between proteins and polysaccharides at the emulsion droplet surface can improve steric stabilization. Droplet size can be smaller if the polysaccharide is present during homogenization, and, therefore, the rate of creaming may be reduced so long as there is no bridging flocculation. Covalent protein–polysaccharide complexation can also provide effective emulsion stabilization. The great improvement in stability arising from the presence of the polysaccharide during emulsification is attributable to the formation of a thicker, stronger steric-stabilizing layer around the droplets.

Tolstoguzov et al. (84) compared the surface properties of BSA and BSA–dextran complexes and the stability of *n*-decane-in-water emulsions prepared with them was evaluated by measuring the volume of the coexisting phases obtained after phase separation, under centrifugation (50 min at

23,000 g). Complete phase separation occurred for emulsions prepared with 0.2 wt% BSA. When BSA–dextran complexes were used (pH 6.0, 0.3 wt% biopolymer concentration), only 40% of the decane separated after centrifugation. Because the emulsification properties of the complexes were strongly dependent on pH and ionic strength, the authors attributed the emulsification power of BSA–dextran complexes to the electrostatic nature of the interactions. Even though both biopolymers carry a net negative charge at pH 7 (BSA–dextran sulfate, 1:3 by weight), a soluble ionic complex can be formed via local electrostatic interaction between the highly charged anionic polymer and positively charged patches on the globular protein. Surface shear viscosity measurements give independent evidence of an interfacial complex between BSA and dextran sulfate.

A similar synergistic effect of protein–polysaccharide complexes in stabilizing emulsions has been reported with corn oil–water emulsions prepared with casein–acidic polysaccharide complexes (85). For a pectin-to-total biopolymers ratio >0.2 , an emulsion stability index of 100% was obtained corresponds to zero creaming of the emulsion after centrifugation for 30 min at 3000 g. Adsorbed complexes at the oil–water interface increased the interfacial viscosity, forming a gellike structure around the oil droplets. Moreover, these emulsions exhibited relatively high thermal stability at 95°C because of the gellike microstructures at the interface. Emulsions prepared with soy proteins–sodium alginate complexes at pH 7.0 and for 10:1 and 4:1 protein-to-polysaccharide ratios (86) exhibited improved thermal stability in comparison to soy protein-stabilized emulsion. The emulsion activity index (EAI) values were 0.801 and 0.953 for a control emulsion (standard emulsion stabilized with soy protein) and for an emulsion prepared with soy proteins–alginate complexes (protein-to-polysaccharide ratio of 4:1), respectively. The improvement of the emulsion stability and activity indices was attributed to the unfolding of the soy protein at the interface that enhances protein–polysaccharide interactions by exposing cationic groups and hydrophobic groups. The newly exposed hydrophobic groups could alter the complex surface properties by providing additional sites for binding lipids, and that allows better anchoring of the amphiphilic macromolecules into the oil phase, resulting in an enhanced emulsion activity and stability indices.

Nevertheless, under specific conditions of pH, ionic strength, and polysaccharide concentration, protein–polysaccharide complexes in emulsions could contribute, in some cases, to a decrease in the emulsion stability. Dickinson and Pawlowsky (87) envisaged the flocculation, creaming, and rheology properties of *n*-tetradecane-in-water emulsions stabilized with BSA– κ -carrageenan complexes. The authors envisaged first the surface properties of soluble complexes by determining the evolution in time of the

surface tension [$\gamma(t)$] at different pH values (Fig. 13). BSA always provided lower γ values at any pH. The higher values of γ obtained with BSA- ι -carrageenan complexes have been attributed to a diminution of the number of free BSA molecules at the interface owing to complex coacervation, to a smaller diffusion coefficient as a result of complex sizes, and to increased viscosity of the solution. The electrostatic nature of BSA- ι -carrageenan complexes was clearly shown and could explain the dependence of the emulsion stability on pH and ionic strength. A relatively poor stability of the emulsion was described for polysaccharide concentrations above 0.01 wt% and was attributed to bridging flocculation of the oil droplets. At high carrageenan content (>0.1 wt%), stability against creaming of the emulsions was increased by the formation of a polysaccharide cross-linked network droplets with gellike rheological properties.

Covalently linked complexes have also shown emulsification capability (88). Because such complexes did not present much interest for food applications, we describe them succinctly. Oleic acid-water emulsions prepared with covalent linked β -lactoglobulin-carboxymethyl dextran conjugates were unaffected by heat treatment up to 80°C , demonstrating the heat stability of the complexes. Dickinson et al. (89) compared the influence of

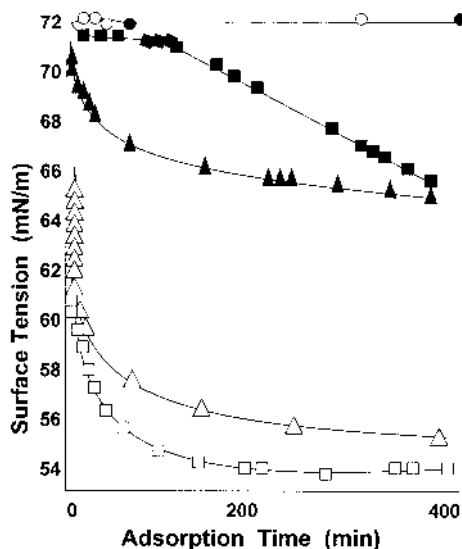


Figure 13 Time-dependent surface tension (γ) of biopolymer solution (5 mM imidazol, 25°C): \circ and \bullet pH = 8.0; \triangle and \blacktriangle pH = 6.5; \square and \blacksquare pH = 6.0. Open and closed symbols refer respectively to 10^{-3} wt% BSA and 10^{-3} wt% BSA + 4.10^{-3} wt% ι -carrageenan. (From Ref. 87).

ionic and covalent protein–polysaccharide interactions on 10 wt% *n*-hexane-in-water emulsions stabilized with BSA, nonionic dextran, and anionic dextran sulfate at neutral pH (Fig. 14). Both BSA–dextran conjugates (curve A) and BSA–dextran sulfate conjugates (curve C), yielded stable emulsions with droplet diameters that remained below 1.5 μm after 3 weeks standing at 25°C. Similar emulsion stability was obtained using a BSA–dextran sulfate mixture (curve D). On the other hand, emulsions prepared with a BSA–dextran mixture were unstable. Conversely conjugating or mixing BSA with amylopectin was not sufficient to stabilize emulsions (curves E and F).

Several scientists envisaged the preemulsification process influence on the emulsifying properties of protein–polysaccharides complexes (90–93). Hydrostatic pressures and preheating of the biopolymers suspensions have been often reported as a useful tool to modify and, to some extent, to enhance the emulsification power of these mixtures.

Heating was reported to increase the surface hydrophobicity of globular proteins such as ovalbumin, but a decrease in surface hydrophobicity was also demonstrated for BSA and β -lactoglobulin (88,91). Conversely, the hydrophobicity of 11S *Vicia faba* globulin was significantly increased by heating the native protein solution to 80°C for 2 min (93). When polysaccharide (i.e., ι -carrageenan) was added to untreated 11S *Vicia faba* globulin or heated at 80°C for 2 min, the surface hydrophobicity of the protein

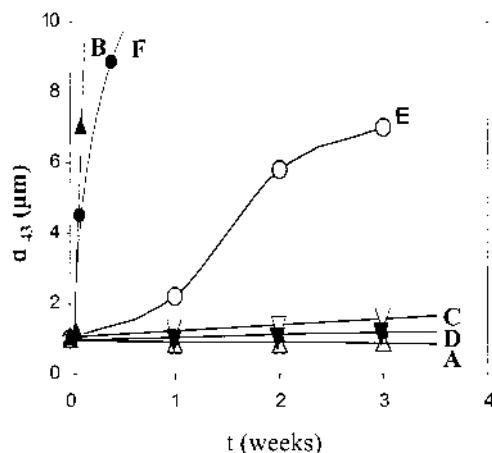


Figure 14 Average droplet diameter d_{43} as a function of time t of emulsions stored at 25°C and stabilized with: (Δ), BSA-dextran conjugate (curve A) (\blacktriangle), BSA dextran mixture (curve B) (∇), BSA–dextran sulfate conjugate (curve C); (\blacktriangledown), BSA dextran sulfate mixture (curve D); (\circ), BSA-amylopectin conjugate (curve E); (\bullet), BSA amylopectin mixture (curve F). (From Ref. 89).

remained unchanged. The temperature treatment of the protein solution induced extensive precipitation, whereas the mixed solution remained clear. It was concluded that ι-carrageenan inhibited the aggregation of the protein molecules by protecting protein-reactive sites.

The influence of temperature treatment on the emulsifying efficiency of 11S *Vicia faba* globulin pure or mixed with ι-carrageenan or κ-carrageenan in 20 wt% *n*-tetradecane-in-water emulsions was also studied (93). Heat treatment was reported to lower the emulsifying power of the protein. To the contrary, polysaccharide addition (protein to polysaccharide ratio of 3.3 to 1) leads to emulsions with smaller droplets at all temperatures. Mixed emulsions prepared with ι-carrageenan (high content of sulfate groups) have been found to be more stable against creaming than those prepared with κ-carrageenan (less sulfated). The average droplet diameters of emulsions were of 5.7 and 8.0 μm, respectively, for mixtures heated for 2 min at 80°C. High-pressure treatment affects significantly the surface hydrophobicity of proteins and protein–polysaccharide blends (90–93). High pressure induces subunit dissociation (quaternary structure) and, to some extent, unfolding of the globular subunits which result in the exposure of new hydrophobic groups within the protein molecules (93). Polysaccharide addition reduced the surface hydrophobicity of the pressurized protein by blocking the hydrophobic site onto the protein surface. In spite of reduced hydrophobicity, mixtures of pressurized κ-carrageenan–protein and ι-carrageenan–protein lead to the formation of stable emulsion with respect to creaming. The same trend as for temperature treatment was observed. The droplet sizes of emulsions prepared with the ι-carrageenan–protein mixture were smaller than those prepared with the κ-carrageenan–protein blend. Conversely, increasing the applied pressure on the protein solution yielded emulsions with larger droplets. This was attributed to protein aggregation by disulfide binding between free-cysteine residues.

C. Double Emulsion Stabilized with Protein–Polysaccharide Hybrids

Recently, we have envisaged the stabilization of double emulsions with some “molecular-recognition” hybrid of whey protein isolate (WPI) and different charged and uncharged polysaccharides (7,94). The emulsifying power of WPI–xanthan gum hybrids was studied. It was found that WPI–xanthan ratio strongly influences the formation and stability of the droplets (Fig. 15). At low protein content (0.5–2 wt%), the droplet size decreases with time due to internal aqueous-phase expulsion. This was attributed to the weakness of the emulsifier film adsorbed onto the external oil–water interface. Microscopic observation revealed that for a WPI–xanthan gum

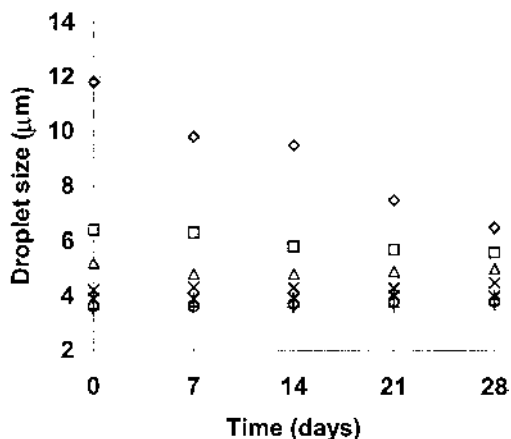


Figure 15 Double-emulsion droplet stability with time at room temperature prepared with 0.5 wt% xanthan gum and increasing amount of WPI as an external emulsifier: 0.5 wt%, \diamond ; 1 wt%, \square ; 2 wt%, \triangle ; 3 wt%, \times ; 4 wt%, $*$; 5 wt%, \circ ; 6 wt%, $+$.

ratio of 0.5/0.5 (w/w), double-emulsion droplets inverted to simple o/w droplets (empty of internal globules) after aging for 28 d at room temperature. At higher protein-to-polysaccharide ratios (3/0.5 to 6/0.5, w/w) double-emulsion droplets exhibited increased stability against creaming and coalescence. Double emulsions were prepared with different whey protein-xanthan ratios. Increasing the xanthan content to 1 wt% decreases the droplets diameter from 11.8 to 3.1 μm (Fig. 16a). It was found that by increasing the protein-to-polysaccharide ratio (region II of the phase diagram), double-emulsion droplets with reduced droplet size and increased stability are formed.

One can conclude that the binodal boundary line corresponds to the limit of complexation of the two biopolymers that will give optimum stabilization. At biopolymer content higher than the binodal composition, the addition of one of the two biopolymers will only slightly affect the double-emulsion droplets' stability and will only add a small depletion stabilizing effect to the emulsion droplets.

1. Rheology

Rheological measurements were performed on double-emulsion droplets. The phase angle, δ , was defined as $\arctan(G''/G')$, where G' is the storage modulus, G'' is the loss modulus, and $\tan(\delta) = G''/G'$. It was found that at

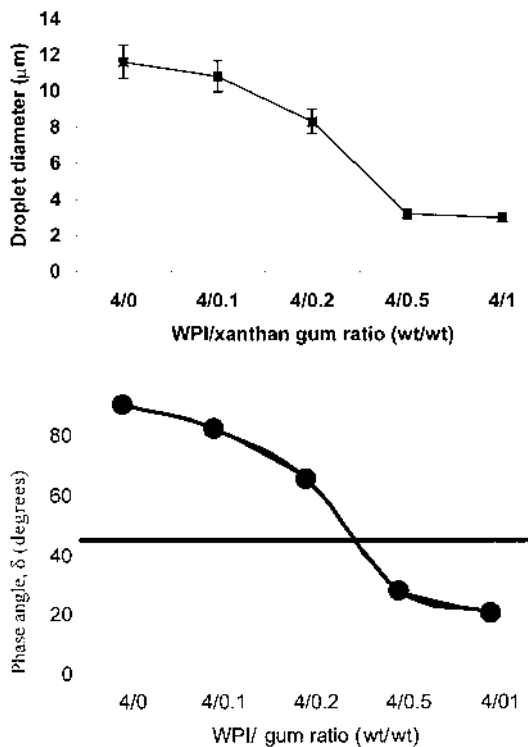


Figure 16 (a) WPI–xanthan gum ratio (w/w) influence on the droplet diameter (μm) of double-emulsion droplets, immediately after preparation. (b) WPI–xanthan gum ratio (w/w) influence on the phase angle δ (degrees) of double-emulsion droplets, immediately after preparation. The phase angle, δ , was defined as $\arctan(G''/G')$, where G' is the storage modulus, G'' is the loss modulus, and $\tan(\delta) = G''/G'$.

low levels of gum (0.1 wt%), the emulsions had high viscosity, with the phase angle (δ) close to 90° , indicating self-assembly of the two biopolymers onto the external oil–water interface. Therefore, the emulsions are stabilized mainly by steric interactions between the “macromolecular-recognition hybrids” adsorbed onto the oil. To the contrary, at a high level of gum (0.3–1 wt%), the emulsions exhibit more elasticity, regarded as a physical property derived from a depletion stabilization mechanism. The protein will preferably adsorb onto the oil–water external interface and the uncomplexed gum will migrate to the bulk and contribute to the stabilization by a depletion mechanism (Fig. 16b). The protein-to-gum ratio of 4/0.5, at which complexation between the protein and the gum takes place,

corresponds to an intermediary viscoelasticity of the system. Microscopic observations and zeta-potential measurements performed on the samples after rheological studies revealed that the emulsion droplets are still multiple droplets and that interactions between the biopolymeric molecules remained unchanged.

At a gum concentration of 0.5 wt%, the protein concentration does not affect the rheological behavior of the double emulsion that conserves its elasticity properties at all ratios with phase angle (δ) values around 25° at all protein contents. At the same time, the yield of preparation of double emulsions prepared with increasing amounts of protein and at 0.5 wt% xanthan gum was 64% for double emulsions stabilized with 6 wt% WPI and increased to 96% with the addition of 0.5 wt% xanthan gum.

2. Effect of pH on Double-Emulsion Stability

The pH is known to influence strongly the net charge of proteins. Therefore, it was important to qualify and to quantify its effect on the protein–polysaccharides interactions in solution and at the oil–water interface in double emulsions. The zeta potential of both solutions and emulsions was determined (Fig. 17). For the WPI–xanthan gum system, the pH affects the protein, the gum, and the combination of the two. The blends behave as the protein alone with very close isoelectric points to pure protein. Once the hybrid is adsorbed onto the oil droplets, the situation is significantly different. The isoelectric point of the protein-stabilized emulsion decreases, indicating unfolding of the protein and screening of its charged residues during

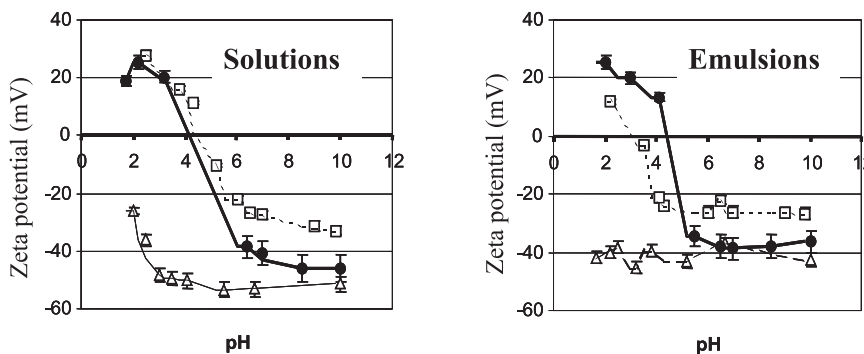


Figure 17 Zeta potential (mV) of solutions (left) and of multiple emulsions (right) prepared with 4 wt% WPI (□), 0.5 wt% xanthan gum (△), and the blend of the two at a weight ratio of 4/0.5 (○).

the emulsification process. At a low pH, one can conclude that the protein is dominant at the interface, and at a high pH, the gum is the dominant one at the interface. In other words, when the pH is reduced to below the isoelectric point of the blend, the steric stabilization is dominant, and when the pH increases, the system is mainly stabilized by a depletion mechanism. The pH also influences strongly the rheological behavior of double emulsions. At a pH below the isoelectric point of the blend [WPI–xanthan gum (4/0.5)], 4.8, the phase angle, δ , is higher than 45° , indicating that the emulsion is viscous and confirming steric stabilization mechanism for these systems. Conversely, at a higher pH (5–10), the system is predominantly elastic (δ close to 25° in all the pH range), indicating a depletion stabilization mechanism. Microscopy observations of emulsion stabilized with a WPI–xanthan gum mixture (4/0.5) at pH 7 reveals a weakness of the film around the oil globules, indicating the presence of uncomplexed biopolymers at the interface. It was concluded that at a pH below the isoelectric point of the blend, the two biopolymers strongly interact and yield fully covered double-emulsion droplets. When the pH of the external aqueous phase increases, at a constant WPI–xanthan gum ratio, the electrostatic interactions between the protein and the gum become weaker around the oil droplets and the “biomolecular-recognition hybrid” film becomes less rigid.

3. Entrapment in Double Emulsions (Vitamin B₁)

Much work was done on the entrapment of addenda in double emulsions, but only a few reports have shown promising results on real systems. In this subsection, we will bring a more recent example drawn from the authors' work.

The formulations stabilized with the mixture of WPI and xanthan gum were used for entrapping vitamin B₁ in the inner aqueous phase. A useful electrochemical method was developed to quantify the amount of vitamin B₁ present in the external aqueous phase. Differential pulse polarography based on the redox properties of the vitamin when it is present in the external aqueous phase allowed the determination of its release profiles under various conditions of pH, protein-to-polysaccharide ratio, and initial concentration of the entrapped addenda. The release profile, as a function of the pH of the external aqueous phase (Fig. 18) reveals that at pH 2, the external interface is better sealed against the release of the entrapped vitamin than at pH 4 and 7. It reconfirmed that there is an extra stability of these double emulsions derived from both electrostatic and steric mechanism stabilization of the external oil–water interface.

At pH 3.5, the increase in the protein-to-polysaccharide ratio also reduces the release rate. As was demonstrated earlier, at high hydrocolloid

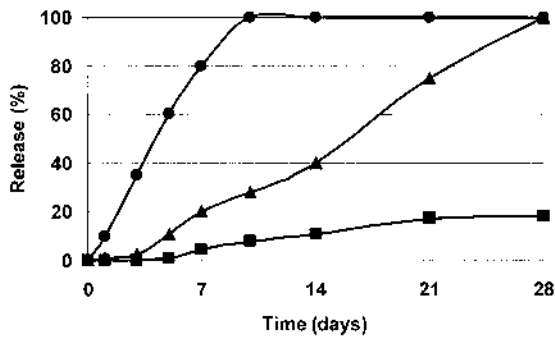


Figure 18 Effect of the external aqueous phase pH on the release profile of vitamin B₁ from multiple emulsions stabilized with WPI-xanthan gum (4/0.5) as the external emulsifier (pH 7, ●; pH 4, ▲; pH 2, ■).

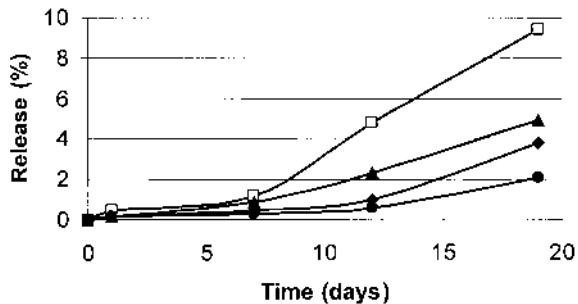


Figure 19 Release profile of vitamin B₁ from multiple emulsions at different WPI-xanthan ratios as the external emulsifier at pH 3.5 (4/0, □; 4/0.1, ▲; 4/0.2, ◆; 4/0.5, ●).

content, the system is stabilized by both electrostatic and steric mechanisms that improve the rigidity of the film around the double-emulsion globules and so delay the vitamin release (Fig. 19).

IX. STABILIZATION BY SOLID PARTICLES

To assist in the stabilization of emulsions, particles (such as fat crystals) must be adsorbed at the emulsion droplet interface, providing a physical barrier to coalescence. It is known that in many emulsified foods, solid particles are necessary for producing stabilization (e.g., ice crystals in ice cream, egg yolk particles in mayonnaise, and fat particles in whipping

cream). The key factors that will determine the influence of fat crystals on emulsion stabilization are (1) the wettability of the crystals at the interface, (2) interfacial film rheology, (3) particle microstructure (polymorphism and morphology), and (4) location of fat crystals [(in the dispersed (o/w emulsion) or continuous phase (w/o emulsion)] (95).

The wetting behavior of particles at the interface is described by contact angles, which are related to the surface tension of each of the three interfaces by Young's equation: $\gamma_{(o/w)} \cos \theta = \gamma_{(o/s)} - \gamma_{(w/s)}$, where θ is the contact angle measured through the water phase and $\gamma_{(o/w)}$, $\gamma_{(o/s)}$, and $\gamma_{(w/s)}$ are the surface tensions of the oil-water, oil-solid, and water-solid interfaces, respectively. $\cos \theta \gamma_{(o/w)}$ is also known as the adhesion tension. Modification of the contact angle (and, therefore, emulsion stability) can be achieved by a modification of the aqueous, oil, or solid phase so as to alter $\gamma_{(o/w)}$, $\gamma_{(o/s)}$, or $\gamma_{(w/s)}$.

In Fig. 20, where water acts as the continuous phase and oil as the dispersed phase, the colloidal particle is partially embedded within the interface at an equilibrium distance dictated by the interparticle forces. With a contact angle less than 90° at the solid-water-oil interface across the water phase, the particle will stabilize o/w emulsions. With contact angles greater

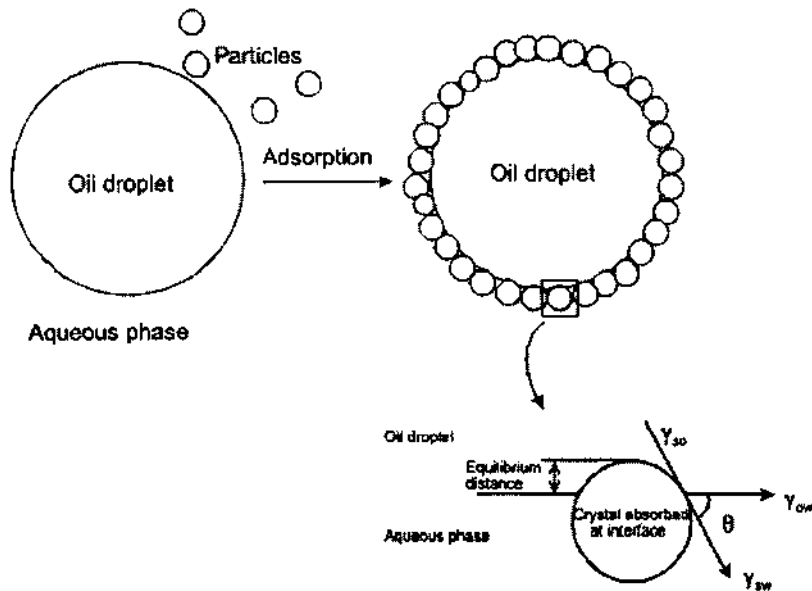


Figure 20 Adsorption and contact angles of fat crystals at the interface of an oil-in-water emulsion.

than 90° , the particles will stabilize a w/o emulsion. If the particles used are completely wetted by either the oil or water phase (and, therefore, the contact angle is 180°), they become fully dispersed in that phase and any emulsion-stabilizing effect is negated. A 90° contact angle means that a crystal is equally wetted by the oil and aqueous phases.

Stabilization of margarine and other similar food emulsions is achieved by partial adsorption of solid fat particles (β' -polymorphs) onto the water–oil interface, bridged by monomeric hydrophobic emulsifiers. The complex stabilization is achieved by “wetting” the oil phase by solid fat particles and emulsifiers (lecithins and monoglycerides of fatty acids). The concept was recently reexamined and reconsidered by Bergenstahl (96,97) and the mechanism was somewhat better elucidated.

The concept of stabilizing emulsions by solid particles (mechanical stabilization) was partially demonstrated in an old and incomplete study (98), showing that colloidal microcrystalline cellulose (CMCC) particles can adsorb in a “solid form” onto oil droplets at the interface of water–oil emulsions and thus improve their stability by mechanical action. Oza and Frank (98) tried the mechanical stabilization concept on double emulsions. The report shows some promise in improving stability and in slowing down the release of drug. This study was, for several years, the only example of applying the concept of mechanical stability on double emulsions. In a most recent article, Khopade and Jain (99) repeated the use of a similar process and managed to stabilize w/o/w emulsions by using MCC (microcrystalline colloidal cellulose) particles at both interfaces. The droplets were small and the yield of the double emulsion was fairly good. The increasing concentration of MCC in either the internal or external phase increased droplet sizes. These systems showed promise in tuberculosis therapy.

Garti et al. (100) carried out several experiments with micronized particles of the α - and β' -polymorphs of tristearin fat together with polyglycerol–polyricinoleate (PGPR) as the internal emulsifiers in double emulsions. Solid fat particles did not sufficiently stabilize the water-in-oil emulsion, and, similarly, the PGPR (at the concentrations used in the formulation) did not provide good stability. However, it was shown that the use of the blend of the two components composed of a solid submicronal fat particles of α - and β' -polymorphs (which are more hydrophilic than the β -form and thus wet the oil–water interface better) “precipitate” onto the water droplets and “cover” them. The fat particles bridge between the water droplets and sinter them only if a lipophilic surfactant (PGPR) was coadsorbed onto the water–oil interface (the w/o emulsion) (Fig. 21). The authors’ interpretation of the results is that “the fat particles adsorb onto the hydrophobic emulsifier film and both, the solid particles and the emulsifier, wet the water and spread at the interface.” The double emulsions

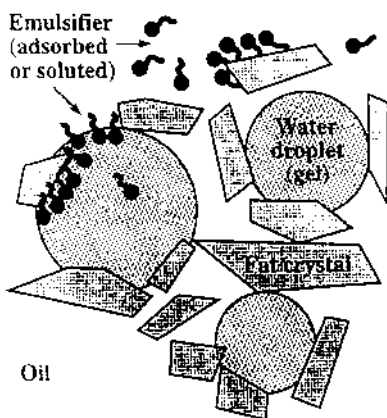


Figure 21 A Schematic of a colloidal margarine structure demonstrating the role of emulsifiers and fat crystals in stabilizing the (w/o) emulsion of margarine by colloidal fat crystals. (From Ref. 100.)

prepared by this technique were more stable than those prepared by monomeric emulsifiers.

Organophilic montmorillonite is an interesting clay that gained some interest in the emulsion technology. Stable *o/w/o* emulsions with components consisting of hydrophilic nonionic surfactant (hydrogenated, ethoxylated castor oil, HCO-60), organophilic montmorillonite, and commercial nonionic surfactant (DIS-14) were made (101). The montmorillonite was added in the second step at the outer *w/o/w* interface. The droplets sizes decreased with the increase of the HCO-60 (0.1–3 wt%) concentration. The viscosity of the double emulsion increased as the concentration of the montmorillonite, and DIS-14 increased, indicating that the excess amount of the inner oil phase is adsorbed by the outer oil phase. The results indicate that the weight fraction of the inner oil phase should not exceed 0.3 wt% for stable *o/w/o* emulsions because the viscosity of the double emulsion is so high that the formulation becomes semisolid.

X. STABILIZATION BY INCREASED VISCOSITY

Most food emulsions are highly complex systems both in terms of composition and structure (102). To control the formation, the stability and rheology of food emulsions require an understanding of the interactions between the various elements present in the system. Recently, progress has been made to understand the interaction behavior at the *o/w* interface between

some of the components found in food emulsions, particularly between different proteins and surfactants, and, to a lesser extent, between proteins and fat crystals. Because fat crystal interactions at the interface are affected by protein, and protein interfacial behavior is affected by small-molecule surfactants, it is important to examine how all of these components interact. As with bulk emulsion properties, the interface can exhibit viscous, elastic, and viscoelastic properties. The ability of an emulsion to resist coalescence will largely depend on the properties of the interface. A highly viscous and rigid interfacial film will retard the rate of film drainage and resist rupture, thereby promoting stability (103). Hence, by controlling interface rheology, one can control the drainage of thin liquid films trapped between coalescing droplets, which may also affect the displacement of crystals away from the interface during droplet coalescence. Kiosseoglou (104) discussed the role of surface-active lipids at the o/w interface on the viscoelastic parameters of BSA, sodium caseinate, and egg yolk films during adsorption at the olive oil-protein solution interface. It was postulated that film viscoelasticity was the result of surface-active lipids interacting with folded and unfolded proteins at the interface.

Restricting the mobility of the active matter in the different compartments of the double emulsion will slow down coalescence and creaming, as well as decrease the transport rates of the drug, or the marker, from the water phase through the oil membrane. Attempts were made to do the following: (1) increase the viscosity of the internal aqueous phase by adding gums/hydrocolloids to the inner water phase, such a thickener may affect also the external continuous phase because the entrapment is not quantitative and the yields of entrapment are limited and are emulsifier dependent, (2) increase the viscosity of the oil phase (fatty acids salts); (3) increase the thickening or gelling of the external water by gums. This process is limited to cosmetic (or similar) applications in which semisolid emulsions are directly applied (Tables 3 and 4). Some of these examples are topical skin care products, creams, and body lotions (105,106).

Double emulsions that were solidified after preparation may suffer from destabilization effects. This phenomenon is scarcely considered but in practice it can occur very often. The solidification occurs because of temperature changes (temperatures can fluctuate from sub-zero of ca -20°C to ca 40°C) during transport or storage. Clause et al. (107,108) studied the phenomena in w/o/w emulsions by microcalorimetric [differential scanning calorimetry (DSC)] techniques. It was concluded that, because of thermodynamic equilibrium, double emulsions may suffer from water transfer during the solidification. This phenomenon occurs even if partial solidification takes place. In addition, a change in the size distribution of emulsion droplets is observed. The mean diameter of the droplets in the

Table 3 Example of w/o/w Multiple Emulsion Stabilized by a Calcium Alginate Gel Layer at the Internal Water Oil Interface

	Hexaglycerol mixed ester	1%
	CSL (calcium stearyl-2-lactylate)	0.75%
Oil phase	Soybean oil	23.25%
Internal aqueous phase	27% Solution sodium alginate, low viscosity	25%
Outer aqueous phase	Polysorbate 20	0.36%
	Water	9.14%
	Vinegar	12%
	Sucrose	6%
	NaCl	2.5%
	Aqueous phase + 1% xanthan gum	20%

Table 4 Composition for Low-Fat Spread Using a w/o/w Formulation

Outer aqueous phase	Salt	1%
	Gelatin	3%
	Maltodextrin DE = 7 ^a	10%
	Water	85%
	Sodium caseinate	1%
w/o emulsion	Water	57.9%
	Rapeseed oil	40%
	PGPR	2%
	Flavor	0.1%

^aDE = dextrose equivalent.

w/o emulsion may shift toward the o/w emulsion and the double emulsion can invert. Therefore, it is not always obvious that increasing viscosity, gelation, or partial solidification improved the emulsion's stability.

XI. MICROCAPSULES OR MICROSPHERES IN THE INTERNAL PHASE

Entrapping the active matter in solid or semisolid particles will dramatically decrease their release rates. Such double emulsions can be stored, before use, for prolonged periods of time without transporting the active matter to the outer interface. Upon use, the double emulsion will be heated or sheared and the solid internal matrix will be ruptured and the active matter should be released. The major problem in practicing such technology is the

difficulties arising in dispersing (and in keeping it stable) the microparticle or nanoparticles in the continuous water phase. Microspheres and nanoparticles using solid encapsulation techniques were tested to replace the classical w/o emulsion. Only a few experiments were carried out showing that release can be slowed down, but the stability of these systems is very limited (109–123). Such methods are applicable only for emulsions that can be freshly prepared prior to their use. It is our hope that more efforts will be made in this direction.

XII. DOUBLE EMULSIONS AS INTERMEDIATES FOR NANOPARTICULATION

Advanced double-emulsion formulations are no longer prepared for the purpose of simple delivery and release of active matter but have changed application directions. Three main new directions can be clearly seen: (1) double emulsions as intermediates for the preparation of solid microspheres or microcapsules, (2) o/w/o double emulsions for improved solubilization and chemical protection of water-insoluble active matter, and (3) double emulsions for selective adsorption of certain compounds for extraction and purification purposes.

Some major examples along with the classical delivery applications in pharmaceuticals and food applications will be described that will emphasize the new emerging applications.

A. Controlled Delivery Applications

The intrinsic instability of the double emulsion caused difficulties for formulators and many of the investigators have decided to abandon this technology (6,7). However, one should bear in mind that the potential applications for double emulsions appear to be enormous, mainly in the areas of food, cosmetics, medicine, and pharmaceuticals. Throughout the years, potential applications have been demonstrated in (1) improved biological availability (parenteral nutrition, anticancer drugs), (2) delivery of drugs (sustained release of narcotic antagonistic drugs, prolonged release of corticosteroids, slow and targeted release of anticancer drugs), and (3) adsorption of toxic compounds. The technology has much promise also in nonpharmaceutical areas of slow and controlled release of materials such as fertilizers and pesticides for agricultural formulations as well as for controlled release for cosmetic, industrial, and food applications (6,7). In fact, most of the applications of double emulsions for controlled delivery are in the field of pharmaceuticals and health.

Double emulsion may offer some advantages for food application mainly with relation to their capability to encapsulate (or entrap) in the internal compartments some water-soluble substances which are then slowly released. The double emulsion can also be used in the food industry where an external water phase is more acceptable in terms of palatability than an oil one (124,125). On this basis, several new products have been patented in the form of w/o/w emulsions, such as salted creams (encapsulation of salt), aromatic mayonnaise, and so for in (126–129). Further food applications are related to the double-emulsion dielectric properties. For example, one can prepare a w/o/w system having the same volume fraction of the dispersed phase and the same texture as a simple emulsion, but with a lower oil content (due to the existence of the aqueous compartments in the food globules) (i.e., low-calorie mayonnaise) (124).

B. Double-Emulsions Solvent-Extraction Techniques for Preparation of Microspheres

Drugs, cosmetic ingredients, and foods additives are microencapsulated for variety of reasons, which include reducing local side effects, controlled release, site-specific (drug) delivery, and drug targeting. A tremendous amount of research work is done in a search of suitable methods to achieve a good encapsulation of water-soluble active matter. The physical characteristics of the microspheres produced largely determine their suitability for use for different objectives. Microspheres are prepared from both natural and synthetic polymers.

Among microencapsulation techniques, the double-emulsion solvent-evaporation method is one of the most useful methods for entrapping water-soluble compounds (109–123). Fig. 22 shows schematically the preparation technique. Over 100 articles and many patents have been published in the course of the last 5 years on the use of this technique. Most of the applications are rather related with pharmaceuticals and drug encapsulation than with foods. We have selected only some examples that are of a more significant value.

The w/o/w emulsions are generally used for encapsulating proteins or peptides. These highly water-soluble molecules are quantitatively introduced in the internal aqueous phase of the multiple emulsions and result in an increased encapsulation efficiency microcapsules in comparison to particles produced by single emulsion solvent-evaporation method. The particular location of the proteins induce a stabilizing effect on the two emulsions, which, in turn, contributes to a successful stabilization of the double emulsion and loading.

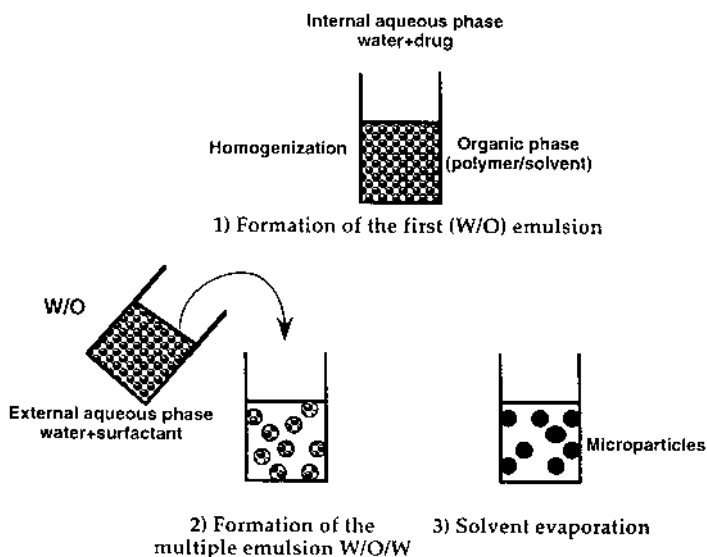


Figure 22 Preparation of microspheres by the multiple-emulsion solvent-evaporation technique.

The double-emulsion solvent-evaporation technique is commonly used to prepare biodegradable hydrophobic microspheres containing hydrophilic pharmaceuticals, proteins, and polypeptides for sustained release applications (111,115–123). In most cases, the microspheres are in the range size of 10–100 μm . However, recently, Blanco-Prieto et al. (116) managed to reduce the microcapsules sizes to less than 5 μm .

Couvreur et al. (115) reviewed the preparation and characterization of many of the different types of the solvent-evaporation microsphere and mostly discussed small poly(lactic-*co*-glycolic acid) microspheres (mean size lower than 10 μm) containing small peptides (Fig. 23). Three main evaporation strategies have been utilized in order to increase the encapsulation capacity an interrupted process, a: continuous process, and the rotary evaporation procedure.

Much work was devoted in recent years to preparing microparticles of narrow size distribution with different biodegradable polymers. The sizes of common microcapsules are 40–50 μm (115–116,121–123).

Liquid–liquid emulsification is a critical step in the double-emulsion microencapsulation process (w/o/w or o/w/o). It was found that the size of these droplets decreases with increasing homogenization intensity and duration. The emulsion droplet size depends, as expected, on viscosity, total volume size, and volume ratio of the continuous phase to the dispersed

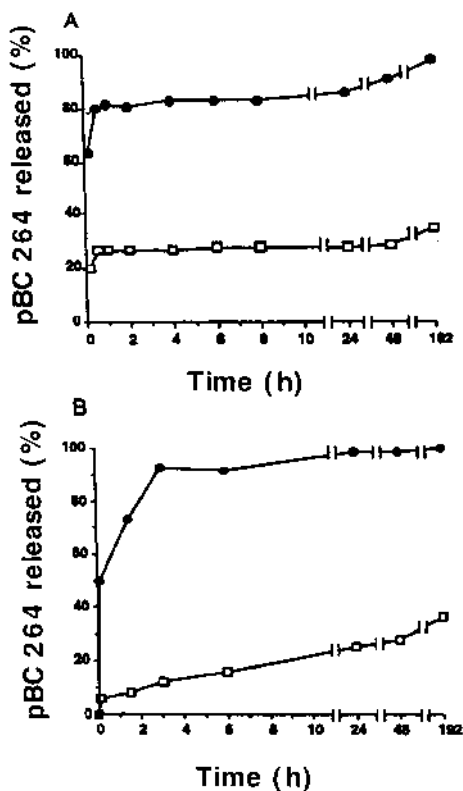


Figure 23 Release kinetic of pBC 264 in phosphate-buffered saline pH 7.4: (top) in vivo and (bottom) in brain tissue from PLGA microspheres prepared with either ovalbumin (●) or Pluronic F-68 (□). (From Ref. 115).

phase: the rotor/stator design was also investigated. All of these physical parameters influence the structure of the microspheres obtained by this technique.

An interesting example is the incorporation of a protein-based drug in microspheres made of a hydrophobic polymer via double liquid-liquid emulsification (w/o/w) or by dispersing a powdered protein in a polymer solution followed by liquid-liquid emulsification (s/o/w) (117). BSA was used as the model protein and poly(methyl methacrylate) (PMMA) was used as the model polymer. The droplets sizes of the w/o emulsion droplets were controlled using rotor/stator homogenization. The size of the microspheres thus prepared was found to increase with the increasing size of the protein powder in the s/o/w system but increase with decreasing size of the

liquid emulsion droplets in the w/o/w system. Empirical correlation can accurately predict the size of the microspheres. Protein loading in the microspheres decreased with respect to increase in w/o emulsion droplet size or in protein powder size.

In a most recent article (122), it was demonstrated that a milk model protein, β -lactoglobulin (BLG), was encapsulated into microspheres prepared by the solvent-evaporation technique. The effect of the pH of the outer aqueous phase on the protein encapsulation and release as well as on the microsphere morphology has been investigated. It was demonstrated that as the amount of BLG increases, the stability of the inner emulsion decreased and the entrapment was less efficient. Therefore, adjusting the combined pH effect and the stability of the inner emulsion may lead to better entrapment. As to the release, it was demonstrated that the “burst effect”, attributed to a morphology change in the microcapsules characterized by the presence of pores, or channels, able to accelerate the release of the BLG, is the most significant release factor. These pores were attributed to the presence of a large amount of BLG on the surface which aggregates during microsphere formation at pH 5.2. It was concluded that it is beneficial to lower the solubility of the protein in the outer phase in order to improve the encapsulation efficiency, although this benefit is provided by a strong adsorption of the protein on microsphere surface. Some more interesting articles on protein entrapments for various oral and other intakes can be found in the literature (117–120). Chitosan porous spherical particles were prepared from o/w/o double emulsions stabilized with a chitosan aqueous solution. The particulation was obtained by a simple evaporation technique (55).

XIII. O/W/O DOUBLE EMULSIONS

Oil-in-water double emulsions were considered to have less potential applications and therefore were less extensively studied. However, in more recent years, several new applications have been mentioned for o/w/o double emulsions which sound interesting and worth being mentioned.

Modulated release of triterpenic compounds from a o/w/o multiple emulsion formulated with dimethicones studied with infrared spectrophotometric and differential calorimetric approaches is one of these examples (130). The authors explored the advantages in the release of triterpenic compounds from o/w/o emulsions. They found two principal advantages: (1) the use of low-molecular-weight silicones decreased the oily touch of the final preparation and (2) due to the large range of viscosity, this excipient influenced the skin distribution of the active matter after the topical

application. The effects of different triterpenic compounds incorporated within multiple emulsions were studied, through in vitro penetration results. The residual film on the skin was also evaluated. Correlations were established between the silicone structure and the distribution of drugs in different skin levels or between the silicone structure and the percutaneous penetration. The incorporation of silicones within o/w/o multiple emulsions seems to be an efficient means of modulating the penetration and the distribution of drugs in the skin.

In another study, the stability of retinol (vitamin A alcohol) was compared in three different emulsions: oil-in-water (o/w), water-in-oil (w/o), and oil-in-water-in-oil (o/w/o) (16). The stability in the o/w/o emulsion was the highest among the three types of emulsion. The remaining percentages, at 50°C after 4 weeks, were 56.9, 45.7, and 32.3, in the o/w/o, w/o, and o/w emulsions, respectively. However, it was also reported that with the increasing peroxide value of o/w and w/o emulsifiers, the remaining percentage of vitamin A palmitate and retinol in the emulsions increased significantly, indicating that peroxides in the formulas accelerate the decomposition of vitamin A. An organophilic clay mineral tan oil gelling agent and a w/o emulsifier also affected the stability of retinol. The stability of retinol in the o/w/o emulsion increased with increasing inner oil-phase ratio, whereas in o/w, it was unaffected by the oil fraction. The encapsulation percentage of retinol in the o/w/o emulsion, the ratio of retinol in the inner oil phase to the total amount in the emulsion, increased with increasing oil fraction. The remaining percentage of retinol in the o/w/o emulsion was in excellent agreement with encapsulation percentage, suggesting that retinol in the inner oil phase is more stable than that in the outer oil phase. Addition of antioxidants (*tert*-butylhydroxytoluene, sodium ascorbate, and EDTA) to the o/w/o emulsion improved the stability of retinol up to 77.1% at 50°C after 4 weeks. The authors concluded that the o/w/o emulsion is a useful formula for stabilizing vitamin A.

Orange oil-in-water emulsions were encapsulated in another oil phase to form a double emulsion with orange oil inside its inner compartment (19). Although the yield was only 44.5%, it is a promising area for further research in the future in order to prevent air oxidation of the oil. Spray-drying of the double emulsion can provide a secondary coating to secure a maximum protection of orange oil and affords a free-flowing flavor powder. Spray-drying of the orange oil double emulsion had a very low destruction effect on its structure, as revealed by light microscopy. This method may have a potential application in different food or pharmaceutical products where maximum protection is required. A secondary coating was applied to the flavor oil already encapsulated in a double emulsion. The spray-drying technique includes spraying a flavor emulsion into a stream of hot air.

The water phase is then evaporated rapidly, leaving the flavor material locked in the carrier.

XIV. MULTIPLE-EMULSION RHEOLOGY

The understanding of the rheological behavior of double emulsions is quite important in the formulation, handling, mixing, processing, storage, and pipeline transformation of such systems. Furthermore, rheological studies can provide useful information on the stability and internal microstructure of the double emulsions. Some attention was given to this subject in recent years and the results are significant because they help to clarify certain aspects on the stability and release properties of the double emulsions (131). Few publications deal with w/o/w double emulsions and only one deals with the o/w/o emulsion. Most of the rheology work is old and do not contribute a new understanding. Therefore, we will bring only recent relevant work.

An interesting characterization of the mechanical properties of the oil membrane in w/o/w emulsions was done by an aspiration technique (132). It was adopted from techniques related to the evaluation of global or cell deformability. The deformability of an individual globule during a total or partial flow into a cylindrical glass tube calibrated under well-controlled conditions of aspiration was determined. An analysis of the behavior of the double emulsion by a migration of the lipophilic surfactant to the interface between the oily and the external aqueous phases was done. It was shown that the elastic shear modulus and the interfacial tension of the oily membrane increased with the lipophilic surfactant concentration. This study also provides an explanation of the mechanism related to the swelling–breakdown process from physical and mechanical considerations.

Grossiord et al. (131–133) applied linear shear flow on the w/o/w double emulsions that contained active matter, and from the rheological patterns, they learned about the bursting effect of the droplets with the release of entrapped substances and the composition of the system. The authors (133) described a set of two types of experiment: oscillatory dynamic tests and a steady-state analysis. They measured the stress and strain of the emulsions by applying sinusoidal shear. These parameters (shear or complex modulus G^* ; the lag phase between stress and strain, δ ; the storage modulus G' and the loss modulus G'') provide a quantitative characterization of the balance between the viscous and elastic properties of the multiple emulsions. At lag phase, $\delta = 0^\circ$, and when $= 90^\circ$, the system is viscoelastic. The shear sweep and the temperature sweep characterize the multiple emulsion at rest. Fig. 24 describes a transition between an elastic behavior and a viscous

behavior, which occurs at critical stress values. The change in this parameters indicate a pronounced structural breakdown. The authors considered the influence of the formulation parameters on the swelling and release kinetics using the rheological properties. Parameters such as the oil nature, the width of the oil membrane, and the lipophilic and the hydrophilic nature of the surfactant have been evaluated. The two main parameters identified to affect the swelling/breakup kinetics were the difference in concentration in water soluble molecules between the internal and the external aqueous phase (Fig. 25), and the lipophilic surfactant concentration. It was also observed that the maximum viscosity values increase with the surfactant ratio (under hypo-osmotic conditions, Fig. 26). The same trend was observed when the release of water-soluble materials, $\beta(t)$, was followed (Fig. 27). The authors concluded that a progressive migration of the excess lipophilic surfactant in the oil phase toward the primary or the secondary interface occurs.

Stroeve and Varanasi (134) also examined the breakup of the multiple-emulsion globules in a simple shear flow and concluded from the critical Weber number $(We)_{cr}$ (Figs. 28 and 29) that the multiple emulsions exhibit behavior that is similar to that of simple emulsions. From Fig. 28, one can see, at least qualitatively, the evolution of $(We)_{cr}$ as a function of p

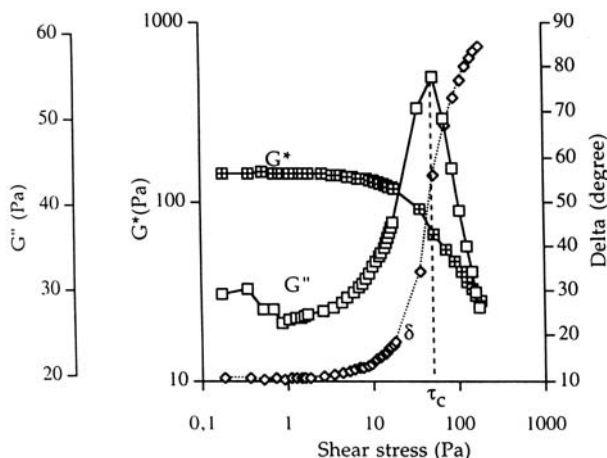


Figure 24 Changes in G^* , G'' and δ for increasing stress at fixed frequency in double emulsions. The double-emulsion composition of the water oil emulsion is 24% oil, various lipophilic surfactant concentrations and 0.7% $MgSO_4$. The o/w/o emulsion contain 80% water in oil, 2% hydrophilic surfactant, and demineralized water. (From Ref. 133.)

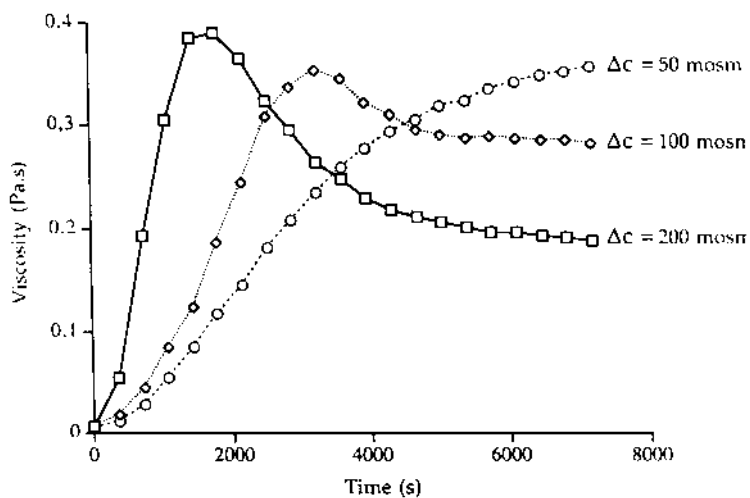


Figure 25 Change in viscosity versus time for different concentration gradients in the inner phase. (From Ref. 133.)

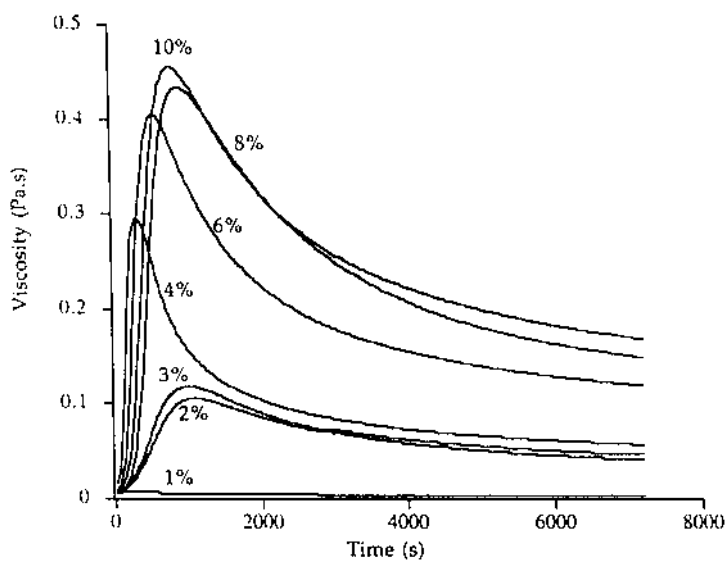


Figure 26 Change in viscosity versus time under hypo-osmotic conditions for different lipophilic surfactant concentrations. (From Ref. 133.)

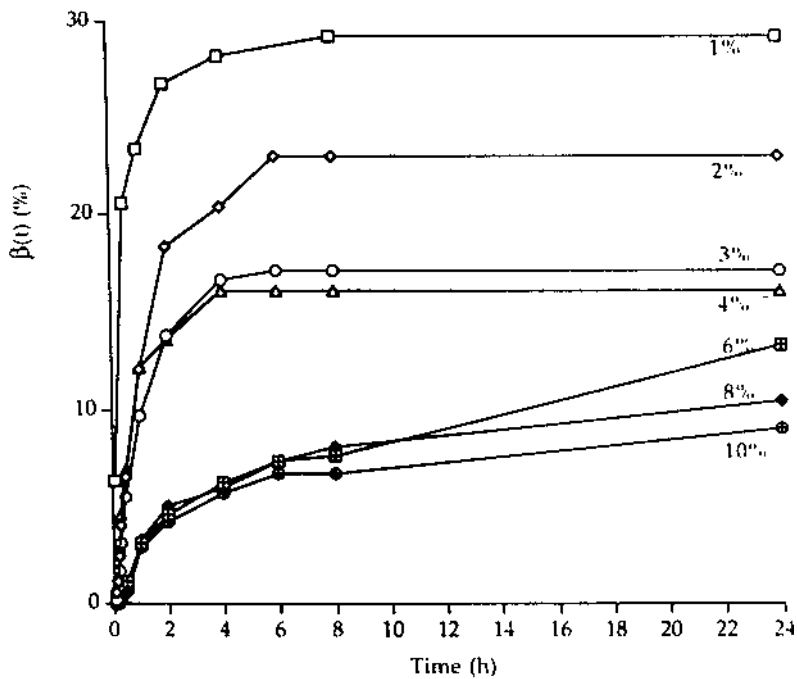


Figure 27 Change in released fraction $\beta(t)$ versus time under hypo-osmotic conditions for different lipophilic surfactant concentrations. (From Ref. 133.)

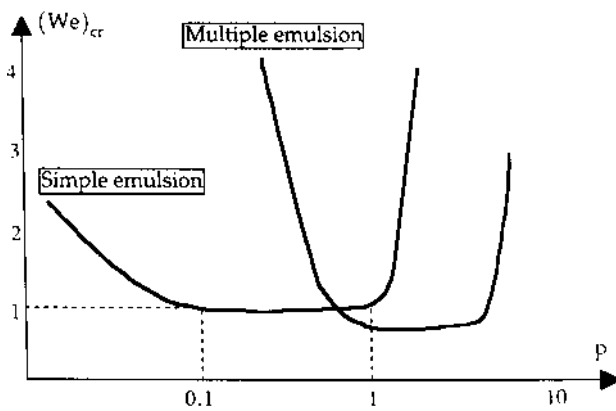


Figure 28 Changes in the critical Weber number $(We)_{cr}$ for simple- and multiple-emulsion disruptions as a function of the viscosity ratio dispersed to the continuous phase. (From Ref. 134.)

(the viscosity ratio between the drop and the continuous phase) for simple and multiple emulsions and that there are some differences between the two emulsions. The double emulsion has more heterogeneous characteristics. From Fig. 29, it is possible to obtain the minimum shear rate value which is able to produce the breakup of the oil globules and the release of water-soluble encapsulated molecules.

The studies showed also that the mechanisms taking place during the breakup were complex and did not always lead to a total release of the entrapped electrolyte. Some phenomena such as a partial leakage of the internal aqueous compartment or the expulsion of the aqueous microglobules covered by a residual lipophilic film were able to restrict the release.

De Cindio and Cacace (125) prepared food double emulsions and studied their rheological behavior by steady shear and oscillatory measurements. They have concluded that the w/o/w appeared to have rheological properties examined to those of a simple o/w emulsion having the same fraction of dispersed phase but lower oil content (Fig. 30). It was also demonstrated that the plot of both storage moduli G' and G'' versus oscillation frequency, ω , are similar in all eight prepared emulsions, and the loss tangent is about 1, and both elastic and viscous contributions to the viscoelastic behavior of double emulsions are of similar magnitude. The similarity of texture between simple and double emulsions is very encouraging, leading to some interesting conclusions and new perspectives. The influence of the mixture of emulsifiers on the double-emulsion stability

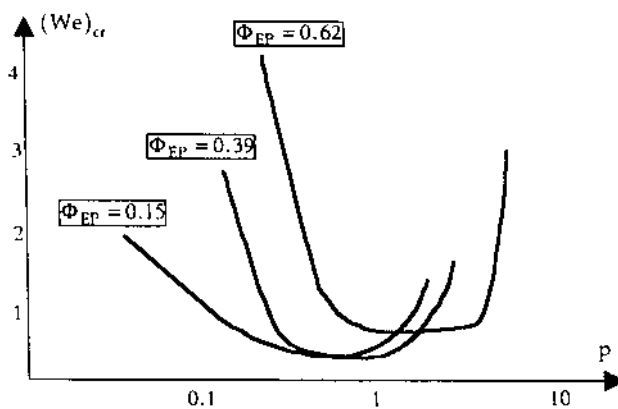


Figure 29 Changes in the critical Weber number $(We)_{cr}$ for multiple-emulsion disruption as a function of the viscosity ratio dispersed to continuous phase, for different primary emulsion volume fractions. (From Ref. 134.)

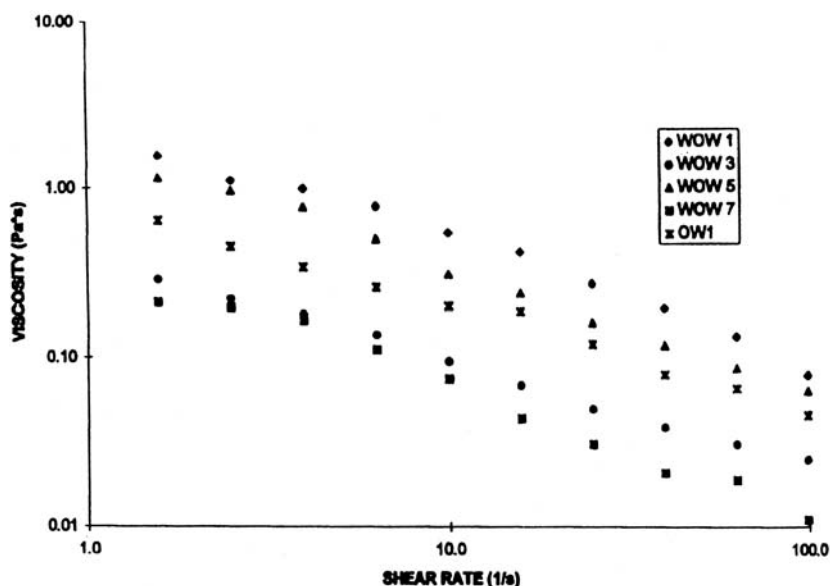


Figure 30 Apparent viscosity versus shear rate for both w/o/w and o/w systems at volume fraction of disperse phase of 0.3. (From Ref. 125).

was studied by an oscillatory ring-surface rheometer from which the interfacial elasticity at the oil–water interface can be evaluated.

Pal (135) studied the rheology of o/w/o double emulsions. The simple o/w emulsions were found to be Newtonian up to a dispersed-phase concentration of 45% by volume and to be non-Newtonian above this volume fraction. All of the double o/w/o emulsions are highly non-Newtonian. The degree of shear thinning increases with the increase in primary o/w emulsion concentration (Fig. 31). The oscillatory measurements indicate that the multiple emulsions are predominantly viscous in that the loss modulus falls above the storage modulus over the entire frequency range investigated (Fig. 32). Upon aging, the storage and loss moduli of the double emulsions show a significant increase. However, the increase in viscosity with aging is only marginal.

The rheological behavior of the w/o/w emulsion studied under a conic plate viscometer has shown a negative thixotropic flow pattern, mostly under a low shear rate. Upon raising the shear rate or the shear time, an increase of the shear stress was observed, which induced phase inversion to a w/o of a semisolid-type emulsion. The hydrodynamic parameters (dissipated energy, kinetic energy, and impulse applied to the emulsion by the rotating cone) causing the phase inversion were determined and a mechanism for

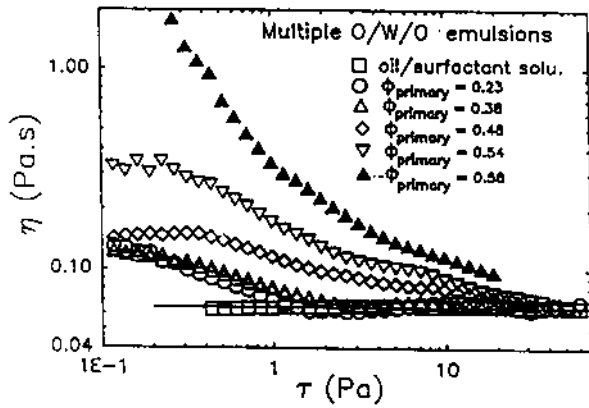


Figure 31 Apparent viscosity as a function of shear stress for multiple o/w/o emulsions. (From Ref. 135.)

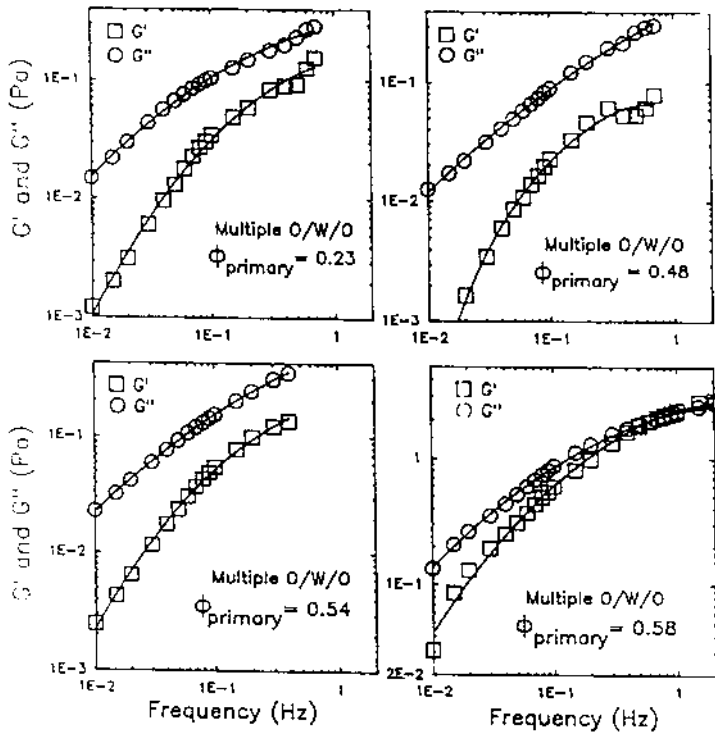


Figure 32 Storage and loss moduli for multiple o/w/o emulsions as functions of frequency. (From Ref. 135.)

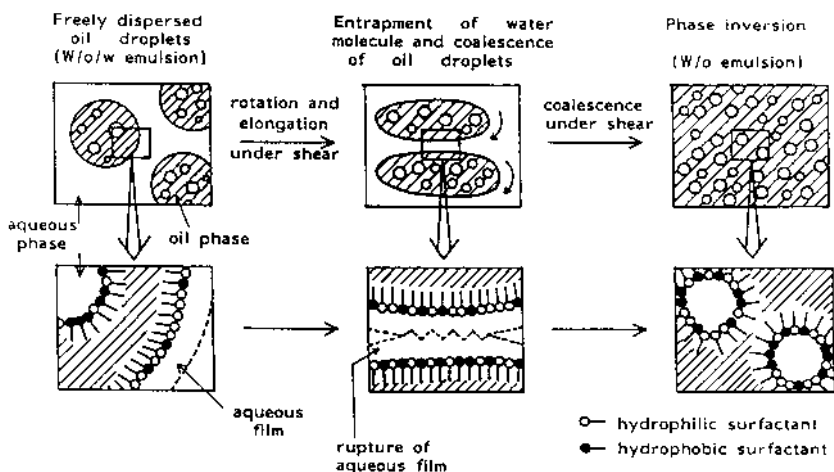


Figure 33 Proposed mechanism of phase inversion under shear. (From Ref. 136.)

such an inversion was suggested. Fig. 33 shows a proposed mechanism for phase inversion under the shear rate (136). Induced shear, causing phase inversion, could serve as a possible technique to release the drug.

XV. CONCLUDING REMARKS

Double emulsions are known for over three decades and were extensively studied in the last 15 years. The internal phase is an excellent reservoir for active matter that needs protection and can be released in a controlled rate. However, the sizes of the droplets and the thermodynamic instability were a significant drawback of this technology.

The use of conventional low-molecular-weight emulsifiers did not solve these problems. However, much progress was made with the introduction of amphiphilic macromolecules as emulsifiers. This multianchoring of flexible macromolecules can improve the steric stabilization by forming, a thick, multilayered coating on the droplets. A variety of hybrids, complexes, adducts, and others between the amphiphiles and coemulsifiers or cosolvents has been suggested. These molecules improved significantly the stability and slowed the release rates. Physical methods of separation, filtration, and extraction also had a positive effect on the release patterns of any drug or active matter. Progress was made also in identifying and characterizing the parameters and mechanisms involved in coalescence, aggregation, and rupture of the double-emulsion droplets. A good control of the rheological

parameters was achieved by a better understanding of their effect on the static and shear-induced stability.

It seems that the double-emulsion technology can now be applied in various application areas, mainly in food, cosmetics, and pharmaceuticals (for nonintravenous applications).

The main goals remain to obtain submicronal double-emulsion droplets with long-term stability (possible by emulsified microemulsions) and to trigger and control the release at will.

Compatible blends of biopolymers (hydrocolloids and proteins) are excellent future amphiphilic candidates which, under certain combinations, will serve both as “release controllers” and “stability enhancers” for the future preparations of double emulsions.

ACKNOWLEDGMENTS

The authors are grateful to Dr. Abraham Aserin for his valuable help and critical reading of the present manuscript.

This work is dedicated to the late Frida and Karl Kissman and supported by the “Kissman Fund for Applied Chemistry,” Jerusalem, Israel.

REFERENCES

1. S. Matsumoto, and W. W. Kang, Formation and applications of multiple emulsions, *J. Dispersion Sci. Technol.* 10, 455–482 (1989).
2. N. Garti, Double emulsions—scope, limitations and new achievements, *Colloids Surf. A: Physicochemical and Engineering Aspects* 123, 233–246 (1997).
3. N. Garti, and A. Aserin, Double emulsions stabilized by macromolecular surfactants, in *Surfactants in Solution*, (A. K. Chattopadhyay and K. L. Mittal, eds.), Surfactant Science Series Vol. 64, Marcel Dekker, New York, 1996, pp. 297–332.
4. N. Garti, Delivery of microparticulated liquid systems in food, in *Handbook of Non-Medical Applications of Liposomes*, (Y. Barenholtz and D. D. Lasic, eds.), CRC, New York, 1996, Vol. 3, pp. 143–199.
5. N. Garti, Influence of the formulation on the characteristics and stability of multiple emulsions, in *Multiple Emulsions: Structure, Properties and Applications* (M. Seiller and J. L. Grossiord, eds.), Editions de santé, Paris, 1998, pp. 81–116.
6. N. Garti, Progress in stabilization and transport phenomena of double emulsions in food applications, *Food Sci. Technol.* 30, 222–235 (1997).
7. N. Garti, and C. Bisperink, Double emulsions: progress and applications, *Curr. Opin. Colloid Interf. Sci.* 3, 657–667 (1998).

8. N. Garti and A. Benichou, Double emulsions for controlled-release applications-Progress and trends, in *Encyclopedic Handbook of Emulsion Technology* (J. Sjoblom, ed.), Marcel Dekker, New York, 2001, pp. 377–407.
9. L. Thill-Francis, Stable double emulsions containing finely divided particles, U.S. patent 93/00007, 1993.
10. A. G. Gaonkar, Method for preparing a multiple emulsion, U.S. patent 5322704, 1994.
11. A. G. Gaonkar, Stable multiple emulsion comprising interfacial gelatinous layer, flavor-encapsulating multiple emulsions and low/no-fat food products comprising the same, U.S. patent 5332595, 1994.
12. Y. Takahashi, T. Yoshida, and T. Takashi, Process for producing a W/O/W type multiple emulsion for medicines, cosmetics, etc., U.S. patent 4985173, 1994.
13. P. Strauel, and G. Friour, Process for preparing photographic emulsions having a low fog level, U.S. patent 94/420106, 1994.
14. C. A. Herb, Rinse-off water-in-oil-in-water compositions. European patent 0717978A2, 1996.
15. G. W. Bams, and W. H. Van Megen, Edible water-in-oil-in-water emulsion, U.S. patent 4650690, 1987.
16. K. Yoshida, T. Sekine, F. Matsuzaki, T. Yanaki, and M. Yamaguchi, Stability of vitamin A in oil-in-water-in-oil-type multiple emulsions, *J. Am. Oil Chem. Soc.* 76(2), 195–200 (1999).
17. S. Y. Kim, and Y. M. Lee, Lipid nanospheres containing vitamin A or vitamin E: Evaluation of their stabilities and in vitro skin permeability, *J. Ind. Eng. Chem.* 5(4), 306–313 (1999).
18. M. Gallarate, M. E. Carlotti, M. Trotta, and S. Bovo, On the stability of ascorbic acid in emulsified systems for topical and cosmetic use, *Int. J. Pharmaceut.* 188, 233–241 (1999).
19. A. Edris, and B. Bergnsthäl, Encapsulation of orange oil in a spray dried double emulsion, *Nahrung Food* 45(2), 133–137 (2001).
20. B. B. C. Youan, J. Gillard, and B. Rollmann, Protein-loaded poly(epsilon-caprolactone) microparticles III. Entrapment of superoxide dismutase by the (water-in-oil)-in-water solvent evaporation method, *STP Pharma Sci.* 9(2), 175–181 (1999).
21. J. L. Grossiord, M. Seiller, I. Pezron, and D. Clause, Multiple emulsions: Vesicular systems with industrial applications, *Oleagineux Corps Gras Lipides* 3(3), 158–162 (1996).
22. T. Uchida, K. Yoshida, and S. Goto, Preparation and characterization of polylactic acid microspheres containing water-soluble dyes using a novel w/o/w emulsion solvent evaporation method, *J. Microencapsulation* 13(2), 219–228 (1996).
23. L. Vigie, Emulsions multiples h/l/h: nouveaux procédés de fabrication et de caractérisation, Graduate thesis, University Paris XI, 1992.
24. J. L. Grossiord, M. Seiller, and A. Silva-Cunha, Obtaining multiple emulsions, in *Multiple Emulsions: Structure, Properties and Applications* (G. Seiller and J. L. Grossiord, eds.), Editions de santé, Paris, 1998, pp. 57–80.

25. E. Pilman, K. Larsson, and E. Torenberg, Inverse micellar phases in ternary systems of polar lipids/fats/water and protein emulsification of such phases to w/o/w–microemulsion–emulsions, *J. Dispersion Sci. Technol.* 1, 267–281 (1980).
26. S. Higashi, M. Shimizu, T. Nakashima, K. Iwata, F. Uchiyama, S. Tateno, S. Tamura, and T. Setoguchi, Arterial-injection chemotherapy for hepatocellular carcinoma using monodispersed poppy-seed oil microdroplets containing fine aqueous vesicles of epirubicin, *Cancer* 75, 1245–1254 (1995).
27. S. Matsumoto, Y. Kida, and D. Yonezawa, An attempt at preparing water-in-oil-in-water multiple-phase emulsions, *J. Colloid Interf. Sci.* 57, 353–361 (1976).
28. S. Matsumoto, M. Koda, and S. Murata, Preparation of lipid vesicles on the basis of a technique for providing w/o/w emulsions, *J. Colloid Interf. Sci.* 62, 149–157 (1977).
29. S. Matsumoto, Y. Ueda, Y. Kita, and D. Yonezawa, Preparation of water-in-oil and oil-in-water multiple emulsions in a eatable form, *Agric. Biol. Chem.* 42, 739–743 (1978).
30. S. Matsumoto, Development of W/O/W-type dispersion during phase inversion of concentrated W/O emulsions, *J. Colloid Interf. Sci.* 94, 362–368 (1983).
31. S. Matsumoto, T. Inoue, M. Koda, and T. Ota, An attempt to estimate stability of the oil layer in water/oil/water emulsions by means of viscometry, *J. Colloid Interf. Sci.* 77, 564–565, (1980).
32. S. Matsumoto, Y. Koh, and A. Michiura, Preparation of water/olive oil/water emulsions in an edible form on the basis of phase inversion technique, *J. Dispersion Sci. Technol.* 6, 507–521 (1985).
33. S. Matsumoto, W/O/W-type multiple emulsions with a view to possible food applications, *J. Texture Studies* 17, 141–159 (1986).
34. M. Frenkel, R. Shwartz, and N. Garti, Stability, inversion, apparent and weighted HLB, *J. Colloid Interf. Sci.* 94, 174–178 (1983).
35. N. Garti, M. Frenkel, and R. Schwartz, Multiple emulsions. Part II: Proposed technique to overcome unpleasant taste of drugs, *J. Dispersion Sci. Technol.* 4, 237–252 (1983).
36. S. Magdassi, M. Frenkel, and N. Garti, On the factors affecting the yield of preparation and stability of multiple emulsions, *J. Dispersion Sci. Technol.* 5, 49–59 (1984).
37. S. Magdassi, M. Frenkel, N. Garti, and R. Kasan, Multiple emulsions II—HLB shift caused by emulsifier migration to the external interface, *J. Colloid Interf. Sci.* 97, 374–379 (1984).
38. S. Magdassi, M. Frenkel, and N. Garti, Correlation between nature of emulsifier and multiple emulsion stability, *Drug Dev. Ind. Pharm.* 11, 791–798 (1985).
39. S. Magdassi, and N. Garti, A kinetic model for release of electrolytes from w/o/w multiple emulsions, *J. Control. Release*, 3, 273–277 (1986).
40. A. J. Khopade, and N. K. Jain, Long-circulating multiple-emulsion system for improved delivery of an anticancer agent, *Drug Delivery* 6(2), 107–110 (1999).
41. M. P. Y. Piemi, M. De Luca, J. L. Grossiord, M. Seiller, and J. P. Marty, Transdermal delivery of glucose through hairless rat skin in vitro: effect of multiple and simple emulsions, *Int. J. Pharm.* 171(2), 207–215 (1998).

42. M. F. Ficheux, L. Bonakdar, F. Leal-Calderon, and J. Bibette, Some stability criteria for double emulsions, *Langmuir* 14(10), 2702–2706 (1998).
43. H. L. Rosano, F. G. Gandolfo, and J. D. P. Hidrot, Stability of W-1/O/W-2 multiple emulsions—Influence of ripening and interfacial interactions, *Colloids Surfaces A: Physicochemical and Engineering Aspects* 138(1), 109–121 (1998).
44. R. G. Stehle, and W. I. Higuchi, In vitro model for transport of solutes in three phase system. I. Theoretical principles. II. Experimental considerations, *J. Pharmaceut. Sci.* 61, 1922–1930 (1972).
45. A. Vaziri, and B. Warburton, Some preparative variables influencing the properties of w/o/w multiple emulsions, *J. Microencapsulation* 11(6), 649–656 (1994).
46. W. Zhang, T. Miyakawa, T. Uchida, and S. Goto, Preparation of stable w/o/w type multiple emulsion containing water-soluble drugs and in-vitro evaluation of its drug releasing properties, *J. Pharm. Soc. Japan.* 112(1), 73–80 (1992).
47. M. Cornec, P. J. Wilde, P. A. Gunning, A. R. Mackie, F. A. Husband, M. L. Parker, and D. C. Clark, Emulsion stability as affected by competitive adsorption between an oil-soluble emulsifier and milk proteins at the interface, *J. Food Sci.* 63(1), 39–43 (1998).
48. E. Fredrokumbaradzi, and A. Simov, Effect of bovine serum albumin (BSA) on release of sulfacetamide sodium from multiple w/o/w emulsions, *Pharmazie* 47(5), 388–389 (1992).
49. N. Garti, A. Aserin, and Y. Cohen, Mechanistic considerations on the release of electrolytes from multiples emulsions stabilized by BSA and nonionic surfactants, *J. Control. Release* 29, 41–51 (1994).
50. E. Dickinson, J. Evison, R. K. Owusu, and A. Williams, Protein stabilized water-in-oil-water emulsions, in *Gums and Stabilizers for the Food Industry* (G. O. Phillips, P. A. Williams and D. J. Wedlock, eds.), IRL Oxford University Press, Oxford, 1994, Vol. 7, pp. 91–101.
51. E. Dickinson, J. Evison, and R. K. Owusu, Preparation of fine protein-stabilized water-in-oil-in-water emulsions, *Food Hydrocolloids* 5, 481–485 (1991).
52. J. Evison, E. Dickinson, R. K. Owusu Apenten, and A. Williams, Formulation and properties of protein-stabilized W/O/W multiple emulsion, in *Food Macromolecules and Colloids* (E. Dickinson and D. Lorient, eds.), Royal Society of Chemistry, Cambridge, 1995, pp. 235–243.
53. A. Koberstein Hajda, and E. Dickinson, Stability of water-in-oil-in-water emulsions containing faba bean proteins, *Food Hydrocolloids* 10(2), 251–254 (1996).
54. P. C. Schulz, M. S. Rodriguez, and L. F. Del Blanco, Emulsification properties of chitosan, *Colloid Polym. Sci.* 276(12), 1159–1165 (1998).
55. T. Adachi, J. Ida, and M. Wakita, Preparation of spherical and porous chitosan particles by suspension evaporation with O/W/O multiple emulsions, *Polym. J.* 31(4), 319–323 (1999).
56. S. C. Yu, A. Bochet, M. Cheron, M. Seiller, J. L. Grossiord, G. Le Bas, and D. Duchene, Design and evaluation of an original o/w/o multiple emulsion

- containing natural cyclodextrins as the emulsifier, *STP Pharm. Sci.* 9(3), 273–277 (1999).
57. A. Benichou, A. Aserin, and N. Garti, Protein–polysaccharide interactions for stabilization of food emulsions. A review, *J. Dispersion Sci. Technol.* 23(1&3), 93–123 (2002).
 58. V. B. Tolstoguzov, Protein–polysaccharide interactions, in *Food Proteins and their Applications* (S. Damodaran and A. Paraf, eds.), Marcel Dekker, New York, 1997, pp. 171–200.
 59. V. B. Tolstoguzov, Functional properties of food proteins and role of protein–polysaccharide interactions, *Food Hydrocolloids* 4, 429–468 (1991).
 60. V. Y. Grinberg, and V. B. Tolstoguzov, Thermodynamic incompatibility of proteins and polysaccharides in solutions, *Food Hydrocolloids* 11, 145–158 (1997).
 61. C. Sanchez, C. Schmitt, V. G. Babak, and J. Hardy, Rheology of whey protein isolate–xanthan mixed solutions and gels. Effect of pH and xanthan concentration, *Nahrung* 41, 336–343 (1997).
 62. P. Walkenstrom, N. Panighetti, E. Windhab, and A. M. Hermansson, Effect of fluid shear and temperature on whey protein gels, pure or mixed with xanthan, *Food Hydrocolloids* 12, 469–479 (1998).
 63. S. I. Laneuville, P. Paquin, and S. L. Turgeon, Effect of preparation conditions on the characteristics of whey protein–xanthan gum complexes, *Food Hydrocolloids* 14, 305–314 (2000).
 64. C. M. Bryant, and D. J. McClement, Influence of xanthan gum on physical characteristics of heat denaturated whey protein solutions and gels, *Food Hydrocolloids* 14, 383–390 (2000).
 65. H. Zaleska, S. G. Ring, and P. Tomasik, Apple pectin complexes with whey protein isolate, *Food Hydrocolloids* 14, 377–382 (2000).
 66. C. Schmitt, C. Sanchez, F. Thomas, and J. Hardy, Complex coarcevation between β -lactoglobulin and acacia gum in aqueous medium, *Food Hydrocolloids* 13, 483–496 (1999).
 67. F. Simonet, C. Garnier, and J. L. Doublier, Partition of proteins in the guar/dextran two-phase systems, *Food Hydrocolloids* 14, 591–600 (2000).
 68. M. M. Alves, C. Garnier, J. Lefebvre, and M. P. Goncalves, Microstructure and flow behavior of liquid water–gelatin–locust bean gum systems, *Food Hydrocolloids* 15, 117–125 (2001).
 69. M. M. Ould Eleya, and S. L. Turgeon, Rheology of κ -carrageenan and β -lactoglobulin mixed gels, *Food Hydrocolloids* 14, 29–40 (2000).
 70. M. M. Ould Eleya, and S. L. Turgeon, The effects of pH on the rheology of β -lactoglobulin/ κ -carrageenan mixed gels, *Food Hydrocolloids* 14, 245–251 (2000).
 71. A. Antonov Yu, and M. P. Goncalves, Phase separation in aqueous gelatin- κ -carrageenan systems, *Food Hydrocolloids* 13, 517–524 (1999).
 72. M. Verheul, and S. Roefs, Structure of whey protein gels, studied by permeability, scanning electron microscopy and rheology, *Food Hydrocolloids* 12, 17–24 (1998).

73. P. Walkenstrom, and A. M. Hermansson, Effect of shear on pure and mixed gels of gelatin and particulate whey protein, *Food Hydrocolloids* 12, 77–87 (1998).
74. P. Walkenstrom, E. Windhalb, and A. M. Hermansson, Shear-induced structuring of particulate whey protein gels, *Food Hydrocolloids* 12, 459–468 (1998).
75. F. Delben, and S. Stefancish, Interaction of food polysaccharides with ovalbumin, *Food Hydrocolloids* 12, 291–299 (1998).
76. C. M. Bryant, and D. J. McClements, Optimizing preparation conditions for heat-denatured whey protein solutions to be used as cold-gelling ingredients, *J. Food Sci.* 65(2), 259–263 (2000).
77. V. B. Galazka, I. G. Summer, and D. A. Ledward, Changes in protein–protein and protein–polysaccharide interactions induced by high pressure, *Food Chem.* 57, 393–398 (1996).
78. P. Paquin, Technological properties of high pressure homogenizers: The effect of fat globules, milk proteins, and polysaccharides, *Int. Dairy J.* 9, 329–335 (1999).
79. N. Lagoueyte, and P. Paquin, Effect of microfluidization on the functional properties of xanthan gum, *Food Hydrocolloids* 12, 365–371 (1998).
80. Y. T. Wu, D. Q. Lin, and A. Q. Zhu, Thermodynamics of aqueous two-phase systems. The effect of polymer molecular weight on liquid–liquid equilibrium phase diagrams by the modified NRTL model, *Fluid Phase Equilibria* 147, 25–43 (1998).
81. J. L. Doublier, C. Garnier, D. Renard, and C. Sanchez, Protein–polysaccharide interactions, *Curr. Opin. Colloid Interf. Sci.* 5, 202–214 (2000).
82. E. Dickinson, The role of hydrocolloids in stabilizing particulate dispersions and emulsions, in *Gums and Stabilisers for the Food Industry* (G. O. Phillips, D. J. Wedlock and P. A. Williams, eds.), IRL Press, Oxford, 1988, Vol. 4, pp. 249–263.
83. V. B. Galazka, E. Dickinson, and D. A. Ledward, Effect of high pressure on ovalbumin–polysaccharide interactions. *High Pressure Res.* 19(1–6), 515–520 (2000).
84. N. A. Larichev, A. N. Gurov, and V. B. Tolstoguzov, Protein–polysaccharide complexes at the interface. I. Characteristics of decane/water emulsions stabilized by complexes of bovine serum albumin with dextran sulfate, *Colloids Surfaces* 6, 27–34 (1983).
85. E. S. Tokaev, A. N. Gurov, I. A. Rogov, and V. B. Tolstogusov, Properties of oil/water emulsions stabilized by casein-acid polysaccharide mixture, *Nahrung* 31, 825–834 (1987).
86. M. S. Lippi, and M. V. Taranto, Soy protein–acidic polysaccharide interaction: Modification of the emulsification properties of soy protein isolate, *Food Sci. Technol.* 14(2), 55–59 (1981).
87. E. Dickinson, and K. Pawlowsky, Effect of τ -carrageenan on flocculation, creaming and rheology of a protein-stabilized emulsion, *J. Agric. Food Chem.* 45, 3799–3806 (1997).

88. K. Nagasawa, K. Takahashi, and M. Hattori, Improved emulsifying properties of β -lactoglobulin by conjugating with carboxymethyl dextran, *Food Hydrocolloids* 10(1), 63–67 (1996).
89. E. Dickinson, and V. B. Galazka, Emulsion stabilization by protein–polysaccharides complexes, in *Gums and Stabilisers for the Food Industry* (G. O. Phillips, D. J. Wedlock and P. A. Williams, eds.), IRL Press, Oxford, 1992, Vol.6, pp. 351–361.
90. V. B. Galazka, E. Dickinson, and D. A. Ledward, Influence of high pressure on interactions of 11S globulin vicia faba with ι -carrageenan in bulk solution and at interfaces, *Food Hydrocolloids* 14, 551–560 (2000).
91. E. Dickinson, and J. D. James, Influence of high-pressure treatment on β -lactoglobulin-pectin associations in emulsions and gels, *Food Hydrocolloids* 14, 365–376 (2000).
92. E. Dickinson, and K. Pawlowsky, Effect of high-pressure treatment of protein on the rheology of flocculated emulsions containing protein and polysaccharide, *J. Agric. Food Chem.* 44, 2992–3000 (1996).
93. V. B. Galazka, E. Dickinson, and D. A. Ledward, Emulsifying Behavior of 11S globulin vicia faba in mixtures with sulphated polysaccharides: Comparison of thermal and high-pressure treatments, *Food Hydrocolloids* 13, 425–435 (1999).
94. A. Benichou, A. Aserin, and N. Garti, Multiple emulsions stabilized by new molecular-recognition hybrids of natural polymers, in *Polymers for Advanced Technologies* 13(10–12), 1019–1031 (2002).
95. D. Rousseau, Fat crystals and emulsion stability—A review, *Food Res. Int.* 33, 3–14 (2000).
96. D. Johansson, B. Bergnstahl, and E. Lundgren, Wetting of fat crystals by triglycerides oil and water. I. The effect of additives, *J. Am. Oil Chem. Soc.* 72, 921–932 (1995).
97. D. Johansson, and B. Bergnstahl, Wetting of fat crystals by triglycerides oil and water. II. Adhesion to the oil/water interface, *J. Am. Oil Chem. Soc.* 72, 933–938 (1995).
98. K. P. Oza, and S. G. Frank, Microcrystalline cellulose stabilized emulsions, *J. Dispersion Sci. Technol.* 7, 543–561 (1986).
99. A. J. Khopade, and N. K. Jain, A stable multiple emulsion system bearing isoniazid: Preparation and characterization, *Drug Dev. Ind. Pharm.* 24(3), 289–293 (1998).
100. N. Garti, A. Aserin, and I. Tiunova, Double emulsions of water-in-oil-in-water stabilized by alpha-form fat microcrystals. Part I: Selection of emulsifiers and fat microcrystalline particles, *J. Am. Oil Chem. Soc.* 76(3), 383–389 (1999).
101. T. Sekine, K. Yoshida, and F. Matsuzaki, A novel method for preparing oil-in-water-in-oil type multiple emulsions using organophilic montmorillonite clay mineral, *J. Surfact. Detergents* 2(3), 309–315 (1999).
102. P. Walstra, On the usefulness of dairy research, *Int. Dairy J.* 8, 155–161 (1998).

103. D. A. Edwards, and D. T. Wasan, A micromechanical model of linear surface rheological behavior, *Chem. Eng. Sci.* 46, 1247–1257 (1991).
104. W. Kiosseoglou, Minor surface-active lipids of olive oil and viscoelasticity of protein films at the olive oil-water interface, *J. Dispersion Sci. Technol.* 13, 135–144 (1992).
105. A. Vaziri, and B. Warburton, Improved stability of w/o/w multiple emulsion by addition of hydrophilic colloid components in the aqueous phase, *J. Microencapsulation* 12(1), 1–5 (1995).
106. S. Susuki, and J. K. Lim, Microencapsulation with carrageenan, locust bean gum mixture in a multiphase emulsification technique for sustained drug-release, *J. Microencapsulation* 11(2), 197–203 (1994).
107. D. Clause, Thermal behavior of emulsions studied by differential scanning calorimetry, *J. Therm. Anal. Calorim.* 51(1), 191–201 (1998).
108. D. Clause, I. Pezron, and L. Komunjner, Stability of w/o and w/o/w emulsions as a result of partial solidification, *Colloids Surfaces A: Physicochemical and Engineering Aspects* 152, 23–29 (1999).
109. Y. Ogawa, Y. M. Yamamoto, H. Okada, H. T. Yashiki, and T. Shimamoto, New technique to efficiently entrap leuprolidine acetate into microcapsules of polylactic acid of poly(lactic/glycolic)acid, *Chem. Pharm. Bull.* 36, 1095–1103 (1988).
110. M. J. Blanco-Prieto, F. Delie, A. Fattal, A. Tartar, F. Puisieux, A. Gulik, and P. Couvreur, Characterization of V3 BRU peptide loaded small PLGA microspheres prepared by a W1/O/W2 emulsion solvent evaporation method, *Int. J. Pharm.* 111, 137–145 (1994).
111. C. H. Schugens, N. Laruelle, N. Nihant, C. Grandfils, R. Jerome, and P. Teyssie, Effect of the emulsion stability on the morphology and porosity of semicrystalline poly-L-lactide microparticles prepared by w/o/w double emulsion evaporation, *J. Control. Release* 32(2), 161–176 (1994).
112. N. Nihant, C. Schugens, C. Grandfils, R. Jerome, and P. Teyssie, Polylactide microparticles prepared by double emulsion-evaporation. 2. Effect of the poly(lactide-co-glycolide) composition on the stability of the primary and secondary emulsions, *J. Colloid Interf. Sci.* 173(1), 55–65 (1995).
113. M. J. Blanco-Prieto, E. Leo, F. Delie, A. Gulik, P. Couvreur, and E. Fattal, Study of the influence of several stabilizing agents on the entrapment and in vitro release of PBC from poly(lactide-co-glycolide) microspheres prepared by a w/o/w solvent evaporation method, *Pharm. Res.* 13, 1137–1139 (1996).
114. R. Cortesi, F. Bortolotti, E. Menegatti, C. Nastruzzi, and E. Esposito, Production and characterization of biodegradable microparticles for the controlled delivery of proteinase inhibitors, *Int. J. Pharm.* 129, 263–273 (1996).
115. P. Couvreur, M. J. Blanco-Prieto, F. Puisieux, B. Roques, and E. Fattal, Multiple emulsions technology for the design of microspheres containing peptides and oligopeptides, *Adv. Drug Delivery Rev.* 28, 85–96 (1997).
116. M. J. Blanco-Prieto, E. Fattal, A. Gulik, B. Dedieu, and P. Couvreur, Characterization and morphological analysis of a cholecystokinin derivative

- peptide-loaded poly(lactide-co-glycolide) microspheres prepared by a w/o/w emulsion solvent evaporation method, *J. Control. Release* 43, 81–87 (1997).
117. Y. Maa, and C. Hsu, Liquid–liquid emulsification by rotor/stator homogenisation, *J. Control. Release* 38, 219–228 (1996).
 118. H. Rafati, A. Coombes, J. Adler, J. Holland, and S.S. Davis, Protein loaded poly(DL-lactide-co-glycolide) microparticles for oral administration: Formulation, structural and release characteristics, *J. Control. Release* 43, 89–102 (1997).
 119. N. Ubrich, J. Ngondi, C. Rivat, M. Pfister, C. Vigneron, and P. Maincent, Selective in vitro removal of anti-A antibodies by adsorption on encapsulated erythrocytes–ghosts, *J. Biomed. Mater. Res.* 37, 155–160 (1997).
 120. Y. F. Maa, and C. C. Hsu, Effect of primary emulsions on microsphere size and protein-loading in the double emulsion process, *J. Microencapsulation* 14, 225–241 (1997).
 121. E. Leo, S. Pecuet, J. Rojas, and P. Couvreur, Changing the pH of the external aqueous phase may modulate protein entrapment and delivery from poly(lactide-co-glycolide) microspheres prepared by a w/o/w evaporation method, *J. Microencapsulation* 15, 421–430 (1998).
 122. M. F. Zambaux, F. Bonneaux, R. Gref, E. Maincent, M. Dellacherie, J. Alonso, P. Labrude, and C. Vigneron, Influence of experimental parameters on the characteristics of poly(lactic acid) nanoparticles prepared by double emulsion method, *J. Control. Release* 50, 31–40 (1998).
 123. T. G. Park, M. J. Alonso, and R. Langer, Controlled release of proteins from poly(L-lactic acid) coated polyisobutylcyanoacrylate microcapsules, *J. Applied Polymer Sci.* 52, 1797–1807 (1994).
 124. B. De Cindio, and D. Cacace, Formulation and rheological characterization of reduced-calorie food emulsions, *Int. J. Food Sci. Technol.* 30, 505–514 (1995).
 125. B. De Cindio, G. Grasso, and D. Cacace, Water-in-oil-in-water emulsions for food applications, *Food Hydrocolloids* 4, 339–353 (1991).
 126. D. K. Asahi, Double emulsified oil-fat composition comprises outer phase of oil and fat inner phase of oil-in-water emulsified fats, and oil and fat phase containing mustard oils, Japanese patent 87016619, 1987.
 127. K. K. Yoshihara Seiyu, Oil and fat cooking product containing double emulsion of liquid oil and fat of above 30°C melting points, Japanese patent 60091939, 1985.
 128. K. Suzuki, K. Uehara, and H. Omura, Oil-in-water-in-oil double emulsified fat or oil composition for cream, spread confectionery or baking use, European patent 425958, 1991.
 129. S. Tsukishima, Double emulsion type filling cream obtained by adding fat or oil to aqueous phase containing saccharides, protein and/or emulsifiers and mixing with plastic fat or oil, Japanese patent 3290152, 1991.
 130. C. Laugel, P. Rafidison, G. Potard, L. Aguadisch, and A. Baillet, Modulated release of triterpenic compounds from a o/w/o multiple emulsion formulated with dimethicones: Infrared spectrophotometric and differential calorimetric approaches, *J. Control. Release* 63(1–2), 7–17 (2000).

131. V. Muguet, M. Seiller, G. Barratt, D. Clausse, J.P. Marty, and J.L. Grossiord, w/o/w multiple emulsions submitted to a linear shear flow: Correlation between fragmentation and release, *J. Colloid Interf. Sci.* 218, 335–337 (1999).
132. S. Geiger, N. Jager-Lezer, S. Tokgoz, M. Seiller, and J.L. Grossiord, Characterization of the mechanical properties of a water/oil/water multiple emulsion oily membrane by a micropipette aspiration technique, *Colloids Surfaces A: Physicochemical and Engineering Aspects*, 157(1–3), 325–332 (1999).
133. J. L. Grossiord, and M. Seiller, Rheology of w/o/w multiple emulsions: formulation, characterization and breakup mechanisms, in *Multiple Emulsions: Structure, Properties and Applications* (J.L. Grossiord and M. Seiller, eds.), Editions de santé, Paris, 1998, pp. 169–192.
134. P. Stroeve, and P. P. Varanassi, An experimental study on double emulsion drop breakup in uniform shear flow, *J. Colloid Interf. Sci.* 99, 360–373 (1984).
135. R. Pal, Multiple O/W/O emulsion rheology, *Langmuir* 12(9), 2220–2225 (1996).
136. Y. Kawashima, T. Hino, H. Takeushi, T. Niwa, and K. Horibe, Rheological study of w/o/w emulsion by a cone-and-plate viscometer: negative thixotropy and shear-induced phase inversion, *Int. J. Pharm.* 72, 65–77 (1991).

11

Structure, Mechanics, and Rheology of Concentrated Emulsions and Fluid Foams

H. M. Princen

Consultant, Flemington, New Jersey, U.S.A.

I. BACKGROUND

Whether enjoying the luxury of a bubble bath or enduring the drudgery of washing dishes, one is likely to be struck by the beauty and intricate structure of foams, froths, or “suds.” Keen observers may even notice the unusual elastic and yield properties, not seen in the constituent aqueous and gaseous phases. Scientifically, the interest in and the study of foams have been truly multidisciplinary and have not been confined to chemists, engineers, and physicists. Foams have traditionally inspired mathematicians for their geometric properties and as equilibrium structures in which the surface area is minimized (1). Metallurgists (2) have realized the similarity between foams and polycrystalline metals, both in their structure and coarsening behavior (grain growth). Similarly, botanists and life scientists in general have noticed strong structural parallels between foams and living tissues (3).

Gas–liquid foams are abundant in nature and their technological applications are numerous. They are used to advantage in fire fighting, enhanced oil recovery, foods (e.g., whipped cream), cosmetics (e.g., shaving cream), and in many other ways. The “world of foams” may be considerably expanded by the realization that concentrated liquid–liquid emulsions, although generally characterized by a much smaller mean size of the dispersed units, are structurally identical to gas–liquid foams, which is readily revealed under the microscope. Macroscopically, they behave like

viscoelastic gels, mayonnaise being a good example. Such emulsions have been variously referred to as high-internal-phase-ratio emulsions (HIPREs), biliquid foams, “aphrons,” or, simply, highly concentrated emulsions. Although they lack the compressibility of gas–liquid foams, they behave similarly in all other respects. Detailed study of such emulsion systems started rather recently and may perhaps be traced to the attempts of Lissant (4–6) and Beerbower et al. (7–10) to design safer aviation and rocket fuels, in which fuel droplets are tightly packed inside a continuous aqueous phase. Reverse (i.e., concentrated water-in-oil) systems can be readily prepared as well. They find application in the high-explosives area, but have particular appeal in the foods and cosmetics industries. What entrepreneur’s mouth would not water at the prospect of being able to sell a product that is at least 90% water and yet is luxuriously rich and creamy? Lissant, in particular, patented numerous potential applications in these areas (e.g., Ref. 11). In yet other applications, the oil phase, either external or internal, can consist of a polymerizable monomer. Subsequent polymerization by heat or radiation can lead to interesting polymers or structurally unique materials (e.g., Refs. 6 and 12–16).

Because of all of these scientific and technological aspects, a thorough understanding of foams and concentrated emulsions is highly desirable. In response to this need, there has lately been a clear upsurge in interest, again from a variety of disciplines, and considerable progress has been and is being made. Several comprehensive textbooks on emulsions and foams have recently been published (17–22). We believe that the overlap with this review is minimal.

II. INTRODUCTION

In general, when a fluid phase (liquid or gas) is dispersed in an immiscible liquid to form drops or bubbles, there is a tendency for the phases to separate again to reduce the augmented surface free energy. With pure phases, this proceeds by rapid coalescence of approaching dispersed entities, as there is no barrier against rupture of the intervening liquid film. Stability or, more correctly, metastability can be conferred by adsorption of surfactants, polymers, or finely divided solid particles at the interface. By this expedient, coalescence can often be suppressed completely. However, this will not prevent ultimate phase separation, as there is another mechanism for reducing the surface area, namely Ostwald ripening. By this mechanism, large bubbles or drops grow at the expense of small ones by dissolution and diffusion of the dispersed phase in response to the higher Laplace pressure in the latter ones. Because gases tend to have greater solubility and diffusivity

in a given continuous liquid than do most other liquids, this process is generally much more rapid in foams than in emulsions. Indeed, whereas most foams will not survive for more than a few hours—even in the absence of coalescence—it is relatively easy to prepare concentrated emulsions whose drop size distribution does not change perceptibly for months or years. They are kinetically or operationally (although not thermodynamically) stable. For this and many other reasons, emulsions may be better characterized and their properties more reliably investigated experimentally than is possible with foams. Thus, to learn about *foam* behavior through experiments, we recommend one look at concentrated emulsions instead. In the same vein, we may use the terms “bubble” and “drop” interchangeably.

In this review, we will only consider stable dispersions, in which coalescence has been totally suppressed. We further restrict ourselves to highly concentrated dispersions, in which the volume fraction of the dispersed phase, ϕ , exceeds a critical value ϕ_0 where the properties start to change drastically. This critical volume fraction corresponds to that of a system of close-packed spheres having the same drop volume distribution as the dispersion. The term “close packed” is somewhat ambiguous and the corresponding volume fraction is not always clearly defined and/or established. Although monodisperse spheres can, in principle, be packed to a maximum density of $\phi_0 = 0.7405$, this value is rarely achieved. In practice, one is more likely to achieve only *random* close packing, which is considerably less dense ($\phi_0 \approx 0.64$) due to the voids created by “arching.” There is a persistent myth that the packing density of a *polydisperse* system is characterized by $\phi_0 > 0.7405$. It is true that the voids in a close-packed system of spheres can be filled sequentially with smaller and smaller spheres of very specific sizes until $\phi_0 \approx 1$. However, this would require a unique multimodal size distribution as well as a unique spatial distribution, neither of which are likely to be ever encountered in practice. It is our experience with typical, unimodal polydisperse emulsions that the spherical droplets arrange themselves at a packing density that, although considerably larger than the 0.64 expected for the random close-packed monodisperse case, is close to but slightly *smaller* than 0.74. Although the actual value must depend somewhat on the details of the size distribution, we estimate that $0.70 < \phi_0 < 0.74$ in most practical cases, where conventional means are used to prepare the emulsion (23,24).

There are reasons why the *effective* value of ϕ , including that of ϕ_0 , may deviate from the apparent value. If the thickness, h , of the stabilized film of continuous phase, separating the dispersed drops or bubbles, is not insignificant compared to the drop or bubble radius, R , then the effective volume of each drop must be augmented by that of a surrounding sheath of thickness $h/2$. This leads to a somewhat larger effective volume fraction,

ϕ_e , which is given (23) by

$$\phi_e = \phi \left[1 - \left(\frac{\phi}{\phi_0} \right)^{1/3} \frac{h}{2R} \right]^{-3} \approx \phi \left(1 + \frac{3.15h}{2R} \right) \quad (1)$$

The latter form is a good approximation for any $\phi > \phi_0$ and $h/R \ll 1$. In most foams, the effect is expected to be minimal, as the bubbles tend to be relatively large. For emulsions of small drop size, however, the effect may be considerable and the peculiar properties resulting from extreme crowding may commence at an apparent volume fraction that is considerably smaller than one would expect for zero film thickness. For example, in an emulsion with droplets of $2R = 1 \mu\text{m}$ and $h = 50 \text{ nm}$, the effective volume fraction already reaches a value of 0.74 at an apparent volume fraction of only about 0.64! The finite film thickness may, for example, result from electrostatic double-layer forces (25) or adsorbed polymers. In what follows, we shall assume zero film thickness, with the understanding that Eq. (1) is to be invoked whenever $h/R \neq 0$.

Another complication arises when strong attractive forces operate between the drops or bubbles. This may lead to a finite contact angle, θ , between the intervening film (of reduced tension) and the adjacent bulk interfaces (23,26–28). Under those conditions, droplets will spontaneously deform into truncated spheres upon contact and can thus pack to much higher densities. For monodisperse drops, the ideal close-packed density, consistent with minimization of the system's surface free energy, is given (23) by

$$\phi_0(\theta) = 0.7405 \left(-\frac{5}{\cos^3 \theta} + \frac{9}{\cos^2 \theta} - 3 \right) \quad (2)$$

which is valid up to $\theta = 30^\circ$, where $\phi_0 = 0.964$. For $\theta = 0$, we recover $\phi_0 = 0.7405$, and ϕ_0 is expected to reach unity when θ exceeds 35.26° (23,28). In the latter limit, all of the continuous phase (except that in the intervening films) should, in principle, be squeezed out spontaneously. In practice, however, one tends to find just the opposite; that is, when θ is large, the droplets spontaneously flocculate into a rather open structure in which $\phi_0 < 0.7405$. The situation is similar to that of a flocculated solid dispersion whose sediment volume is generally greater than that of a stable dispersion. Apparently, the strong attractive forces prevent the droplets from sliding into their energetically most favorable positions, leaving large voids in the otherwise dense structure. Nevertheless, the structure may be irreversibly densified to approach the condition prescribed by Eq. (2) by centrifugation and subsequent relaxation (23,27). Foams and emulsions in which $\theta \neq 0$ have only been studied occasionally and will rarely be touched upon in this review.

III. STRUCTURAL ELEMENTS

As discussed earlier, the nature and properties of fluid–fluid dispersions start to change drastically when the volume fraction approaches or exceeds ϕ_0 . A certain rigidity sets in, because the drops or bubbles can no longer move freely past each other.

As the volume fraction is raised beyond ϕ_0 , the drops lose their sphericity and are increasingly deformed while remaining separated by thin stable films of continuous phase. At sufficiently high ϕ , the drops become distinctly polyhedral, albeit with rounded edges and corners. At this stage, the continuous phase is confined to two structural elements: *linear* Plateau borders with an essentially constant cross section over some finite length, and *tetrahedral* Plateau borders, where four linear borders converge (Fig. 1a).

Each linear border is generally curvilinear and fills the gap between the rounded edges of three adjoining polyhedral drops. In cross section, its sides are formed by three arcs, each pair of which meets tangentially to form the thin film separating the corresponding droplet pair (Fig. 1b). The pressures in the drops are related to the mean curvatures of the intervening films through

$$\begin{aligned} p_1 - p_2 &= 2\sigma C_{12} \\ p_2 - p_3 &= 2\sigma C_{23} \\ p_3 - p_1 &= 2\sigma C_{31} \end{aligned} \quad (3)$$

where σ is the interfacial tension between the continuous and dispersed phases and the sign of each film curvature C is taken positive (negative)

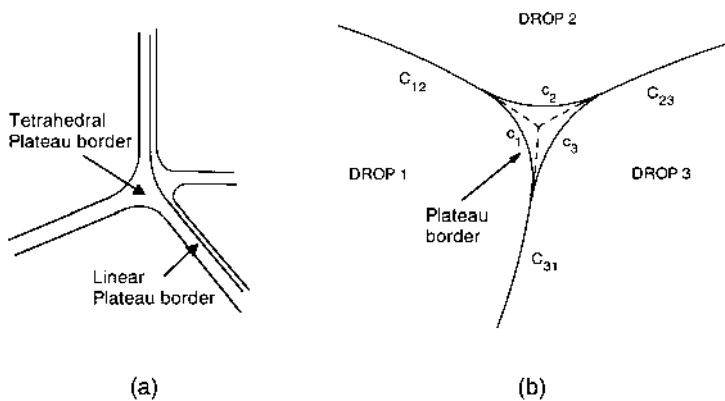


Figure 1 (a) Four linear Plateau borders meeting in a tetrahedral plateau border; (b) cross section through a linear Plateau border and its three associated films and drops.

if the pressure in the drop indicated by the first index is the higher (lower) one. Adding Eqs. (3) leads to the following relationship between the three mean film curvatures:

$$C_{12} + C_{23} + C_{31} = 0 \quad (4)$$

The pressure inside the linear Plateau border, p_b , is given by

$$p_b = p_1 - \sigma c_1 = p_2 - \sigma c_2 = p_3 - \sigma c_3 \quad (5)$$

where c_1 , c_2 , and c_3 are the curvatures of the border walls and are all counted as positive. Since all Plateau borders are connected, they are in hydrostatic equilibrium.

Normally, an ambient gaseous atmosphere of pressure P surrounds the dispersion. Relative to this ambient pressure, p_b is lower and given (29) by

$$p_b = P - \sigma_c |C_t| \quad (6)$$

where $|C_t|$ is the absolute value of the curvature of the free continuous-phase surface at the dispersion–atmosphere boundary (i.e., *between* the exposed bubbles) and σ_c is the *surface tension* of the continuous phase [$\sigma_c = \sigma$ for foams, but $\sigma_c \neq \sigma$ for emulsions (29) unless the “ambient atmosphere” consists of bulk dispersed liquid].

The excess pressures in the drops, relative to that in the interstitial continuous phase, p_b , are often referred to as their *capillary pressures*, p_c . For example,

$$(p_c)_1 = p_1 - p_b = \sigma c_1 \quad (7)$$

It is clear that, in general, the capillary pressure varies from drop to drop.

When Eqs. (3) are combined with Eqs. (5), the following relationships between the curvatures of the films and those of the Plateau border walls are obtained:

$$\begin{aligned} 2C_{12} &= c_1 - c_2 \\ 2C_{23} &= c_2 - c_3 \\ 2C_{31} &= c_3 - c_1 \end{aligned} \quad (8)$$

For each film to be stable, it must be able to develop an internal, repulsive *disjoining pressure* Π_d to counteract the capillary suction acting at the film–Plateau border junction. At equilibrium, it can be readily shown

from the above that

$$\begin{aligned}
 (\Pi_d)_{12} &= \frac{\sigma(c_1 + c_2)}{2} \\
 (\Pi_d)_{23} &= \frac{\sigma(c_2 + c_3)}{2} \\
 (\Pi_d)_{31} &= \frac{\sigma(c_3 + c_1)}{2}
 \end{aligned} \tag{9}$$

Thus, the disjoining pressures in three confluent films are, in general, unequal. It turns out that the difference in the disjoining pressures in two of the films is defined by the curvature of the third film. For example, from Eqs. (9) and (8),

$$(\Pi_d)_{31} - (\Pi_d)_{23} = \frac{\sigma(c_1 - c_2)}{2} = \sigma C_{12} \tag{10}$$

[The inequality of the disjoining pressures implies that the films may have slightly different equilibrium thicknesses and tensions. In extreme cases (30), this may lead to sensible deviations from Plateau’s first law of foam structure, stated below.]

As the volume fraction approaches unity, the linear Plateau border shrinks into a line. In this “dry-foam” limit, mechanical equilibrium demands that the three films—of presumed equal tensions—meet pairwise at angles of 120° along this line (Plateau’s first law of foam structure). However, even when the Plateau border is finite and the films do not really intersect, the principle may well hold when applied to the virtual line of intersection that is obtained when the films, while maintaining their curvatures, are extrapolated into the border (dashed lines in Fig. 1b). A rigorous proof has been published by Bolton and Weaire (31) for two-dimensional (2D) foams, in which the Plateau borders are rectilinear. To our knowledge, no proof has yet been presented for the more general case of curvilinear borders in three-dimensional (3D) space. In fact, because the Plateau border can be viewed as a line with a line tension (32), this broader statement of Plateau’s first law may *not* strictly apply when the border has some finite longitudinal curvature.

A *tetrahedral* Plateau border is formed by the confluence of four linear Plateau borders (Fig. 1a). It fills the gap between the rounded corners of four adjoining polyhedral drops. The pressure in the tetrahedral border is, of course, equal to that in each of the outgoing linear borders, which sets the curvature of each of its four bounding walls. In the dry-foam limit ($\phi \rightarrow 1$), the tetrahedral border reduces to a point (“vertex” or “node”),

where the four linear borders meet pairwise at the angle of $\cos^{-1}(-1/3) = 109.47^\circ$ (Plateau's second law of foam structure). The principle probably remains valid for finite borders, when applied to the point where the four virtual lines of film intersection (see Fig. 1) meet upon extension into the tetrahedral border.

IV. OVERALL STRUCTURE AND OSMOTIC PRESSURE

Having described the structural elements of foams approaching the dry-foam limit ($\phi \rightarrow 1$), it is still a daunting task to describe the structure and properties of the system as a whole. The task is even more difficult for systems in which ϕ_0 is exceeded, but the polyhedral regime has not yet been reached. In this case, the drops have exceedingly complex shapes, and linear and tetrahedral Plateau borders, as defined earlier, are not present. Much can be learned about the qualitative behavior by considering *2D model systems*, in which the drops do not start out as spheres but as parallel circular cylinders and tetrahedral plateau borders do not arise. We shall first consider the particularly simple, perfectly ordered monodisperse case, with a subsequent gradual increase in complexity.

[Lest the reader think that 2D foams are just figments of the imagination, it must be pointed out that they can be generated—or at least closely approximated—by squeezing a 3D foam between two narrowly spaced, wetted, transparent plates (2,33–37). Structurally, even closer realizations may be obtained in phase-coexistence regions of insoluble monolayers of surface-active molecules at the air–water interface (38), where the role of surface tension is taken over by the line tension at the phase boundaries.]

A. Monodisperse, Perfectly Ordered 2D System

Such a system has been discussed in detail in Ref. 39. In the absence of gravity, the circular cylinders of radius R arrange in hexagonal packing (Fig. 2a) at a volume fraction $\phi_0 = \pi/2\sqrt{3} = 0.9069$. In cross section, each circular drop can be thought to be contained within a regular hexagon of side length $a_0 = 2R/\sqrt{3}$. As the volume fraction is increased, the drop is flattened against its six neighbors to form a hexagon of side length a ($< a_0$) but with rounded corners described by circular arcs of radius r (Fig. 2b). At constant drop volume, one finds

$$\frac{r}{R} = \left(\frac{\phi_0}{1 - \phi_0} \right)^{1/2} \left(\frac{1 - \phi}{\phi} \right)^{1/2} \quad (11)$$

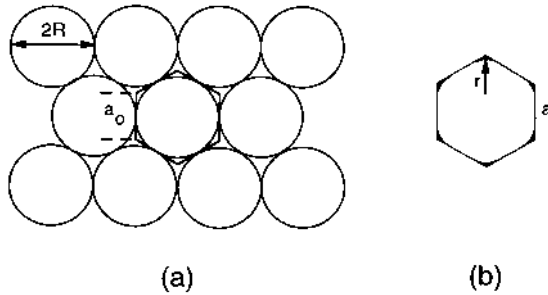


Figure 2 (a) Uncompressed cylindrical drops in hexagonal close packing ($\phi = \phi_0 = 0.9069$); (b) compressed drop ($0.9069 < \phi < 1$).

The capillary pressure in each drop is given by $p_c = \sigma/r$ or, when scaled by the initial capillary pressure $(p_c)_0 = \sigma/R$, by

$$\tilde{p}_c = p_c / (p_c)_0 = R/r \quad (12)$$

In the above process, the surface area of each drop, per unit of length, increases from $S_0 = 2\pi R$ to $S = 6(a - 2r/\sqrt{3}) + 2\pi r$, which, at constant drop volume, can be shown to lead to

$$\frac{S}{S_0} = \frac{1}{(\phi_0\phi)^{1/2}} [1 - (1 - \phi_0)^{1/2}(1 - \phi)^{1/2}] \quad (13)$$

This function has been plotted in Fig. 3. In the limit of $\phi = 1$, the scaled surface area reaches a maximum that is given by

$$\frac{S_1}{S_0} = \frac{1}{\phi_0^{1/2}} = 1.0501 \quad (14)$$

The scaled surface area and its variation with ϕ are of crucial importance in the definition and evaluation of the *osmotic pressure*, Π , of a foam or emulsion. We introduced the concept in Ref. 39, where it was referred to as the “compressive pressure,” P . It has turned out to be an extremely fruitful concept (24,29,40). The term “osmotic” was chosen, with some hesitation, because of the operational similarity with the more familiar usage in solutions. In foams and emulsions, the role of the solute molecules is played by the drops or bubbles; that of the solvent is played by the continuous phase, although it must be remembered that the nature of the interactions is entirely different. Thus, the osmotic pressure is defined as the pressure that needs to be applied to a semipermeable, freely movable

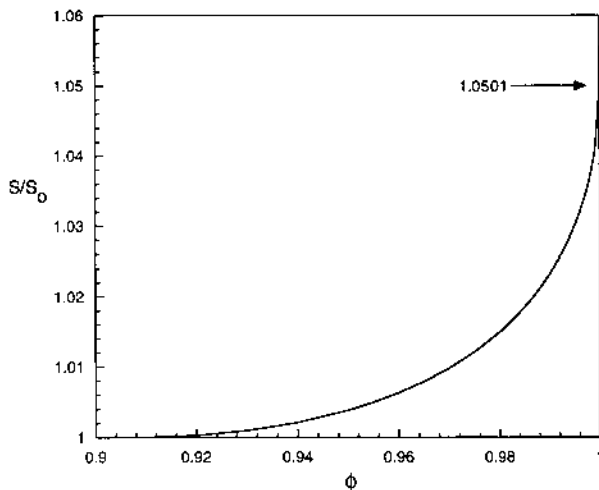


Figure 3 Scaled surface area, S/S_0 , for monodisperse 2D drops as a function of volume fraction.

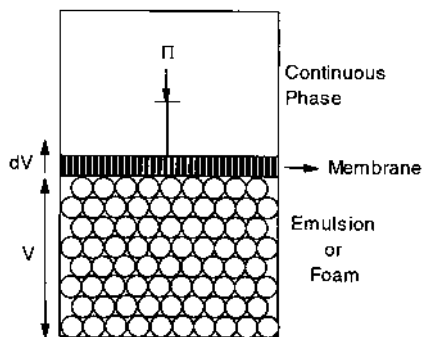


Figure 4 Semipermeable membrane separating dispersion from continuous phase; pressure to prevent additional continuous phase from entering the dispersion is the “osmotic” pressure, Π . [From Ref. 40. Copyright (1986) American Chemical Society.]

membrane, separating a fluid–fluid dispersion from its continuous phase, to prevent the latter from entering the former and to thereby reduce the augmented surface free energy (Fig. 4). The membrane is permeable to all of the components of the continuous phase but not to the drops or bubbles. As we wish to postpone discussion of compressibility effects in foams until later, we assume that the total volume (and therefore the volume of the dispersed phase) is held constant.

As long as the membrane is located high up in the box in Fig. 4, the emulsion or foam may be characterized by $\phi < \phi_0$ and $\Pi = 0$. As the membrane moves down, a point is reached where $\phi = \phi_0$. Any further downward movement requires work against a finite pressure Π , reflecting the increase in the total surface area as the drops are deformed; that is,

$$-\Pi dV = -\Pi dV_2 = \sigma dS \quad (\text{constant } V_1) \quad (15)$$

where V is the dispersion volume, V_1 is the volume of the dispersed phase, V_2 is the volume of the continuous phase in the dispersion, and σ is assumed to be constant. Because $V = V_1 + V_2$ and $\phi = V_1/V$, Eq. (15) leads to the completely general expression

$$\Pi = \sigma \phi^2 \frac{d(S/V_1)}{d\phi} = \sigma \phi^2 \frac{S_0}{V_1} \frac{d(S/S_0)}{d\phi} \quad (16)$$

where S/V_1 is the surface area per unit volume of the dispersed phase. Alternatively, as shown in Ref. 29, Π may be equated to the pressure difference between an ambient atmosphere and the continuous phase in the dispersion, or from Eq. (6):

$$\Pi = P - p_b = \sigma_c |C_l| \quad (17)$$

For yet a third useful way to express Π , see Refs. 24, 29, and 40.

For the special case of a monodisperse 2D system,

$$\frac{S_0}{V_1} = \frac{2}{R} \quad (18)$$

which, when combined with Eqs. (16) and (13), results in

$$\Pi = \frac{\sigma}{R} \left(\frac{\phi}{\phi_0} \right)^{1/2} \left[\left(\frac{1 - \phi_0}{1 - \phi} \right)^{1/2} - 1 \right] \quad (19)$$

or, in reduced form,

$$\tilde{\Pi} \equiv \frac{\Pi}{\sigma/R} = \frac{\Pi}{(p_c)_0} = \left(\frac{\phi}{\phi_0} \right)^{1/2} \left[\left(\frac{1 - \phi_0}{1 - \phi} \right)^{1/2} - 1 \right] \quad (20)$$

where $\phi_0 = 0.9069$. Figure 5 shows the dependence of $\tilde{\Pi}$ on ϕ .

The suggestion has been made (Exerowa, personal communication, 1990), since withdrawn (20,41), that Π and p_c are really identical. It is

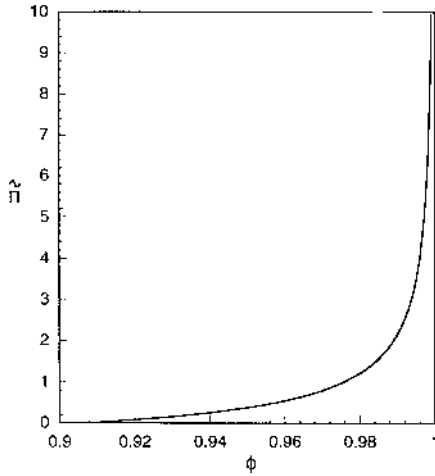


Figure 5 Reduced osmotic pressure as a function of ϕ for a perfectly ordered 2D system.

clear from the above that this is not so. In fact, examination of Eqs. (20), (11), and (12) shows that, at least for this simple model system,

$$\tilde{p}_c - \tilde{\Pi} = \left(\frac{\phi}{\phi_0}\right)^{1/2} \quad (21)$$

At $\phi = \phi_0$,

$$\tilde{p}_c - \tilde{\Pi} = 1 \quad (22)$$

At the upper limit of $\phi = 1$,

$$\tilde{p}_c - \tilde{\Pi} = \phi_0^{-1/2} = \frac{S_1}{S_0} = 1.0501 \quad (23)$$

Both \tilde{p}_c and $\tilde{\Pi}$ tend to infinity in this limit, but the *relative* difference between them tends to zero. This is the regime of concern in much of the interesting work of Exerowa et al. (e.g., Refs. 42 and 43), where the difference between the capillary and osmotic pressures may therefore, indeed, be safely ignored (41). However, this is not so in general and we shall demonstrate in Sect. V that $\tilde{\Pi}$ is a much more useful and informative parameter than \tilde{p}_c .

Before leaving this topic, it should be mentioned that modifications of most of the above expressions have been derived to take account of finite film thickness, finite contact angle at the film–Plateau border junction, or

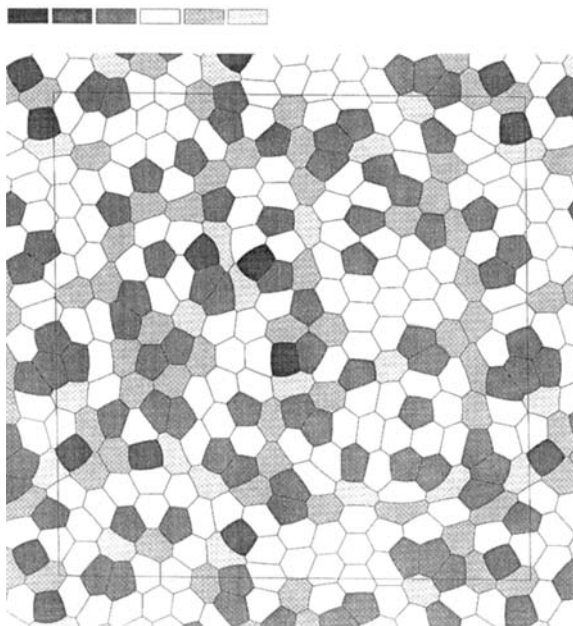


Figure 6 Topologically disordered, but volumetrically monodisperse 2D system ($\phi = 1$) with periodic boundaries; each shade corresponds to drops with a certain number of sides (e.g., the unshaded drops all have six sides). (Courtesy of T. Herdtle and A. M. Kraynik.)

both (39). Finally, it must be realized that a monodisperse 2D system does not necessarily pack in the perfectly ordered, hexagonal state depicted in Fig. 2. Herdtle et al. (personal communication, 1993) have constructed highly disordered, yet monodisperse 2D dry foams with periodic boundaries (Fig. 6), in which all films meet at angles of 120° and all film curvatures satisfy Eq. (4). In a sense, these systems are monodisperse only in a *volumetric* sense, but are *topologically* disordered or “polydisperse.” They are equilibrium structures, whose surface energy, although at a *local* minimum, must be higher than that of the perfectly ordered hexagonal system. Because the bubble pressures are not the same, such a system is bound to coarsen, thereby reducing its total surface energy. In practice, disorder of this type may be imposed by the finiteness of any system with bounding walls. If the walls are wetted by the continuous phase, then the outer films must be directed normal to the walls, which is generally incompatible with a perfectly ordered internal structure. As we shall see, this complication arises in 3D foams as well.

B. Polydisperse 2D Systems

In the last decade or so, much progress has been made toward a more complete understanding of these disordered structures. Most work relies on the computer generation of disordered (volumetrically) polydisperse structures with periodic boundary conditions, in which the film angles and curvatures obey the rules set forth in Sect. III. For a recent review, see Ref. 33. An example, taken from Ref. 44, is shown in Fig. 7. The structure contains many bubbles that are not hexagons, but it is readily proven that the *average* number of sides is still six (44). Simpler and very special types of (volumetric) polydispersity and disorder have been considered by Khan and Armstrong (45) and Kraynik et al. (46). In these cases, illustrated in Fig. 8, the topology is preserved. All bubbles are still hexagons and all films remain flat; the bubbles, therefore, do not coarsen with time. The first system (Fig. 8a) is simply bimodal and is obtained by increasing or decreasing the height of all bubbles in a given row. The second system (Fig. 8b) is much more disordered and can be generated from the monodisperse system by randomly increasing (or decreasing) each bubble area, as illustrated in Fig. 9, with the limitation that no vertices ever touch or cross over, lest Plateau's first law be violated and resultant (so-called T1) rearrangements lead to a much more complex structure. The total surface area is not affected by such transformations, so that, as in the monodisperse case,

$$\frac{S_1}{S_0} = 1.0501 \quad (24)$$

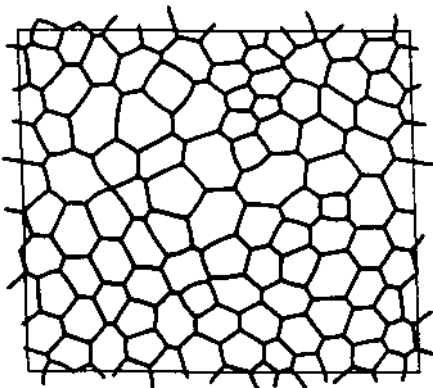


Figure 7 Computer-generated, topologically disordered and volumetrically polydisperse 2D system ($\phi=1$) with periodic boundaries. (From Ref. 44, with permission from Taylor & Francis Ltd.)

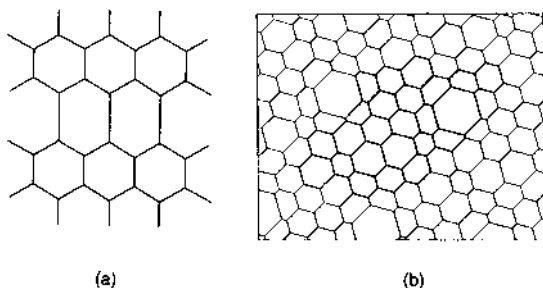


Figure 8 (a) Simplest case of volumetrically bimodal 2D system; (b) more highly disordered, volumetrically polydisperse hexagonal 2D system ($\phi = 1$). The cluster of darkly outlined drops forms the repeating unit. (Courtesy of A. M. Kraynik. Similar structures appear in Ref. 46.) In both cases, the system is topologically “monodisperse.”

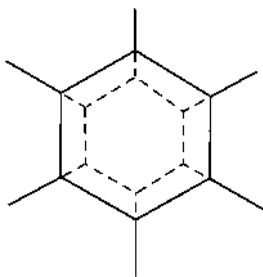


Figure 9 Recipe for creating a volumetrically polydisperse (but topologically monodisperse) hexagonal system from perfectly ordered 2D system; total surface energy remains unchanged.

This is not necessarily true for the more general structures such as that in Fig. 7, which is both volumetrically and topologically polydisperse. Unfortunately, although presumably available as a result of the numerical simulations, the value of S_1/S_0 and how it varies with the details of the size distribution appear not to have been reported for these cases.

Starting from a dry-foam system as in Fig. 7, the volume fraction can be lowered by “decorating” each vertex with a Plateau border, whose wall curvatures obey the rules set forth in Sect. III (31). As the volume fraction is lowered by increasing the size of the Plateau borders, a point is soon reached where adjacent Plateau borders “touch” and subsequently merge into single four-sided borders. Bolton and Weaire (47) have followed this process down

to the volume fraction ϕ_c , where all bubbles are spherical and structural rigidity is lost. This is perhaps the most satisfactory definition of ϕ_0 . Their finding suggests that, for that particular system, ϕ_c equaled 0.84 (not 0.9069), which happens to be close to the random packing density of (monodisperse) circular disks. Using similar computer simulations, Hutzler and Weaire (48) calculated the osmotic pressure and found it to obey Eq. (19) closely in the “drier” regime. It started to deviate at lower volume fractions and did not reach zero until ϕ dropped to about 0.82, which is close to ϕ at the rigidity loss transition.

C. Monodisperse 3D Systems

Ideally, uniform spheres arrange in “hexagonal close” packing, which is face-centered cubic (fcc), at $\phi_0 = \pi\sqrt{2}/6 = 0.7405$. The role of the circumscribing hexagon in monodisperse 2D systems is taken over by the rhombic dodecahedron (Fig. 10). As the volume fraction is raised, each drop flattens against its 12 neighbors. This process has been described by Lissant (4,5), who considered the drop to be transformed into a truncated sphere and each

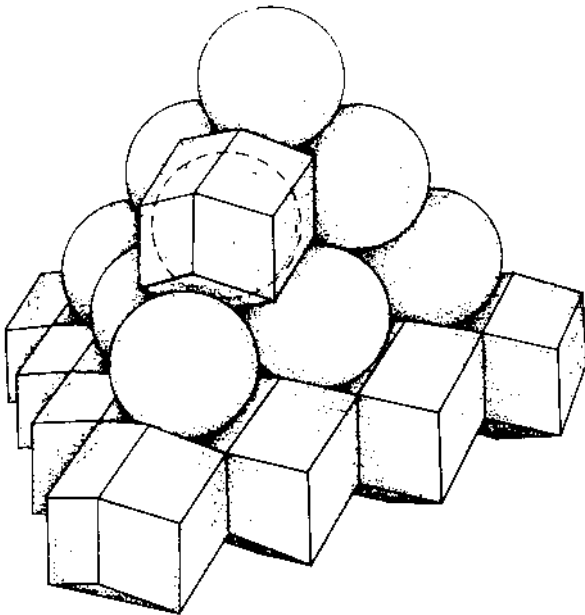


Figure 10 Spheres in hexagonal close packing (fcc), each occupying a rhombic dodecahedron. (From Ref. 4, with permission from Academic Press.)

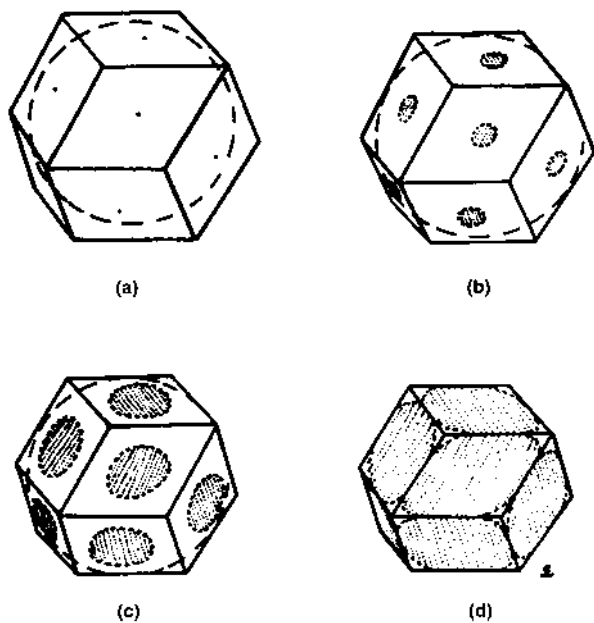


Figure 11 Each drop flattens against its neighbors as the volume fraction increases; a stable thin film of continuous phase separates neighboring drops. (From Ref. 4, with permission from Academic Press.)

film to be circular, at least until it reaches the sides of the diamond faces (Fig. 11). This is incompatible with a zero contact angle at the film edge. Moreover, at constant drop volume, this model would imply *decreasing* capillary (and osmotic) pressure with increasing ϕ , which is clearly inconsistent. In reality, the problem is much more complicated; the drop cannot remain spherical and the films must be noncircular. Using Brakke's now famous "Surface Evolver" computer software (49), Kraynik and Reinelt (50), and Lacasse et al. (51) have correctly and accurately solved this problem for this and other structures (discussed later in this subsection).

As suggested already by Lissant (4,5), the packing is likely to change above some critical value of ϕ . It is clear that if the dodecahedral packing were to persist up to $\phi=1$, Plateau's second law would be violated at 6 of the 14 corners of the polyhedron, because 8 linear borders would converge there, rather than the mandatory 4. Lissant proposed that the structure changes to a body-centered cubic (bcc) packing of planar tetrakaidecahedra (truncated octahedra; see Fig. 12a). However, such a structure satisfies neither of Plateau's laws. In this dry-foam regime, Kelvin's "minimal

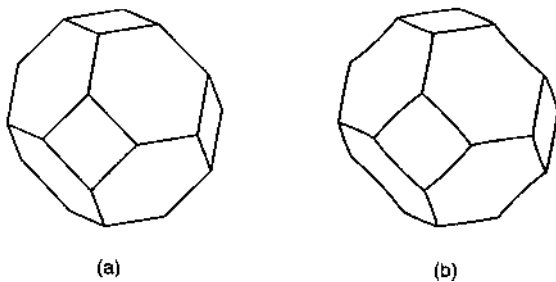


Figure 12 (a) Planar tetrakaidecahedron (or truncated octahedron); (b) Kelvin's minimal tetrakaidecahedron (bcc).

tetrakaidecahedron” (Fig. 12b), which is obtained by slight distortion of its planar counterpart, solves this problem and has long been considered as the most satisfactory candidate for the drop shape. It has 6 planar quadrilateral faces, 8 nonplanar hexagonal faces of zero mean curvature, and 36 identical curved edges. In a space-filling ensemble of such polyhedra, Plateau’s first and second laws are fully satisfied. Kelvin derived approximate expressions for the shape of the hexagons and the sides (52–54). Based on that model, Princen and Levinson (55) calculated the length of the sides and the surface areas of the quadrilateral and hexagonal faces, relative to those of the parent planar tetrakaidecahedron of the same volume. They arrived at the following result for the increase in surface area as a spherical drop transforms into a Kelvin tetrakaidecahedron of the same volume:

$$\frac{S_1}{S_0} = 1.0970 \quad (25)$$

(This compares to values of 1.0990 for the planar tetrakaidecahedron, 1.1053 for the rhombic dodecahedron, and 1.0984 for the regular pentagonal dodecahedron. The latter—although often considered as a unit cell in foam modeling—is not really a viable candidate either, as it not only violates Plateau’s laws but is also not space filling.)

More recently, Reinelt and Kraynik (56) have carried out more exact numerical calculations on the Kelvin cell, leading to the slightly higher value of

$$\frac{S_1}{S_0} = 1.0972 \quad (26)$$

Kelvin’s polyhedron would indeed represent the ideal drop shape in the dry-foam limit by effecting, in Kelvin’s own words, “a division of space with

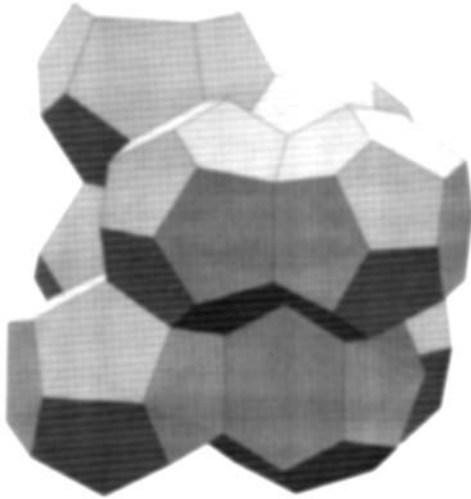


Figure 13 Unit cell in Weaire–Phelan structure, containing 2 pentagonal dodecahedra and 6 tetrakaidecahedra, each having 12 pentagonal and 2 hexagonal faces. (Courtesy of A. M. Kraynik.)

minimum partitional area,” if he had added the proviso that this division is to be accomplished with identical cells. It has recently been proven by Weaire and Phelan (57) that at least one structure of even lower energy exists, if this restriction is lifted. The Weaire–Phelan structure (Fig. 13), whose surface area is about 0.34% lower than that of Kelvin (i.e., $S_1/S_0 = 1.0936$), has repeating units that contain 8 equal-volume cells: 2 identical pentagonal dodecahedra and 6 identical tetrakaidecahedra that each have 12 pentagonal and 2 hexagonal faces. The pressure in the dodecahedra is slightly higher than that in the tetrakaidecahedra. Perhaps surprisingly, neither the Kelvin nor the Weaire–Phelan structure is rarely, if ever, encountered in actual monodisperse foams (3). The reason for this may lie in small deviations from monodispersity or, more likely, in the disturbing effects of the container walls, as alluded to already in connection with 2D foams. Alternatively, as the continuous phase is removed from between the initially spherical drops in fcc packing, slight irregularities in this drainage process may force the system to get trapped in a less-ordered structure that may be at a local surface area minimum but is separated from the lower-energy Kelvin and Weaire–Phelan structures by a significant barrier [cf. the difficulty one encounters in trying to build a 15-bubble cluster that has a Kelvin polyhedron at its center (58)].

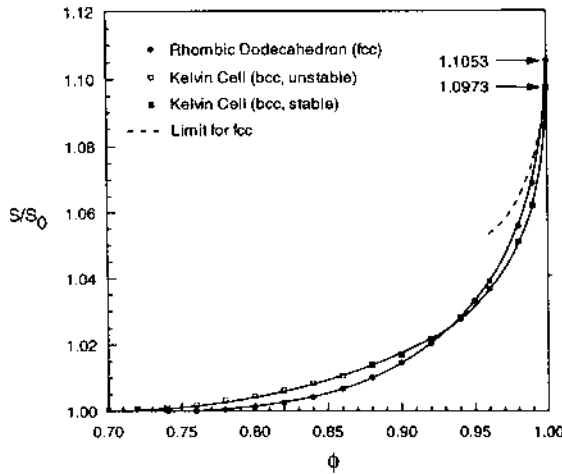


Figure 14 Scaled surface areas as a function of volume fraction for the rhombic dodecahedral (fcc) and Kelvin structures (bcc). (From data kindly provided by A. M. Kraynik and D. A. Reinelt.)

Kraynik and Reinelt (50) and Lacasse et al. (51) have accurately computed the changes in surface area as a drop transforms from a sphere into a regular dodecahedron (fcc) or a Kelvin cell (bcc) with increasing volume fraction while maintaining zero contact angle. Expressed in terms of S/S_0 , the results are shown in Fig. 14. The Kelvin structure is internally unstable below $\phi \approx 0.87$. The results further indicate that the Kelvin cell becomes the more stable structure above $\phi \approx 0.93$. Also indicated is the limiting law for $\phi \rightarrow 1$ for the dodecahedron. In that regime, linear Plateau borders of constant cross section run along the edges of the polyhedron. Their volumes and surface areas can be evaluated as a function of ϕ , whereas the volumes and surface areas of the tetrahedral borders become negligible. For the rhombic dodecahedron (24), this leads to

$$\frac{S}{S_0} = 0.0686[1 - 1.892(1 - \phi^{1/2})]^3 + 1.0367 \quad (\phi \rightarrow 1)$$

Kraynik and Reinelt (50) also evaluated the all-important osmotic pressure $\Pi(\phi)$, which, for 3D structures, is given by [cf. Eq. (16)]

$$\Pi = \sigma \phi^2 \frac{S_0}{V_1} \frac{d(S/S_0)}{d\phi} = \frac{3\sigma \phi^2}{R} \frac{d(S/S_0)}{d\phi}$$

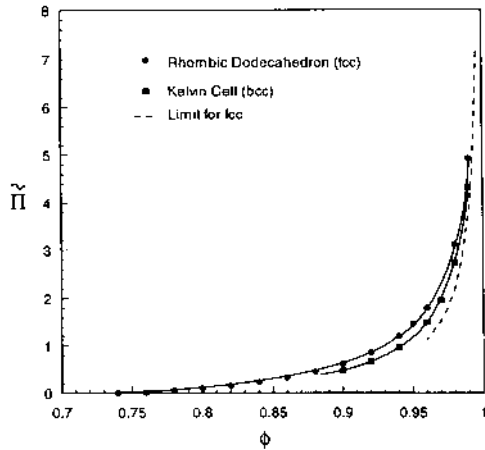


Figure 15 Reduced osmotic pressure as a function of volume fraction for the rhombic dodecahedral and Kelvin structures. (From data kindly provided by A. M. Kraynik and D. A. Reinelt.)

where R is the radius of the initially spherical drops, or

$$\tilde{\Pi} \equiv \frac{\Pi}{\sigma/R} = 3\phi^2 \frac{d(S/S_0)}{d\phi} \quad (27)$$

For the dodecahedron, the appropriate limiting law for $\phi \rightarrow 1$ is given (24) by

$$\tilde{\Pi} = \frac{\Pi}{\sigma/R} = 0.5842\phi^{1/3} \frac{[1 - 1.892(1 - \phi)^{1/2}]^2}{(1 - \phi)^{1/2}} \quad (\phi \rightarrow 1) \quad (28)$$

Figure 15 shows $\tilde{\Pi}(\phi)$ for the dodecahedron and Kelvin cell.

Detailed numerical calculations have been carried out by Bohlen et al. (59) for the transition of monodisperse spheres in simple *cubic* packing ($\phi_0 = 0.5236$) to cubes ($\phi = 1$), for both zero and finite contact angles. Unfortunately, although the results are interesting, this kind of packing is not realistic for foams and emulsions and will not be discussed further.

D. Polydisperse 3D Systems

This is, of course, the system of greatest interest from a practical point of view. The detailed structure is exceedingly complex. As mentioned earlier,

even the value of ϕ_0 is not precisely defined and is expected to depend somewhat on the details of the size distribution. Nevertheless, there is clear experimental evidence (23,24) that ϕ_0 is close to—or slightly smaller than—0.7405 for “typical,” polydisperse, unimodal emulsions.

In the dry-foam limit, each polyhedral drop must satisfy Euler’s formula; that is,

$$v - e + f = 2 \quad (29)$$

where v is the number of vertices, e is the number of edges, and f is the number of faces. For an infinite number of space-filling polyhedra that are subject to Plateau’s rules, a number of statistical relationships can be derived from Eq. (29) (60–62). Perhaps the most interesting of these is

$$\langle f \rangle = \frac{12}{6 - \langle e \rangle} \quad (30)$$

where $\langle f \rangle$ is the average number of faces per cell and $\langle e \rangle$ is the average number of edges per face. Equation (30) is consistent with what is expected for a monodisperse “Kelvin foam,” where $\langle f \rangle = f = 14$ and $\langle e \rangle = (6 \times 4 + 8 \times 6)/14 = 5.143$, or a Weaire–Phelan structure, where $\langle f \rangle = (2 \times 12 + 6 \times 14)/8 = 13.5$ and $\langle e \rangle = [2 \times 12 \times 5 + 6 \times (12 \times 5 + 2 \times 6)]/108 = 5.111$. As mentioned earlier, Matzke (3) found that, in a real, supposedly monodisperse foam, Kelvin’s polyhedra did not occur and that pentagonal faces were predominant. He found that $\langle f \rangle = 13.70$ and $\langle e \rangle = 5.124$, which is, again, consistent with Eq. (30). For a real polydisperse dry foam, Monnereau and Vignes-Adler (63) found $\langle f \rangle = 13.39 \pm 0.05$ and $\langle e \rangle = 5.11$, again in close agreement with Eq. (30). These authors did not encounter any Kelvin cell (or Weaire–Phelan structure) either.

For $\phi_0 < \phi < 1$, the drops go through a complex transition from spheres to pure polyhedra. In this most general system, the osmotic pressure is given by

$$\Pi(\phi) = \sigma \phi^2 \frac{S_0}{V_1} \frac{d(S/S_0)}{d\phi} = \frac{3\sigma \phi^2}{R_{32}} \frac{d(S/S_0)}{d\phi} \quad (31)$$

where R_{32} is the surface/volume or Sauter mean radius of the initially spherical drops:

$$R_{32} \equiv \frac{\sum n_i R_i^3}{\sum n_i R_i^2} = \frac{3V_1}{S_0} \quad (32)$$

Although R_{32} can be readily measured for any practical system, the complex geometry does not allow the evaluation of $S(\phi)/S_0$ and $\Pi(\phi)$ from first principles. Instead, in the next section, we shall show how these and other important functions can be derived from experiment.

V. UTILITY AND EXPERIMENTAL EVALUATION OF THE OSMOTIC PRESSURE

We have repeatedly emphasized the importance and utility of the osmotic pressure Π of foams and concentrated emulsions. Once known as a function of ϕ , it may be used to quantitatively link and predict a large number of other important properties. Some of these are listed in this section. In addition, these considerations lead to a convenient method for evaluating $\Pi(\phi)$ experimentally (see Sec. V.D).

A. Motion of Continuous Phase Between Different Systems in Contact

Let two concentrated dispersions with the same type of continuous phase [e.g., an aqueous foam and an oil-in-water emulsion, or two different o/w emulsions] be brought into contact, either directly or via a freely movable semipermeable membrane. If the osmotic pressures are unequal (e.g., as a result of differences in the volume fractions, mean drop size, interfacial tension, or combinations thereof), it is obvious that the (common) continuous phase will flow from the dispersion with the lower osmotic pressure into that with the higher osmotic pressure until the two pressures are equalized. The final volumes and volume fractions of the two dispersions may be predicted in a straightforward manner, once $\tilde{\Pi}(\phi)$ is known. It is important to point out that equality of the (mean) *capillary pressures* does not necessarily rule out flow nor does their inequality imply it.

B. Vapor Pressures of Continuous and Dispersed Phases

It can be shown (29) that the vapor pressure, p_v^c , of the continuous phase is reduced to below that of the bulk continuous phase, $(p_v^c)_0$, according to

$$p_v^c = (p_v^c)_0 \exp\left(\frac{-\Pi \bar{V}_2}{\Re T}\right) \quad (33)$$

where \bar{V}_2 is the partial molar volume of the solvent, \Re is the gas constant, and T is the absolute temperature.

Similarly, the vapor pressure of the dispersed phase, p^d , in a concentrated emulsion can be related to that of the bulk dispersed phase, $(p_v^d)_0$ by

$$p_v^d \approx (p_v^d)_0 \exp\left(\frac{2\sigma \bar{V}_1 S}{R_{32} \mathfrak{R} T S_0}\right) \quad (34)$$

where σ is the interfacial tension, R_{32} is the Sauter mean drop radius, \bar{V}_1 is the molar volume of the dispersed liquid, and S/S_0 is the relative increase in surface area at the volume fraction ϕ . For $\phi < \phi_0$, where $S/S_0=1$, we recover a variant of Kelvin's equation; for $\phi > \phi_0$, the increased vapor pressure is augmented further by the appearance of the factor S/S_0 in the exponent, with S/S_0 being related to $\Pi(\phi)$ through Eq. (31).

C. Gradient in ϕ in Gravitational Field

So far, we have assumed that gravity is absent or negligible, so that the volume fraction is uniform throughout the system. In gravity, however, a sufficiently tall column will develop a significant gradient in ϕ (24). Even if each individual drop is small enough to be essentially unaffected by the field (i.e., when the Bond number is very small), the combined buoyant force of the underlying drops causes increasing drop deformation (and volume fraction) in the higher regions (Fig. 16). At the boundary between the dispersion and the bulk continuous phase, where $z=0$, we have $\phi=\phi_0$, and the drops are purely spherical. At higher z , they increasingly deform until, as $z \rightarrow \infty$, they acquire a purely polyhedral shape and $\phi \rightarrow 1$. It is

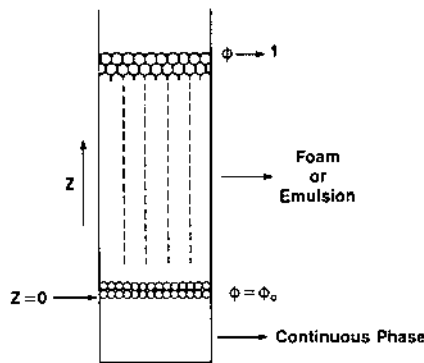


Figure 16 Transition from spherical to polyhedral drops in vertical column. [From Ref. 40. Copyright (1986) American Chemical Society.]

clear that, at any level, the combined buoyant force of all underlying drops per unit area must equal the local osmotic pressure:

$$\Pi(\phi) = \Delta\rho g \int_0^z \phi dz \quad (35)$$

or

$$\tilde{\Pi}(\phi) = \frac{\Delta\rho g R_{32}}{\sigma} \int_0^z \phi(z) dz = \int_0^{\tilde{z}} \phi(\tilde{z}) d\tilde{z} \quad (36)$$

where $\Delta\rho$ is the density difference between the phases, g is the acceleration due to gravity, $\tilde{\Pi}(\phi)$ is the reduced osmotic pressure

$$\tilde{\Pi}(\phi) = \frac{\Pi(\phi)}{\sigma/R_{32}} \quad (37)$$

and \tilde{z} is the reduced height

$$\tilde{z} \equiv \frac{R_{32}z}{a_c^2} \quad (38)$$

where $a_c = [\sigma/(\Delta\rho g)]^{1/2}$ is the capillary length.

In all of the above, it is assumed that there is no gravitational segregation by drop size, that is, the drop size distribution does not vary with height.

Thus, once $\tilde{\Pi}(\phi)$ is known, $\phi(\tilde{z})$ can be evaluated from Eq. (36) in the form

$$\tilde{z}(\phi) = \int_0^{\tilde{\Pi}} \frac{d\tilde{\Pi}(\phi)}{\phi} = \int_{\phi_0}^{\phi} \frac{1}{\phi} \left(\frac{d\tilde{\Pi}(\phi)}{d\phi} \right) d\phi \quad (39)$$

As mentioned earlier, the only system for which $\tilde{\Pi}(\phi)$ is known exactly is the monodisperse 2D system [cf. Eq. (16)]. When Eq. (39) is applied to this case, we find

$$\tilde{z}(\phi) = \frac{1}{(\phi_0\phi)^{1/2}} \left[1 + \left(\frac{1-\phi_0}{1-\phi} \right)^{1/2} (2\phi-1) \right] - 2 \quad (40)$$

where $\phi_0 = 0.9069$. This result has been obtained also by Pacetti (64). The volume fraction profile is shown in Fig. 17.

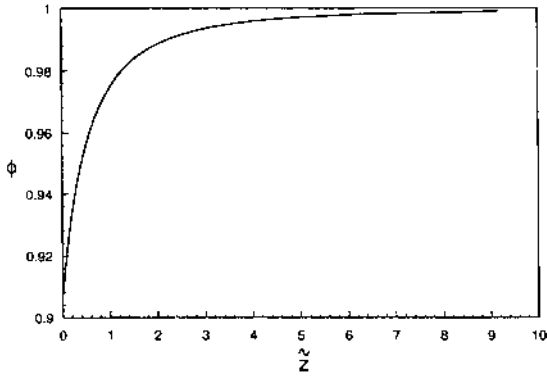


Figure 17 Volume fraction versus reduced height for perfectly ordered 2D case.

D. Experimental Determination of $\tilde{\Pi}(\phi)$ for Real Systems

From the above, it is clear that $\tilde{\Pi}(\phi)$ may be evaluated experimentally from Eq. (36) by determining the volume fraction as a function of height in an equilibrated (i.e., completely drained) dispersion column. This has been done very carefully for a typical, well-characterized polydisperse emulsion of paraffin oil in water (24). The emulsion had a Sauter mean drop radius of $R_{32} = 44.7 \mu\text{m}$, an interfacial tension of 7.33 mN/m , and a density difference of 0.144 g/cm^3 . The experimental profile $\phi(\tilde{z})$ is given in Fig. 18 and may be compared with that in Fig. 17 for the monodisperse 2D system. It could be numerically fitted to the following equations, covering three different ranges of ϕ :

“Low”-volume fraction ($0.715 < \phi < 0.90$ or $0 < \tilde{z} < 0.5$):

$$\tilde{z} = 0.237 \left(\frac{\phi - 0.715}{1 - \phi} \right) \quad (41)$$

or

$$\phi = \frac{\tilde{z} + 0.169}{\tilde{z} + 0.237} \quad (42)$$

This leads to

$$\tilde{\Pi}(\tilde{z}) = \tilde{z} - 0.068 \ln(\tilde{z} + 0.237) - 0.098 \quad (43)$$

which, upon substitution for \tilde{z} according to Eq. (41), leads to $\tilde{\Pi}(\phi)$. Equation (41) shows that $\phi = \phi_0 = 0.715$ at $\tilde{z} = 0$. This is one of our

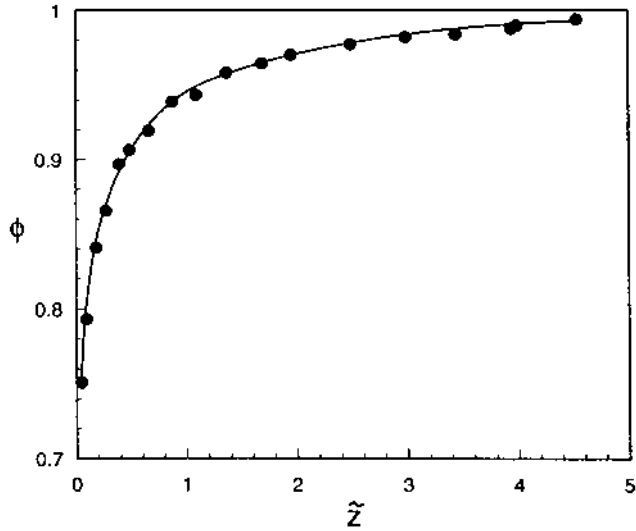


Figure 18 Experimental profile of volume fraction versus reduced height for typical polydisperse emulsion. [From Ref. 24. Copyright (1987) American Chemical Society.]

reasons for concluding that typical polydisperse systems pack slightly less tightly than ideally close-packed monodisperse systems, where $\phi_0 = 0.7405$.

Intermediate-volume fraction ($0.90 < \phi < 0.99$ or $0.5 < \tilde{z} < 4.0$):

$$\phi = 1.037[1 - (117.6\tilde{z} + 4.0)^{-1/2}] \quad (44)$$

and

$$\tilde{\Pi} = \frac{0.00819\phi^2}{(1 - 0.9639\phi)^2} \quad (45)$$

High-volume fraction ($0.99 < \phi < 1$ or $\tilde{z} > 4.0$):

$$\tilde{z} \approx \tilde{\Pi} = 0.5842 \frac{[1 - 1.892(1 - \phi)^{1/2}]^2}{(1 - \phi)^{1/2}} \quad (46)$$

which is the appropriate limiting solution for the polyhedral system.

Equations (42), (43), (45), and (46) describe the dependence of $\tilde{\Pi}$ on ϕ , as shown in Fig. 19. It may be compared with that for the monodisperse 2D

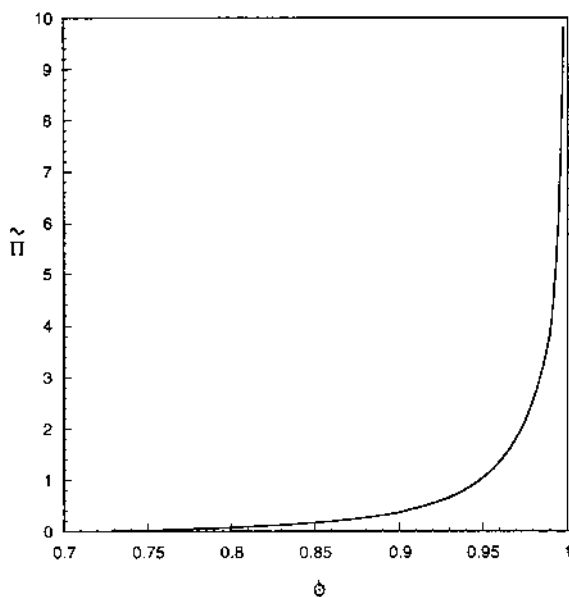


Figure 19 Reduced osmotic pressure as a function of volume fraction for typical polydisperse emulsion. [From Ref. 24. Copyright (1987) American Chemical Society.]

and 3D systems in Figs. 5 and 15, respectively. Close examination shows that the experimental osmotic pressure is consistently lower than those for the idealized structures in Fig. 15.

Even though these relationships were derived for one particular emulsion, its size distribution was “typical,” so that we believe that they can be applied with reasonable confidence in most practical situations. Nevertheless, more work remains to be done to elucidate the effect of the details of the size distribution. There is a particular need for the equivalent expressions for the *monodisperse* system, which would serve as a benchmark. Bibette’s (65) novel way of preparing emulsions of low polydispersity ($\pm 10\%$ in radius) has opened up experimentation along these lines. Unfortunately, the technique appears to be capable only of generating emulsions of extremely small drop size ($R < 1 \mu\text{m}$), which complicates matters in several ways. First, estimates of the effective volume fractions [cf. Eq. (1)] become questionable, unless detailed quantitative information is available on the equilibrium film thickness as a function of the apparent volume fraction (or capillary pressure). This is usually not the case, potentially leading to significant errors. Second, droplets of such small size are Brownian, which may lead to an entropic contribution to the osmotic

pressure, in addition to the energetic contribution considered so far. These and other factors may be responsible for some of the differences between the above results and those of Mason et al. (66), who measured $\Pi(\phi)$ for an oil-in-water “Bibette emulsion” of $R = 0.48 \mu\text{m}$. To cover the whole range of ϕ , they used three different ways to generate the osmotic pressure: gravitational compaction, centrifugation, and dialysis of the emulsion against the continuous phase containing various levels of dextran, a polymer to which the dialysis membrane is impermeable. The osmotic pressure was found to rise at an estimated effective ϕ of $(\phi_0)_e \approx 0.60$ (rather than 0.715). This is close to 0.64, the value for random close packing of uniform spheres. Up to $\phi_e = 0.80$, the data could be fitted well to

$$\tilde{\Pi} \propto \phi^2(\phi - 0.60) \quad (\phi < 0.80).$$

For $\phi > 0.80$, the results of the two studies appear to be quite consistent, in spite of the disparity in the degree of polydispersity of the emulsions employed. The apparent discrepancy at the lower volume fractions may be entirely due to the large difference in mean drop size, for the reasons cited earlier.

E. Gravitational Syneresis or Creaming

In the absence of gravity (or with fluids of matched densities), a perfectly stable emulsion or foam with $\phi > \phi_0$ will remain uniform and not “phase separate”, (i.e., it will not exude a bottom layer of continuous phase). In a gravitational (or centrifugal) field, such syneresis may occur, however, as a result of compaction in the upper region (assuming that we are dealing with a foam or o/w emulsion; the continuous phase would separate at the *top* in w/o emulsions). In a consumer product, such behavior could be detrimental, as it might suggest instability, breakdown, and limited shelf life, even though simple shaking would restore (temporary) uniformity. With the knowledge contained in the previous subsection, it is possible to predict exactly when such syneresis will in fact occur (67). For a container of constant cross section, the parameters of importance are the overall volume fraction, $\bar{\phi}$, and the reduced height of the sample, \tilde{H} , defined by

$$\tilde{H} \equiv \frac{HR_{32}}{a_c^2} = HR_{32} \Delta\rho \frac{g}{\sigma} \quad (47)$$

where H is the actual height of the sample. It is clear that, for any $\bar{\phi}$, there must be a critical reduced sample height, \tilde{H}_{cr} , above which syneresis will

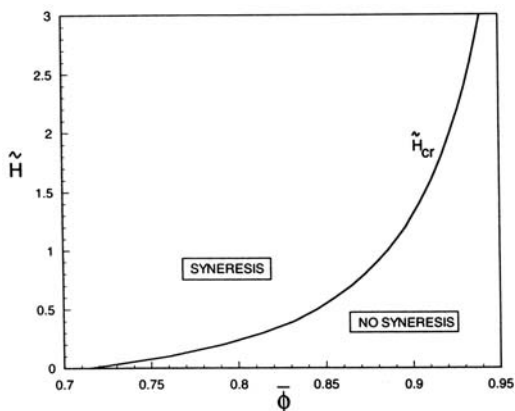


Figure 20 Critical sample height for occurrence of syneresis as a function of overall volume fraction.

occur and below which it will not. From a material balance and Eq. (36), it is readily shown that \tilde{H}_{cr} must obey the condition

$$\tilde{H}_{cr} = \frac{\tilde{\Pi}(\tilde{H}_{cr})}{\phi} \quad (48)$$

Figure 20 shows how the resulting $\tilde{H}-\bar{\phi}$ diagram is bisected by $\tilde{H}_{cr}(\bar{\phi})$. Reference 67 provides procedures for determining the height of the separated layer of continuous phase, if any, as well as the precise variation of ϕ with height in the sample. The method may be extended to containers with varying cross section (67). The following general conclusions may be drawn: (a) Everything else being equal, syneresis is less likely the higher the overall concentration of the dispersed phase, $\bar{\phi}$; of course, when $\bar{\phi} < \phi_0$, syneresis will *always* occur; (b) For given $\bar{\phi}$ ($> \phi_0$), the tendency toward syneresis is less pronounced the smaller \tilde{H} {i.e., for small drop size, high interfacial tension, small density difference, and small sample height [cf. Eq. (47)]}; (c) For a foam or typical o/w emulsion, the tendency toward syneresis is reduced if the container is shaped with its widest part at the bottom. The reverse is true for typical w/o emulsions.

F. Increase in Specific Surface Area with ϕ

We have seen that the osmotic pressure is directly linked to the scaled specific surface area, S/S_0 , as ϕ increases from ϕ_0 through Eq. (31). For the mono-disperse 2D system, S/S_0 is given by Eq. (13) and is plotted in Fig. 3.

To the extent that the real emulsion studied in Ref. 24 is representative of typical polydisperse 3D systems, one can derive S/S_0 from the expressions for $\bar{\Pi}(\phi)$ in Section V.D. The results (24) are as follows:

For $0.715 < \phi < 0.90$,

$$\frac{S}{S_0} = 1 + \frac{1}{3} \left[\frac{0.084}{\phi} - \frac{0.068}{\phi} \ln(1 - \phi) - 0.237 \right] \quad (49)$$

For $0.90 < \phi < 0.99$,

$$\frac{S}{S_0} = \frac{0.00283}{1 - 0.9639\phi} + 0.989 \quad (50)$$

For $0.99 < \phi < 1$,

$$\frac{S}{S_0} = 1.014 + 0.0686[1 - 1.892(1 - \phi)^{1/2}]^3 \quad (51)$$

The combined results are shown in Fig. 21, where it is seen that the transition from spheres to completely developed polyhedra is accompanied by an increase in surface area of 8.3%. As mentioned earlier, for the *monodisperse* case, one predicts an increase in surface area of 9.7% on the basis of

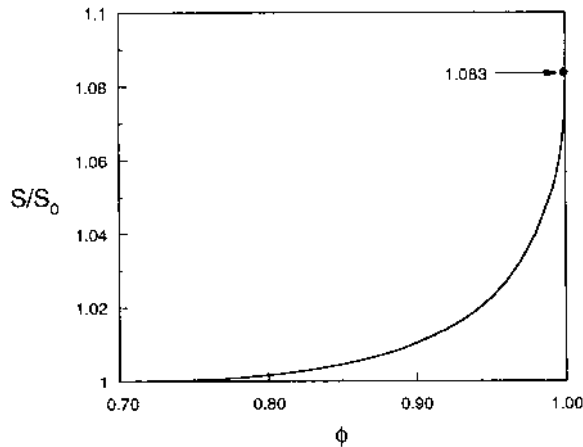


Figure 21 Scaled specific surface area as a function of volume fraction for typical polydisperse emulsion. [From Ref. 24. Copyright (1987) American Chemical Society.]

Kelvin’s polyhedron as the ultimate drop shape, or 9.4% for the Weaire–Phelan structure. Polydispersity appears to give rise to an even somewhat *smaller* overall change in surface area. Recent computer simulations of various monodisperse and polydisperse structures by Kraynik et al. (68) confirm this result almost quantitatively.

G. Surface Area in Films Versus Total Surface Area

At any given volume fraction ϕ , a fraction S_f/S of the total surface area forms part of the films separating the droplets, and the remainder is still “free” in the Plateau borders ($S_f/S=0$ at $\phi=\phi_0$; $S_f/S=1$ at $\phi\rightarrow 1$). This parameter may play an important role in problems relating to the stability of, and mass transfer in, such systems. We have shown (29) that

$$\frac{S_f}{S} = \frac{S_1/S_0 f(\phi)}{S/S_0 \phi^{2/3}} \approx \frac{1.083 f(\phi)}{\phi^{2/3} S/S_0} \quad (52)$$

where S/S_0 is given by Fig. 21 and $f(\phi)$ is the fraction of a confining wall that is “contacted” by the flattened parts of the drops pushing against it, under the assumption that the wall is perfectly wetted by the continuous phase. This fraction, which varies from $f=0$ at ϕ_0 to $f=1$ at $\phi=1$, can be measured experimentally (69) and was found empirically to be given by

$$f(\phi) = 1 - \frac{3.20}{(\phi/(1-\phi) + 7.70)^{1/2}} \quad (53)$$

for $\phi_0 < \phi < 0.975$. (By solving for ϕ at $f=0$, we again obtain evidence that $\phi_0 \approx 0.72$ for real, polydisperse systems.) For $\phi > 0.975$, we expect that $f(\phi)$ is given, to a good approximation (40), by

$$f(\phi) = [1 - 1.892(1-\phi)^{1/2}]^2 \quad (54)$$

Combining Eqs. (53) and (54) with Eq. (52) leads to the approximate dependence of S_f/S on ϕ as shown in Fig. 22.

These are just some of the examples of where and how the osmotic pressure, or its related properties, can be used to define the overall equilibrium behavior of these complex fluids, even though their detailed microscopic structure may not be fully known. Other examples are presented in Section VI, where we describe the only properties that are unique to foams as a result of the compressibility of their dispersed phase.

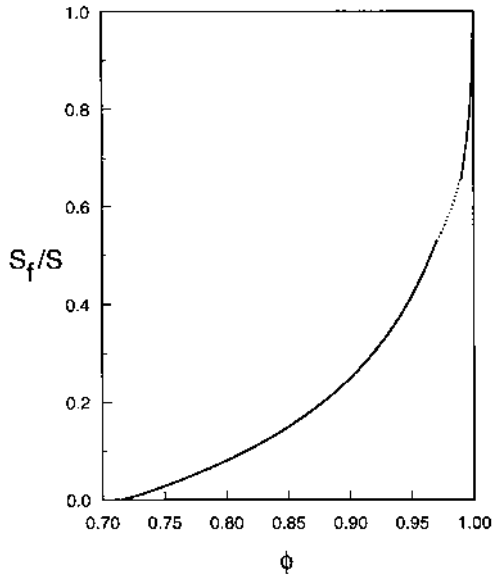


Figure 22 Fraction of total surface area contained in films as a function of volume fraction for typical polydisperse emulsion. Solid curve at right is limiting solution for fcc; the dashed curve connects it to the lower experimental region. [From Ref. 29. Copyright (1988) American Chemical Society.]

VI. FOAMS: INTERNAL PRESSURE, EQUATION OF STATE, AND COMPRESSIBILITY

Up to this point, we have emphasized the common structural and other properties of concentrated emulsions and foams. However, because of their gaseous dispersed phase, foams are compressible and, just as gases themselves, can be characterized by an equation of state that relates their volume, external pressure, and temperature.

A. Dry-Foam Limit ($\phi = 1$)

For a polydisperse dry foam, one can define an average *internal pressure* \bar{p}_i that is given by

$$\bar{p}_i = \frac{\sum p_i v_i}{\sum v_i} = \frac{\sum p_i v_i}{V} \quad (55)$$

where p_i and v_i are the pressure and volume of bubble i , respectively, and V is the total foam volume. Derjaguin (70) has shown that

$$\bar{p}_i = P + \frac{2\sigma S_1}{3V} \quad (\phi = 1) \quad (56)$$

where P is the external pressure and S_1/V is the specific surface area of the foam. Assuming ideality of the gas phase, this leads to the *equation of state*

$$\left(P + \frac{2\sigma S_1}{3V}\right)V = n\mathfrak{R}T \quad (\phi = 1) \quad (57)$$

where n is the number of moles of gas in the foam. The same results were later obtained by Ross (71).

Morrison and Ross (72) have indicated that although Eqs. (56) and (57) are undoubtedly correct for monodisperse foams, a rigorous proof of their validity for *polydisperse* systems was lacking. Such proof has since been provided by Hollinger (73), Crowley (74), and Crowley and Hall (75).

Derjaguin (70) further showed that the compression modulus K is given by

$$K \equiv -V \frac{dP}{dV} = \frac{P + 2\bar{p}_i}{3} = P + \frac{4\sigma S_1}{9V} \quad (\phi = 1) \quad (58)$$

which compares to $K=P$ for a simple ideal gas.

The specific surface area in Eqs. (56)–(58) may be replaced by

$$\frac{S_1}{V} = \frac{S_1 S_0}{S_0 V} = \frac{3}{R_{32}} \frac{S_1}{S_0} \quad (59)$$

where, as earlier, R_{32} is the Sauter mean bubble radius and $S_1/S_0 \approx 1.083$ is the increase in surface area associated with the transition from spherical to polyhedral bubbles at equal volume.

B. Foams with Finite Liquid Content ($\phi < 1$)

We have shown (29) that, for this general case, Eqs. (56)–(58) are to be modified as follows:

$$\bar{p}_i = P + \frac{1-\phi}{\phi} \Pi + \frac{2\sigma S}{3V_1} \quad (60)$$

$$\left(P + \frac{1-\phi}{\phi} \Pi + \frac{2\sigma S}{3V_1}\right)\phi V = n\mathfrak{R}T \quad (61)$$

$$K = \frac{1}{\phi} \left[P + \frac{1-\phi}{3\phi} \Pi + (1-\phi)^2 \frac{d\Pi}{d\phi} + \frac{4\sigma S}{9V_1} \right] \quad (62)$$

where Π is the osmotic pressure, V_1 is the volume of the dispersed gas phase, and V is the total foam volume ($V_1 = \phi V$). For $\phi = 1$, Eqs. (56)–(58) are recovered.

Equations (60)–(62) may be written in the form

$$\bar{p}_i - P = \frac{\sigma}{R_{32}} \left(\frac{1-\phi}{\phi} \tilde{\Pi} + 2 \frac{S}{S_0} \right) \quad (63)$$

$$\left[P + \frac{\sigma}{R_{32}} \left(\frac{1-\phi}{\phi} \tilde{\Pi} + 2 \frac{S}{S_0} \right) \right] \phi V = nRT \quad (64)$$

$$K = \frac{1}{\phi} \left[P + \frac{\sigma}{R_{32}} \left(\frac{1-\phi}{3\phi} \tilde{\Pi} + (1-\phi)^2 \frac{d\tilde{\Pi}}{d\phi} + \frac{4}{3} \frac{S}{S_0} \right) \right] \quad (65)$$

where $\tilde{\Pi}$ is the reduced osmotic pressure. The terms within the parentheses depend on ϕ only and can be evaluated from the above-presented data. It may be shown (29) that the “osmotic” terms, although significant, provide only a rather small correction ($< 6\%$) to the dominant “Derjaguin terms” in S/S_0 . Of perhaps trivial but greater significance is the correction for the volume fraction outside the brackets of Eqs (61), (62), (64), and (65).

VII. MECHANICAL AND RHEOLOGICAL PROPERTIES

It has long been realized that the crowding of deformable drops and bubbles in concentrated emulsions and foams gives rise to interesting mechanical and rheological properties, not shown by the separate constituent fluid phases. When subjected quasistatically to a small stress, these systems respond as purely elastic solids, characterized by a static elastic modulus, G . Under dynamic conditions, the modulus has a real, elastic component (the storage modulus, G') and a complex, viscous component (the loss modulus, G''). Once a critical or yield stress is exceeded, the systems flow and behave as viscoelastic fluids, whose effective viscosity decreases from infinity (at the yield stress) with increasing shear rate. Thus, in rheological terms, they are *plastic* fluids with viscoelastic *solid* behavior below the yield stress and viscoelastic *fluid* behavior above the yield stress.

A number of early experimental studies have provided qualitative evidence for some or all of these behavioral aspects (e.g., Refs. 4 and 76–82), but the techniques employed were usually crude and/or the systems were poorly characterized, if at all. This makes it impossible to use these early experimental data to draw conclusions as to the quantitative relationships between the rheological properties, on the one hand, and important

system variables, such as volume fraction, interfacial tension, mean drop size (and size distribution), fluid viscosities, shear rate, and so forth, on the other hand. In the last decade or so, interest in this area has intensified and much progress has been and is being made along several fronts: theoretical modeling, computer simulation, and careful experimentation. For other recent, although by now somewhat outdated, reviews, see Refs. 83–86.

A. Theoretical Modeling and Computer Simulation

In view of the exceedingly complex structure of 3D systems—even when monodisperse—initial efforts were confined almost exclusively to their 2D analogs. Although unrealistic in some ways, these models provide important kinematic insights and their behavior may be extrapolated, with caution and limitations, to real systems. At first, for the sake of mathematical tractability, the complexity was reduced even further by considering perfectly ordered, *monodisperse* 2D systems. Gradually, the degree of complexity has been increased by allowing disorder. It is only very recently that some intrepid investigators have begun to tackle the 3D problem in earnest.

1. Elastic and Yield Properties: Shear Modulus and Yield Stress

Two-Dimensional Systems. For the perfectly ordered case, the unstrained equilibrium structure has been discussed earlier. The (cylindrical) drops are arranged on a perfectly ordered hexagonal lattice, decorated at its vertices with Plateau borders, whose wall curvatures are determined by the drop size and volume fraction according to Eq. (11). The system can be thought to be confined between two parallel plates, with rows of drops being forced to align with the plates. As one of the plates is now moved within its own plane to induce shear, all drops respond by being deformed identically. In the process, the surface area increases. With the assumption of constant interfacial tension, this results in a force (stress) versus deformation (strain) behavior that has been analyzed in detail, using straightforward geometrical arguments, by Princen (87) for any value of $\phi \geq \phi_0$. The simplest dry-foam case of $\phi = 1$ has been considered independently by Prud'homme (88).

The sequence of events in the dry-foam limit is illustrated in Fig. 23 for a single unit cell (i.e., the parallelogram formed by the centers of four adjacent drops). As the cell is strained at constant volume, the angle between the films must remain at 120° , which causes the central film to shorten until its length shrinks to zero. At that point, four films meet in a line. The resulting instability resolves itself by a rapid so-called T1 rearrangement or “neighbor switching.” In the process, new film is generated from the center to restore the original, unstrained configuration. A different, perhaps clearer, view of the system as it moves through such a cycle is shown in

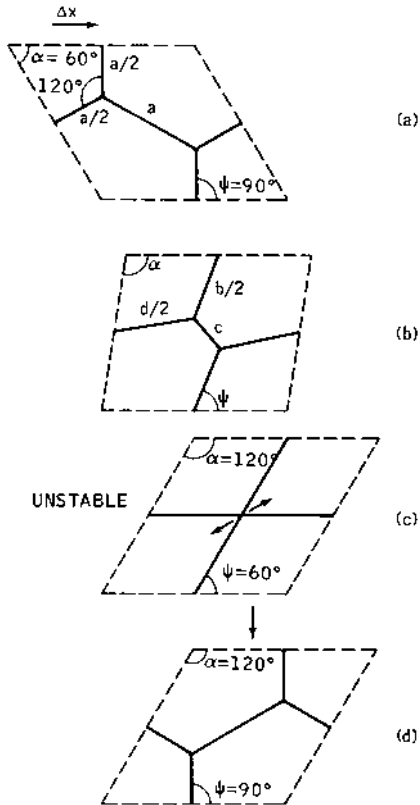


Figure 23 Shear deformation of unit cell of perfectly ordered 2D system in dry-foam limit ($\phi = 1$); the transition from (c) to (d) is rapid and is often referred to as a T1 rearrangement or neighbor switching. (From Ref. 87, with permission from Academic Press.)

Fig. 24. At any stage, the stress per unit cell is given by the horizontal component of the tension of the originally vertical films; that is,

$$F = 2\sigma \cos \psi \quad (66)$$

where ψ is the angle between these films and the horizontal shear direction. The resulting stress-strain curve per unit cell is given by curve 8 in Fig. 25, where \tilde{F} is the dimensionless stress per unit cell:

$$\tilde{F} = \frac{F}{2\sigma} = \cos \psi \quad (67)$$

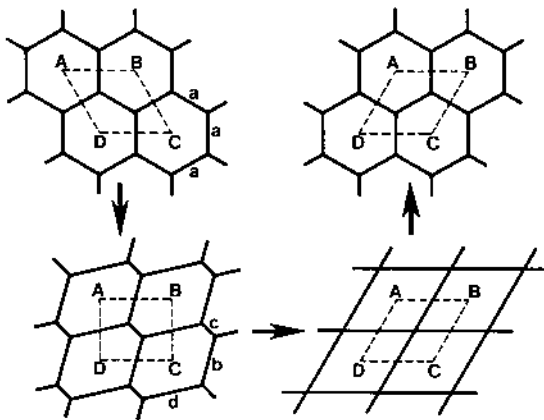


Figure 24 Alternative view of shear strain cycle. (From Ref. 87, with permission from Academic Press.)

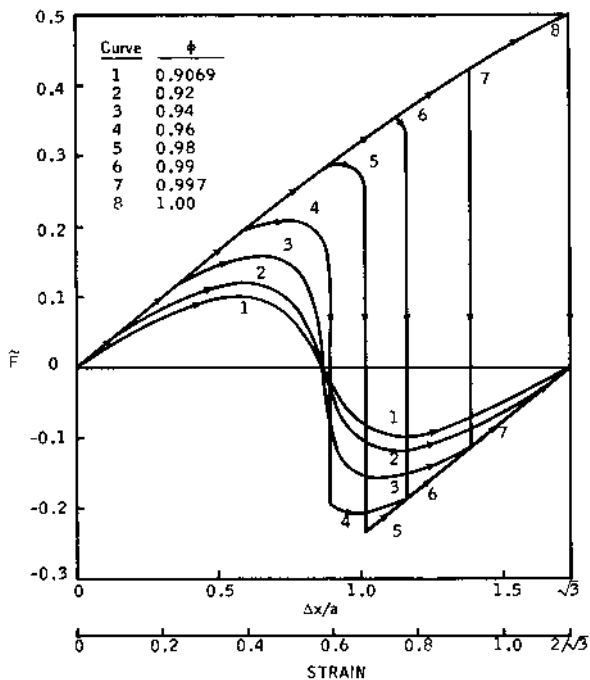


Figure 25 Shear stress per unit cell versus shear strain for perfectly ordered 2D system at different volume fractions. (From Ref. 87, with permission from Academic Press.)

Khan and Armstrong (45,89,90), using a slightly different analysis, arrived at the following simple analytical result for curve 8:

$$\tilde{F} = \frac{\gamma}{(\gamma^2 + 4)^{1/2}} \quad (68)$$

where γ is the imposed strain, which varies from zero to $2/\sqrt{3}$ at the point of instability. The cycle then repeats itself.

When $\phi < 1$, the situation is considerably more complicated (Fig. 26). As long as the two Plateau borders within the unit cell remain separated (Mode I), the stress per unit cell is unaffected. However, beyond a given strain, which depends on ϕ , the Plateau borders merge to form a single, four-sided border. In this Mode II regime, the films no longer meet at 120° , and the stress-strain curve deviates from that for the dry-foam limit.

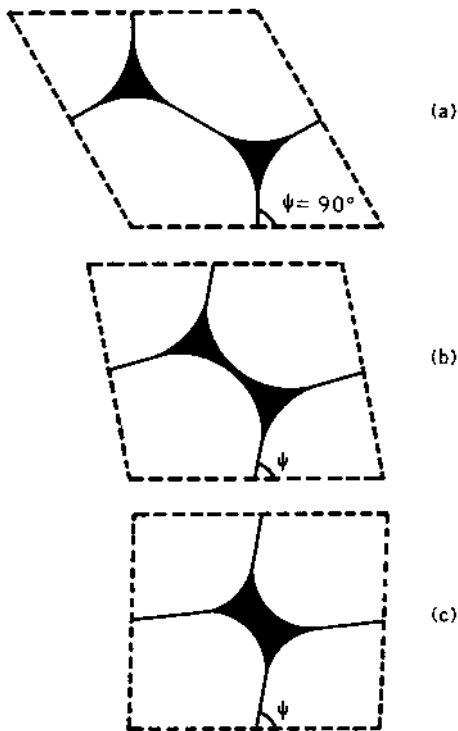


Figure 26 Increasing strain for systems with $0.9069 < \phi < 1$. Between (a) and (b), the system is in Mode I; between (b) and (c), the system is in Mode II. (From Ref. 87, with permission from Academic Press.)

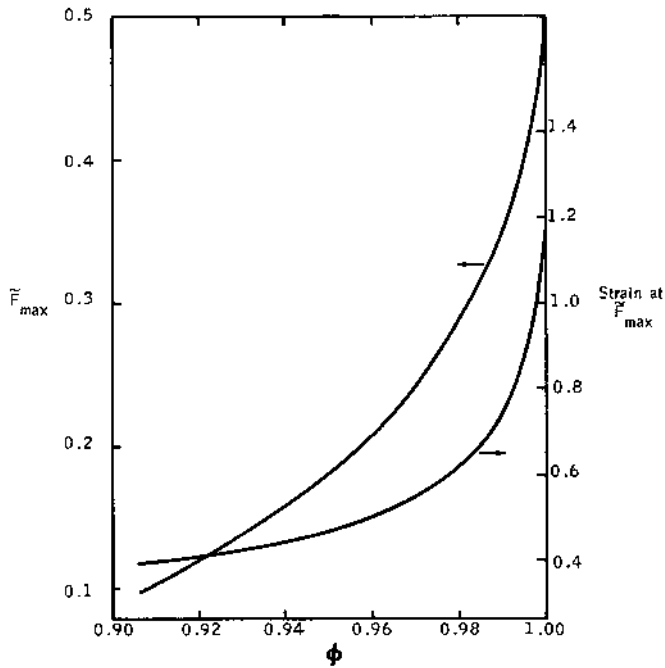


Figure 27 Static yield stress per unit cell and yield strain as a function of volume fraction for a perfectly ordered 2D system. (From Ref. 87, with permission from Academic Press.)

It passes through a (lower) maximum and ultimately reverses sign, either continuously or via a T1 rearrangement (87). The resulting curves are collected in Fig. 25. In each case, the maximum \tilde{F}_{\max} corresponds to the static *yield stress* per unit cell. It is plotted in Fig. 27 as a function of ϕ , together with the corresponding yield strain. Realizing that there are $1/a\sqrt{3}$ unit cells per unit of length in the shear direction and that a may be expressed in terms of the more practical drop radius R and volume fraction ϕ , one finds for the stress(τ)–strain(γ) relationship

$$\tau = 1.050 \frac{\sigma}{R} \phi^{1/2} \tilde{F}(\gamma, \phi) \quad (69)$$

whereas the *yield stress*, τ_0 , is given by

$$\tau_0 = 1.050 \frac{\sigma}{R} \phi^{1/2} \tilde{F}_{\max}(\phi) \quad (70)$$

where $\tilde{F}_{\max}(\phi)$ may be read from Fig. 27. It is expected to start deviating from zero when adjacent layers of close-packed drops or bubbles can freely slide past each other (i.e., at $\phi = \pi/4 = 0.7854$).

The small-strain, static *shear modulus*, G , is defined as

$$G \equiv \left(\frac{d\tau}{d\gamma} \right)_{\gamma=0} \quad (71)$$

and can be obtained from Eqs. (69) and (68):

$$G = 1.050 \frac{\sigma}{R} \phi^{1/2} \left(\frac{d\tilde{F}}{d\gamma} \right)_{\gamma=0} = 0.525 \frac{\sigma}{R} \phi^{1/2} \quad (\phi > \phi_0) \quad (72)$$

The model predicts zero shear modulus for $\phi < \phi_0$.

Both the yield stress and the shear modulus scale with σ/R , but, although the yield stress increases strongly with volume fraction, the shear modulus is affected only very weakly through $\phi^{1/2}$. In the dry limit of $\phi = 1$, both reach identical limiting values of

$$\tau_0 = G = 0.525 \frac{\sigma}{R} \quad (\phi = 1) \quad (73)$$

The analysis may be extended to systems in which the film thickness, h , or the contact angle, θ , between the films and the Plateau border walls are finite (87). The effect of a finite film thickness is to increase the effective volume fraction [cf. Eq. (1)], which raises the yield stress and shear modulus in a predictable fashion. The effect of a finite contact angle on the shear modulus is to simply reduce it by a factor of $\cos \theta$. The effect on the yield stress is more complex. In most but not all cases, the yield stress is increased. Furthermore, a finite contact angle can give rise to interesting new instability modes and to hysteretic behavior. The reader is referred to Ref. 87 for further details.

Subsequently, Khan and Armstrong (89,90) and Kraynik and Hansen (91) considered the effect of the orientation of the unit cell, relative to the shear direction, for the dry-foam case. They found that the shear modulus is unaffected, but that the yield stress is sensitive to the orientation. In addition, they considered planar extension as well as shear.

The sudden jump of the shear modulus from zero to a finite value at ϕ_0 and its subsequent weak sensitivity to ϕ for $\phi > \phi_0$ are rather peculiar and appear to be associated with the perfect order of the model. The pure cyclical character of the stress-strain curves is—by itself—a symptom of

“perfection pathology.” Real systems do not exhibit these particular features, because they are invariably disordered, which causes T1 rearrangements to occur even at very small strains, as well as randomly throughout the system, rather than simultaneously at all vertices.

The shear modulus of polydisperse hexagonal systems of the type depicted in Fig. 8b, is still given by Eq. (72) when R is replaced by $R_{\text{av}} = (\sum R_i^2/n)^{1/2}$, a characteristic drop radius that is based on the average drop area (46). However, as expected, the “elastic limit” (i.e., the stress and strain where the first T1 rearrangement occurs) is reduced relative to that of the monodisperse case of the same volume fraction.

The elastic and yield properties of 2D systems with the most general type of disorder (cf. Fig. 7) have been simulated by Hutzler et al. (92) for both dry and wet systems. Indeed, as the number of polydisperse drops in the simulation is increased, the jumps in stress associated with individual or cooperative T1 rearrangements become less and less noticeable. Instead, the stress increases smoothly with increasing strain until it reaches a plateau that may be identified with the yield stress. The yield stress was found to increase sharply with increasing volume fraction, very much as in the monodisperse case. Furthermore, the shear modulus for the dry system ($\phi = 1$) was essentially identical to that for the monodisperse case, as given by Eq. (73) with R_{av} , as defined earlier, replacing R . Its dependence on ϕ was very different from that in Eq. (72), however. When expressed in our terms, their results for $1 > \phi > 0.88$ could be fitted to

$$\frac{G}{\sigma/R_{\text{av}}} = 0.51 - 21(1 - \phi)^2 \quad (74)$$

Assuming that this relationship continues to hold for $\phi < 0.88$ (where their simulations ran into difficulties because of the large number of T1 processes the program had to deal with), the authors (92) concluded that G reaches zero at $\phi = \phi_0 \approx 0.84$. As mentioned earlier, this “rigidity-loss transition” can be identified as the random close packing of hard disks. The drop in G with decreasing ϕ could further be correlated with the average number of sides of the Plateau borders, which gradually increased from three close to $\phi = 1$ to about four at $\phi = 0.84$. Although these simulations involved a rather small number of drops and leave some questions unanswered, they do indicate a type of elastic behavior that—as we will see later—much more closely reflects that of real systems. Clearly, disorder plays a critical role.

Three-Dimensional Systems. The first expression for the shear modulus of random dry foams (and emulsions) was derived by Derjaguin (93). It is based on the assumption that the foam is a collection of randomly

oriented films of constant tension 2σ and negligible thickness and that each film responds affinely to the applied shear strain, as would an imaginary surface element in a continuum. Evaluating the contribution to the shear stress of a film of given orientation and averaging over all orientations then leads to

$$G = \frac{4}{15} \sigma \frac{S_1}{V} \quad (\phi \approx 1) \quad (75)$$

where S_1/V is the surface area per unit volume. Because $S_1/V \approx 1.083 S_0/V = 3.25/R_{32}$, this may be written as

$$G \approx \frac{13}{15} \frac{\sigma}{R_{32}} \approx 0.87 \frac{\sigma}{R_{32}} \quad (\phi \approx 1) \quad (76)$$

Much later, Stamenović and Wilson (94) rediscovered Eq. (75), using similar arguments but pointing out at the same time that it probably represents an overestimate. Indeed, using 2D arguments, Princen and Kiss (95) concluded that the affine motion of the individual films violates Plateau's laws and leads to an overestimate of G by a factor of 2, at least in 2D. (Kraynik, in a private communication, pointed out an internal inconsistency in Ref. 95 and concluded that G is overestimated by a factor of only 3/2). Furthermore, Derjaguin's model does not allow for T1 rearrangements; it does not predict a yield stress nor does it have anything to say about the effect of ϕ in "wet" systems. On the other hand, the model correctly predicts that G scales with σ/R .

Stamenović (96) analyzed the deformation of an idealized single foam vertex, where four Plateau borders meet and concluded that

$$G = \frac{1}{6} \sigma \frac{S_1}{V} \approx 0.54 \frac{\sigma}{R_{32}} \quad (\phi \approx 1) \quad (77)$$

As pointed out by Reinelt and Kraynik (56), however, the idealized vertex does not adequately represent an equilibrium structure. Similar reservations apply to the work of Budiansky and Kimmel (97), who considered the behavior of an isolated foam cell in the form of a regular pentagonal dodecahedron and obtained a shear modulus between the two above values.

Using Brakke's Surface Evolver (49), Reinelt and co-workers (56,68,98–102) have explored in detail the elastic response of monodisperse, perfectly ordered structures, both "dry" and "wet," to extensional and shear strain. Structures considered included the rhombic dodecahedron, the regular ("planar") tetrakaidecahedron, the Kelvin cell, and the Weaire–Phelan

Table 1 Shear Moduli of Dry Systems

	$G_1/\sigma V^{-1/3}$	$G_2/\sigma V^{-1/3}$	$G_{av}/\sigma V^{-1/3}$	$G_{av}/\sigma R^{-1}$
Regular tetrakaidecahedron	0.5525	0.9696	0.8028	0.4980
Kelvin	0.5706	0.9646	0.8070	0.5006
Weaire–Phelan	0.8902	0.8538	0.8684	0.5387
Random (monodisperse)			0.78 ± 0.08	0.48 ± 0.05

structure. Some degree of disorder was introduced by considering bidisperse Weaire–Phelan systems (103), in which the relative volumes of the dodecahedra and tetrakaidecahedra were varied, as well as random, although monodisperse, systems (68). As in the 2D case, the stress–strain behavior depends on the cell orientation relative to the strain direction. Because of the multitude of edges and faces of each cell, a variety of T1 transitions may occur at increasing strain, leading to very complex behavior. Some of their results for the shear moduli of dry systems ($\phi = 1$) are listed in Table 1.

The ordered structures are all anisotropic, have cubic symmetry, and can be characterized by two shear moduli, G_1 and G_2 . To simulate orientational disorder, the authors introduced an “effective isotropic shear modulus,” $G_{av} = (2/5)G_1 + (3/5)G_2$, which is obtained by averaging over all orientations. The first three columns of Table 1 give the moduli in units of $\sigma V^{-1/3}$, where V is the cell volume; the last column is given in units of σ/R , where $R = (3V/4\pi)^{1/3}$. The orientation-averaged results are surprisingly close to the 2D prediction of $G/\sigma R^{-1} = 0.525$ [cf. Eq. (73)], Stamenović’s prediction of $G/\sigma R^{-1} = 0.54$ [cf. Eq. (77)], and the extrapolated experimental result of Princen and Kiss (95) for polydisperse emulsions, which indicated that $G/\sigma R_{32}^{-1} = 0.509$ (see Sect. VII.B.3). The small influence of polydispersity is also suggested by the finding that G_{av} varies less than 0.5% when the volume ratio of the two types of cells in bidisperse Weaire–Phelan structures is varied between 0.039 and 2.392 (103).

Simulations of this type can pinpoint an “elastic limit” where the first (or subsequent) T1 transition(s) take(s) place. It depends extremely strongly on orientation, as does the “dynamic yield stress” (i.e., the stress integrated over a complete strain cycle). The relevance to the yield stress of real disordered systems is therefore quite limited (100). As in 2D simulations, simulations on more highly disordered systems will undoubtedly bring increased insight.

Simulations on “wet” rhombic dodecahedra and Kelvin cells have been carried out by Kraynik and colleagues (68,102). The effective isotropic shear moduli were found to depend slightly on the volume fraction but did not show the linear dependence on $\phi - \phi_0$ found experimentally for

disordered systems (95). Again, simulations on highly disordered wet systems should improve our understanding.

Buzza and Cates (104) also addressed the question of whether disorder or the increased dimensionality from two to three dimensions is responsible for the observed experimental behavior of the shear modulus. In particular, they explored the lack of the sudden jump in G from zero to a finite value at $\phi = \phi_0$ that is predicted by the perfectly ordered 2D model. We have seen earlier that disorder appears to remove that abrupt jump in two dimensions (92). For drops on a simple cubic lattice, Buzza and Cates analyzed the drop deformation in uniaxial strain close to $\phi = \phi_0$, first using the model of “truncated spheres.” (For reasons given earlier, we believe this to be a very poor model.) They showed that this model did not eliminate the discontinuous jump in G . An exact model, based on a theory by Morse and Witten (105) for weakly deformed drops, led to $G \propto 1/\ln(\phi - \phi_0)$, which gets rid of the discontinuity but still shows an unrealistically sharp rise at $\phi = \phi_0$ and is qualitatively very different from the experimentally observed linear dependence of G on $\phi = \phi_0$. Similar conclusions were reached by Lacasse and co-workers (51,106). A simulation of a disordered 3D model (106) indicated that the droplet coordination number increased from 6 at ϕ_0 to 10 at $\phi = 0.84$, qualitatively similar to what is seen in disordered 2D systems (92). Combined with a suitable (anharmonic) interdroplet force potential, the results of the simulation were in close agreement with experimental shear modulus and osmotic pressure data. Therefore, it appears again that disorder is responsible for many of the features of real systems.

2. Shear Viscosity

Compared to the quasistatic elastic and yield behaviors of concentrated emulsions and foams, the rate-dependent viscous properties are even more complex and relatively unexplored. Formally, the shear stress, τ , may be expressed as a function of the shear rate, $\dot{\gamma}$, as

$$\tau(\dot{\gamma}) = \tau_0 + \tau_s(\dot{\gamma}) \quad (78)$$

where τ_0 is the (elastic) yield stress and $\tau_s(\dot{\gamma})$ is the contribution from any rate-dependent dissipative processes; or, in terms of the effective shear viscosity, μ_e ,

$$\mu_e \equiv \frac{\tau(\dot{\gamma})}{\dot{\gamma}} = \frac{\tau_0}{\dot{\gamma}} + \frac{\tau_s(\dot{\gamma})}{\dot{\gamma}} \quad (79)$$

The first term is, to a large extent, responsible for the shear-thinning behavior of these systems. As is clear from the previous discussion, τ_0 is determined primarily by σ , R and ϕ , whereas the size distribution may play a secondary

role. The dynamic stress, τ_s , is expected to depend on these and other variables (e.g., the shear rate, the viscosities of the continuous and dispersed phases, and surface-rheological parameters). So far, the predictive quality of theoretical and modeling efforts has been very restricted because of the complexity of the problem.

Buzza et al. (107) have presented a qualitative discussion of the various dissipative mechanisms that may be involved in the small-strain linear response to oscillatory shear. These include viscous flow in the films, Plateau borders, and dispersed-phase droplets (in the case of emulsions), the intrinsic viscosity of the surfactant monolayers, and diffusion resistance. Marangoni-type and “marginal regeneration” mechanisms were considered for surfactant transport. They predict that the zero-shear viscosity is usually dominated by the intrinsic dilatational viscosity of the surfactant monolayers. As in most other studies, the discussion is limited to small-strain oscillations, and the rapid events associated with T1 processes in steady shear are not considered, even though these may be extremely important.

It is now generally recognized that surfactants are indeed crucial, not only in conferring (meta)stability to the emulsion or foam but also in controlling the rate-dependent rheology of the film surfaces and that of the system as a whole. Several early, spatially periodic 2D models neglected this aspect and made other simplifying assumptions. Khan and Armstrong (45,89,90) and Kraynik and Hansen (108) assumed that all of the continuous phase resides in the films (i.e., there were no Plateau borders) and that there is no exchange of fluid *between* the films. The film surfaces were assumed to be completely mobile (no surfactant!). When such a system is strained globally, the uniform films respond with simple planar extension (or compression) at constant volume. This mechanism predicts significant structural changes but leads to viscous terms in Eqs. (78) and (79) that are insignificant compared with the elastic terms up to extremely high shear rates that are unlikely to be encountered in practice. Experimentally, one finds a much more significant contribution (see Sect. VII.B.3).

A more complete 2D analysis of simple shear is that of Li et al. (109). It solves the detailed hydrodynamics in the drops, films, and Plateau borders for the case of equal viscosities of the continuous and dispersed phases. Again, large structural changes are predicted. However, surfactants (and surface tension gradients) are assumed to be absent, which severely limits the practical implications of the analysis. An interesting conclusion is that, under certain conditions, shear flow can stabilize concentrated emulsions, even in the total absence of surfactants.

An approach that is almost diametrically opposed to the earlier models of Khan and Armstrong, and Kraynik and Hansen, was advanced by Schwartz and Princen (110). In this model, the films are negligibly thin,

so that all of the continuous phase is contained in the Plateau borders and the surfactant turns the film surfaces immobile as a result of surface tension gradients. Hydrodynamic interaction between the films and the Plateau borders is considered to be crucial. This model, believed to be more realistic for common surfactant-stabilized emulsions and foams, draws on the work of Mysels et al. (111) on the dynamics of a planar, vertical soap film being pulled out of, or pushed into, a bulk solution via an intervening Plateau border. An important result of their analysis is commonly referred to as Frankel's law, which relates the film thickness, $2h_\infty$, to the pulling velocity, U , and may be written in the form

$$\frac{h_\infty}{r} = 0.643(3Ca^*)^{2/3} \quad (80)$$

where $Ca^* = \mu U / \sigma$ ($\ll 1$) is the film-level capillary number, μ and σ are the viscosity and surface tension of the liquid (the "continuous phase"), and r is the radius of curvature of the Plateau border where it meets the film and is given by capillary hydrostatics, $r = (\sigma / 2\rho g)^{1/2}$, where ρ is the density of the liquid and g is the gravitational acceleration.

Frankel's law has its close analogs in a number of related problems (112–114) and has been verified experimentally (115,116) in the regime where the drawn-out film thickness, $2h_\infty$, is sufficiently large for disjoining-pressure effects to be negligible. Below some critical speed, the thickness of the drawn-out film equals the finite equilibrium thickness, $2h_{eq}$, which is set by a balance of the disjoining pressure, $\Pi_d(h)$, and the capillary pressure, σ/r , associated with the Plateau border. Thus, Frankel's law and the following analysis apply only as long as $1 \gg Ca^{*2/3} \gg h_{eq}/r$. It is expected to break down as the capillary number approaches zero. Disjoining pressure effects may, in principle, be included (e.g., Ref. 117) but at the expense of simplicity and generality of the model.

The interesting hydrodynamics and the associated viscous energy dissipation are confined to a transition region between the emerging, rigidly moving film and the macroscopic Plateau border. The lubrication version of the Stokes equation may be used in this region, as the relative slope of the interfaces remains small there.

It is reasonable to assume that the same basic process operates in moving emulsions and foams. Lucassen (118) has pointed out that for such systems to be stable to deformations such as shear, the dilatational modulus of the thin films must be much greater than that of the surfaces in the Plateau border. However, this is equivalent to the assumption of inextensible film surfaces that underlies Frankel's law. Therefore, it may well be that, by implication, emulsions and foams that are stable to shear (and we

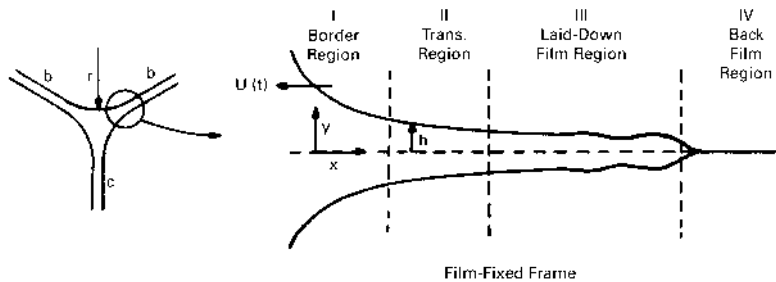


Figure 28 Film being pulled out of a Plateau border with velocity $U(t)$; all viscous dissipation occurs in the transition region (II). (From Ref. 110, with permission from Academic Press.)

are interested in such systems only) have the appropriate surface rheology for Frankel's law to apply. Of course, in emulsions and foams, each Plateau border of radius r (set by drop size and volume fraction) is now shared by three films. At any given moment, one or two of the films will be drawn out of the border while the other(s) is (are) pushed into it, at respective quasi-steady velocities $U(t)$ that are dictated by the macroscopic motion of the system (Fig. 28). Using a perfectly ordered 2D system, Schwartz and Princen (110) considered a periodic uniaxial, extensional strain motion of small frequency and amplitude, so that inertial effects are negligible and complications due to the merger of adjacent Plateau borders and associated rapid T1 processes are avoided. They proceeded by calculating the instantaneous rate of energy dissipation in the transition region of each of the three films associated with a Plateau border and integrated the results over a complete cycle. When the effective strain rate is related to the frequency of the imposed motion, the result can be expressed as an effective viscosity that is given by*

$$\mu_e = 5.3\mu Ca^{-1/3} \quad (81)$$

where the macroscopic capillary number $Ca \equiv \mu a \dot{\gamma} / \sigma$, a is the length of the hexagon that circumscribes a drop or bubble, and μ is the viscosity of the continuous phase. Because of the small amplitude of the imposed motion,

*In the original article (110), the numerical coefficient was given as 6.7. This and a few other minor numerical errors were pointed out by Reinelt and Kraynik (119, and private communication).

the result does not depend on the volume fraction. It was further argued that in the case of emulsions, the effect of the dispersed-phase viscosity, μ_d , is relatively insignificant. Reinelt and Kraynik (120) later estimated that this is a good approximation as long as

$$\frac{\mu_d}{\mu} \ll \text{Ca}^{-1/3} \quad (82)$$

Apart from a change in the numerical coefficient, Eq. (81) is expected to apply also to a periodic, small-amplitude *shearing* motion. However, in *steady shear*, rapid film motions associated with the T1 processes, whose effect has so far not been analyzed, periodically interrupt the above process. Further, as the strain at the instability depends on the volume fraction (Fig. 27), the viscous term may become ϕ dependent. Provided that the effect of the T1 jumps may be neglected or the associated viscous contribution also scales with $\mu\text{Ca}^{-1/3}$, this model would then predict for the shear viscosity,

$$\mu_e = \frac{\tau_0}{\dot{\gamma}} + C(\phi)\mu\text{Ca}^{-1/3} = \frac{\tau_0}{\dot{\gamma}} + C'(\phi)\frac{\mu^{2/3}\sigma^{1/3}}{R^{1/3}}\dot{\gamma}^{-1/3} \quad (83)$$

or, for the shear *stress*,

$$\tau = \tau_0 + C(\phi)\frac{\sigma}{a}\text{Ca}^{2/3} = \tau_0 + C'(\phi)\frac{\mu^{2/3}\sigma^{1/3}}{R^{1/3}}\dot{\gamma}^{2/3} \quad (84)$$

where $C(\phi)$ and $C'(\phi)$ are of order unity and the yield stress τ_0 is given by Eq. (70). Equations (83) and (84) describe a particular type of ‘‘Herschel–Bulkley’’ behavior, characterized in general by $\tau = \tau_0 + K\dot{\gamma}^n$ and $\mu_e = \tau_0/\dot{\gamma} + K\dot{\gamma}^{n-1}$. The special case of $n = 1$ is referred to as ‘‘Bingham plastic’’ behavior. Occasionally, foams and concentrated emulsions are claimed to behave as Bingham fluids. As we shall see, this is not so. (In fact, it is extremely unlikely that *any* fluid, when examined carefully, can be described as such.)

Reinelt and Kraynik (119) improved on the above model by including structural changes that result from the fact that the film tensions deviate from the equilibrium value of 2σ as they are being pulled out of or pushed into the Plateau border. These changes are of order $(\text{Ca}^*)^{2/3}$, as already pointed out by Mysels et al. (111). As the values and signs of Ca^* at any instant are different for the three films emanating from a Plateau border, their tensions are generally unequal and the angles between them deviate from 120° , and the Plateau border radius, r , is also affected. However, these refinements do not alter the qualitative conclusion of the original model, as embodied in Eq. (81), for either planar-extensional or shear deformations.

Applying this approach to uniform dilatation of a foam, Reinelt and Kraynik (119) also derived an expression for the dilatational viscosity, which again scales with $\mu\text{Ca}^{-1/3}$. Using a different surface-rheological description, Edwards and co-workers (121–123) arrived at alternative expressions for the dilatational viscosity of wet and dry foams.

In yet another extension, Reinelt and Kraynik (120) applied the approach to *steady shearing* and *planar-extensional* flow of perfectly ordered 2D systems for $0.9069 < \phi < 0.9466$. This is the range of “very wet” systems, for which the shear stress varies continuously with strain over a complete strain cycle (cf. Fig. 25), so that rapid film events associated with T1 processes are avoided. They also investigated the effect of orientation, and structural effects due to changes in film tension were again included. As earlier, the effective viscosity was found to be proportional to $\mu\text{Ca}^{-1/3}$. Interestingly, the model indicates that the effective viscosity increases with increasing volume fraction, which parallels practical experience.

Okuzuno and Kawasaki (124) simulated the shear rheology of dry, random 2D systems, using their “vertex model” in which the films are uncurved and do not generally meet at 120° angles. Although Plateau’s condition is therefore violated, the model offers the advantage of being computationally more efficient than other, more realistic models. By solving the “equations of motion” for all the vertices, while taking account of T1 rearrangements and using the energy-dissipation approach of Schwartz and Princen (110), these authors tentatively concluded that the system behaves like a Bingham plastic fluid. However, because the number of simulations was quite limited, they did not rule out Herschel–Bulkley behavior with $n \neq 1$ (see above discussion). In a later study, the same investigators (125) observed violent flows like that of an avalanche in their simulations in the large strain regime at small shear rate. Similar avalanchelike flows are observed in simulations by Jiang et al. (126).

This review is not exhaustive by any means. Other studies have been and are being published regularly, as the topic continues to enjoy considerable interest. It appears, however, that theoretical analyses and computer simulations can only go so far. There is a need for careful experimental work in order to establish the *actual* behavior of real systems. As has been the case in the past, further progress will be optimal when the two approaches go hand in hand.

B. Experimental Approaches and Results

The rheological parameters of primary scientific and practical concern are the static and dynamic shear modulus, the yield stress, and the shear-rate-dependent viscosity. The aim is to understand and predict how these

depend on the system parameters. In order to accomplish this with any hope of success, there are two areas that need to be emphasized. First, the systems studied must be characterized as accurately as possible in terms of the volume fraction of the dispersed phase, the mean drop size and drop size distribution, the interfacial tension, and the two bulk-phase viscosities. Second, the rheological evaluation must be carried out as reliably as possible.

1. System Characterization

The bulk phases are generally Newtonian and their *viscosities* can be measured with great accuracy with any standard method available.

The *nominal volume fraction* of the dispersed phase can be obtained very accurately from the relative volumes (or weights) of the phases used in the preparation of a highly concentrated emulsion (69). A series of emulsions, differing only in volume fraction, may be conveniently prepared by dilution of a mother emulsion with varying known amounts of the continuous phase (69). Alternatively, if the phases differ greatly in volatility, the volume fraction may be obtained, albeit destructively, from the weight loss associated with evaporation of the more volatile phase, usually water (127). Another destructive method is to destroy the emulsion by high-speed centrifugation in a precision glass tube, followed by accurate measurement of the relative heights of the separated liquid columns (24). To arrive at the *effective volume fraction*, the nominal volume fraction may need to be corrected for a finite film thickness according to Eq. (1). Because all rheological parameters depend more or less strongly on the volume fraction, it is important that the vertical gradient in volume fraction due to gravity be kept to a minimum, if reliable rheological evaluations are to be expected. The gradient in volume fraction may be predicted quantitatively (67). Because the drop size and the density difference between the phases are generally much larger in foams than in emulsions, the gradient in ϕ is usually much more pronounced in the former than in the latter. The rheologies of both types of system being governed by identical laws, it is preferable—for this and many other reasons (see next paragraph)—to use *emulsions*, rather than foams, to learn about *foam* rheology.

The *mean drop size* and *drop size distribution* can be measured to within a few percent accuracy with a number of techniques, such as the “Coulter Counter” (69,95,128) and dynamic light scattering. The Coulter Counter is eminently suitable for oil-in-water emulsions but has a lower practical limit of about 1 μm . Various light-scattering techniques are equally suitable for oil-in-water and water-in-oil (w/o) emulsions and afford a larger dynamic range. In either case, the concentrated emulsion must be diluted with the continuous phase to a level where coincidence counting or multiple

scattering, respectively, is avoided. One popular method that should perhaps be avoided is optical microscopy, which is not only tedious but also relatively inaccurate when applied to polydisperse systems because of depth-of-focus limitations and wall effects. At any rate, a practical lower limit for accurate, quantitative optical microscopy is well in excess of $1\ \mu\text{m}$. Whatever method is used, it is desirable that complete size distributions be reported. At the very least, when only a mean drop size is reported, the *type* of mean should be specified. Finally, it appears that size determinations are much easier to obtain in emulsions than in foams. Moreover, although it is easy to prepare emulsions whose drop size distribution changes imperceptibly over a period of months, the bubble size distribution in foams changes very rapidly as a result of Ostwald ripening. It is, therefore, almost impossible to have accurate knowledge of the bubble size distribution at the moment a rheological measurement is being made. These are yet additional reasons for using emulsions in order to investigate foams.

The *interfacial tension* may be determined to within about 1% accuracy with the spinning drop method (129,130). It is an absolute and static method that requires only small samples and, in contrast to most other methods, does not depend on the wettability of a probe, such as a ring or Wilhelmy plate. The stabilizing surfactant is commonly used at concentrations in the bulk continuous phase that are far above the critical micelle concentration (cmc). This ensures that the concentration remains above the cmc after adsorption onto the vastly extended interface has taken place, which is clearly needed to maintain emulsion stability. It is tempting, therefore, to assume that the interfacial tension in the finished emulsion equals that between the unemulsified bulk phases and that it remains constant when a “mother emulsion” is diluted with continuous phase in order to create a series of emulsions in which only ϕ is varied (69). This may be a reasonable assumption when a pure surfactant is used, but there is evidence that this may not be so when impure commercial surfactants are employed (95,128).

2. Rheological Evaluation

Most studies have used standard rheological techniques, such as rotational viscometers of various types and geometries, such as concentric-cylinder, cone-and-plate, and parallel-plate rheometers, each of which may be operated in various modes [constant stress, constant strain, steady shear, or dynamic (i.e., oscillatory) shear]. The relative advantages and/or limitations of these and other techniques may be found in any standard textbook on practical rheometry (e.g., Ref. 131). When applied to highly concentrated emulsions and foams—or suspensions in general, for that matter—these

techniques are fraught with many difficulties and pitfalls that are often overlooked, leading to results of questionable validity. Some of these difficulties are the following.

Wall-induced Instability. Princen (69) has reported that otherwise very stable oil-in-water emulsions showed extremely erratic behavior when sheared in a commercial concentric-cylinder viscometer with stainless-steel parts. The problem could be traced to the “coalescence” of the dispersed oil droplets with the steel walls and the formation of a thick oil layer. Apparently, the thin films of continuous phase separating the walls from the first layer of individual droplets were unstable and ruptured. Coating all relevant parts with a thin film of silica, which assured adequate film stability and complete wetting of the steel by the continuous phase, solved the problem (69). Later, an even more satisfactory solution consisted of replacing the steel inner and outer cylinders with glass parts, combined with other improvements in design (95,128,132). Some of the glass cylinders were highly polished; others were roughened and equipped with vertical grooves to eliminate or reduce wall slip (see below). Wall-induced instability may or may not be a problem, depending on the wall material, the emulsion (w/o or o/w), and surfactant type.

End and Edge Effects. In the analysis of raw data obtained with any type of rotational viscometer, it is assumed that the flow field is known and simple. For example, in the conventional concentric-cylinder viscometer, it is assumed that the fluid moves in concentric cylindrical layers that extend unchanged from the precise top to the precise bottom of the inner cylinder. This is true only when the cylinders are infinitely long. For cylinders of finite length, complications at the top are usually minor and can often be neglected. In the lower region of the viscometer, however, the flow is seriously disturbed. In addition, the bottom of the inner cylinder may contribute a substantial fraction of the total measured torque. This can lead to serious errors. Various suggestions have been made to deal with the problem (131), but their practical value is questionable. In addition to making other improvements, including the use of a *hollow* inner cylinder, Princen and Kiss (95,128,132) effectively isolated the bottom region by filling it with a layer of mercury. In that way, the sample of interest is strictly confined to the space between the cylinders. As long as its effective viscosity is much greater than that of mercury, flow between the cylinders is undisturbed and the torque on the bottom of the inner cylinder is negligible. The arrangement is shown schematically in [Fig. 29](#).

In the cone-and-plate viscometer, there are similar, although perhaps somewhat less severe, problems associated with the outer edge (131).

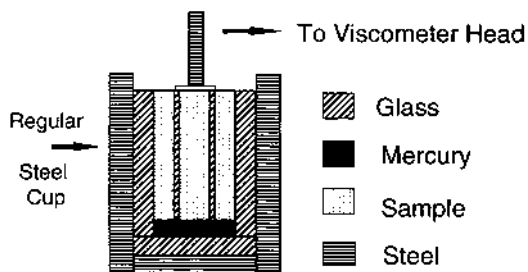


Figure 29 Modified concentric-cylinder viscometer with glass outer cylinder, hollow glass inner cylinder, and pool of mercury to confine the sample to the gap and thus to minimize the end effect.

Wall Slip. Along with wall-induced instability, the occurrence of slip between the sample and the viscometer walls is one of the most serious and prevalent, although often neglected, problems one encounters in assessing the rheology of dispersed systems, in general, and concentrated emulsions in particular. Because concentrated emulsions have a yield stress, wall slip—if present—can be readily demonstrated by painting a thin line of dye on top of the sample in a wide-gap rotating-cylinder viscometer (69). As long as the yield stress is not exceeded at the inner cylinder wall, the sample is not sheared at all but is seen to move around in the gap as an elastically strained solid! In this regime, shear is confined to the thin films of continuous phase separating the wall from the adjacent droplets. For a sufficiently smooth wall, it is possible to estimate the thickness of these films from the measured wall stress and angular velocity (69).

It is obvious that neglect of wall slip may lead to meaningless conclusions as to the system's rheology. There are two different approaches to dealing with this particular problem. First, one can try to eliminate slip by roughening the viscometer surfaces. Princen and Kiss (95) successfully used roughened and grooved glass cylinders to determine the static shear modulus of concentrated emulsions. This worked well in the low-stress, linear elastic regime, although, even here, some wall creep did occur (which could be readily corrected for). However, massive wall slip was noted to commence at shear stresses exceeding only about one-half of the bulk yield stress. Thus, even though the roughness was commensurate with the drop size and served the intended purpose, the arrangement would have been inadequate for determining the yield stress and shear viscosity. Therefore, the question remains how rough a surface must be to eliminate slip up to the maximum shear stress considered. As an extreme case, large radial vanes have been recommended, at least for yield stress

measurements (133). Although undoubtedly effective in preventing slip, the vanes do lead to some uncertainty in the strain field.

Many published rheological studies declare that wall slip was checked for and found to be absent. Unless solid evidence is provided, it behooves the reader to approach such assertions with a healthy dose of skepticism.

A second approach is to permit slip and to correct for it. This usually involves running the sample in two or more viscometer geometries (e.g., at different gap widths) (131,134,135). Doubts have been expressed as to the validity of this approach (136). At any rate, the procedure is rather tedious and may not be very accurate. In an alternative method, Princen and Kiss (128), using their improved design with polished glass cylinders, established empirically that the torque versus angular velocity data for concentrated emulsions may be linearized over most of the all-slip/no-flow regime. The stress at which the data deviated from this linear behavior was identified as the yield stress. Under the further, reasonable assumption that the linearized slip behavior persists above the yield stress, where flow commences, the angular velocity could be corrected for wall slip. Following standard rheological procedures for yield-stress fluids in a wide-gap concentric-cylinder viscometer, the dependence of the effective viscosity on shear rate could then be determined.

It is clear from the above discussion that extreme care must be exercised in the characterization and rheological evaluation of concentrated emulsions. Few, if any, commercial viscometers are designed to give reliable results for non-Newtonian fluids. Not only are modifications of the hardware often called for, but also the software of automated instruments is generally incapable of dealing with yield stress fluids, end effects, and wall slip. For example, to correct for end effects, it will not do to use a calibration or “instrument factor” for any but Newtonian fluids. Unfortunately, there are no shortcuts in this field!

3. Experimental Results

For reasons indicated earlier, accurate physical characterization and rheological evaluation of *foams* is extremely difficult. Indeed, although there is much published material on foams that is qualitatively consistent with what one would expect (and much that is not), we are not aware of any such studies that can stand close quantitative scrutiny. Therefore, we shall restrict ourselves to what has been learned from *highly concentrated emulsions*, whose rheology is, in any case, expected to be identical to that of foams in most respects. However, even in the emulsion area, the number of carefully executed studies is severely limited. Admittedly not without some prejudice, we shall concentrate on the systematic experimental work

by two groups that were active at different times at the Corporate Research Laboratory of Exxon Research and Engineering Co. [i.e., Princen and Kiss (69,95,128) and Mason et al. (66,127,137,138)]. Both groups used oil-in-water emulsions, but whereas Princen and Kiss used “typical” polydisperse emulsions with a mean radius of 5–10 μm , Mason and co-workers opted for submicron, monodisperse “Bibette emulsions.” The term “monodisperse” is relative; there remained some polydispersity in drop radius of about 10% and the emulsions were structurally disordered on a macroscopic scale. The mean drop size in Princen’s emulsions was at least an order of magnitude greater, which may account for some of the differences in the results. Princen and Kiss used their customized concentric-cylinder viscometer exclusively, either in steady shear with wall slip (to give the yield stress and viscosity) or as a constant-strain device without wall slip (to give the static shear modulus). Mason and co-workers were more eclectic in choosing their techniques (concentric-cylinder and cone-and-plate geometries in steady-shear and dynamic modes, as well as optical techniques).

Shear Modulus. Princen and Kiss (95) used a series of well-characterized, polydisperse oil-in-water emulsions of essentially identical Sauter mean drop size, R_{32} , and drop size distribution but varying dispersed-phase volume fraction, ϕ . Their modified Couette viscometer was purposely equipped with ground and grooved glass cylinders to eliminate wall slip,* and the emulsion was strained by turning the outer cylinder over a small, precisely measured angle in the linear elastic regime. From the measured stress at the inner cylinder, the static shear modulus, G , can be obtained in a straightforward manner. The results in Fig. 30 show that over the range considered ($0.75 < \phi < 0.98$), $GR_{32}/\sigma\phi^{1/3}$ varies linearly with ϕ , and we can write

$$G = 1.77 \frac{\sigma}{R_{32}} \phi^{1/3} (\phi - 0.712) = 1.77 \frac{\sigma}{R_{32}} \phi^{1/3} (\phi - \phi_0) \quad (85)$$

where $\phi_0 = 0.712$ can be identified as the “rigidity-loss transition” for the particular size distribution in these emulsions. This is surprisingly close to that for ideal close packing of monodisperse spheres ($\phi_0 = 0.7405$) but clearly in excess of that for random close packing of monodisperse spheres ($\phi_0 \approx 0.64$). The exact value of ϕ_0 is expected to depend somewhat on the details of the drop size distribution.

*This fact was unfortunately misrepresented in Ref. 66.

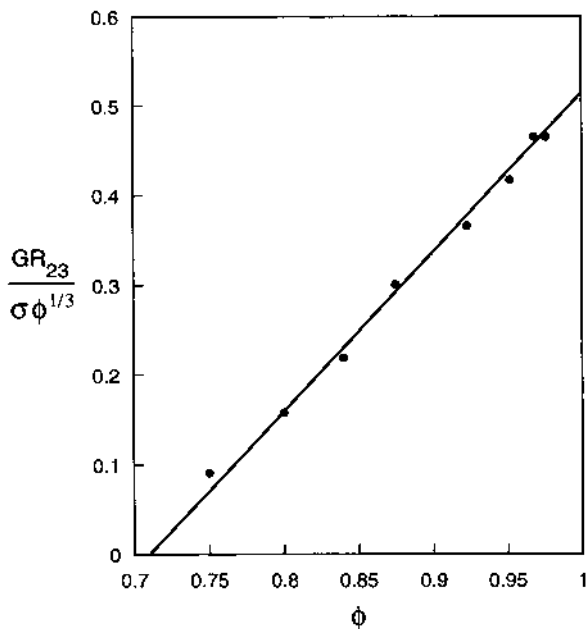


Figure 30 Scaled static shear modulus, $GR_{32}/\sigma\phi^{1/3}$, versus ϕ for typical polydisperse emulsions. Solid points are experimental data; the solid line is drawn according to Eq. (85). (From Ref. 95, with permission from Academic Press.)

In the “dry-foam” limit ($\phi = 1$), Eq. (85) reduces to

$$G_{\phi=1} = 0.509 \frac{\sigma}{R_{32}} \quad (86)$$

As indicated earlier, this is in close agreement with various theoretical estimates.

It may be argued which mean drop size is most appropriate for describing the rheology of polydisperse systems. The selection of R_{32} is based on limited evidence (69) and some other mean might ultimately turn out to be preferable. (See, however, the postscript in Sect. IX.)

A simple extension of the perfectly ordered 2D model to a 3D model would have suggested that $G = 0$ for $\phi < \phi_0 = 0.74$, with a sudden jump to an almost constant, finite value of $G \propto \sigma\phi^{1/3}/R$ for $\phi > 0.74$ [cf. Eq. (72)]. As discussed earlier, it is now generally agreed that the absence of the discontinuity and the essentially linear dependence on ϕ above ϕ_0 , found experimentally, is due to structural disorder.

Mason et al. (66) used small-amplitude, dynamic, oscillatory methods (both in cone-and-plate and concentric-cylinder geometries) to probe the viscoelastic properties [i.e., the storage (elastic) and loss (viscous) moduli, G' and G'' , respectively] as a function of frequency, ω . No mention is made of wall-induced instability or end and edge effects. Having roughened the viscometer walls, the authors claim that wall slip was nonexistent. At low frequencies, G' reached a plateau that may be equated with the static shear modulus, G . Plots of the scaled modulus, GR/σ , versus the effective volume fraction, ϕ_e , for four emulsions of different drop size essentially overlapped, as expected. The drops were so small that significant corrections had to be made to the nominal volume fractions to account for the finite (estimated) film thickness, h , according to Eq. (1). In the dry-foam limit ($\phi_e = 1$), the scaled modulus approached a value of about 0.6, which is reasonably close to Princen's value of 0.51, but even for $\phi < 1$, the data of the two groups are remarkably similar. For example, for $\phi_e = 0.85$ and 0.75, Mason et al. show values for GR/σ of about 0.30 and 0.10, respectively, whereas Eq. (85) yields 0.23 and 0.061, respectively, for GR_{32}/σ . The differences are roughly commensurate with the scatter in Mason's data. At any rate, the difference in polydispersity in the two sets of emulsions, or some experimental factor in either study (end/edge effects?), may well explain these minor systematic discrepancies.

Overall, Mason et al. found that their data can be described by

$$G \approx 1.7 \frac{\sigma}{R} \phi (\phi - 0.64) = 1.7 \frac{\sigma}{R} \phi (\phi - \phi_0) \quad (87)$$

where $\phi_0 \approx 0.64$ is the value for random close packing of monodisperse spheres. Except for the difference in ϕ_0 , this is very similar to Eq. (85).

Because of the limited sensitivity of their viscometer and the increased potential effect of a gradient in ϕ due to gravity, Princen et al. did not explore the range of $\phi < 0.75$ and reasonably assumed that the linear behavior in Fig. 30 continues down to $G = 0$ at $\phi = \phi_0 \approx 0.71$. It is unclear what significance, if any, must be attached to the apparent difference in ϕ_0 found in the two studies. Had it been possible to properly explore that regime, Princen's data might have shown some curvature for $\phi < 0.75$ and a similar smooth decline in G toward zero at $\phi_0 \approx 0.64$. More likely, the difference is real and simply attributable to the differences in polydispersity and associated random packing density. Another factor of potential significance is the large difference in mean drop size. The drops in Mason's emulsions were submicron and, therefore, Brownian, which may contribute an entropic (thermal) component to the modulus, as well as affect the packing density.

Direct support for Eq. (85) has been reported by, among others, Taylor (139), Jager-Lézer et al. (140), Pal (141), and Coughlin et al. (142). Indirect support has been obtained by Langenfeld et al. (143), who compared the specific surface areas of a number of water-in-oil emulsions as determined by two independent methods: (a) from the measured shear modulus—which yields R_{32} from Eq. (85), and thus the specific surface area from $3\phi/R_{32}$ —and (b) from small-angle neutron scattering. The agreement was very satisfactory.

Yield Stress and Shear Viscosity. Using their modified concentric-cylinder viscometer—equipped in this case with polished glass inner and outer cylinders to allow unimpeded wall slip and a mercury pool to eliminate the lower end effect—Princen and Kiss (128) determined the yield stresses, τ_0 , and effective viscosities, $\mu_e(\dot{\gamma})$, of a series of well-characterized, polydisperse oil-in-water emulsions. They empirically established that in all cases, the all-slip/no-flow regime at slow steady shear was characterized by a linear dependence of τ_1 on ω/τ_1 (where τ_1 is the stress on the inner cylinder and ω is the angular velocity of the outer cylinder). The stress at which the data deviated from this linearity was identified as the yield stress. At higher angular velocity, it was reasonably assumed that the same linear slip behavior continued to operate, which permitted a straightforward slip correction. Using conventional rheometric analyses, the stress and viscosity were finally obtained as a function of shear rate.

The yield stress data could be expressed in the form

$$\tau_0 = \frac{\sigma}{R_{32}} \phi^{1/3} Y(\phi) \quad (88)$$

The experimental values of $Y(\phi)$ are shown in Fig. 31 and can be empirically fit to

$$Y(\phi) = -0.080 - 0.114 \log(1 - \phi) \quad (89)$$

Equation (89) should be used only within the range considered (i.e., $0.83 < \phi < 0.98$).

Data by Pal (141) support Eqs. (88) and (89), once the volume fraction is corrected for a finite film thickness of 90 nm. Earlier data by Princen (69) are consistently somewhat higher, probably because of significant end effects in the original, unmodified viscometer.

Figures 32 and 33 show the fully corrected plots of shear stress versus shear rate. Taking account of small differences in the measured interfacial tensions, all data could be accurately represented by

$$\tau = \tau_0 + 32.0(\phi - 0.73) \frac{\sigma}{R_{32}} \text{Ca}^{1/2} = \tau_0 + 32.0(\phi - 0.73) \left(\frac{\sigma \mu \dot{\gamma}}{R_{32}} \right)^{1/2} \quad (90)$$

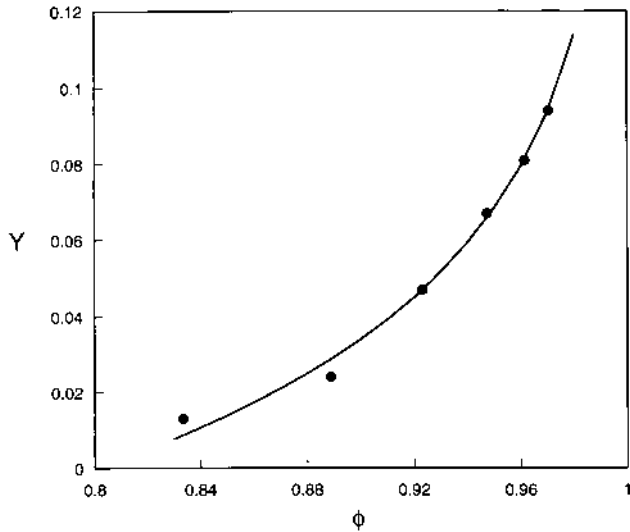


Figure 31 Yield stress function $Y(\phi) = \tau_0 R_{32} / \sigma \phi^{1/3}$ versus ϕ for typical polydisperse emulsions. Solid points are experimental data; the curve is drawn according to Eq. (89). (From Ref. 128, with permission from Academic Press.)

where μ is the viscosity of the continuous phase and Ca is the capillary number

$$Ca \equiv \frac{\mu R_{32} \dot{\gamma}}{\sigma} \quad (91)$$

which did not exceed a value of 10^{-4} in any of the experiments.

For the effective viscosity, this leads to

$$\mu_e \equiv \frac{\tau}{\dot{\gamma}} = \frac{\tau_0}{\dot{\gamma}} + 32.0(\phi - 0.73)\mu Ca^{-1/2} = \frac{\tau_0}{\dot{\gamma}} + 32.0(\phi - 0.73) \left(\frac{\sigma \mu}{R_{32} \dot{\gamma}} \right)^{1/2} \quad (92)$$

where τ_0 is given by Eqs. (88) and (89). Again, Eq. (92) should not be used outside the range considered. It is interesting to point out that, as with so many other properties, the viscous term tends to zero at $\phi = \phi_0 \approx 0.73$.

It is encouraging that Eqs. (90) and (92) have the same form as Eqs. (84) and (83), respectively, except for the exponent of the capillary number. Several reasons for this difference have been advanced (128), including the neglect of T1 rearrangements and disjoining pressure effects

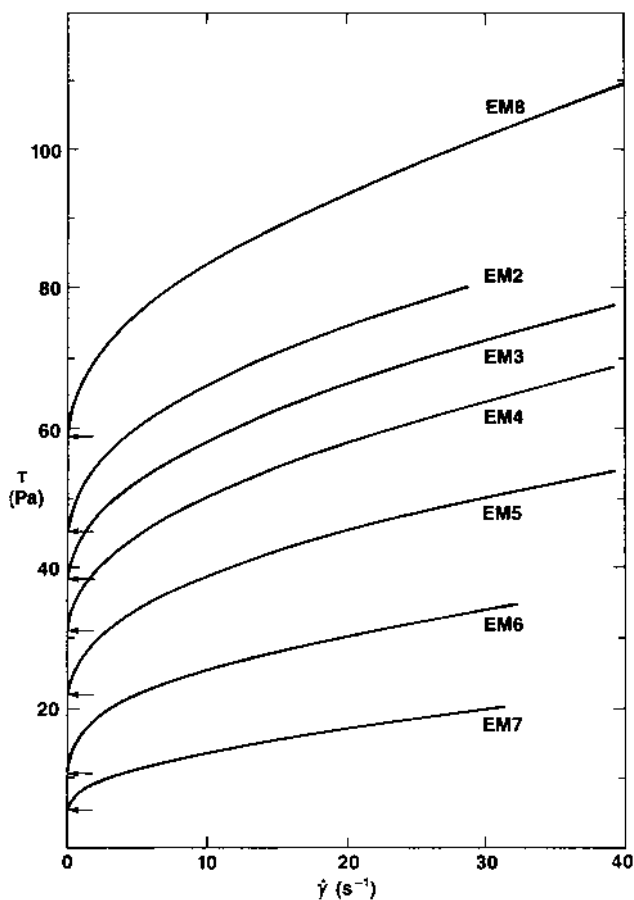


Figure 32 Fully corrected plots of shear stress vs shear rate for series of typical polydisperse emulsions. Arrows indicate the yield stress, τ_0 . Emulsions EM2–7 have the same drop size ($R_{32} = 10.1 \pm 0.1 \mu\text{m}$) but different volume fractions ($\phi = 0.9706, 0.9615, 0.9474, 0.9231, 0.8889, \text{ and } 0.8333$, respectively). For EM8, $R_{32} = 5.73 \mu\text{m}$ and $\phi = 0.9474$. (From Ref. 128, with permission from Academic Press.)

in the original model. At any rate, considering that this is the first and only systematic study of its kind, it is not yet clear how generally applicable Eqs. (90) and (92) will turn out to be. Although some other qualitative experimental support exists (144–146), there is a great need for additional, careful studies to explore this area further. It may be significant in this context that Liu et al. (147), using diffusing-wave spectroscopy [a novel light-scattering

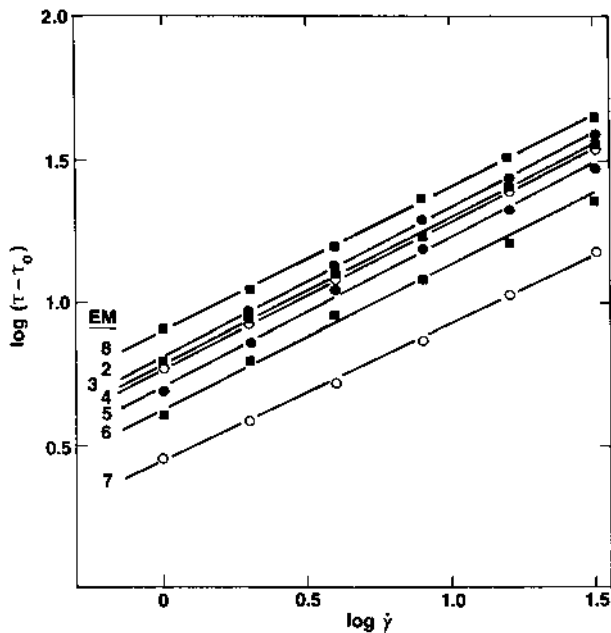


Figure 33 Plots of $\log(\tau - \tau_0)$ versus shear rate for same emulsions as in Fig. 32. In all cases, the slope is very close to 1/2. (From Ref. 128, with permission from Academic Press.)

technique (148)] have found a contribution to the dynamic shear modulus that is proportional to $\omega^{1/2}$ (or $Ca^{1/2}$) and increases roughly linearly with volume fraction. Mason et al. (138) investigated the steady-shear behavior of some monodisperse emulsions in the low- ϕ range. They found that the viscous stress contribution varies as $\dot{\gamma}^{2/3}$ for $\phi=0.58$ and as $\dot{\gamma}^{1/2}$ for $\phi=0.63$. For $\phi>0.65$, no clear power-law behavior was observed. These authors claim that meaningful steady-shear measurements cannot be made on emulsions of higher volume fractions because of the occurrence of “inhomogeneous” strain rates. They presumably refer to the fact that, for example, in a concentric-cylinder viscometer, only part of the emulsion (i.e., within a given radius) is being sheared, whereas the outer part is not. However, this situation, common to all yield-stress fluids, has been well recognized and analyzed in the rheology literature and can be handled in a quite straightforward manner (128).

Mason et al. (138) determined the yield stresses and yield strains of a series of monodisperse emulsions, using either a cone-and-plate or double-wall Couette geometry in oscillatory mode. Wall-induced coalescence and

wall slip were claimed to be absent, but no mention is made of attempts to reduce end or edge effects. Estimated film thicknesses were used to arrive at the effective volume fractions. Their data for the yield stress could be fit to

$$\tau_0 = 0.51 \frac{\sigma}{R} (\phi - 0.62)^2 \quad (93)$$

and, for high ϕ , are claimed to be “about an order of magnitude greater than those measured for polydisperse emulsions,” as given by Eqs. (88) and (89). This appears to be a misrepresentation. It is readily demonstrated that the two sets of data are, in fact, quite comparable. For example, for $\phi = 0.85$ and $\phi = 0.95$, the values of the scaled yield stress, $\tau_0 R / \sigma$, are 0.027 and 0.055 according to Eq. (93), and 0.013 and 0.067 according to Eq. (88). In fact, as $\phi \rightarrow 1$, Mason et al. predicted that the scaled yield stress reaches a limiting value of 0.074, whereas extrapolation of Princen and Kiss’s data in Fig. 31 suggest a value that is well in excess of 0.1 and perhaps as high as 0.15 [the yield stress must remain finite in this limit and use of Eq. (89) is unwarranted in this regime]. Mason et al. further assert that, at high ϕ , the yield *strain* of their monodisperse emulsions is also over an order of magnitude greater than that of the polydisperse emulsions of Princen and Kiss. This conclusion appears to be equally unfounded. In fact, the rheological behavior of concentrated emulsions appears to be remarkably unaffected by polydispersity.

We are not aware of any other systematic experimental studies that meet the criteria set out above and there remains a great need for additional careful work in this fascinating area.

VIII. ADDITIONAL AREAS OF INTEREST

Although this review covers many aspects of highly concentrated emulsions and foams, it does not deal with a number of issues that are of considerable interest. Foremost is the issue of emulsion and foam stability. A great deal of information can be gleaned from recent books on foams and conventional emulsions (17–22). Stability of highly concentrated emulsions is a rather more delicate and specialized problem. The reader may consult a number of recent publications that specifically deal with this subject (149–154).

One of the main driving forces for the recent upsurge in interest in foams—and one that has been responsible for the entrance of so many physicists into the field—has been their presumed usefulness in modeling grain growth in metals. The coarsening of foam through gas diffusion (a special form of Ostwald ripening) is thought to follow similar laws.

This, among other things, inspired the first computer simulations of foams by Weaire and co-workers and remains an active area of research (33).

As indicated, highly concentrated emulsions provide attractive starting materials for the synthesis of novel materials (e.g., polymers and membranes). Ruckenstein has been particularly active in this area. In addition to the references cited earlier (6,12–16), the reader may wish to consult a recent comprehensive review of this area (155).

IX. POSTSCRIPT

Except for some minor editing, this review is identical to [Chapter 11 in Ref. 156](#). Since then, further progress has been made. Two noteworthy examples are the following.

In a recent tour de force, Kraynik, Reinelt, and van Swol (personal communication, 2002) have carried out numerous computer simulations on the shear modulus of truly disordered, 3D, dry-foam systems, in which the degree of polydispersity was varied by over two orders of magnitude. Their work comes to two important conclusions: (a) The surface volume or Sauter mean radius R_{32} leads to a true numerical constant in Princen's Eq. (86). The choice of other means, such as the simple average radius, appears to lead to a numerical factor that varies significantly with the degree of polydispersity. Moreover, Kraynik et al. have developed strong theoretical grounds for this conclusion. Although Princen's initial choice of this particular mean was based mostly on intuition, and on very limited experimental evidence, that choice now appears to have been justified. (b) With R_{32} as the mean, Kraynik et al. found that the appropriate value of the numerical factor in Eq. (86) is 0.511, in remarkable agreement with Princen's experimental value of 0.509! Because the error in both values is estimated to be a few percent, it can be stated with considerable confidence that the constant equals 0.51 ± 0.01 . Unfortunately, the case of "wet" foams ($\phi < 1$) appears to be computationally too intensive to be similarly simulated in the foreseeable future.

In a recent *experimental* study, Ponton et al. (157) measured the shear moduli of a series of laboratory-prepared, polydisperse water-in-oil emulsions of varying volume fraction. R_{32} was used as the characteristic mean radius. The results were in very close agreement with Eq. (85) in that the value of ϕ_0 was found to be 0.714, instead of Princen's reported value of 0.712. Again, we see remarkable agreement! Unfortunately, the authors failed to measure the interfacial tension in these emulsions, so that the value of the numerical factor in Eq. (85) could not be ascertained.

ACKNOWLEDGMENTS

Special thanks are due to A. M. Kraynik for the many stimulating discussions we have had over the years, for keeping me informed on recent developments, and for kindly providing some of the unpublished results and illustrations. I have also benefited from illuminating discussions with P.-G. de Gennes and D. Weaire. My interest in these fascinating systems goes back to my years at Unilever Research, where E. D. Goddard and M. P. Aronson provided invaluable and much appreciated support and collaboration.

LIST OF SYMBOLS

Latin Symbols

a	Side of hexagon circumscribing compressed 2D drops in perfect order
a_o	Side of hexagon circumscribing uncompressed (circular) 2D drops in perfect order
a_c	Capillary length = $[\sigma/(\Delta\rho g)]^{1/2}$
c_i	Mean curvature of surface between Plateau border and drop i
C_{ij}	Mean curvature of film between drops i and j
C_t	Mean curvature of free surface of continuous phase at dispersion-atmosphere boundary
Ca	Macroscopic capillary number = $\mu a \dot{\gamma} / \sigma$ or $\mu R_{32} \dot{\gamma} / \sigma$
Ca*	Film-level capillary number = $\mu U / \sigma$
e	Number of edges of a polyhedral drop
f	Number of faces of a polyhedral drop
$f(\phi)$	Fraction of surface of confining wall “in contact” with dispersed drops
F	Stress per unit cell
F_{\max}	Maximum or yield stress per unit cell
g	Acceleration due to gravity
G	Static shear modulus
G'	Storage modulus
G''	Loss modulus
h	Film thickness
h_{eq}	Equilibrium film thickness
h_{∞}	Half the film thickness pulled out of Plateau border
H	Sample height
H_{cr}	Critical sample height for separation of continuous phase
K	Compression modulus
p_b	Pressure in Plateau border

p_c	Capillary pressure
p_i	Pressure in drop i
p_v^c	Vapor pressure of continuous phase in dispersion
$(p_v^c)_0$	Vapor pressure of bulk continuous phase
p_v^d	Vapor pressure of dispersed phase in dispersion
$(p_v^d)_0$	Vapor pressure of bulk dispersed phase
P	External pressure
r	Radius of Plateau border surfaces in 2D close-packed drops
R	Radius of spherical or circular drop
R_{av}	Average drop radius
R_{32}	Surface volume or Sauter mean drop radius
\mathfrak{R}	Gas constant
S	Surface area of compressed drops
S_0	Surface area of uncompressed (spherical or circular) drops
S_f	Surface area contained in films
T	Absolute temperature
U	Film velocity
v	Number of vertices of a polyhedral drop
V	Dispersion volume
V_1	Volume of the dispersed phase
V_2	Volume of the continuous phase in the dispersion
\bar{V}_1, \bar{V}_2	Partial molar volume of phase 1 and 2, respectively
$Y(\phi)$	Yield-stress function
z	Vertical height in dispersion column

Greek Symbols

γ	Strain
$\dot{\gamma}$	Rate of strain
$\Delta\rho$	Density difference
θ	Contact angle at film–Plateau border junction
μ	Viscosity of continuous phase
μ_d	Viscosity of dispersed phase
μ_e	Effective viscosity of dispersion
Π	Osmotic pressure
Π_d	Disjoining pressure
ρ	Density
σ	Surface or interfacial tension
τ	Stress
τ_0	Yield stress
τ_s	Stress due to dissipative processes
ϕ	Volume fraction of dispersed phase in emulsion or foam

ϕ_0	Volume fraction of close-packed spherical drops
ϕ_e	Effective volume fraction, after correction for finite film thickness
ψ	Angle between films and shear direction
ω	Frequency or angular velocity

REFERENCES

1. F. J. Almgren and J. E. Taylor, *Sci. Am.* 235, 82 (1976).
2. C. S. Smith, *Metall. Rev.* 9, 1 (1964).
3. E. B. Matzke, *Am. J. Bot.* 33, 58, 130 (1946).
4. K. J. Lissant, *J. Colloid Interf. Sci.* 22, 462 (1966).
5. K. J. Lissant, *J. Soc. Cosmet. Chem.* 21, 141 (1970).
6. K. J. Lissant and K. G. Mayhan, *J. Colloid Interf. Sci.* 42, 201 (1973).
7. A. Beerbower, J. Nixon, and T. J. Wallace, *J. Aircraft* 5, 367 (1968).
8. A. Beerbower, J. Nixon, W. Philippoff, and T. J. Wallace, *SAE Trans. Sec. 2* 76, 1446 (1968).
9. J. Nixon, A. Beerbower, and T. J. Wallace, *Mech. Eng.* 90, 26 (1968).
10. J. Nixon, and A. Beerbower, *Preprints, Div. Petrol. Chem. Am. Chem. Soc.* 14, 49 (1969).
11. K. J. Lissant, U.S. patent No. 3,892,881.
12. K. J. Lissant, B. W. Peace, S. H. Wu, and K. G. Mayhan, *J. Colloid Interf. Sci.* 47, 416 (1974).
13. J. M. Williams, *Langmuir* 4, 44 (1988).
14. E. Ruckenstein and K. Kim, *J. Appl. Polym. Sci.* 36, 907 (1988).
15. E. Ruckenstein, *Colloid Polym. Sci.* 267, 792 (1989).
16. E. Ruckenstein and J. S. Park, *Chem. Mater.* 1, 343 (1989).
17. J. Sjöblom (ed.), *Emulsions and Emulsion Stability*, Surfactant Science Series Vol. 61, Marcel Dekker, New York; 1996.
18. R. K. Prud'homme and S. A. Khan (eds.), *Foams: Theory, Measurements, and Applications*, Surfactant Science Series Vol. 57, Marcel Dekker, New York, 1996.
19. L. L. Schramm (ed.), *Foams: Fundamentals and Applications in the Petroleum Industry*, Advances in Chemistry Series No. 242, American Chemical Society, Washington, DC, 1994.
20. D. Exerowa and P. M. Kruglyakov (eds.), *Foam and Foam Films: Theory, Experiment, Application*. Studies in Interface Science Vol. 5, Elsevier, Amsterdam, 1998.
21. D. Weaire and S. Hutzler, *The Physics of Foams*, Clarendon Press, Oxford, 1999.
22. J. F. Sadoc and N. Rivier (eds.) *Foams and Emulsions*, Kluwer Academic, Dordrecht, 1999.
23. H. M. Princen, M. P. Aronson, and J. C. Moser, *J. Colloid Interf. Sci.* 75, 246, (1980).
24. H. M. Princen and A. D. Kiss, *Langmuir* 3, 36 (1987).

25. D. M. A. Buzza and M. E. Cates, *Langmuir* 9, 2264 (1993).
26. M. P. Aronson and H. M. Princen, *Nature* 286, 370 (1980).
27. M. P. Aronson and H. M. Princen, *Colloids Surfaces* 4, 173 (1982).
28. H. M. Princen, *Colloids Surfaces* 9, 47 (1984).
29. H. M. Princen, *Langmuir* 4, 164 (1988).
30. A. V. Neimark and M. Vignes-Adler, *Phys. Rev. E* 51, 788 (1995).
31. F. Bolton and D. Weaire, *Phil. Mag.* B 63, 795 (1991).
32. V. V. Krotov and A. I. Rusanov, *Mendeleev Commun.* 177 (1998).
33. J. A. Glazier and D. Weaire, *J. Phys.: Condens. Matter* 4, 1867 (1992).
34. J. A. Glazier and J. Stavans, *Phys. Rev. A* 40, 7398 (1989).
35. J. A. Glazier, S. P. Gross, and J. Stavans, *Phys. Rev. A* 36, 306 (1987).
36. J. Stavans and J. A. Glazier, *Phys. Rev. Lett.* 62, 1318 (1989).
37. J. Stavans, *Phys. Rev. A* 42, 5049 (1990).
38. J. Lucassen, S. Akamatsu, and F. Rondelez, *J. Colloid Interf. Sci.* 144, 434 (1991).
39. H. M. Princen, *J. Colloid Interf. Sci.* 71, 55 (1979).
40. H. M. Princen, *Langmuir* 2, 519 (1986).
41. P. M. Kruglyakov, D. R. Exerowa, and K. I. Khrystov, *Langmuir* 7; 1846 (1991).
42. K. Khrystov, P. Kruglyakov, and D. Exerowa, *Colloid Polym. Sci.* 257, 506 (1979).
43. K. Khrystov, D. Exerowa, and P. M. Kruglyakov, *Colloid J. (Engl. Transl.)* 50, 765 (1988).
44. D. Weaire and J. P. Kermode, *Phil. Mag. B* 50, 379 (1984).
45. S. A. Khan and R. C. Armstrong, *J. Non-Newtonian Fluid Mech.* 25, 61 (1987).
46. A. M. Kraynik, D. A. Reinelt, and H. M. Princen, *J. Rheol.* 35, 1235 (1991).
47. F. Bolton and D. Weaire, *Phil. Mag. B* 65, 473 (1992).
48. S. Hutzler and D. Weaire, *J. Phys: Condens. Matter.* 7, L657 (1995).
49. K. A. Brakke, *Exp. Math.* 1, 141 (1992).
50. A. M. Kraynik and D. A. Reinelt (private communication; to be published).
51. M.-D. Lacasse, G. S. Grest, and D. Levine, *Phys. Rev. E* 54, 5436 (1996).
52. W. Thomson (Lord Kelvin), *Phil. Mag.* 24, 503 (1887).
53. W. Thomson (Lord Kelvin), *Acta Math.* 11, 121 (1887–1888).
54. W. Thomson (Lord Kelvin), *Mathematical and Physical Papers*, Cambridge University Press, London, 1911, Vol. V, p 297.
55. H. M. Princen and P. Levinson. *J. Colloid Interf. Sci.* 120, 172 (1987).
56. D. A. Reinelt and A. M. Kraynik, *J. Colloid Interf. Sci.* 159, 460 (1993).
57. D. Weaire and R. Phelan, *Phil. Mag. Lett.* 69, 107 (1994).
58. S. Ross and H. F. Prest, *Colloids Surfaces* 21, 179 (1986).
59. D. S. Bohlen, H. T. Davis and L. E. Scriven, *Langmuir* 8, 892 (1992).
60. H. W. Schwartz, *Rec. Trav. Chim.* 84, 771 (1964).
61. H. Aref, and T. Herdtle, in *Topological Fluid Mechanics*, (H. Moffat and A. Tsinober, eds.), Cambridge University Press, New York, 1990, p. 745.
62. T. Herdtle, Ph.D. thesis, University of California, San Diego, 1991.
63. C. Monnereau and M. Vignes-Adler, *Phys. Rev. Lett.* 80, 5228 (1998).

64. S. D. Pacetti, Masters thesis, University of Houston, 1985.
65. J. Bibette, *J. Colloid Interf. Sci.* 147, 474 (1991).
66. T. G. Mason, M.-D. Lacasse, G. S. Grest, D. Levine, J. Bibette, and D. A. Weitz, *Phys. Rev. E* 56, 3150 (1997).
67. H. M. Princen, *J. Colloid Interf. Sci.* 134, 188 (1990).
68. A. M. Kraynik, M. K. Neilsen, D. A. Reinelt, and W. E. Warren, in *Foams and Emulsions*. (J. F. Sadoc and N. Rivier, eds.), Kluwer Academic, Dordrecht, 1999, pp. 259–286.
69. H. M. Princen, *J. Colloid Interf. Sci.* 105, 150 (1985).
70. B. V. Derjaguin, *Kolloid Z.* 64, 1 (1933).
71. S. Ross, *Ind. Eng. Chem.* 61, 48 (1969).
72. I. D. Morrison and S. Ross, *J. Colloid Interf. Sci.* 95, 97 (1983).
73. H. B. Hollinger, *J. Colloid Interf. Sci.* 143, 278 (1991).
74. T. L. Crowley, *Langmuir* 7, 430 (1991).
75. T. L. Crowley and D. G. Hall, *Langmuir* 9, 101 (1993).
76. M. Blackman, *Trans. Faraday Soc.* 44, 205 (1948).
77. J. O. Sibree, *Trans. Faraday Soc.* 30, 325 (1934).
78. A. David and S. S. Marsden, in *44th Annual Meeting, Society of Petroleum Engineers*, 1969, paper 2544.
79. V. Sanghani and C. U. Ikoku, *Trans. ASME* 105, 362 (1983).
80. B. J. Mitchell, *Oil Gas J.* 96 (1971).
81. S. H. Raza and S. S. Marsden, *Soc. Petrol. Eng. J.* 7, 359 (1967).
82. R. J. Mannheimer, *J. Colloid Interf. Sci.* 40, 370 (1972).
83. J. P. Heller and M. S. Kuntamukkula, *Ind. Eng. Chem.* 26, 318 (1987).
84. J. H. Aubert, A. M. Kraynik and P. B. Rand, *Sci. Am.* 254, 58 (1986).
85. A. M. Kraynik, *Annu. Rev. Fluid Mech.* 20, 325 (1988).
86. D. Weaire and M. A. Fortes, *Adv. Phys.* 43, 685 (1994).
87. H. M. Princen, *J. Colloid Interf. Sci.* 91, 160 (1983).
88. R. K. Prud'homme, in *Annual Meeting of the Society of Rheology*, 1981.
89. S. A. Khan, Ph.D. thesis, Massachusetts Institute of Technology, 1985.
90. S. A. Khan and R. C. Armstrong, *J. Non-Newtonian Fluid Mech.* 22, 1 (1986).
91. A. M. Kraynik and M. G. Hansen, *J. Rheol.* 30, 409 (1986).
92. S. Hutzler, D. Weaire, and F. Bolton, *Phil. Mag.* B 71, 277 (1995).
93. B. Derjaguin, *Kolloid Z.* 64, 1 (1933).
94. D. Stamenović and T. A. Wilson, *J. Appl. Mech.* 51, 229 (1984).
95. H. M. Princen and A. D. Kiss, *J. Colloid Interf. Sci.* 112, 427 (1986).
96. D. Stamenović, *J. Colloid Interf. Sci.* 145, 255 (1991).
97. B. Budiansky and E. Kimmel, *J. Appl. Mech.* 58, 289 (1991).
98. D. A. Reinelt, *J. Rheol.* 37, 1117 (1993).
99. A. M. Kraynik and D. A. Reinelt, *Forma* 11, 255 (1996).
100. D. A. Reinelt and A. M. Kraynik, *J. Fluid Mech.* 311, 327 (1996).
101. A. M. Kraynik and D. A. Reinelt, *J. Colloid Interf. Sci.* 181, 511 (1996).
102. A. M. Kraynik and D. A. Reinelt, *Proceedings of the XIIIth International Congress on Rheology*, 1996, p. 625.
103. A. M. Kraynik and D. A. Reinelt, *Chem. Eng. Commun.* 148/150, 409 (1996).

104. D. M. A. Buzza and M. E. Cates, *Langmuir* 10, 4502 (1994).
105. D. C. Morse and T. A. Witten, *Europhys. Lett.* 22, 549 (1993).
106. M.-D. Lacasse, G. S. Grest, D. Levine, T. G. Mason, and D. A. Weitz, *Phys. Rev. Lett.* 76, 3448 (1996).
107. D. M. A. Buzza, C.-Y. D. Lu, and M. E. Cates, *J. Phys. II (France)* 5, 37 (1995).
108. A. M. Kraynik and M. G. Hansen, *J. Rheol.* 31, 175 (1987).
109. X. Li, H. Zhu and C. Pozrikidis, *J. Fluid. Mech.* 286, 379 (1995).
110. L. W. Schwartz and H. M. Princen, *J. Colloid Interf. Sci.* 118, 201 (1987).
111. K. J. Mysels, K. Shinoda, and S. Frankel, *Soap Films: Studies of Their Thinning and a Bibliography*, Pergamon Press, New York, 1959.
112. L. Landau and B. Levich, *Acta Physicochim. URSS* 17, 42 (1942).
113. F. P. Bretherton, *J. Fluid Mech.* 10, 166 (1961).
114. L. W. Schwartz, H. M. Princen, and A. D. Kiss, *J. Fluid Mech.* 172, 259 (1986).
115. K. J. Mysels and M. C. Cox, *J. Colloid Interf. Sci.* 17, 136 (1962).
116. J. Lyklema, P. C. Scholten, and K. J. Mysels, *J. Phys. Chem.* 69, 116 (1965).
117. G. F. Teletzke, H. T. Davis, and L. E. Scriven, *Rev. Phys. Appl.* 23, 989 (1988).
118. J. Lucassen, in *Anionic Surfactants: Physical Chemistry of Surfactant Action*. (E. H. Lucassen-Reijnders, ed), Surfactant Science Series Vol. 11, Marcel Dekker, New York, 1981, p. 217.
119. D. A. Reinelt and A. M. Kraynik, *J. Colloid Interf. Sci.* 132, 491 (1989).
120. D. A. Reinelt and A. M. Kraynik, *J. Fluid Mech.* 215, 431 (1990).
121. D. A. Edwards, H. Brenner, and D. T. Wasan, *J. Colloid Interf. Sci.* 130, 266 (1989).
122. D. A. Edwards and D. T. Wasan, *J. Colloid Interf. Sci.* 139, 479 (1990).
123. D. A. Edwards and D. T. Wasan, in *Foams: Theory, Measurements, and Applications*. (R. K. Prud'homme and S. A. Khan, eds), Surfactant Science Series Vol. 57, Marcel Dekker, New York, 1996, p189.
124. T. Okuzuno and K. Kawasaki, *J. Rheol.* 37, 571 (1993).
125. T. Okuzono and K. Kawasaki, *Phys. Rev. E* 51, 1246 (1995).
126. Y. Jiang, P. J. Swart, A. Saxena, M. Asipauskas, and J. A. Glazier, *Phys. Rev. E* 59, 5819 (1999).
127. T. G. Mason, J. Bibette, and D. A. Weitz, *Phys. Rev. Lett.* 75, 2051 (1995).
128. H. M. Princen and A. D. Kiss, *J. Colloid Interf. Sci.* 128, 176 (1989).
129. H. M. Princen, I. Y. Z. Zia, and S. G. Mason, *J. Colloid Interf. Sci.* 23, 99 (1967).
130. J. L. Cayias, R. S. Schechter, and W. H. Wade. in *Adsorption at Interfaces* (K. L. Mittal, ed), ACS Symposium Series No. 8, American Chemical Society, Washington, DC, 1975, p. 234.
131. R. W. Whorlow, *Rheological Techniques*, Ellis Horwood, Chichester, 1980.
132. H. M. Princen, *J. Rheol.* 30, 271 (1986).
133. P. V. Liddell and D. V. Boger, *J. Non-Newtonian Fluids* 63, 235 (1996).
134. A. S. Yoshimura and R. K. Prud'homme, *Soc. Petrol Eng.* 735 (1988).
135. A. S. Yoshimura and R. K. Prud'homme, *J. Rheol.* 32, 53 (1988).
136. P. Brunn, M. Müller and S. Bschorer, *Rheol. Acta* 35, 242 (1996).
137. T. G. Mason and D. A. Weitz, *Phys. Rev. Lett.* 74, 1250 (1995).

138. T. G. Mason, J. Bibette, and D. A. Weitz, *J. Colloid Interf. Sci.* 179, 439 (1996).
139. P. Taylor, *Colloid Polym. Sci.* 274, 1061 (1996).
140. N. Jager-Lézer, J.-F. Tranchant, V. Alard, C. Vu, P. C. Tchoreloff, and J.-L. Grossiord, *Rheol. Acta* 37, 129 (1998).
141. R. Pal, *Colloid Polym. Sci.* 277, 583 (1999).
142. M. F. Coughlin, E. P. Ingenito, and D Stamenović, *J. Colloid Interf. Sci.* 181, 661 (1996).
143. A. Langenfeld, F. Lequeux, M.-J. Stébé, and V. Schmitt, *Langmuir* 14, 6030 (1998).
144. F. van Dieren, in *Theoretical and Applied Rheology*. (P. Moldenaers and R. Keunings, eds.), *Proceedings of the XIth International Congress on Rheology* Elsevier, Amsterdam 1992, p. 690.
145. Y. Otsubo and R. K. Prud'homme, *Soc. Rheol. (Japan)* 20, 125 (1992).
146. Y. Otsubo and R. K. Prud'homme, *Rheol. Acta* 33, 303 (1994).
147. A. J. Liu, S. Ramaswamy, T. G. Mason, H. Gang, and D. A. Weitz, *Phys. Rev. Lett.* 76, 3017 (1996).
148. D. J. Pine, D. A. Weitz, P. M. Chaikin, and E. Herbolzheimer, *Phys. Rev. Lett.* 60, 1134 (1988).
149. E. Ruckenstein, G. Ebert, and G. Platz, *J. Colloid Interf. Sci.* 133, 432 (1989).
150. H. H. Chen and E. Ruckenstein, *J. Colloid Interf. Sci.* 138, 473 (1990).
151. H. H. Chen and E. Ruckenstein, *J. Colloid Interf. Sci.* 145, 260 (1991).
152. M. P. Aronson, K. Ananthapadmanabhan, M. F. Petko, and D. J. Palatini, *Colloids Surfaces A* 85, 199 (1994).
153. M. P. Aronson and M. F. Petko, *J. Colloid Interface Sci.* 159, 134 (1993).
154. J. Bibette, D. C. Morse, T. A. Witten and D. A. Weitz, *Phys. Rev. Lett.* 69, 2439 (1992).
155. E. Ruckenstein, *Adv. Polym. Sci.* 127, 1 (1997).
156. H. M. Princen, in *Encyclopedic Handbook of Emulsion Technology*. (J. Sjöblom, ed.), Marcel Dekker, New York, 2000, p. 243.
157. A. Ponton, P. Clément, and J. L. Grossiord, *J. Rheol.* 45, 521 (2001).

12

Beverage Emulsions

Chee-Teck Tan

Consultant, Middletown, New Jersey, U.S.A.

I. INTRODUCTION

Since the late 1990s, the beverage market in the United States had gone beyond providing beverages for refreshment to health and wellness claims. Beverages are also found to be the most successful and popular means of delivering functional benefits (1). These new beverages are flavored tea, flavored water, juice drinks, dairy-based juice drinks, and fortified beverages. In the United States, by the flavor category, the market statistic shows cola ranks first, and lemon-lime and orange are second and third, respectively. However, worldwide, orange flavor is the favorite of consumers (2). These citrus flavor products are based primarily on the essential oils from the peel of the fruits (e.g., orange oils, lemon oils, etc.). Like all essential oils, they are not water miscible. They cannot be mixed directly with a sugar solution to make a beverage. There are two methods of incorporating these flavors into soft drinks. The first method involves separating out the water-soluble fraction of the flavor from the essential oils by extraction and distillation. The second method involves converting the oil into a water-dispersible emulsion (i.e., a beverage emulsion).

Beverage emulsions are a unique class of emulsions. They are different from other food emulsions in that they are to be consumed in a highly diluted form, rather than in their original concentrate form. They are first prepared as an emulsion concentrate, which is later diluted in a sugar

solution to produce the finished beverage—the soft drink. The soft drink prepared can be either a noncarbonated still drink or a carbonated drink. In soft drinks, the beverage flavor emulsion provides flavor, color, and cloudy appearance for the beverage, or just simply the cloudiness when the beverage cloud emulsion is used. These characteristics of beverage emulsions are what make them a unique class of emulsions. In the preparation of the finished beverages, the beverage emulsion concentrate is diluted in a sugar solution to produce the finished soft drinks; it is usually diluted several hundred times. The emulsions in both the concentrate and diluted forms must have a high degree of stability. They must be stable for at least 6 months, as required by the beverage industry. Other examples of emulsions consumed in a diluted form are coffee whitener and dairy cream for coffee. However, these emulsions are consumed almost immediately after dilution; the stability of the diluted form is required only for a short time. Therefore, dairy cream and coffee whiteners do not have the same stability problem as encountered by beverage emulsions for soft drinks. In this chapter, we will deal mainly with beverage emulsions for soft drinks.

II. DEFINITION

Beverage emulsions can be divided into two categories: beverage flavor emulsions and beverage cloud emulsions. Beverage flavor emulsions provide the beverage with flavor, cloudiness, and color as in certain formulas. Beverage cloud emulsions provide only cloudiness with no flavor. Both beverage emulsions are composed of an oil phase and a water phase, and they are classified as oil-in-water (o/w) emulsions. The oil phase consists of flavor oils and weighting agents. Flavor oils are usually composed of essential oils or citrus oils. Weighting agents can also be called density-adjusting agents, because they are added to flavor oils to increase the oil-phase density. They are materials that are oil soluble, which have no flavor of their own and have densities higher than the flavor oils. For beverage cloud emulsions, the oil phase contains only flavorless oils and the weighting agent. The flavorless oil can be orange terpenes or other flavorless oils, such as vegetable oils or edible waxes. The water phase usually consists of various types of hydrocolloid, acid, preservative, and coloring. The most commonly used hydrocolloids are gum arabic. During the shortage of gum arabic in the mid-1980s, blends of different hydrocolloids and modified food starches were developed for uses as gum arabic replacements.

III. INGREDIENTS

A. Oil Phase

1. Oils

In most of the beverage flavor emulsions, the flavor oils is the major component of the oil phase. It is responsible for providing the flavor and may produce some of the cloud in the beverage. The flavor oil in the emulsions is composed of several types of citrus oil in different proportion to produce a well-balanced flavor. Citrus oils are characterized by the presence of more than 90% of monoterpenes and a smaller amount of sesquiterpenes. They are not miscible with water. To compose a total flavor for a beverage, other flavor chemicals, such as alcohol, aldehyde, ketone, and esters, are compounded. These minor ingredients are responsible for the characteristic aroma and flavor profiles. These chemicals are important for the flavor of the products but have different degrees of solubility in water and do not behave as the typical oil phase in the emulsion (3).

In the beverage cloud emulsions, because terpenes possess little intrinsic odor or flavor, terpene hydrocarbons are used often as the oil component in the emulsions. Pure and deodorized vegetable oils are also commonly used with terpenes in the cloud emulsions. In addition to vegetable oils, edible waxes can also be used in the beverage cloud emulsions. When a stronger cloudifying strength is needed in some beverage flavor emulsions, terpene or vegetable oils are added to the flavor oils in order to produce more clouds in the emulsions (4,5).

Although citrus oils and other oils are important for the beverage emulsions, they also present a major problem for the emulsions because of their low density. In general, citrus oils have a specific gravity in the range of 0.845 to 0.890 g/cm³. The specific gravity of a 10–12% sugar solution of soft drink is about 1.038–1.046 g/cm³. The low specific gravity and insolubility of citrus oils in water indicate that it is difficult to mix the oils into the sugar solution to make a stable dispersion of the oils. Therefore, weighting agents are needed to add to the oils to increase the specific gravity.

2. Weighting Agents

Weighting agents are a group of materials added to the essential oils to increase their specific gravity and help to maintain a stable dispersion of the oil in sugar solution. In the beverage industry, weighting agents are also called density-adjusting agents. The criteria for a good weighting agent are as follows:

- Oil soluble, but relatively insoluble in sugar solution
- Has specific gravity sufficiently higher than that of essential oils

- Contributes no undesirable flavor, odor, or color to the finished product
- Approved by the food regulatory agency of the country in which the product is to be consumed

In the 1940s, brominated vegetable oil (BVO) was first used in soft drinks as the weighting agents for orange oils. In 1970, the United Kingdom and several other European countries withdrew their permission for the use of BVO. The United States and Canada restricted the permitted level of use to 15 ppm (6–10). These limitations have given the soft drink industry difficulty in producing flavor emulsions for soft drinks. Since then, a large variety of materials have been investigated for use as weighting agents for citrus oils.

As the result of the limitations placed on BVO use in 1970, the commonly used weighting agents are ester gum, sucrose acetate isobutyrate (SAIB), and damar gum. These materials have been approved individually by various countries; however, none has been approved universally by all countries.

Ester gum. Ester gum is a hard, pale-amber-colored resin produced by the esterification of pale wood rosin with food-grade glycerol and purified by steam stripping. Wood rosin is a solid resinous material which occurs naturally on the oleoresin of pine trees. There are three major sources for rosin (11):

Gum rosin. Obtained by collection of the exudate of living pine trees followed by heating and stripping of the volatile terpenes and turpentine compounds

Wood rosin. Obtained by solvent extraction of aged pine stumps following by solvent refining of the extracted material

Tall oil. Obtained as a by-product of the Kraft process for wood pulp production followed by depitching and distillation

All three types of rosin are similar in nature and are composed of approximately 90% resin acids and 10% nonacidic neutral compounds.

The acid fraction is a complex mixture of isomeric diterpenoid mono-carboxylic derivatives of alkylated hydrophenanthrenes having the typical molecular formula $C_{20}H_{30}O_2$. These acids are classified into two types: the abietic type and the pimaric type. The distribution of these resin acids can vary slightly according to botanical origin. Resin acids containing conjugated dienes and dehydro-, dihydro-, and tetrahydroabietic acids are classified as being of the abietic type. These differ from pimaric type acids in location of the double bonds and in type and configuration of the alkyl groups attached to C-13. The two double bonds of the abietic-type acids

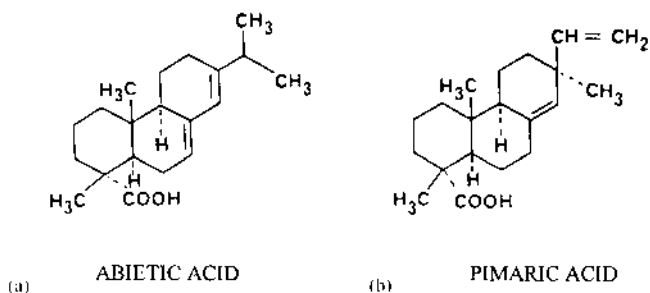


Figure 1 The structural formulas of (a) abietic acid and (b) pimaric acid.

are conjugated, whereas those of the pimaric type cannot be because of the quarternary nature of the carbon atom at position 13. The presence of the conjugated double bond of abietic acid makes it readily oxidizable, isomerized by heat and acids. The structural formulas of abietic acid and pimaric acid are shown in Fig. 1. A typical analysis of gum and wood resins shows that the abietic acid content is in the range 55–68%.

In the neutral fractions of gum, wood, and tall oil rosins, one feature in common is that each is composed of approximately 60% of ester of resin and fatty acids. The resin acids are those found in the acid fraction of rosin. The fatty acids are those found in other neutral products. The fatty acids are predominantly the C-18 acids (i.e., oleic, linoleic, linolenic, and stearic). The alcohol portion of the esters is unidentified.

Ester gum is made by esterification of wood rosin with glycerol. The structurally hindered nature of the resin acid carboxyl group attached to a tertiary carbon atom makes it necessary to use higher temperatures or generally more drastic conditions to bring about esterification. This hindrance is, in turn, responsible for the unusual resistance of the ester linkage to cleavage by water, acid, or alkali. The ester gum with optimum physical properties is glycerol triabietate, which is produced from 3 mol of resin acid combined with 1 mol of glycerol. In commercial practice, it is difficult to obtain such a perfect ester. Commercially, the esterification process produces a mixture of monoglycerides, diglycerides, and triglycerides. Excess glycerol is removed by vacuum distillation and the remaining ester gum is steam-sparged until-odor free. Ester gum produced in this manner has the following typical properties (12):

Softening point (°C)	90
Color, USDA rosin scale	WG
Acid number	6.5
Density at 25°C (g/cm ³)	1.08

Ester gum is produced in flaked and rock forms in the past. The flaked form is easier to use. Because of the large surface area present on the flaked form, flaked-form resins are also prone to gradual oxidation. This usually induces darkening in color and decreasing solubility in terpenes and other organic solvents. In 1997, the manufacturer of ester gum started to produce the ester gum in pastilles shape and packaged in multilayered bags to protect the product. It is claimed that the barrier bag protected the product properties for at least 8 month (13).

The use of ester gum (glyceryl abietate) in orange oil terpene fractions to obtain a stabilized orange drink was first proposed in 1967 (14). Ester gum is considered the best agent for creating cloudy emulsions when it is used in combination with other emulsifying agents (5). Because ester gum is prone to oxidation, hydrogenated abietic acid and esters were proposed for use in cloud emulsions but are still pending government approval (15). Glycerol ester of wood rosin or ester gum is approved by the United States, Canada, and a number of other countries as a food additive. As specified in the U.S. Code of Federation Regulations, Title 21, under Section 172.735 (Glycerol ester of wood rosin), ester gum is permitted for use in nonalcoholic carbonated beverages at 100 ppm. Ester gum is known in the European Union under food additive number E445. It has been evaluated by the Scientific Committee for Food of the EEC, who established an acceptable daily intake (ADI) of 12.5 mg/kg body weight/day. The JECFA (Joint Expert Committee on Food Additives) of the FAO/WHO listed ester gum in the codex Alimentary as E445, glycerol ester of wood rosin (16,17).

Sucrose Acetate Isobutyrate. Sucrose acetate isobutyrate (SAIB) is a mixture of sucrose esters containing approximately 2 mol acetate and 6 mol isobutyrate per mole of sucrose. The major constituent of the mixture is 6,6'-diacetyl- 2,3,4,1'3'4'-hexaisobutyryl sucrose. The structure formula of pure sucrose acetate isobutyrate is shown in Fig. 2. SAIB is manufactured by esterification of sucrose with acetic anhydride and isobutyric anhydride in the presence of a barium hydroxide catalyst. After the removal of unreacted acids and anhydrides by steam-stripping under vacuum, the crude product is decolorized with activated carbon and purified by molecular distillation (18).

Sucrose acetate isobutyrate is a tasteless, odorless, and colorless viscous substance. It has a viscosity of 100,000 cps and a specific gravity of 1.146 g/cm³ at 25°C. SAIB is very soluble in various solvents, such as orange terpenes, ethanol, and median-chain triglycerides. Being fully saturated, it has excellent oxidative stability. The viscosity of SAIB decreases when it is mixed with a solvent and, similarly, the viscosity will drop from 100,000 to 105 cps when the temperature is raised from 30°C to 100°C (19). The typical

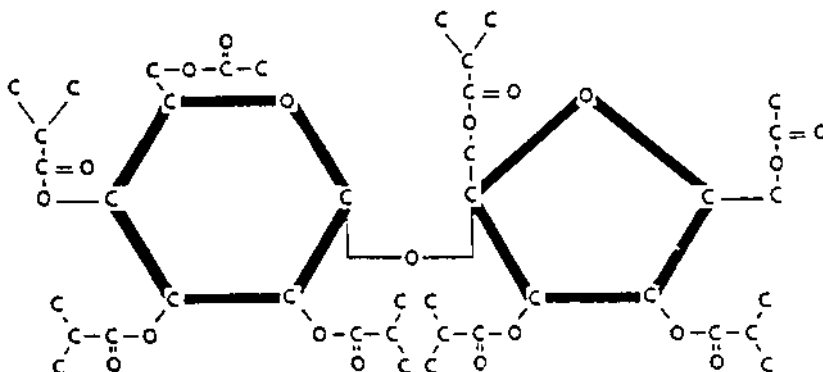


Figure 2 The structural formula of sucrose acetate isobutyrate (SAIB).

properties of SAIB are as follows:

Color, Gardner Scale:	1
Refractive index, n 20/D:	1.154
Specific gravity, at 25°C (g/cm ³)	1.146
Flash point, Tag closed cup (°C)	226
Solubility in water, at 25°C (wt%)	0.1
Shelf life (years)	2

A study conducted by Eastman Chemical Company determined the stability of SAIB in beverages. The study was performed at various values for the pH from 2.46 to 4.01 and for the temperature from 20°C and 40°C. SAIB was very stable under all conditions for 2 months. Minimal degradation of SAIB was observed in the beverages and beverage bases. The study was concluded. The stability of the emulsion containing acacia gum can be improved by the addition of six to eight parts per million of dioctyl sodium sulfosuccinate (DSS), based on the final beverage (20).

Sucrose acetate isobutyrate is metabolized to sucrose, acetic, and isobutyric acids. Metabolic studies indicate that the primary urinary metabolites in humans are lower acetylated sucrose and free sucrose. In 1968, a patent was issued in the United Kingdom for SAIB to be used for mixing with essential oils to facilitate the emulsification of these oils in water for the manufacture of soft drinks (21). Since then, many studies have been made on the biochemical effect and metabolism of SAIB in the rat and man. In general, the results of the studies show that the use of SAIB as a food additive is unlikely to constitute a toxicological problem with respect to its metabolic fate in man (22–24). SAIB is now being used as a weighting agent in beverage emulsions in many countries. In June 1999, the United States Food Drug Administration

(FDA) approved SAIB for use in nonalcoholic beverages at a maximum level of 300 ppm in the finished beverage (25). SAIB is approved globally in more than 40 countries. In most of the countries of the European Union, the permitted level is 300 ppm or 300 mg/L. In the United States, SAIB can be listed as SAIB or sucrose acetate isobutyrate. In the European Union countries, SAIB is designated as E444 (26).

Damar Gum. Damar is the general name given to a group of natural exudates from shrubs of the *Caesalpinaceae* and *Dipterocarpaceae* families and other families belonging to the genera Dammar (27). These plants are indigenous to Malaysia, Indonesia, and the East Indies. The materials of the resins are known as Pale Bold Indonesia Dammar, Dammar Mata Kuching, or Cat Eye Dammar (28).

Damar resin contains an acidic fraction and a neutral fraction. The neutral fraction of the resin is subdivided into ethanol-soluble and ethanol-insoluble fractions, which are designated α -resene and β -resene, respectively. The β -resene has been shown to be a polymeric material of low molecular weight. The remainder of the resin is principally a complex mixture of neutral and acidic triterpenes. The main neutral triterpenes are dammadienone, dammadienol, hydroxydammarenes, and hydroxyhopanone. All of these substances are tetracyclic compounds.

In the acidic fraction, the following acids have been identified: dammarolic acid, ursonic acid, and dammarenic acid, dammar-enonic acid. Methyl esters mixture of the above acids are found with the acids (28,29).

Damar gum is completely soluble in essential oils, benzene, toluene, petroleum ether, carbon tetrachloride, and chloroform. It is partially soluble in ethanol and acetone, and it is insoluble in water. It has been used in coating varnishes for many years. Because of its high solubility in essential oils, it is used as a weighting agent for edible oil to produce beverage clouds emulsions (30). Damar gum can be used in the crude form if it is of top quality; small amounts of impurities that consist of insoluble materials, such as fine bark chips, can be removed by simple filtration after the solution is made. However, in most cases, the crude form will impart a terpene note to the product. A deodorized material can be made through solvent extraction (28,29,31) or by fractional distillation (32).

The typical characteristics of damar gum for use as weighting agent are as follows (27):

Appearance:	Off-white to pale yellow to brown
Weight loss:	5% at 105°C for 18 h
Melting point range:	90–110°C
Insoluble matters:	0.5%
Specific gravity:	1.05–1.08 g/cm ³ at 20°C

Damar gum is permitted for use in beverages as an all-natural non-chemically modified vegetable gum resin; it is classified under the name AGATIS D'AMMARA (Classification N3), number 16 of the Single List of Natural Flavoring Substances, countersigned by 21 countries belonging to the Council of Europe.

Brominated Vegetable Oils. Brominated vegetable oil (BVO) was first used as the weighting agent for essential oils in beverages in the 1940s. It is made by the addition of bromine molecules to the olefinic bonds of the unsaturated fatty acid moieties of vegetable oils.

Commercial BVOs are made from vegetable oils with an iodine number of 80–90, such as olive oil, which produces a BVO with a specific gravity about 1.24 g/cm^3 at 20°C . Vegetable oils with an iodine number of 105–125, such as sesame oil, corn oil, soybean oil, or cottonseed oil, give a BVO with a specific gravity of about 1.33 g/cm^3 at 20°C . The BVO for beverage use is a dark brown color, viscous liquid with bland odor and bland taste.

It is the high specific gravity of BVO that makes it unique as an important weighting agent for citrus oils in soft drinks. It balances the specific gravity of citrus oils and, at the same time, provides cloudiness or opacity to the beverages. In 1966, the Joint FAO/WHO Expert Committee on Food Additives expressed particular concern about the possibility of bromine storage in body tissue when BVOs were used in food. In 1970, permission to use BVOs in soft drinks was withdrawn in the United Kingdom, after being permitted for use for some 30 years. In the same year, the U.S. government limited the use of BVO to 15 ppm in the finished beverage (6).

Other Weighting Agents. Since the use of brominated vegetable oil was banned or limited in different countries, the soft drinks industry has been faced with the problem of finding alternatives to replace BVO. In addition to ester gum, SAIB, and damar gum mentioned earlier, the following potential weighting agents have been proposed and are still being evaluated by the soft drink industry and metabolism and toxicology studies (4):

- Sucrose octa-isobutyrate
- Sucrose octa-acetate
- Sucrose hepta-isobutyrate
- Sucrose octa-propionate
- Propylene glycol dibenzoate
- Glycerol tribenzoate
- Glycerol ester of hydrogenated rosin
- Methyl ester of hydrogenated rosin

B. Water Phase

1. Water

In beverage emulsions, water is the major component. In most beverage emulsions, the water content is about 60–70%, and in certain formulations, it can be as high as 80%. The importance of good quality water in an emulsion is no less than that in soft drinks. Standard water treatment for soft drink water should be applied to the water intended for beverage emulsion. The treatment should remove colloidal and suspended matter, undesirable taste, odor, and micro-organisms. The carbonate hardness or alkalinity of water should be reduced. Highly alkaline water neutralizes the acid in the soft drink and causes the beverage to “go flat” and taste insipid. It will also affect the stability of the beverage emulsion due to the neutralization of the electrostatic charge carried by the emulsion particles. The effect of high water hardness or alkalinity on emulsion stability is much more obvious in the finished soft drink than in the emulsion concentrate because of the very high volume ratio of water to emulsion in the finished drink. Although there is no industrial standard set for hardness or alkalinity for water used in soft drinks, the major soft drink companies have been using the maximum hardness level at 50 mg of CaCO_3 per liter for cola drinks and 100 mg of CaCO_3 per liter for other products (33,34). For beverage emulsions, the water hardness level is recommended to have the same quality—not to exceed 50 mg of CaCO_3 per liter. Public municipal water supplies are not necessarily acceptable for soft drinks or emulsions without treatment. The water treatment at the public water plant is to produce safe potable water and it does not necessarily have the quality required for the soft drink industry. Public water companies depend on reservoirs for water supplies. Water quality varies, because different water sources feed into the reservoirs. Seasonal variation is another influence on the quality of the water in the reservoirs. The additional treatment applied to municipal water at the soft drink plant is to ensure that the quality of water used throughout the year is the same. In the preparation of beverage emulsion, the following steps further treat the raw municipal water: cartridge filtration (5 μm), cation exchange, anion exchange, and ultrafiltration (0.22 μm). This water must be of such quality described as “ultrapure” (35).

2. Hydrocolloids

Hydrocolloids are water-soluble biopolymers consisting of high-molecular-weight polysaccharides with rigid backbone and totally hydrophilic polyol

(sugar) moieties. Some hydrocolloids serve as the stabilizer in the oil-in-water emulsions (36). The basic mechanisms for emulsion stabilization by hydrocolloids are viscosity effect, film formation, steric hindrance, and electrostatic interaction. These stabilization mechanisms will be discussed in detail later. To perform as an effective stabilizer for beverage emulsion, the hydrocolloid must have the following properties:

- Readily soluble with high solubility in cold water
- Low viscosity in water
- High emulsifying property
- Will not thicken or gel on aging

Gum Arabic. Gum arabic or gum acacia is the most well-known hydrocolloid for use in beverage emulsions. It is a dried exudate from the stems and branches of trees of the genus *Acacia*, which belong to the botanical family Leguminosae. About 80% of the acacia of commerce are from *Acacia senegal*, with *Acacia seyal* providing about 10%, with other minor species making up the difference. The best commercial grades designated for good uses are those giving clear, viscous, colorless, or pale yellow solutions that are as tasteless and odorless as possible (37). Gum arabic is a very complex substance with many unique features and properties. Supposedly, its chemical structure is composed of a main skeleton of 18–20 galactose units, with arabinose and rhamnose units limited to the side chains and uronic residues existing as sodium, potassium, and magnesium salts, which tend to give the molecule a buffering capability. The geometry is such that around 50% of these units are believed to be internal in the molecule (38). Composition ranges for the more commonly occurring *Acacia* species are as follows (37):

Ash	3–4 %
Nitrogen	0.14–1.11%
Glucuronic acid	9–16%
pH, solution at 25%	4.4
Intrinsic viscosity	12.1–20.7 ml/g
Molecular weight	$(312–950) \times 10^3$

Gum arabic is almost completely soluble in twice its weight of water and has very low viscosity in water with regard to concentration. A 30% solution has a viscosity of about 100 cps (39,40). Solutions of gum arabic show essentially Newtonian flow properties below about 40% concentration (41). The pH of a 10% gum solution is about 4.6–5.5. The addition of salts or electrolytes affects the consistency of the gum solution as does the pH. Gum arabic solutions become most viscous near pH 6–7. The high solubility

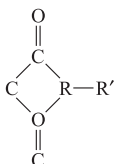
and low viscosity allow for the preparation of solutions containing a high concentration of gum solids.

Gum arabic is well known as an emulsion stabilizer and emulsifier. It is most effective in stabilizing oil-in-water emulsions. It has been reported that gum arabic has a hydrophile-lipophile balance (HLB) value of 8.0 (42); another researcher gave it another value of 11.9 (43). These values indicate that gum arabic is an efficient emulsifier for oil-in-water emulsions. Gum arabic reduces the interfacial tension between oil and water and facilitates the formation of fine oil droplets in the emulsion (94). It has the ability to form an adsorbed film at the oil-water interface whose surface viscoelasticity is rather insensitive to dilution of the aqueous phase. The formation of a thick layer of film around emulsion droplets enable the flavor oil emulsion to be sterically stabilized both in a concentrate and in a diluted beverage (44). It has been reported that it is the protein-containing high-molecular weight-fraction which adsorbs most strongly at the oil-water interface and is probably mainly responsible for the emulsifying and stabilizing properties of the gum acacia (45). In a functionality study of fractionated gum arabic, it was reported that the higher-protein, high-molecular-weight fraction makes the best emulsions. All fractions except the lowest-molecular-weight fraction (about 5% of the whole gum) make reasonably good emulsions and perform well in model beverage (46).

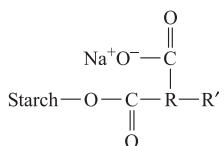
Spray-dried gum arabic is a cleaned gum in a spray-dried powder form. It is used commonly for the preparation of beverage emulsions. In producing spray-dried gum, the raw gum is crushed, dissolved in water, foreign materials of the gum in solution removed by filtration or centrifugation, and then pasteurized and spray-dried into powder. A standard spray-dried gum arabic contains approximately 50% of particles less than 75 μm . A recent development in the gum industry is to make the powder into a fine granulated form for dust-free flowing and faster dissolution in water.

Modified Food Starches. The most widely accepted alternative to gum arabic for use as a beverage emulsion stabilizer is modified starches. They are a group of specially designed starch derivatives with balanced lipophilic and hydrophilic groups on the starch molecules. The starch derivatives are also converted to low-viscosity starches by acid degradation or by enzyme digestion. Caldwell and Wurzburg (47) and Richard and Bauer (48) developed the modification processes. The starch derivative is prepared by a standard esterification reaction in which the reagent and the starch suspended in water are mixed under alkaline conditions. The reagent is a substituted cyclic dicarboxylic acid anhydride having the following

structural formula:



where R is a dimethylene or trimethylene radical and R' is the substituent group, usually a long hydrocarbon chain. Examples are the substituted succinic acid anhydrides in which the substituent lipophilic chain is an alkyl or alkenyl group containing 5–18 carbon atoms. The acid ester of starch may be represented by the following structural formula:



where R is a dimethylene or trimethylene radical and R' is the substituent lipophilic group.

The octenylsuccinic acid anhydride-treated starches, generally referred to as sodium starch octenyl succinates, have been approved for food use by the U.S. FDA and by several other countries. The maximum level of the anhydride treatment allowed is 3%. The approximate degree of substitution is about 0.02 (49). These starches are widely used in the food and pharmaceutical products.

This type of modified starch is a white or yellowish-white bland-tasting, odorless powder. It is cold water soluble and the solution is very low in viscosity. At a concentration less than 20%, its solution has a viscosity about equal to that of gum arabic at the same concentration. The low viscosity of this starch in solution is an important attribute for it to be used as a beverage emulsion stabilizer. Another important property is the emulsifying power derived from the lipophilic modification of the starch molecules. In comparing the use of modified starch to gum arabic, modified starch is a cleaner material, as it contains fewer foreign substances. It is as easy to handle as gum arabic. The emulsion made with some of the earlier developed modified starch had the tendency to develop higher viscosity or form gel in storage at refrigerated temperatures due to retrogradation of the starch. This shortcoming has been overcome by recent developments (50,51).

There are several advantages to using modified starch as the stabilizer in the emulsions. The most important one is that the raw material for manufacturing this starch is corn, which is grown in several areas of the world and the overall supply is less likely to be affected by climatic conditions than that of gum arabic. The second is that in formulation, a smaller amount of modified starch than gum arabic can be used to stabilize the emulsions. A drawback of using modified starch is that it cannot be considered as natural an ingredient as gum arabic.

Gum Tragacanth. Gum tragacanth is known to have the excellent stabilization mechanisms of colloidal suspensions even at relatively low concentrations (of the order of 10 ppm). Gum tragacanth is commonly used with gum arabic as the stabilizer for emulsions because of its high viscosity. When it is used in conjunction with gum arabic, the mixture is a very effective stabilizer for emulsions. The viscosity of a solution of gum tragacanth and gum arabic tends to be lower than that of either constituent solution. A minimum viscosity is attained in a mixture consisting of 80% tragacanth and 20% arabic (52). The viscosity of gum tragacanth is most stable at pH 4 to 8 (53). In solution, it takes 48 h to develop to its maximum viscosity. The viscosity of the tragacanth solution is reduced by the addition of acids, alkalis, or electrolytes. It is also affected by the manner in which the solution is prepared.

Gum tragacanth is not a completely soluble gum. It is compatible with other plant hydrocolloids as well as carbohydrates and proteins. Because of the high price of this gum and its slow hydration rate with slow viscosity development, it is not commonly used commercially in beverage emulsions.

Other Hydrocolloids. Other hydrocolloids which have been reported to be useful in beverage emulsions are some “underutilized” species of Acacia, such as *Acacia verec* and gum arabic from the *Acacia senegal* species, and locust bean gum (54). The successful performance of these gums depends very much on their formulations. There are reports on using hydrocolloid materials such as propylene glycol alginate, xanthan gum, pectin, gellan gum, ghatti gum, and carboxymethylcellulose to enhance the stability of flavor and cloud emulsions. These materials are used as a thickener or blend of thickeners in diluted beverages. They cannot be used to replace gum arabic or modified starch in the emulsion concentrate. The beverage emulsions prepared using these hydrocolloid materials do not have the required stability for the emulsion concentrate and in the finished soft drinks. In general, polysaccharides are usually added to oil-in-water emulsions to enhance the viscosity of the aqueous phase, which produces desirable textural characteristics and retards the creaming of oil droplets. Nevertheless, at certain concentrations, polysaccharides

have been shown to accelerate creaming instability by promoting droplet flocculation through the depletion mechanism (55,56).

3. Acids

Acid is an important ingredient in a soft drink because it provides the taste and controls the pH. In a beverage emulsion, acid plays an important role in controlling the pH to prevent the growth of micro-organisms. It is used to bring the emulsion to pH below 4.5. The reason is that most bacteria grow best at a pH range of 6.0–8.5, and pathogens do not grow well below pH 4.5.

Citric acid is used most commonly in beverage emulsions because it is closely related to citrus products and citrus flavor is the most popular flavor of beverage emulsions. There is an additional benefit of using citric acid because its sequestering power for chelating metallic ions may be present in water (57). Citric acid is usually produced in crystal or powder form and is readily soluble in water. Other acids, such as phosphoric acid, is used in cola emulsion but is not permitted in beverages which claim a fruit juice content. Malic, tartaric, acetic, and lactic acids have been used somewhat rarely as a replacement for citric acid for producing acidity.

4. Preservatives

Benzoic acid or sodium benzoate is added to beverage emulsion as a preservative. Other approved preservatives can also be used. Because of the low solubility of benzoic acid, its sodium or potassium salt is most commonly used. The preservative effect of benzoic acid is largely influenced by the pH. It is greatly increased by a corresponding decrease in pH because it is the undissociated form of benzoic acid which exhibits the preservative action. The preservation of beverages by benzoic is most effective when acidity is less than pH 4.5.

5. Colorings

FD&C colors are commonly used for citrus flavor emulsions. FD&C Yellow 6 and FD&C Red 40 are used for an orange shade. Natural colors, such as α - and β -carotenes and marigold extracts, are used for their yellow or orange shades. However, the stability of natural colors is never as good as the FD&C colors. In cola-flavored soft drinks, caramel color is used. Because of the high acidity in the beverage, the acid-stable double-strength caramel color is used. When the emulsion is a cloudifier, usually no colors are added. The natural color of cloudifiers is just milky white. Because titanium dioxide is an acceptable food additive, the water-dispersible form of it has been used to improve the opaque appearance of oil-in-water

emulsion for short-term stability (58,59). Because of the high specific gravity of titanium dioxide it has the tendency to settle out in the beverage.

III. PREPARATION OF BEVERAGE EMULSIONS

In general, the preparation of a beverage emulsion can be divided into the following steps:

A. Step 1. Preparation of the Water Phase and Oil Phase

For the water phase, it is simple to dissolve the proper amounts of preservative, citric acid, coloring, and gum in water and make a complete solution. It is important to follow the proper order of the addition of these ingredients to assure their full dissolution in water. For the oil phase, the weighting agent is dissolved completely in the oil. The ratio of the weighting agent to the oil is governed by the legitimate permissible amount in the finished beverages. Usually, the maximum quantity of the permissible amount of weighting agent is used to fully utilize the benefit of the weighting agent.

B. Step 2. Prehomogenization

In this step, the oil phase is mixed with the water phase to make a crude emulsion or "premix." It breaks the oil phase into small oil droplets in the water phase. The quality of the premix of prehomogenization being supplied to the homogenizer can greatly influence the quality of the finished emulsion. A good premix fed to the homogenizer produces a better emulsion than a poor premix (60). The reason for this is quite easy to understand. At any given homogenizing pressure, a fixed amount of energy is available for transmission to the product; this energy is the means by which particle size reduction is achieved. If a significant portion of this energy is needed to reduce very large particles, then there will not be enough energy left over to work on the smaller particles and reduce them even further.

As a general rule, the premix should have a droplet size less than 20 μm to avoid a polydispersed final emulsion (61). In practice, it is preferable to have the premix droplet size smaller than 10 μm . Usually, this step can be achieved by the use of a high-speed mixer, colloid mill, homomixer, or making one pass through the homogenizer.

C. Step 3. Homogenization

This is the most important step of the process. In this step, the crude emulsion or premix is pumped through the homogenization valves of the homogenizer at high pressure. The high pressure forces the liquid to pass through the valves at a high velocity, which creates turbulence and cavitation forces that shatter the oil droplets into fine particles (62,63). Single-stage or two-stage homogenizers are usually used for this procedure. For beverage emulsions, a two-stage homogenizer is preferred. In a two-stage homogenizer, the second stage provides controlled back-pressure to ensure the optimum efficiency of homogenization. An additional benefit of the second-stage valve is its ability to delay or prevent reagglomeration of the particles after leaving the first stage. The second-stage valve also provides a means of controlling the viscosity of the product (64). The pressure setting for the first-stage homogenization valve usually varies from one emulsion to the other and is dependent on the composition of the emulsion. This first-stage pressure can vary from 2000 psi to 5000 psi, or from 140 to 350 kg/cm², and in certain cases, 7000 psig or 500 kg/cm². In general, the second-stage pressure is set between 300 and 500 psi (20 and 35 kg/cm²) or set at 10% of the first-stage pressure.

Because beverage emulsions usually require either a very small average particle size and a very uniform particle size distribution, it is simply not possible to reach these goals in a single pass through a homogenizer. Generally, two passes of the emulsion through the homogenizer are performed in order to obtain a more uniform particle size distribution in the emulsion. Because beverage emulsions vary in their formulations, there is no set operational procedure for all emulsion preparations. However, the ideal operating procedures for each emulsion can be designed according to the basic principles of a stable emulsion.

IV. STABILITY PROBLEMS

In 1970, the use of BVO in soft drinks has been banned or regulated. The use of BVO in the soft drinks is limited to 15 ppm in the United States and a few other countries. In many countries, its use is completely prohibited. For this reason, the soft drink industry has been trying to find other appropriate materials to take the place of BVO for use as the weighting agent for citrus oils in beverage emulsions. Although ester gum, SAIB and damar gum can be used as the weighting agents in place of BVO, they have their shortcomings and limitations. All of these weighting agents do not have a specific gravity as high as that of BVO. The specific gravity of ester gum

is 1.08 g/cm^3 , that for SAIB is 1.15 g/cm^3 , and that for damar gum is 1.05 g/cm^3 . They all have government regulations on the amount can be used in beverages. Under these regulations and the low specific gravity of weighting agents, a stable beverage emulsion has become difficult to make than when BVO could be used without limitation.

The instability of beverage emulsion observed in both the concentrates and the finished soft drinks may lead to the following occurrences (65): creaming (ringing), flocculation, and coalescence.

A. Creaming

Creaming is a term adopted from the separation of cream from unhomogenized milk. In the soft drink industry, the common term for creaming of the soft drink in bottles is “ringing.” This is because in the beverages, the flavor oil particles separate from the beverage and float to the top and it is seen as a white creamy ring at the neck of the bottle. Creaming or ringing is related to flocculation. It can be considered as a separation of one emulsion into two emulsion sections. One section is richer in the oil phase than the original emulsion, and the other section is richer in the water phase than the original emulsion. When creaming occurs in a bottle of beverage, the emulsion richer in the oil phase rises to the top and forms a creamy layer or just a ring at the neck of the bottle. It is not only unsightly to have the ring at the neck of the bottle but it indicates the breakdown of the distribution of the flavor oil in the bottle of beverage.

In relation to creaming, two other phenomena not commonly observed in bottles of soft drink are “lifting” and “striation.” Lifting occurs when the emulsion in the bottle of beverage lifts up from the bottom and shows a clear layer of liquid at the bottom. Striation occurs when the emulsion in the bottle shows two or more distinctive layers of different degrees of cloudiness. It looks as if the emulsion in the bottle has separated itself into two or more different particle size or density fractions. Lifting and striation only show in bottles that have been held in an upright position undisturbed for a long period of time. They are more often seen in bottles that are kept in the refrigerator where the temperature is low and the Brownian movement and thermal convection of the emulsion particles are less active.

A rather special and rare situation found in soft drinks is “sedimentation.” Sedimentation is also called “downward creaming” by the soft drink industry. It happens only when the weighting agent is overused or supersaturated in the oil. In such case, the excess weighting agent will separate gradually from the flavor oil and precipitate in the beverages (66). When the

gum arabic or starch used in preparing the emulsion has not been purified properly, the impurities or foreign materials will precipitate as sediments.

B. Flocculation

Flocculation occurs when oil droplets of the dispersed phase form aggregates or clusters without coalescence. At this stage, the droplets still retain their original identities. The forces which draw these droplets together to form aggregates are primarily the long-range London–van der Waals forces and electrostatic forces around the droplets (67). From the creaming point of view, these aggregates behave as simple large droplets. The rate of creaming is accelerated in systems in which the density difference of the aggregates from the continuous phase is sufficiently large. In the emulsion concentrate, a perceptible increase in emulsion viscosity can be observed when flocculation occurs. Although flocculation generally changes the physical properties of the emulsion, the particle size distribution remains unchanged. In the finished beverage system, the droplet concentration is so low that the flocculation is often reversible. The aggregates can be readily redispersed because the interaction forces between the droplets are weak. This phenomenon can be observed by lightly shaking a bottle of beverage that has a ring in the neck. The ring quickly disappears after the shaking.

C. Coalescence

In this stage, there is localized disruption of the sheaths around neighboring droplets of the aggregates, and the oil droplets merge together to form a large droplet. This leads to a decrease of the number of oil droplets and eventually causes the breakdown of the emulsion. When a proper hydrocolloid is used in the water phase, the breakdown of the emulsion will seldom reach this stage. The reason is that the hydrocolloid, such as gum arabic, has a good film-forming ability and will form film around the oil droplets in addition to providing viscosity in the water phase (68). More about the film-forming property of gum arabic will be discussed later in this chapter.

V. STABILIZATION OF BEVERAGE EMULSIONS

For a beverage emulsion, the most critical criterion of stability is its stability in the finished beverage, where the emulsion concentrate is further dispersed in sugar solution. The stability of the emulsion in the concentrate is much easier to achieve than in the finished beverage. This is because, in the

concentrate, the viscosity is high due to the high concentration of a hydrocolloid, which acts as a stabilizer. In the beverage, the emulsion concentrate is redispersed in sugar solution at a very high dispersion ratio. The dispersion ratio could vary from 1/300 to 1/1000 depending on the flavor strength or the cloud strength in the emulsion concentrate. It can almost be described as the emulsion concentrate being dispersed in a second water phase i.e., from a gum-solution water phase to a sugar-solution water phase. The following discussion will emphasize the principles involved in stabilizing beverage emulsions in sugar solutions such as ready-to-drink beverages.

A. Stokes' Law

The "Ringing Test" is the most popular method used to evaluate the stability of beverage emulsions in soft drinks. It is a simple test in which bottles of soft drinks containing the beverage emulsion are held in an upright or horizontal position for observation of ringing. If the emulsion in the soft drink bottle is not stable and will ring, it will form ring faster in the horizontal position than at the upright position. The reason is simply that the oil droplets in the bottle have a much longer distance to travel to the top surface than in the bottle at horizontal position. The rate of ringing or creaming of an oil droplet in sugar solution may be determined by equating the force of gravitation with the opposing hydrodynamic force as given by Stokes' law:

$$v = \frac{2gr^2(\rho_2 - \rho_1)}{9\eta_1} \quad (1)$$

In Eq. (1), v is the rate of creaming or sedimentation, g is the acceleration of gravity, r is the droplet radius, ρ_2 is the density of the oil phase, ρ_1 is the density of the water phase, and η_1 is the viscosity of the water phase. In an o/w emulsion or a soft drink, the oil density, ρ_2 , is lower than that of the water phase, ρ_1 . The resulting sign, v , is negative; hence, creaming or ringing will occur.

As an example of the use of Stokes' law, consider the case of the orange flavor emulsion used to make a beverage. Orange oils are the major components of orange flavor. Typically, orange oils have a density of 0.846 g/cm³ and the sugar solution in the soft drink has a density of 1.040 g/cm³ for a 10% sugar solution or 1.048 g/cm³ for a 12% sugar solution. Applying these density data to Stokes' law, the resulting v carries a negative sign, which indicates that the emulsion will ring in the bottle. Stoke's law shows that the velocity of a droplet, v , is directly proportional to

the density difference between the oil phase and the water phase and to the square of the radius of the droplet. It is also inversely proportional to the viscosity of the water phase. The equation clearly shows that if one can make orange oils with a density equal to that of the sugar solution, there will be no creaming or ringing in the finished beverage because when $\rho_2 = \rho_1$, $\rho_2 - \rho_1 = 0$ and, therefore, $v = 0$. Because orange oil is lighter in density than the sugar solution in the soft drink, weighting agents must be added to orange oil to increase the density. However, the government regulates the use of weighting agents. These regulations make it impossible to adjust the density of the orange oil to equal to that of the sugar solution. For example, an equal weight of ester gum added to orange oil can only bring the density of orange oil from 0.85 to 0.95 g/cm³. A density of 0.95 g/cm³ is still a large difference from 1.05 g/cm, the density of a 12% sugar solution. According to Stokes' law, an emulsion with these components will cause a ringing problem in the soft drink. Because of the consumer's preference for the strength of the orange flavor and the 10–12% sugar sweetness level in the beverages, there is little a beverage processor can do to narrow the density difference between the oil phase and the water phase, because the amount of weighting agent added to the orange oil is reaching the regulated limit in the finished beverage. The exception is in making diet drinks, where artificial sweeteners are used and the density of the water solution is almost equal to 1.

As shown in Stokes' law, if $\rho_2 - \rho_1$ and η_1 equal to constants, where gravity, g , is also a constant, the velocity of an oil droplet moving upward will be in direct proportion to r^2 . It demonstrates that reducing the droplet size is one effective way to control the creaming velocity when the adjustment of oil density has reached the maximum limit permitted. For instance, in a bottle of beverage, a particle 0.1 mm in diameter will travel upward at a velocity 100 times slower than a particle 1.0 mm in diameter. This example shows the importance of controlling the particle size, keeping it small.

B. Adsorption at Interfaces

Most beverage emulsions are made with a water phase composed of gum arabic or other hydrocolloids and water. It has been known for many years that gum arabic solution produces a film at the oil–water interface. Shotton and White reported that gum arabic solution formed a film on paraffin oil and showed this interfacial film to be viscoelastic (68). Dickinson et al. reported that gum arabic forms film and stabilizes an oil-in-water emulsion containing gum arabic and *n*-tetradecane. They also reported that the surface rheology of gum arabic films is relatively insensitive to dilution of the aqueous phase (69). In the case of modified starch, such as sodium

starch octenyl succinates, because it contains both lipophilic and hydrophilic groups, the starch molecules are attracted to the oil–water interface and form a film about the oil droplets (49).

Because citrus oils are most commonly used in beverage emulsions, we conducted a study of the characteristics of films formed at the interface of orange oil droplets dispersed in a gum arabic solution. In order to simulate closely to the conditions of commercial beverages, the orange oil was weighted with ester gum to a density of 0.95 g/cm. The study was repeated using modified starch, sodium starch octenyl succinates, in the water phase. The films formed by both gum arabic and modified starch are viscoelastic. Under the microscope, they appeared as elastic interfacial film or shield on the oil droplets. The elastic property of the films formed by gum arabic and modified starch on orange oil droplets are seen on the shrunk bubble of oil droplet shown in Figs. 3 and 4 (70). The film or shield protects droplets from coalescence when they collide with each other. Aging of the interfacial film in the gum or starch solution seemed to strengthen the film on the droplets (68,70).

Finished beverages were prepared using emulsions containing orange oil with ester gum as the weighting agent with gum arabic or modified starch according to the standard formula and procedure. The aging study of these emulsions in the finished beverage was conducted by storing them on a shelf at ambient temperature for 6 months with weekly checking of their particle size changes. The results show that there was no rinking in the bottle with no significant change in particle size as analyzed by Coulter Model LS-130 particle analyzer (70). In this study, the orange oil/gum arabic emulsion in the beverage had a mean particle size of 0.364 μm when freshly prepared and 0.410 μm after being aged for 6 months. The orange oil/modified starch

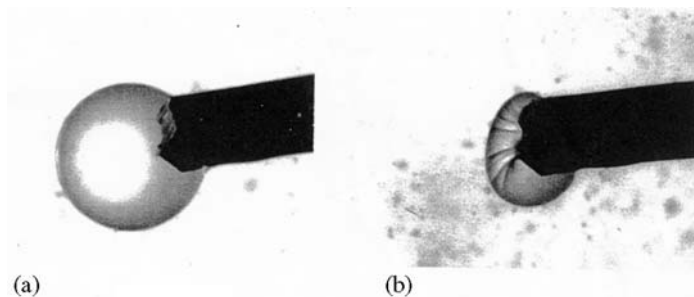


Figure 3 Orange oil droplet in gum arabic solution: (a) full oil droplet; (b) oil droplet shown with wrinkled membrane after oil had been partially withdrawn. (From Ref. 70 with permission.)

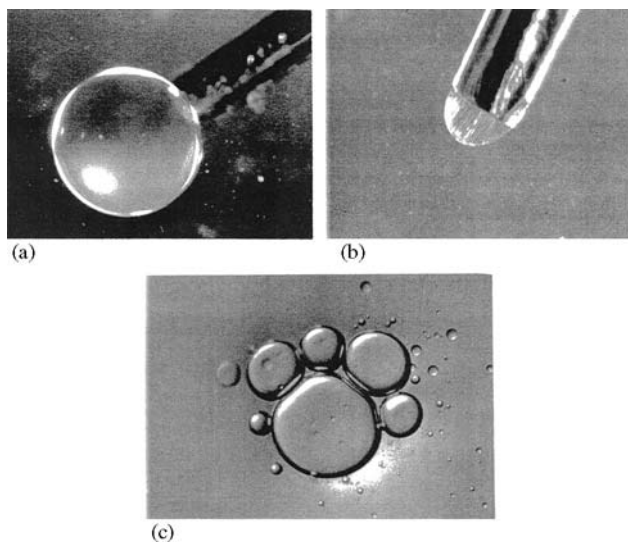
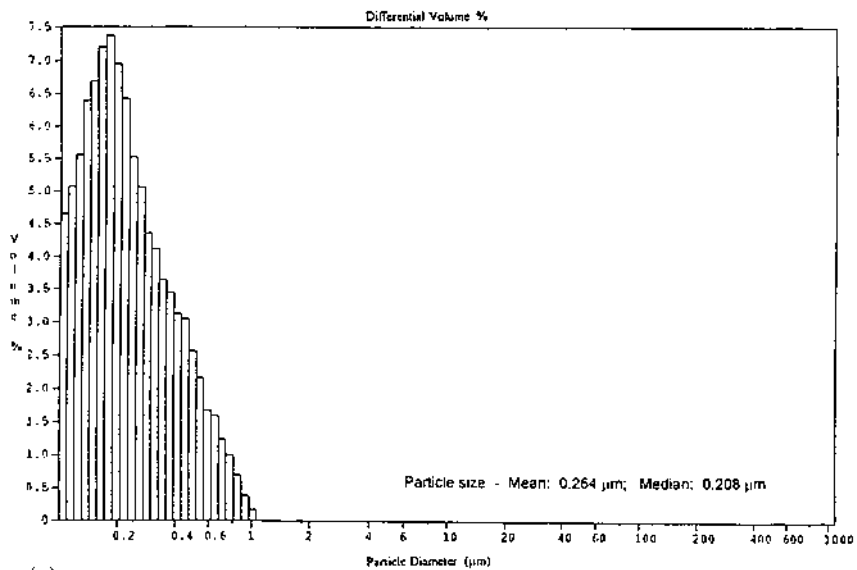


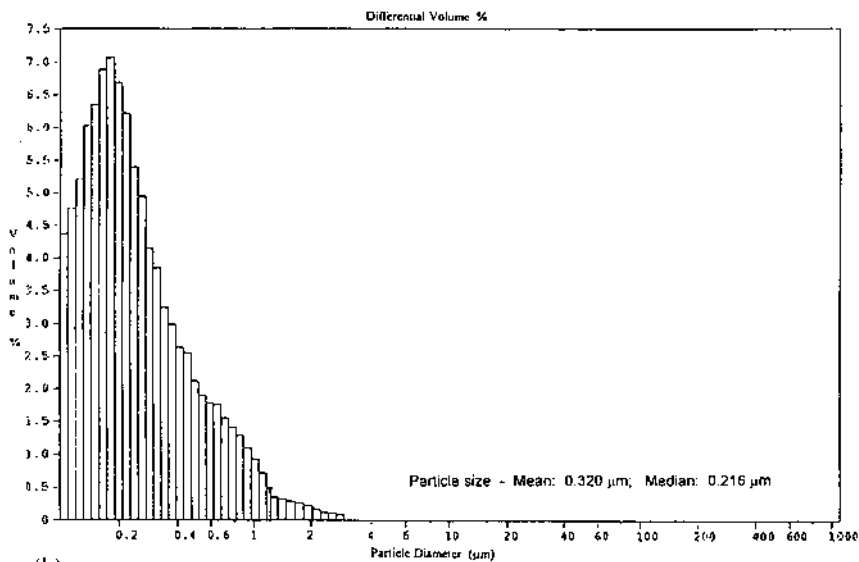
Figure 4 Orange oil droplet in sodium octenyl succinated starch solution: (a) full oil droplet; (b) oil droplet shown with wrinkled membrane after oil had been partially withdrawn; (c) orange oil droplets with membrane aged in sodium succinated starch solution and showed no coalescence. (From Ref. 70.)

emulsion in the beverage had a mean particle size of $0.264\ \mu\text{m}$ when freshly prepared and $0.320\ \mu\text{m}$ after 6 months of aging. The changes are so small and the effect to the emulsion stability in beverage is negligible. The histograms of these two emulsions in beverages when freshly prepared and after 6 months in storage are shown in Figs. 5 and 6. These histograms show that there is no significant change in the particle size distribution patterns.

Because gum arabic or modified starch is heavier than water, a layer of hydrated gum arabic or starch will provide an added weight to the oil droplet and actually change the density of the total droplet—the oil droplet plus the hydrocolloid film—to a higher value. When an oil droplet is smaller, the percentage of weight contributed by the hydrocolloid layer to the total droplet weight will be larger than that for a larger droplet. This further indicates that to achieve emulsion stability in the finished beverage, the oil droplets of the emulsion should be made small. When oil droplets are small, they will gain more of the additional weight benefit contributed by the gum or starch layer on the particles. This theory answers partially the question commonly asked in the industry: “Why in orange oil weighted with a weighting agent to a density of only about $0.95\ \text{g/cm}^3$ could the emulsion

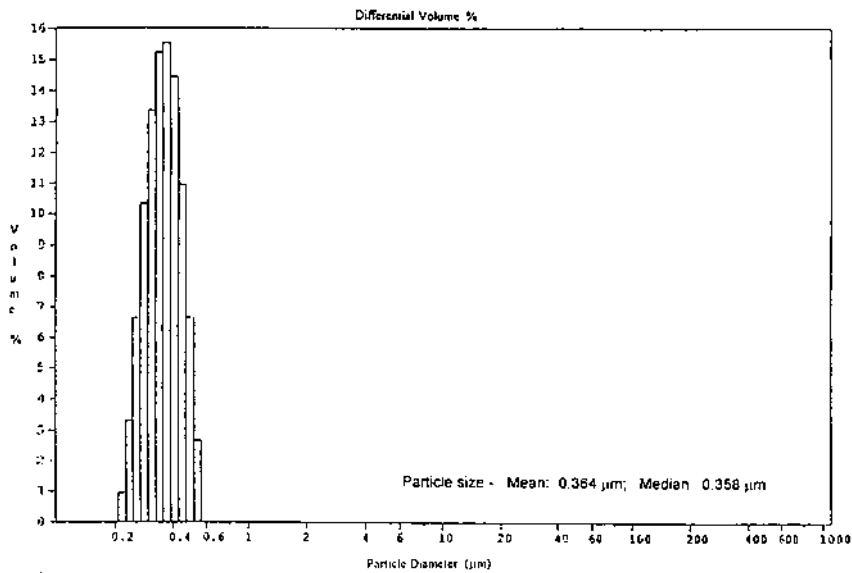


(a)

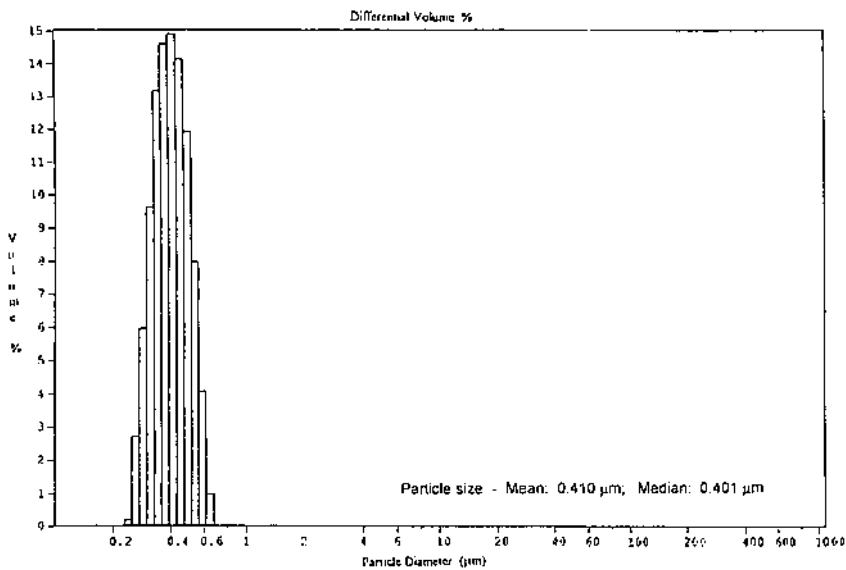


(b)

Figure 5 Particle size distribution histogram of an orange oil/gum arabic emulsion in beverage stored at room temperature: (a) 2 days old and (b) 6 months old. (From Ref. 70.)



(a)



(b)

Figure 6 Particle size distribution histogram of an orange oil/modified starch emulsion in beverage stored at room temperature: (a) 2 days old and (b) 6 months old. (From Ref. 70.)

still be made stable in a solution of density of 1.05 g/cm^3 ?" This is because the additional weight of the film brings up the density of the particle close to that of the sugar solution when the particles are small enough to take the advantage of the weight of film.

The formation of the interfacial film by gum arabic or other hydrocolloid polymers on the oil droplets also helps to stabilize the emulsion in another way. It is the hydrocolloid material adsorbed on the surface of the oil droplets which prevents oil droplets from coalescence and the formation of larger droplets. Coalescence may eventually lead to emulsion breakdown. It may be described as the adsorbed hydrocolloid layer on droplets keeping the droplets far enough apart such that the van der Waals attraction force is minimized (67,71). In this way, the droplets will remain dispersed. When an emulsion is stabilized sterically by adsorbed polymers, the mechanism is considered "polymeric steric stabilization" (72,73).

In many classic emulsions in which emulsifiers or surfactants are used, the emulsifiers are adsorbed on the interface of oil droplets as a closely packed monomolecular film and reduce the surface tension. In citrus-flavor beverage emulsions, Walford proposed using a blend of Atmos 300/Tween-80 (HLB 11.5) to prepare a stable clouding agent (74). Kaufman and Garti studied the use of a different combination of Span/Tween emulsifiers to stabilize oil-in-water emulsions (75). They reported that the type of emulsifier, the required HLB, oil concentration, amount of emulsifier, and the method of preparation affect emulsion stability. However, because of flavor and their non-natural status, little or no emulsifier is being used in the present commercial beverage products. In citrus-flavor soft drinks, which have a delicate flavor, the off-flavor imparted from the emulsifier can be detrimental to taste.

In the beverage emulsion, when gum arabic or sodium starch octenyl succinate is used, they perform as an emulsifier but in a weaker manner as compared to true emulsifiers. It is because these hydrocolloids do not have the distinctive polar and nonpolar groups that, the real emulsifiers have (42,43,49).

C. Electrostatic Interaction

In an oil-in-water emulsion, the oil particle may acquire an electric charge through the ionization of an adsorbed surface charged group. In beverage emulsions, gum arabic is used in the water phase. Gum arabic is an acidic polysaccharide. The carboxyl (COO^-) ions are at the periphery of the molecule and are very active in creating an anionic environment (76). Surface charge may also be acquired through the adsorption of the dissolution of small ions in the water phase. Anions have a greater tendency to be

adsorbed than cations, because cations are normally more hydrated and prefer to stay in the aqueous bulk solution. The electrical charge may also be acquired through a possible friction mechanism. An empirical physical rule may be applied to this theory. It states that a substance having a high dielectric constant is positively charged when in contact with another substance that has a lower dielectric constant (77). Because water has a dielectric constant higher than oil, oil droplets will have a negative charge. These charges cause a repulsive force among the oil droplets which prevents flocculation, therefore contributing to the stability of emulsion.

As mentioned earlier, dispersed oil droplets may acquire an electric charge through the ionization of surface groups. Oppositely charged ions (counterions) are preferentially attracted toward the surface, and ions of the same charge (co-ions) are repelled from the surface. The region of unequal counterion and co-ion concentrations near the charged surface is called the electrical double-layer. The double layer may be regarded as consisting of two regions: an inner region of strongly adsorbed ions and an outer region where ions are diffusely distributed according to a balance between electrical forces and random thermal motion (78). At some point in the double-layer region, corresponding more or less to the potential at the zone of shear, the electrical potential is called the zeta potential (83). The determination of the zeta potential is important in the study of emulsion stability. It is an important parameter for both achieving emulsion stability and destroying emulsion stability. Gum arabic solutions generally have a zeta potential about -23 mV (71,79,80). However, one cannot categorically state that an emulsion will or will not be stable at a given zeta potential, as some other factors should be taken into consideration. It is especially true in the case of beverage emulsion; two other important factors are the density difference between the two phases and the droplet sizes. It should be stressed that the zeta potential reflects both the electrolyte's presence in the system and the dissociated ions accompanying the original colloid particles. When a cation electrolyte is added to an emulsion containing a dispersed phase carrying negative charges, the electrolyte will be adsorbed and neutralize the zeta potential. This, in turn, will cause aggregation to occur due to the London-van der Waal's forces. This electrolyte effect on emulsion stability is much more evident in soft drinks than in the emulsion concentrates, because the emulsion concentrate contains a high concentration of gum arabic and gum arabic is known to produce stable emulsions over a wide range of pH and in the presence of electrolytes (68,70). In soft drinks, the emulsion is in a very diluted form and the gum arabic concentration is very low; therefore, the electrolyte effect is more obvious.

In the adsorption and desorption of electrolyte ions causing the change of zeta potential, the higher the valency of the ions, the greater

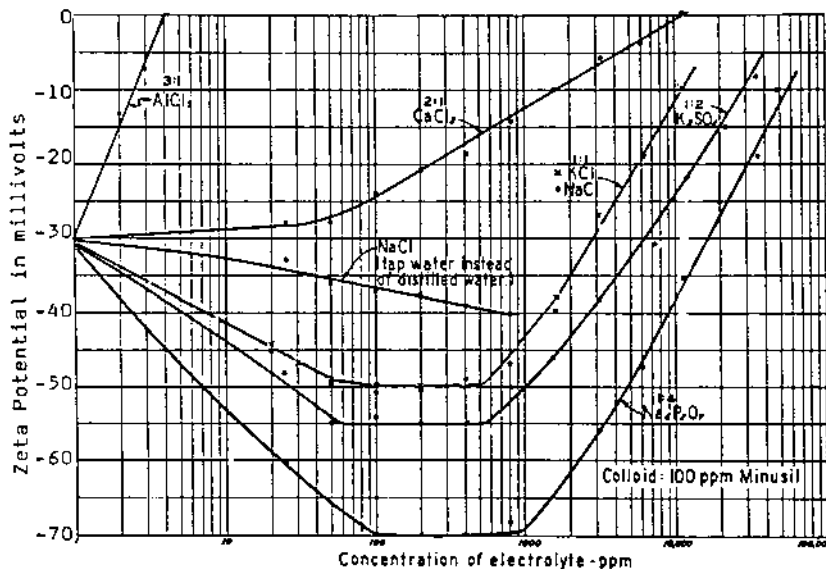


Figure 7 The effect of electrolytes on the zeta potential of a colloidal dispersion. (Courtesy of Zeta-Meter, Inc., New York.)

the effect of compressing the electrical double layer around the droplets and changing the zeta potential (81); that is, the higher the cation valence, the lower the zeta potential, and the higher the ion concentration, the greater the decrease in the negative zeta potential (82). Trivalent ions, such as aluminum ions, have 10–100 times the effect of equivalent concentrations of divalent ions, like calcium, which have 10–100 times the effect of equivalent concentrations of univalent ions. The effect of different electrolytes on the zeta potential of a colloidal dispersion is shown in Figure 7 (83). For the above reason, the soft drink industry usually uses only treated water to make emulsions and the finished beverages.

VI. PARTICLE SIZE CHARACTERIZATION

To achieve good emulsion stability, it is important to control the oil droplet size. This is especially true for beverage emulsions because their particles have to be stable in both the concentrate and the diluted finished soft drink. This means that the same oil phase must be stable in two water phases of different composition. In controlling the particle size, it is essential to know the average size of the oil phase particles and the size distribution of these

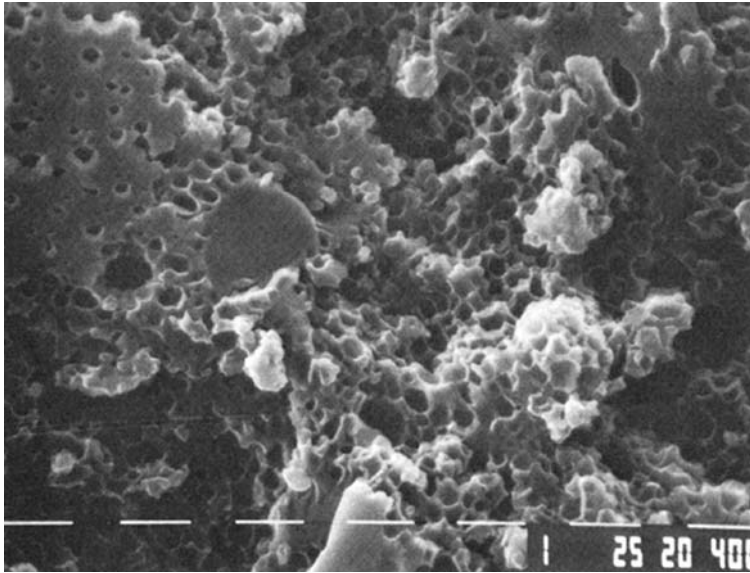


Figure 8 Scanning electron microphotograph of a dehydrated stable beverage emulsion concentrate.

particles in the emulsions. Two emulsions may have the same average particle size and yet have dissimilar stability because of the difference in their distributions of particle size.

A scanning electron microscopic photograph of a dehydrated stable emulsion that originally contained 70% moisture is shown in Fig. 8. In this microphotograph, the holes are the sites of oil droplets. Because the emulsion was dried at room temperature, the droplets did not change in size. The holes represent the actual size of the droplets. They show that almost all of the droplets have a diameter smaller than $1\ \mu\text{m}$.

For the beverage emulsion, the determination of particle size distribution serves two purposes: One is to estimate the quality of the emulsion concentrate and the other—even more important—is to predict the stability of the emulsion when it is made into the finished beverage at a future date. The latter is for quality control. It is to predict the stability of an emulsion by comparing its particle size data with the quality control standard established previously for this product.

There are many methods available for the determination of particle size and size distribution. Groves and others (84,85) have reviewed these methods of particle characterization. Groves' review emphasizes those methods that have practical use for emulsions containing smaller particles.

The beverage industry commonly uses the following methods for product development and quality control: optical microscopic method, transmittance measurement, and laser diffraction technique.

A. Optical Microscopy

The optical microscope is one of the most valuable tools for observing the microstructure of emulsions (86). It is invaluable for a quick examination of the emulsion when there is no other particle size measurement instrument available. Although the microscope is mainly used for examination of the oil particles, it is also useful for checking the gum solution. If there are insoluble materials or underdissolved gum particles in the solution, they can be seen under microscope. Because beverage emulsions are oil particles dispersed in a transparent liquid and they have very similar refractive indexes, a conventional bright-field optical microscope is not suitable for examining oil-in-water emulsions. A microscope equipped with a phase-contrast attachment is best for this purpose. A microscope equipped with a dark-field attachment can be used also. Both phase-contrast and dark-field microscopes will enhance the edge contrast of the image of oil droplets (87). When using the phase-contrast microscopy, an experienced technician can view and estimate the particles down to $0.5\ \mu\text{m}$ at $1000\times$ magnifications with a micrometer. The theoretical limit of resolution of an optical microscope is about $0.2\ \mu\text{m}$, but, in practice, it is difficult to obtain reliable measurements below about $1\ \mu\text{m}$. The experience of routine use of an optical microscope is essential in particle characterization, even if it is used only to examine the state of dispersion for making crude measurements. In practice, it is common to use a microscope in conjunction with other instrumental analysis. Using an optical microscope for objective measurement is almost impossible. A statistically significant count of particles, allowing a 5% error and at 95% confidence level, would need 2960 particles. In general, the emulsion has to be diluted before being placed on the microscope slide. Brownian movement of particles usually is a problem for particle counting under the microscope. To slow down the Brownian movement, a gelatin solution, low-viscosity sodium carboxymethylcellulose (CMC) solution, or glycerin in water are commonly used to dilute the emulsion in place of pure water.

B. Light-Scattering Determination

In general, two types of light scattering method are used: (a) angular light scattering, where the intensity of the scattered light is measured as a function of the scattering angle, and (b) transmittance or turbidity measurement,

where the intensity of the transmitted light is measured. In principle, the angular light-scattering method contains more information, but turbidity measurement is easier to carry out using a spectrophotometer (88,89). For routine particle size analysis or stability tests, where precision is not highly critical, turbidity provides a convenient monitor of the state of the emulsion. However, turbidity measurement only translates to average particle size.

In the soft drink industry, turbidity or transmittance measurement is used as a quick method to check the quality of the emulsion. Some other methods are measuring the spectral absorption of diluted emulsion at two wavelengths, such as 850 nm and 450 nm, or 800 nm and 400 nm, and using the ratio of the readings as stability indices (90,91).

C. Laser Diffraction Technique

The particle counting technique has been known for many years in emulsion science and pharmaceutical research (92). Providing adequate care in sampling and preparing the electrolyte solution, particle size analysis can produce accurate and reproducible results (84,92). In our study we found that there is good corelationship of the data of emulsion particle size distribution obtained from the particle size analysis with the stability of the emulsion in beverage (65). It is generally agreed that the particle size analyzer is capable of making a unique and valuable contribution to the subject of particle size characterization (84,93). With the development in the laser diffraction technique, several instrument manufacturers have developed more sensitive and accurate particle size analyzers. These instruments can determine particle size down to 0.01 μm with the upper size limit to 1000 μm . It is important to have an instrument with the upper size limit at 1000 μm as to make it useful for determine the oil droplet size in premix or crude emulsions. These instruments measure particle size distributions by measuring the pattern of laser light scattered by the particles in the sample. Arrays of photodetectors detect and measure the intensity of the scattered light. Each particle's scattering pattern is characteristic of its size. The pattern measured by the instrument is the sum of the pattern scattered by each constituent particle in the sample. When the duration of the measurement is long enough that the flux pattern accurately represents the contributions from all particles, an analysis of the resulting pattern will yield the particle size distribution of the sample. Because the measurement procedure is fully automated, once the emulsion sample has been placed in the instrument, it takes only a few minutes to complete. The data generated have proven to be invaluable for quality control and troubleshooting the processing of the emulsion.

For expressing the particle size distribution of an emulsion, it is preferable to use volume percentage distribution rather than population percentage distribution. The reason is that volume percentage distinctively shows the quantity in volume of the large particles present in the emulsion. It can be clearly illustrated in the following example. In one emulsion, there are 100,000 dispersed particles of 1 μm diameter and 100 particles of 10 μm diameter. By percentage in population, 100, 10- μm -diameter particles are only 0.1% in number of the total particle population. When expressed in volume percentage, these 10- μm -diameter particles represent 50% of the total volume of all the particles. This is because the volume of 100,000, 1- μm -diameter particles is equal to that of the 100, 10- μm diameter particles. In the beverage, if these 10- μm -diameter particles float to the surface and ring, it represents 0.1% of the particles population in the bottle. The percentage of 0.1% is almost insignificant in the ratio of the population. However, in reality, it represents 50% of the total oil volume and it presents a serious ringing problem.

There is another way to express the particle size distribution data—that is, the total “surface area,” in square meter (m^2), of the particles in each size category (93). When one oil particle is broken to many smaller particles, the total area of these particles will increase according to their reduced size. However, this method of data presentation is not as commonly used as the volume percentage method. The reason is that it is not as easy and simple to associate the data with the quality of the emulsion as the volume percentage.

VII. STABILITY CRITERIA SETTING

To set the criteria of particle size distribution for determining the stability of an emulsion, one has to realize that the criteria are different for each emulsion because each emulsion has a different composition which influences the physical and chemical properties of the product. Examples of particle size distributions of a typical stable emulsion and an unstable emulsion of orange oil with ester gum in gum arabic solution are shown in Figs. 9 and 10. In Fig. 9, the particle volume percentage of the most critical channel, channel 2 (0.4–0.5 μm), is over 50%, and the total volume percentage of channels 1–5 (0.32–1.0 μm) is over 80%. In Fig. 10, the particle volume percentage of channel 2 is slightly over 30%, and the total volume percentage of channels 1–5 is only over 60%, and there is a heavy-tail portion of particles larger than 1.0 μm . Figure 11 is the composite picture of three histograms. The top one shows the particle size distribution in volume percent of an unstable emulsion. This emulsion was used to make a soft drink. On standing, this bottle of soft drink developed a ring in the

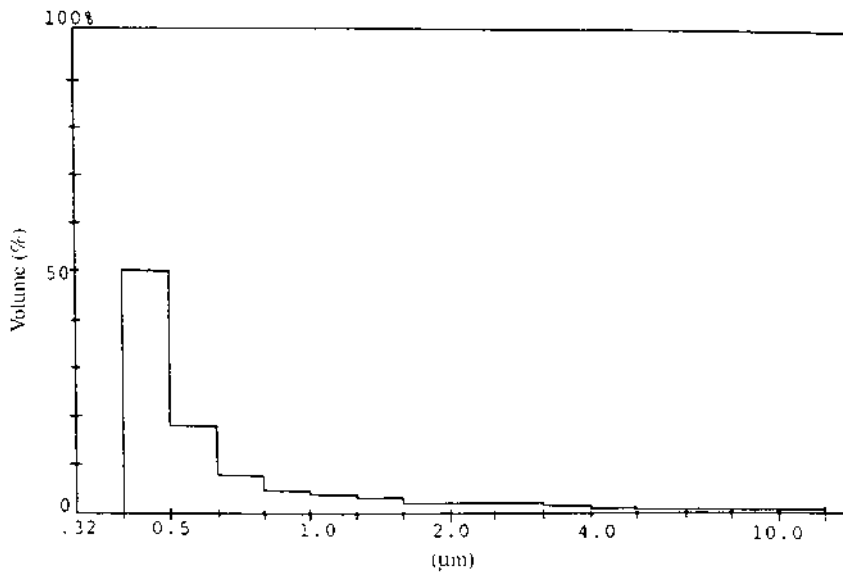


Figure 9 Particle size distribution histogram in volume percentage of a stable emulsion of orange oil plus ester gum in gum arabic solution.

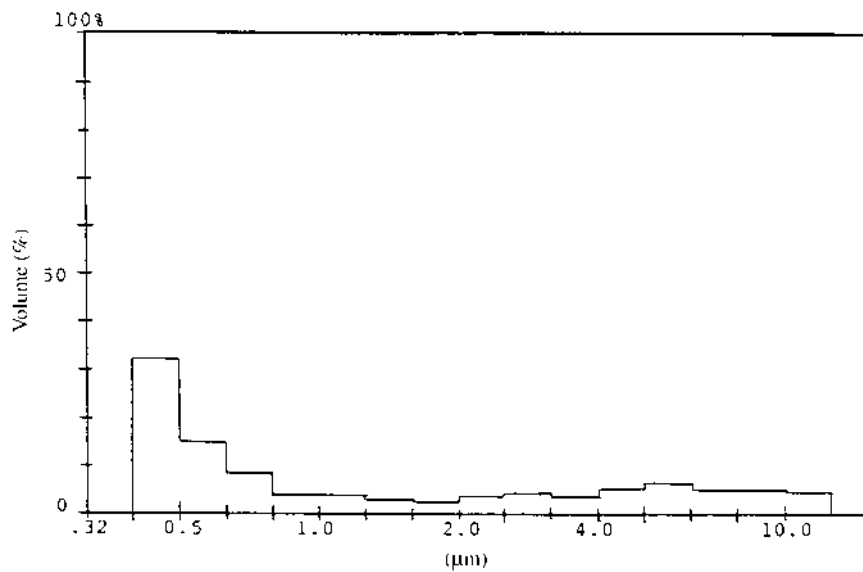


Figure 10 Particle size distribution histogram in volume percentage of an unstable emulsion of orange oil plus ester gum in gum arabic solution.

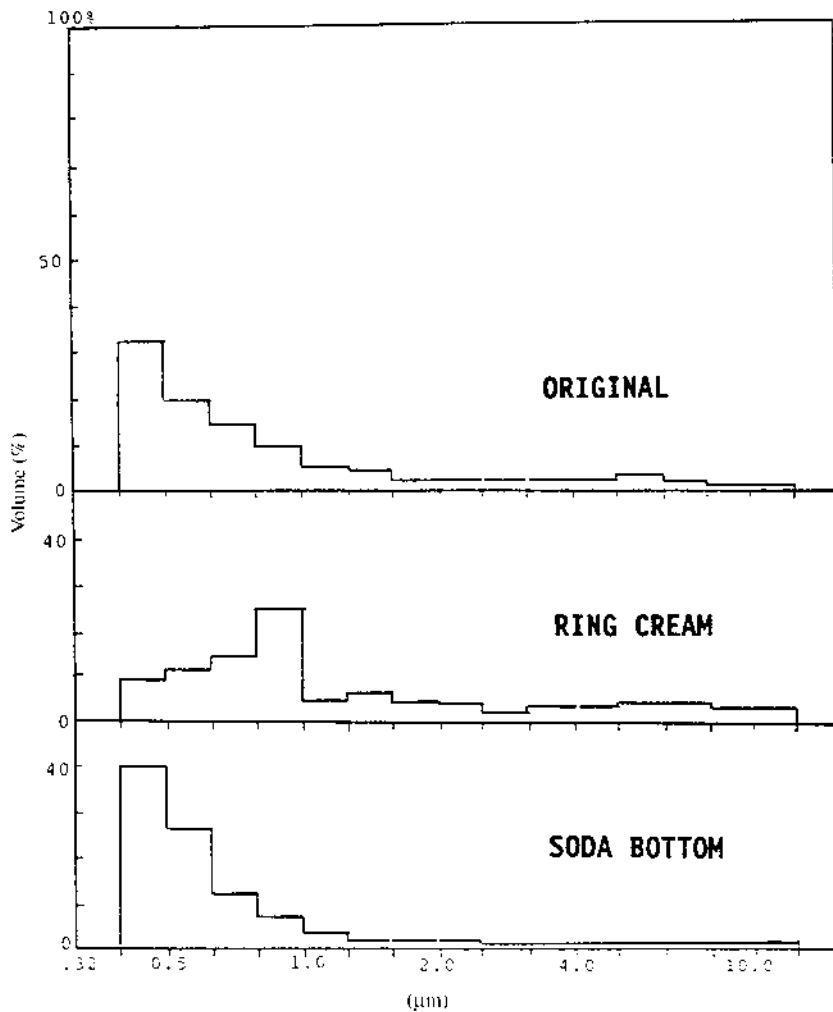


Figure 11 Particle size distribution histogram of (top) an unstable emulsion; (middle) the ringing cream section from a soft drink prepared from the above emulsion; (below) the stable section of the soft drink in the same bottle.

neck of the bottle. The particle size distribution in volume percent of the creamlike ringing material in the neck region is shown in the middle histogram. The bottom histogram shows the particle size distribution in volume percent of the stable emulsion in the nonringing portion of the bottle. The middle and bottom histograms clearly illustrate the particle

size distributions difference of the stable portion and the unstable portion of the soft drink made of an unstable emulsion. It has been determined that the particle size distribution shown in the bottom histogram can be used as the criterion for stability for this particular emulsion. No matter which particle size distribution criterion is used, it is first necessary to collect a series of data with regard to the relationship of different particle size distribution patterns to their degrees of ringing. After these data have been obtained from the soft drink system, then the stability criteria can be developed.

VIII. SUMMARY

Beverage emulsions are a unique class of emulsion. They are prepared in the concentrated form first and then diluted in order to prepare the finished beverage. It has to be stable in both the concentrated and the diluted forms, as the water phases are of different compositions. The stability of the emulsion can be achieved by the application of colloidal chemistry principles.

ACKNOWLEDGMENTS

The author thanks Ms. Joanna Wu Holmes for her excellent technical assistance. The constructive comments on the preparation of this chapter by Dr. Chi-Tang Ho are greatly appreciated.

REFERENCES

1. J. Holleran, New beverage trend: the changing face of fortified beverages, *Stagnito's New Product Mag.* July 28–30 (2000).
2. Anon, Beverage Industry, October, 14 (1987).
3. M. E. Carey, T. Asquith, R. S. T. Linforth, and A. J. Taylor, Modeling the partition of volatile aroma compounds from a cloud emulsion, *J. Agric. Food Chem.* 50, 1985 (2002).
4. H. D. Preston, Clouding agents and heading liquors, in *Developments in Soft Drink Technology, Volume 1* (L. F. Green, ed.), Applied Science, London, 1978, p. 87.
5. V. R. Kaufman and G. Garti, Effect of cloudy agents on the stability and opacity of cloudy emulsions for soft drinks, *J. Food Technol.* 19, 225 (1984).
6. T. J. Coomes, Cloud stability in soft drinks, *Proc. Inst. Food Sci. Technol.* 4(1), 33 (1971).
7. A. Oppenheimer, Clouding agents for the food industry, *Food Prod. Dev.* 5(3), 90 (1971).

8. A. Oppenheimer, Clarifying the clouding agent picture, *Food Prod. Dev.* 8(5), 60 (1974).
9. U.S. Food and Drug Administration, Glycerol ester of wood rosin, Code of Federal Regulations, Title 21, Section 172.735.
10. U.S. Food and Drug Administration, Soda water; identity; label statement of optional ingredients, Code of Federal Regulations, Title 21, Section 165.175.
11. H. I. Enos, G. C. Harris, and G. W. Hedrick, Rosin and rosin derivatives, in *Encyclopedia of Chemical Technology, Volume 17*, Interscience Encyclopedia, New York, 1970, p. 475.
12. Anon., *Hercules Ester Gum 8BG*, Product Data No. 7043-4, Hercules, Inc., Wilmington, DE, (1999).
13. Anon., *Hercules Ester Gum 8BG—Glycerol Ester of Wood Rosin*, Hercules, Inc., Wilmington, DE, (1997).
14. C. K. Simon (to Dominion Products, Inc.), U.S. patent No. 3,353,961, 1967.
15. Polak's Frutal Works, Inc., British patent No. 1,537,160, 1978.
16. World Health Organization, *Food Additives Series 1974*, No. 6,186, WHO, Geneva, 1974.
17. U.K. Food Advisory Committee, *Report on the Review of the Use of Additives to Cloud Soft Drinks*, London: U.K. Food Advisory Board, 1985.
18. R. H. Goins and H. E. Davis (to Eastman Kodak Co.), U.S. patent No. 3,096,324, 1963.
19. Anon., *Sucrose Acetate Isobutyrate*, Product Bulletin, Eastman Chemical Products, Inc., 1983.
20. S. J. Byrd, SAIB—The oldest new ingredient for the beverage market, in *2001 Annual Meeting of the Institute of Food Technologists*, 2001.
21. Bush Boake Allen, Ltd., U.K. patent No. 1 118 019, 1968.
22. W. J. Krasavage, G. D. Di Vincenzo, B. D. Astill, R. L. Roudabush, and C. J. Terhaar, Biological effects of sucrose acetate isobutyrate in rodents and dogs, *J. Agric. Food. Chem.* 21, 473 (1973).
23. B. G. Procter, P. Dussault, and C. I. Chappel, Biochemical effects of sucrose acetate isobutyrate (SAIB) on the liver, *Proc. Soc. Exp. Biol. Med.* 142, 595 (1973).
24. J. C. Phillips, J. Kingsnorth, I. Rowland, S. D. Gangolli, and A. G. Lloyd, Studies on the metabolism of sucrose acetate isobutyrate in the rat and in *Man*, *Food Cosmet. Toxicol.* 14, 375 (1976).
25. U.S. Food and Drug Administration, Sucrose Acetate Isobutyrate. Code of Federal Register, Title 21, Section 172.833 (1999).
26. Anon., *Frequently Asked Questions about SAIB Food-Grade*, Kingsport, TN: Eastman Chemical, 2000.
27. Anon., Resinogum DD, Product Bulletin Q 19, Rouen: Iranex France S.A., 1979.
28. J. S. Mills and A. E. A. Werner, The chemistry of dammar resin, *J. Chem. Soc.* 51, 3132 (1955).

29. J. S. Mills, The constitution of the neutral tetracyclic triterpenes of dammar resin, *J. Chem. Soc.* 52, 2196 (1956).
30. Hasegawa Co., Japanese patent No. 4 834 233, 1973.
31. G. de Haas, Dutch patent No. 65,604, 1950.
32. R. L. Jolly, French patent No. 2 095 093, 1972.
33. N. H. Mermelstein, Water purification for beverage processing, *Food Technol.* 26, 47 (1972).
34. Anon., Production and Quality Control Manual, Dr. Pepper Co., Dallas, Texas, in *Beverages: Carbonated and Non-carbonated* (J. G. Woodroof and G. F. Phillips, eds.), AVI, Westport, CT, 1981.
35. C. D. Morelli, Product water-beverage, in *Water Manual*, 3rd ed. Beverage World Publication, Great Neck, NY, 1994, Chap. 5.
36. N. Garti, Hydrocolloids as emulsifying agents for oil-in-water emulsions, *J. Dispers. Sci. Technol.* 20(1&2), 327 (1999).
37. D. M. W. Anderson, Water-soluble plant gum exudates—Part 1: Gum arabic, *Process Biochem.* 12, 24 (1977).
38. W. Balke, Types of gum acacia and their uses, in *Meeting of the Society of Soft Drink Technologists*, 1979.
39. K. L. Krumel and N. Sarkar, Flow properties of gums useful to the food industry, *Food Technol.* 29(4), 36 (1975).
40. M. Glicksman, Present and future uses of hydrocolloids in foodstuffs, in *Gums and Hydrosoluble Natural Vegetal Colloids, Fourth International Symposium*, Iranex, Paris, 1976.
41. O. E. Araujo, Effect of certain preservatives on the aging characteristics of acacia, *J. Pharm. Sci.*, 21, 535 (1966).
42. A. H. C. Chun, R. S. Joslin, and A. N. Martin, The high hydrophile-lipophile balance of gums, Part I, *Drug Cosmet. Ind.* 82, 164 (1958).
43. W. L. Guess, Determination of the hydrophile-lipophile balance of acacia using various surfactants, *J. Pharm. Sci.* 50, 238 (1961).
44. E. Dickinson, V. B. Galazka, and D. M. W. Anderson, Emulsifying behavior of gum arabic. Part 2: Effect of the gum molecular weight on the emulsion droplet-size distribution, *Carbohydr. Polym.* 14, 373 (1991).
45. E. Dickinson, V. B. Galazka, and D. M. W. Anderson, Emulsifying behavior of gum arabic. Part 2: Effect of the gum molecular weight on the emulsion droplet-size distribution, *Carbohydr. Polym.* 14, 385 (1991).
46. A. K. Ray, P. B. Bird, G. A. Iacobucci, and B. C. Clark, Functionality of gum arabic. Fractionation, characterization and evaluation of gum fraction in citrus oil emulsions and model beverages, *Food Hydrocolloids*, 9(2), 122 (1995).
47. C. G. Caldwell and O. B. Wurzburg (to National Starch and Chemical Co), U.S. patent No. 2,661,349, 1953.
48. C. Richard and C. Bauer (to Anheuser Busch, Inc.), U.S. patent No. 4,035,235, 1977.
49. P. C. Trubiano, Succinate and substituted succinate derivatives of starch, in *Modified Starches: Properties and Uses* (O. B. Wurzburg, ed.), CRC Press, Boca Raton, FL, 1986.

50. C. Chiu, (to National Starch and Chemical Co.), U.S. patent No. 5,185,176, 1993.
51. T. Otera, H. Tsubomoto, and P. C. Trubiano (to National Starch & Chemical Co.), EC patent No. EP1149845, 2001.
52. D. M. W. Anderson, *Gums and Stabilizers for the Food Industry* (G.O. Philips, D. J. Wedlock and P. A. Williams, eds.), Elsevier Applied Science, London, 1986, Vol. 3, p. 79.
53. K. A. Coia and K. R. Stouffer, Shelf life study of oil/water emulsions using various commercial hydrocolloids, *J. Food Sci.* 52, 166 (1987).
54. F. Thevenet, Natural sources of gum arabic, in *Conference Londres*, 1980.
55. E. Dickinson, J. Ma, and M. J. W. Povey. Creaming of concentrated oil-in-water emulsions containing xanthan, *Food Hydrocolloids*, 8(5), 481 (1994).
56. D. J. McClements, Comments on viscosity enhancement and depletion flocculation by polysaccharides, *Food Hydrocolloids* 14, 173 (2000).
57. T. E. Furia, Sequestrants in food, in *Handbook of Food Additives* (T. E. Furia, ed.), CRC Press, Boca Raton, FL, 1972, p. 271.
58. W. Chantrapornchai, F. M. Clydesdale, and D. J. McClements, Optical properties of oil-in-water emulsion containing titanium dioxide particles, *Colloids Surfaces A: Physicochem. Eng. Aspects* 166, 123 (2000).
59. M. E. Carlotti, M. Gallarate, M. Trotta, and V. Canova, On the use of saccharose esters in the preparation of O/W emulsions with liquid crystals, *J. Dispers. Sci. Technol.* 21(1), 31 (2000).
60. W. D. Pandolfe, Effect of premix condition, surfactant concentration, and oil level on the formation of oil-in-water emulsions, *J. Dispers. Sci. Technol.* 16(7), 633 (1995).
61. Anon., Homogenization and emulsification, *APV Gaulin Technical Bulletin*. No. 67, 1983.
62. W. D. Pandolfe, Effect of dispersed and continuous phase viscosity on droplet size of emulsions generated by homogenization, *J. Dispers. Sci. Technol.* 2, 459 (1981).
63. W. D. Pandolfe and R. R. Kinney, Recent developments in the understanding of homogenization parameters, in *1983 Summer National Meeting*, 1983.
64. Anon., The effect of the second stage homogenizing valve, *AVP Gaulin Technical Bulletin* No. 33, 1974.
65. C. T. Tan and J. W. Holmes, Stability of beverage flavor emulsions, *Perf. Flavor* 13(1), 1 (1988).
66. R. Chanamai and D. J. McClements, Impact of weighting agents and sucrose on gravitational separation of beverage emulsions, *J. Agric Food Chem.* 48, 5561 (2000).
67. T. F. Tadros and B. Vincent, Emulsion stability, in *Encyclopedia of Emulsion Technology, Volume 1, Basic Theory* (P. Becher, ed.), Marcel Dekker, New York, 1983.
68. E. Shotton and R. F. White, Stabilization of emulsions with gum acacia, in *Rheology of Emulsions* (P. Sherman, ed.), Pergamon Press, Oxford, 1963.
69. E. Dickinson, D. J. Elverson, and B.S. Murray, On the film-forming and emulsion-stabilizing properties of gum arabic: Dilution and flocculation aspects, *Food Hydrocolloids* 3(2), 101 (1989).

70. C. T. Tan, Beverage flavor emulsion—A form of emulsion liquid membrane microencapsulation, in *Food Flavors: Formation, Analysis and Packaging Influences*, (E.T. Contis et al., eds.), Elsevier Science, Amsterdam, 1998, p. 29.
71. D. Silber and S. Mizrahi, Coalescence of orange oil droplets at oil–gum solution interface and some relationships to emulsion stability, *J. Food Sci.* 40, 1174 (1975).
72. D. J. McClements, General features of polymeric steric stabilization, in *Food Emulsions—Principles, Practice, and Techniques*, CRC Press, Boca Raton, FL, 1999.
73. R. Chanamai and D. J. McClements, Comparison of gum arabic, modified starch and whey protein isolate as emulsifiers: Influence of pH, CaCl₂ and temperature, *J. Food Sci.* 67(1), 120 (2002).
74. J. Walford, Stabilisers for essential oils in flavour formations, *Food Manuf.* 51(2), 35 (1976).
75. V. R. Kaufman and N. Garti, Spectral absorption measurements for determination of ease of formation and stability of oil in water emulsions, *J. Dispers. Sci. Technol.* 2(4), 475 (1981).
76. F. Thevenet, Acacia gums—Stabilizers for flavor encapsulation, in *Flavor Encapsulation* (S. Risch and G. Reineccius, eds.), ACS Symposium Series 370, American Chemical Society, Washington, D.C, 1988.
77. P. Becker, *Emulsions: Theory and Practice*, Robert E. Krieger, New York, 1977, p. 119.
78. E. Dickinson and G. Stainsby, *Colloid in Food*, Applied Science, London, 1982, p. 44.
79. M. L. Layme, D. E. Dunstan, and M. L. Gee, Zeta potentials of gum arabic stabilized oil-in-water emulsions, *Food Hydrocolloids* 13, 459 (1999).
80. S. C. Charma, Gums and hydrocolloids in oil-in-water emulsions, *Food Technol.* 35(1), 59 (1981).
81. T. A. Iranloye, N. Pilpel, and M. J. Groves, Some factors affecting the droplet size and charge of dilute oil-I-water emulsions prepared by self-emulsification, *J. Dispers. Sci. Technol.* 4, 109 (1983).
82. S. Usui, Y. Imamura, and E. Barouch, Destabilization of oil-in-water emulsion with inorganic electrolytes in the absence and the presence of sodium dodecyl sulfate, *J. Dispers. Sci. Technol.* 8(4), 359 (1987).
83. T. M. Riddick, *Control of Colloid Stability Through Zeta-Potential*, Zeta-Meter, Inc., New York, 1968, p. 22.
84. M. J. Groves, Particle size characterization in dispersions, *J. Dispers. Sci. Technol.* 1(1), 97 (1980).
85. M. Kalab, P. Allan-Wojtas, and S. S. Miller, Microscopy and other imaging techniques in food structure analysis, *Trends Food Sci. Technol.*, 6, 180 (1995).
86. R. J. Mikula, Emulsion characterization, in *Emulsions: Fundamentals and Applications in the Petroleum Industry* (L. L. Schramm, ed.), American Chemical Society, Washington, DC, 1992, Chap. 3.
87. J. M. Aguilera and D. W. Stanley, *Microstructural Principles of Food Processing and Engineering*, Elsevier, Amsterdam, 1990.

88. P. Walstra, Estimating globule size distribution of oil-in-water emulsion by spectrophotometry, *J. Colloid Interf. Sci.* 27, 493 (1968).
89. W. D. Pandolfe and S. F. Masucci, An instrument for rapid spectroturbidimetric analysis, *Am. Lab.* 40, (1984).
90. K. Horie, S. Tanaka, and T. Akabori, Determination of emulsion stability by spectral absorption I: Relationship between surfactant type, concentration, and stability index, *Cosmet. Toilet.* 93, 53 (1978).
91. V. R. Kauffman and N. Garti, Spectral absorption measurements for determination of ease of formation and stability of oil-in-water emulsion, *J. Dispers. Sci. Technol.* 2(4), 475 (1981).
92. P. J. Lloyd, J. I. T. Stenhouse, and R. E. Buxton, Comparison of the errors due to sampling and analysis by Coulter Counter, in *Particle Size Analysis* (M. J. Groves, ed.), Heyden & Son, London, 1978.
93. J. K. Johnson, Droplet size analysis of soft drink emulsions by Coulter Counter, in *Proceedings of 29th Annual Meeting of the Society of Soft Drink Technologists.* 1982, p. 121.
94. B. Warburton, *The Rheology and Physical Chemistry of Some Acacia Systems*, Monograph No. 24, Society of the Chemical Industry, 1966.

13

Dressings and Sauces

Larry D. Ford

Kraft Foods, Memphis, Tennessee, U.S.A.

Raju P. Borwankar

Kraft Foods, East Hanover, New Jersey, U.S.A.

David Pechak and Bill Schwimmer

Kraft Foods, Glenview, Illinois, U.S.A.

I. INTRODUCTION

Dressings and sauces include mayonnaise, spoonable and pourable salad dressings, condiment sauces (e.g., ketchup, barbecue sauce, spaghetti sauce). The Association for Dressings and Sauces (ADS) reports the U.S. sales of dressings (including mayonnaise) in 2000 was \$2.9 billion (U.S.) with a growth rate of 3.9%.

Food dressings vary widely in their composition, texture, and flavor. A listing of some of the most widely known dressings and their fat compositions is given in [Table 1](#). Dressings cover a broad spectrum of oil–water composition and some products are defined on the basis of their oil content. In the United States, standards of identity require that mayonnaise contain at least 65% vegetable oil by weight (some brands of mayonnaise contain 80% or more oil), a minimum of 2.5% acetic acid (vinegar for microbial preservation; citric and malic acids may also be used provided they are not greater than 25% of the weight of acetic acid), and egg-yolk-containing ingredients which may be liquid, frozen, or dried (the yolk provides emulsifying properties and, in addition, gives the mayonnaise a pale yellow color). Spoonable salad dressings may be very similar to

Table 1 Typical Fat Contents of Dressings and Sauces

Sample	Percentage
Mayonnaise	75–84
Italian	50–60
Salad dressing (spoonable)	30–60
Blue cheese	30–40
French	36–40
Russian	30–40
Thousand Island	30–45
Italian (low calorie)	0–3
Barbecue sauce	1–2
Ketchup	0.1–0.2

mayonnaise, but the standard of identity for these products requires a minimum of 30% vegetable oil and allows the use of starches as a thickening agent (products generally contain 35–50% oil). Pourable salad dressings, such as French dressing, may contain less oil and may contain gums (1).

The Nutrition Labeling and Educational Act of 1990 (NLEA) allows for nutrient content claims on the food labels in the United States. The U.S. regulations for foods are published each year in Code of Food Regulations 21 CFR Part 101. The three claims of particular interest here are Reduced, Low, and Free as applied to calories, sodium, fat, saturated fat, and cholesterol. Additionally, the NLEA standardized the serving sizes for each product. [Table 2](#) provides the definitions of these claims. Standards vary by country.

Some fat-free salad dressings contain no oil and are not even emulsions. For the purpose of this chapter, all “full-fat” dressings and sauces are considered as “classic” emulsions and their corresponding reduced-fat and fat-free counterparts are considered as “nonclassic” emulsions. The rationale behind this classification as opposed to the one based on fat level is that all so-called nonclassic emulsion-based products need to be formulated and processed to approach in attributes to their corresponding classic emulsion-based counterparts. This need for matching the attributes presents its own unique and difficult challenges. In other words, challenges in making a 6% fat Ranch dressing are quite different than the challenges in making a 6% fat mayonnaise. This chapter includes a special section on challenges encountered with nonclassic emulsion based dressings and sauces.

Table 2 Nutrition Labeling and Educational Act Claims

Claim	Definition	Example
Reduced	A nutritionally altered product contains at least 25% less of a nutrient or 25% fewer calories than a reference food	Reduced calorie (25% fewer calories than reference food) Reduced sodium (25% less sodium than reference food)
Low	A reference amount (and 50 g of food if reference amount is small) contains ≤ 40 cal, ≤ 140 mg of sodium, ≤ 3 g of fat, ≤ 1 g of saturated fat, and $\leq 15\%$ of calories from saturated fat, or ≤ 20 mg of cholesterol	Low calorie (≤ 40 cal per reference amount of per 50 g, if the reference amount is ≤ 30 g or 2 tablespoons, whichever is greater) Low saturated fat (≤ 1 g of saturated fat per serving or 50 g, whichever is greater, and $\leq 15\%$ calories from saturated fat)
Free	A serving and the reference amount contains no or physiologically inconsequential amount: < 5 cal, 5 mg of sodium, < 0.5 g of fat, < 0.5 g of saturated fat, and < 0.5 g trans fatty acids, < 2 mg of cholesterol, or < 0.5 g of sugars	Fat free (< 0.5 g per serving) Sodium free (< 5 mg of sodium) Sugar free (< 0.5 g of sugars)

A. Microstructure of Dressings and Sauces

There is limited literature on the microstructure of sauces and dressings. Chang et al. (2) used, transmission electron microscopy (TEM) to examine the interfacial film surrounding emulsified lipid droplets in diluted samples of mayonnaise. They concluded that the film or membrane is composed of coalesced low-density lipoprotein of egg yolks and microparticles of egg yolk granules. They postulated that the stability of the lipid droplets is attributed to the high degree of plasticity of particles and to fibrous membranes on droplet surfaces.

Tanaka and Fukuda (3) demonstrated using scanning electron microscopy (SEM) that the addition of xanthan gum to French salad dressing inhibited lipid droplet fusion, which extended the shelf life up to 6 months. Tung and Jones (4), using light and electron microscopy, determined particle size (lipid droplet) in mayonnaise and a spoonable, starch-based salad dressing. The interfacial film on lipid droplets of diluted mayonnaise was described. The morphology of the continuous phase could not be determined, however, because of the preparation techniques that were used. Using SEM, they were able to describe the nonlipid material found between droplets of a spoonable salad dressing (Fig. 1). Flukiger (5) studied internal phase volume dependence in mayonnaise using light microscopy. It was shown that clumping of lipid was dependent on the concentration of emulsifiers.

Darling and Birkett (6) studied the role of fat crystallization in the reduction of emulsion stability in oil-in-water emulsions. Using freeze-fracture TEM, they showed the mechanism by which fat crystals penetrate the interfacial membrane resulting in the breakdown of the emulsion.

The application of confocal scanning laser microscopy (CSLM) has enabled Heertje et al. (7) to perform optical sectioning of mayonnaise. This instrument allows a disturbance-free observation of internal structure with relatively minor preparative steps for the sample. [Nine parts of a mayonnaise sample were mixed with one part of a Nile Blue solution (0.1%) and the stained mayonnaise was placed between two glass slides for observation.] The lipid droplets within the sample were tightly packed together, causing the outline of the droplets to be hexagonal in shape. Although the continuous phase was easily distinguishable, its structural components could not be determined because of relatively low resolution caused by magnification limitations.

Through a slight modification of an agar microencapsulation technique developed by Salyaev (8) (see also Refs. 9–11), high-resolution TEMs of liquid and visocous samples in their near-natural or native states can be achieved.

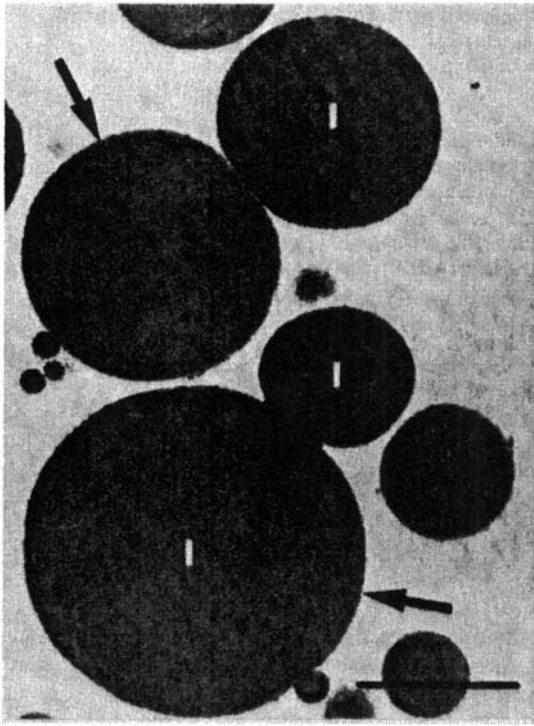


Figure 1 Salad dressing containing 49% oil viewed with scanning electron microscopy. Lipid droplets (l) are embedded within a reticulum of amorphous and fibrillarlike (arrows) material. The amorphous material is assumed to be cooked starch paste. Scale bar equals 10 μm . (Courtesy of Dr. Marvin A. Tung.)

B. Rheology of Dressings and Sauces

The discussion in this chapter will concentrate on applications to dressings and sauces and will not address the basic concepts which have been discussed elsewhere (see, e.g., [Chapter 4](#) in F. 12, and Ref. 13). The techniques used for rheological evaluation of dressings and sauces have depended on the nature of the particular products.

Most dressings and sauces exhibit viscoelastic rheological behavior, although some “thinner” products are primarily viscous in their flow behavior. Mayonnaise and spoonable (or semisolid or viscous) salad dressings are examples of products which show viscoelastic rheological behavior and also possess a yield stress. Pourable salad dressings, such as French salad dressing varieties and Thousand Island dressing, are primarily viscous in

their flow behavior, but exhibit varying degrees of thixotropy and often a measurable yield stress as well.

C. Stability of Dressings and Sauces

The emulsion stability of food dressings is a relative concept. All emulsions in dressings are thermodynamically unstable and, given enough time, will separate. Therefore, the formulator is fighting a losing battle and can never develop a dressing with an indefinite shelf life. Indeed, the destabilization may even be involved in the release of flavor and the perception of mouth-feel. In addition, there are different types of emulsion stability. Some emulsions are formulated to give maximum stability against coalescence (mayonnaise) whereas other emulsions are formulated to give maximum stability against creaming (pourable salad dressings). Flocculation or aggregation, considered as instability in dispersion science, may actually be desirable in dressings and sauces.

In some emulsions, maximum stability is desired to keep product integrity under adverse conditions (e.g., mayonnaise with an internal phase volume of 80%, which is past the point of hexagonal close packing of spheres at 74.05%). In other emulsions such as Italian dressing, only short-term stability is necessary.

There are three main methods for stabilizing emulsions based on electrostatic, steric, and particle stabilization mechanisms. The theoretical treatments of these mechanisms are considered elsewhere (see [Chapter X](#)). In this chapter, a brief outline of the mechanisms and their relevance to salad dressings will be discussed.

D. Processing of Dressings and Sauces

Many of the dressings and sauces, being emulsions, involve an emulsification step. The energy imparted varies with the type of product—the desired droplet size being of primary importance. Shear, turbulence, and cavitation alone or in combination are involved. Different types of emulsification device are employed, colloid mill being the most common. This section is added to this revised edition to discuss key factors controlling this critical unit operations and present guidelines for the selection of emulsification equipment.

E. Nonclassic Dressings and Sauces

Many of the dressings and sauces are high in fat and of nutritional concern to the consumers. As a result, the Better-For-You segment of these

products is growing. As the fat is reduced or eliminated and replaced by other nonlipid ingredients, the need to match the appearance, texture, mouth-feel, flavor, and performance (in recipes, if relevant) attributes of the nonclassic products with their classic counterparts presents unique challenges. The prevalent thinking during the early development of fat-free products was that one must look for the magic replacement ingredient that delivers all characteristics of fat. This was subsequently replaced by a systems approach where specific technologies are leveraged for different functions of fat to create a system that works in a synergistic fashion. The most critical remaining challenge to be overcome in the nonclassic dressings and sauces is around flavor—deliver the right flavor impact and maintain its stability over the shelf life of the product.

II. MICROSTRUCTURE OF DRESSINGS AND SAUCES

A. Introduction

The tools and techniques used to investigate the microstructure of foods are vast and in some manner only limited to the imagination and creativity of the investigator. Relatively simple methods based on routine light microscopy techniques have been demonstrated by Flint (14), where she separates methods based on what information is being sought in the investigations of food emulsions. If the ingredients present in a product are the main focus, the methods can allow for significant disruption of the product, selected optical setup (i.e., polarized optics) and selective stains (i.e., Oil Red O, toluidine blue, iodine) and result in a quick diagnosis. If, on the other hand, the information being sought requires the product to remain intact, other methods are demonstrated using vapors such as iodine for starch and osmium tetroxide for oils. For these methods, the samples are prepared just prior to observation and the degree of success is in part based on the skill and experience of the investigator.

Other methods utilizing only slightly more sophisticated light microscopes employ the use of fluorescence optics. The sample preparation times can be as simple and quick as those for routine light microscopy but with the added specificity of molecular markers that can detect minute concentrations of minor emulsion components. A detailed description of fluorescence microscopy as a technique applied to food systems can be found in Ref. 15.

An example of the use of fluorescence microscopy being used to investigate the proteins at the interface of emulsions can be found in the work of Sengupta and Damodaran, although this work is not specific to dressings

and sauces, the methodology could just as easily be adapted to these food systems. The authors used epifluorescence microscopy to demonstrate phase separation of mixed-protein films. By labeling each protein with a different fluorescent compound, the authors were able to demonstrate that the initial saturated monolayer exhibited a homogeneous mix of proteins but films that were allowed to age for several days exhibited a redistribution of the proteins at an air–water interface.

To answer questions not addressed by the previously described techniques requires a significant increase in time and capital investment. Although the use of fixatives and embedding materials has allowed for thin sections of emulsions to be routinely achieved, the investment in sample preparation time and tools to perform the methodology is significant. Such methodology does, however, allow one to address new and possibly more challenging questions. The introduction of glutaraldehyde and plastic embedding resins opens the door to fine-structure analysis that can take advantage of transmission electron microscopy as well as light microscopy observations.

Again, as with the light microscopy methods described earlier, the details of the methodology employed is greatly dependent on the questions being asked. The use of agar to entrap mayonnaise prior to fixation and embedment was sufficient in the work of Tung and Jones (4), where the lipid droplets and their associated interfacial film were the main focus of study even though the long-range microstructure was lost.

Other more elaborate techniques have been developed in an attempt to preserve long-range structure. One such method, developed by Salyaev (8), was designed for preparation of liquid, semiviscous, and viscous samples. The critical element in this beautifully simple technique is the production of small, delicate, agar cylinders within which the sample is placed. The cylinders are then sealed at both ends and processed intact for examination using standard methods. Samples processed in this manner remain in their natural or near-natural morphological state and the introduction of artifact is kept to a minimum. The best example of well-preserved morphology is with mayonnaise. Using this method, the tightly packed lipid droplets retain their hexagonal morphology when viewed in cross section (Fig. 2a).

Confocal laser scanning microscopy (CLSM) has the advantage of allowing multifocal plane imaging of intact, often unprocessed samples. Although used extensively in the biomedical realm, its use in food science has been more slowly embraced. Heertje et al. (7) showed its potential in food systems, and, later, they (17) demonstrated its usefulness in studying the dynamics of emulsifier displacement at an oil–water interface. More recently and as an example of how microscopy data can

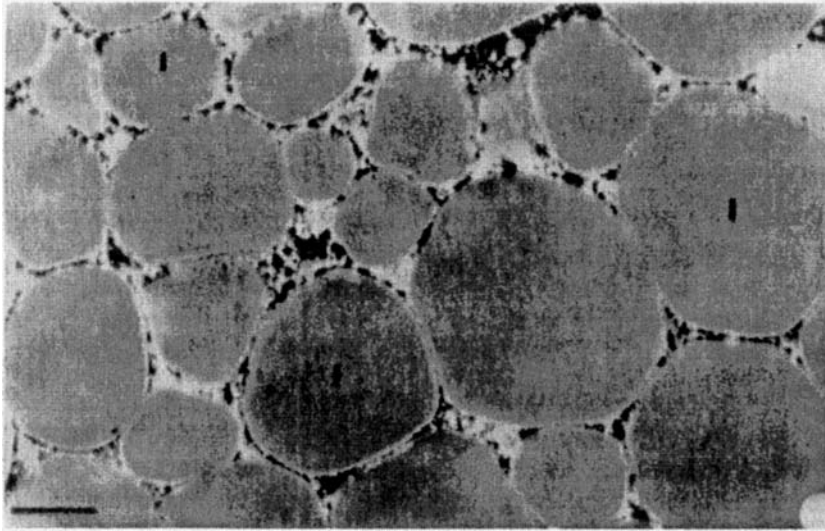


Figure 2 The microstructure of mayonnaise containing 80% oil. Low-magnification transmission electron micrograph showing the tight packing of lipid droplets (l) within sample. Note electron dense material between droplets. Scale bar equals 2 μm . (Courtesy of R. S. Unger.)

benefit from incorporation in a multifaceted approach utilizing image analysis and rheological and sensory data, Langton et al. (18) studied texture variations in mayonnaise. They varied the homogenization and temperature levels, as well as the amount of egg yolk to produce products that had defined organoleptic differences and then analyzed them using CLSM and freeze-fracture TEM methods. Whereas, CLSM utilized intact wet samples and the freeze-fracture TEM method utilized a quick-freeze method, they both avoid the more typical methods that disrupt the sample or allow for extensive repositioning of mayonnaise components. The authors were able to correlate fat droplet size and egg yolk distribution with storage modulus and perceived texture.

The most common morphological feature of dressings and sauces is the lipid droplet. Although there is great variation in the size of the droplets (Table 3), all are coated with an interfacial film. When viewed in profile at high magnification with an electron microscope, the interfacial film appears as a thin electron-dense band. The width of the film ranges from 100 to 200 \AA depending on the type of sauce or dressing. An aqueous phase surrounds the lipid droplets. This phase is continuous and,

Table 3 Lipid Droplet Size in Dressing and Sauces Determined by Light Microscopy

Sample	Size ^a (μm)	Variance
Blue cheese	10.8	±6.06
Thousand Island	14.8	±7.05
Russian	35.8	±20.98
Italian (low calorie)	26.2	±13.13
French	38.0	±19.17
Italian	41.3	±28.24
Salad dressing (spoonable)	1.96	±1.37
Barbecue sauce	13.19	±3.31
Mayonnaise	2.64	±1.97

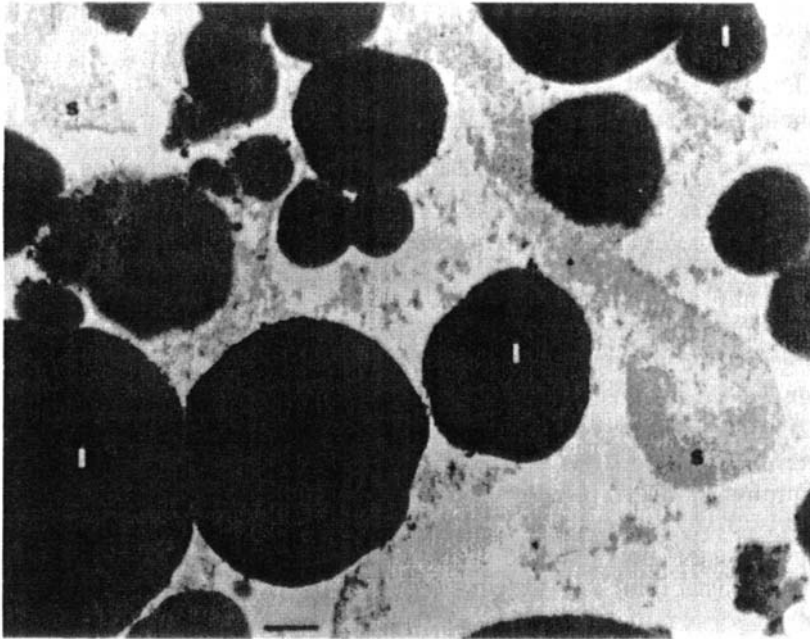
^aSize measured as mean diameter.

in dressings, contains the spices and plant material that enhance flavor of the product.

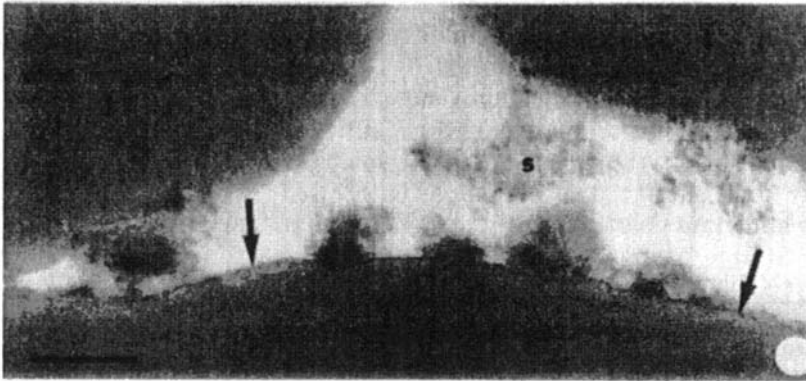
Polymorphic masses of starch are present in the continuous phase of some spoonable salad dressings (Fig. 3). In mayonnaise, fragments of egg yolk granules are the predominant structure in the continuous phase. These fragments or particles adhere to the interfacial film and to each other, resulting in the formation of a protein network. The network increases the viscosity of the product and enhances stability of the emulsion. Sauces such as ketchup and barbecue sauce contain a low percentage of lipid and a high percentage of water and plant material. In ketchup, the plant material is presumed to be tomato cell walls. As a result of processing, the cellulose fibers that once comprised the cell walls become disassociated from each other and form a fine network that can only be visualized with the electron microscope.

B. Mayonnaise and Spoonable Salad Dressings

Mayonnaise is an oil-in-water emulsion that is difficult to examine ultra-structurally because of its high lipid content (Table 1) and the fragility of its interfacial film. Special techniques (described earlier), must be employed to avoid the introduction of artifact caused by specimen preparation. Properly prepared mayonnaise will contain lipid droplets that are tightly packed together and hexagonal in shape (Fig. 2). Lipid droplets in the sample examined have a mean diameter of 2.64 μm (±2.0 SD, Table 3) and are surrounded by an interfacial film that is approximately 140 Å in width (Fig. 2). The continuous phase, located between lipid droplets, is composed of electron-dense particles in an aqueous environment. The particles are



(a)



(b)

Figure 3 The microstructure of starch-stabilized salad dressing. Low-magnification transmission electron micrograph showing the wide size distribution of lipid droplets (l) within the sample. Note aggregates of starch (s) with the continuous phase. Scale bar equals 1.0 μm . (Courtesy of D. Dylewski and R. Martin.)

polymorphic in shape, average 550 Å in size, and are presumed to be fragments of egg yolk granules. The protein particles adhere to one another, forming “bridges” between lipid droplets and also forming a layer or coating on the interfacial film. The protein bridges undoubtedly influence the rheological properties of mayonnaise, and the coating of the film should enhance emulsion stability.

The spoonable salad dressing examined in this study is an oil-in-water emulsion that contains 46% lipid (Table 1). Some spoonable salad dressings have a starch base. Lipid droplets in these samples are spherical to angular in outline and have a mean diameter of 1.9 μm (Table 3). The interfacial membranes are continuous, approximately 120 Å in width, and appear electron dense. Polymorphic aggregates of starch are present in the continuous phase (Figure 3). At high magnification, small particles of starch adhering directly to the interfacial membrane can be resolved. The presence of starch in the continuous phase is thought to increase the stability of the emulsion.

C. Pourable Salad Dressings

Pourable salad dressings are emulsions that share one common morphological feature, the lipid droplet. Because lipid droplets frequently and rapidly coalesce, depending on the type of dressing, morphological descriptions are difficult from a technical standpoint. Phase separation further adds to the difficulty and can only be overcome by using methods that are rapid. Differential interference light microscopy and freeze-fracture transmission electron microscopy are the methods of choice.

The lipid droplets are spherical in shape, surrounded by an interfacial film of various widths and composition, and vary in size (Table 3). Lipid droplet size is specific for each type of dressing and is determined by the stabilizers used and the method of processing.

Based on lipid droplet size, the pourable salad dressings examined in this study can be divided into two classes. Blue cheese, Ranch, and Thousand Island are included in the first class of “creamy dressings” with droplets that range from 10 to 15 μm in size or even lower. The second class contains droplets that are from 25 to 40 μm in size and includes “oily dressings” such as Russian, Italian, and French dressings.

D. Sauces

1. Ketchup

The samples of commercial ketchup that were examined were composed primarily of tomato cell fragments (Figs. 4a and 4b). Large fragments of



Figure 4 The microstructure of ketchup. (a) Light micrograph of a thick section showing tomato cell fragments (arrows). Scale bar equals 10 μm . (b) Transmission electron micrograph showing aggregates of plant cell fragments (arrows). Note: Cell fragments appear to be embedded within a matrix of fine fibrillarlike material (arrowheads). Scale bar equals 0.5 μm . (Courtesy of D. Dylewski and R. Martin.)

cell walls and aggregates of intercellular material all within the size range of 10 μm or less could be resolved using light microscopy. Although the ketchup was known to contain 0.1% oil, distinct droplets were not detected in the sample.

Examination of thin sections using TEM revealed the presence of a major structural/functional component of ketchup that was not resolvable at the light microscopic level. This component is a fine fibrillarlike material that is dispersed throughout the sample and presumed to be cellulose fibers

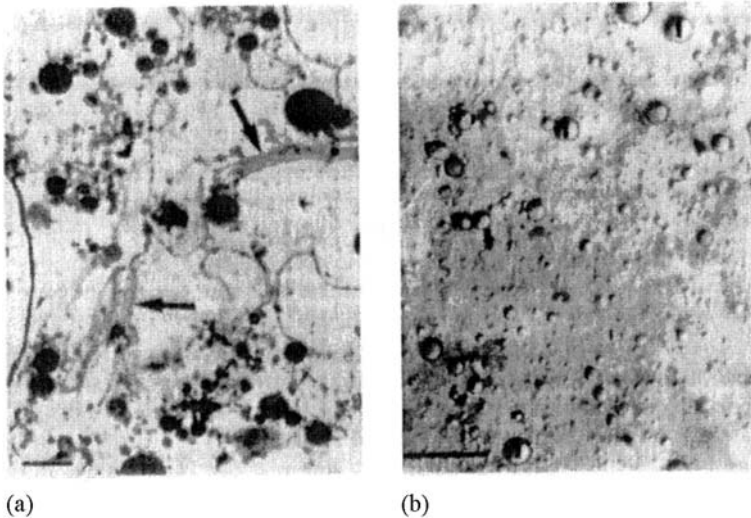


Figure 5 The microstructure of barbecue sauce containing 1.5% oil. (a) Thick section of sample viewed with bright field light microscopy. Lipid droplets (l) appear to be entrained within plant cellular debris (arrows). Scale bar equals 10 μm . (b) Differential interference micrograph showing fine dispersion of lipid droplets (l). Scale bar equals 50 μm . (Courtesy of D. Dylewski and R. Martin.)

from disrupted plant cell walls. The fibers form a matrix within which intracellular fragments are embedded. Occasionally, the fibers are aggregated with their long axes oriented in the same direction. We speculate that these aggregates are partially disrupted cell walls. The fibers function as water-binding agents, much like gums.

2. Barbecue Sauce

The barbecue sauce presented in this study is an emulsion that contains approximately 1.5% oil (Table 1). The mean diameter of the lipid droplets is 13.9 μm (Table 3), and they appear spherical in shape (Figs. 5a and b). The continuous phase of the sauce is composed primarily of plant cell fragments, presumably cell walls of tomatoes.

III. RHEOLOGY OF DRESSINGS AND SAUCES

A. Introduction

Over a very long time, Heinz ketchup commercials have depicted the thickness of their ketchup as an important and differentiating quality attribute

versus the competition. Barbecue sauces have, time and again, touted thickness as a good thing. Indeed, consumer acceptance of dressings and sauces is at least somewhat dependent on their texture. One very important reason to measure the rheology of dressings and sauces then is because the rheological properties are related to the product texture.

Texture of dressings and sauces is very complex, multidimensional term and consumer liking of product texture is an overall effect stemming from evaluations across all relevant textural attributes. In fact, as depicted in some Heinz ketchup commercials, the slowness with which the ketchup pours out of a bottle gives a visual assessment of the product thickness (textural attribute) and viscosity (rheological attribute). Thus, multiple senses are involved in the assessment of texture. Hence, the need for many different approaches and techniques to measure the rheological behavior of these products.

Even when considering a single attribute, and a simple one at that, such as thickness, the perception of that attribute is a combination of several different ways in which the attribute can be perceived. As discussed by Borwankar (19), consumer perception of the thickness of barbecue sauce is a combination of perception of viscosities from several different sensory cues: how the sauce pours out of the bottle, perception during basting, its cling, and, finally, its mouth-feel. Because the steady-state rheological behavior of the sauce is non-Newtonian, the viscosities relevant in these different applications are different because different shear rates are relevant (Fig. 6). This highlights the central difficulty encountered when one attempts to draw correlations between rheology and sensory perception: For a reasonable chance of success, only one means of sensory assessment of the texture attribute should be emphasized, a feat not easily accomplished in practice.

Perhaps the most emphasized viscosity characteristic for dressings and sauces is the viscosity relevant in the mouth. According to Shama and Sherman (20), the relevant shear stresses and shear rates involved are dependent on the product's viscosity itself, ranging from very high shear rates

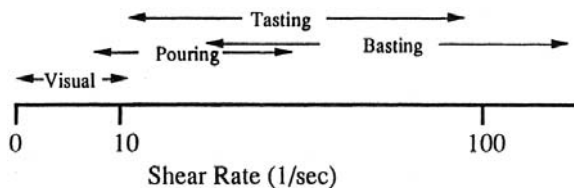


Figure 6 Shear rates operating under different processes involved in sensory perception of barbecue sauce.

corresponding to the shear stress of about 100 dyn/cm^2 for very thin systems to shear rate of about 10 s^{-1} for very thick systems. For typical pourable dressings and sauces, the shear rate range in question is about s^{-1} . For spoonable dressings, firmness or thickness is perhaps more related to the yield stress rather than viscosity.

A more complex but often mentioned textural attributes, again especially for spoonable salad dressings, is creaminess. Creaminess likely has more than just textural connotations. Even as a textural term, its sensorial assessment is complicated and not fully understood. Nevertheless, Kokini (21) suggested that creaminess is determined by thickness and smoothness, which he modeled via fluid mechanical models. He obtained a reasonably good correlation between creaminess and rheological properties across several product categories.

B. Rheological Measurements

Viscosity is the characteristic most commonly used in salad dressing quality control (22) and the rheology of dressings and sauces has been the subject of many articles. Although these have appeared in a number of scientific and technical journals, the reader is referred especially to the *Journal of Texture Studies* and the *Journal of Dispersion Science and Technology*.

The techniques used for rheological evaluation of dressings and sauces have depended on the nature of the particular product. For viscoelastic mayonnaise or spoonable salad dressings, various authors have employed creep compliance (see, for example, Refs. 23–28) and other dynamic testing (see, for example, Refs. 29–32). Coaxial cylinder viscometers and extrusion rheometers have been used to evaluate both the viscoelastic products and the more fluid dressings and sauces (see, for example, Refs. 33–34).

Atkin and Sherman (23), from creep compliance studies, found that mayonnaise exhibits nonlinear viscoelastic behavior at stresses of about $10,000 \text{ dyn/cm}^2$. Later, Kisseoglou and Sherman (25) concluded from creep compliance measurements at about 70 dyn/cm^2 that mayonnaise exhibited linear viscoelastic behavior. Gladwell et al. (38) studied the dependence of the rheological behavior of soy oil in water emulsions upon oil concentration and Gladwell et al. (39) studied the dependence of the creep/recovery behavior of oil-in-water emulsions upon disperse phase concentration. In each of those studies, regions of linear viscoelastic behavior and regions of nonlinear viscoelastic behavior were also found. This illustrates the importance of carefully specifying the measurement conditions. Similarly, Rao (40) noted that Boger and Tiu (41) observed

time-dependent shear thinning (thixotropic) behavior with mayonnaise, were Blake and Moran (33) did not. Rao (40) gave that example to demonstrate the necessity for determining whether a given sample has time-complicating factor in the measurement of viscosity of thick systems such as mayonnaise is the occurrence of wall slip effects. The presence of these have been demonstrated by Pascual et al. (42), who recommend the use of serrated configurations to minimize these and improve the reproducibility of measurements.

Although Barnes and Walters (43) have argued convincingly that "...given accurate measurements, no yield stress exists," the yield stress concept is useful in characterizing many dressing and sauces. As quoted by Barnes and Walters (43), Scott Blair (44) defined yield stress as "that stress below which no flow can be observed under the conditions of experimentation." Following this definition, various dressings and sauces do exhibit yield stresses when one considers the "conditions of experimentation" to be the conditions of use by the consumer. Although many different ways are available for measuring the yield stress of a spoonable salad dressing, perhaps the simplest method is the vane method. This method is best described by Alderman et al. (45). Park, et al. (46) (see also Ref. 47) used a falling-needle viscometer and a rotating-concentric-cylinder viscometer to determine the yield stress of several samples, including tomato ketchup. The falling-needle viscometer data led to a yield stress of 10.85 N/m². Perhaps the best technique to measure the yield stress of pourable dressings such as Ranch is using a controlled-stress rheometer.

Recently, a spate of new rheological methods is being applied to food systems, especially dressings. Accounts of extensional viscosity measurements and tribology (thin layer) measurements are appearing in the literature (see Refs. 48 and 49, respectively). These are emerging areas and the significance of these rheological properties for food scientists and engineers will become clearer as these techniques are more widely utilized.

C. Emulsion Rheology

For a good overview of emulsion rheology, refer to the work of Sherman (12, [Chapt. 4](#); 50, 51). A general representation of viscosity of emulsions can be written as

$$\eta = f(\eta_0, \phi, d, A) \quad (1)$$

where η is the viscosity of emulsion, η_0 is the continuous phase viscosity, ϕ is the phase volume fraction of the dispersed phase, d is the drop size, and A is the state of aggregation of the emulsion. This equation is a very good way of

thinking about emulsion viscosity, although it clearly is a simplification. The emulsion viscosity increases with the phase volume fraction of the dispersed phase in a non-linear manner. The phase volume fraction of the dispersed phase includes contribution from the thickness of the emulsifier layer whose contribution increases as the drop size decreases.

The effects of drop size and aggregation are primarily seen with relatively concentrated emulsions ($\phi > 0.2-0.4$). The viscosity of the emulsion decreases with increasing drop size. This is due to a number of reasons: hydrodynamic resistance dependent on the average separation distance between drops, contribution from interfacial rheology, electroviscous effects, increased aggregation seen in finer emulsions, and contribution of interfacial layer thickness mentioned earlier.

Aggregation increases the emulsion viscosity. The interdroplet interaction determines if the aggregates are relatively open or compact. Open aggregates entrain large amounts of continuous phase and hence have higher viscosity than the compact ones. Open aggregates occur when there is a strong attractive interaction between droplets, and compact aggregates are formed when the attraction is weak (see Ref. 52). The aggregation state of an emulsion is clearly dependent on the shear rate and, for thixotropic (time-dependent) system, on shear history. As the shear rate increases, aggregates are broken down to smaller and smaller sizes and the emulsion viscosity decreases. Hence, concentrated emulsions often show a shear thinning (non-Newtonian) behavior.

Thus, the shear thinning seen in dressings and sauces is attributable to progressively breaking aggregates with shear. Gums and stabilizers can play a role as well (see Section IV.C). The time-dependent or thixotropic behavior arises if the kinetics of breaking and forming aggregates is slow. Chan Man Fong and De Kee (53) have modeled this behavior and shown that the model explains transient rheological properties of mayonnaise fairly well. Amemiya and Shoemaker (54) have shown that, for model dispersions, thixotropy increases with increasing phase volume fraction and decreasing drop size.

The viscosity of emulsion increases as the continuous phase viscosity increases. Typically, gums and stabilizers are added to pourable dressings and salad dressings to increase the continuous phase viscosity and, hence the viscosity of the emulsion. Gums and stabilizers have non-Newtonian rheology and they impart non-Newtonian character to the emulsion even when the amount of the dispersed phase is low.

Equation (1) can actually be generalized to any rheological property, not just viscosity. For yield stress and shear modulus of concentrated emulsions, Princen (55) derived equations theoretically that directionally confirm the drop size and phase volume fraction effects. In their model, which did

not account for aggregation, yield stress and shear modulus are a result of packing the emulsion beyond the close-packing limit. Aggregation can actually produce finite yield stresses and shear moduli even below the close-packing limit. Similarly, gums and stabilizers if added can have yield stress and shear modulus as well themselves.

The above discussion actually suggests that aggregation can be used to one's advantage in formulating dressings and sauces. An aggregated system will have a higher viscosity than a nonaggregated system. Thus, one can formulate a dressing (or a sauce) with less oil and/or less gums and stabilizers by causing controlled aggregation. As discussed in Section IV and in other chapters in the book, aggregation leads to an increase in creaming and coalescence. The control lies in devising an aggregated system that is otherwise stable to creaming and coalescence.

IV. EMULSION STABILITY OF DRESSINGS AND SAUCES

A. Introduction

Dressings cover a broad spectrum of oil–water composition, as is seen in [Table 1](#); from mayonnaise, a 65–84% oil-in-water emulsion, to fat free dressings, which may contain no oil. Most commercially important sauces contain little oil and, therefore, will not be considered in this section.

Dressings also cover a diverse range of products. For discussion purposes, dressings are divided into three categories: semisolid, pourable, and nonclassic. Each category has its own requirements for emulsion stability, but each product shares the need to maintain the emulsion integrity during processing, packing, transportation, storage, consumer preparation, and consumption. Of these dressings, only mayonnaise, salad dressing, and French have their own standard of identity. Mayonnaise must have at least 65% fat and salad dressing and French dressing must have 30% and 35% fat, respectively. The oil phase volumes of these and other dressings are evident from viewing [Figs. 1–5](#).

As previously mentioned, the emulsion stability of food dressings is a relative term due to the fact that all emulsions in dressings are thermodynamically unstable and, given enough time, undergo phase separation. However, in a kinetic sense, the emulsions in dressings can be made stable through an acceptable shelf life and still maintain appearance, texture, and flavor that are desirable to the consumer. For individual dressings, emulsion stability may be concerned with any or all aspects of flocculation, creaming, and coalescence. The half-life of dressing emulsions may range from seconds for a product like separating Italian dressing to years for mayonnaise.

B. Theoretical Considerations

As discussed in [Chapters 1](#) and [2](#), the primary modes of destabilization of emulsions involve creaming, flocculation, and coalescence. These processes occur concurrently and tend to build upon each other. Coalescence is promoted in cream layers and in flocs. Coalescence and flocculation lead to increased creaming rates. Differential creaming promotes flocculation. Although traditionally considered as a mode destabilization in dispersions, flocculation or aggregation is not necessarily bad in itself. Flocculation can, in fact, be beneficial if it does not lead to visual separation and/or coalescence. This is because aggregation leads to increased rheological properties and, thus, can provide a cost-savings opportunity (see above).

Emulsions are typically stabilized against creaming by the use of stabilizers such as gums and starches. The primary factor leading to stability is the increase in continuous phase viscosity, which can proportionally reduce creaming velocities, and, at times, the presence of a yield stress, which can completely suppress creaming. Gums are known to actually promote aggregation by either bridging or depletion mechanisms, depending on whether the gum attaches to the interface or not. Nevertheless, the suppression of creaming due to increased continuous phase rheological properties far exceeds any increase caused by promotion of aggregation.

Stability toward coalescence in the emulsions derives from the use of emulsifiers which are surface-active agents and/or particles. For coalescence to occur, the drops must encounter each other and the thin film trapped between the drops plays a crucial role. The drainage and stability of the intervening thin film controls whether or not coalescence will occur in such encounters. The film can be stabilized either by reduction or elimination of the driving force due to repulsive interactions between droplets that can counteract the forces that are pushing the drops together or by slowing down the drainage rates.

Kinetic stability against coalescence can be obtained via a decrease in the rate of drainage of the intervening thin films due to suppressed interfacial mobility. This is achieved either due to persistence of interfacial tension gradients that suppress mobility, the Gibbs–Marangoni effect, and/or the interfacial viscoelasticity [see, for example, the reviews by Ivanov, (56), Ivanov and Dimitrov (54), and Wasan (58)]. These changes reduce the rate of drainage of the thin film between emulsion droplets, thus suppressing coalescence. Although there has been considerable amount of work done on drainage and subsequent rupture of thin films, the timescales involved in these processes are so short (seconds to minutes in most reported studies) that the kinetic mechanism is likely not important in providing the shelf stability to dressings and

saucers.* Rather, one relies on changing the interaction between the droplets by enhancing repulsion. The primary means of stabilization are electrostatic, steric, structuring and particle stabilization. Several of these mechanisms are commonly recognized and are also described in [Chapter 1](#) and are only briefly covered here. Perhaps the one exception is structuring, which will be described in Section IV.B.3. These stabilization mechanisms rely on altering the interactions between droplets to render emulsions metastable.

1. Electrostatic Stabilization

The attractive forces of the van der Waals interactions and the electrostatic repulsion forces due to the diffuse electrical double layer are the basis for the DLVO (Derjaguin, Landau, Verwey, and Overbeek) theory of colloid stability.

The electrostatic repulsive force is derived from the local accumulation of counterions at a charged surface, the concentration of these ions being strongly dependent on the ionic strength (a function of salt concentration and valence of the ions) of the medium. The thickness of the diffuse layer of counterions around the charged particle surface is compressed by the salt and hydrogen ion concentrations normally found in dressings to such a degree as to make the repulsive force ineffective in stabilizing the emulsion. Even though complex ionic surfactants such as proteins are commonly used, their method of stabilization extends beyond that of electrical repulsive forces and will be covered in the next section. Therefore, electrostatic stabilization plays only an indirect role in dressing emulsion stabilization by its effect on protein structure.

2. Steric Stabilization

As two emulsion droplets approach closely, the adsorbed surfactant layers interact. For macromolecules adsorbed to the surface of emulsion droplets, only a portion of the large molecule is at the surface. Much of hydrated structure remains in the aqueous phase. Therefore, as two emulsion droplets with adsorbed macromolecules approach each other, the chains of the macromolecules interact in at least two ways. First, the number of configurations that the molecular chains can attain is reduced (along with their

*On the other hand, this mechanism is likely to be very important in the formative stages of the emulsion in preventing recoalescence (see later). The studies of thin film drainage in the early stages of emulsion formation are lacking due to the inherent difficulties involved. However, recently, some of the nonequilibrium effects involved have been investigated.

entropy). Additionally, the hydrated portion of the chains has associated water molecules which, when forced from the chain, create a local osmotic gradient (increases the enthalpy) which tends to force the particles apart.

For small-molecule nonionic emulsifiers, the lack of hydrated structures extending from the surface reduces the entropic and enthalpic forces until they are often too weak to provide adequate stability. However, small-molecule nonionic emulsifiers such as the polysorbates are used in pourable dressings with good results. Here, stabilization may instead be caused by the structured packing of micelles in the continuous phase between approaching droplets.

3. Structuring

In [Chapters 1](#) and [2](#), the formation of liquid crystals was considered as one of the ways that emulsifier structures can stabilize emulsions. A relatively new mechanism recognized over the last decade or so is the stratification phenomena seen in various systems. The presence of micelles, particles, or similar discrete entities in the bulk can lead to stratification in the thin films separating emulsion droplets. This phenomenon has been discovered and developed by Wasan, Ivanov, and co-workers (see, for example, Refs. 58–60). The ordered structure occurs in thin films and leads to a stabilizing interaction. This has been shown to occur in food dispersions as well (61).

4. Particle Stabilization

Emulsions can also be stabilized by adsorption of particles at the droplet interface (62). It is the balance of energies at the solid–liquid and liquid–liquid interfaces which determine the effectiveness of the particle stabilization. In other words, both the oil and the water phases should prefer contact with the solid particle rather than with each other. Theoretically, the optimum stabilization occurs when the oil and water phases have equal preference for the particle and the contact angle at the droplet surface is 90°C . For practical purposes though, the contact angle should be between 60 and 70°C to overcome instability which could result from perturbations at the interface. Contact angles can be changed by adding surfactants which adsorb preferentially to one interface.

Particle stabilization is thought to be present in several dressing systems. For example, in dressing systems, finely ground spice particles such as mustard have been attributed to enhancing emulsion stability. Also, in mayonnaise, small particles from the egg yolk have been attributed as providing the major stabilizing force.

C. Emulsifiers and Stabilizers

As discussed later in Section V, the formation of droplets in dressing emulsions has little value if the droplets are not protected from coalescence by emulsifiers (the half-life of emulsions without emulsifiers is about 1 s). Typically, stabilization is divided into two processes: transient (at the time of formation) and long term (over shelf life). Small-molecule surfactants seem to impart better transient stability (due to their ability to migrate along the droplet surface), whereas large-molecule surfactants function best at long-term stability. However, surfactants are seldom additive in their effects on emulsion stability. In fact, when more than one surfactant is present, they compete for the interface. Under equilibrium conditions, the surfactant with the greatest ability to lower the interfacial tension is preferentially adsorbed, and if present in sufficient quantity to cover all available interfacial area, it can effectively prevent adsorption of other surfactants. Small molecules often adversely affect the long-term storage because they preferentially adsorb to the interface and inhibit adsorption of the large-molecule surfactants, which are actually better at providing long-term stability.

Three general types of surfactants are used in dressings: substituted polysaccharides, polyoxyethylene derivatives of sorbitan fatty acid esters (polysorbates), and proteins (Table 4). The substituted polysaccharides such as propylene glycol alginate are used in various salad dressings to provide low levels of emulsion activity and stability. Low-molecular-weight surfactants such as the polyoxyethylene derivatives of sorbitan fatty—acid esters—the polysorbates [high HLB (hydrophile–lipophile balance)] are used in pourable dressings, where greater emulsion stability is desired. Proteins are present in many dressing emulsions and are an important class of food surfactant. The manner in which proteins adsorb and rearrange at the droplet interface is critical to emulsion stability.

Table 4 Sources of Emulsifiers

Emulsifier type	Ingredients
Protein	Buttermilk, sour cream, skim milk, nonfat dry milk, whole milk, sodium caseinate, whey, whole eggs (fresh, salted, frozen), egg whites (fresh, frozen, dried), egg yolks (fresh, salted, sugared, dried)
Phospholipids	Egg yolks, whole milk, sour cream
Particle	Mustard flour
Synthetic	Polysorbate
Chemical modified	Propylene glycol alginate

Proteins form a film around the surface of oil droplets to give stable oil-in-water emulsions. The interfacial activity of a protein proceeds through the following stages: (1) native protein molecule diffuses to the interface, (2) protein penetrates the interface, and (3) molecules rearrange to achieve minimum energy. Stage 1 of emulsification by proteins is a diffusion-dependent process; therefore, any variables such as temperature, shape of the protein, and viscosity of the medium will affect this stage. In stage 2, the protein molecule arrives at the oil–water interface and causes a reduction in interfacial tension as it establishes the interface. As a general rule, the interfacial tension should be lowered below 10 dyn/cm for effective emulsification to take place (63).

After the proteins establish the interface, a slow change in interfacial tension with time is observed. Graham (64) explains that this change is a consequence of the molecular rearrangements within the protein film. Rearrangement is fast for flexible proteins, such as casein, and slow for rigid globular proteins, such as lysozyme. Interfacial films from globular molecules have more residual structures, such as helices, therefore allowing more cross-linking and chain entanglement. This greater extent of cross-linking and entanglement produces a greater resistance to shear and dilation, thus resulting in greater resistance to shear and dilation thus resulting in greater viscoelasticity and stability. Globular proteins tend to form more cohesive films than flexible proteins. Films containing globular proteins will be more stable than films containing flexible molecules because lateral cohesion of the globular proteins will tend to heal defects in the films. For prevention of coalescence in protein-stabilized emulsions, the pH should be away from the isoelectric point and the interfacial layers need to be heavily hydrated and electrically charged. The role of the thickness of the protein layer, however, is a point of controversy.

As already mentioned, mayonnaise has an extremely high dispersed oil phase volume ranging from around 75% to 82% in commercial samples. Due to this high dispersed volume, the droplets are mostly in contact with each other and the spherical shape of the oil droplets has become deformed until the drops actually resemble the polyhedral figures seen more often in foams. Obviously, whatever forms the barrier between adjacent droplets must be mechanically strong, rugged, and present a high-energy barrier to coalescence. There are two mechanisms left to impart stability to the emulsion: steric and particle. For steric stability, macromolecular surfactants such as protein are needed. For particle stability, particles with a polar portion for water and a nonpolar portion for the oil (perhaps a complex of lipid/polar-lipid/protein) are required. Fortunately, a natural emulsifier exists which contains components for both methods of stabilization—the egg. Typically, the batch process for making mayonnaise involves starting

Table 5 Polysaccharides and Their Use in Dressings

Gums/starches	Comments
Xanthan	Most widely used gum; salt, acid, and heat resistant; suspending agent; stabilizer; gelling reaction with locust bean gum and guar gum
Sodium alginate	Gels with Ca^{2+} ions; high viscosity with heat
Propylene glycol alginate	Stabilizer; emulsifier; thickener; some gelling with Ca^{2+} ions; pH tolerant;
Locust bean gum	Thickener; gels with xanthan; insensitive to Ca^{2+} ions
Guar gum	Thickener; insensitive to Ca^{2+} ions; cost-effective
Gum arabic	Some emulsifier activity; thickener; stabilizer
Gum acacia	Suspending agent; forms films at interface
Starch	Thickener; retrogradation a problem
Modified starch	Inhibits retrogradation; thickener
Microcrystalline cellulose	Adds body and mouth-feel

with an aqueous phase of egg yolks, vinegar, salt, sugar, and mustard grains to which vegetable oil is added slowly until a seed emulsion of desired viscosity is formed. Then, the remainder of the oil may be incorporated rapidly.

Gums and/or starches (see Table 5) are added to most dressings for a variety of reasons. These polysaccharides are not surface active (with the exception of PGA) but act to thicken the dressing which affects mouth-feel, cling, and so for (refer to Section III. C). Most importantly, stabilizers can improve the emulsion stability of the dressing. Of course, by making the continuous phase more viscous, oil droplets encounter each other less often. More importantly, it is the creation of a yield stress which increases emulsion stability by minimizing or eliminating creaming of the oil droplets under the relatively low force of gravity (65).

D. Natural Ingredient Effects

1. Eggs

There have been numerous studies on eggs and egg yolks, with regard to their composition as well as the emulsifying properties. For an excellent review, the readers are referred to Refs. 66 and 67. Egg yolks are the most functional components of the whole egg as far as the emulsifying functionality in dressings and sauces is concerned. Egg yolk owes its emulsifying activity to a lecithin protein complex (lipoproteins). Egg whites (albumen) are less functional. Egg yolk is a suspension of particles in protein

solution. Although liquid egg yolk has been a standard raw material for decades, many suppliers today are promoting egg yolk powders with excellent flavor and functionality. Today's egg yolk powders owe this to a gentle spray-drying process used that prevents heat abuse. The egg yolk powders have longer shelf life and do not deteriorate in performance and taste when stored correctly. These can be readily hydrated prior to use.

Egg yolk contain components which contribute to emulsion stability by both steric and particle mechanisms. The particle mechanism is evident in mayonnaise in the micrograph shown in Fig. 2, where protein particles are found at the interfaces between oil droplets. The isoelectric point of egg whites and egg yolks are 5.4 and 5.3, respectively (68). At neutral pH these egg fractions are negatively charged but at the pH's of most salad dressings (pH 2.8–pH 4.0), they are positively charged. However, due to the rather high ionic strengths of dressings due to high salt content, electrostatic stabilization is not likely.

2. Mustard Flour

Salad dressings typically contain mustard flour. Chang et al. (2) note that, according to Corran (69), powdered mustard is an effective emulsifier.

Fischbach and Kokini (24) examined the effects of variable mustard flour levels on oil-in-water emulsion stability and rheology. They found that adding lower levels, (up to 0.5%) of mustard flour increased stability, but higher levels of mustard flour (0.75% and 1.0%) led to decreased emulsion stability, possibly due to formation of a xanthan gum–mustard protein complex. Creep parameters also reached a maximum at lower levels of mustard flour, depending on the age of the emulsion. Mustard flour is added to products for its flavor contribution, but it is also thought to contribute to emulsion stability, possibly by a particle mechanism.

3. Dairy Proteins

Today, more and more salad dressings contain dairy ingredients incorporated in them. Dairy proteins are mainly of two kinds: caseins and whey proteins. Depending on the dairy ingredient used, whey proteins may or may not be included. If cheese is used, proteolytic fractions of caseins may be included. All of the caseins and a whey protein, α -lactalbumin, have an isoelectric point in the range of 4.1–4.5 (70). The other major whey protein, β -lactoglobulin, has an isoelectric point of 5.3. As a result, the environment of many dressings is very close to the isoelectric point of these proteins and these proteins may be nonfunctional as emulsifiers in dressings. Worse yet, they may compete with the functional emulsifiers such as egg yolk for the interface and actually cause emulsion stability issues.

E. Practical Considerations

As previously mentioned, in order to more easily understand the characteristics and requirements of emulsion stability for food dressings, it is worthwhile to consider dressings as three categories: semisolid, pourable, and reduced-calorie dressings.

Semisolid dressings are, by definition, very viscous emulsions (refer to section III. C). In mayonnaise, this is due to a high phase volume of oil, whereas in salad dressing, the effect of phase volume is augmented through the use of stabilizers (starches) which thicken the continuous phase. Due to the high oil content of the mayonnaise emulsion, the oil droplets are forced close together, and in extreme cases, the spherical shape of the droplets becomes deformed (see Fig. 2). This close proximity precludes concern for flocculation, and emulsion stability must instead be concerned with preventing coalescence. Because in many cases droplets are actually in contact with neighboring drops, coalescence can only be delayed by employing tough, pliable membranes around the oil droplets. In semisolid dressings, this membrane is formed from protein and polar lipid components of egg yolk.

Pourable dressings are, of course, much less viscous than semisolid dressings and as such are susceptible to creaming. The oil phase volume normally ranges from 30% to 50% oil, but can be as high as 60–65% for the creamy style dressings. Due to this lower ratio of oil to water, the oil droplets are spaced apart from each other and flocculation, which could lead to coalescence, is also of concern.

Low-fat and fat-free dressings are generally based on the full-fat dressings with the addition of starches and gums to replace the oil. Of course, as the oil is reduced, the emulsion stability does not become a problem; however, maintaining the low amounts of oil in a fully dispersed state throughout the dressing can be challenging in lower-viscosity pourable dressing types. Special considerations have to be given to imparting a full-fat flavor and texture for these products as well. These are considered in more detail in Section VI.

A prediction of the food emulsion's stability without actually going through shelf life is very desirable. Typical measurements have evolved around accelerated aging tests but must be viewed carefully because many forces caused by the "aging" test would have never been experienced by a normally aged emulsion. One must realize that the accelerated physical stability tests do not consistently accelerate many processes occurring through normal aging (e.g., oxidation and hydrolysis), which are just as important in determining product shelf life. Nevertheless, the assessment of emulsion stability is often necessary. A typical protocol for assessing product's emulsion stability should include several methods: shelf-life

testing at normal storage temperature, abuse testing at elevated and/or colder temperatures than normal to simulate warehouse and consumer abuse and abuse testing vibration to simulate distribution abuse; perhaps even freeze–thaw cycles. Accelerated testing such as the centrifugal test may be used as well, but with the above caution. The science behind the various tests is not completely understood, making them an art rather than truly scientific, but, often times, practitioners have developed enough product experience that well-designed abuse tests can serve them well.

There is a real need for a more scientific prediction of emulsion stability, especially as new products and cost-reduced products are developed at a frantic pace. Common methods based on the partitioning behavior of surfactants such as HLB and PIT (phase inversion temperature) are of little use in most dressing systems. This is because the major stabilizing forces are usually due to proteins and adsorption of small-molecule surfactants interferes with their adsorption. Currently, of the four most promising areas of predicting emulsion stability, two are based on properties of the interface between the oil and water. For years, the correlation of interfacial rheology and emulsion stability has been claimed, but as discussed, the suppression of the drainage rate that the interfacial rheology causes is not large enough to provide long shelf stability. More recently, Darling and Birkett (6) have given acclaim to the thickness of the interfacial layer as a predictor of emulsion stability. The new area of structuring in the thin film is likely to emerge as the most definitive predictor of stability. The final predictor of emulsion stability is based on particle size and distribution and how these change over time. It is actually an old method, but due to recent refinements in resolution, it allows the researcher to follow coalescence in its earliest stages.

The challenge to the food emulsion scientist is to comprehend the food system on its many levels—not only those of emulsion science (molecular structure of surfactants; assemblies and aggregates at the interface and in the bulk; rheology; and stability) but their consequential effect on the organoleptic properties of the food as well (correlated with sensory evaluation).

V. PROCESSING OF DRESSINGS AND SAUCES

The primary goal of emulsion processing for dressings and sauces is to produce a uniform, physically stable product with desired textural attributes. Although emulsion processing often has its greatest effect on product texture and stability, important changes in product flavor, color, and sheen may also occur. In general, reducing the mean internal-phase particle size and narrowing the particle size distribution will increase product stability,

viscosity, and yield. However, smaller oil droplets also refract light differently than larger droplets and will result in a product that is lighter in color and greater in opacity. Additionally, smaller oil droplets may release flavors differently than larger oil droplets, possibly reducing the intensity and delaying the impact of flavor as the product is tasted. Therefore, the benefits of producing a more stable product by reducing droplet size must be weighted against the impact of texture, flavor, and color.

As discussed by Walstra (71), breakage of the larger droplets into smaller ones is not the only process occurring during emulsification. Many other processes occur simultaneously. Adsorption of the emulsifier on to newly formed droplet surface is a key process that needs to occur during the timescale of emulsification, otherwise the newly formed droplets that are not adequately stabilized by the emulsifier will recombine and all the disruption is for a naught. In order to adequately stabilize the newly formed emulsion droplets against recombination, first and foremost the emulsifier must be present in sufficient quantity to provide minimally monolayer coverage on the interface and, second, the monolayer coverage must be reached during the timescale of the emulsification process. If the adsorption is too slow, recombination cannot be prevented.

Thus, as described in Fig. 7, drop breakage, emulsifier adsorption, and recombination of the droplets are the three processes of importance. The final droplet size of the emulsion is governed by the balance of the breakage and the recombination processes. The droplet breakage is primarily governed by the time, amount, and distribution of energy input into the system. The recombination step is primarily impacted by the type, amount, and adsorption kinetics of the emulsifier. Efforts to optimize emulsification must account for the interdependencies between the functional properties of the emulsifier and the processing equipment.

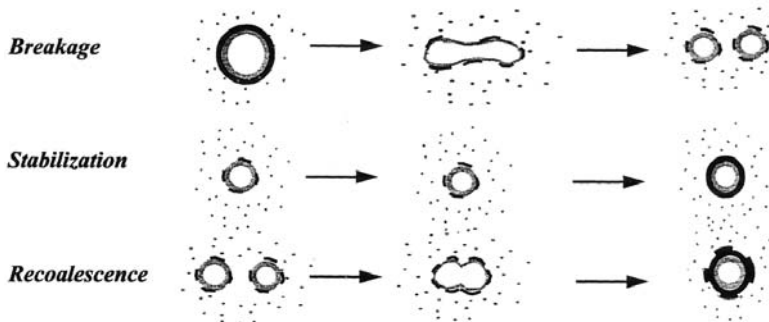


Figure 7 Processes occurring during emulsification. (Adapted from Ref. 71.)

The main steps in an emulsification process are (1) preparation of the oil and aqueous phases with proper incorporation of emulsifiers, hydrocolloids, and other dry ingredients, (2) mixing the phases to form a uniform premix, which may be in the form of either a coarse emulsion or an unstable dispersion, (3) applying shear or other forces to form droplets of the internal phase and reduce the mean droplet size, and (4) allowing sufficient time in the shear zone to adequately cover the internal phase with emulsifier to stabilize the droplets. With the correct emulsifier, food emulsions can be produced with very little mechanical energy input; dressings and sauces have been prepared for hundreds of years using no more than a bowl and a whisk. However, the use of more complex emulsification devices enables product attribute optimization at the lowest cost. Generally, dressings and sauces that are dispersions as opposed to emulsions (typically low- and no-fat dressings and sauces) may be produced on the same process that is used to produce emulsions, although different considerations may take priority, such as the shear rate needed to create a uniform product in the case of a dispersion being of greater importance than the amount of time in the shear zone necessary for emulsifier adsorption in the case of an emulsion.

A. Drop Breakage

Drop breakage occurs in emulsification devices under laminar, turbulent, or cavitation modes, or combinations thereof. Elongational flow is encountered under some conditions. For an excellent account of the drop breakage under these various conditions, the reader is referred to [Chapter 1](#) of Ref. 12.

Studies carried out by Taylor (72) on single droplets under laminar conditions have shown that the drop undergoes steady deformation under shear up to a point at which breakage can occur into smaller fragments. The extent of deformation is characterized by a dimensionless number called the Weber number, We^L , which is defined as the ratio between the deforming shear forces and conservative interfacial forces, which tend to restore the spherical, undeformed shape of the drop:

$$We^L = \frac{\tau}{p_c} = \frac{\tau d}{4\gamma} \quad (2)$$

Here, τ is the shear stress, p_c is the capillary pressure, γ is the interfacial tension and d is the drop diameter. At a certain critical Weber number, a critical deformation state is reached at which rupture occurs.

The critical Weber number is a function of the viscosity ration of the two phases:

$$\text{We}_{\text{crit}}^{\text{L}} = f\left(\frac{\eta_d}{\eta_c}\right) \quad (3)$$

Figure 8 shows the variation of We_{crit} with the viscosity ratio. Thus, the maximum size of the drop that can withstand rupture is given

$$d_{\text{max}} = \frac{4\gamma\text{We}_{\text{crit}}^{\text{L}}}{\tau} \quad (4)$$

Equation (4) shows that selection of both the proper emulsifier to lower interfacial tension and process to provide a high shear rate will aid in achieving a small d_{max} . It is also clear then that in order to cause droplet breakage under laminar conditions, the maximum droplet size that can survive rupture depends strongly on the viscosity ratio. A viscosity ratio of near unity gives the smallest droplet sizes for a given shear input and is the most energy-efficient situation.

Turbulent flow is characterized by eddies of a wide size range. Overall liquid movement is due to the large eddies of the order of the energy-transmitting device such as the agitator. These eddies transfer kinetic energy to the small eddies where viscous dissipation occurs. If a droplet in turbulent

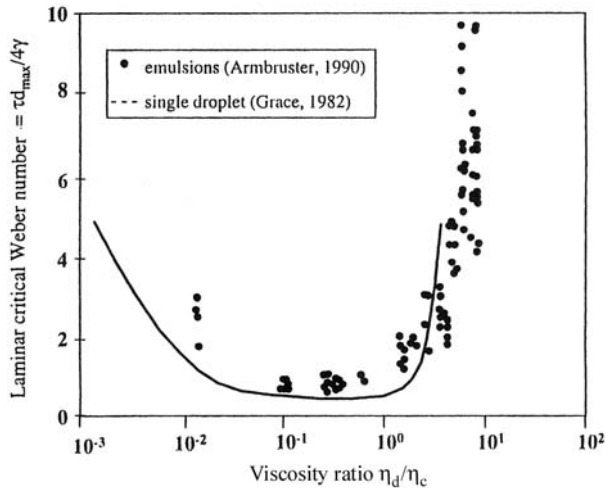


Figure 8 Variation of critical Weber number with viscosity ratio. (From Ref. 75.)

flow is much smaller than the eddy, it follows the movement of the eddy. If, however, it is of a size similar or larger than the eddy, fluctuating velocity gradients at the droplet surface cause droplet deformation, which can lead to rupture. In analogy to the laminar conditions, a turbulent Weber number can be defined as the ratio between the deforming turbulent forces and the restoring interfacial forces:

$$\text{We}^T = \frac{\rho_c v'^2 d}{4\gamma} \quad (5)$$

where ρ_c is the continuous phase density and v' is the eddy velocity. According to the Kolmogoroff theory of isotropic turbulence, we get

$$\text{We}^T \propto \frac{\rho_c \varepsilon^{2/3} d^{5/3}}{\gamma} \quad (6)$$

Rupture, again, occurs when the Weber number exceeds a critical value:

$$\text{We}^T > \text{We}_{\text{crit}}^T \quad (7)$$

Thus,

$$d_{\text{max}} \propto \frac{\gamma^{3/5}}{\rho_c^{3/5} \varepsilon^{2/5}} \quad (8)$$

Equation (8) is valid for d_{max} larger than the size of the small energy-dissipating eddies, which is commonly the case in a simple emulsification device without homogenization facilities.

When the viscosity of the system is large or the drops are very small, Shinnar (73) has suggested that the drop breakage even under highly turbulent conditions occurs due to viscous stresses rather than the inertial stresses, and

$$d_{\text{max}} \propto \left(\frac{\gamma^2}{\rho_c \eta_c \varepsilon} \right)^{1/2} \quad (9)$$

This equation is not fully tested experimentally, perhaps because the high-pressure homogenization condition that are perhaps necessary to achieve small drops involve multiple mechanisms and not simple turbulent shear for drop breakage.

Finally, cavitation is the phenomenon of formation and collapse of small vapor bubbles in a liquid. A high-velocity fluid produces locally negative pressures which lead to the formation of a cavity at that point. As the cavity implodes, it produces a macroscopic shock wave. A nearby droplet can get sucked into the shrinking void and the resultant droplet deformation may lead to its rupture. Cavitation is implicated in ultrasonic emulsification and, perhaps, in a high-pressure homogenization, although Phipps (74), has rejected this notion.

The above equations describing drop breakage assume that the drop stays in a high-energy zone for sufficiently long time for it to deform and break. This critical deformation time depends on the drop viscosity and the excess deforming stress above the conservative interfacial stress

$$t_{\text{def}} = \frac{\eta d}{\tau - p_c} \quad (10)$$

For a drop size reduction by a factor of 10, approximately 10 consecutive disruption steps are necessary, assuming that each disruption step results in two drops of size $(d/2)^{1/3}$. The overall residence time in the high-energy zone must be longer than the sum of individual critical deformation times. The influence of the residence time is particularly evident under turbulent conditions.

B. Emulsifier Effect

Given that the emulsifier is capable of stabilizing the emulsion in the first place, the conditions needed to be met to minimize recoalescence are that the emulsifier is present in sufficient quantity to adsorb on the newly formed surfaces to provide minimally a monolayer coverage and that the kinetics of adsorption are rapid. The approximate monolayer coverage for low-molecular-weight lipid based emulsifiers such as polysorbates is of the order of 5×10^{-10} mol/m² and for macromolecular emulsifiers such as proteins it is of the order of 2–8 mg/m². Based on the interfacial area generated, one can calculate the amount needed for adsorption. The adsorbed emulsifier is in equilibrium with the emulsifier in the bulk. If the adsorption isotherm is known, one can calculate precisely the minimum amount of emulsifier needed. Otherwise, one can add a little excess over the amount needed at the interface.

Adsorption kinetics are governed primarily by the size of the emulsifier molecule. When the emulsifier adsorbs rapidly, the situation is what is called a mechanically limited dispersion. Here, the above drop breakage equations apply, with γ being the equilibrium interfacial tension at the emulsifier concentration involved (this approaches γ_{min} , the minimum

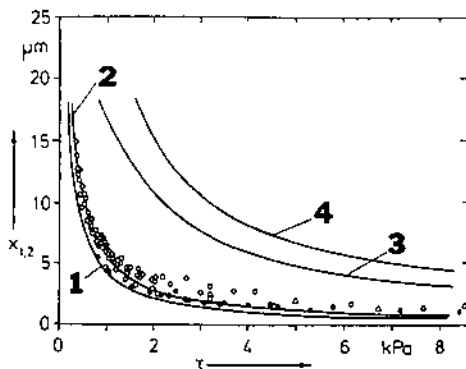


Figure 9 Droplet diameter as a function of shear stress for a fast emulsifier, LEO-10. (From Ref. 75.)

achievable interfacial tension for the emulsifier in question if the emulsifier is present in sufficient excess). When the emulsifier adsorbs slowly, the interfacial tension in the above equations is not the equilibrium interfacial tension at the emulsifier concentration involved but is, in fact, quite a bit higher, resulting in a larger drop size. This situation is described as kinetically limited dispersion. Furthermore, without sufficient adsorption of the emulsifier, the recoalescence process is not completely prevented, further increasing the droplet size obtained. Under laminar conditions, the larger emulsifier molecules show slow adsorption kinetics. Figures 9 and 10 show the droplet sizes obtained for a fast emulsifier LEO-10, lauryl alcohol 10(ethylene oxide) ether, and a slow emulsifier, egg yolk (75).^{*} These data are the first such data known to the authors showing the effect of adsorption kinetics of emulsifier on the final droplet size obtained during emulsification.

Although it is understandable that the larger emulsifier molecules show slow adsorption kinetics under laminar conditions, Walstra (65) has suggested that the exact opposite may be applicable under turbulent conditions, especially when the emulsifier molecular sizes approach the size of the drops. The phenomenon of capture during collisions is then likely involved. Capture efficiencies are expected to be significantly higher for such large emulsifier molecules. No experimental data similar to those of Armbruster are available under turbulent conditions to verify this assertion.

^{*}The lines in the figures are theoretical calculations based on Eq. (4) with the area average diameter estimated to be $d_{\max}/2.4$ for critical Weber numbers estimated from the viscosity ratios (not shown).

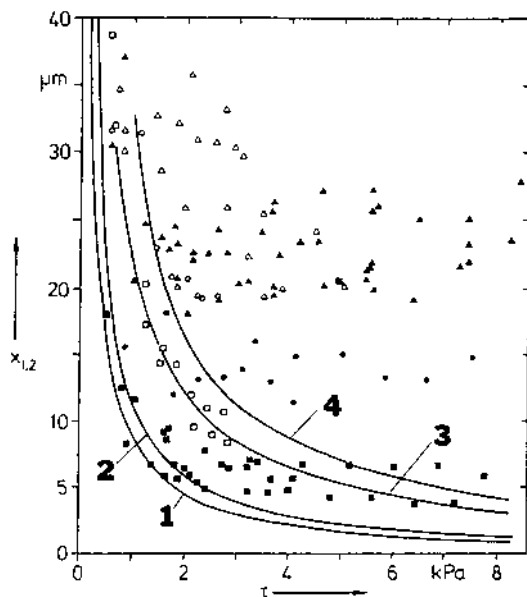


Figure 10 Droplet diameter as a function of shear stress for a slow emulsifier, egg yolk. (From Ref. 75.)

The Weber relationships discussed earlier suggest that droplet size may be reduced by (a) reducing interfacial tension and by (b) increasing process shear rate in the case of laminar flow or fluid velocity in the case of turbulent flow. However, following the above discussion, depending on whether a system is a kinetically or mechanically limited there may be limits on droplet size reduction available in a given system that will drive process developer to modify the selection and operating procedures of emulsification equipment. For example, it is possible to show that when using a homogenizer to process a slow emulsifier system at a constant emulsifier level, there exists an inverse relationship between homogenization pressure and droplet size for low-fat systems such that processing at progressively higher pressures will deliver progressively smaller droplets. However, using the same process and emulsifier systems at a higher fat level, progressively higher pressures will initially yield smaller droplets, but an asymptote will be reached where higher pressures will not reduce droplet size further. Although the initial droplet size may be the same at high pressures for the different fat levels, the extremely short residence time in the homogenizer limits the extent of emulsifier adsorption in the shear zone. Therefore, recoalescence is more likely to occur in the high fat/high surface area system resulting in an asymptotic

relationship between particle size and homogenization pressure such that no further droplet size reduction is possible beyond a certain pressure. If smaller droplets were desired in a high-fat system, it would be necessary to either change the type of emulsifier or equipment to make the system mechanically limited.

C. Process Design and Equipment Selection

Important considerations in designing a food emulsion process include process type (batch versus continuous), order of addition of ingredients, process temperature, and process shear rates. The decision of whether to use a batch or continuous process is driven by consideration of run-time length, space, frequency of manual ingredient additions, and capital requirements. Processes which have a high number of product changeovers and/or a significant number of ingredient additions are ordinarily designed as batch processes. Continuous processes are typically used in cases of long run times and offer advantages of reduced labor and space requirements.

The selection of the final emulsification device that will achieve the minimum droplet size and produce the finished product is of great importance. Although the feed to this device may consist of either a coarse emulsion or an unstable dispersion, a coarse emulsion is often used. The benefit of the coarse emulsion is the partial reduction in droplet size and enhanced uniformity of feed to the final emulsification device. When preparing the feed to this unit operation, a coarse emulsion may be obtained using an emulsifier soluble in the continuous phase and adding the discrete phase to the continuous phase (typically, the discrete phase will be oil and the continuous phase will be aqueous). In a batch process, a mixing tank may be used prior to the shear device to provide the coarse emulsion. A variety of agitator types may be found in the industry, including axial-, radial-, and disk-type impellers. In continuous or semicontinuous processes, the oil and aqueous streams are joined and sheared via in-line mixers to form the coarse emulsion prior to the final emulsification device. Many in-line mixers are also commercially available for this application.

Although many choices are available for the emulsification unit operation, they generally fall into two categories: (1) devices that reduce droplet size via shear forces in laminar flow and (2) devices that reduce droplet size via cavitation and/or shear in turbulent flow (a number of devices employ both methods). Shear forces result from velocity gradients; most shear devices generate shear forces by passing fluid at high velocities through small stationary or moving gaps or by passing fluid from a region of high to low pressure. In general, a higher shear rate will produce a smaller and more uniform droplet size, although there is a point of diminishing returns

and the temperature rise at very high shear rates may be detrimental to the product. Commonly used shear devices include colloid mills, toothed-disk rotor/stator mixers, and pin mixers. Colloid mills utilize a single conical rotor–stator pair in which the rotor surface geometry and the gap between the rotor and stator may be adjusted to vary shear rate. Toothed-disk rotor–stator devices generally consist of three or more sets of rotors/stators in which the tooth geometry, rotor/stator gap size, and rotor may be adjusted to modify shear rate. As discussed earlier, cavitation refers to the implosion of vapor bubbles within a fluid; the resultant shock waves create droplets. Shear generated in turbulent flow may contribute to droplet formation and size reduction due to intense fluid mixing and localized pressure differences. The most common example of this method is homogenization in which vapor bubbles are formed by pressure differential in fluid flow.

The choice of equipment may be driven by formulation. As discussed earlier, products using slow emulsifiers and high oil levels may be better suited to equipment which provides sufficient residence time to allow for droplet stabilization, whereas products using fast emulsifiers and/or low-fat levels may be better suited to equipment such as a homogenizer, which provides significant droplet size reduction with very little residence time in the unit (although for all equipment, residence time is on the order of seconds).

For oil-based dressings and sauces, attention must also be paid to minimizing oxidation of the oil content through the processing and packaging operations. In addition to formulation methods including the use of sequestrants and antioxidants, common methods include processing in an inert-gas environment and the use of barrier packaging materials to displace oxygen from the product and prevent its reintroduction.

Table 6 lists some of the product-impact parameters that should be considered when choosing an emulsification device. Manufacturing considerations such as flexibility in modifying shear rates, sanitary design, CIP ability, energy usage, maintenance costs, changeover flexibility, and ergonomics in disassembly must also be considered and may often define the choice between equipment that has similar effects on product attributes.

It is a common misconception to assume that the central role of an emulsification device is to provide energy input needed because one is increasing the interfacial area, and hence, the interfacial energy of the system. In reality, only a small fraction of the energy input actually goes toward the interfacial energy. Most of it is dissipated as heat. Estimates are that only 0.01% of the energy used in a homogenizer is converted to the interfacial energy. That is why many of the high-energy emulsification devices cause a significant temperature rise in the emulsion, sometimes necessitating a cooling scheme. In fact, a good estimate of the energy

Table 6 Criteria of Emulsification Equipment Selection

Type of machine	Agitated vessel	Colloid mill	Toothed disk dispersers	Homogenizers
Comminution mechanisms	Turbulent shear	Laminar turbulent shear	Turbulent shear	Turbulent shear/cavitation
Energy consumption (W/m ³)	10 ³ –10 ⁵	10 ⁶ –10 ¹¹	10 ⁸ –10 ⁹	10 ¹¹ –10 ¹³
Residence time (s)	Undefined	10 ⁻³ –10 ⁻¹	10 ⁻³ –10 ⁻²	10 ⁻⁵ –10 ⁻⁴
Droplet size (μm)	5–100	2–20	2–20	0.5–5
Suitable for high-fat o/w emulsions	±	+	+	–
Suitable for low viscosities	–	±	±	+
Suitable for high viscosities	±	+	+	–
Addition of particulates	+	–	±	–
Indirect heating/cooling	+	±	±	–
Direct steam injection	+	±	±	–
Continuous processing	–	+	+	+
Batch processing	+	+	+	–

input by an emulsification device can be made from the temperature rise obtained if no cooling is provided or from a heat balance if cooling is provided. In the case of a homogenizer, for every 1000 psi homogenizing pressure, the temperature rise is approximately 3° F.

VI. NONCLASSIC DRESSINGS AND SAUCES

In previous sections, the full-fat versions of traditional emulsion-based products have been presented and, in this chapter, will be referred to as classic emulsions. In this section, nonclassic emulsions will be considered as no-fat to low-fat versions of standard full-fat products.

On a chronological basis, spoonable salad dressings developed in the 1930s can be considered as a first-generation, reduced fat mayonnaise-like dressing. Oil levels were reduced from 80% in mayonnaise to 45–50% in salad dressing. With this substantial reduction in dispersed phase volume, significantly thinner texture was supplemented through the use of starches. Flavor changes were masked through targeting a tarter, sweeter, and more spicy profile.

During the mid-1980s, “light” dressings were introduced. Gums were included in formulations to add texture such as mouth-feel, cling, firmness, slipperiness, and so forth that could not be provided in an acceptable manner through merely increased levels of starch.

Then, during the early 1990s, fat-free dressings were developed. In most cases, starches and gums used alone or in conjunction with each other were not able to deliver the texture and flavor necessary to gain satisfactory consumer acceptance. Fat replacers or fat mimetics were the technologies developed for the most part to provide the additional texture and appearance characteristics needed.

The progression of fat/emulsion phase reduction is readily apparent in a microscopic investigation. The loss of a significant portion of the fat in the move to fat free is evidenced in the example of spoonable salad dressings in which the increasing role of starch and fibrillarlike fat replacers are shown as the fat/emulsion phase is reduced from full fat (48%), light (23%), and fat free (2–3%) (Figs. 11–11c).

Earliest fat replacers were built on the concept of non-digestible fat like molecules. Olestra from Procter and Gamble was developed in the 1960s from sugar and fatty acids to produce sucrose hexa, hepta and octa fatty acid esters. This fat replacer was designed to replace oil on a one-to-one basis, functioning as the hydrophobic phase in emulsions and even capable of fried and cooked applications. However, its non digestibility and macro ingredient status raised issues concerning fat-soluble vitamin depletion and

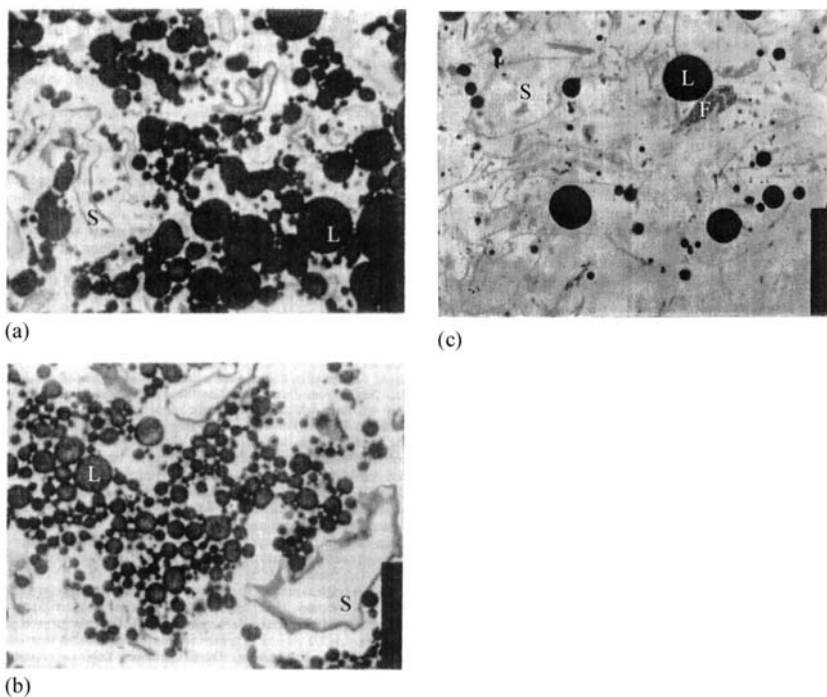


Figure 11 The microstructure of spoonable salad dressing. (a) Section of stained, full-fat sample viewed with bright-field light microscopy. Lipid droplets (L) are numerous and are separated by some starch granules. Scale bar equals 25 μm . (b) Section of stained, “light” sample viewed with bright-field light microscopy. Lipid droplets (L) are significantly less numerous and are separated by more starch granules. Scale bar equals 25 μm . (c) Section of stained, fat-free sample viewed with bright-field light microscopy. Lipid droplets (L) are scant and are separated by starch granules and fibrillarlike material. Scale bar equals 25 μm .

the body’s ability to handle it as waste. A number of similar products have been developed such as esterified polysaccharides, carboxylate esters, and so forth by various companies but none of them are in use in dressings and sauces.

During the late 1980s a paradigm shift occurred such that rather than trying to replace all of the functionality of fat with a fatlike molecule, of perhaps some of the functionality of fat could be substituted through micro-particulates. The original product based on this concept was Simplese from the NutraSweet Company. Using egg and dairy protein as source materials, a creamy material was produced which was composed of spherical protein

particles in the 0.5–2.0- μm diameter range. It was claimed that the particulates produced a ball-bearing effect in the mouth. Later, larger particles were also found to work if soft and compressible. This concept was soon transferred to carbohydrate-based materials and their gels. Starch and gum technologies were reevaluated and novel textures were developed to supplement conventional usages. It was this paradigm shift in the 1980s that led to the successful introduction of fat-free products.

The original approach for replacing the functionality of the fat from the emulsion phase was to search for a “magic bullet” ingredient which would target all the product needs. This approach was only somewhat successful in products which fat contributed in fairly straightforward and minor ways to texture and where the product had strongly characterizing flavors which were mostly independent on fat contribution or interaction. A systems approach was soon adopted to replace specific product functionality of the fat by specific fat-replacement technology. The impact of fat in the emulsion phase is evidenced in the product in appearance, texture, mouth-feel, stability, handling, and, most importantly, flavor (Fig. 12).

Flavor character, release, and stability continued to be a major hurdle in the nonclassic emulsion dressings. Fat is known to play an important role in the flavor perception of foods. It influences the temporal profile, flavor impact, perception of flavor notes, and the order of their occurrence (76). The fat replacers in use today are composed of proteins and carbohydrates, which interact with the flavor compounds differently than fat does (77,78). For example, flavors are known to bind to proteins (79) and starches (80).

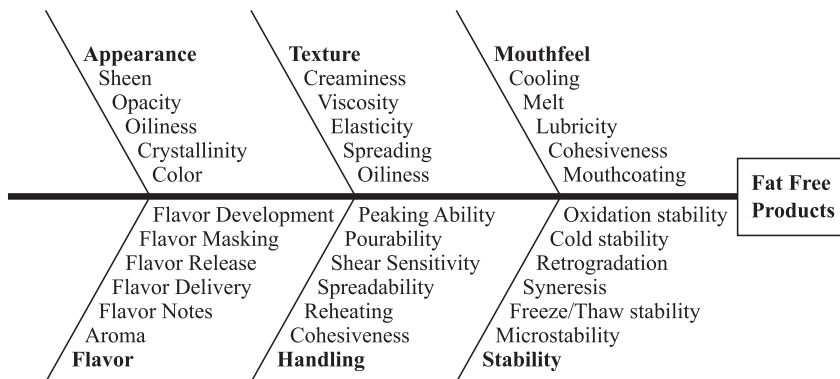


Figure 12 Functional considerations in the development of fat free products. (Adapted from *Prepared Foods*, December 1992, p. 21.)

The influence of the oil phase in the emulsion of classic emulsions on the production, perception, and preservation of flavors was considerable and presented many challenges for replication in nonclassic dressings. The near absence of fat in fat-free products posed a difficult challenge in achieving full-fat flavor (Table 1). An understanding of these flavor effects now became necessary.

The overwhelming majority of food flavors are complex mixtures of compounds. These flavors come to dressings through ingredients, product processing during manufacturing, flavor addition, chemical reactions during storage, physical changes including repartitioning of and/or loss of phases, and final food preparation.

Preception of flavor depends not only on the presence of proper flavor compounds at the appropriate intensity but the timing of the flavor release and masking effects as well. In nonclassic emulsions, the increased presence of water and the hydrophilic molecules of starch, gum, and other fat replacers dramatically affects the partitioning of volatile hydrocarbon flavor compounds. This effect significantly affects flavor intensity perception and release rates. The masking effect of the dispersed oil in the emulsion of classic emulsions plays an important role in rounding flavor perception and covering low-level off-flavors. Also, the presence of fat affects the binding of flavors by various hydrophobic sites in carbohydrates and proteins. Quality gaps in fat-free products along with low regulatory hurdles have recently opened the door for reduced-calorie fats. Products such as Caprenin and Salatrim are special triglycerides based on specific fatty acid profiles which digest at lower caloric values. These products could allow for an intermediate approach of using lower levels (but not fat free) of a fat ingredient at a significantly reduced calorie impact.

VII. CONCLUSIONS AND PROGNOSTICATION

There are four significant trends in the dressings and sauces industry. First is the introduction of increasing number of low-fat and fat-free dressings and the continuing effort to improve these products. Second is a steady launch of new products, especially new flavors, especially in sauces and pourable dressings categories. Third is the growing need to cut the cost of production. Fourth are next trends of healthy foods—for example, based on new fats and oils such as diacyl glycerols (DAGs) such as Enova oil recently introduced in the market by ADM Kao. Accomplishing this will involve changes in formulation and processing. Developing products scientifically would necessitate application of disciplines such as rheology, microscopy, and emulsion stability theory; the objective data provided

by such disciplines will have to be correlated with sensory evaluation of the products.

Particularly critical is the advancement of fundamental understanding of emulsion stability. Successful predictive tests for emulsion stability can significantly reduce the product development cycle time. We believe here that the role of thin films in the stability of emulsions is an emerging field of study that is likely to be the key to predicting emulsion stability of dressings and sauces over the shelf life as well to their processing.

Microscopy of foods has come a long way in recent years. For a recent review of available techniques, see Ref. 81. Significant technical advances in the field of microscopy include cryo-fixation methods, which will replace chemical fixation with a reduction in processing time and elimination of artifacts. Expanded applications will be made of immunocytochemical methods to determine the location of target proteins in various food systems. Computer-aided image analysis and enhancement systems will allow more objective, rapid, and accurate analysis of microscopic data than current morphometric and stereological methods. Application will be made of confocal microscopy and the “optical sectioning” capability of that technique. The scanning tunneling microscope [and the atomic force microscope (AFM)] will be used to resolve structure at a molecular level.

Advances in theory and instrumentation have allowed rigorous viscoelastic characterization of food products. As discussed, newer techniques are being developed to characterize extensional properties and tribology of the products.

With better microscopic and rheological techniques, it will be possible to relate microstructure to rheology and, finally, sensory textural characteristics of the product, a goal which has heretofore remained elusive. These techniques, and others, will be used to understand and predict the emulsion stability of dressings and sauces.

REFERENCES

1. N. N. Potter, *Food Science*, 4th ed. AVI, Westport, CT, 1986, pp. 457–458.
2. C. M. Chang, W. D. Powrie, and O. Fennema, Electron microscopy of mayonnaise, *Can. Inst. Food Sci. Technol. J.* 5, 134–137 (1972).
3. M. Tanaka and H. Fukuda, Studies on the texture of salad dressings containing xanthan gum, *Con. Inst. Food Sci. Technol. J.* 130–134 (1976).
4. M. A. Tung and L. J. Jones, Microstructure of mayonnaise and salad dressing, *Scanning Electron Micros.* 3 523–530 (1981).
5. W. Flukiger, Die fliesseigenschaften von emulsonen, *Fette-Seifen Anstrichmittel* 69, 449–452 (1967).

6. D. F. Darling and R. J. Birkett, Food colloids in practice, in *Food Emulsions and Foams* (E. Dickinson, ed.), Royal Society of Chemists, London, 1986, 1–29.
7. I. Heertje, P. van der Vlist, J. C. G. Blonk, H. A. C. Hendricks, and G. J. Brakenhoff, Confocal scanning laser microscopy in food research: Some observations, *Food Microstruct.* 6, 115–120 (1987).
8. R. K. Salyaev, A method of fixation and embedding of liquid and fragile materials in agar microcapsulae, in *Proc. 4th European Regional Conf. Electron Microscopy*, 1968, pp. 37–38.
9. M. Kalab, Electron microscopy of milk products: A review of techniques. *Scanning Electron Microsc.* 3, 453–472 (1981).
10. P. Allan-Wojtas and M. Kalab, Fixation of fat globules in whole milk yogurt for electron microscopy, *Milchwissenschaft* 39, 323–327 (1984).
11. M. Liboff, R. D. Goff, Z. Haque, and J. E. Kinsella, Changes in the ultrastructure of emulsions as a result of electron microscopy preparation procedures, *Food Microstruct.* 7, 67–74 (1988).
12. P. Sherman (ed.), *Emulsion Science*, Academic Press, New York, 1968.
13. S. D. Holdsworth, Applicability of rheological models to the interpretation of flow and processing behavior of fluid food products, *J. Texture Studies*, 2, 393–418 (1971).
14. O. Flint, Food emulsions, in *Food Microscopy A Manual of Practical Methods, Using Optical Microscopy*, Bios Scientific, 1987, pp. 113–118.
15. L. Munck (ed.) *Fluorescence Analysis in Foods*, Wiley New York, 1989.
16. T. Sengupta, and S. Damodaran, Lateral phase separation in adsorbed binary protein films at the air-water interface, *J. Food Chem.* 49 (6), 3087–3091 (2001).
17. I. Heertje, J. Nederlof, H. A. C. M. Hendricks, and E. H. Lucassen-Reynders, The observation of the displacement of emulsifiers by confocal scanning laser microscopy, *Food Struct.* 9, 305–316 (1990).
18. M. Langton, A. Astrom, and A.-M. Hermansson, Microscopy in relation to the textural properties of mayonnaise, in *Food Emulsions and Foams: Interfaces, Interactions and Stability* RSC, Cambridge, 1999, pp. 366–376.
19. R. P. Borwankar, Food texture and rheology: A tutorial review, *J. Food Eng.* 16, 1–16 (1992).
20. F. Shama and P. Sherman, Identification of stimuli controlling the sensory evaluation of viscosity. I. Oral methods. *J. Texture Studies*, 111–118 (1973).
21. J. L. Kokini, Fluid and semi-solid texture and texture taste interactions, *Food Technol.* 39(11), 86–94 (1985).
22. R. L. McDermott, W. J. Harper, and R. Whitley, A centrifugal method for characterization of salad dressing emulsions, *Food Technol.* 98, 81–87 (1981).
23. G. Atkin and P. Sherman, Further application of the modified gel rigidity modulus apparatus, *J. Texture Studies* 10, 253–259 (1980).
24. R. Fischbach and J. L. Kokini, Effect of aging and mustard flour on rheological properties of model O/W emulsion, *J. Food Sci.* 52, 1748–1749 (1987).
25. V. D. Kiosseoglou and P. Sherman, The influence of egg yolk lipoproteins on the rheology and stability of o/w emulsions and mayonnaise. 1. Visco-elasticity

- of groundnut oil-in-water emulsions and mayonnaise, *J. Texture Studies* 14, 397–417 (1983).
26. J. I. Lewis and C. F. Shoemaker, A method for measurement of the transient response of semisolid foods under steady shear, *J. Food Sci.* 49, 741–755 (1984).
 27. E. J. Vernon-Carter and P. Sherman, Rheological properties and applications of mesquite tree (*Prosopis juliflora*) gum. 4. Rheological properties of mesquite gum films at the oil water interface, *J. Dispers Sci. Technol.* 2, 399–413 (1981).
 28. E. J. Vernon-Carter and P. Sherman, Rheological properties and applications of mesquite tree (*Prosopis juliflora*) gum. 5. The rheological properties and stability of corn oil-in-water emulsions stabilized by blends of mesquite gum and Tween 60, *J. Dispers Sci. Technol.* 2, 415–431 (1981).
 29. K. K. Bistany and J. L. Kokini, Comparison of steady shear rheological properties and small amplitude dynamic visco-elastic properties of fluid food materials, *J. Texture Studies* 14, 113–124 (1983).
 30. M. Dervisoglu and J. L. Kokini, Steady shear rheology and fluid mechanics of four semi-solid foods, *J. Food Sci.* 51, 541–546 (1986).
 31. J. H. Elliott and A. J. Ganz, Salad dressings—Preliminary rheological characterization, *J. Texture Studies* 8, 369–371 (1977).
 32. J. L. Kokini and A. Dickie, A model of food spreadability from fluid mechanics, *J. Texture Studies*, 13, 211–227 (1981).
 33. J. A. Blake and J. J. Morn, A new approach to capillary extrusion rheometry, *J. Texture Studies* 5, 227–239 (1975).
 34. O. H. Campanella and M. Peleg, Analysis of the transient flow of mayonnaise in a coaxial viscometer, *J. Rheol.* 31, 439–452 (1987).
 35. O. H. Campanella and M. Peleg, Determination of the yield stress of semiliquid foods from squeezing flow data, *J. Food Sci.* 52, 214–215 (1987).
 36. V. D. Kiosseoglou and P. Sherman, The rheological conditions associated with judgment of pourability and spreadability of salad dressings, *J. Texture Studies* 14, 277–282 (1983).
 37. P. Kovacs and B. D. Titlow, Stabilizing cottage cheese creaming emulsions with a xanthan blend, *Am. Dairy Rev.* 34J–34M (1976).
 38. N. Gladwell, M. J. Grimson, R. R. Rahalkar, and P. Richmond, Rheological behavior of soy oil-water emulsions: Dependence upon one concentration, *J. Food Sci.* 60, 440–443 (1985).
 39. N. Gladwell, M. J. Grimson, R. R. Rahalkar, and P. Richmond, Linear visco-elastic behavior of sterically stabilized oil-water emulsions, *J. Chem. Soc., Faraday Trans 2* 81, 643–652 (1985).
 40. M. A. Rao, Measurement of flow properties of fluid foods—developments, limitations, and interpretation of phenomena, *J. Texture Studies*, 8, 257–282 (1977).
 41. Boger and Tiu 1974.
 42. C. Pascual, M. C. Alfaro, and J. Munoz, *Food Emulsions and Foams: Interfaces, Interactions and Stability*. E. Dickinson and J. M. Rodriguez Patino, eds.), RSC, Cambridge, 1998, pp. 356–365.

43. H. A. Barnes and K. Walters, The yield value myth? *Rheol. Acta* 24, 323–326 (1985).
44. G. W. Scott Blair, *J. Appl. Phys.* 4, 113 (1933).
45. N. J. Alderman, G. H. Meeten, and J. D. Sherwood, Vane rheometry of bentonite gels, *J. Non-Newtonian Fluid Mech.* 39, 291–310 (1991).
46. N. A. Park, R. G. Irvine, Jr., and F. Gui, Yield stress measurements with the falling needle viscometer, *Xth Int. Cong. on Rheology*, 1988.
47. N. A. Park and T. F. Irvine, Jr., The falling needle viscometer: A new technique for viscosity measurements. *Am. Lab.* 58–63 (1988).
48. J. Plucinski, R. K. Gupta, and S. Chakrabarti, Shear and extensional rheology of mayonnaises *Second International Meeting of Shear and Extensional Flow of Polymer Fluids from the Solution to the Melt*, 1994.
49. S. Giasson, J. Israelachvili, and H. Yoshizawa, Thin film morphology and tribology of food emulsions *J. Food Sci.* 62, 640–646 (1997).
50. P. Sherman (ed.), *Rheology of Emulsions*, Pergamon Press, Oxford, 1963.
51. P. Sherman (ed.), *Food Texture and Rheology*, Academic Press, New York, 1978.
52. R. J. Hunter, *Introduction to Modern Colloid Science*, Oxford Science, Oxford, 1993.
53. C. F. Chan Man Fong, G. Turcotte, and D. De Kee, Modelling steady and transient rheological properties, *J. Food Eng.* 27, 63–70 (1996).
54. J. I. Amemiya and C. F. Shoemaker, Measurement of thixotropy of model food colloidal suspensions with step change shear rate, in *Rheology of Foods* (R. P. Borwankar and C. F. Shoemaker, eds.), Elsevier, New York, 1992, pp. 17–24.
55. H. M. Princen, Rheology of foams and highly concentrated emulsions. J. Elastic properties and yield stress of a cylindrical model system. *J. Colloid Interf. Sci.* 91, 160–175 (1983).
56. I. B. Ivanov, Effect of surface mobility on the dynamic behavior of thin liquid films. *Pure Appl. Chem.* 52, 1241–1261 (1980).
57. I. B. Ivanov and D. S. Dimitrov, Thin film drainage, in *Thin Liquid Films* (I. B. Ivanov, ed.), Marcel Dekker, New York, 1988.
58. D. T. Wasan, Interfacial transport processes and rheology: Structure and dynamics of thin liquid films. *Chem. Eng. Ed.* 104, (1992).
59. A. D. Nikolov and D. T. Wasan, Ordered micelle structuring in thin films formed from anionic surfactant solutions: part I—Experimental. *J. Colloid Interf. Sci.* 133, 1–12 (1989).
60. A. D. Nikolov, P. A. Krachevsky, I. B. Ivanov, and D. T. Wasan, Ordered micelle structuring in thin films formed from anionic surfactant solutions: Part II—Model development. *J. Colloid Interf. Sci.* 133, 13–22 (1989).
61. K. Koczó, A. D. Nikolov, D. T. Wasan, R. P. Borwankar, and A. Gonsalves, Layering of sodium caseinate sub-micelles in thin liquid films. *J. Colloid Interf. Sci.* 178(2), 694–702 (1996).
62. S. U. Pickering, *J. Chem. Soc.* 91, 2001 (1907).
63. W. D. Harkins and N. Sollman, Interfacial tension and emulsification. I. The effects of bases, salts, and acids upon the interfacial tension

- between aqueous sodium oleate solutions and benzene, *J. Am. Chem. Soc.* 48, 69 (1926).
64. P. Graham, The conformation of proteins at interfaces and their role in stabilizing emulsions, in *Theory and Practice of Emulsion Technology* (A. L. Smith, ed.), Academic Press, New York, 1976, pp. 75–98.
 65. P. Walstra, Overview of emulsion and foam stability, in *Food Emulsions and Foams* (E. Dickinson, ed.), Royal Society of Chemists, London, 1987.
 66. W. D. Powrie and S. Nakai, The chemistry of eggs and egg products in *Egg Science and Technology* (W. J. Stadelman and O. J. Cotterill, eds.), Food Products Press, 1990, pp. 97–139.
 67. R. E. Baldwin, Functional properties of eggs in foods in *Egg Science and Technology* (W. J. Stadelman and O. J. Cotterill eds.), Food Products Press, 1990, pp. 345–383.
 68. T. M. Riddick, *Control of Colloid Stability Through Zeta Potential*. Zeta-Meter, Inc., 1968, p. 150.
 69. J. W. Corran, Emulsification by mustard, *Spice Mill* 57, 175 (1934).
 70. B. H. Webb, A. H. Johnson, and J. A. Alford, *Fundamentals of Dairy Chemistry*, 2nd ed. AVI Westport, CT, 1983, p. 90.
 71. P. Walstra, Formation of emulsions, in *Encyclopedia of Emulsion Technology, Vol. I: Basic Theory*, (P. Becher, ed.), Marcel Dekker, New York, 1983.
 72. G. I. Taylor, *Proc. R. Soc. London A* 146, 501 (1934).
 73. R. Shinnar, On the behavior of liquid dispersions in mixingvessels, *J. Fluid Mech.* 10, 259–275 (1961).
 74. L. Phipps, *The High Pressure Dairy Homogenizer*, National Institute for Research in Dairying, Reading, PA, 1985.
 75. H. Armbruster, Untersuchungen zum kontinuierlichen Emulgierprozess in Kolloidmuhlen unter Berücksichtigung spezifischer Emulgatoreigenschaften und Stromungsverhältnissen im Disperfierspalt. Dissertation, University of Karlsruhe, Karlsruhe, Germany.
 76. L. C. Hatchwell, *Implication of Fat on Flavor in Flavor–Food Interactions* (R. J. McGorin and J. V. Leland, eds.), ACS Symposium Series 633, American Chemical Society, Washington, DC, 1996, pp. 14–23.
 77. J. Bakker, Flavor interactions with the food matrix and their effects on perception in *Ingredient Interactions* (A. G. Gaonkar, ed.), Marcel Dekker, New York, 1995, 411–439.
 78. G. A. Reineccius, Flavor fat replacer Interactions in foods, in *Ingredient Interactions* (A. G. Gaonkar, ed.), Marcel Dekker, New York, 1995, pp. 441–450.
 79. T. E. O’Neill, *Flavor Binding by Food Proteins: An Overview in Flavor–Food Interactions* (R. J. McGorin and J. V. Leland, eds.), ACS Symposium Series, 633 American Chemical Society, Washington, DC, 1996, pp. 59–74.
 80. M. Y. M. Hau, D. A. Gray, and A. J. Taylor, *Binding of volatiles to Starch in Flavor–Food Interactions* (R. J. McGorin and J. V. Leland, eds.), ACS Symposium Series 633 American Chemical Society, Washington, DC, 1996, pp. 109–117.

81. M. G. Smart, R. G. Fulcher, and D. G. Pechak, Recent developments in the microstructural characterization of foods, in *Characterization of Foods: Emerging Methods* (A. G. Gaonkar, ed.), Elsevier, New York, 1995, pp. 233–275.
82. J. Sestak, R. Zitny and M. Houska, Simple rheological models food liquids for process design and quality assessment, *J. Fodo Eng.* 35–49 (1983).

14

Analysis of Droplet Characteristics Using Low-Intensity Ultrasound

John N. Coupland

*The Pennsylvania State University, University Park,
Pennsylvania, U.S.A.*

D. Julian McClements

The University of Massachusetts, Amherst, Massachusetts, U.S.A.

I. INTRODUCTION

A. Introduction

Sensory and bulk physicochemical properties of food emulsions, such as texture, stability, appearance, and taste are largely determined by the characteristics of the droplets that they contain (i.e., particle size distribution, disperse phase volume fraction, physical state, and colloidal interactions) (1). For example, the rate at which droplets cream or sediment due to gravitational forces is strongly dependent on their size. The characteristics of the droplets in a particular emulsion are governed principally by the ingredients it contains, the homogenization technique used to prepare it, and the environmental conditions it experiences during manufacture, storage, and consumption and may change appreciably during the lifetime of the product due to various instability mechanisms. For these reasons and because it is impossible to accurately predict the structure/functionality for many real systems, it is important to have analytical techniques that can be used to measure the characteristics of the droplets in emulsions.

The compositional and microstructural complexity of food emulsions often makes traditional methods of droplet characterization unreliable (e.g., microscopy, light scattering, and electrical pulse counting). Consequently, the development of novel methods of characterizing droplet characteristics in food emulsions has gained impetus in recent years. The ideal analytical technique for measuring droplet characteristics would be non-destructive, simple to use, versatile, rapid, reproducible, and reasonably priced. It would also be valuable to be able to make measurements on emulsions during the manufacturing process, so the technique should meet hygienic processing standards and be robust enough to survive in a factory environment. Analytical techniques based on ultrasound meet many of these requirements.

B. Ultrasonic Propagation in Food Emulsions

Analytical techniques based on ultrasound use high-frequency mechanical vibrations (typically between 20 kHz and 200 MHz) to provide information about the composition, structure, or dynamics of materials (2). Ultrasonic waves are qualitatively similar to sound waves, but their frequencies are too high for the human ear to detect. Ultrasonic waves propagate through materials as small deformations in the thermal–mechanical properties (i.e., as small deviations in the average temperature and pressure of the material). The power levels used in the ultrasonic analysis of food emulsions are so low that the deformations caused in the material are extremely small and reversible, which means that the technique is nondestructive.

In general, the most commonly used ultrasonic waves for characterizing materials are *longitudinal* waves and *shear* waves. In longitudinal waves, the deformations occur parallel to the direction of transmission of the wave, whereas in shear waves, the deformations occur perpendicular to the direction of transmission. The longitudinal ultrasonic properties of a material are fundamentally a function of the compressibility of a material and the amount of material to be compressed (i.e., density). Shear waves are highly attenuated in most fluids and so they are rarely used to characterize food emulsions and are not discussed further here.

The parameters that are most commonly measured in an ultrasonic experiment are the ultrasonic velocity, c , and the ultrasonic attenuation coefficient, α :

$$c = \frac{d}{t} = \lambda f \quad (1)$$

$$\frac{A}{A_0} = e^{-\alpha d} \quad (2)$$

where d is the distance traveled by the wave in t , λ is the wavelength of the ultrasonic wave, f is the frequency of the ultrasonic wave, and A and A_0 are the initial and final amplitudes of the ultrasonic wave. The overall ultrasonic characteristics of a material are represented by the complex propagation constant, $k = \omega/c + i\alpha$, where ω is the angular frequency ($=2\pi f$) and i is $\sqrt{-1}$. Velocity and attenuation are fundamental physical properties of the emulsion but are only useful if they can be measured accurately and related to the droplet properties of interest.

During recent years, there have been considerable advances in the development of mathematical theories to describe the propagation of ultrasonic waves through emulsions (3–5). These theories can be used to relate the measurable ultrasonic properties of an emulsion (i.e., c , α , or k) to the droplet characteristics of the emulsion (e.g., particle size distribution and dispersed phase volume fraction). A simplified version of the theory is presented here, which is suitable for application to relatively dilute emulsions containing nonfloculated droplets in the long-wavelength limit (i.e., $r \ll \lambda$) (5):

$$\left(\frac{K}{k_1}\right)^2 = \left(1 - \frac{3i\phi A_m}{(k_1 r)^3}\right) \left(1 - \frac{9i\phi A_d}{(k_1 r)^3}\right), \quad (3)$$

where K is the complex propagation constant of the emulsion ($=\omega/c + i\alpha$), k_1 is the complex propagation constant of the continuous phase, ϕ is the dispersed phase volume fraction, and A_m and A_d are the monopole and dipole scattering coefficients, respectively, individual droplets. Scattering coefficients appropriate for fluid-in-fluid colloidal dispersions and for solid-in-fluid colloidal dispersions are available in the literature (6). Nevertheless, calculation of these coefficients requires knowledge of many physiochemical properties of the oil and water phases (e.g., ultrasonic velocity, attenuation coefficient, specific heat capacity, thermal conductivity, density, and cubical expansion coefficient). The need for all of this information in order to interpret ultrasonic measurements is currently one of the major drawbacks of ultrasonic analysis techniques, although an increasing amount of data is being tabulated in the literature (7). The ultrasonic velocity and attenuation coefficient of an emulsion are determined from the complex propagation constant using the following relationships: $c = \omega/\text{Re}(K)$ and $\alpha = \text{Im}(K)$.

It is informative to examine the physical significance of the scattering coefficients (A_m and A_d) that appear in the theories used to model the ultrasonic properties of emulsions.

1. Monopole Scattering Coefficient, A_m

The droplets and surrounding liquid expand and contract to different extents in the presence of the pressure fluctuations associated with an ultrasonic wave (Fig. 1a). Consequently, the droplet pulsates relative to the surrounding liquid, thus generating a monopole pressure wave that propagates into the surrounding liquid. Most of this monopole wave is not detected in the forward direction, which leads to an increase in the attenuation of the emulsion referred to as the *monopole scattering loss*. In addition, because of pressure–temperature coupling, there is a fluctuating temperature gradient between the droplet and surrounding liquid that causes heat to flow backward and forward across the droplet interface. This process is usually irreversible because the heat flow into the droplet is less than the heat flow outward. As a result, some of the ultrasonic energy is converted to heat, which leads to an increase in the attenuation of the emulsion referred to as the *thermal absorption loss*. The distance that the thermal wave propagates into the surrounding liquid is characterized by the *thermal skin depth*, δ_T :

$$\delta_T = \sqrt{\frac{2\tau_1}{\rho_1 C_P \eta_1 \omega}} \quad (4)$$

where the angular frequency is ω , the density is ρ , the specific heat capacity is C_P , the thermal conductivity is τ , and the viscosity is η (subscript 1 refers to the continuous phase). This equation indicates that the thickness of the thermal wave increases as the frequency of the ultrasonic wave decreases.

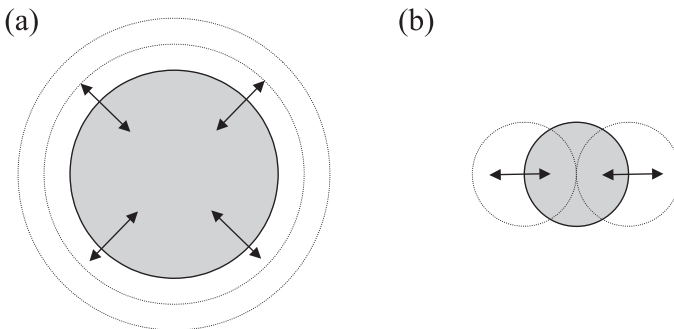


Figure 1 Diagram (not to scale) illustrating models of ultrasonic scattering from an emulsion droplet: (a) thermal (monopolar) scattering; (b) viscous (dipolar) scattering.

The thermal absorption loss is much greater than the monopole scattering loss in the long-wavelength limit.

2. Dipole Scattering Coefficient, A_d

As an ultrasonic wave passes through an emulsion, it causes the droplets to oscillate backward and forward because of the density difference between them and the surrounding liquid (Fig. 1b). The movement of the droplets relative to the surrounding liquid leads to the generation of a dipolar pressure wave. Most of this dipole wave is not detected in the forward direction, which leads to an increase in the attenuation of the emulsion referred to as the *dipole scattering loss*. In addition, the oscillation of the droplet is damped because of the viscosity of the surrounding liquid, and so some of the ultrasonic energy is lost as heat, which leads to an increase in the attenuation of the emulsion referred to as the *viscoinertial absorption loss*. The distance that the viscoinertial wave propagates into the surrounding liquid is characterized by by *viscoinertial skin depth*, δ_S :

$$\delta_S = \sqrt{\frac{2\eta_1}{\rho_l\omega}} \quad (5)$$

This equation indicates that the thickness of the viscoinertial wave also increases as the frequency of the ultrasonic wave decreases (8). The viscoinertial absorption loss is much greater than the dipole scattering loss in the long-wavelength limit.

3. Limitations of the Theory

The above theory assumes that the emulsions are dilute enough so that multiple-scattering effects are unimportant and that the thermal and viscoinertial waves generated by one droplet do not overlap those generated by neighboring droplets (9). Multiple-scattering and viscoinertial overlap effects are usually quite small in food emulsions, but thermal overlap effects can be appreciable and lead to a significant reduction in the attenuation coefficient compared to that predicted by Eq. (3), (9). The deviations between theory and experiment increase as the ultrasonic frequency decreases, the particle size decreases, and the droplet concentration increases. For example, in Fig. 2, the simple theory set out in Eq. (3) predicts that attenuation should increase with droplet concentration, whereas the experimental observations indicate a maximum close to $\phi = 50\%$. Beyond this concentration, the thermal layers of adjacent droplets begin to overlap and each individual particle is less able to convert sound energy to heat;

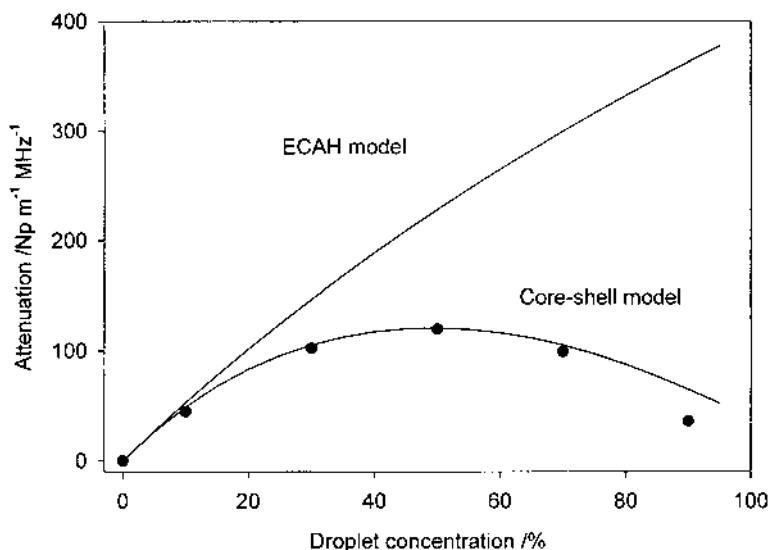


Figure 2 Ultrasonic attenuation coefficient (at 10 MHz) of an *n*-hexadecane oil-in-water emulsion ($r_{32}=0.2\mu\text{m}$) as a function of emulsion concentration. Two theoretical lines are shown alongside the data: the Epstein–Carhart–Alegra–Hawley (ECAH) model and a more sophisticated core–shell scattering theory described in the text.

hence, the total attenuation is reduced. Similarly, when considering the attenuation spectra of different concentrations of fine (Fig. 3a) and coarse emulsions (Fig. 3b), the simple theory in Eq. (3) gives an adequate fit when the skin overlap is not significant (i.e., large, dilute particles at high frequency).

Recently, a number of methods of incorporating thermal overlap (10) and visco-inertial overlap (11) effects into the ultrasonic scattering theory have been proposed and combined to produce a comprehensive core–shell scattering theory that gives a good description of the ultrasonic properties of emulsions over a wide range of conditions (Fig. 2; the core–shell theory also gives a good description of the data in Fig. 3, but these lines are not shown here).

Another major limitation of the theory is that it assumes that the droplets are randomly dispersed in the emulsion. If the droplets undergo flocculation, then there may be an appreciable deviation between the ultrasonic scattering theory and experimental measurements because of thermal overlap and scattering effects. In a flocculated emulsion, the droplets are in close proximity, which leads to a greater degree of thermal overlap and a

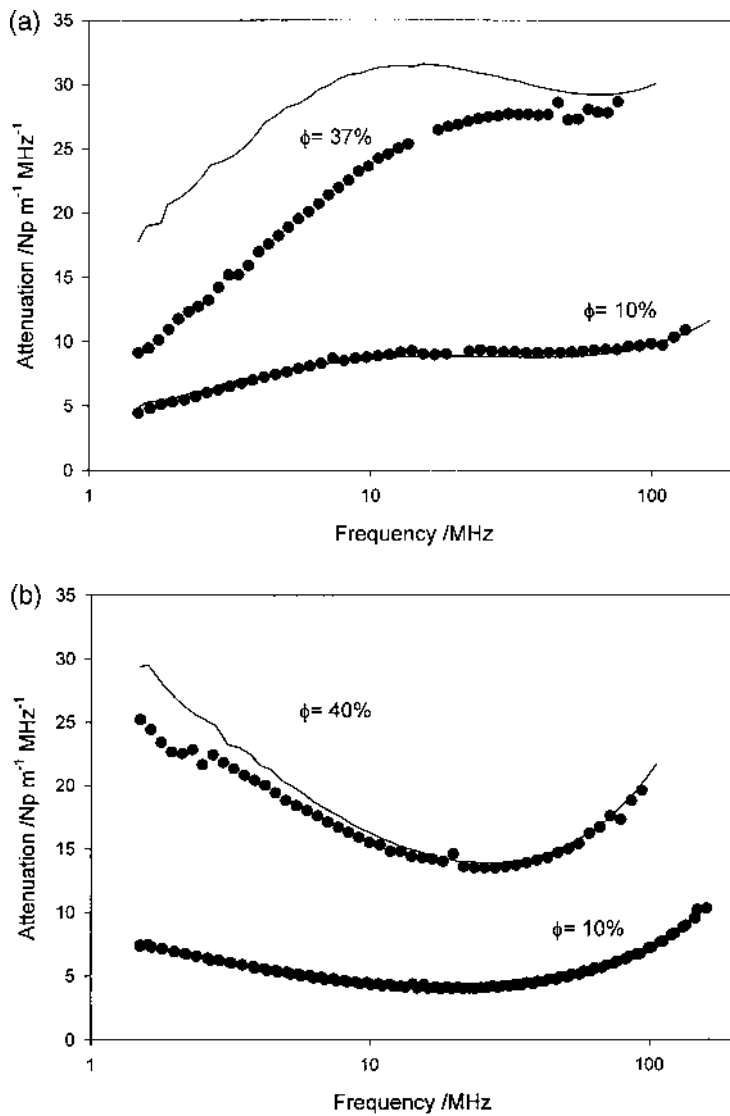


Figure 3 Ultrasonic attenuation spectra for different concentrations of silicone oil in water emulsions: (a) fine ($r=0.1\ \mu\text{m}$) droplets and (b) coarse ($r=0.56\ \mu\text{m}$). Theoretical prediction from ECAH multiple-scattering theory is shown alongside the experimental data.

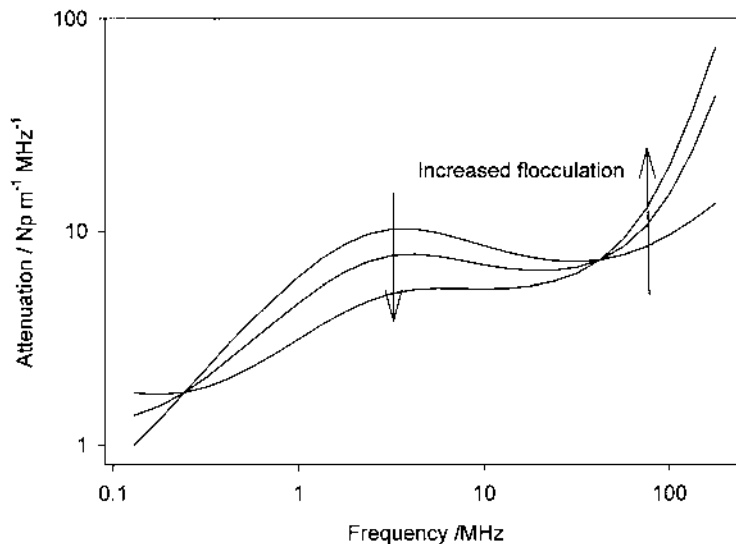


Figure 4 Theoretical prediction of the attenuation spectra of 10% silicone oil in water emulsions flocculated to different extents. The primary particle size is $0.25\ \mu\text{m}$ and the floc size is taken as $5\ \mu\text{m}$, with a packing fraction of droplets inside the flocs of 63%.

decrease in the attenuation at low ultrasonic frequencies. In addition, the effective particles in a flocculated emulsions are larger than in a nonflocculated emulsion, which leads to increased scattering and attenuation at high frequencies (9) (Fig. 4). Recently, a theory has been developed to relate the ultrasonic properties of flocculated emulsions to floc characteristics, such as concentration, size, and internal packing (9). This theory assumes that a flocculated emulsion can be treated as a two-phase system, which consists of spherical “particles” (the flocs) dispersed in a continuous phase. The flocs are treated as an “effective medium” whose properties depend on the size, concentration, and packing of the droplets within them. The ultrasonic properties of a flocculated emulsion are calculated using a two-stage procedure. First, the thermophysical and ultrasonic properties of the effective medium within the flocs are calculated using a core-shell theory. Second, the ultrasonic properties of a suspension of these flocs dispersed in a continuous phase are calculated using ultrasonic scattering theory. Sample theoretical predictions of the attenuation spectra of flocculated emulsions are presented in Fig. 4. These were calculated assuming varying proportions of the droplets (diameter = $1\ \mu\text{m}$) were present in flocs (diameter = $10\ \mu\text{m}$). This theory has been shown to give good agreement with experimental measurements of flocculated oil-in-water emulsions (12).

Finally, it should be mentioned that the development, refinement, and validation of theories suitable for interpreting ultrasonic spectra of emulsions and other types of colloidal suspension is currently a highly active area of research (13–16). Therefore it is likely that further developments will occur in the near future.

C. Ultrasonic Measurements

Many of the ultrasonic methodologies developed for fluids characterization (17–21) are suitable for food emulsions. A typical experimental setup includes an electrical signal generator that is used to excite an ultrasonic transducer to produce an acoustic wave which, after passing through the emulsion, is detected by a second transducer. (Alternatively, a single transducer and a reflector plate may sometimes be used.) These components are arranged in two main groups: pulse and resonance methods.

1. **Pulse methods.** A pulse of ultrasound is measured after transmission through a known path length of emulsion. This ultrasonic velocity is determined by measuring the time taken for the pulse to travel a fixed distance [Eq. (1)], and the attenuation coefficient is determined by measuring the reduction in amplitude of the pulse after it has traveled through the emulsion [Eq. (2)] (17,22). The frequency dependence of the ultrasonic properties of an emulsion can be determined using two different pulsed techniques: tone burst and Fourier transform. In the tone-burst method, a pulse containing a number of cycles of ultrasound at a single frequency (actually a narrow range of frequencies) is applied to the sample, and the ultrasonic velocity and attenuation coefficient of the sample are determined at this specific frequency. This procedure is then repeated using ultrasonic waves with different frequencies. In the Fourier transform method, a broadband pulse of ultrasound, which contains a range of different frequency components, is applied to the sample. Fourier transformation is then used to determine the velocity and attenuation of the ultrasonic wave over the frequency range of the transducer. The major advantage of the Fourier transform method is that a spectrum can be obtained using a single ultrasonic pulse, which speeds up the analysis (22).
2. **Resonance Methods.** Analytical instruments based on the resonator method use a continuous ultrasonic wave, rather than an ultrasonic pulse, to determine the ultrasonic properties of a sample. One transducer measures signal intensity and the other generates a continuous wave of either constant wavelength while

the path length is varied or variable frequency across a fixed path length. In a fixed-path-length resonator, a continuous wave containing a single, slowly increasing ultrasonic frequency is transmitted across the measurement cell. When the cell path length is an integer number of whole wavelengths, constructive interference occurs and there is a maximum in the detected energy (20,21,23). The shape and position of these resonance peaks can be used to calculate the ultrasonic velocity and attenuation coefficient of the liquid in the cell to very high precision.

Traditionally, analytical instruments for characterizing emulsion properties had to be constructed by researchers', however, a number of instrument manufacturers now supply analytical instruments based on ultrasound that are specifically designed for characterizing emulsion properties. There are a number of important practical considerations that should be taken into account when developing or selecting an analytical instrument for characterizing emulsion properties.

- The ultrasonic properties of most liquids are strongly temperature dependent and so it is important to use an instrument in which the temperature is precisely controlled (i.e., $\pm 0.2^\circ\text{C}$ or better).
- The measurement volume of commercial ultrasonic analytical instruments can vary from a few milliliters to several liters, which may be important if a sample is expensive or in limited supply.
- The measurement time may be important in systems where rapid kinetic measurements are required. Data acquisition is usually much faster for Fourier transform spectrometers than for 'tone-burst' or resonance spectrometers, enabling faster kinetic processes to be monitored.
- Many commercial spectrometers will automatically calculate particle size distribution and disperse the phase volume fraction of an emulsion from its measured ultrasonic spectrum. The theories used by commercial instruments to make this calculation vary widely and it is essential to ensure that the theory has been validated for the types of system under investigation.
- Whereas both velocity and attenuation can be readily measured, velocity tends to be more affected by imprecision in temperature and composition, so attenuation is often more useful for structural measurements.
- Probably the single most common reason for poor-quality ultrasonic measurements is the presence of small air bubbles trapped within liquids. The large impedance mismatch between air cells and the surrounding emulsion leads to extensive scattering of

ultrasound that can obscure the effects of the emulsion itself. In many cases, air cells can be eliminated by judicious use of gentle centrifugation or degassing prior to measurement.

II. APPLICATIONS

Studies over many years, usually using custom-built ultrasonic instrumentation, has demonstrated the potential of the ultrasonic technique for characterizing the properties of emulsion droplets (e.g., droplet size, droplet concentration, droplet crystallization, and creaming stability). Ultrasound has advantages over many alternative technologies because measurements are rapid, nondestructive, and noninvasive and can be made in concentrated or optically opaque materials. Recently, analytical instruments based on ultrasonic spectrometry that are specifically designed for characterizing emulsion properties have become commercially available. Consequently, many of the potential benefits of ultrasonic technology for characterizing food emulsions have become available to scientists working in the food industry. Nevertheless, it is important for users of these commercial instruments to be aware of the theoretical basis of the ultrasonic technique, because improper measurement procedures or data interpretation can lead to appreciable errors.

A. Droplet Concentration

Analysis of droplet concentration is one of the simplest and most successful applications of low-intensity ultrasonic techniques to food emulsions. This application is based on there being an appreciable difference in the ultrasonic velocities of the oil and aqueous phases when ultrasonic velocity measurements are used or there being a significant amount of attenuation of the ultrasonic wave due to the presence of the emulsion droplets when attenuation coefficient measurements are used. The influence of droplet concentration on the ultrasonic velocity and attenuation of a model food emulsion is shown in Fig. 2. The droplet concentration of an emulsion can be determined by developing an empirical calibration curve or by using an appropriate theoretical model. The ultrasonic scattering theory described earlier [ECAH theory, Eq. (3)] adequately predicts the effects of droplet concentration on the ultrasonic properties of emulsions, provided that thermal overlap effects are not appreciable (24,25) (i.e., $\phi < 10\%$ in this case), but when thermal overlap becomes important (small droplet sizes, low ultrasonic frequencies, or high droplet concentrations), a more sophisticated theory must be applied (24). Criteria for deciding whether these effect should be taken

into account have been published in the literature (24). Ultrasonic measurements have previously been used to measure the droplet volume fraction of emulsified vegetable oil (26), milk (27), and salad dressings (28, 29).

B. Particle Size

Analytical instruments based on ultrasonic spectroscopy are gaining increasing acceptance for measuring the droplet size distribution of concentrated food emulsions. These instruments normally measure the ultrasonic attenuation coefficient (and sometimes the ultrasonic velocity) over a range of frequencies and then compute the particle size distribution (and volume fraction) that gives the best agreement between the measured spectra and that predicted by ultrasonic scattering theory. The suitability of a given instrument for a particular application largely depends on how accurately the scattering theory it uses to analyze the measured spectrum represents the ultrasonic properties of the emulsion being analyzed. In relatively dilute nonfloculated emulsions, there is excellent agreement between theory and experiment, and the measured particle size distributions are in close agreement with those measured by other technologies (24,25). However, when thermal overlap effects are important (e.g., in concentrated or flocculated emulsions), there may be appreciable differences between theory and experiment (Figs. 2 and 3), which would lead to large errors in any measured particle size distributions. For example, if the ECAH theory was used to characterize the concentrated emulsion in Fig. 3a, it would attempt to calculate the particle size (r) in Eq. (3) that would cause the theoretical line to best approach the measured data. However, under these conditions, the ECAH theory does not well describe the emulsion (particularly at low frequencies), so the particle size calculated would be meaningless. Therefore, one should always ensure that the ultrasonic scattering theory being used to interpret the data is appropriate for all sizes, concentrations, and frequencies (24).

One should also be aware that in order to compute the droplet characteristics from the measured ultrasonic spectrum in a reasonable time, it is often necessary to make some simplifying assumption about the shape of the particle size distribution (e.g., it is monomodal or bimodal or has a log-normal form). Only if these assumptions about the shape of the particle size distribution are incorrect will the final data be inaccurate. Despite these limitations, ultrasonic spectroscopy is currently one of the few practical methods of measuring the droplet size distribution of concentrated emulsions in situ [other techniques include nuclear magnetic resonance (NMR), electroacoustics, diffuse optical reflectance, and dielectric spectroscopy] (1). The ultrasonic technique has been used to determine particle size

distributions in a number of food products, including emulsified vegetable oils (30), salad cream (29), and milk fat globules (27).

C. Droplet Flocculation

The bulk physicochemical properties of many food emulsions are strongly influenced by droplet flocculation (e.g., creaming and rheology) (1). It is therefore important to have analytical techniques capable of providing information about the extent of droplet flocculation and about the structural characteristics of the flocs formed. Characterization of floc properties in most food emulsions is extremely difficult because their delicate structure is disrupted by the sample preparation procedures required by many analytical techniques (e.g., dilution or stirring in light scattering, electrical pulse counting, or microscopy techniques). A number of studies have shown that the ultrasonic properties of emulsions change appreciably when the droplets become flocculated (8,31–33) and ultrasonic attenuation spectroscopy has been used to study droplet flocculation in oil-in-water emulsions induced by diverse mechanisms (12,34,35) in the light of recent theoretical developments (9).

The same ultrasonic spectroscopy technique has been used to study the disruption of flocs in a shear field (36). As the emulsions are exposed to higher shear rates, the flocs become disrupted and their attenuation spectra becomes closer to that of nonflocculated droplets. The sensitivity of ultrasonic spectra to droplet flocculation and the fact that ultrasonic techniques can be applied nondestructively and noninvasively opens up the potential for “rheo-acoustic” techniques (37,38). These techniques measure the rheology of colloidal dispersions using a conventional rheometer while obtaining information about the structure and concentration of flocs using an ultrasonic spectrometer. Thus, it is possible to correlate changes in dispersion rheology to changes in floc structure as the shear rate applied to the system is varied in a controlled manner.

D. Gravitational Separation

Creaming leads to a change in oil distribution throughout a product. Ultrasonic velocity (or attenuation) can be used to measure the concentration of oil in an emulsion (see Sect. II.A) as a function of height using a simple one-dimensional imaging apparatus. A stepper motor moves an ultrasonic transducer along the vertical axis of the emulsion and a series of ultrasonic measurements are made at different heights and times (39). The ultrasonic measurements can then be converted into oil concentrations using a calibration curve or ultrasonic scattering theory. A typical creaming profile

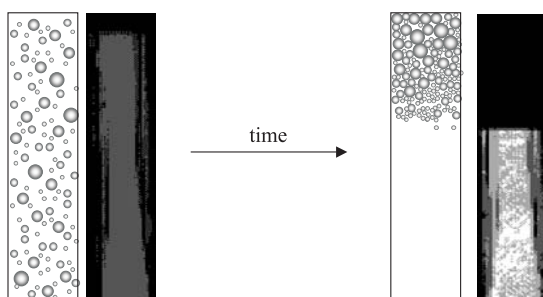


Figure 5 Diagrams and ultrasonic images illustrating creaming in oil-in-water emulsions. In the ultrasonic images, light regions indicate low oil content and dark regions indicate high oil content. Initially, the droplets are evenly dispersed and the ultrasonic image shows no detail. After storage, the droplets accumulate at the top of the container and a clear light/dark band is seen in the ultrasonic image.

for emulsified corn oil is shown in Fig. 5. In this case, the ultrasonic data are given as a two-dimensional image taken across a sample of emulsion at different times after preparation. Light areas indicate a higher oil concentration. This type of approach often has limited spatial resolution because the sound beam has a significant width (often ~ 1 cm) and averages the ultrasonic properties over that distance. It would be possible to achieve better resolution with a focused transducer or more sophisticated signal processing. It is important to remember that converting an ultrasonic measurement to oil concentration is not straightforward, as both particle size and oil concentration can vary within a cream layer and both can affect the ultrasonic signal (40–43). Even with these limitations, the use of ultrasonics to probe the structure of cream layers is a powerful tool and one of the unique applications of the technique. Conventional measurements of creaming are often based on visual identification of the boundary between an oil-rich layer and an oil-poor layer and can easily miss details of fine structure. For example, xanthan gum can cause an emulsion to cream due to depletion flocculation (8), but there are a variety of structures formed within the cream layer not evident to the naked eye. Ultrasonic imaging of the process was also able to detect the influence of added salt on the structure of the cream layer induced in the emulsion by xanthan gum (44).

E. Droplet Crystallization

Ultrasound has proved to be a highly sensitive method for monitoring the melting and crystallization for emulsion droplets (45,46). The physicochemical basis of the utilization of ultrasound for this purpose is the relatively

large difference in physical and ultrasonic properties of solid and liquid droplets.

The influence of heating and cooling on the ultrasonic velocity and attenuation coefficient of an *n*-hexadecane oil-in-water emulsion is shown in Fig. 6. When an emulsion containing crystalline fat droplets is heated, there is a sharp decrease in the ultrasonic velocity around the melting point of the bulk fat because the solid phase has a higher ultrasonic velocity than the liquid phase. When the same emulsion containing liquid oil droplets is cooled, the droplets exhibit a high degree of supercooling before they crystallize and the ultrasonic velocity returns to the starting solid-fat line. The emulsion droplets do not crystallize until they are cooled well below their thermodynamic melting point because the impurities that normally promote heterogeneous nucleation in bulk oils are distributed throughout such a very large number of droplets that each individual droplet is free of impurities. Consequently, nucleation tends to take place by a homogeneous mechanism (or sometimes a surface heterogeneous mechanism) in emulsions rather than be promoted by impurities as in bulk oils (47). To a first approximation, the fraction of crystalline material within the droplets (Φ) at a particular temperature can then be calculated as

$$\Phi = \left(\frac{1}{c^2} - \frac{1}{c_l^2} \right) / \left(\frac{1}{c_s^2} - \frac{1}{c_l^2} \right) \quad (6)$$

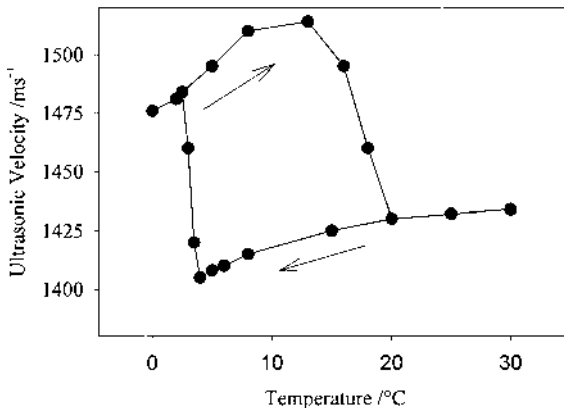


Figure 6 The effect of a cooling–heating cycle on the ultrasonic velocity in a 20% hexadecane-in-water emulsion. The speed of sound in the emulsion decreases with temperature and there is an abrupt change corresponding to the phase transition in the droplet oil. Supercooling of the liquid oil is responsible for the hysteresis loop observed.

where c is the measured ultrasonic velocity of the emulsion and c_s and c_l are the ultrasonic velocities in the emulsion when the droplets are completely solidified or completely liquefied oil, respectively, extrapolated to the measurement temperature (48). Equation (6) is based on the assumption that solid fats and liquid oils have similar densities and behave ideally as a mixture (49). Ultrasonic methods have been successfully used to measure the supercooling of emulsified triacyl glycerols (45,48), margarine and butter (50), and milk fat (49).

A similar hysteresis loop occurs in the attenuation coefficient of an emulsion during the melting and freezing of the droplets (51). However, in the experiment reported in Fig. 6 there was a large attenuation peak and extensive velocity dispersion at the melting point of the dispersed phase. This occurs because pressure–temperature fluctuations associated with the acoustic wave perturb the solid–liquid equilibrium and some of the ultrasonic energy is lost as heat. The magnitude of the attenuation peak is dependent on the frequency of the ultrasound. At low frequencies, the temperature–pressure gradients associated with the ultrasonic wave are small and so the equilibrium is maintained and attenuation is low. At high frequencies, the changes in temperature and pressure occur so rapidly that there is no time for the system to respond and the ultrasonic absorption is also low. However, at intermediate frequencies, the temperature–pressure gradients are sufficiently large and persist for a sufficiently long time that an appreciable amount of material is able to undergo an ultrasonically induced phase transition. The energy required to rapidly crystallize and melt a proportion of the fat leads to the significant absorption of the ultrasonic wave observed. The excess absorption is related to the dynamics of the phase transition (52).

III. CONCLUSIONS

The ultrasonic properties of emulsions are relatively easy to measure to good precision, particularly considering the wide commercialisation of acoustic spectrometers suitable for fluids characterization. The development of off-the-shelf instrumentation has been accompanied by advances in the theory describing ultrasonic spectra of emulsions in terms of particle size, concentration, association, and distribution. By comparing theory and experiment, it is possible to measure dispersed phase volume fraction, particle size (and, to some extent, particle size distribution), degree of flocculation, and creaming. Although examples of these measurements have been reported in the literature, rarely have multiple unknowns been deconvoluted from a single acoustic spectrum and so comprehensive ultrasonic characterization of droplet properties remains elusive. It is probably

more practical to use ultrasound in conjunction with other established methods that can measure other properties (e.g., density measurements to calculate dispersed phase volume fraction and light scattering to calculate primary particle size) and then use the acoustic data to measure emulsion properties not otherwise readily accessible (e.g., flocculation).

Very often our understanding of the world jumps forward when we develop a new way of looking at it. As an example, consider the widespread introduction of static light-scattering instruments into food emulsions laboratories over the past 20 years. The theories and phenomena important in food emulsion science did not change, but the explanations used began to more specifically describe events in terms of the size of the structures present. In this example, the principles of light scattering had a long history, but the difficulty of making measurements and the complexity of the mathematics prevented widespread application until they were integrated into a convenient package.

Ultrasonic instruments for particle characterization are in a similar position now as light-scattering instruments were 20 years ago and we can expect a similar pattern of development. Using these methods, we can reasonably measure realistic concentrations of fat in a relatively undisturbed state and, hence, evaluate the real properties of delicate structures that our existing techniques necessarily disrupt in sample preparation. It is our hope that this chapter will go some way to encouraging food emulsion scientists to gain the benefits of the new approaches while avoiding some of the pitfalls of poor measurement technique or extension of a theory beyond its assumptions.

REFERENCES

1. D. J. McClements, *Food Emulsions: Principles, Practice, and Techniques*, CRC Press, Boca Raton, FL, 1999.
2. M. J. W. Povey, *Ultrasonic Techniques for Fluids Characterization*, Academic Press, San Diego, CA, 1997.
3. A. S. Dukhin, P. J. Goetz, T. H. Wines, and P. Somasundaran, Acoustic and electroacoustic spectroscopy, *Colloids Surfaces A* 173, 127–158 (2000).
4. D. J. McClements, Principles of ultrasonic droplet size determination in emulsions, *Langmuir* 12, 3454–3461 (1996)
5. D. J. McClements and J. N. Coupland, Theory of droplet size distribution measurements in emulsions using ultrasonic spectroscopy, *Colloids Surfaces A* 117, 161–170 (1996).
6. J. A. Allegra and S. A. Hawley, Attenuation of sound in suspensions and emulsions: Theory and experiments, *J. Acoust. Soc. Am.* 51, 1545–1564 (1971).

7. J. N. Coupland and D. J. McClements, Physical properties of liquid edible oils, *J. Am. Oil Chem. Soc.* 74, 1559–1564 (1997).
8. D. J. McClements Ultrasonic determination of depletion flocculation in oil-in-water emulsions containing a non-ionic surfactant, *Colloids Surfaces A* 90, 25–35 (1994).
9. D. J. McClements, W. Herrmann, and Y. Hemar, Influence of flocculation on the ultrasonic properties of emulsions: theory, *J. Phys. D* 31, 2950–2955 (1998).
10. D. J. McClements, Y. Hemar, and N. Herrmann, Incorporation of thermal overlap effects into multiple scattering theory, *J. Acoust. Soc. Am.*, 105, 915–918 (1999)
11. A. Dukhin and P. Goetz, Acoustic and electroacoustic spectroscopy characterizing concentrated dispersions emulsions, *Adv. Colloid Interf. Sci.* 92, 73–132 (2001).
12. R. Chanamai, N. Herrman, and D. J. McClements, The influence of flocculation on the ultrasonic properties of emulsions: *J. Phys. D* 31, 2956–2963 (1998).
13. O. G. Harlen, M. J. Holmes, M. J. W. Povey, Y. Qiu, and B. D. Sleeman, A low frequency potential scattering description of acoustic propagation in dispersions, *SIAM J. Appl. Math.* 61, 1906–1931 (2001).
14. P. D. M. Spelt, M. A. Norato, A. S. Sangani, and L. L. Tavlarides. Determination of particle size distributions from acoustic wave propagation measurements, *Phys. Fluids* 11, 1065–1080, (1999).
15. P. D. M. Spelt, M. A. Norato, A. S. Sangani, M. S. Greenwood, and L. L. Tavlarides, Attenuation of sound in concentrated suspensions: theory and experiments, *J. Fluid Mech.* 430, 51–86 (2001).
16. F. Vander Meulen, G. Feuillard, O. B. Matar, F. Levassort, and M. Lethieco, Theoretical and experimental study of the influence of the particle size distribution on acoustic wave properties of strongly inhomogeneous media, *J. Acoust. Soc. Am.* 110, 2301–2307 (2001).
17. D. J. McClements and P. Fairley, Frequency scanning ultrasonic pulse echo reflectometer, *Ultrasonics* 30, 403–405, (1992).
18. E. P. Papadakis, The measurement of ultrasonic velocity, *Ultrasonic Measurement Methods* (R.N. Thurston and A.D. Pierce, eds.), Academic Press, San Diego, CA, 1990, pp. 81–106.
19. E. P. Papadakis, The measurement of ultrasonic velocity, *Ultrasonic Measurement Methods* (R.N. Thurston and A.D. Pierce, eds.), Academic Press, San Diego, CA, 1990, pp.107–155.
20. A.P. Sarvazyan, Development of methods of precise ultrasonic measurements in small volumes of liquids, *Ultrasonics* 20, 151–154 (1982).
21. A. P. Sarvazyan and T. V. Chalikian, Theoretical analysis of an ultrasonic interferometer for precise measurements at high pressures, *Ultrasonics* 29, 119–124, (1991).
22. D. J. McClements and P. Fairley, Ultrasonic pulse echo reflectometer, *Ultrasonics* 29, 58–62, (1991).
23. J. Blitz, *Ultrasonics: Methods and Applications*, Butterworths, London, 1971.

24. R. Chanamai, N. Herrman, D. J. McClements, Influence of thermal overlap effects on the ultrasonic attenuation spectra of polydisperse oil-in-water emulsions, *Langmuir* 15, 3418–3423 (1999).
25. N. Herrmann and D. J. McClements, Ultrasonic propagation in highly concentrated oil-in-water emulsions, *Langmuir* 15, 7937–7939 (1999).
26. D. J. McClements and M. J. W. Povey, Scattering of ultrasound by emulsions, *J. Phys. D: Appl. Phys.* 22, 38–47 (1989).
27. C. A. Miles, D. Shore, and K. R. Langley, Attenuation of ultrasound in milks and creams, *Ultrasonics* 28, 394–400 (1990).
28. R. Chanamai, F. Alba, and D. J. McClements, Ultrasonic spectroscopy study of salad dressings, *J. Food Sci.* 65, 507–513 (2000).
29. D. J. McClements, M. J. W. Povey, M. Jury, and E. Betsanis, Ultrasonic characterization of a food emulsion, *Ultrasonics* 28, 266–272 (1990).
30. J. N. Coupland and D. J. McClements, Droplet size determination in food emulsions: comparison of ultrasonic and light scattering methods, *J. Food Eng.* 50, 117–120, (2001).
31. Y. Hermar, N. Herrmann, P. Lemarechal, R. Hocquart, and F. Lequeux, Effective medium model for ultrasonic attenuation due to the thermo-elastic effect in concentrated emulsions, *J. Phys. II* 7, 637–647 (1997).
32. D. Hibberd, A. Holmes, M. Garrood, A. Fillery-Travis, M. Robbins, and R. Challis, Ultrasonic monitoring of oil-in-water emulsions undergoing depletion flocculation, *J. Colloid Interf. Sci.* 193, 77–87, (1997).
33. D. J. Hibberd, B. H. Robinson, and M. M. Robins, Ultrasonic characterisation of colloidal dispersions: detection of flocculation and adsorbed layers, *Colloids Surfaces B* 12, 359–371 (1999)
34. R. Chanamai, N. Herrmann, and D. J. McClements, Probing floc structure by ultrasonic spectroscopy, viscometry, and creaming measurements, *Langmuir* 16, 5884–5891 (2000).
35. N. Herrmann, Y. Hemar, P. Lemarechal, and D. J. McClements, Probing particle–particle interactions in flocculated oil-in-water emulsions using ultrasonic attenuation spectrometry, *Eur. Phys. J. E* 5, 183–188 (2001).
36. R. Chanamai, N. Herrmann, and D. J. McClements, Ultrasonic spectroscopy study of flocculation and shear-induced floc disruption in oil-in-water emulsions. *J. Colloid Interf. Sci.* 204, 268–276 (1998).
37. L. Haider, P. Snabre, and M. Boynard, Rheo-acoustical study of the shear disruption of reversible aggregates. Ultrasound scattering from concentrated suspensions of red cell aggregates, *J. Acoust. Soc. Am.* 107, 1715–1726 (2000).
38. P. Snabre, L. Haider, and M. Boynard, Ultrasound and light scattering from a suspension of reversible fractal clusters in shear flow, *Eur. Phys. J. E.* 1, 41–53 (2000).
39. T. K. Basaran, K. Demetriades, and D. J. McClements, Ultrasonic imaging of gravitational separation in emulsions, *Colloids Surfaces A* 136, 169–181 (1998).
40. V. J. Pinfield, E. Dickinson, and M. J. W. Povey, Modeling of concentration profiles and ultrasonic velocity profiles in a creaming emulsion: importance of scattering effects, *J. Colloid Interf. Sci.* 166, 363–374 (1994).

41. V. J. Pinfield, M. J. W. Povey, and E. Dickinson, The application of modified forms of the Urick equation to the interpretation of ultrasonic velocity in scattering systems, *Ultrasonics* 33, 243–251 (1995).
42. V. J. Pinfield, M. J. W. Povey, and E. Dickinson, Interpretation of ultrasonic sound velocity in creaming profiles, *Ultrasonics* 34, 695–698 (1996).
43. V. J. Pinfield, M. J. W. Povey, and E. Dickinson, Modeling of combined creaming and flocculation in emulsions, *J. Colloid Interf. Sci.* 186, 80–89 (1997).
44. E. Dickinson, J. Ma, and M. J. W. Povey, Creaming of concentrated oil in water emulsions containing xanthan, *Food Hydrocolloids* 8, 481–497 (1994).
45. W. Kloek, P. Walstra, and T. Van Vliet, Nucleation kinetics of emulsified triglyceride mixtures, *J. Am. Oil Chem. Soc.* 77, 643–652 (2000).
46. D. J. McClements, E. Dickinson, and M. J. W. Povey, Crystallization of hydrocarbon-in-water emulsions containing a mixture of solid and liquid droplets, *Chem. Phys. Lett.* 172, 449, (1990).
47. D. J. McClements, S. R. Dungan, J. B. German, C. Simoneau, and J. E. Kinsella, Droplet size and emulsifier type affect crystallization and melting of hydrocarbon-in-water emulsions, *J. Food Sci.* 58, 1148 (1993).
48. J. N. Coupland, E. Dickinson, D. J. McClements, M. J. W. Povey, and C. Rancourt de Mimmerand, Crystallization in simple paraffins and monoacid saturated triacylglycerols dispersed in water, (E. Dickinson and P. Walstra, eds.), *Food Colloids and Polymers: Stability and Mechanical Properties*, Royal Society of Chemistry, London, 1993.
49. C. A. Miles, G. A. J. Fursey, and R. C. D. Jones, Ultrasonic estimation of solid/liquid ratios in fats, oils, and adipose tissue, *J. Sci. Food Agric.* 36, 218–228 (1985).
50. D. J. McClements, The use of ultrasonics for characterizing fats and emulsions, Ph.D. dissertation, Leeds University, 1988.
51. D. J. McClements, M. J. W. Povey, and E. Dickinson, Absorption and velocity dispersion due to crystallization and melting of emulsion droplets, *Ultrasonics* 31, 433–437 (1993).
52. A. J. Matheson, *Molecular Acoustics*, Wiley, London, 1971.

15

NMR Studies of Emulsions with Particular Emphasis on Food Emulsions

Balin Balinov

Amersham Health, Oslo, Norway

Francois Mariette

Cemagref, Rennes, France

Olle Söderman

University of Lund, Lund, Sweden

I. INTRODUCTION

Very early in the development of colloid science, emulsions received considerable attention. This is due to the fact that emulsions are of great fundamental as well as technical importance. They occur in a multitude of situations ranging from the extraction of crude oil to various food products. Therefore, it is not surprising that the practical knowledge about emulsions is quite extensive. People engaged in the production generally know how to produce emulsions with desired properties such as droplet-size distributions and shelf-life. The same level of empirical knowledge is at hand for the opposite process of breaking an emulsion. When it comes to the basic scientific understanding of emulsions, we are a little worse off. It is quite clear that several fundamental properties of emulsions, such as what factors determine the stability of emulsions, what is the importance of the properties of the continuous phase, and so on, are not fully understood. To some extent, we also lack or have not yet applied suitable techniques in the study of emulsions.

The majority of emulsions are stabilized by surfactants and Bancroft, one of the pioneers in emulsion science, realized that the stability of an emulsion was related to the properties of the surfactant film. This insight has become important during the latter years, when attempts have been made to draw on the rather detailed and profound understanding that today exists about bulk surfactant systems in the description of emulsions (1). This high level of understanding about bulk surfactant systems stems not the least from the application of modern physicochemical techniques such as scattering methods and nuclear magnetic resonance (NMR). It seems reasonable to expect that the application of these techniques to emulsion systems would lead to an increased basic understanding of central emulsion properties.

In this contribution, we will attempt to show how NMR can be used to study various emulsion systems and how NMR may be used in emulsion applications. We focus in particular on food emulsions, which, by their very nature, cover a very wide area in practical applications. One finds “semi-solid” varieties such as margarine and butter as well as liquid ones such as milk, sauces, dressings, and various beverages. In addition, food emulsions also include an array of products that contain both solids and/or gases in addition to two liquid phases such as in ice cream. Because of the complexity in their chemical composition and their heterogeneous structure, the use of NMR techniques in the study of food emulsions are up until now relatively limited. This is in contrast to the many studies dealing with biopolymers and their structure modification induced by food processing. The first applications of NMR to food emulsions were in the determination of solid-fat content and emulsion composition. These methods are based on the relative NMR signal intensities. Somewhat surprisingly, the relaxation time variation as a function of fat and/or water phase structure and composition has received little attention. Since the development of new benchtop NMR spectrometers, new applications using both relaxation time parameters and self-diffusion coefficient have been suggested and introduced.

We first discuss the NMR technique as such, with special emphasize on features important for the study of emulsions. Subsequently, we treat some important examples of how NMR can be used to obtain important information about central aspects of emulsions, in general, and food emulsions, in particular.

II. THE NMR TECHNIQUE

A. Fundamentals

Nuclear magnetic resonance is a spectroscopic technique and as such it is very well suited for investigations of topics such as molecular arrangements

and molecular dynamics. NMR has gone through a dramatic development over the last decades. For this reason, there are numerous monographs treating many different aspects of the method (2–4). Here, we will attempt to introduce the technique from the point of view of emulsion science.

Nuclear magnetic resonance spectroscopy is based on the fact that some nuclei possess a permanent nuclear magnetic moment. When placed in an external magnetic field, they take a certain well-defined state, which correspond to distinct energy levels. Transitions between neighboring energy levels take place due to absorption of electromagnetic radiation at radio-frequencies. In NMR, the signal is obtained by a simultaneous excitation of all transitions with radio-frequency pulses, followed by detection of the irradiation emitted as the system returns to the equilibrium state. The recorded free-induction decay (FID) may be used as such, but Fourier transformation of the time-resolved FID is usually performed to obtain the NMR spectrum.

Modern NMR spectrometers, operating at 500–800 MHz for protons, have a high resolution that allows one to identify up to several hundreds of lines in a complex NMR spectrum. In most cases, only a limited number of lines are used to obtain the information needed. In some applications, the spectral resolution is not a necessary step in the data analyses and the information may be obtained from the time dependence of the amplitude of the FID. The FID reflects all of the nuclei of a given type (e.g., protons) and is used to obtain information on the average relaxation phenomena of the nuclei of interest. For this type of signal detection, 10–20-MHz NMR spectrometers for protons is an option suitable for many industrial applications.

Nuclear magnetic resonance is a very versatile spectroscopic technique for three main reasons. (1) It is not a destructive technique. Thus, the system may be studied without any perturbation that influences the outcome and interpretations of the measurements. The system can be characterized repeatedly with no time-consuming sample preparations in between runs. (2) There are a large number of spectroscopic parameters that may be determined by NMR relating to both static and dynamic aspects of a wide variety of systems. (3) A large number of atomic nuclei carry nuclear spins, and for essentially any element in the periodic table, it is possible to find at least one suitable nucleus. This has the important consequence that for systems that show local segregation (such as surfactant and emulsion systems), it is possible to investigate different domains of the microheterogeneous system by studying different nuclei.

The most commonly used nucleus in NMR is ^1H , but also ^{13}C , ^{19}F , ^{23}Na and ^{31}P are of importance. These nuclei are naturally occurring isotopes and need not be inserted chemically. Another very useful nucleus

is ^2H ; however, the natural abundance of this species is, in general, too small to allow for reasonable measuring times. Therefore, this nucleus is usually inserted by chemical labeling. This can, in fact, be used to an advantage because the ^2H nucleus can be directed to a particular part of the molecule, hence making it possible to investigate different parts of a molecule.

It is convenient to divide the parameters obtained from NMR spectra into dynamic and static parameters.

B. Static Parameters

The static parameters are obtained from the observed resonance frequencies. The general frequency range where a particular nucleus shows a spectroscopic line is determined by the magnetogyric ratio, which is a nuclear property without chemical interest. However, the precise value of the resonance frequency is determined by molecular properties. For isotropic systems, the two most important parameters determining the resonance frequency is the chemical shift and the scalar spin–spin coupling.

The chemical shift is determined by the screening due to the electrons in the vicinity of the investigated nucleus. This, in turn, is determined mainly by the primary chemical structure of the molecule but also other factors such as hydrogen-bonding, conformation, and the polarity of the environment influence the chemical shift. In systems with local segregation, such as emulsions, this has the consequence that one may observe two separate signals from the same molecule if it resides in two different environments. This occurs if the exchange of the molecule between the two environments is slow on the relevant timescale, which is given by the inverse of the shift difference between the two environments. This feature of the experiment gives us the possibility to investigate the distribution of molecules and exchange rates in microheterogeneous systems.

The scalar coupling is exclusively of intramolecular origin and of little importance in emulsion systems.

Another static parameter of importance is the integrated area under a given peak. This quantity is proportional to the number of spins contributing to a given peak, and hence (relative) concentrations can be determined. This, as will be shown in Sect. VI, has some important applications in emulsion science.

C. Dynamic Parameters

Dynamic processes on the molecular level influence the nuclear spin system by rendering the spin Hamiltonian time dependent. Depending on the relation between the characteristic times of the molecular motions, τ_c , and the

strength of the modulated interaction, ω_I (expressed in frequency units), one can identify different regimes.

For slow motions, when $\tau_c\omega_I \gg 1$, the system is in the solid regime and ω_I contributes to the resonance frequencies observed. This is the situation encountered in anisotropic liquid crystals, where the NMR spectra are usually dominated by static effects.

In the other extreme, when $\tau_c\omega_I \ll 1$, the phenomenon of motional narrowing occurs. Here, the spin relaxation is characterized by a limited number of time constants, the most readily observed are the longitudinal, T_1 , and transverse, T_2 , relaxation times. The first of these characterizes the decay of the M_z magnetization to equilibrium and the second characterizes the return of the $M_{x,y}$ magnetization to equilibrium (where M_z is perpendicular to the polarizing magnetic field and $M_{x,y}$ lies in a plane perpendicular to M_z). Measurements of the relaxation times require that the sample is perturbed by various pulse sequences. The one most often used for measuring T_1 is the inversion recovery sequence (or variations of it), and different echo sequences are usually used for measuring T_2 .

For the case when $\tau_c\omega_I \approx 1$, the shape of the NMR spectral line is strongly affected by the characteristic features of the molecular motions.

We shall make two remarks concerning features, which are peculiar to the topic of NMR and emulsions. The first deals with the fact that an emulsion system may actually contain molecules that fulfill more than one of the motional regimes described earlier. Consider, for instance, molecules in the continuous phase. For them, the condition $\tau_c\omega_I \ll 1$ holds. For molecules residing at the interface between the two liquids of the emulsion, the situation may be different, and depending on the size of the emulsion droplet, they may experience any of the three time domains described earlier.

Our second remark deals with the effect of diamagnetic susceptibility variations. In heterogeneous structures, the magnetic field is perturbed in the vicinity of regions of differing susceptibilities. As a consequence, the random motions of the molecules in this spatially varying magnetic field induces relaxation effects. T_1 and T_2 relaxation require fluctuations at the Larmor frequency, whereas, in addition, T_2 relaxation is also sensitive to slower fluctuations. Because the fluctuations brought about by diffusion in the locally varying field typically occur with rates, which are slower than the Larmor frequencies, $T_2 \ll T_1$ for this effect. Peculiar to systems with spherical structures, such as reasonably dilute emulsions, is that the gradient of the magnetic field *inside* the droplet is not affected. Thus, the above-described effect only operates for the continuous phase, which can be used to identify whether an emulsion is of the oil-in-water or water-in-oil type in a straightforward manner (5).

D. Measurement of Self-Diffusion

A very important dynamic molecular process is that of the transport of molecules due to thermal motion. This can conveniently be followed by the NMR pulsed field gradient (PFG) method. Because this approach has been of particular importance in the field of microheterogeneous surfactant systems, in general, and in emulsion systems, in particular, we will spend some time introducing this application of NMR. The technique has recently been described in a number of review articles (cf. Refs. 2 and 6–8), so here we will merely state that the technique requires no addition of probes, thus avoiding possible disturbances that addition of probes may cause, and that it gives component resolved self-diffusion coefficients with great precision in a minimum of measuring time. The main nucleus studied is the proton, but other nuclei, such as Li, F, Cs, and P, are also of interest.

The method monitors transport over macroscopic distances (typically in the micrometer regime). Therefore, when the method is used to study colloidal systems, the determined diffusion coefficients reflect aggregate sizes and obstruction effects for colloidal particles. This is the origin of the success the method has had in the study of microstructures of surfactant solutions and also forms the basis of its applications to emulsion systems. We expect that the PFG method will also be increasingly important in the study of emulsion systems and, therefore, we will discuss the method in some detail, with particular focus on its application to emulsions.

The fact that the information is obtained without the need to invoke complicated models, as is the case for the NMR relaxation approach, is particularly important. In this context, it should be stressed that the PFG approach measures the self-diffusion rather than the collective diffusion coefficient, which is measured by, for instance, light-scattering methods.

In its simplest version, the method consists of two equal and rectangular gradient pulses of magnitude g and length δ , one on either side of the 180° radio-frequency(rf)-pulse in a simple Hahn echo experiment. For molecules undergoing free (Gaussian) diffusion characterized by a single diffusion coefficient of magnitude D , the echo attenuation due to diffusion is given by (9,10)

$$E(\Delta, \delta, g) = E_0 \exp \left[-\gamma^2 g^2 \delta^2 \left(\Delta - \frac{\delta}{3} \right) D \right] \quad (1)$$

where Δ represents the distance between the leading edges of the two gradient pulses, γ is the magnetogyric ratio of the monitored spin, and E_0

denotes the echo intensity in the absence of any field gradient. By varying either g , δ , or Δ (while at the same time keeping the distance between the two Rfpulses constant), D can be obtained by fitting Eq. (1) to the observed intensities.

As mentioned earlier, the key feature of PFG diffusion experiments is the fact that the transport of molecules is measured over a time Δ , which we are free to choose at our own will in the range of from a few milliseconds to several seconds. This means that the length scale over which we are measuring the molecular transport is in the micrometer regime for low-molecular-weight liquids. When the molecules experience some sort of boundary with regard to their diffusion during the time Δ , the molecular displacement is lowered as compared to free diffusion, and the outcome of the experiment becomes drastically changed (2,11,12).

This situation applies to the case of restricted motion inside an emulsion droplet. In this case, the molecular displacements cannot exceed the droplet size, which indeed often is in the micrometer regime. Until recently, no analytical expressions that describe the echo decay in restricted geometries for arbitrary gradient pulses have been available. However, Barzykin(13) and Codd and Callaghan(14) have developed two approaches that work for arbitrary gradient pulses. This is an important step and will undoubtedly lead to an increased applicability of the method. Because the application of these approaches are somewhat numerically cumbersome and PFG work performed up until now mainly rely on one of two approximate schemes, we will describe these schemes below.

In one of these, one considers gradient pulses, which are so narrow that no transport during the pulse takes place. This has been termed the short gradient pulse (SGP) (or narrow gradient pulse, NGP) limit. This case leads to a very useful formalism whereby the echo attenuation can be written as (2)

$$E(\delta, \Delta, g) = \iint \rho(\mathbf{r}_0) P(\mathbf{r}_0|\mathbf{r}, \Delta) \exp[i\gamma g \delta(\mathbf{r} - \mathbf{r}_0)] d\mathbf{r} d\mathbf{r}_0 \quad (2)$$

where $P(\mathbf{r}_0|\mathbf{r}, \Delta)$ is the propagator, which gives the probability of finding a spin at position \mathbf{r} after a time Δ if it was originally at position \mathbf{r}_0 .

As discussed by Kärger and Heink(15) and Callaghan (2), Eq. (2) can be used to obtain the displacement profile, which is the probability for a molecule to be displaced dz during Δ in the direction of the field gradient, irrespective of its starting position. Modern NMR spectrometers are capable of producing gradient pulses with durations less than 1 ms and with

strengths around 10 T/m. Under these conditions, the SGP limit is often valid. The challenge is to design $E(\delta, \Delta, g)$ experiments that are sensitive to a particular type of motion in a system of interest. The study topics include free diffusion in the continuous phase in emulsions, restricted diffusion inside emulsion droplets, molecular exchange between emulsion droplets in highly concentrated emulsions, or drug release from emulsion droplets. Some of those examples will be considered in this chapter.

For the case of free diffusion, $P(\mathbf{r}_0|\mathbf{r}, \Delta)$ is a Gaussian function, and if this form is inserted in Eq. (2), Eq. (1) with the term $\Delta - \delta/3$ replaced with Δ is obtained, which is the SGP result for free diffusion. For cases other than free diffusion, alternate expressions for $P(\mathbf{r}_0|\mathbf{r}, \Delta)$ have to be used. Tanner and Stejskal (16) solved the problem of reflecting planar boundaries; however, the case of interest to us in the context of emulsion droplets, (i.e. that of molecules confined to a spherical cavity of radius R) was presented by Balinov et al. (17). The result is

$$\begin{aligned}
 E(\delta, \Delta, g) = & \frac{9[\gamma g \delta R \cos(\gamma g \delta R) - \sin(\gamma g \delta R)]^2}{(\gamma g \delta R)^6} \\
 & + 6(\gamma g \delta R)^2 \sum_{n=0}^{\infty} [j'_n(\gamma g \delta R)]^2 \\
 & \times \sum_m \frac{(2n+1)\alpha_{nm}^2}{\alpha_{nm}^2 - n^2 - n} \exp\left(-\frac{\alpha_{nm}^2 D \Delta}{R^2}\right) \frac{1}{[\alpha_{nm}^2 - (\gamma g \delta R)^2]^2} \quad (3)
 \end{aligned}$$

where $j_n(x)$ is the spherical Bessel function of the first kind and α_{nm} is the m^{th} root of the equation $j'_n(\alpha) = 0$. D is the bulk diffusion of the entrapped liquid, and the rest of the quantities are as defined earlier. The main point to note about Eq. (3) is that the echo amplitudes do indeed depend on the radius, and thus the droplet radii can be obtained from the echo decay for molecules confined to reside in a sphere, provided that the conditions underlying the SGP approximation are met.

The second approximation used is the so-called Gaussian phase distribution. Originally introduced by Douglass and McCall (18), the approach rests on the approximation that the phases accumulated by the spins on account of the action of the field gradients are Gaussian distributed. Within this approximation and for the case of a steady gradient, Neuman (19) derived the echo attenuation for molecules confined within a sphere, within a cylinder and between planes. For spherical geometry, Murday and Cotts (20) derived the equation for pulsed field gradients in the Hahn echo experiment described earlier.

The result is

$$\begin{aligned}
& \ln[E(\delta, \Delta, g)] \\
&= -\frac{2\gamma^2 g^2}{D} \sum_{m=1}^{\infty} \frac{\alpha_m^{-4}}{\alpha_m^2 R^2 - 2} \\
&\quad \times \left(2\delta - \frac{2 + \exp[-\alpha_m^2 D(\Delta - \delta)] - 2\exp(-\alpha_m^2 D\delta)}{\alpha_m^2 D} \right) \\
&\quad - \frac{2\exp(-\alpha_m^2 D\Delta) + \exp[-\alpha_m^2 D(\Delta + \delta)]}{\alpha_m^2 D}
\end{aligned} \tag{4}$$

where α_m is the m^{th} root of the Bessel equation $(1/(\alpha R))J_{3/2}(\alpha R) = J_{5/2}(\alpha R)$. Again, D is the bulk diffusion coefficient of the entrapped liquid.

Thus, we have at our disposal two equations with which to interpret PFG data from emulsions in terms of droplet radii, neither of which are exact for all values of experimental and system parameters. As the conditions of the SGP regime are technically demanding to achieve, Eq. (4) (or limiting forms of it) have been used in most cases to determine the droplet radii. A key question is then under what conditions Eq. (4) is valid. That it reduces to the exact result in the limit of $R \rightarrow \infty$ is easy to show and also obvious from the fact that we are then approaching the case of free diffusion, in which the Gaussian phase approximation becomes exact.

Balinov et al. (17) performed accurate computer simulations aimed at further testing its applicability over a wide range of parameter values. An example is shown in Fig. 1. The conclusion reached in Ref. 17 was that Eq. (4) never deviates by more than 5% in predicting the echo attenuation for typically used experimental parameters. Thus, it is a useful approximation and we will use it in Section III.

As pointed out earlier, the NMR echo amplitude E depends on the droplet's radius, which can be estimated by measuring E at different durations of δ and/or magnitudes g of the pulsed gradient. Typical echo attenuation profiles, generated by using Eq. (4), are presented in Fig. 2, which demonstrates the sensitivity of the NMR self-diffusion experiment to resolve micrometer droplet sizes.

We end this section by noting that the above discussion applies to the situation when the dispersed phase cannot exchange between droplets or between the droplets and the continuous medium (at least on the relevant timescale). This is the case for most emulsions. However, for some concentrated emulsions, this is not necessarily the case and the molecules of the dispersed phase may actually exchange between droplets during the characteristic time of the measurement. This leads to special effects, which will be discussed in Section III.

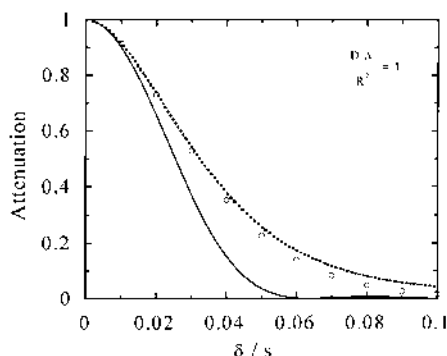


Figure 1 Results of a simulation of the diffusion of water molecules inside an emulsion droplet of radius R , given as the echo amplitude, versus the duration δ of the field gradient pulse. The ratio $D\Delta/R^2$ is 1. The dotted line is the prediction of the Gaussian phase approximation [Eq. (4)], whereas the solid line is the prediction of the SGP [Eq. (3)]. (Adapted from Ref. 17.)

III. STUDIES OF DIFFUSION AND FLOW IN EMULSIONS

A. Determination of Emulsion Droplet Radii by Means of the NMR Diffusometry Method

As pointed out earlier, the echo attenuation curve for the PFG experiment when applied to molecules entrapped in an emulsion droplet is a signature of the size of the emulsion droplet (cf. Fig. 2). As a consequence, droplet sizes can be determined by means of the PFG experiment.

The NMR sizing method, which was apparently first suggested by Tanner in Ref. 10 has been applied to a number of different emulsions ranging from cheese and margarines to crude oil emulsions (21–27).

When applied to a real emulsion one has to consider the fact that the emulsion droplets in most cases are polydisperse in size. This effect can be accounted for if the molecules confined to the droplets are in a slow-exchange situation, meaning that their lifetime in the droplet must be longer than Δ . For such a case, the echo attenuation is given by

$$E_{poly} = \frac{\int_0^{\infty} R^3 P(R) E(R) dR}{\int_0^{\infty} R^3 P(R) dR} \quad (5)$$

where $P(R)$ represents the droplet size distribution function and $E(R)$ represents the echo attenuation according to Eq. (4) [or, within the SGP approximation, Eq. (3)] for a given value of R .

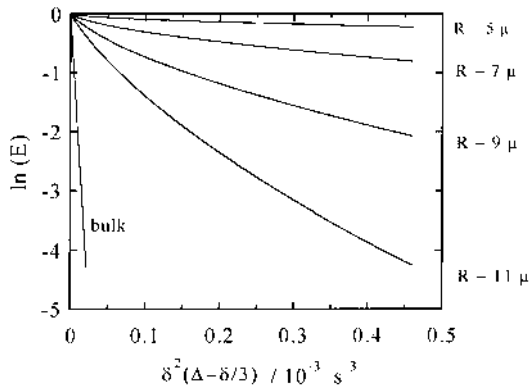


Figure 2 The echo attenuation as a function of $\delta^2(\Delta-\delta/3)$ for different radii of emulsion droplets [according to Eq. (4)] with $\Delta = 0.100$ s, $\gamma g = 10^7$ rad/m/s, and $D = 2 \times 10^{-9}$ m²/s.

The principle goal is to extract the size distribution function $P(R)$ from the experimentally observed $(E(\delta, \Delta, g))$ (henceforth referred to as E) profiles. Two approaches have been suggested. In the first, one assumes the validity of a model size distribution with a given analytical form (26,27), whereas in the second, the size distribution which best describes the observed experimental E profiles is obtained without any assumption on the form of the size distribution (28,29).

A frequently used form for the size distribution (26,27) is the log-normal function as defined in Eq. (6), as it appears to be a reasonable description of the droplet size distribution of many emulsions:

$$P(R) = \frac{1}{2R\sigma\sqrt{2\pi}} \exp\left[-\frac{(\ln 2R - \ln d_0)^2}{2\sigma^2}\right] \quad (6)$$

In addition, it has only two parameters, which makes it convenient for modeling purposes. In Eq. (6), d_0 represents the diameter median and σ is a measure of the width of the size distribution.

To illustrate the method and discuss its accuracy, we will use as an example some results for margarines (low-calorie spreads) (21). This system highlights some of the definite advantages of using the NMR method to determine emulsion droplet sizes, because other nonperturbing methods hardly exist for these systems.

Given in Fig. 3 is the echo decay for the water signal of a low-calorie spread containing 60% fat. These systems are w/o emulsions and as can be

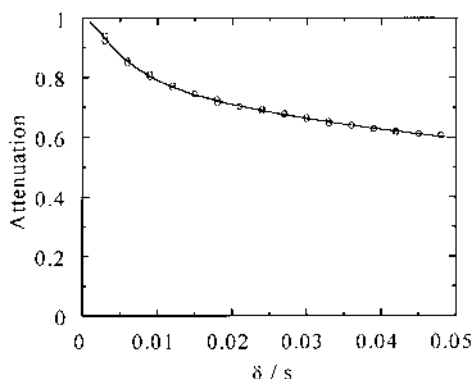


Figure 3 Echo intensities for the entrapped water in droplets formed in a low-calorie spread containing 60% fat versus δ . The solid line corresponds to the predictions of Eqs. (4)–(6). The results from the fit are $d_0=0.82\ \mu\text{m}$ and $\sigma=0.72$. (Adapted from Ref. 21.)

seen the water molecules do experience restricted diffusion (in the representation of Fig. 3, the echo decay for free diffusion would be given by a Gaussian function). Also given in Fig. 3 is the result of fitting Eqs. (4)–(6) to the data. As is evident, the fit is quite satisfactory and the parameters of the distribution function obtained are given in the figure caption. However, one might wonder how well determined these parameters are, given the fact that the equations describing the echo attenuation are quite complicated. To test this matter further, Monte Carlo calculations were performed in Ref. 21. Thus, random errors were added to the echo attenuation and the least squares minimization was repeated 100 times, as described previously (30). A typical result of such a procedure is given in Fig. 4. As can be seen in Fig. 4 the parameters are reasonably well determined, with an uncertainty in R (and σ , data not shown) of about $\pm 15\%$.

In the second approach, Ambrosone et al. (28,29) have developed a numerical procedure based on a solution of the Fredholm integral equation to resolve the distribution function $P(R)$ without prior assumptions of its analytical type. The method involves the selection of a generating function for the numerical solution, which may not be trivial in some cases. The method was tested by computer simulation of E for a hypothetical emulsion with a bimodal droplet size distribution (31). Figure 5 shows the reconstruction of the true droplet size distribution from the synthesized E data.

Creaming or sedimentation of emulsions with droplet sizes above $1\ \mu\text{m}$ cause some experimental difficulty because of the change of the total amount of spins in the NMR active volume of the sample tube during the

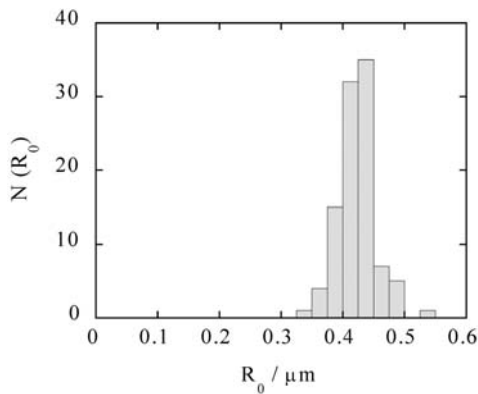


Figure 4 A Monte Carlo error analysis of the data in Fig. 3. The value of the parameter d_0 in Eq. (6) is $d_0 = 0.82 \pm 0.044 \mu\text{m}$ (note that $R_0 = d_0/2$ is plotted). (Adapted from Ref. 21.)

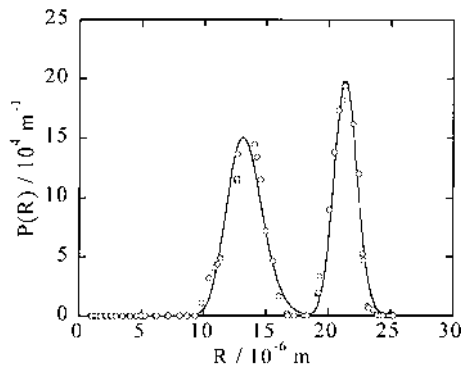


Figure 5 Determination of the size distribution function in the case of a bimodal distribution. The solid line represents the “true” volume fraction distribution function. The dots represents its values evaluated from the generated NMR data. (Adapted from Ref. 31.)

experiment. This can be accounted for by extra reference measurements with no gradient applied before and after each NMR scan at a particular value of δ or g . In addition, such reference measurements may provide information on the creaming rate, which is a useful characteristic of emulsions. Creaming or sedimentation is not a problem in the study of most food emulsions (such as low-calorie spreads) and highly concentrated emulsions.

Emulsion droplet sizes in the range from 1 μm up to 50 μm can be measured with rather modest gradient strengths of about 1 T/m. Note that the size determination rests on determining the molecular motion of the dispersed phase, so the method cannot be applied to dispersed phases with low molecular mobility. In practice, oils with self-diffusion coefficients above $10^{-12} \text{m}^2/\text{s}$ are required for sizing of o/w emulsion. Of course, w/o emulsions with most conceivable continuous media can be sized.

Emulsion droplets below 1 μm in size can often be characterized by the Brownian motion of the droplet as such (exceptions are concentrated emulsions or other emulsions where the droplets do not diffuse). This is the approach taken in the study of microemulsion droplets, where the diffusion behavior of the solubilized phase is characterized by the droplets (Gaussian) diffusion.

In conclusion, we summarize the main advantages of the NMR diffusion method as applied to emulsion droplet sizing. It is nonperturbing, requiring no sample manipulation (such as dilution with the continuous phase), and nondestructive, which means that the same sample may be investigated many times, which is important if one wants to study long-time stability or the effect of certain additives on the droplet size. It requires small amounts of sample (typically on the order of a few 100 mg). Moreover, the total NMR signal from the dispersed phase in emulsions is usually quite intense because of the large amount of spins. This fact allows for rapid measurements with a single scan per δ/g point.

B. Applications of NMR Techniques to Investigate Diffusion and Flow in Food Emulsions

Most of the applications of NMR diffusimetry on food emulsion are focused on the droplet size measurement described earlier. Over the years, several groups have established (21,26,27) the usefulness of the method when applied to margarine and low-calorie spreads (cf. Fig. 3 and 4) and the method is now available on commercial benchtop NMR spectrometers from Bruker, Oxford Instruments, or Universal Systems. However, in the open literature, there are relatively few articles that have been published dealing with droplet sizing of food emulsion. One contribution presents water self-diffusion and fat self-diffusion in cheese (23). Callaghan et al. found no significant difference in the value of the diffusion coefficients between Swiss and cheddar cheese. The water self-diffusion coefficient was about one-sixth of the value of bulk water at 30°C and it was suggested that water diffusion is confined to the protein surface. The self-diffusion of fat was reduced because of restrictions induced by the droplets.

Another study deals with the mobility of lipid contained in bread as a function of water content and temperature (32). The self-diffusion coefficient obtained at 30°C is of the same order as the one measured for the diffusion of lipids in bulk milk fat and was slightly affected by a change in water content (from 6% to 9%). The self-diffusion corresponds to the intrinsic motion within the lipid globule, and the distances probed were too small to allow the molecules to reach the droplet interface.

Because certain NMR experiments are sensitive to motion, flow can be measured with appropriate experimental protocols. These techniques are referred to as NMR velocimetry. The advantage of this technique is that a velocimetry profile or map can be obtained without assumptions of the uniformity of the shear rate. Because many food products exhibit complex non-Newtonian rheological properties, NMR velocimetry across the annular gap of a Couette cell allows for the visualization of nonuniform behavior. For example, the effect of the temperature on the rheology of butter fat and margarine has been studied (33). The results show the effect of the temperature on the heterogeneity of the rheological status of the sample. Moreover, the transition from heterogeneous to homogeneous viscosity as a function of the temperature was dependent on the emulsion composition and structure.

IV. NMR DIFFUSION STUDIES OF CONCENTRATED EMULSIONS

The above discussion applies to the case where the molecules are confined to the droplets on the timescale of the experiment. This is a reasonable assumption for many emulsions and it can in fact be tested by the NMR diffusion method by varying Δ . However, there are some interesting emulsion systems where this is not always the case. These are the so-called highly concentrated emulsions (often termed “high internal phase ratio” or “gel emulsions”) (34,35), which may contain up to (and in some cases even more than) 99% dispersed phase. Here, the droplets are separated by a liquid film, which may be very thin (on the order of 0.1 μm) and which may, in some instances, be permeable to the dispersed phase.

The case when the persistent time of the dispersed phase in the droplet is of the same order of magnitude as Δ is particularly interesting. Under these conditions, one may in some cases obtain one (or several) peak(s) in the plot of the echo amplitudes versus the quantity q (which is defined as $q = \gamma g \delta / 2\pi$). This is a surprising result at first sight, as we are accustomed to observe a monotonous decrease of the echo amplitude with q , but it is actually a manifestation of the fact that the diffusion is no longer Gaussian.

Such peaks can be rationalized within a formalism related to the one used to treat diffraction effects in scattering methods (36), and the analysis of the data may yield important information regarding not only the size of the droplets but also the permeability of the dispersed phase through the thin films as well as the long-term diffusion behavior of the dispersed phase. In Fig. 6, we show the results, which display diffractionlike effects in a concentrated emulsion system. The particular example pertains to a concentrated three-component emulsion based on a nonionic surfactant with the composition $C_{12}E_4/C_{10}H_{22}/H_2O$ (1 wt % NaCl) (3/7/90 wt%). The concentrated emulsion was made according to a protocol described in Ref. 37.

The data in Fig. 6 are presented with the value of the quantity q (defined earlier) on the abscissa. This quantity has the dimension of inverse length and it is, in fact, related to the scattering vector used in describing scattering experiments. In fact, the inverse of the value of the position of the peak can be related to the center-to-center distance of the droplets. In the example given in Fig. 6, this value is roughly $1.8\mu\text{m}$, which is in rough agreement with twice the droplet radii as judged from microscope pictures taken of the emulsion.

In order to analyze the data in more detail, one needs access to a theory for diffusion in these interconnected systems. One such theory was developed by Callaghan and co-workers (12). It assumes that the SGP limit

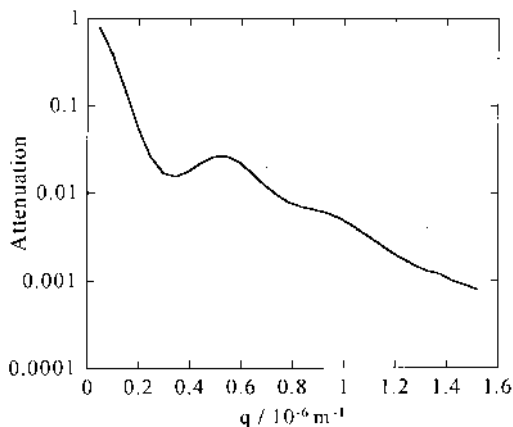


Figure 6 Diffractionlike effects in a concentrated emulsion system based on a nonionic surfactant with the composition $C_{12}E_4/C_{10}H_{22}/H_2O$ (1 wt% NaCl), (3/7/90 wt%).

described earlier is valid and it is based on a number of underlying assumptions of which pore equilibration is perhaps the most serious one. This latter assumption implies that an individual molecule in a droplet samples all of the positions in the interior of the droplet fully before it migrates to a neighboring droplet. The echo amplitude profile for such a case is given by the product of a structure factor for the single pore and a function that depends on the motion of the molecules between the pores. The pore-hopping formalism takes as input the radius of the sphere, the long-time diffusion coefficient, the center-to-center distance between the droplets, and, finally, a spread in the center-to-center distance (to account for polydispersity of the droplets). The prediction of the pore-hopping theory for the data in Fig. 6 is included as a solid line obtained with theoretical pore-to-pore distance of 1.2 μm , spread of the pore size of 0.2 μm , and the long-time diffusion coefficient $D = 9 \times 10^{-11} \text{ m}^2/\text{s}$. The agreement is not quantitative (the difference most likely owing to problems in defining a relevant structure factor for our system of polydisperse droplets), but the main features of the experimental data are certainly reproduced. A value for the lifetime of water molecule in a droplet (approximately 3 ms) was obtained from the values of the above pore-hopping parameters.

A different starting point in the analysis of the data such as the one in Fig. 6 is to make use of Brownian simulations (38). These are essentially exact within the specified model, although they do suffer from statistical uncertainties. For the present case, one lets a particle perform a random walk in a sphere with a semipermeable boundary. With a given probability, the particle is allowed to leave the droplet, after which it starts to perform a random walk in a neighboring droplet. That the approach yields peaks in the echodecay curves can be seen in Fig. 7 (38). The simulation scheme yields essentially the same kind of information as the pore-hopping theory. Thus, one obtains the droplet size and the lifetime of a molecule in the droplet (or quantities related to this, such as the permeability of the film separating the droplet).

Clearly, data such as those presented in Fig. 6 can be used to study many aspects of concentrated emulsions of which a few were exemplified earlier. It can also be used to study the evolution of the droplet size with time (recall that the method is nonperturbing) and also as a function of changes in external parameters such as temperature, which is an important variable for the properties of nonionic surfactant films.

Finally, we note that concentrated emulsions are excellent model systems in the development of the PFG methods as applied to the general class of porous systems, where the method has a great potential in providing relevant and important information.

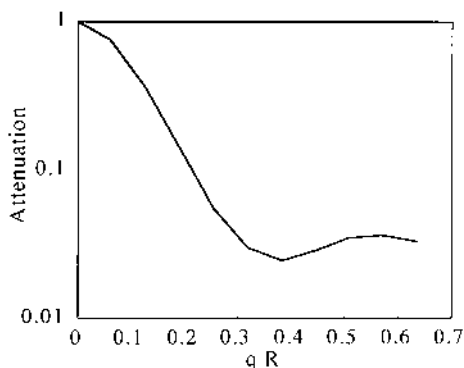


Figure 7 Brownian dynamic simulations of the echo decay at various qR for various $q = \gamma g \delta / 2\pi$ [$R = 4 \mu\text{m}$, $P_{\text{wall}} = 0.032$ (the probability of a molecule to penetrate the film), $\Delta = 100 \text{ ms}$]. The simulation scheme yields essentially the same kind of information as the pore-hopping theory. (Adapted from Ref. 38.)

V. NMR DIFFUSION STUDIES OF MULTIPLE EMULSIONS

Multiple emulsions usually refer to series of complex two-phase systems that result from dispersing an emulsion into its dispersed phase. Such systems are often referred to as water-in-oil-in-water (w/o/w) or oil-in-water-in-oil (o/w/o) emulsions, depending on the type of internal, intermediate, and continuous phase. Multiple emulsion were early recognized as promising systems for many industrial applications, such as in the process of immobilization of proteins in the inner aqueous phase (39) and as liquid membrane systems in extraction processes (40). The w/o/w emulsions have been discussed in a number of technical applications [e.g., as prolonged drug delivery systems (41–46), in the context of controlled-release formulations (47), and in pharmaceutical, cosmetic, and food applications (48)].

Multiple emulsions have a complex morphology and various important parameters for their preparation and characterization have been described (41,49). Examples are the characteristics of the w/o globules in w/o/w systems, such as their size and volume fraction, water/oil ratio inside the w/o globules, and average number and size of water droplets inside the w/o globules. The time dependence of those parameters is closely related to the stability of multiple emulsions and their morphology. Other important features are transport properties of substances encapsulated into discrete droplets and the permeability of the layer separating the internal from the external continuous phase. As was shown earlier, the NMR PFG method is a sensitive tool for studying structure and complex

dynamic phenomena, therefore, it is a promising technique in the study of multiple emulsions.

An example of possible uses of the method is demonstrated in Fig. 8, where the echo signal from the water in a w/o emulsion (panel a) and from the resulting double emulsion obtained when the original w/o emulsions is emulsified in water (panel b) are displayed (5). Also given are the resulting size distributions (panel c). The state of the water in multiple w/o/w emulsions was examined by recoding the water proton spectra (50). A narrow signal indicated water in a simple emulsion, whereas a broad signal indicated a multiple emulsion containing dispersed water.

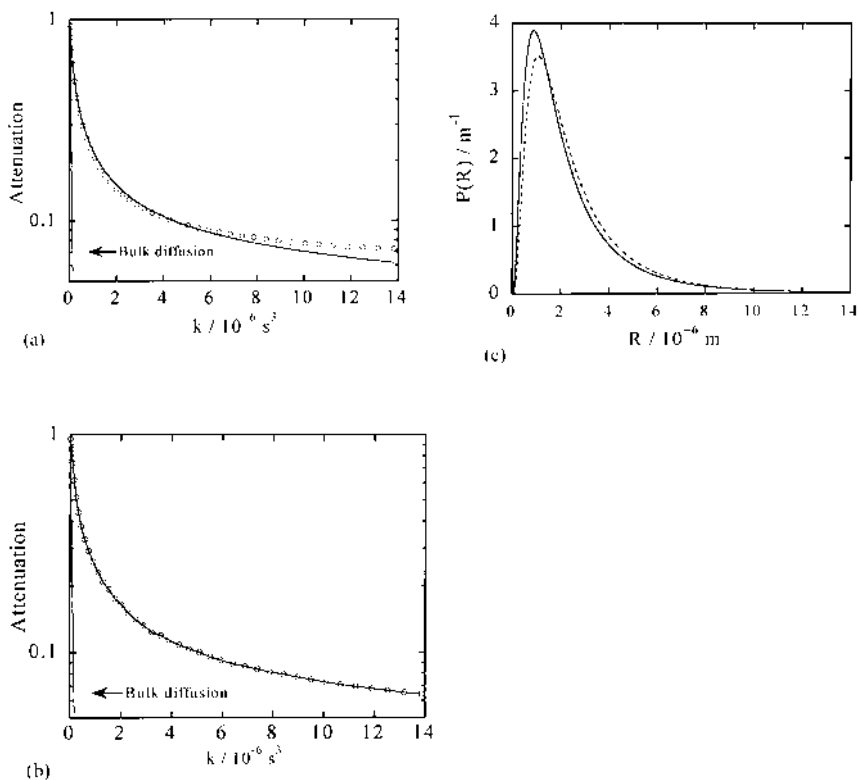


Figure 8 The echo signal from the water in a w/o emulsion (panel a), and from the resulting double emulsion obtained when the original w/o emulsions is emulsified in water (panel b). Also given in panel c are the resulting size distributions (— is w/o emulsion; --- is w/o/w emulsion). Please note that the size distribution is not normalized. (Adapted from Ref. 5.)

For studies of these complex systems, NMR is very well suited, as few other methods exist that can determine such basic properties as the state of water and the size distribution of internal emulsion droplets. In addition, the NMR PFG method may convey information about the molecular transport from emulsion droplets, a quantity that is relevant in the context of release mechanisms and rates from such emulsion carriers.

VI. DETERMINATION OF THE EMULSION COMPOSITION

Many industrial emulsion systems, such as cosmetic or pharmaceutical formulations, have well-defined compositions, whereas for other systems, the composition and nature of the ingredients may be unknown. An example of the latter is constituted by some food emulsions. The high sensitivity of the NMR experiment and ability to identify substances by their characteristic spectra may be used to quantify the emulsion composition. This method relies on the fact that the NMR spectra appears as a set of separated signals corresponding to the nuclei of interest and where the separation is due to the varying electronic environment within the molecule. The intensity of each signal, determined from the area under the signal, is proportional to the number of equivalent protons. Many emulsion systems are based on water and hydrocarbon oils, which have well-resolved lines even in quite primitive NMR spectrometers. This fact allows one to quantify the emulsion ingredients of interest (such as oil, water surfactant, or additives) without the need to separate the dispersed from the continuous phase. This quantitative characterization of emulsion systems may be particularly valuable for quality or process control, where an accurate and rapid analysis of the emulsion composition is a major requirement.

The determination of fat and water content in food emulsions with low-field NMR spectrometer requires that the relaxation time (T_2 or T_1) from each fraction are different. This situation is often at hand when the fraction of nonfat dry matter is either sufficiently large to decrease the water relaxation time, as in seeds or powders (51), or sufficiently low, as in dressings. If the discrimination is not possible, the NMR measurement should be performed before and after drying of the sample. A more sophisticated technique has been proposed in Ref. 52, which is based on the difference between the water and the fat self-diffusion. By choosing appropriate parameters of the NMR sequence, it was possible to determine both the water and the fat content in the sample.

Other methods proposed are based on the chemical shift difference between the hydroxyl group from water and methyl groups from lipid. Tellier et al. (53) demonstrated that reliable NMR determinations of water

and fat in minced meat can also be obtained under flowing conditions, a finding which suggests future on-line applications. Small variations in the water content ($< 4\%$) can be detected with a time response of less than 1 min. However, the reliability of these measurements depends on the capacity of maintaining a constant temperature in the sample. Because high-resolution NMR detects only liquid signals, temperature variations, which affect the solid/liquid ratio of the fat, induce signal fluctuation. A high-field spectrometer is not always necessary; fat and water content have also been determined with a low-field high-resolution spectrometer (54). The accuracy of the method was controlled on different meat products and cooked sausage. The main advantage of the technique is that the measurement protocol did not depend on the type of fat present. At low and medium resolution, anhydrous CuSO_4 can be added in order to relax the large water resonance and enhance detection of the much weaker oil resonance. This approach was used in studies of French salad dressing (55). These methods have been implemented on a magnetic resonance imaging (MRI) scanner to provide a tool to directly control the water and fat content of a bottle of French-style dressing (56). The method is a proton density projection using a spin-echo imaging sequence with the phase encode gradient turned off. The accuracy of the MRI method is within $\pm 2\%$. A MRI method for simultaneous determination of water and fat in cheese has also been proposed (57). The MRI sequence was a chemical shift selective sequence (CHESS). This sequence provides separately the fat- and water-enhanced images. Other MRI sequences have been also evaluated on dairy cream (58). The accuracy of these methods depends strongly on the main magnetic field strength, which may constitute a limitation for industrial applications. More recently, the MRI method has been developed for the control of the stability of the emulsion. When the relaxation time for oil–water emulsion is known, the volume fraction of each component phase can be calculated using

$$\frac{1}{T_{1\text{obs}}} = \frac{\phi_{\text{oil}}}{T_{1\text{oil}}} + \frac{\phi_{\text{water}}}{T_{1\text{water}}} \quad (7)$$

where ϕ_{oil} and ϕ_{water} are the volume fractions of oil and water, respectively. A fast spatially localized technique was developed for T_1 determination. Volume fractions along the profile of a 40% (v/v) oil–water emulsion were calculated several times during creaming to establish the dynamics of the process (59). This method is based on the assumption that the relaxation time of the fat and water phase was independent of the volume fraction.

The NMR characterization of emulsion composition may be quite valuable also in fundamental studies of emulsion systems and their applications. Various emulsion processing, such as creaming, solvent evaporation,

and extraction of substances by emulsions often require a quantitative analysis of the emulsion components, which can be performed with high precision using NMR techniques.

VII. ESTIMATING THE CREAMING OR SEDIMENTATION RATE

It is difficult to measure an absolute value for the creaming (or sedimentation) rate of an emulsion, as there is often a broad size distribution of the emulsion droplets. For an isolated droplet in a continuous medium, the creaming/sedimentation rate is dependent on the difference in density between the droplet and the continuous medium, the size of the droplet to the second power, and the viscosity of the continuous medium. It is obvious that different droplet sizes will give different creaming/sedimentation rates (assuming that there is a density difference between droplet and the continuous medium). We note two NMR methods that may be principally valuable in obtaining information on emulsion creaming or sedimentation. The first one is based on the quantitative analysis of the amount of dispersed phase. Emulsions containing large droplets gradually redistribute in a test tube and the creaming or sedimentation of the emulsion can be studied by determining the amount of droplet phase suspended in the emulsion at a fixed position as a function of time. This could be done directly in the NMR tube or by analyzing the amount of dispersed phase in a sample withdrawn from a fixed position of the test tube at distinct time intervals (60). Additional centrifugation of the emulsion, followed by NMR comparison of the composition of the lower and the upper fraction is a preferred method for more stable emulsions. The second method for estimating the sedimentation rate is based on flow measurements by NMR PFG. The method is sensitive to flow rates in the range of micrometers per second along the direction of the gradient of the magnetic field.

In many cases, the creaming or sedimentation occurs simultaneously with coalescence and is related to emulsion stability. In the next section, we will briefly consider the assessment of emulsion shelf life by NMR.

VIII. DETERMINATION OF EMULSION SHELF LIFE AND EMULSION STABILITY

Traditionally, emulsion stability is characterized by evaluating the droplet size distribution as a function of time and relating the results to various formulation parameters. On the basis of such studies, the thermodynamic instability of conventional emulsions is understood and well

documented (61–63). As discussed earlier, the NMR PFG is able to yield the evolution of the droplet size distribution of the same sample over time without any destruction of the sample. The change in size distribution may then be interpreted in terms of the change in the average droplet size or the total droplet area. There are two mechanisms for the decrease in the total droplet area. The first is the coalescence of two droplets involving the rupture of the film formed in the contact region of two neighboring droplets. The second process is Ostwald ripening involving the exchange of the molecules of the dispersed phase through the continuous phase. For concentrated o/w emulsions [at least the ones the present authors have investigated (64)], the permeability across the thin liquid film between the droplets is so slow that the stability is given by the film rupture mechanism. Given in Fig. 9 is the total droplet area as a function of time for a concentrated emulsion consisting of 98 wt% heptane, water, and cetyl trimethylammonium bromide (CTAB). As can be seen, there is a rapid initial decrease in the area, which levels out after about 12 h. From the initial part of the curve, the film rupture rate may be obtained, and for the data in Fig. 9, the value is $4 \times 10^{-5} \text{ s}^{-1}$. At longer times, the emulsion becomes remarkable stable, and there is little or no further decrease in the total droplet area during a period of 1 year.

In some concentrated emulsions, molecular exchange between the emulsion droplets occurs on a time-scale defined by the value of Δ . This situation is at hand if the dispersed phase crosses the film by some mechanism, the detailed nature of which need not concern us here. We are then dealing with a system with permeable barriers (on the relevant

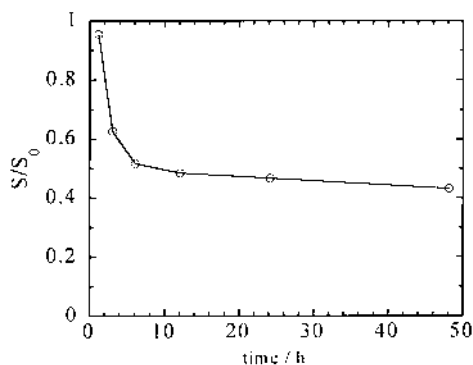


Figure 9 Decrease of the relative droplet surface area (S/S_0) with time for a highly concentrated o/w emulsion containing 98 wt% heptane and 0.4 wt% CTAB as emulsifier. S/S_0 is calculated from the droplet size distribution as obtained by the NMR self-diffusion technique. The initial slope corresponds to a film rupture rate of $J = 4 \times 10^{-5} \text{ s}^{-1}$. (Adapted from Ref. 64.)

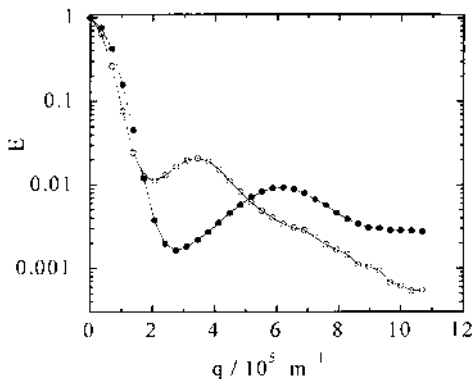


Figure 10 Normalized intensities versus q for one diffusion time ($\Delta = 50$ ms) at 2 (solid circles) and 8.5 (open circles) h after emulsion preparation. Parameters used in the experiment were $\delta = 3$ ms and a maximum gradient strength of 8.37 T/m. (Adapted from Ref. 65.)

timescale), and the system can now be regarded as belonging to the general class of porous systems. As was shown earlier, the interpretation of the NMR PFG signal in this case also gives a information on the droplet size. Given in Fig. 10 is the droplet size determined at two different instances (65), demonstrating that the stability of a concentrated emulsion with time can be conveniently followed by this method.

IX. STUDIES OF THE DISPERSED AND CONTINUOUS PHASE

A. Identification of the Dispersed Phase in Emulsions

Emulsions are formed by mixing two liquids, a process which creates discrete droplets in a continuous phase. During emulsification (e.g., by applying mechanical agitation), both liquids tend to form droplets, resulting in a complex mixture of o/w and w/o emulsions. Which of the components form the continuous phase depends on the emulsifier used because one type of the droplets is unstable and coalesce. Therefore, there is a need to identify the continuous phase in emulsion systems not only in the final emulsion system but also at short times after emulsion formation or even during the emulsification process. The NMR self-diffusion method may easily distinguish the continuous and dispersed phases based on the transport properties of its molecules. For example, molecules confined in the discrete droplets have an apparent diffusion coefficient, which is much lower than the corresponding value in the bulk phase. Molecules in the continuous phase, on the other

hand, have an apparent diffusion coefficient similar to the value in the corresponding bulk phase and this fact can be used to identify the type of continuous phase. This is particularly relevant in the case of emulsification by the phase-inversion technique (66), where a single surfactant may form either o/w or w/o emulsions depending of the formulation conditions. In many cases, the inversion of the emulsion from o/w to the w/o type (or from w/o to o/w) is a required and important step of emulsion formation. Due to its sensitivity to the transport properties of the dispersed phase, the NMR self-diffusion method is a useful tool for studying the phase-inversion process.

B. Study of the Properties of the Continuous Phase

Extensive work has been carried out in order to establish a relationship between emulsion properties and the properties of surfactant systems. The classical HLB (hydrophile–lipophile balance) concept is widely used in emulsion science to describe the balance of the hydrophilic and lipophilic properties of a surfactant at oil–water interfaces. The HLB value determines the emulsion-inversion point (EIP) at which an emulsion changes from one type to the other. This is of particular importance for nonionic surfactants that change their properties with changes in the temperature (66). Various NMR techniques have given significant contributions to the basic understanding of surfactant systems and some of those were reviewed in Ref. 8. The usefulness of NMR in studying surfactant solutions lies in the direct information they provide about the microstructure of microheterogeneous systems (8,67–71). It is beyond the scope of this chapter to summarize the use of NMR techniques to study surfactant systems, but we will present some representative examples related to emulsions.

In order to study the influence of the microstructure of the continuous phase on the stability of emulsions, two of the present authors investigated the system sodium dodecyl sulfate (SDS)/glycerolmono(2-ethylhexyl)ether/decane/brine (3 wt% NaCl) (72). In this system, emulsions of the o/w or w/o type can be made depending on the ratio between surfactant and cosurfactant. The total amount of surfactant and cosurfactant is kept constant at 5 wt%. The samples are made with equal weights of brine and decane and with a varying ratios between surfactant and cosurfactant. The emulsions in this system are made in two-phase areas of the phase diagram which for the o/w emulsions consists of an oil-rich phase and a phase of normal micelles and for the w/o emulsions consist of a water-rich phase and a micellar phase of reversed micelles. The micellar phase is the continuous medium for both types of emulsion. In order to determine the structure of the continuous medium, the emulsion samples were allowed to

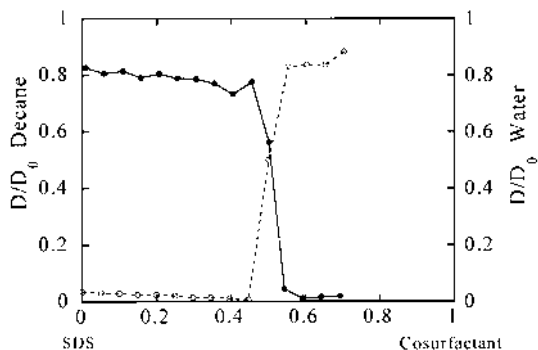


Figure 11 Microemulsion structure in the continuous phase studied by the diffusion coefficients (D) divided by the diffusion coefficients (D_0) for the neat liquid versus the relative amount of SDS in the SDS surfactant mixture. ○: decane diffusion; ●: water diffusion. (Adapted from Ref. 73.)

cream (or sediment) and the clear continuous medium was separated from each sample. These solutions were then characterized by the NMR self-diffusion method and the diffusion coefficients of both the oil and the water were determined. The result is shown in Fig. 11, where the reduced diffusion coefficients (D/D_0 , where D is the actual diffusion coefficient and D_0 is the diffusion coefficient of the neat liquid at the same temperature) for the oil and the water are plotted versus the ratio between cosurfactant and surfactant. For the o/w emulsion where SDS is the only surfactant, one finds that the continuous medium consists of small spherical micelles, that the water diffusion is fast [slightly lowered relative neat water due to obstruction effects (74)], and that the oil diffusion is low and corresponds to a hydrodynamic radius of the oil swollen micelle of about 50 Å (according to Stokes law). When the cosurfactant is introduced and its amount is increased, the size of the micelles is increased, as can be inferred from the diagram by the lowered value of the reduced diffusion coefficient of the oil. Close to the three-phase area, the continuous medium is bicontinuous, as the value of the reduced diffusion coefficient is almost the same for both the oil and the water and is equal to approximately 50% of the value for the bulk liquids. When the amount of cosurfactant is increased further, one passes over to the w/o emulsion region, where the continuous medium is bicontinuous near the three-phase area and then changes to closed reversed micellar aggregates, as can be seen from the reverse in order of the magnitudes of the values of oil and water diffusion coefficients. The hydrodynamic radius of the inverse micelles is about 70 Å.

In another study (75), NMR self-diffusion measurements of the continuous oil phase show that a stable highly concentrated w/o emulsion is

formed when the continuous phase is a reverse micellar solutions, whereas unstable emulsions were formed when the continuous phase is a bicontinuous microemulsions.

C. ^{31}P -NMR of Emulsion Components

The linewidths of ^{31}P -NMR can be used to characterize the properties of phospholipids. In emulsions, the linewidths are affected by the aqueous phase pH, size, or dispersion states of particles and methods of emulsification. The hydrophilic head-group motions of emulsified egg yolk phosphatidyl-cholin (PC) and lyso PC are examined by ^{31}P -NMR to evaluate their phospholipid states and stability. The results suggest that the head-group motions of phospholipids are related to emulsion stability (76,77).

Many emulsion systems are stabilized by phospholipids that form various self-organized structures in the continuous phases. Examples are fat emulsions containing soy triacylglycerols and phospholipids that are used for intravenous feeding. Studies have shown that these emulsions contain emulsion droplets and excess phospholipids aggregated as vesicles (liposomes), which remain in the continuous phase upon separation of the emulsion droplets by ultracentrifugation. The lamellar structure of the vesicles in the supernatant was characterized by ^{31}P -NMR (78) that distinguishes lipids in the outer and inner lamellae. ^{31}P -NMR was used (79) to confirm that the resulting structures in lipid emulsions are emulsion droplets rather than lipid bilayers. The composition of the fat particles of parenteral emulsions was obtained by ^{31}P -NMR (80). Analysis of the data identified the ratio of phospholipid/triacylglycerol in various fractions of emulsion droplets separated by centrifugation. ^{31}P -NMR showed (81) that approximately 48 mol% of the phospholipid emulsifier in a model intravenous emulsion forms particles smaller than 100 nm in diameter.

^{31}P -NMR and ^{13}C -NMR may be used to study the emulsifier properties at the o/w interface. The analysis of T_1 relaxation times of selected ^{13}C and ^{31}P nuclei of β -casein in oil-water emulsions indicates (82) that conformation and dynamics of the N-terminal part of β -casein are not strongly altered at the oil-water interface. A large part of the protein was found in a random coil conformation with restricted motion with a relatively long internal correlation time.

D. Molecular Organization from Relaxation Measurements

In addition to the NMR signal intensity, values of T_1 and T_2 have been used to characterize food emulsions. Indeed, the relaxation time T_2 for the water phase is sensitive to biopolymer conformation changes through chemical

exchange mechanisms. Monitoring the water phase T_2 relaxation provides information on the effects of emulsion formation, addition of surfactants, and temperature on the biopolymer structure at the fat droplet surface. For example, large differences in the modification of T_2 induced by the formation of emulsions have been observed when adding Na-casein or β -lactoglobulin (83). Because of the initial conformation of the protein, the effect of the fat-protein interaction at the interface on the protein structure was different. The sensitivity of the relaxation time depends on the biopolymer ratio between the amount fixed at the droplet surface and the amount dispersed in the aqueous phase. If the biopolymer content in the water phase is in large excess, then the relaxation will not be sensitive to the interface. This is illustrated by the relaxation time behavior in cheese (84). In that case, the water relaxation is related to the protein/water ratio and independent of the fat content, and the T_2 relaxation time of the water phase is sensitive to the molecular and microstructural organization of the protein gel (85). The molecular structure of the protein gel induced during ripening could be monitored with T_2 relaxation measurements or T_2 maps obtained from MRI. With appropriate image analysis methods, the volume of the nonmature part and the mature part in cheese could be quantified (86) and related to sensory properties of the cheese (87,88).

The relaxation times of fat have also been studied. When the fat is in the liquid state, the relaxation time T_2 is influenced by the carbon chain length and by the degree of unsaturation (89). As many fats in food are a complex mixture of triglycerides, the NMR signal can be described by a broad distribution of relaxation times (84) and the interpretation of such behavior in food is difficult. In contrast to this situation, large changes in the longitudinal relaxation time of solid fat according to the polymorphic state have been observed in triglycerides (90). The longitudinal relaxation time was 12 s at 25°C for the polymorphic β form and decreases to 0.6 s when polymorphic α is formed. Measurement of T_1 provides a method of following the time course of the polymorphic transformation upon, for example, aging. Such variations have also been observed between fat in bulk and in emulsions for model food emulsions (83) or for real food products such as ice cream mix (91). However, because of the complexity of fat composition, the interpretation in terms of polymorphism modification is difficult.

X. DEGREE OF SOLIDIFICATION OF THE DISPERSED PHASE

Many emulsion-based formulations also contain solid particles. Typical examples in the area of food products are margarine and salad dressing.

In the food industry, the determination of the amount of solid fat is an essential part of process control. An example is the monitoring of the fat hardening in margarine after its formation as a w/o emulsion. Close control of the solid fat content (SFC) is needed to give the margarine its characteristic properties. The NMR methods used in the determination of the SFC will be briefly described in Section X.A. We conclude the chapter by discussing NMR methods in the context of emulsion stability.

A. Determination of the Solid Fat Content

The determination of the SFC content by pulsed NMR is based on the fact that the transverse magnetization of solid fat decays much faster than oil. The spin-spin relaxation time (T_2) of solid fat is about $10\ \mu\text{s}$ and that of oil is about $100\ \text{ms}$. The NMR signal, derived from the amplitude of the FID, of partially crystallized fat after a 90° radio-frequency (RF) pulse is schematically shown in Fig. 12. The magnetization of the solid fat decays very fast. As a consequence, its contribution to the signal is far less than 0.1% of the initial value after about $70\ \mu\text{s}$. The decrease of the liquid-oil signal at this moment ($70\ \mu\text{s}$) is smaller than 1% and, therefore, the signal intensity will be well proportional to the number of protons in the liquid.

Two pulsed NMR methods exist for measuring the SFC of edible oils: the direct and indirect methods. The direct method determines the SFC from the signals corresponding to the total amount of solid and liquid fat (measured at time $t \approx 0$) and the amount of liquid fat (measured at long

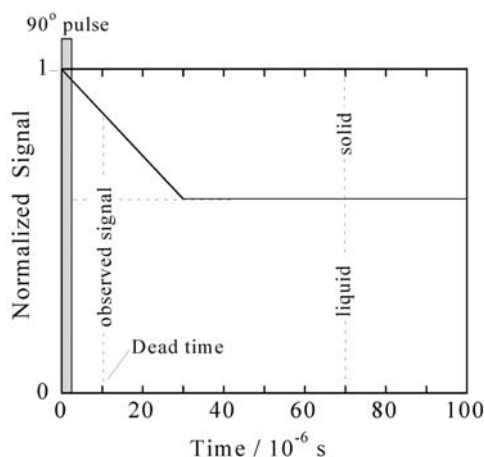


Figure 12 The NMR signal of partially crystallized fat after a 90° RF pulse.

enough time). The indirect method, determines the SFC, S_{ind} , by comparing the signal from the liquid fraction I_l with the signal I_m from completely melted fat. We have

$$S_{\text{ind}} = \frac{cI_m - I_l}{cI_m} \times 100\% \quad (8)$$

where the factor c corrects the signal for the temperature dependence of both the equilibrium magnetization and the Q -factor of the receiver coil. The correction factor $c = I_{0l}/I_{0m}$ is obtained by measuring the signals I_{0l} and I_{0m} of a reference liquid sample at both the measuring temperature and the melting temperature, respectively. The indirect method is mainly used as a reference for the direct method when the signals from both the liquid and the solid fat are processed. The indirect method is similar to the previously used continuous-wave (wide-line) technique that has some disadvantages compared to the pulsed NMR approaches. For example, saturation conditions are needed to obtain a sufficiently large signal-to-noise ratio. Even with a well-chosen reference sample, the systematic error is in the range of 1–2% (92). The wide-line analyses give only the narrow peak from the liquid fat, which should be compared to the signal of melted fat. This requires a second measurement to be performed after at least 1 h and automation of the measurement is hardly possible.

The direct method solves these problems and measures the SFC based on the processing of both the liquid and the solid signal (93). The measurement procedure may be fully automated and the percentage of solid is displayed immediately after the measurements. The measuring time is a few seconds and the SFC is determined with a standard deviation of about 0.4%. The signal can be obtained directly from the magnetization decay of the solid-fat protons and is equal to the signal immediately after the 90° pulse; see Fig. 12. Due to the dead time of the receiver, it is not possible to measure the initial signal height of solid and liquid, $s + l$, but only a signal $s' + l$ after a certain time of about $10 \mu\text{s}$ after the 90° pulse. To determine the SFC, the “true” NMR signal from solid fat, s , may be obtained from the measured signal, s' , from the solid fraction multiplied with the correction factor f which depend on the T_2 of the solid fat protons. The solid fat fraction S can be expressed in terms of s' (equal to the difference between the observed and liquid signal according to Fig. 12) as

$$S = \frac{fs'}{l + fs'} \times 100\% \quad (9)$$

The correction factor $f = s/s'$ can be determined from the measured s' and the solid fraction s obtained by the indirect method [Eq. (8)] using a

reference sample. The calibration should be performed once for a series of similar samples.

The direct method is very fast and reproducible and the time for sample preparation is minimal. Only one NMR measurement is needed to obtain a SFC value.

Commercial spectrometers are available that convert the NMR signal to the percentage of SFC in fats and margarine. Examples of NMR spectrometers that are suitable for the characterization of SFC are PC100, NMS100, the Minispec from Bruker, QP20+ from Oxford Instruments, and Maran Ultra from Universal Systems. Determination of SFC by NMR is a recognized international ISO standard (94).

In contrast to calorimetric methods, NMR allows the determination of the SFC both under isothermal conditions and as a function of temperature. Consequently, many studies have been carried with the aim of understanding the effect of the fat blend on the SFC, mainly focusing on dairy fat (95–97) and cacao butter (98). The NMR method was used also for process control of the crystallization behavior (99,100). For example, effects of minor components (101), effects of surfactants (102), effects of interesterification (103,104), and effects of protein–fat interactions (102) on the crystallization of dairy fat and complex fat mixtures have been studied.

The use of the direct method and the use of calibrated standards allow for the determination of SFC expressed in mass fraction. Further assumptions made are that the hydrogen nuclei contents and relaxation properties (T_2) of the liquid and the standards are similar. For phase behavior studies, molar fractions, rather than mass fractions, of the solute in solvent are required. When all of the molecules in a sample blend are of similar molecular weight, the standard mass SFC provides a good approximation of the molar SFC. However, when the molecular weights of the blend solute and solvent differ, mass SFC can differ greatly from molar SFC (105).

The direct or indirect methods are only valid for anhydrous fat on account of the complication posed by the presence of water protons contributing to the signal. The relaxation of water is somewhat faster than that of oil, but not enough to distinguish the oil and water contributions to the signal (95). Two strategies have been proposed to tackle this problem, one is based on water suppression and the other subtracts the water phase signal from the total liquid signal. The water signal could be saturated by selecting short repetition time between the pulses (106). However, accurate results with this method assume that the liquid-fat signal is not affected by the short repetition time. In Ref. 102, it was proposed to replace water by heavy water. This method is based on the assumption that the presence of D_2O does not alter the behavior of the emulsion. Another method is to change

the relaxation time of water by adding paramagnetic ions (Cu^{2+} , Mn^{2+}), the addition of which causes the relaxation time of water to become so small that the liquid-fat signal could be estimated. This method has been used in Ref. 107 on cream, where the water phase signal was damped by adding MnCl_2 , whereas Walstra and van Beresteyn (108) used CuSO_4 . This method requires measurements of the water phase signal separately as well as knowledge of the exact fat fraction of the cream. Moreover, this method assumes that the water and fat signals are additive. This latter assumption has been validated in Ref. 109, where no interference between the signals were found. In order to study the influence of surfactant on ice cream mix emulsions, Barfod et al. performed two measurements: one on a water phase sample containing all water-soluble components and the other on the emulsion (110). Knowing the fat content of the mixture, the SFC could be calculated from

$$\% \text{SFC} = \frac{fs \times 100}{fs + (l - xI_{\text{H}_2\text{O}})} \quad (10)$$

l represents the liquid signal, $I_{\text{H}_2\text{O}}$ is the liquid signal from the water phase, and x is the water fraction. This latter method was recently used to study the effect fat crystallization on the behaviors of protein and lipids at a lipid-water interface (111).

As noted earlier, the determination of the SFC is based on the sampling of two points from the NMR signal: one after the dead time of the probe (11 μs) and the next one at 70 μs . This method assumes that the relaxation time of the solid part is temperature independent and independent of the fat composition when using an external reference. This assumption is not always valid. For example, the precise analysis of the free-induction signal of milk fat at 5°C shows that an intermediate phase, characterized by a relaxation time T_2^* varying in the 50–250- μs range, could be detected (112). This intermediate phase represents about 4% of the entire fat content and, consequently, it should be considered when absolute values of SFC are required. An alternative is to analyze the complete NMR signal. This approach provides a precise determination of the relaxation time of the solid phase and the signal intensity is deduced without the need to correct for probe dead time. This method has been successfully applied on fat blends (113), on model food emulsions (83,114), on cheese (84) and ice cream mix (91).

The NMR method for determining SFC has been implemented on a MRI scanner (115). The procedure to quantify the rate of crystallization is essentially the same as for the indirect method in spectroscopic NMR experiments. The method has been used to study the fat signal intensity

from pure chocolate bars as a function of the cooling rate (116). The variation in the signal intensity was interpreted in terms of variations in the solid/liquid ratio of the cacao butter; hence, the existence of different polymorphic forms in the two samples was suggested. Differential Scanning Calorimetry (DSC) experiments confirmed this interpretation. Applied on adipose tissues from pig carcasses, a strong linear relationship was found between the SFC and the fat composition and this allowed for an accurate mapping of the solid/liquid ratio in animal subcutaneous adipose tissues and in intermuscular fat tissues from different pieces (117). The primary information obtained from MRI studies of lipid crystallization is the crystal growth rate (115,118). Oil-weighted MR images were obtained using a T_1 -weighed spin-echo sequence. The water signal was attenuated by using a small delay between the RF pulses. The crystallization dynamics was quantified from localized spectroscopy using a stimulated echo-pulse sequence. The method was then evaluated on model system both in bulk and in emulsion system. The results show that the rate of lipid crystallization differs significantly from bulk to the oil-water emulsion state and that difference is dependent on the nature of the triglycerides (115). From NMR and MRI studies, the crystal growth has been empirically modeled and revealed a significant trilaurin-location dependence, confirming that the rates of the nucleation processes were affected both by the concentration of trilaurin and the heat transfer properties of the sample and vessel (118).

B. Studies of the Emulsion Stability

It was demonstrated (119,120) that pulsed NMR may be used to measure the extent of oil solidification during cooling of oil-in-water emulsions. Pulsed proton NMR can distinguish between the oil and aqueous phases because of the large differences between the relaxation times of oil and water protons. On cooling, the NMR signal obtained for the aqueous phase is relatively small compared to the oil phase during the entire cooling cycle. For example, the water signal was approximately 10 times lower than the water signal for o/w emulsion containing approximately 50% hydrogenated oil (121). When the lipid phase containing the lipophilic emulsifier is cooled, the NMR signal decreases as the sample solidifies. The NMR signals from the different types of protons of the emulsion system are approximately additive (the sum of the aqueous and oil phases). In practice, the signal obtained for the supercooled emulsion is always larger than expected from a mixture with a solid fat and water, indicating that emulsification has had an inhibiting effect on fat solidification. The dispersion of fat into small droplets suppresses the rate of solidification under supercooling due to

nucleation phenomena in confined emulsion droplets (122–124). The extent of solidification at supercooling is high for very large emulsion droplets and correlates with a low emulsion stability. Unstable emulsions show little supercooling, but those that are relatively stable to creaming and phase separation are resistant to oil solidification. The greater the degree of dispersion, the slower the rate of phase separation. A correlation was made between the emulsion stability and the NMR signal from the emulsion when compared to the NMR signal from the fat and water phase alone (121). A parameter called “percent interaction” was derived from the NMR signal (120), the value of which correlated well with actual resistance of the emulsion to creaming and phase separation during storage. For example, the NMR signals from an emulsion and its corresponding fat phases were determined for an emulsion containing 48% hydrogenated oil, 1% acetylated monoglyceride (a 49% total fat phase), 1% Tween-20, and 50% water (a 51% aqueous phase) (121) as follows:

Fat phase signal	$71.5 \times 0.49 = 35.0$
Aqueous phase signal	$7.51 \times 0.51 = 3.8$
Expected emulsion signal	38.8
Observed emulsion signal	41.5

The “interaction percentages” (Int%) were calculated using

$$\text{Int}\% = \left(\frac{s_1 + l + w}{s + w} - 1 \right) \times 100\% \quad (11)$$

where the observed emulsion signal ($s_1 + l + w$) corresponding to the signal from the solidified fat fraction, s_1 , and not solidified fat, l , and water, w , was compared to the expected emulsion signal ($s + w$) corresponding to solid fat and water.

An emulsion is considered to be relatively stable if the observed NMR is more than 30% larger compared to the sum of the NMR signal from corresponding bulk water and oil (121). Pulsed NMR cooling curve measurements on emulsions offer an improved method for prediction of emulsion stability. By using a flow-through cell in the NMR magnet, the rate and extent of phase separation was measured accurately (120). The method is useful in selection of optimum types and levels of emulsifiers for each system (119). NMR measurements can also assist in optimizing surfactant blends to obtain stable emulsion. At the optimum emulsion formulation for a particular oil, the “interaction percentage” will be at a maximum, which indicates higher emulsion stability.

XI. CONCLUSIONS

In the above sections, we have presented various applications of the NMR technique in the study of emulsions. NMR is a versatile spectroscopic technique. This is also reflected in the span of questions pertaining to various aspects of emulsions that can be addressed with the NMR technique. The topics covered there include the determination of droplet size distributions, aspects of emulsion stability, crystallization of fat, and determination of fat and water contents in food emulsions.

It seems quite clear that emulsions will become increasingly important in more specialized applications in the future. In such applications, the demands for accurate design of properties of the emulsion systems, process, and quality control will be a major challenge. As should be clear from the above, NMR will become increasingly important in this regard. Controlled delivery of drugs as well as the use in the administration of pesticides is two examples of emulsion technology that will require accurate and reproducible characterization.

Due to its insensitivity to the physical nature of the sample and to its nonperturbing character, it seems likely that different NMR methods will find increasing use in studies of emulsions that are important in various types of food.

ACKNOWLEDGMENT

The work was financially supported by the Swedish Board for Industrial and Technical Development (NUTEK).

REFERENCES

1. A. Kabalnov and H. Wennerström, *Langmuir* 12, 276–292 (1996).
2. P. T. Callaghan, *Principles of Nuclear Magnetic Resonance Microscopy*, Clarendon Press, Oxford, 1991.
3. R. R. Ernst, G. Bodenhausen, and A. Wokaun, *Principles of Nuclear Magnetic Resonance in One and Two Dimensions*, Oxford University Press, Oxford, 1987.
4. D. Canet, *Nuclear Magnetic Resonance. Concepts and Methods*, Wiley, Chichester, 1996.
5. I. Lönnqvist, B. Håkansson, B. Balinov, and O. Söderman. *J. Colloid Interf. Sci.* 192, 66–73 (1996).
6. P. T. Callaghan, C. M. Trotter, and K. W. Jolley, *J. Magn. Reson.* 37, 247–259 (1980).
7. P. Stilbs, *Prog. Nucl. Magn. Reson. Spectrosc.* 19, 1–45 (1987).

8. O. Söderman and P. Stilbs, *Prog. Nucl. Magn. Reson. Spectrosc.* 26, 445–482 (1994).
9. E. O. Stejskal and J. E. Tanner, *J. Chem. Phys.* 42, 288–292 (1965).
10. J. E. Tanner, Thesis, University of Wisconsin–Madison, 1966.
11. P. T. Callaghan and A. Coy, in *NMR Probes of Molecular Dynamics*, (P. Tycko, ed.), Kluwer Academic, Dordrecht, 1993.
12. P. T. Callaghan, A. Coy, T. P. J. Halpin, D. MacGowan, J. K. Packer, and F. O. Zelaya, *J. Chem. Phys.* 97, 651–662 (1992).
13. A. V. Barzykin, *Phys. Rev. B* 58, 14,171–14,174 (1998).
14. S. L. Codd and P. T. Callaghan, *J. Magn. Reson.* 137, 358–372 (1999).
15. J. Kärgler and W. Heink, *J. Magn. Reson.* 51, 1–7 (1983).
16. J. E. Tanner and E. O. Stejskal, *J. Chem. Phys.* 49, 1768–1777 (1968).
17. B. Balinov, B. Jönsson, P. Linse, and O. Söderman, *J. Magn. Reson. A* 104, 17–25 (1993).
18. D. C. Douglass and D. W. McCall, *J. Phys. Chem.* 62, 1102 (1958).
19. C. H. Neuman, *J. Chem. Phys.* 60, 4508–4511 (1974).
20. J. S. Murday and R. M. Cotts, *J. Chem. Phys.* 48, 4938–4945 (1968).
21. B. Balinov, O. Söderman, and T. Wörnheim, *J. Am. Oil Chem. Soc.* 71, 513–518 (1994).
22. B. Balinov, O. Urdahl, O. Söderman, and J. Sjöblom, *Colloids Surfaces* 82, 173–181 (1994).
23. P. T. Callaghan, K. W. Jolley, and R. Humphrey, *J. Colloid Interf. Sci.* 93, 521–529 (1983).
24. X. Li, J. C. Cox, and R. W. Flumerfelt, *AIChE J.* 38, 1671–1674 (1992).
25. I. Lönnqvist, A. Khan, and O. Söderman, *J. Colloid Interf. Sci.* 144, 401–411 (1991).
26. K. J. Packer and C. Rees, *J. Colloid Interf. Sci.* 40, 206–218 (1972).
27. J. C. van den Enden, D. Waddington, H. Van Aalst, C. G. Van Kralingen, and K. J. Packer, *J. Colloid Interf. Sci.* 140, 105–113 (1990).
28. L. Ambrosone, A. Ceglie, G. Colafemmina, and G. Palazzo, *J. Chem. Phys.* 110, 797–804 (1999).
29. L. Ambrosone, A. Ceglie, G. Colafemmina, and G. Palazzo, *J. Chem. Phys.* 107, 10,756–10,763 (1997).
30. P. Stilbs and M. Moseley, *J. Magn. Reson.* 31, 55–61 (1978).
31. L. Ambrosone, G. Colafemmina, M. Giustini, G. Palazzo, and A. Ceglie, *Prog. Colloid Polym. Sci.* 112, 86–88 (1999).
32. G. Roudaut, D. van Dusschoten, H. van As, M. A. Hemminga, and M. Lemeste, *J. Cereal Sci.* 28, 147–155 (1998).
33. M. M. Britton and P. T. Callaghan, *J. Texture Studies* 31, 245–255 (2000).
34. K. J. Lissant, *J. Colloid Interf. Sci.* 22, 462–468 (1966).
35. H. M. Princen, *J. Colloid Interf. Sci.* 91, 160–175 (1983).
36. P. T. Callaghan, A. Coy, D. MacGowan, K. J. Packer, and F. O. Zelaya, *Nature (London)* 351, 467–469 (1991).
37. R. Pons, I. Carrera, P. Erra, H. Kunieda, and C. Solans, *Colloids Surfaces A* 91, 259–266 (1994).

38. B. Balinov, P. Linse, and O. Söderman, *J. Colloid Interf. Sci.* 182, 539–548 (1996).
39. R. H. Engel, S. J. Riggi, and M. J. Fahrenbach, *Nature* 219, 856–857 (1968).
40. N. N. Li and A. L. Shrier, in *Recent Developments in Separation Science* (N. N. Li, ed.), Chemical Rubber Co., Cleveland, OH, 1972.
41. S. Matsumoto, in *Nonionic Surfactants* (M. Schick, ed.), Marcel Dekker, New York, 1987.
42. P. J. Taylor, C. L. Miller, T. M. Pollack, F. T. Perkins, and M. A. Westwood, *J. Hyg. (London)* 67, 485–890 (1969).
43. L. A. Elson, B. C. Mitchlev, A. J. Collings, and R. Schneider, *Rev. Eur. Etudes Clin. Biol.* 15, 87–90 (1970).
44. C. J. Benoy, L. A. Elson, and R. Schneider, *Br. J. Pharmacol.* 45, 135–136 (1972).
45. A. F. Brodin, D. R. Kavaliunas, and S. G. Frank, *Acta Pharm. Suec.* 15, 1–12 (1978).
46. D. Whitehill, *Chem. Drug* 213, 130–135 (1980).
47. R. K. Owusu, Z. Qinhong, and E. Dickinson, *Food Hydrocolloids* 6, 443–453 (1992).
48. E. Dickinson, J. Evison, and R. K. Owusu, *Food Hydrocolloids* 5, 481–485 (1991).
49. M. Frenkel, R. Shwartz, and N. Garti, *J. Colloid Interf. Sci.* 94, 174–178 (1983).
50. A. Rabaron, P. A. Rocha-Filho, C. Vaution, and M. Seiller, Study and demonstration of multiple w/o/w emulsions by nuclear magnetic resonance, in *Fifth International Congress on the Technology of Pharmaceuticals*, 1989.
51. R. E. Hester and D. E. C. Quine, *J. Dairy Res.* 44, 125–130 (1977).
52. H. Berg, Determination of fat and water content in meat with NMR, in *Fifth International Conference on Applications of Magnetic Resonance in Food Science*, 2000.
53. C. Tellier, M. Trierweiler, J. Lejot, and G. J. Martin, *Analisis* 18, 67–72 (1990).
54. J. P. Renou, A. Briguët, P. Gatellier, and J. Kopp, *Int. J. Food Sci. Technol.* 22, 169–172 (1987).
55. P. Fairbrother and D. N. Rutledge, *Analisis* 21, 113–117 (1993).
56. J. R. Heil, W. E. Perkins, and M. J. McCarthy, *J. Food Sci.* 55, 763 (1990).
57. R. Ruan, K. Chang, P. L. Chen, R. G. Fulcher, and E. D. Bastian, *J. Dairy Sci.* 80, 9–15 (1998).
58. S. L. Duce, M. H. G. Amin, M. A. Horsfield, M. Tyszka, and L. D. Hall, *Int. Dairy J.* 5, 311–319 (1995).
59. R. J. Kauten, J. E. Maneval, and M. J. McCarthy, *J. Food Sci.* 56, 799–801 (1991).
60. M. Gangoda, B. M. Fung, and E. A. O’Rear, *J. Colloid Interf. Sci.* 116, 230–236 (1987).
61. C. Washington, *Int. J. Pharm.* 66, 1–21 (1990).
62. J. Boyd, C. Parkinson, and P. Sherman, *J. Colloid Interf. Sci.* 41, 359–370 (1972).
63. N. Weiner, *Drug Dev. Ind. Pharm.* 12, 933–951 (1986).

64. O. Söderman and B. Balinov, in *Emulsions and Emulsion Stability* (J. Sjöblom, ed.), Marcel Dekker, New York, 1996.
65. B. Håkansson, R. Pons, and O. Söderman, *Langmuir* 15, 988–991 (1999).
66. L. Marszall, in *Nonionic Surfactants* (M. Schick, ed.), Marcel Dekker, New York, 1987.
67. B. Lindman, O. Söderman, and H. Wennerström, in *Novel Techniques to Investigate Surfactant Solutions* (R. Zana, ed.), Marcel Dekker, New York, 1987.
68. B. Balinov, U. Olsson, and O. Söderman, *J. Phys. Chem.* 95, 5931–5936 (1991).
69. B. Lindman and P. Stilbs, in *Microemulsion Systems* (H.L. Rosano and M. Clause, eds.), Marcel Dekker, New York, 1987.
70. B. Lindman, K. Shinoda, U. Olsson, D. Andersen, G. Karlström, and H. Wennerström, *Colloids Surfaces* 38, 205–224 (1989).
71. A. Khan, in *Specialist Periodical Reports, Nuclear Magnetic Resonance* (G. A. Webb, ed.), The Royal Society of Chemistry, Cambridge, 1993.
72. K. Shinoda, H. Kunieda, T. Arai, and H. Saijo, *J. Phys. Chem.* 88, 5126–5129 (1984).
73. O. Söderman, I. Lönnqvist, and B. Balinov, in *Emulsions—A Fundamental and Practical Approach*, (J. Sjöblom, ed.), Kluwer Academic, Dordrecht, 1992.
74. B. Jönsson, H. Wennerström, P. Nilsson, and P. Linse, *Colloid Polym. Sci.* 264, 77 (1986).
75. C. Solans, R. Pons, S. Zhu, H. T. Davis, D. F. Evans, K. Nakamura, and H. Kunieda, *Langmuir* 9(6), 1479–1482 (1993).
76. K. Chiba and M. Tada, *Nippon Nogei Kagaku Kaishi* 62, 859–865 (1988).
77. K. Chiba and M. Tada, *Agric. Biol. Chem.* 53, 995–1001 (1989).
78. M. Rotenberg, M. Rubin, A. Bor, D. Meyuhas, Y. Talmon, and D. Lichtenberg, *Biochim. Biophys. Acta* 1086, 265–272 (1991).
79. J. Drew, A. Liodakis, R. Chan, H. Du, M. Sadek, R. Brownlee, and W. H. Sawyer, *Biochem. Int.* 22, 983–992 (1990).
80. J. Férézou, T. L. Nguyen, C. Leray, T. Hajri, A. Frey, Y. Cabaret, J. Courtieu, C. Lutton, and A. C. Bach, *Biochim. Biophys. Acta* 1213, 149–158 (1994).
81. K. Westesen and T. Wehler, *J. Pharmaceut. Sci.* 82, 1237–1244 (1993).
82. L. C. ter Beek, M. Ketelaars, D. C. McCain, P. E. Smulders, P. Walstra, and M. A. Hemminga, *Biophys. J.* 70, 2396–2402 (1996).
83. F. Mariette, S. Querangal, M. Cambert, C. C. Lopez, and A. Riaublanc, in Protein structural changes at the O/W interface emulsion studied by NMR relaxometry, *Fifth International Conference on Applications of Magnetic Resonance in Food Science*, 2000.
84. B. Chaland, F. Mariette, P. Marchal, and J. de Certaines, *J. Dairy Res.* 67, 609–618 (2000).
85. B. Chaland, Thesis, University of Rennes, France, 1999.
86. B. Chaland, F. Mariette, P. Marchal, and J. de Certaines, Macro structural and morphological changes during soft cheese ripening by MRI, in *Fifth International Conference on Applications of Magnetic Resonance in Food Science*, 2000.

87. F. Mariette, G. Collewet, P. Marchal, and J. M. Franconi, in *Advances in Magnetic Resonance in Food Science* (P. Belton, B. Hills, and G. A. Webb, eds.), The Royal Society of Chemistry, Cambridge, 1999.
88. F. Mariette, G. Collewet, P. Fortier, and J. M. Soulie, in *Magnetic Resonance in Food Science—A View to the Future* (G. A. Webb, P. Belton, A. M. Gil, and I. Delgadillo, eds.), The Royal Society of Chemistry, Cambridge, 2001.
89. D. J. LeBotlan and I. Helie, *Analisis* 22, 108–113 (1994).
90. I. J. Colquhoun and A. Grant, Solid State NMR spectroscopy of fats, in *Eurofood Chem V*, 1989.
91. T. Lucas, S. Dominiawsyk, F. Mariette, and G. Alvarez, ¹H NMR assessment of water behaviour in ice cream, in *Engineering Food, Eighth ICEF International Conference Proceedings*, 2000.
92. A. J. Haighton, K. van Putte, and L. F. Vermaas, *J. Am. Oil Chem. Soc.* 49, 153–156 (1972).
93. K. van Putte and J. van den Enden, *J. Phys. E: J. Sci. Instrum.* 6, 910–912 (1973).
94. ISO 8292: 1991, Animal and vegetable fats and oils: determination of solid fat content, pulsed nuclear magnetic resonance method, International Organization for Standardization (1991).
95. B. K. Mortensen, in *Developments in Dairy Chemistry — 2. Lipids* (P. F. Fox, ed.), Applied Science, London, 1983.
96. N. M. Barfod, in *Characterization of Food: Emerging Methods* (A. G. Gaonkar, ed.), Elsevier, New York, 1995.
97. M. L. Herrera, M. D. Gatti, and R. W. Hartel, *Food Res. Int.* 32, 289–298 (1999).
98. H. K. Leung, G. R. Anderson, and P. J. Norr, *J. Food Sci.* 50, 942–945 (1985).
99. K. E. Kaylegian and R. C. Lindsay, *J. Dairy Sci.* 75, 3307–3317 (1992).
100. B. Breitschuh and E. J. Windhab, *J. Am. Oil Chem. Soc.* 73, 1603–1610 (1996).
101. A. J. Wright, R. W. Hartel, S. S. Narine, and A. G. Marangoni, *J. Am. Oil Chem. Soc.* 77, 463–475 (2000).
102. N. M. Barfod and N. Krog, *J. Anal. Org. Chem. Soc.* 64, 112–119 (1987).
103. A. G. Marangoni and D. Rousseau, *J. Am. Oil Chem. Soc.* 75, 1265–1271 (1998).
104. D. Rousseau, K. Forestiere, A. R. Hill, and A. G. Marangoni, *J. Am. Oil Chem. Soc.* 73, 963–972 (1996).
105. A. G. Marangoni, A. J. Wright, S. S. Narine, and R. W. Lencki, *J. Am. Oil Chem. Soc.* 77, 565–567 (2000).
106. S. Shanbhag, M. P. Steinberg, and A. I. Nelson, *J. Am. Oil Chem. Soc.* 48, 11 (1971).
107. E. G. Samuelson and J. Vikelsoe, *Milchwissenschaft* 26, 621–625 (1971).
108. P. Walstra and E. C. H. Van Beresteyn, *Netherlands Milk Dairy J.* 29, 36–65 (1975).
109. M. A. J. S. Van Boekel, *J. Am. Oil Chem. Soc.* 51, 316–320 (1974).
110. N. M. Barfod, N. Krog, G. Larsen, and W. Buchheim, *Fat Sci. Technol.* 1, 24–29 (1991).

111. T. Sugimoto, T. Mori, J. Mano, T. A. Mutoh, Y. Shiinoki, and Y. Matsumura, *J. Am. Oil Chem. Soc.* 78, 183–188 (2001).
112. D. Le Botlan and I. Helie, *Anal. Chim. Acta* 311, 217–223 (1995).
113. J. Van Duynhoven, I. Dubourg, G. J. Goudappel, and E. Roijers, *J. Am. Oil Chem. Soc.* 79, 383–388 (2002).
114. D. Le Botlan, J. Wennington, and J. C. Cheftel, *J. Colloid Interf. Sci.* 226, 16–21 (2000).
115. C. Simoneau, M. J. McCarthy, R. J. Kauten, and J. B. German, *J. Anal. Org. Chem. Soc.* 68, 481–487 (1991).
116. S. L. Duce, T. A. Carpenter, and L. D. Hall, *Lebensm. Wiss. Technol.* 23, 545–590 (1990).
117. A. Davenel, P. Marchal, A. Riaublanc, and G. Gandemer, in *Advances in Magnetic Resonance in Food Science* (P. Belton, B. Hills, G. A. Webb, eds.), The Royal Society of Chemistry, Cambridge, 1999.
118. S. Ozilgen, C. Simoneau, J. B. German, M. J. McCarthy, and D. S. Reid, *J. Sci. Food Agric.* 61, 101–108 (1993).
119. J. Trumbetas, J. A. Fioriti, and R. J. Sims, *J. Am. Oil Chem. Soc.* 53(12), 722–726 (1976).
120. J. Trumbetas, J. A. Fioriti, and R. J. Sims, *J. Am. Oil Chem. Soc.* 55(2), 248–251 (1978).
121. J. L. Cavallo and D. L. Chang, *Chem. Eng. Prog.* 86, 54–59 (1990).
122. D. Turubull, *J. Chem. Phys.* 20, 411 (1952).
123. J. P. C. Cordiez, G. Grange, and B. Mutaftschiev, *J. Colloid Interf. Sci.* 85, 431–441 (1982).
124. D. Clause, in *Encyclopedia of Emulsion Technology*, (P. Becher, ed.), Marcel Dekker, New York, 1985.